



# Space engineering

## Spacecraft mechanical loads analysis handbook

ECSS Secretariat  
ESA-ESTEC  
Requirements & Standards Division  
Noordwijk, The Netherlands

Foreword

This Handbook is one document of the series of ECSS Documents intended to be used as supporting material for ECSS Standards in space projects and applications. ECSS is a cooperative effort of the European Space Agency, national space agencies and European industry associations for the purpose of developing and maintaining common standards.

The material in this Handbook is defined in terms of description and recommendation how to organize and perform mechanical loads analyses of spacecraft and payloads.

This handbook has been prepared by the ECSS-E-HB-32-26 Working Group, reviewed by the ECSS Executive Secretariat and approved by the ECSS Technical Authority.

## Disclaimer

ECSS does not provide any warranty whatsoever, whether expressed, implied, or statutory, including, but not limited to, any warranty of merchantability or fitness for a particular purpose or any warranty that the contents of the item are error-free. In no respect shall ECSS incur any liability for any damages, including, but not limited to, direct, indirect, special, or consequential damages arising out of, resulting from, or in any way connected to the use of this document, whether or not based upon warranty, business agreement, tort, or otherwise; whether or not injury was sustained by persons or property or otherwise; and whether or not loss was sustained from, or arose out of, the results of, the item, or any services that may be provided by ECSS.

Published by: ESA Requirements and Standards Division  
ESTEC, P.O. Box 299,  
2200 AG Noordwijk  
The Netherlands

Copyright: 2013© by the European Space Agency for the members of ECSS

## Change log

---

ECSS-E-HB-32-26A 19 February 2013	First issue
--------------------------------------	-------------

## Table of contents

<b>Change log .....</b>	<b>3</b>
<b>Acknowledgements .....</b>	<b>12</b>
<b>Preface.....</b>	<b>13</b>
<b>1 Scope.....</b>	<b>15</b>
<b>2 References .....</b>	<b>15</b>
<b>3 Terms, definitions and abbreviated terms.....</b>	<b>16</b>
3.1    Terms from other documents .....	16
3.2    Terms specific to the present document .....	17
3.3    Abbreviated terms.....	18
<b>4 Overview of the loads analysis process.....</b>	<b>22</b>
4.1    Introduction.....	22
4.2    Loads cycles.....	23
4.3    Logic and sequence of loads analysis.....	24
4.4    Loads and verification approach (prototype or protoflight).....	25
4.5    Loads and levels of assembly .....	27
4.6    Mechanical loads for design and verification.....	28
4.6.1    Spacecraft flight environments and dynamic loads.....	28
4.6.2    Vibration environments and frequency range .....	28
4.6.3    Introduction to analysis and test types for verifying mechanical requirements .....	29
4.6.4    Static and quasi-static loads.....	31
4.6.5    Static loads test.....	33
4.6.6    Spacecraft-launcher coupled loads analysis .....	34
4.6.7    Sine vibration .....	35
4.6.8    Spacecraft design loads and test predictions versus LV/SC CLA results .....	37
4.6.9    Random vibration and vibro-acoustic environment.....	38
4.6.10    Shock testing .....	40
4.7    Basic principles, criteria and assumptions in structure and loads verification .....	41

4.7.1	Introduction .....	41
4.7.2	Equivalence criteria for loads and environments .....	41
4.7.3	Criteria for assessing verification loads .....	44
4.7.4	Main inconsistencies of the loads verification process.....	44
4.8	Notching in sine and random vibration testing.....	45
4.8.1	Introduction .....	45
4.8.2	Example of requirements .....	45
4.8.3	Basic principles .....	45
4.8.4	Response and force limiting .....	46
4.8.5	Criteria for notching justification .....	48
4.8.6	Conclusions on notching in sine and random vibration testing .....	50
4.9	References .....	50
<b>5</b>	<b>Background on structural dynamics .....</b>	<b>52</b>
5.1	Introduction.....	52
5.1.1	The dynamic environment.....	52
5.1.2	Types of structural analysis.....	53
5.1.3	List of topics .....	54
5.1.4	Principal notations.....	54
5.2	Dynamic environments – analysis and specifications.....	56
5.2.1	Generalities.....	56
5.2.2	Example - the maiden flight of Ariane 1 .....	57
5.2.3	Sine environment .....	59
5.2.4	Transient environment .....	64
5.2.5	Random environment.....	67
5.2.6	Sine-equivalent dynamics .....	76
5.2.7	Combined environments .....	85
5.3	Dynamic analysis.....	88
5.3.1	Frequency domain analysis.....	88
5.3.2	Modal approach .....	90
5.3.3	Effective mass models .....	94
5.3.4	Craig-Bampton models .....	95
5.4	Coupled analysis and notching in sine tests.....	109
5.4.1	FRF coupling.....	109
5.4.2	Modal approach .....	110
5.4.3	Simple example .....	111
5.4.4	Use of the shock response spectrum .....	113
5.5	Primary and secondary notching.....	117
5.5.1	Modes concerned by primary notching.....	117
5.5.2	Secondary notching .....	117

5.5.3	Simple example .....	118
5.5.4	Conclusions on notching in sine tests .....	120
5.6	Random tests .....	120
5.6.1	Issues on random tests .....	120
5.6.2	Mechanical equivalence example.....	121
5.6.3	Notching in random vibration tests .....	123
5.7	Practical aspects of modal effective masses.....	126
5.8	Conclusions .....	128
5.9	References .....	128
<b>6</b>	<b>Launcher / spacecraft coupled loads analysis .....</b>	<b>131</b>
6.1	Introduction.....	131
6.1.1	General aspects.....	131
6.1.2	Launch loads and terminology used in the CLA process .....	132
6.1.3	The role of the CLA within the loads cycle.....	134
6.2	The phases of the CLA process.....	135
6.2.1	Introduction .....	135
6.2.2	Parameters driving the CLA process .....	136
6.2.3	Mathematical model verification and database integration .....	136
6.2.4	Finite element model reduction .....	136
6.2.5	Checks on the Craig-Bampton matrices and OTM .....	137
6.2.6	Frequency cut-off for computed modes .....	137
6.2.7	Coupling of the launcher and spacecraft models.....	137
6.2.8	Calculation of the generalized responses.....	137
6.2.9	Determination of the physical responses.....	137
6.2.10	Post-processing .....	137
6.2.11	Uncertainty factors .....	138
6.3	CLA output and results evaluation .....	139
6.3.1	Overview .....	139
6.3.2	Guidelines to response parameter selection.....	140
6.3.3	Equivalent sine input.....	140
6.3.4	Computation of static components from OTM .....	140
6.3.5	Relative displacements .....	141
6.3.6	Interface mechanical fluxes and overfluxes .....	141
6.3.7	Results review, verification and validation .....	146
6.3.8	Use of CLA results for structural verification.....	147
6.3.9	Reporting .....	147
6.4	Ariane 5 coupled loads analysis.....	150
6.4.1	Introduction to Ariane 5 CLA .....	150
6.4.2	Mission analysis organization and management .....	151

6.4.3	CLA events and load cases.....	152
6.4.4	Concomitant events and load cases combination.....	161
6.4.5	Flight phases and CLA standard load cases .....	162
6.4.6	Aspects of the Ariane 5 CLA methodology .....	165
6.5	The Arianespace spacecraft qualification process .....	167
6.5.1	Introduction .....	167
6.5.2	Quasi-static loads .....	168
6.5.3	Dynamic environment .....	170
6.6	Space Shuttle coupled loads analysis.....	176
6.6.1	Overview.....	176
6.6.2	CLA load events.....	177
6.6.3	Elements of the design and verification process for Space Shuttle payloads .....	178
6.7	References .....	181
<b>7</b>	<b>Static loads .....</b>	<b>182</b>
7.1	Introduction.....	182
7.2	Quasi-static loads .....	182
7.2.1	General aspects.....	182
7.2.2	Equivalence between dynamic conditions and CoG net accelerations ...	183
7.2.3	Quasi-static loads specification .....	184
7.2.4	Prediction of QSL and mechanical environment by base-drive analysis.....	186
7.3	Static test philosophy and objectives .....	186
7.4	Definition of static test configuration and load cases.....	187
7.4.1	Introduction .....	187
7.4.2	Boundary conditions.....	188
7.4.3	Loading systems .....	188
7.4.4	Load cases .....	189
7.4.5	Instrumentation .....	190
7.5	Static test evaluation.....	190
7.6	References .....	192
<b>8</b>	<b>Sine vibration .....</b>	<b>201</b>
8.1	Introduction.....	201
8.2	Sine vibration levels specification .....	201
8.2.1	Sine loads for spacecraft.....	201
8.2.2	Sine loads for payload and equipment .....	202
8.3	Simulation / test prediction.....	203
8.3.1	Introduction .....	203
8.3.2	Boundary conditions.....	203

8.3.3	Damping .....	204
8.3.4	Notch assessment.....	204
8.4	Sine vibration test .....	205
8.4.1	Objectives .....	205
8.4.2	Notching process .....	206
8.4.3	Test preparation.....	208
8.4.4	Sine test campaign.....	221
8.5	References .....	231
<b>9</b>	<b>Random vibration and vibro-acoustics .....</b>	<b>232</b>
9.1	Introduction.....	232
9.1.1	Overview.....	232
9.1.2	Random vibration loads .....	233
9.1.3	Vibro-acoustic loads.....	233
9.2	Requirements .....	236
9.3	Random vibration specification .....	236
9.3.1	Introduction .....	236
9.3.2	Component vibration environment predictor, Spann method .....	236
9.3.3	Specifications derived from random and vibro-acoustic test data .....	238
9.3.4	VibroSpec .....	240
9.3.5	Test/analysis extrapolation method.....	242
9.4	Random vibration analysis.....	244
9.4.1	Finite element analysis and Miles' equation .....	244
9.4.2	Finite element analysis.....	245
9.4.3	Guidelines for FE random vibration response analysis .....	247
9.5	Random vibration testing .....	249
9.5.1	Introduction .....	249
9.5.2	Notching.....	249
9.6	Vibro-acoustic analysis .....	266
9.6.1	Introduction .....	266
9.6.2	Boundary element analysis .....	266
9.6.3	Statistical energy analysis .....	269
9.6.4	General guidelines for vibro-acoustic analyses .....	272
9.7	Acoustic testing .....	274
9.7.1	Introduction .....	274
9.7.2	Test plan/procedure .....	274
9.8	Verification of compliance.....	276
9.8.1	General aspects.....	276
9.8.2	An example based on the vibration response spectrum .....	277
9.9	Special topics in random vibration .....	280

9.9.1	Simulation of the random time series .....	280
9.9.2	Prediction of random acoustic vibration of equipment mounted on panels .....	283
9.9.3	Quick way to predict fatigue life (Steinberg method).....	287
9.10	References .....	290
<b>10 Shock</b>	<b>293</b>	
10.1	Introduction.....	293
10.2	Shock environment.....	293
10.3	Shock design and verification process .....	294
10.3.1	Shock input derivation to subsystems .....	295
10.3.2	Shock verification approach .....	296
10.3.3	Shock damage risk assessment.....	299
10.4	References .....	302
<b>11 Dimensional stability</b>	<b>303</b>	
11.1	Introduction.....	303
11.2	Dimensional stability analysis .....	304
11.2.1	Thermo-elastic distortion analysis .....	305
11.2.2	1g-0g transition (gravity release) .....	312
11.2.3	Moisture absorption / release .....	313
11.3	Dimensional stability verification .....	315
11.3.1	Introduction .....	315
11.3.2	Thermal distortion test.....	315
11.3.3	Gravity release test .....	321
11.4	Material property characterisation testing .....	322
11.4.1	Coefficient of Thermal Expansion (CTE) characterisation .....	322
11.4.2	Coefficient of Moisture Expansion (CME) characterisation .....	323
11.5	References .....	324
<b>12 Fatigue and fracture control</b>	<b>325</b>	
12.1	Introduction.....	325
12.2	Definitions.....	328
12.3	List of events .....	328
12.4	Load spectra per event .....	332
12.4.1	General .....	332
12.4.2	Existing load curves .....	332
12.4.3	Measured load curves .....	334
12.4.4	Calculating load curves .....	336
12.5	Generation of fatigue spectra.....	340
12.6	References .....	341

<b>13 Micro-gravity and micro-vibrations.....</b>	<b>343</b>
13.1 Introduction.....	343
13.1.1 Background.....	343
13.1.2 Scope.....	344
13.2 Micro-gravity .....	344
13.2.1 General aspects.....	345
13.2.2 Derivation of micro-gravity specifications .....	356
13.2.3 Micro-gravity environment verification .....	364
13.3 Micro-vibration .....	371
13.3.1 General aspects.....	371
13.3.2 Micro-vibration analysis.....	373
13.3.3 Micro-vibration budget assessment.....	381
13.3.4 Pointing error synthesis.....	384
13.3.5 Micro-vibration verification test.....	385
13.4 Micro-gravity and micro-vibration disturbance sources .....	390
13.4.1 Scope.....	390
13.4.2 Review of potential disturbance sources .....	390
13.4.3 Characterisation of the disturbance sources forcing functions.....	400
13.5 References .....	437
<b>14 Soft stowed packaging.....</b>	<b>439</b>
14.1 Introduction.....	439
14.2 Packaging guidelines .....	440
14.3 Materials for packaging.....	441
14.3.1 Physical properties.....	441
14.3.2 Attenuation data for foam packed items .....	447
14.4 Soft stowed equipment verification flow .....	453
14.4.1 Hardware categories and criticality.....	453
14.4.2 General verification aspects .....	453
14.4.3 Off-the-shelf (OTS) items and already existing equipment .....	458
14.4.4 New equipment / hardware .....	460
14.2 References .....	465
<b>15 Nonlinear structures.....</b>	<b>466</b>
15.1 Introduction.....	466
15.2 Common spacecraft structure nonlinearities .....	466
15.2.2 Damping .....	467
15.2.3 Contact .....	468
15.2.4 Nonlinear stiffness.....	469
15.3 Nonlinearity detection .....	470

15.4 Handling of spacecraft structure nonlinearities.....	471
15.4.1 Introduction .....	471
15.4.2 Guidelines for testing .....	472
15.4.3 Nonlinearity characterisation and parameter estimation .....	474
15.4.4 Guidelines for structure modelling and analysis .....	476
15.4.5 Impact of nonlinearities on CLA flight load predictions .....	481
15.5 References .....	483
<b>16 Finite element models.....</b>	<b>484</b>
16.1 Introduction.....	484
16.2 Requirements for structure mathematical models .....	485
16.3 Introduction to V&V in computational mechanics .....	485
16.4 Spacecraft finite element model complexity and validation test.....	488
16.5 Uncertainty quantification during load cycles .....	489
16.5.1 Overview.....	489
16.5.2 Dynamic variability or uncertainty factor $K_v$ .....	489
16.5.3 Model factor $K_M$ .....	491
16.6 Verification and quality assurance for spacecraft finite element analysis .....	491
16.7 Mathematical model validation.....	493
16.7.1 General concepts and terminology.....	493
16.7.2 Why a mathematical model validation process.....	494
16.7.3 Categorization of the uncertainty and sources of disagreement between simulation and experimental outcomes .....	495
16.7.4 Specific aspects of the validation of spacecraft FEM for coupled loads analysis.....	495
16.7.5 Error localization and model updating by sensitivity and optimization.....	500
16.7.6 Specific aspects concerning base-drive sine vibration testing and “real-time” model validation .....	501
16.7.7 Stochastic approaches for model validation .....	502
16.8 References .....	503

## Acknowledgements

The following persons were actively involved in the development of this handbook:

G. Aglietti, University of Surrey

J. Albus, Astrium

M. Bellini, TAS-I

J. Buffe, TAS-F

D. Burtin, ArianeSpace

A. Calvi, ESA-ESTEC (Convenor)

A. Capitaine, Astrium

E. Cavro, Intespace

J. Dupré, ArianeSpace

C. Fabriès, TAS-F

S. Fransen, ESA-ESTEC

D. Gangloff, CNES

A. Girard, Intespace (retired)

N. Gualtieri, TAS-I

A. Itta, TAS-I

G. Kerschen, University of Liege

W. Konrad, Astrium

S. Laborde, Astrium

R. Morisset, Astrium

P. Nali, TAS-I

A. Newerla, ESA-ESTEC

F. Quagliotti, TAS-I

A. Rittweger, Astrium

N. Roy, Top Modal

J. San Juan Molla, ArianeSpace

G. Sinnema, ESA-ESTEC

R. Ullio, TAS-I

J-B Vergniaud, Astrium

R.P.G. Veul, NLR

J. J. Wijker, NSO

Comments concerning the technical content of this handbook are welcomed by the European Cooperation for Space Standardization, Noordwijk, the Netherlands, [www.ecss.nl](http://www.ecss.nl).

## Preface

The ECSS-E-HB-32-26 "Spacecraft Mechanical Loads Analysis Handbook" has been developed with the aim to harmonize methodologies, procedures and practices currently applied for the conduct of spacecraft and payloads loads analysis. It makes available to the European Space Community a set of well proven methods, procedures and guidelines for the prediction and assessment of structural design loads and for the evaluation of the test loads. In particular, recent advances in the area of structural dynamics and vibrations, in both methodology and performance, have the potential to make spacecraft system analysis and testing more effective from technical, cost, and hardware safety points of view. However, application of advanced analysis methods varies among the Space Agencies and their contractors. Identification and refinement of the best of these methodologies and implementation approaches has been an objective of the Working Group.

The handbook is intended to be a practical guide rather than a theoretical treatise. The emphasis is on dynamic environments of spacecraft, however other mechanical environments are addressed and often the principles are broad enough to be applicable in many cases to launch vehicles as well. It is assumed that the reader has a general knowledge of spacecraft structures and structural dynamics without necessarily being an expert in these disciplines.

This first edition represents a collection of contributions by a number of engineers from throughout the European Space Community. It reflects the insight gained from their practical experience. The contributions have been harmonised and the handbook completed by the "harmonization team". The level of treatment varies among topics, depending on the issues each author feels is critical and the overall assessment performed by the harmonization team concerning the level of detail in each topic that is important to the loads analysis process.

The book is not intended as a selfstanding textbook since in some cases it is rather complementary to other ECSS documents and more in general to textbooks and publications on spacecraft structures and structural dynamics. It can be a key tool for spacecraft designers, system and structural engineers who need to find out more about mechanical loads analysis and for those in charge of developing requirements and specifications.

The reader benefits best by reading the book sequentially, although most of the chapters are selfcontained, with references to other parts of the book provided as needed. An overview of the chapters is presented below:

- Chapter 4 gives an overview of the loads analysis process aimed at establishing appropriate loads for design and testing.
- Chapter 5 presents a summary of the principles of structural dynamics addressed throughout the different chapters of the present handbook.
- Chapter 6 addresses the launcher / spacecraft coupled loads analyses performed to check that a spacecraft design is compliant with the overall mechanical environment generated by a launcher during all flight phases and to ensure that the mission can be achieved.

- Chapters 7 to 10 deal with analysis and testing related to the various types of mechanical environments generated by the launcher: static in chapter 7, sine vibrations in chapter 8, random vibrations (including vibro-acoustic environment) in Chapter 9, shocks in chapter 10.
- Chapter 11 is devoted to dimensional stability i.e. the behaviour of highly accurate structures to maintain their dimensions under all kinds of conditions.
- Chapter 12 deals with fracture control and fatigue life verification, discussing the various aspects involved in deriving fatigue load spectra to perform analyses or tests.
- Chapter 13 addresses the micro-gravity and micro-vibration environment for which the spacecraft systems should be designed and operated such that limit acceleration levels are not exceeded.
- Chapter 14 is related to soft stowed equipment and the verification process of items packed in foam, to assess the compatibility of the cargo item with the attenuated environments.
- Chapter 15 tackles the problems generated by a nonlinear behaviour of the structures, which can significantly affect the verification process.
- Chapter 16 addresses the mathematical models used for loads analysis, with emphasis on finite element analysis quality and acceptance of the results.

Funding and resources for the handbook were provided by the European Cooperation for Space Standardization leading to the creation of the initial Working Group. However the number of contributors soon increased with time and substantial additional volunteer support was provided by individuals and organizations.

These additional resources have been crucial to the successful accomplishment of the “handbook project”. All the volunteer contributors that have sacrificed their time are gratefully acknowledged, as well as the contributors that made an effort beyond the allocated resources. This first edition of handbook is thus the result of two and a half years of effort by the “enlarged” Loads Analysis Working Group.

A substantial effort has been made to eliminate mathematical and factual errors. Nevertheless it is possible (and likely) that some errors will be found through readers’ use of the handbook. Detected errors along with any omissions, corrections or comments may be sent to either the ECSS Secretariat or to the addresses below. If, as hoped, the book is of use to the space community, it could be updated and made more useful and practical.

**1****Scope**

---

The ECSS-E-HB-32-26 recommends engineering practices for European programs and projects. It may be cited in contracts and program documents as a reference for guidance to meet specific program/project needs and constraints.

The target users of this handbook are engineers involved in design, analysis and verification of spacecraft and payloads in relation to general structural loads analysis issues. The current know-how is documented in this handbook in order to make this expertise available to all European developers of space systems.

It is a guidelines document; therefore it includes advisory information rather than requirements.

**2****References**

---

Due to the structure of the document, each chapter includes at its end the references called in it.

# 3

## Terms, definitions and abbreviated terms

### 3.1 Terms from other documents

For the purpose of this document, the terms and definitions from ECSS-S-ST-00-01 apply.

For the purpose of this document, the following terms and definitions from ECSS-E-ST-32 apply:

buckling  
design allowable  
design factor  
design limit load (DLL)  
design load (DL)  
design parameters  
design ultimate load (DUL)  
design ultimate stress  
design yield load (DYL)  
design yield stress  
detrimental deformation  
factor of safety (FOS)  
failure  
limit load (LL)  
relieving loads  
residual stress  
stiffness  
structural design  
structure  
ultimate strength  
yield strength

For the purpose of this document, the following terms and definitions from ECSS-E-ST-32-10 apply:

local design factor (KLD)  
margin policy factor (KMP)  
model factor (KM)  
project factor (KP)  
test factors (KA and KQ)  
ultimate design factor of safety (FOSU)  
yield design factor of safety (FOSY)

## 3.2 Terms specific to the present document

### 3.2.1 Fundamental mode

Same as primary mode

### 3.2.2 Global mode

Mode which corresponds to a global movement

NOTE A global mode can be a secondary mode e.g. when opposed motion is present.

### 3.2.3 Load factor

Dimensionless multiple of the gravitational acceleration that represents the inertia force acting on a structure

### 3.2.4 Local mode

Mode which corresponds to a local movement

NOTE A local mode can be a primary mode e.g. tank mode.

### 3.2.5 Notching

Reduction of acceleration input levels around resonant frequencies, to avoid over testing

### 3.2.6 Primary mode

Mode associated with a large effective mass

NOTE No cut-off criterion can be given. Primary modes are identified in relative terms by examination of the table of modal effective masses. In practice there are 1 or 2 primary modes in the lateral directions and perhaps more in the axial direction.

### 3.2.7 Quasi-static loads

Combination of static and dynamic loads into an equivalent static load specified for design purposes

NOTE 1 quasi-static loads are equivalent to (or interpreted by the designer as) static loads, typically expressed as equivalent accelerations at the CoG.

NOTE 2 in some contexts quasi-static loads are understood as: "loads associated to a quasi-static event".

### 3.2.8 Quasi-static acceleration

Depending on the context the following definitions are in use:

- quasi-static load expressed as equivalent acceleration at the CoG (general)
- quasi-static component of the acceleration (specific, e.g. in LV/SC CLA terminology)
- acceleration associated to a quasi-static event (specific)

### 3.2.9 Quasi-static component

Component of a parameter (e.g. force or acceleration) which does not include the vibration

### **3.2.10 Quasi-static event**

Event generated by external forces which change slowly with time so that the dynamic response of the structure is not significant

### **3.2.11 Secondary mode**

Mode that is not primary i.e. with small effective mass

### **3.2.12 Static acceleration**

Acceleration of constant magnitude and direction with respect to the structure

NOTE in the LV/SC CLA terminology it is normally understood as CoG “mean acceleration” (i.e. no vibration included) of the LV/SC system assumed as rigid body. This is equivalent to the quasi-static component of the acceleration.

### **3.2.13 Static load**

Load of constant magnitude and direction with respect to the structure

NOTE examples are loads caused by joint preloads, clamping, and constant thrust

### **3.2.14 Steady load**

Same as static load

### **3.2.15 Steady-state acceleration**

Same as static acceleration

### **3.2.16 Steady-state vibration**

Vibration which exists in a system if the velocity of each particle is a continuing periodic quantity

## **3.3 Abbreviated terms**

For the purpose of this document, the abbreviated terms from ECSS-S-ST-00-01 and the following apply:

<b>Abbreviation</b>	<b>Meaning</b>
<b>AL</b>	Acceptance Test Load
<b>ATM</b>	Acceleration Transformation Matrix
<b>ATV</b>	Automated Transfer Vehicle
<b>BE</b>	Boundary Elements
<b>BEM</b>	Boundary Element Method
<b>CDR</b>	Critical Design Review
<b>CE</b>	Cargo Element
<b>CLA</b>	Coupled Loads Analysis
<b>CNES</b>	<i>Centre National d'Etudes Spatiales</i> – French National Space Agency
<b>COF</b>	Cross-Orthogonality Factor

Abbreviation	Meaning
<b>CoG</b>	Centre of Gravity
<b>CME</b>	Coefficient of Moisture Expansion
<b>CTE</b>	Coefficient of Thermal Expansion
<b>CTM</b>	CoG Transformation Matrix
<b>DAAR</b>	<i>Dispositif d'Accrochage Arrière</i> - Lower Attachment Device
<b>DAAV</b>	<i>Dispositif d'Accrochage Avant</i> - Forward Attachment Device
<b>DCI</b>	<i>Document de Contrôle d'Interface</i> – Interface Control Document
<b>DIAS</b>	<i>Dispositif A Souplisseur</i> – Softening Device
<b>DLL</b>	Design Limit Load
<b>DOF</b>	Degree of Freedom
<b>DOP</b>	Duct OverPressure
<b>DRD</b>	Document Requirement Definition
<b>DTM</b>	Displacement Transformation Matrix
<b>DUL</b>	Design Ultimate Load
<b>DYL</b>	Design Yield Load
<b>EAP</b>	<i>Etage d'Accélération à Poudre</i> – Solid Rocket Booster
<b>EPC</b>	<i>Etage Principal Cryotechnique</i> - Cryogenic Main Core Stage
<b>EPS</b>	<i>Etage à Propergols Stockables</i> – Storable Propellant Stage
<b>EQM</b>	Engineering Qualification Model
<b>ESC-A</b>	<i>Etage Supérieur Cryotechnique type A</i> – Upper Cryogenic Stage type A
<b>ESA</b>	European Space Agency
<b>ESI</b>	Equivalent Sine Input
<b>ESTEC</b>	European Space Research and Technology Centre
<b>FCLA</b>	Final Coupled Loads Analysis
<b>FDS</b>	Fatigue Damage Spectrum
<b>FE</b>	Finite Element
<b>FEA</b>	Finite Element Analysis
<b>FEM</b>	Finite Element Model
<b>FM</b>	Flight Model
<b>FMD</b>	Force Measurement Device
<b>FRF</b>	Frequency Response Function
<b>FOS</b>	Factor of Safety
<b>FOSU</b>	Ultimate Design Factor of Safety
<b>FOSY</b>	Yield Design Factor of Safety
<b>HSB</b>	Handbuch Struktur Berechnung
<b>I/F</b>	Interface

<b>Abbreviation</b>	<b>Meaning</b>
<b>IOP</b>	Ignition OverPressure
<b>IRF</b>	Impulse Response Function
<b>ISS</b>	International Space Station
<b>ITAR</b>	International Traffic in Arms Regulation
<b>KA</b>	Acceptance Test Factor
<b>KQ</b>	Qualification Test Factor
<b>LL</b>	Limit Load
<b>LTM</b>	Load Transformation Matrix
<b>LV</b>	Launch Vehicle
<b>MA</b>	Mode Acceleration (method)
<b>MAC</b>	Modal Assurance Criterion, Mass Acceleration Curve
<b>MD</b>	Mode Displacement (method)
<b>MEFE</b>	Maximum Expected Flight Environment
<b>MoS</b>	Margin of Safety
<b>MPLM</b>	Multi-Purpose Logistics Module
<b>MST</b>	Modal Survey Test
<b>MTA</b>	Mode Truncation Augmentation (method)
<b>MUA5</b>	Ariane 5 User's Manual
<b>NASA</b>	National Aeronautics and Space Administration
<b>NLR</b>	<i>Nationaal Lucht- en Ruimtevaartlaboratorium</i> – National Aerospace Laboratory
<b>NSO</b>	Netherlands Space Office
<b>OASPL</b>	Overall Sound Pressure Level
<b>OTM</b>	Output Transformation Matrix
<b>PCLA</b>	Preliminary Coupled Loads Analysis
<b>PFM</b>	Protoflight Model
<b>POC</b>	<i>Plan d'Opérations Combinées</i> – Combined Operations Plan
<b>PSD</b>	Power Spectral Density
<b>QL</b>	Qualification Test Load
<b>QM</b>	Qualification Model
<b>QS</b>	Quasi-Static
<b>QSL</b>	Quasi-Static Load
<b>RAL</b>	<i>Revue d'Aptitude au Lancement</i> - Launch Readiness Review
<b>RAMP</b>	<i>Revue d'Analyse de Mission Préliminaire</i> – Preliminary Mission Analysis Review
<b>RAMF</b>	<i>Revue d'Analyse de Mission Finale</i> – Final Mission Analysis Review

Abbreviation	Meaning
<b>RAV</b>	<i>Revue d'Aptitude au Vol</i> - Launch vehicle flight readiness review
<b>RMS (rms)</b>	Root Mean Square
<b>RRS</b>	Random Response Spectrum (also called VRS)
<b>SAMF</b>	<i>Spécification d'Analyse de Mission Finale</i> – Final Mission Analysis Specification
<b>SARO</b>	<i>Système Amortisseur du Réservoir Oxygène</i> – Oxygen Tank Damping System
<b>SC</b>	Spacecraft
<b>SDOF</b>	Single Degree of Freedom
<b>SEA</b>	Statistical Energy Analysis
<b>SYLDA</b>	<i>Système de Lancement Double Ariane 5</i> - Ariane 5 Double Launch System
<b>SM</b>	Structural Model
<b>SPL</b>	Sound Pressure Level
<b>SRB</b>	Solid Rocket Booster
<b>SRS</b>	Shock Response Spectrum
<b>STM</b>	Structural-Thermal Model
<b>STM</b>	Stress Transformation Matrix
<b>SSV</b>	Space Shuttle Vehicle
<b>TAS-F</b>	Thales Alenia Space France
<b>TAS-I</b>	Thales Alenia Space Italy
<b>UDHM</b>	Unsymmetrical Dimethyl Hydrazine (propellant)
<b>VLA</b>	Verification Loads Analysis
<b>VRS</b>	Vibration Response Spectrum (also called RRS)

## 4

# Overview of the loads analysis process

## 4.1 Introduction

Loads analysis substantially means establishing appropriate loads for design and testing. That is the task of loads analysis. The goal or purpose of loads analysis is nearly always to support design or to verify requirements for designed or built hardware.

Every event in the life of a spacecraft introduces structural loads. The challenge is to identify the events that may be critical, predict loads caused by each of the independent sources of loads for these events, and then combine the predicted loads in a manner suitable for design. Launch generates the highest loads for most spacecraft structures, but other events can be critical for parts of the structure [1].

There are many sources of loads during launch, in lateral as well as in axial directions. Some loads can be predicted as a function of time (deterministic loads), others can only be estimated statistically (random loads).

Predicting appropriate loads is one of the most challenging aspects of design. Structural loads depend on complex, random environments and on the designs of the spacecraft and launch vehicle, and the predicted loads which are used for design depend on how well the forcing environments and the model of the structure are mathematically simulated.

In practice the major sources of uncertainties are:

- Transient forcing functions and acoustic environments, usually based on flight and test data
- Mathematical models used for loads analysis

To account for uncertainty in design environments and mathematical models, uncertainty factors are applied to calculated loads.

Loads analysis is a crucial task in design a space structure. Loads analysis is doubly important because it is the basis for static and sine test loads used to verify strength of primary and many secondary structures. On the other hand predicting responses is important not only to assess the structure ability to survive but also to provide design and test environments and requirements for units and subsystems. Here it is worth to recall that ground testing is supposed to envelop mission environments, with margin.

A mistake in the loads analysis can mean that the structure is designed and tested to the wrong loads. For this reason it is important to be confident in the loads analysis, which means checking the sensitivity of the assumptions and validation of critical analysis. In particular the loads analysis which are at the basis of strength analysis and static or sine testing should be validated. Moreover, before reacting to loads analysis results, the engineering team should review them to make sure they are error free and reasonable [1].

## 4.2 Loads cycles

In most cases, structural loads are dependent not only on the external environment but also on the structural properties of the spacecraft or payload. This means the sizing of structural members can influence the loads. At the same time, the sizing is often governed by the need to withstand the loads. As a result, structural design and loads analysis are normally an iterative process [2]. This cycle, called “loads cycle”, is the iterative process of predicting and assessing structural loads. It basically consists of generating coupled mathematical models, calculating loads, assessing the loads, and identifying necessary design changes.

According to [1] a loads cycle is the process of:

- Generating and combining mathematical models for a proposed or established design
- Assembling or developing forcing functions, load factors, or other mathematical expressions to simulate the critical loading environments
- Calculating design loads and displacements for all significant ground, launch, and mission events
- Assessing the results to identify design modifications or risks
- Modifying the design accordingly or choosing to accept the risks

A loads analysis cycle should be performed whenever there is no sufficient confidence in the loads used to design the structure. This might be the case when:

- The structural design changes significantly from the last loads cycle
- The design environments change because of new flight or test data
- The mathematical models change significantly, e.g. following test results and the model validation process

Spacecraft programs typically perform a number of loads cycles, for example one each for preliminary design, final design, and final verification. The latter is done with “test correlated” mathematical models.

The verification loads cycle differs from design loads cycles only in that, instead of identifying required design changes, the adequacy of a structure that has already been built and tested is assessed. In practice the verification criteria are assessed not only for analysis but also for test. This also includes the reassessment of the analysis used to predict the acoustic and random vibration loads that occur simultaneously with maximum transients.

The primary steps in a typical launch vehicle-payload load cycle analysis process are shown in Figure 4-1. A similar approach may be used for any dynamic loading event [2].

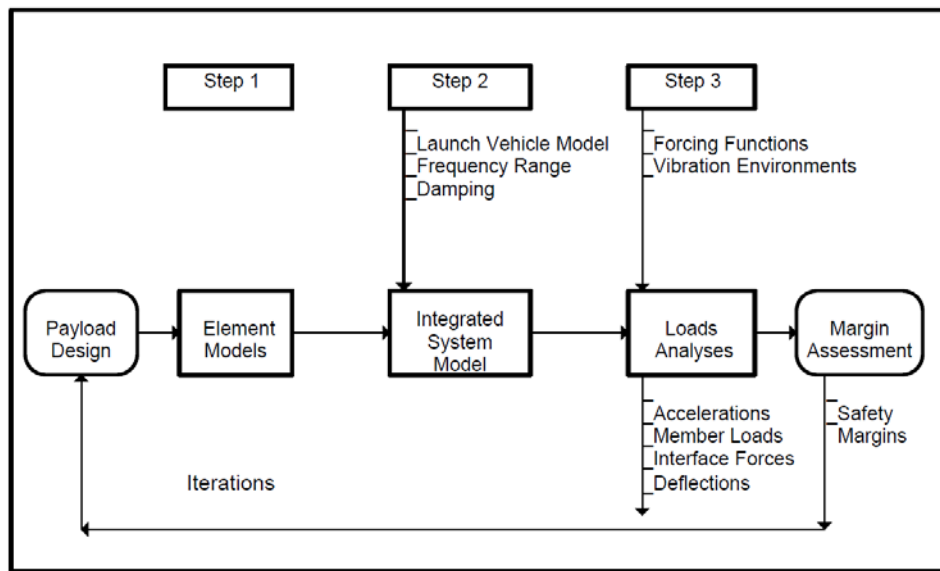


Figure 4-1: The Load Cycle Analysis Process [2]

### 4.3 Logic and sequence of loads analysis

The logic and sequence of the spacecraft loads analysis process depends on many factors strictly related to the general design, development and verification plan. In practice no general approach can be proposed. The whole process and the specific sequences within the loads cycles are strongly depending on the project and on the phase and maturity of the project itself. Nevertheless some "milestones" can be identified.

In the early stages of the project:

- Identification of structure architecture
- Dimensioning by preliminary loads assumptions. In particular for the primary structure by using the load factors taken from the launch vehicles user's guides
- Development of preliminary FEMs, in particular to verify stiffness
- Definition of technical specifications for equipment and identification of pre-qualified units (heritage)
- Frequency response analysis at spacecraft level, simulating the sine vibration test, for the evaluation of the structural response and for the preliminary definition of the primary notching
- Preliminary LV/SC CLA. This is usually performed "as soon as possible"

Starting from the phase B and during phases C-D the following activities are normally performed:

- Development of more detailed FEMs
- Refinement of the primary structure design
- Frequency response analysis. Not necessarily the technical specifications are changed
- (Base-drive) Random vibration analysis for reassessment of test specifications and test predictions
- Vibro-acoustic analysis at system level (FEM-BEM SEA). However it is not always performed
- (Intermediate &) Final LV/SC CLA
- Verification of compliance

## 4.4 Loads and verification approach (prototype or protoflight)

The verification philosophy, protoflight or prototype, has an important impact on the loads. This impact can be illustrated by Figure 4-2 and Table 4-1, here reported from [7]. However it should be noted that the interpretation which follows is slightly beyond the original (and normative) meaning of Figure 4-2 and Table 4-1 as reported in [7]. Nevertheless it well illustrates the effects of the verification philosophy on the loads.

Let us assume the left hand column of Figure 4-2, indicated as "Satellites test logic", together with the satellite coefficients reported in Table 4-1, reports the effects of the protoflight approach on the loads.

Similarly, let us assume the right hand column of Figure 4-2, indicated as "Launch vehicles test logic", together with the launch vehicles coefficients reported in Table 4-1, reports the effects of the prototype approach on the loads.

The major impact on the loads can be noted to be the different "design factor", i.e. "coefficient A": the protoflight approach suffers the penalty of the coefficient KQ for the definition of the design loads. This is evident on the protoflight model since it experiences the qualification loads.

Note 1: Figure 4-2 has the advantage of showing a compact overview of the common design logic together with the verification approaches by test. However, a visual comparison of the test loads levels for protoflight and prototype in line with the big arrow on the left side could be misleading. In fact it should be clear (looking in particular to Table 4-1) that the test levels, for protoflight and prototype, make reference to different values of design loads.

### Example

Using Table 4-1, interpreting "satellite" as "protoflight" and "launch vehicle" as "prototype" and finally assuming for sake of simplicity LL=100, , KQ=1.25, FOSU=1.25 (and all the other involved factors equal to unity):

Protoflight: LL=100; DLL=125; QL=125; DUL=156.25

Prototype: LL=100; DLL=100; QL=125; DUL=125

In conclusion the design ultimate loads are higher for the protoflight approach. This should be clear considering that the qualification loads are part of the loads to be experienced by the flight hardware.

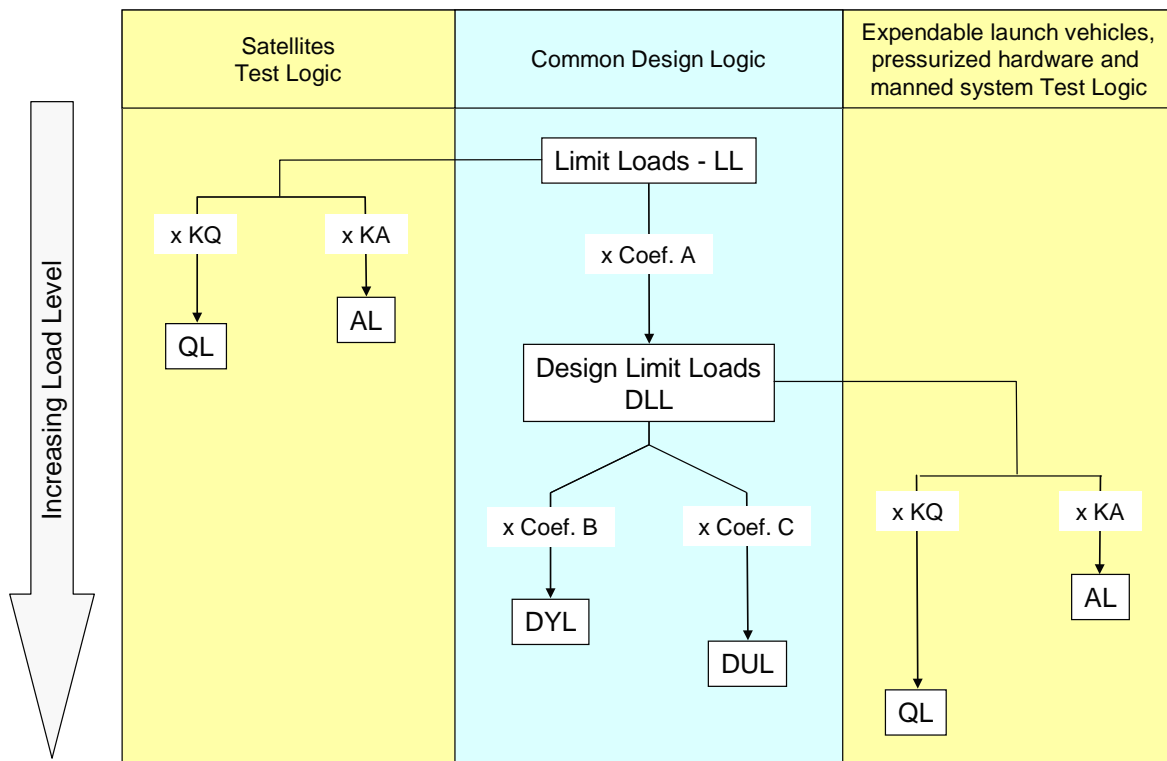


Figure 4-2: Logic for Factors of Safety application

Table 4-1: Relationship among (structural) factors of safety, design factors and additional factors

Coefficient	Satellite	Launch vehicles and pressurized hardware	Man-rated systems
Coef A or Design factor	KQ x K <sub>P</sub> x K <sub>M</sub>	K <sub>P</sub> x K <sub>M</sub>	K <sub>P</sub> x K <sub>M</sub>
Coef B	FOSY x K <sub>LD</sub>	FOSY x K <sub>MP</sub> x K <sub>LD</sub>	FOSY x K <sub>LD</sub>
Coef C	FOSU x K <sub>LD</sub>	FOSU x K <sub>MP</sub> x K <sub>LD</sub>	FOSU x K <sub>LD</sub>

Note 2: Definitions and numerical values for the factors reported in Table 4-1 are reported in [7].

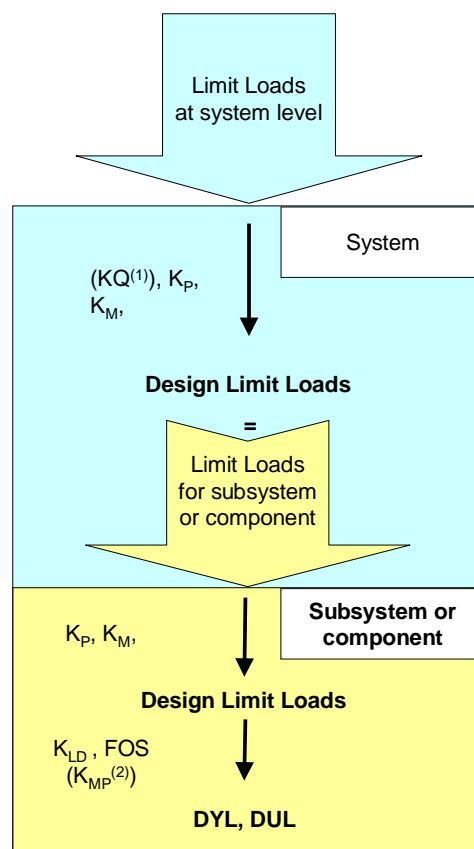
Note 3: The ECSS logic for factors of safety, as presented in Figure 4-2 and Table 4-1 and more in general in the ECSS documentation [7], is different, at least formally, from the logic in the NASA technical standard [18]. In particular the ECSS documentation makes a distinction between Limit Load and Design Limit Load, which is not the case in [18], where only LL is considered and DLL would be understood as synonymous. LL and DLL are also normally considered synonymous in the American technical literature, as for example in [1].

Note 4: The general guidelines for verification can be found in [6].

## 4.5 Loads and levels of assembly

The prediction of dynamic environments, as well as the formulation of design criteria and test specifications, is often accomplished for hardware at various levels of assembly. In fact because of the long lead times necessary to design and fabricate the parts, subassemblies, components, and subsystems used to produce a system, the hardware items at each level of assembly are usually tested separately to provide confidence that they function properly at the next level of assembly. However, the types of dynamic excitations of concern from a testing viewpoint can be different for different levels of assembly. The dynamic environment for every system and its constituent elements is carefully evaluated to establish the excitations that are relevant at each level of assembly.

The impact of the levels of assembly on the loads is illustrated by Figure 4-3, here reported from [7].



$KQ^{(1)}$ : for satellite  
 $K_{MP}^{(2)}$ : for launch vehicles

**Figure 4-3: Factors of Safety and levels of assembly**

The application logic for factors of safety as given in Figure 4-2 is applied in a “recursive” manner from system level to subsystem level or lower levels of assembly. DLL computed at each level are used as LL for analysis at their own level to compute the DLL for the next lower levels of assembly. In practice additional  $K_F$  and  $K_M$  factors are included at each lower level of assembly. This is graphically shown in Figure 4-3. For satellite,  $KQ$  is used only at system level in order to avoid repetitive application of qualification margins.

## 4.6 Mechanical loads for design and verification

### 4.6.1 Spacecraft flight environments and dynamic loads

Launch consists of a series of events, each of which has several independent sources of load for the launch vehicle and payload. The flight environments that generate static and dynamic loads on spaceflight hardware are normally categorized as follows (e.g. [1] [2]):

- The static acceleration, generated by constant external forces or which change slowly with time so that the dynamic response of the structure is not significant (also called quasi-static acceleration associated to a quasi-static event).
- The low-frequency dynamic response, typically from 0 Hz to 100 Hz, of the launch vehicle/payload system to transient flight events. However for some small launch vehicles the range of low-frequency dynamic response can be up to 150 Hz.
- The high-frequency random vibration environment, which typically has significant energy in the frequency range from 20 Hz to 2000 Hz, transmitted from the launch vehicle to the payload at the launch vehicle/payload interfaces.
- The high frequency acoustic pressure environment, typically from 20 Hz to 8000 Hz, inside the payload compartment. The payload compartment acoustic pressure environment generates dynamic loads on components in two ways: (1) by direct impingement on the surfaces of exposed components, and (2) by the acoustic pressure impingement upon the component mounting structures, which induces random vibrations that are mechanically transmitted to the components.
- Shock events. The energy spectrum is usually concentrated at or above 500 Hz and is measured in a frequency range of 100 Hz to 10 KHz [15].

Combinations of these loads may occur at different times in flight.

Once on-orbit, the spacecraft structural response to the micro-vibration environment, characterised by very low acceleration levels transmitted by the spacecraft structure, can be important for verifying the mission performances, for example compliance with pointing requirements of optical instruments.

### 4.6.2 Vibration environments and frequency range

One of the main issues related to the spacecraft structural analysis is that the phenomena (excitation sources and structural response) occur over a wide frequency range, from very low frequency up to medium and high frequency.

It should be noted that in this context “low frequency” refers to the range of frequencies from “static” (zero Hz) up to the first modes of vibration of the structure; whereas “high frequency” is where the structural response is characterised by high modal density and high modal overlap. Hence this terminology is not absolute but depends upon the particular structure’s characteristics. In fact, for a very stiff (and light) structure (e.g. equipment as a small electronic box) with lowest resonance frequency at a few hundred Hz this frequency range would be “low frequency” whereas for other structures, like large satellites, where the first modes can be in the region of e.g. 10 Hz, the range of frequency around 100 Hz and above could be referred to as high frequency; and low frequency would refer to a range of up to a few 10’s of Hz.

Currently there is not a single structural analysis technique which is able to describe accurately the structural behaviour in the whole frequency range.

In the low frequency region the FEM is able to predict the structural behaviour with good confidence. However, the prediction accuracy generally decreases as frequency increases. This can be for computational reasons linked to the mathematical modelling but also due to more physical causes.

For example, to maintain the computational effort within the limitation of the available computer technology often the mesh is not sufficiently fine to appropriately capture the short wavelength deformations typical of high frequency dynamics. In addition, computational techniques like mode superposition can introduce further inaccuracy due to the effects of modal truncation.

The more physical reasons for the inaccuracy of high frequency deterministic predictions (FE and other methods) are that the physical response becomes very sensitive to structural details (e.g. imperfections); some of which are unavoidable manufacturing and assembly tolerances. The practical result of this is that nominally identical physical structures tend to have different behaviour at high frequency, and this has been confirmed by the experience with the 5 satellites of the Rapideye constellation [13]. Also, authors in other areas of engineering, e.g. [14], have shown that nominally identical structures (the chassis of cars) from the same production line, at medium and high frequency, can display very different dynamic response properties.

Figure 4-4 illustrates the influence of the frequency content on the dynamic behaviour of spacecraft structures and the relevant structural analysis methodologies which are used.

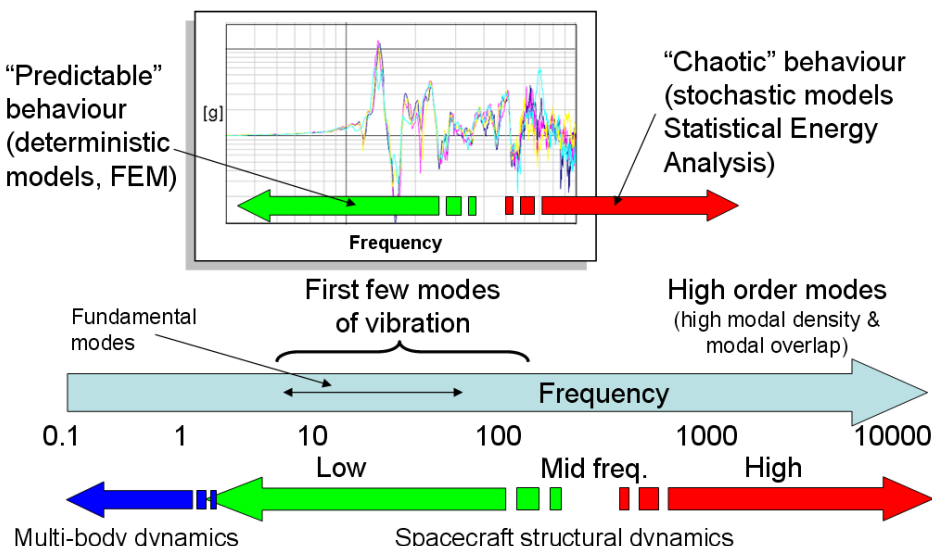


Figure 4-4: Dynamic behaviour and analysis methodologies w.r.t. frequency range

#### 4.6.3 Introduction to analysis and test types for verifying mechanical requirements

The spacecraft design process begins with an initial estimate of loads based on past experience with similar launch configurations. These preliminary design load factors are used to size the load-carrying structure. Once the preliminary design and corresponding drawings of the spacecraft are complete, they can be used to create a structural finite-element model. This model is in turn used to derive the condensed dynamic model and internal load recovery equations [16]. This information is used in the preliminary design load cycle, for example in the preliminary LV/SC CLA. In fact simultaneous steady-state and transient forces (which excite the structure low frequency modes of vibration) during launch usually cause most of the loads in the larger structures of the spacecraft.

Moreover, both individually and in combination, the mechanical environments of pressure, vibration, shock, and thermal gradients impose design requirements on many structural components. Ensuring

the survivability of the hardware poses challenges that in general can be met only by extensive pre-flight tests encompassing acoustic, shock, vibration, and thermal environments [15]. Table 4-2 provides a summary of analysis and test types that are normally used for verifying mechanical requirements.

Environmental testing is performed at varying magnitudes and durations to verify the design of space systems and to screen flight hardware for quality of workmanship. The first step in this process is the definition of the maximum expected environments during launch and on-orbit operation. Data from previous flights and ground tests are analysed to generate predictions for a specific mission. These environments are then flowed down from the space vehicle level to the various subsystems and components for use as design requirements and, later, as test requirements [15].

To account for uncertainties in mission environments and variations between the test article and the flight article, environments during qualification testing are more severe than at any time during the mission. Thus test environments may drive the design. This is especially true for secondary structures that are loaded most by high frequency vibrations.

Recent progress in the area of computational mechanics allows predicting and assessing the effects of medium and high frequency vibrations. However environmental testing, such as random vibration, acoustic and shock, has proven necessary for instruments and units because, in general, structural responses become more difficult to predict as the size of the structure decreases and the vibration frequency increases. Also, thickness, strength, and fatigue resistance are harder to control for tiny structures [1].

Objectives of the system level testing (i.e. environmental tests of the fully assembled spacecraft) are:

- To verify the spacecraft mechanical and electrical connections
- To measure the spacecraft responses (e.g. during acoustic testing) and verify that the environments used to qualify the spacecraft units were high enough.
- To be protected against unexpected phenomena (e.g. parametric instability of pressurized propellant tanks)
- To determine the dynamic contributions to the design inertia loads

It should be noted that the sine vibration test is commonly considered an environmental test, however in principle it is not. In fact normally the responses are monitored and the input forces are monitored as necessary to make sure the target responses or member loads are not exceeded (see Section 4.8).

A final remark is that the dynamic environments for space vehicle hardware are typically multiple-axis, i.e., the excitations occur simultaneously along all three orthogonal axes of the hardware. Acoustic tests naturally simulate a multiple-axis excitation, but shock and vibration test facilities are commonly uniaxial. Multiple axis test facilities designed to simulate low frequency shock and vibration environments (generally below 100 Hz) are available. For space vehicle hardware, however, it is more common to perform shock and vibration tests using machines that apply the excitation sequentially along one axis at a time. The potential error caused by simulating a multiple-axis shock and/or vibration excitation with sequentially applied single-axis excitations is widely debated [3].

**Table 4-2: Analysis and test types used for verifying mechanical requirements**

Load	Verification by analysis	Verification by test
Static & Quasi-static	Static analysis	Static test Sine burst test Sine vibration test
Transient environment in low frequency range	Transient analysis Frequency response analysis	Sine vibration test
Quasi harmonic loads in low frequency range	Frequency response analysis Transient analysis	Sine vibration test
Broad band vibration (random & acoustic)	Random vibration analysis Vibro-acoustic analysis	Random vibration test Acoustic noise test
Shock & high frequency transient	Transient analysis Shock propagation assessment Semi-analytical approaches	Shock test
Pressure	Static analysis Thermal-functional analysis Venting analysis	Proof pressure test Thermal-functional test
Thermo-elastic	Thermo-elastic analysis	Thermo-elastic test

#### 4.6.4 Static and quasi-static loads

The preliminary design of a spacecraft primary structure is typically based on loads factors provided in the launch vehicle user's manual.

The design load factors are represented by the Quasi-Static Loads (QSL) that are the more severe combinations of dynamic and static accelerations that can be encountered at any instant of the mission including ground and flight operations. For example the flight limit levels of QSL for a spacecraft launched on Ariane 5 and complying with the spacecraft fundamental frequency requirements and with the static moment limitation are given in Table 4-3 [8].

**Table 4-3: QSL (flight limit levels) for a spacecraft launched on Ariane 5**

Acceleration (g) <b>Critical flight events</b>	Longitudinal		Lateral	Additional line load (N/mm)
	Static	Dynamic	Static + Dynamic	
Lift-off	- 1.8	$\pm$ 1.5	$\pm$ 2	26
Aerodynamic phase	- 2.7	$\pm$ 0.5	$\pm$ 2	23
Pressure oscillations / SRB end of flight	- 4.40	$\pm$ 1.6	$\pm$ 1	37
SRB jettisoning *	-0.7	$\pm$ 3.2	$\pm$ 0.9	0

It is important to point out that launch load factors provided by the launcher user's manual:

- normally apply only if the spacecraft fundamental frequencies are above some specified values
- cover only steady-state accelerations and the effects of low-frequency transient
- normally are not high enough to envelope the effects of transient on secondary and tertiary structures
- in some cases may not be fully adequate for the design of primary structures. This can happen for dynamic loading which cannot be properly represented by quasi-static loads (e.g. in presence of out-of-phase motion or fundamental local modes).

In practice additional quasi-static load cases are often derived from dynamic analyses. For example they correspond to the dynamic levels seen by the main instruments and the tank. These load cases are taken into account for the design of the spacecraft structure. They correspond to the loading of the main sub-systems of the spacecraft independently, or simultaneously. Normally the instruments are also designed to sustain the loads mentioned.

Finally it should be noted that dedicated quasi-static load cases can be specified to cover other events such as air transportation or the transportation of the spacecraft in horizontal position in the container.

If more than a specific launcher is identified for the mission, all quasi-static load cases provided by the launcher manuals are considered for spacecraft design and verification. For example Figure 4-5 reports the envelope of the quasi-static loads at qualification level for the satellite Sentinel 3 as induced by Vega and Rockot launch vehicles.

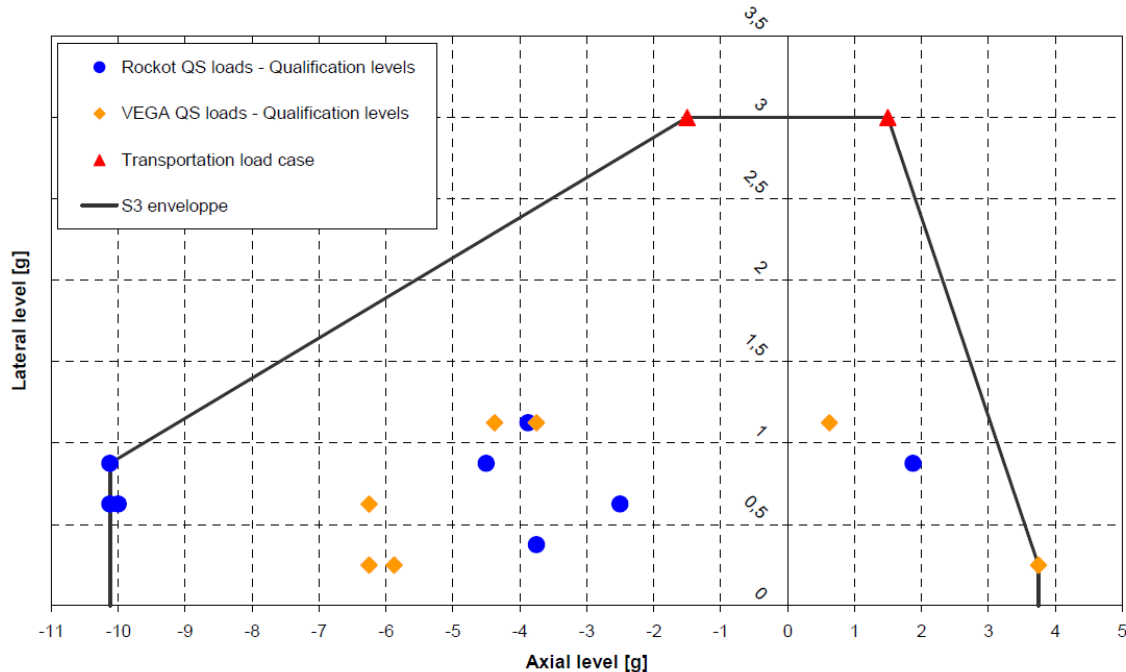


**Figure 4-5: Sentinel-3 quasi-static loads at qualification level induced by Vega and Rockot launch vehicles [9]**

Static and quasi-static loads can be verified by analysis and test. Simultaneous multi axes verification can be obtained by static analysis and static test. In case of vibration tests such as sine sweep or sine burst, the target loads are normally reached on one specific axis at the time.

## 4.6.5 Static loads test

### 4.6.5.1 General

A static test is a common test for verifying the strength of spacecraft structures. In particular static load tests are performed to confirm the design integrity of the primary structural elements of the spacecraft platform. Loads are applied with dead weights or hydraulic jacks. The test typically consists of several load cases, each of which tests a different part of the structure. In a prototype qualification static test, each case includes a *yield test*, in which the structure ability to withstand a certain level of load without detrimental deformation is verified, and an *ultimate test*, in which the structure withstands a higher level of load without rupture or collapse (see Section 7.4.4).

A properly designed static test is very effective in verifying strength, since all potential failure modes can be tested, and in verifying stiffness. However statically simulating the launch loads can be a real challenge. The target is to develop load cases that are as severe as the combined effects of the design limit loads (i.e. in practice the “worst case conditions”), and then increase them by appropriate or applicable factors.

It should be noted that the test conditions of a controlled-loads test, such as the static tests, are based on the predictions of the structure response to a specific environment. Thus a single mistake in the loads analysis can mean that the structure is designed and tested to the “wrong” loads. Clearly it is important to be very confident in the loads analysis, which means to check the sensitivity of the assumptions and validate the loads analysis [1].

### 4.6.5.2 Example of strategy for defining the static test load cases

This section reports the basic strategy which has been used to define the test load cases for the qualification of the Sentinel 3 protoflight structure [10].

The main objectives of the Sentinel 3 PFM static load test campaign have been:

- To verify the structural integrity by means of selected static test load cases which qualify the spacecraft structure including a number of interfaces
- To verify the global stiffness, axially and laterally, by means of uni-axial and qualification load cases

The structural analyses of the spacecraft have identified the critical structural elements and the corresponding design load case. Based on that, the definition of the test load cases has considered that the design limit loads are in general 1.32 times higher than the qualification loads, since the applicable factors are  $K_P = 1.1$  and  $K_M = 1.2$ . Thus for the static test the loads have been adjusted to reflect the fact that nominally qualification load levels are imposed to the specimen.

In practice a key aspect for the definition of the test load cases, and the associated levels, is the comparison between the Design, Qualification and Test Loads and relevant margins of safety. Within the Sentinel 3 project a “colour code” has been used which helps to identify the test loads and their resulting margins of safety with respect to the design and qualification values. The colour code is reported in Table 4-4 which explains the meaning of the colours. The following nomenclature is used:

D – Design (DLL) Values

Q – Qualification Values

T – Test Values

**Table 4-4: "Colour Code": Load levels and relevant MoS [10]**

<b>D &gt; T &lt; Q</b>	The Test load is lower than the Design and Qualification load. It means that the Test load case MoS is higher than the Design and Qualification MoS.
<b>D &gt; T &gt; Q</b>	The Test load is higher than the Qualification load but lower than the Design load. It means that the Test Load case MoS is lower than Qualification MoS but higher than the Design case MoS.
<b>D &lt; T &gt; Q</b>	The Test load is higher than both the Design and Qualification load. It means that the Test load case MoS is lower than both the Design and Qualification case MoS.

The “green” situation corresponds, in principle, to the condition which qualifies the structure without jeopardizing the structure. The “yellow” situation corresponds to a test load level which is insufficient to qualify, for example, a specific structural item. In this case the adequacy of the test load is assessed with respect to the objectives of the test, for example the structural item could result qualified by similarity and the selected test load be adequate. The “red” situation involves load levels in the structure higher than those corresponding to the design limit loads and this implies a dedicated reassessment of the margins of safety.

Since Sentinel 3 adopted a PFM approach (in practice the specimen used for the static test is refurbished as flight model), a key successful criterion for the test has been “no yield” and “no rupture” at qualification loads. Of course different approaches and success criteria are possible within a prototype approach (see Section 7.4.4).

#### 4.6.6 Spacecraft-launcher coupled loads analysis

The structural response of the spacecraft to transient flight events (low frequency mechanical environment) is simulated by spacecraft-launcher coupled dynamic analysis, which is a key task of the loads cycle process. The coupled loads analysis is a transient (or harmonic) analysis performed by using the mathematical models of the spacecraft and launcher, merged together, and by applying the forcing functions for the different launch events.

The main objective of the CLA is to calculate the loads on the spacecraft, where the term “loads” refers to the set of internal forces, displacements and accelerations that characterise the structural response to the applied forces. The loads of the spacecraft derived from the analysis are taken as a basis to verify the dimensioning of the spacecraft itself.

The low frequency domain typically ranges from 0 to up 100 Hz and corresponds to the frequency content of the forcing functions used in the CLA. The excitation may be of aerodynamic origin (wind, gust, buffeting at transonic velocity) or may be induced by the propulsion system (e.g. thrust build up or tail-off transient, acoustic loads in the combustion chambers). Of primary interest are the spacecraft interface accelerations and interface forces. The interface accelerations can be used to derive an equivalent sine spectrum at the spacecraft interface. The interface forces can be employed to calculate the “equivalent accelerations” at the spacecraft centre of gravity (quasi-static accelerations). Of large interest is also the recovery of the internal responses which are used to verify the structural integrity of the spacecraft and its components. The computed responses and their deduced minimum and maximum levels can be employed within the design, verification and test phases of the spacecraft. For example, secondary structures and flexible components such as solar arrays, booms, instruments and propellant tanks are also designed (and test verified) to withstand the dynamic environment induced at the base of the spacecraft. The dynamic loads (e.g. accelerations, forces, stresses) on these

components can be verified directly by means of the CLA (apart from acoustic loads under the fairing which are analysed separately).

In the test verification phase of the spacecraft, the equivalent sine spectrum computed by means of the CLA is often used to assess and justify the reduction, at specific resonant frequencies, of the spectrum specified by the launcher authority. This might be required to avoid possible damage to the spacecraft structure itself or its components (e.g. solar arrays, booms).

## 4.6.7 Sine vibration

### 4.6.7.1 Overview

In a number of situations sine-wave excitations are used for qualification and protoflight testing of space vehicle hardware, even though the “mission” dynamic excitation being simulated is not periodic [3]. In particular the low frequency transient is often simulated at the subsystem and system assembly level using a swept-sine vibration test over a frequency range up to about 100 Hz. The magnitude and sweep rate for the resulting vibration are selected supposedly to cause the hardware response to be similar to the response predicted for the transient. Some common procedures to derive such a test are also reported in [3].

The use of a swept-sine excitation to simulate a transient excitation can result in the unique situation of causing a simultaneous undertest and overtest of the hardware. The undertest is due to exciting only one hardware resonance at a time during the sweep-sine test, as opposed to the simultaneous excitation of multiple resonances of the hardware, as would be induced by the transient excitation. The potential overtest is due to applying a larger number of stress cycles to the hardware during the swept-sine test than occurs during the transient excitation. Of course, in this case, the amount of overtesting can be reduced by increasing the sweep rate.

However the main cause of potential overtesting is the difference in structure boundary conditions between test and flight configurations. During a vibration test, the test article is usually attached to a very rigid fixture and it is excited or driven along a single linear direction, with the structure being completely restrained along the other five degrees-of-freedom (DOF). This generates a response of the test item in its “clamped natural modes” and not in the coupled modes as exhibited during the flight [4] [5].

For example in the flight configuration the spacecraft is attached to a mounting structure (i.e. adapter and launcher) that normally exhibits some flexibility in all six DOF in the frequency range of interest. The flexibility difference in the direction of excitation is the main contributor to the overtesting phenomenon. In the flight configuration, the acceleration at the interface between the mounting structure and the test article drops at certain frequencies, resulting in valleys in the acceleration spectra. These frequencies correspond to the resonance frequencies of the test article when attached to a rigid support (such as a shaker). This phenomenon is known as the vibration absorber effect. In other words, during a vibration test, the structure is excited with a specified input acceleration that is the envelope of the flight interface acceleration, despite the amplitude at certain frequencies drops in the flight configuration. This results in exaggerated amplification of input forces, and internal stresses, at the resonance frequencies of the test article. In practice, because the input spectrum does not consider the actual flight behaviour and excites the spacecraft modes, the structural response of the spacecraft would exceed the spacecraft design capability and the values encountered during the launch simulations.

To avoid such effects, the sine test input spectrum needs to be notched. However, it should be clear that the criteria used for notching do not have to generate an input spectrum that can jeopardize the flightworthiness of the spacecraft. For example this can happen if the testing levels are not coherent

with the levels required by the CLA. As a general rule, the notching should be kept to a minimum and the input spectrum to be applied to the spacecraft as much as possible similar to the one requested by the launcher authority. The reason is that this spectrum provides robustness to the spacecraft design compliant with it since it covers a wide range of responses found in past spacecraft-launcher CLA and in addition it provides a sweep over the frequency band of interest, therefore covering possible deviations of local modes.

#### **4.6.7.2 Spacecraft sine vibration test**

The objective of the spacecraft sine vibration tests is to verify the strength of secondary (and in case also primary) structure.

The spacecraft qualification test consists of one sweep through the specified frequency range and along each axis. The acceleration amplitudes are specified in the launcher user's manual and applied successively on each axis. Normally a notching procedure may be agreed on the basis of the latest coupled loads analysis available at the time of the tests to prevent excessive loading of the spacecraft structure or equipment. This is done without jeopardizing the tests objective to demonstrate positive margins of safety with respect to the flight loads. Also the required sweep rates may be modified on a case-by-case basis depending on the actual damping of the spacecraft structure. This is done while maintaining the objective of the test.

If more than a specific launcher is identified for the mission, the envelope of the sine environments provided by the launcher manuals are considered for spacecraft design and verification.

Primary notching (Section 4.8.1) is computed in order to limit the forces and moments at the LV/SC interface to the ones corresponding to the maximum axial and lateral QS levels specified by the launcher manuals. In practice the calculation of maximum loads at the interface is performed by means of the spacecraft total mass, CoG position and the specified QS accelerations. For what concerns the notching in the lateral directions the resultant forces and moments are taken into account.

Secondary notching (Section 4.8.1) is computed in order to limit the acceleration or the load levels at some locations of the spacecraft. The limits used in order to compute the secondary notching correspond normally to the qualification levels of the corresponding subsystems or units.

For example the primary and secondary notching computed at CDR for the satellite Sentinel 3 under the VEGA sine vibration environment in longitudinal ("axial") direction is plotted in Figure 4-6 (in blue and dashed green, respectively).

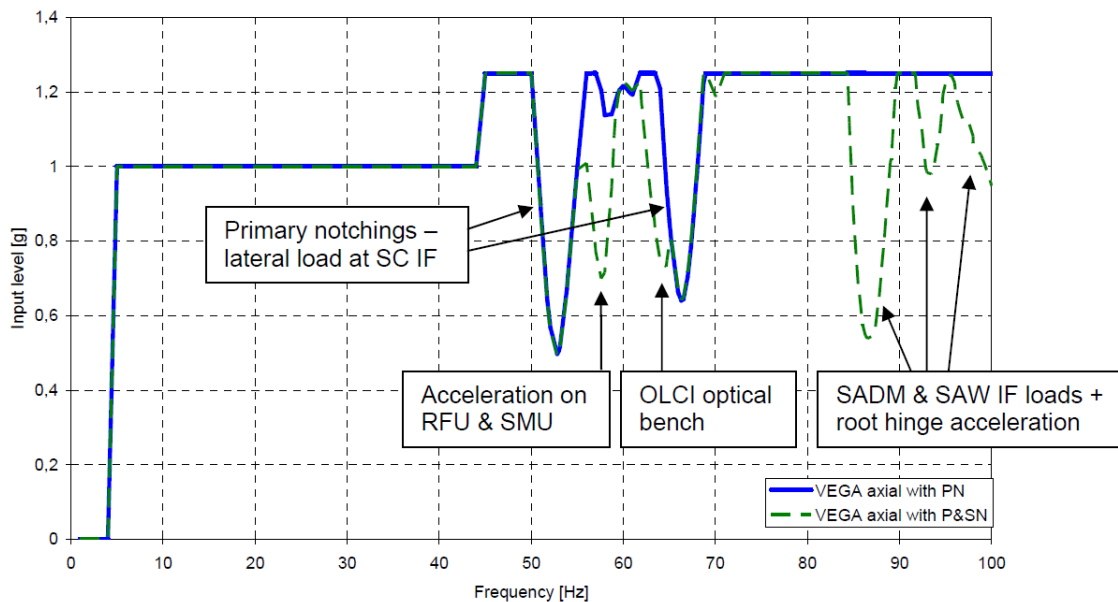


**Figure 4-6: Primary (PN) and secondary notching (SN) for Sentinel 3 under VEGA sine axial environment [9]**

#### 4.6.8 Spacecraft design loads and test predictions versus LV/SC CLA results

An important step of the loads cycle is the comparison of design loads and the test predictions, such as sine and static qualification tests, with the results of the LV/SC coupled loads analysis. The comparison is crucial to assess if design changes are needed (within a design loads cycle), or if the structure that has already been built and tested is adequate (in the verification loads cycle). The above mentioned comparison can also be used to assess the adequacy of the static (and also sine) test load cases. In practice the following data are normally compared:

- Quasi-static loads and maximum interface loads
- Tensile and compressive fluxes at the LV/SC interface
- Sine test levels vs. sine-equivalent dynamics at the SC interface
- Equivalent quasi-static loads at main sub-systems
- Acceleration levels inside the spacecraft (minimum and maximum accelerations are compared for example to further assess the notching adequacy in the sine vibration test)
- Other load levels (e.g. platform/solar array wing interface loads)

The aim of the comparison is to assess that the loads and the accelerations that are reached during the qualification tests cover the ones coming from the LV/SC CLAs with margins.

Figure 4-7 shows an example of compatibility assessment of the notching in sine qualification testing, which refers to the satellite Sentinel-3. The predicted notching is compared to sine-equivalent levels ( $Q=20$ ) coming from the satellite/VEGA launcher CLA.

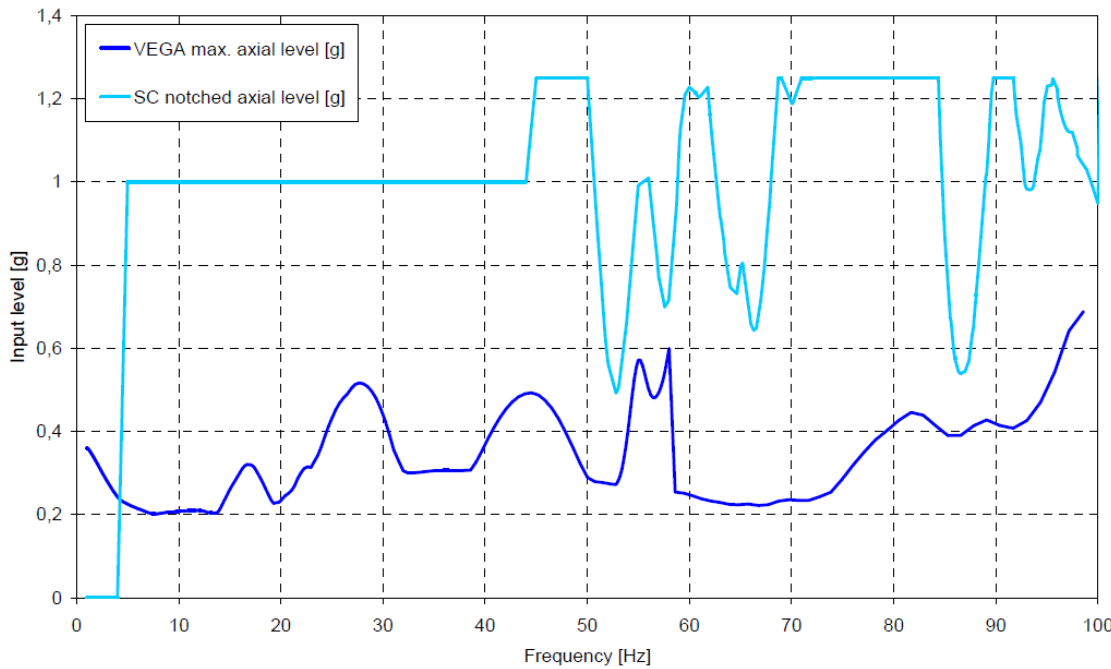


**Figure 4-7: Sentinel 3 sine test predicted notching compared to sine-equivalent levels coming from LV/SC CLA – Axial direction [9]**

## 4.6.9 Random vibration and vibro-acoustic environment

### 4.6.9.1 Random vibration analysis and testing

Some load environments are treated as random phenomena, when the forces involved are controlled by non-deterministic parameters [2]. Examples include high frequency engine thrust oscillation, aerodynamic buffeting of fairing, and sound pressure on the surfaces of the payload.

Random vibration analysis describes the forcing functions and the corresponding structural response statistically. It is generally assumed that the phasing of vibration at different frequencies is statistically uncorrelated. The amplitude of motion at each frequency is described by a power spectral density function. In contrast to transient analysis which predicts time histories of response quantities, random vibration analysis generates the power spectral densities of these response quantities. From the power spectral density, the root mean square (rms) amplitude of the response quantity is calculated. The root-mean-square acceleration is the square root of the integral of the acceleration PSD over frequency. Random vibration limit loads are typically taken as the "3-sigma load" (obtained by multiplying the rms load by 3).

Random vibration testing helps demonstrate that hardware can withstand the broad-band high frequency vibration environment. The tests are conducted on an electrodynamic vibration machine or "shaker," which consists of a mounting table for the test item rigidly attached to a drive-coil armature. A control system energizes the shaker to the desired vibration level. Feedback for the control system is provided by a series of accelerometers, which are mounted at the base of the test item [15]. Similarly to sine testing, adequate control approaches and strategies are used to avoid overtesting and to ensure realistic structural responses.

Heritage flight data, test data and analytical methods are used to predict vibration test levels. In most cases the predicted environments are verified later with system-level acoustic tests.

#### 4.6.9.2 Vibro-acoustic response analysis

Acoustic pressure fluctuations under the fairing are generated by engine operation (plume impingement on the pad during lift-off) and by unsteady aerodynamic phenomena during atmospheric flight (i.e. shock waves and turbulence inside the boundary layer), which are transmitted through the upper composite structures. The sound field under the fairing is normally assumed as diffuse.

Structures vibrate randomly in response to acoustics. The structures that respond the most are light in weight and large in surface area, such as skin panels, solar arrays and antenna dishes. Relatively small, heavy structures have very little direct response to acoustics, but they vibrate because of excitation from more responsive structures. This vibration is often the driving environment for a spacecraft electrical, electro-mechanical and electronic components [1].

Vibro-acoustic response analysis is basically performed for two reasons:

- To assess the strength and life of acoustically sensitive structures
- To predict random vibration environments for spacecraft components

Since the most severe acoustic environment for a spacecraft is during ground testing, typically the spacecraft vibro-acoustic response analysis is performed by considering the vibro-acoustic test environment. This is described by a plot of sound pressure level (SPL) over a frequency range.

Recent developments in the area of computational mechanics allow performing vibro-acoustic response analysis of a complete spacecraft. The analysis can be performed by combining the FE method and the BE method with SEA approach, and allows the random levels on units and instruments to be compared to technical specifications or qualification levels. For example Figure 4-8 reports the calculated random vibration levels for the Sentinel 3 Solar Array Drive Mechanism (SADM) compared to level required by the test specification.

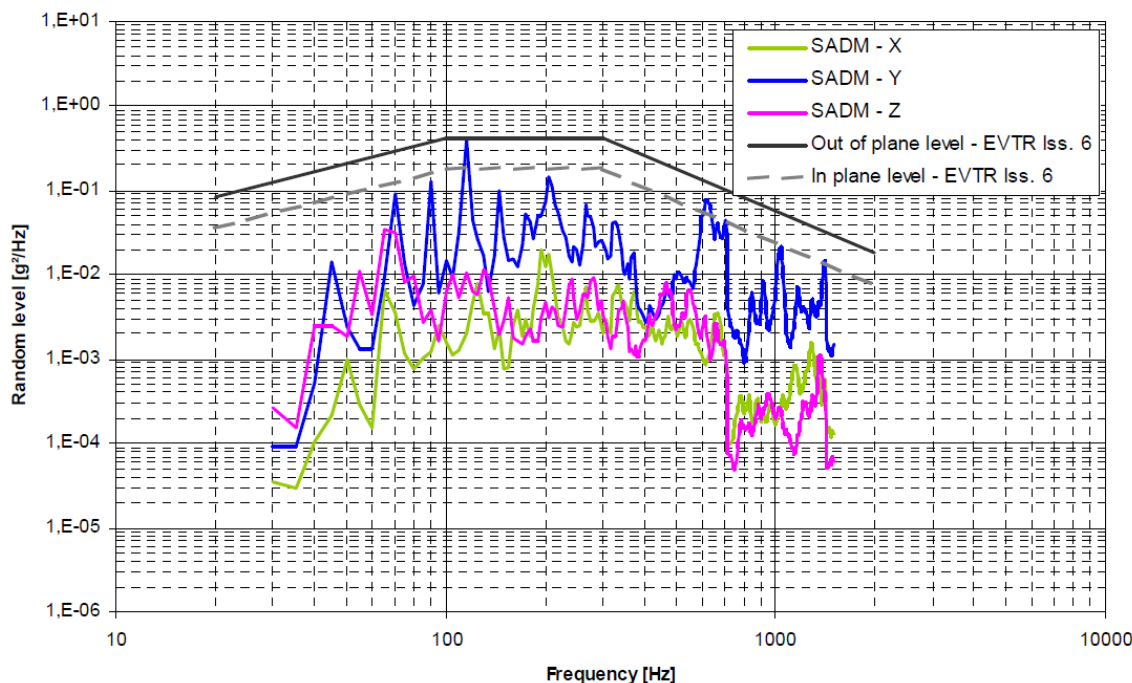


Figure 4-8: Random vibration levels for Sentinel 3 SADM [9]

Another important advantage of performing a vibro-acoustic analysis at spacecraft level is that the results can be compared to the ones from a base drive random vibration test predictions, for example of an instrument, and to assess if some adjustments of the levels (e.g. secondary notching) are possible.

#### **4.6.9.3 Acoustic testing**

Acoustic testing of space vehicles or major subsystems strives to simulate the acoustic pressure expected during lift-off and subsequent mission phases. Space vehicles also contain complex components that are susceptible to acoustic noise, and these are tested to ensure all potential failure modes and workmanship defects have been properly screened out prior to system integration. In a typical acoustic test, the test specimen is positioned in an acoustic chamber. The chamber is a large room with thick walls and a smooth interior surface that permits high reverberation. The test article is placed on a fixture or suspended from bungee cords. In some cases, the test item may be attached to larger metal plates to simulate actual mounting on the spacecraft structure, thereby creating a more realistic profile of the interface vibration. Loudspeakers or horns supply the acoustic energy, with four or more microphones strategically placed to control and record the sound level within the room. Numerous acceleration transducers are installed on the test item to measure the vibration at the mounting interfaces of critical components; then PSD curves are derived and finally compared with those used to test components. Many of these critical components are also functionally monitored during the test. The measurements are compared with the appropriate design specifications for the components to assess their qualification for flight [15].

The acoustic test levels for a particular space vehicle or subsystem are usually derived from measurement data on similar structures on past flights and ground tests. In qualification testing the flight limit spectrum is increased by the appropriate qualification factor.

The test lasts at least one minute to establish a duration margin of four times the exposure in flight. Additional test time may be accumulated depending on the program requirements.

Summarizing, the main objectives of acoustic testing at spacecraft level are:

- To verify adequacy of electrical connections
- To validate the random vibration environments used to qualify components
- To determine the random vibration contribution to the design inertia loads
- To qualify large appendages (e.g. solar arrays, antennae) with representative boundary conditions.

#### **4.6.10 Shock testing**

Shocks are a transient mechanical loading characterised by very short duration, high frequency content and high acceleration amplitudes with rapid initial rising times.

During the launch and deployment operations in the very early orbit phase the spacecraft is subjected to several energetic shock events: launcher stages separation, fairing jettisoning, separation of the satellite from the launcher (e.g. clamp-band release), and deployment of appendages such as solar arrays, antennas or scientific instruments on deployable booms.

Shocks are mainly caused by the actuation of pyrotechnic devices such as release mechanisms for stage and satellite separation, and deployable mechanisms for solar arrays.

For example spacecraft launched by Ariane 5 are subjected to noticeable shocks during the following events [8]:

- the launch vehicle upper stage separation
- the fairing jettisoning
- the spacecraft separation

The shocks generated by the upper stage separation and the fairing jettison are propagated from their source to the base of the spacecraft through the launch vehicle structures. For these events, the envelope of the shocks levels at the spacecraft interface is normally presented in the launch vehicle user's manual.

The spacecraft separation shock is directly generated at the base of the spacecraft and its levels depend on the adapter type, since the interface diameter and the separation system have a direct impact.

System level shock tests are generally performed with the actual shock generating equipment (e.g. clamp band release) or by using of sophisticated pyro-shock generating systems (e.g. SHOGUN for Ariane 5 payloads). In this way a direct simulation of the mission event is provided and the tests do not include any amplitude margin. System-level shock tests provide an excellent opportunity to measure shocks incident on components throughout the space vehicle.

Unit-level shock tests are accomplished using one of several methods, which generally entail securing the component to a fixture that is then subjected to impact. This "ringing plate" approach has provided the best practicable simulation of unit exposure to shock. In addition, vibration shakers are used in some applications to impart a transient shock. Shock testing is typically not performed as a unit workmanship screen, but is deferred to the system level for greater detection of functional defects [15].

Summarizing, the main objectives of shock testing are:

- to demonstrate the ability of a specimen to withstand the shock loads
- to validate equipment qualification loads during tests at spacecraft level

## 4.7 Basic principles, criteria and assumptions in structure and loads verification

### 4.7.1 Introduction

This section summarizes some important principles, criteria and assumptions which are normally (or often) applied for spacecraft structure verification, with a special emphasis to the loads analysis.

It is worth recalling that the verification criteria are the ground rules that, if properly defined and then satisfied before launch, prove that a spacecraft can meet its requirements. There are criteria for design (including analysis) and test. Verification criteria in practice often become contractual requirements.

### 4.7.2 Equivalence criteria for loads and environments

The parameter most commonly used in the industry to define the motion of a mechanical system is the acceleration. The reason is mainly that accelerations are directly related to forces/stresses and "easy" to specify and measure. In practice accelerations are used as a measure of the severity of the mechanical environment. The loads are usually specified in terms of:

- Equivalent accelerations at the CoG, for the quasi-static loads
- Sine spectra of the acceleration, for the low frequency transients and harmonic loads

- Power spectral densities (usually of the acceleration), for the broad band random vibrations
- Shock response spectra for the shock loads

The main parameters are levels but also durations. The duration is a significant parameter for random vibrations. For swept-sine vibration tests, the duration is determined by the sine sweep rate. Of course the damage potential depends both on the load levels and duration, the latter being especially relevant for structural life verification.

The subject of the equivalence criteria for dynamic environments, which are often crucial for establishing appropriate loads, is very complex, and normally the “equivalence” is limited and it can have some drawbacks. Since in general the equivalence has some limitations, enveloping techniques and conservativeness are often applied. In the following just some basic concepts are recalled. Relevant information can also be found in [3].

It should be noted that a very first “equivalence criterion” is implicit in the way the loads are defined. For example it is implicitly assumed that two mechanical shocks are “equivalent” if they are represented by the same SRS, even if there are some reserves. Similar considerations can be made both for random vibration environments defined by PSD of the input accelerations and duration, and also for low frequency transients defined by sine spectra and sweep rate.

For example two random vibration environments are equivalent if, assuming they have equal durations, they are represented by the same acceleration PSD, regardless the differences in the time histories. On the other hand, it is a common mistake to use the rms value of the input acceleration as a measure of its severity. The problem with the rms value is that it depends strongly on the values of the PSD at very high frequencies and on the upper frequency limit, which are often irrelevant. The most appropriate measure of the severity of a random vibration test is the PSD value at the resonant frequencies of the item [11]. The maximum PSD value is important only if it is related to the main resonances.

Establishing an equivalence between different environments, or identifying which is the most severe, typically involves the evaluation and comparison of the (expected) structural responses. This is very important since on the basis of environment comparisons, decisions can be made, for example, on the status of compliance or on the most adequate tests which should be performed and included in the structural verification plan.

The procedure which allows to establish an *equivalence between a low frequency transient and the “sine equivalent dynamics”* (see Section 5.2.6) is very important in practice, since some launcher authorities make decisions on the acceptability of a “notched profile” also on the basis of the “equivalent sine” of the predicted accelerations at the spacecraft/launcher interface. It should be noted that this approach has some important limitations and inconsistencies (e.g. [4]).

The equivalence criteria which allow establishing the *equivalence between the base-driven random vibration environment with the vibro-acoustic environment* are also very important in practical applications. The “equivalence” which can be established is indeed rather limited since the two environments are intrinsically different due to the different physical nature, i.e. purely mechanical and acoustic, of the excitation (see Section 5.6). In practice, for large spacecraft, it should be noted that the specified levels and duration for the acoustic noise test are, usually, highly conservative. On the basis of that assumption, the base-driven random vibration environments for lower levels of assembly (e.g. instruments and units) can be derived by enveloping the predicted response in terms of acceleration PSDs, when the spacecraft is loaded by the vibro-acoustic environment specified by the launcher authority for the acoustic noise test. For small and compact spacecraft, random tests can be more severe on some areas than the acoustic noise test.

In some cases an *equivalence is established between the random vibration environment and the shock environment*. Typically the random environment is used to cover the shock environment. This practice

is based on the fact that the random vibration input is a single event generating vibration levels on a wide frequency range. In this sense it is "similar" to a shock event even if the latter is much shorter. In order to allow the comparison, the random vibration environment expressed as an acceleration PSD is converted in a sort of SRS, such as for example a random response spectrum, RRS (see Section 5.2.5.4). More information can be found in [12].

In a number of situations, for example for primary or secondary notching definitions, it is crucial *to compare the random vibration environment with the quasi-static loads* specified for the structural item. It is a common mistake, and unfortunately an usual industrial approach, to consider the "3-sigma" output acceleration as equivalent (or in any case comparable) to a quasi-static load. This is in general incorrect since:

- QSL are equivalent accelerations at the CoG, this is not usually the case for the random acceleration considered.
- The rms value of the acceleration depends strongly on the values of the PSD at very high frequencies and on the upper frequency limit, which are often irrelevant.

The latter point can be illustrated by the following considerations.

The response displacement, as well as force and stress, spectral densities have the same "general shape" as the response acceleration spectral densities but their higher-frequency peaks are, in general, significantly lower in proportion to the lower-frequency peaks. In other words the first modes account for nearly all of the total displacement, force and stress. In mathematical terms it can be explained by noting that the displacement PSD is proportional to the acceleration PSD by a factor  $1 / \omega^4$ . In more "physical" terms, this effect can also be explained by considering that the fundamental modes, e.g. the ones that have the largest effective masses and that establish the "force-link", are usually at lower frequency. Finally a global argument is the following: QSL and random loads do not have the same distribution in the item, depending on the frequency content compared to the eigenmodes. In other words, QSL implies a "quasi-rigid" behaviour which is not far from the first global mode in each direction, but the quasi-rigid behaviour is quite different with respect to the other modes, i.e. upper global modes and local modes.

Summarizing the following criteria are applied in industrial applications.

Two mechanical environments are considered equivalent if they have the same SRS (for random vibrations the same RRS). In this case the equivalence is established on the base of the SDOF response. This criterion is often applied to structure with base excitation.

Another criterion is based on the evaluation and comparison of the structural response to the mechanical environments. The comparison is often performed in terms of accelerations and interface forces. In this case the equivalence is established on the base of the response of the actual structure.

Both criteria are based on structural responses, either from the SDOF system or from the actual structure. The advantage of the SDOF system is that it is a simple and "standard" structure which can be used not only to characterize the environment but also to estimate the response of the actual structure, albeit with assumptions. The advantage of using the response of the actual structure is that the solution is "exact", but the calculations are more costly and the results are valid only for the given structure. The practice depends on the industrial context, schematically:

- If the structure is "unknown", the SRS approach should be applied. This approach is simple but with assumptions, so with some risk.
- If the structure is "known", it is recommended to compute its actual response. This approach is more costly but also more reliable.

As a conclusive remark on equivalent loads and environments, in general it is always dangerous to replace an environment by another of different type and relevant structural analyses of the item should be performed.

### **4.7.3 Criteria for assessing verification loads**

The following criteria are normally applied for strength verification [1]:

- Analysis: margins of safety greater than or equal to zero.
- Test, for structures qualified by static or sinusoidal testing: test loads or stresses (in practice it means “as predicted” by validated mathematical models and test conditions) are compared with the total predicted loads during the mission, including flying transients, acoustics, random vibration, pressure, thermal effects and preloads. In other words this is evidence that the applied test loads have been sufficiently high, including qualification margins.
- Test, for structures qualified by acoustic or random vibration testing: test environments are compared with random-vibration environments derived from system-level acoustic testing. In other words this is evidence that the applied random vibration test levels, at lower level of assembly, were high enough, including qualification margins.
- Test, for structures qualified by shock testing: test environments are compared with shock environments derived from system-level shock testing. In other words this is evidence that the applied shock test levels, at lower level of assembly, were high enough, including qualification margins.

### **4.7.4 Main inconsistencies of the loads verification process**

The main “inconsistencies” and potential issues in the loads verification process are here summarized:

- Uni-axial vibration and shock test facilities while the dynamic environments for space vehicle hardware are typically multiple-axis. In practice, tests are performed axis by axis.
- Tests are performed environment by environment, even if they occur simultaneously. For this reason loads superposition techniques are applied and the verification of the structural integrity by analysis is normally required to prove the qualification of the spaceflight hardware. For example the vibration and acoustic tests contribute to the qualification through validation of mathematical models and through measurement of dynamic responses.
- Low frequency transient often simulated at the subsystem and system assembly level using a swept-sine vibration test, mainly because of its simplicity in specification and testing.
- Infinite mechanical impedance of the shaker and the standard practice of specifying the input acceleration as the frequency envelope of the flight interface acceleration (despite the presence of antiresonances or dips in the flight configuration). This is the major cause of over testing in aerospace vibration tests.
- Vibro-acoustic environment often simulated at the subsystem and units assembly level using a random vibration test.
- Test levels largely based on computational analyses. For this reason it is important to validate critical loads analyses.

## 4.8 Notching in sine and random vibration testing

### 4.8.1 Introduction

This section reports basic principles, logic and criteria concerning notching in sine and random vibration testing.

Notching is the reduction of acceleration input levels around resonant frequencies, to avoid over testing. "Notching" can be distinguished in "primary notching" and "secondary notching".

The primary notching is performed to limit the shaker-test specimen interface forces to the target values, normally qualification or acceptance loads. This is basically the same as to limit the equivalent accelerations to the centre of gravity of the test item.

The secondary notching is performed to limit local accelerations with the purpose of protecting equipment, instruments or sub-systems.

Primary notching in sine testing of the spacecraft is mainly justified by the fact that the real environment in flight is of transient nature and is simulated on shaker by a sine sweep based on an envelope of LV/SC interface levels foreseen in the considered frequency band. This envelope doesn't account for the possible reactions of the spacecraft which can produce level reductions in some frequency bands.

These potential level reductions (with respect to a rigid spacecraft) are due to a high spacecraft dynamic mass at LV/SC interface which reduces the effect of the exciting forces according to the Newton's law. This high dynamic mass is generated by eigenmodes with high effective masses with respect to the interface. As the primary notching is related to interface forces, the unique criterion for mode selection in this case should be based on the modal effective masses.

The secondary notching is related to level reduction on critical areas inside the spacecraft. In this case, the frequency response function involved is the spacecraft dynamic transmissibility between the considered area and the LV/SC interface, and the unique criterion for mode selection should be based on the modal effective transmissibilities.

Similar concepts apply to random notching.

### 4.8.2 Example of requirements

Examples of requirements concerning notching in sine and random vibration testing are the following:

- *Notching criteria and implementation (for sine and random vibration tests) shall be approved by the customer and, if relevant by the launcher authority.*
- *Primary notching may be done.*
- *Secondary notching shall be approved by the customer.*

*NOTE: Secondary notching is generally not allowed.*

### 4.8.3 Basic principles

The following basic principles can be established.

Notching can be considered when it can be demonstrated that an "unreasonable" over testing with respect to the target loads (e.g. qualification loads) occurs if an adequate reduction of the input spectrum in some frequency bands is not applied.

In this context the term “unreasonable” is important. In fact by using sine sweep and random vibration tests the risk of overtesting (as well as undertesting) with respect to the maximum expected flight environment (including margin) cannot be completely removed. This is due to differences between “flight” and “test” conditions which can hardly be removed (e.g. sine sweep excitations used to simulate transient, base drive random test used to simulate vibro-acoustic environment, multi-axis excitations vs. single axis test facilities, differences in boundary conditions etc.).

In order to minimize the risk of under testing, and then of mission failure, the general recommendation of minimizing the practice of notching can often be imposed by explicit (or “implicit”) requirements, for example by the launcher authority or by the customer. On the other hand it should be noted that, especially in the case of PFM, it is normally a “common interest” to limit as much as possible any overtesting and unjustified risk of structural failures.

Other important aspects are the following. The need for primary notching is generally “well understood”, i.e. it is due to the specific dynamic behaviour of the test specimen on the shaker produced by the modes with large effective masses. In addition the frequency bands involved are normally narrow and relatively easy to localize. The agreement on the depth and width of the notches is usually rather straightforward.

More complex is the scenario for the definition of the secondary notching. In fact the secondary notching is, in its own essence, a revision of the applicable mechanical environment; it means a change of the applicable test specifications. The arguments are then not only technical, but also contractual, since they involve the sharing of responsibility and risk between customer and contractor. However, within a cooperative scenario, the crucial question remains technical: is the test specimen, or part of it, going to suffer an unreasonable overtesting, if the notching is not applied?

In practice secondary notching opens the door to a systematic reassessment of the test specifications by comparing the predicted dynamic response in the test with the expected “flight” mechanical environment. This is potentially in conflict with the logic of producing the test specifications by “enveloping” the expected mechanical environment at the interface, which has demonstrated during the years to be a robust approach. Moreover the systematic reassessment of the mechanical loads induced by the possibility of performing secondary notching generally induces inefficiencies and complexities in the process of mechanical analyses.

This explains why it is often recommended to limit the practice of secondary notching to the critical items which indeed need to be protected. This handbook supports the recommendation.

In short, the notching on the input spectrum can be considered as far as it does not “jeopardise” the aim of the test, for example the qualification of the test specimen. However the application of the basic principles is not straightforward. Adequate approaches and criteria are crucial and some of them are hereafter reported.

#### **4.8.4 Response and force limiting**

To alleviate the overtesting problem and to define the notched spectra, two basic approaches are used:

- methods based on measurement of accelerations, also referred as “response limiting”
- methods based on measurement of forces, also referred as “force limiting”

Response-limiting consists of analytically predicting, usually through coupled loads analysis, the in-flight response at critical locations on the test article, measuring these responses during the test, and reducing or notching the input acceleration at the critical resonance frequencies so that measured responses do not exceed the predicted limits.

The main problems or disadvantages with the response limiting approach are the following (e.g. [5] [17]):

1. The coupled loads analysis for response-limiting prediction is based on FE models of both the test article and the mounting structure. The models are used to predict the in-flight response at the critical locations, however the accuracy of the prediction is usually questionable, particularly in the higher frequency range.
2. It may sometimes be complicated to take measurements at some critical locations. For example some of these locations may simply not be accessible.
3. For a large structure, the number of critical locations may be quite large, and there might be in the order of tens or even hundreds of instrumentation channels. This results in higher cost of test set-up and instrumentation, and complicates the definition of control strategy for the tests.
4. Considering its empirical nature, the process of getting agreement on acceptable values for response limits by all parties involved may sometimes be very tedious and may involve lengthy analysis and discussions.

In the force limited vibration approach, response-limiting is replaced by limiting the reaction force at the interface between the test article and the shaker.

By contrast, compared on a point-by-point basis with the above problems of response-limiting, the force limited vibration notching approach has the following advantages [5].

1. The interface force prediction depends less or not at all on the FEM of the test article and the mounting structure. First, since the interface forces are global parameters, thus "averaged" characteristics of the structure, they can be predicted analytically with more confidence than the single-point responses. Consequently, good prediction may be obtained with a less detailed and smaller sized FE model. Second, since the parameters of the test article and the mounting structure required for predicting force limits may be obtained experimentally, if the hardware of the mounting structure is timely available, the force limits could be predicted without the need of any FE model.
2. Force sensors are incorporated at the interface attachments between the test article and the shaker (or fixture). These are physical locations that are normally easily accessible.
3. Force-limiting typically only requires one to six instrumentation channels (three forces and three moments at the interface between the test article and the shaker). Often, only the reaction force in the direction of excitation is required.
4. Force Limited Vibration provides a theoretically sound basis for input-limiting, which, once understood, should be acceptable to all parties and thus should reduce the effort of coming to an agreement on this sometimes serious issue.

In practice often a hybrid approach which includes both response and force-limiting is implemented.

An exhaustive discussion on the methods used to alleviate the overtesting problem in vibration testing is beyond the purpose of the present section. See Section 8.4.2 for a practical discussion concerning the FMD.

## 4.8.5 Criteria for notching justification

### 4.8.5.1 Overview

Notching should be accepted when:

- Loads coming from the coupled system are demonstrated (with margins)
- Target loads of the tests would be exceeded

In practice the assessment is based on the following approaches.

For sine vibration tests:

- sine test analytical predictions (and during the test campaign the expected test response based on lower level test runs) are compared to the results of the coupled loads analysis. Typically the comparison is performed in terms of interface forces, max-min accelerations and equivalent sine input, the latter being normally available at satellite system level.

For random vibration tests:

- random test analytical predictions (and during the test campaign the expected test response based on lower level test runs) are compared to the results of the system-level vibro-acoustic analysis. Typically the comparison is performed in terms of PSDs of the interface forces, interface accelerations and accelerations at critical locations. Unfortunately reliable and detailed analyses are not always available.

The general criterion of not exceeding the QSLs during the vibration test is generally accepted, however the accurate evaluation of the equivalent acceleration at CoG can be a difficult task, especially for secondary notching.

Specific criteria which are generally accepted are reported in the following sections.

### 4.8.5.2 Primary notching in sine vibration test

Criterion 1: Primary notching can be considered in the frequency bands where the shaker-test item I/F forces are predicted to be higher than the relevant target loads.

Criterion 2: Primary notching based on measured accelerations and FE analysis data can be considered when the adequacy of I/F forces estimation method can be proved.

### 4.8.5.3 Secondary notching in sine vibration test

Criterion 1: Secondary notching can be considered when it can be demonstrated that the severity of the structural response during the base drive sine test is expected to be higher than the target loads (e.g. for qualification test the target loads could be assumed to be the coupled loads analysis response multiplied by the applicable qualification factor. Both quasi-static loads and equivalent sine spectra, if available, should be considered for the comparison).

Note 1: the notched input acceleration spectra are usually considered acceptable when they envelope the predicted equivalent sine spectra (which include the qualification factor, if applicable) calculated in the coupled loads analysis.

Criterion 2: Secondary notching should be minimized in order to reduce the risk of under testing within the concerned frequency bands. It means that moderate over testing is acceptable if positive margins can be shown.

Note 2: justification of secondary notching based on “under specification” of sine vibration environment or QS loads at lower level of assembly in principle is not acceptable. In other words, flow-up of notching is not in itself a justification.

Note 3: local dynamic response higher than the item QS loads does not necessarily mean that the QS loads (i.e. equivalent CoG accelerations) are exceeded.

Note 4: if no modal identification is performed, the secondary notching based only on analytical predictions is difficult to assess and justify. In this context it is recommended to properly instrument the relevant critical items.

#### 4.8.5.4 Primary notching in random vibration test

Criterion 1: Primary notching based on measured interface forces can be considered when they are predicted to be higher than the target loads.

Criterion 2: Primary notching based on measured accelerations can be considered when the adequacy of the I/F forces estimation method can be proved.

Criterion 3: Width and depth of the notches in the relevant frequency bands should be identified with the goal of minimizing the risk of under testing.

#### 4.8.5.5 Secondary notching in random vibration test

Criterion 1: Secondary notching in random vibration tests can be considered when it can be demonstrated that the severity of the structural response of the test item during the random vibration test is expected to be higher than the acoustic response which is intended to simulate (e.g. satellite acoustic noise qualification test).

Note 1: it means that measured accelerations PSDs in all locations are expected to be higher than the predicted acceleration PSDs in the system-level vibro-acoustic analysis.

Note 2: justification of secondary notching based on “under specification” of random vibration environment or QS loads at lower level of assembly in principle is not acceptable. In other words, flow-up of notching is not in itself a justification.

Criterion 2: Secondary notching in random vibration test should be minimized in order to reduce the risk of under testing within the concerned frequency bands. It means that moderate over testing is acceptable if positive margins can be shown.

Note 3: local dynamic response higher than the item QS loads does not necessarily mean that the QS loads (i.e. equivalent CoG accelerations) are exceeded (see Section 4.7.2).

#### 4.8.5.6 Notching and verification approach (prototype or protoflight)

Ideally the same principles, criteria, methods and procedures apply regardless the verification approach, prototype or protoflight. In practice the fact that the test specimen be flight hardware or a qualification model can substantially drive a number of decisions about the acceptance of a specific notched input spectrum.

For flight hardware, PFM or FM, it is a primary goal not to overtest the structure, therefore all precautions are taken in order not to damage the test specimen due to an overtesting. In particular the margins policy can be carefully reconsidered with respect to risk of damaging the test specimen. Of course decisions should be taken without jeopardising the aim of the test.

For qualification models, e.g. STM or SM, the goal not to overtest the structure could be in some cases less stringent and test strategies can be put in place to assess the robustness and more realistic margins

of the structure. For examples a delta-qualification run with reduced or no notching could follow a preliminary qualification.

#### **4.8.5.7 Reporting**

Before testing the following information should be included in the supporting documentation:

- Prediction by analysis of the notched spectrum
- Documentation of the FE analysis response (“active output”) which is used for predicting the notched spectrum and relevant limitations to be applied (“plateaus” or “thresholds”)

After testing the following information should be included in the supporting documentation:

- Analytical predictions validated by test results (e.g. test results at low and intermediate levels should show that the FE model is valid for the intended use).
- Documentation of the computational methods which are used to complement the test measurements (e.g. forces estimated by measured accelerations and FE analysis data).

### **4.8.6 Conclusions on notching in sine and random vibration testing**

The following criteria and information are considered for notching justification:

- Computational methods and procedures for notching predictions are documented. In particular:
  1. “Active” output parameters and relevant “thresholds” (e.g. accelerations and forces)
  2. Methods to recover or estimate QS loads (e.g. units CoG equivalent accelerations)
- Notching predictions are validated by lower level test runs
- Primary notching is justified versus coupled loads analysis results
- Secondary nothing should be minimized (and limited to sensitive units)
- Secondary notching in random vibration should be justified versus satellite vibro-acoustic analysis results
- Post-test assessments are performed

## **4.9 References**

- [1] Sarafin T.P. (editor), Spacecraft Structures and Mechanisms-from Concept to Launch, Kluwer Academic Publishers, Dordrecht, The Netherlands, 1995
- [2] Load Analyses of Spacecraft and Payloads, NASA-STD-5002, June 1996
- [3] Dynamic Environmental Criteria, NASA-HDBK-7005, March 2001
- [4] Calvi A., Nali P. – Some Remarks on the Reduction of Overtesting during Base-Drive Sine Vibration Tests of Spacecraft – Proc. of the ECCOMAS Conf. on Computational Methods in Structural Dynamics and Earthquake Engineering - Rethymno, Crete, Greece, June 2007
- [5] Y. Soucy, A. Coté – Reduction of Overtesting during Vibration Tests of Space Hardware – Canadian Aeronautics and Space Journal, Vol. 48, No 1, March 2002

- [6] Spacecraft Engineering, Verification guidelines, ECSS-E-HB-10-02 A, Noordwijk, The Netherlands, December 2010
- [7] Space engineering , Structural factors of safety for spaceflight hardware, ECSS-E-ST-32-10C Rev. 1, Noordwijk, The Netherlands, March 2009
- [8] ArianeSpace, "Ariane 5 User's Manual", Issue 5, Revision 1, July 2011
- [9] R. Knockaert - Sentinel 3 Mechanical Qualification Philosophy, Thales Alenia Space document S3-TN-TAF-SC-02066, Issue 1, 01/06/2011
- [10] V. Penman - Sentinel 3 Spacecraft Structure, PFM Static Load Test, Justification Test Report, RUAG document S3-RP-OSZ-SC-0013, Issue 1, 8-12-2010
- [11] Steinberg, D.S., "Vibration Analysis for Electronic Equipment", Third edition, 2000, John Wiley and Sons, ISBN 0-471-37685-X
- [12] ESSB-HB-E-005, "ESA Mechanical Shock Design and Verification Handbook", Issue 1, April 16 2012
- [13] SSTL Document N ST0134360 in reply to the ESA ITT "Methodology for Analysis of Structure-Borne Micro-Vibration", 24th September 2009
- [14] Kompella, M.S., Bernhard, B.J., "Measurement of the statistical variation of structural acoustic characteristics of automotive vehicles", Proc. SAE Noise and Vibration Conf., Warrendale, USA, 1993
- [15] E. Perl, T. Do, A. Peterson, J. Welch – Environmental Testing for Launch and Space Vehicles - Crosslink, The Aerospace Corporation Magazine for Advances in Aerospace Technology, <http://www.aero.org/publications/crosslink/fall2005/02.html>
- [16] A. M. Kabe, M. C. Kim, C. E. Spiekermann – Loads Analysis for National Security Space Missions – Crosslink, The Aerospace Corporation Magazine for Advances in Aerospace Technology, <http://www.aero.org/publications/crosslink/winter2004/04.html>
- [17] T.D. Scharton - Force Limited Vibration Testing Monograph - NASA Reference Publication RP-1403, May 1997
- [18] Structural Design and Test Factors of Safety for Spaceflight Hardware, NASA-STD-5001, June 1996

# 5

## Background on structural dynamics

### 5.1 Introduction

This chapter presents a summary of the principles of structural dynamics addressed throughout the different chapters of the present handbook. Further details concerning the majority of the concepts presented in this chapter may be found in [1].

This introduction starts with a general description of the dynamic environment of the LV/SC system and the associated types of analysis, followed by a presentation of the topics covered in the chapter along with the corresponding notations.

#### 5.1.1 The dynamic environment

During the course of a launch, the LV/SC system is excited by various sources of which the launcher engines play a particularly important role.

Generally speaking, these excitation sources are transmitted to the spacecraft via two distinct load paths:

- Structural or mechanical-borne transmission via the launcher structure in which the spacecraft is excited by mechanical forces at its interface with the launcher.
- Acoustic or air-borne transmission via the ambient air in which the spacecraft is excited by the acoustic pressure field inside the fairing and acting on all exposed surfaces.

These two load paths are clearly very different and moreover may occur simultaneously such as during lift-off or transonic flight, in which case we speak of a vibro-acoustic environment. At higher altitudes with decreasing air density the environment progressively becomes purely structural.

These vibration sources can comprise several regimes:

- Harmonic – This case is rather rare but very important due to the high amplification of motion that can result.
- Transient – In fact all excitations are transient, however we restrict this term to a relatively short excitation which can last from several milliseconds for pyrotechnic events (i.e. shock) to several tenths of seconds for transient thrust loads.
- Random – Beyond certain durations a deterministic analysis becomes impossible in which case the behaviour must be considered in a probabilistic manner. This is the case for most of the excitations caused by various sources which are more or less independent.

Regardless of the type of regime, the frequency content is particularly important. In the frequency domain, related to the time domain by the Fourier transform, the spectral content of the excitation with respect to the structure under consideration may be:

- Low frequency – The excitation produces structural responses with relatively simple shapes whose wavelengths are of the same order as the dimensions of the structure itself. More specifically the low frequency domain involves a small number of normal modes (stationary vibrational shapes related to the structure and associated with specific frequencies) permitting efficient analysis techniques.
- Wide band – In the higher frequencies the number of modes increases as well as the complexity of their shapes, therefore reducing the significance of each individual mode and rendering the analysis more difficult. This is the case of the vibro-acoustic environment producing wide band random vibrations, as well as the shock environment whose behaviour is more propagative than stationary. In general, the higher the frequency, the more the environment excites structures of smaller size.

Depending on the flight events under consideration, the type of structural dynamic analysis employed may be quite different.

### 5.1.2 Types of structural analysis

Subjected to a given environment, a structure responds. The analysis of its dynamic behaviour depends on various factors:

- Linear vs. Nonlinear Analysis – The behaviour of the structure may be linear (proportional to the excitation, etc.) or nonlinear for several reasons. In the latter case the analysis is much more difficult unless some type of linearisation is performed.
- Low frequency vs. Wide band – In the low frequency range, the modal approach provides an efficient analysis technique known as mode superposition. Each mode behaves as a “spring-mass” or one degree-of-freedom (DOF) system. In the wide band range, the number of modes becomes excessive, requiring the use of more suitable analysis techniques which are in general more complex, less accurate and used less widely.
- Time vs. Frequency Domain – Analyses may be performed in the time or frequency domains. In the frequency domain the relations between excitations and responses are called frequency response functions (FRF) which can be manipulated with ease leading to several advantages.
- Continuous vs. Discrete – Apart from particular cases, it is advantageous to represent a structure using a mathematical model discretised using a finite element approach in which case the equations of motion are expressed in terms of matrices.
- Global vs. Modular – Direct analysis using finite elements can become numerically burdensome when dealing with a large number of DOF. If the structure is modular (i.e. composed of distinct components connected at localized interfaces), each component may be analysed separately before assembly. This coupling technique known as substructuring, may be performed using FRF (Frequency Response Synthesis) or modes (Component Mode Synthesis).

These different analyses can be followed by an optimisation procedure to improve the dynamic behaviour of the structure if design margins are available, or a model updating procedure with respect to test data to obtain a more representative and therefore more reliable model.

### 5.1.3 List of topics

As a result of the above discussion, the following topics are covered in this chapter:

- Section 5.2 is dedicated to the characterisation of the dynamic environment, necessary for subsequent analysis in the different regimes and for the elaboration of specifications.
- Section 5.3 presents the different analysis techniques in order to determine the structural response to the environment. This is accomplished using a frequency domain analysis followed by a modal approach with effective mass models and by Craig-Bampton models for coupled loads analysis.
- Section 5.4 applies the previous considerations to the analysis of the coupled LV/SC system and its consequences on the qualification of the structures by sine testing which requires the use of the notching technique.
- Section 5.5 makes the distinction between primary notching, justified by coupled analysis, and secondary notching related to the maximum loads of subsystems and equipment.
- Section 5.6 addresses random testing used for qualifying structures with respect to mechanical or acoustic environments.

### 5.1.4 Principal notations

#### 5.1.4.1 Matrix conventions

By general convention,  $\mathbf{X}_{ab}$  designates a matrix of dimension  $(n,p)$  whose  $n$  rows and  $p$  columns correspond to the degrees of freedom (DOF)  $a$  and  $b$  respectively.

This convention implies the use of certain precautions detailed in [1] which are not stated here for simplicity.

#### 5.1.4.2 Scalars or matrices

$A$	Amplitude
	Amplification
$C, c$	Viscous damping
$F$	Force
$f$	Frequency
$G$	Flexibility (displacement/force)
$H$	Frequency response function (FRF)
	Dynamic amplification factor
$I$	Identity
$K, k$	Stiffness (force/displacement)
$L$	Modal participation factor
$M, m$	Mass (force/acceleration)
$P$	Probability
$p$	Probability density
$q$	Modal displacement
$Q$	Amplification at resonance: $Q = 1 / (2\zeta)$
$R$	Sweep rate (generally expressed in oct/min)
	Reaction force
	Auto or cross-correlation
$S$	Response spectrum (SRS or RRS)

---

$T$	Transmissibility (displacement/displacement, etc.)
	Dynamic transmissibility factor
	Period or duration
$t$	Time
$u$	Physical displacement
$W$	Power spectral density (PSD)
$\eta$	Structural damping factor
$\zeta$	Viscous damping factor
$\sigma$	Standard deviation
$\tau$	Delay
$\Psi$	Normal mode
$\Phi$	Junction mode
$\omega$	Circular frequency: $\omega = 2\pi f$

#### 5.1.4.3 Subscripts

$i$	Internal
$c$	Connection
$e$	Excitation
$j$	Junction (boundary)
$k$	Normal Mode
$o$	Observation
$p$	Residual (pseudo) mode
$r$	Rigid (statically determinate) junction
$res$	Residual

#### 5.1.4.4 Other notations

$\tilde{X}$	Effective parameter
$x^*$	Conjugate of $x$
$\dot{x}, \ddot{x}$	$dx/dt, d^2x/dt^2$
$\bar{x}$	Average of $x$

## 5.2 Dynamic environments – analysis and specifications

### 5.2.1 Generalities

Details on the analysis and the specification of dynamic environments may be found in Vol. 1-5 of [2].

The characterisation of a dynamic environment for its analysis leading to specifications depends on its regime:

- Harmonic – The characterisation of a harmonic environment poses no particular problem since a sine is simply defined by its frequency and amplitude, which can be considered to vary slowly with time.
- Random – Signal processing, including the Fourier transform to convert to the frequency domain, provides a satisfactory characterisation under certain conditions.
- Transient – The Fourier transform leads to a characterisation in the frequency domain, however this approach is not well adapted to the need of specifying a test for qualification of the structure. Indeed, because of the phase which accompanies the amplitude, this transformation lacks the notion of severity used to compare environments and to elaborate an envelope. To conserve the severity, an alternative characterisation must be considered.

The idea generally adopted for a transient regime is to characterise it by its effect on a reference structure, the 1-DOF system, defined by two parameters (natural frequency and damping ratio) of which the natural frequency provides a characterisation in the frequency domain. This leads to the concept of the response spectrum which can be used in two different contexts, depending on the failure mode considered for the structure:

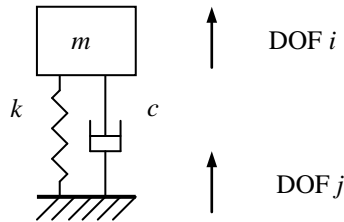
- Failure by exceeding maximum allowable stress – In this case the maximum response levels are considered leading to the shock response spectrum (SRS) which is particularly well adapted to the transient regime but can also be used for other regimes making the SRS a general tool for comparison and envelopes of environments. This type of spectrum, especially easy to obtain for the harmonic regime, is developed in Section 5.2.4.3 for transients, and extended to random excitation in Section 5.2.5.4.
- Failure by fatigue – Although often less critical for launch due to the limited duration of the events, this failure mode is potentially dangerous. Severity in this case is based on the number of cycles of the response associated with an endurance curve of the material leading to the fatigue damage spectrum (FDS). This type of spectrum is particularly useful in the random regime with long durations but can also be used in the harmonic regime to determine equivalent environments although not without risk due to required assumptions. The FDS is not treated in this chapter due to its specific nature, however details can be found in Vol. 4 of [2].

Figure 5-1 describes the 1-DOF system (reference structure) which is used throughout this chapter in regards to various spectra and normal modes.

- It is characterised by three physical parameters: the mass,  $m$ , the stiffness,  $k$  and the viscous damping constant,  $c$  relating the dissipative force to the relative velocity.
- It can be excited by a force  $F_i$  acting on its internal DOF,  $i$ , and/or by an acceleration  $\ddot{u}_j$  imposed on its junction DOF,  $j$ .

- As a result of the above excitations, it responds by an acceleration  $\ddot{u}_i$  at its internal DOF,  $i$ , and by a reaction force at its junction DOF,  $j$ .

These mnemonic notations are further developed for the general case in Section 5.3.



**Figure 5-1: The 1-DOF system**

Before examining the above characterisations for the different regimes, let us consider an illustrative example using the first qualification flight of the Ariane launcher which took place on Dec. 24 1979.

### 5.2.2 Example - the maiden flight of Ariane 1

Figure 5-2 shows the acceleration time history at the LV/SC interface during the 1<sup>st</sup> and 2<sup>nd</sup> stage (N2O4/UDHM) flight segments in the axial and lateral directions. Only the lower and upper envelopes are plotted in order to simplify the responses.

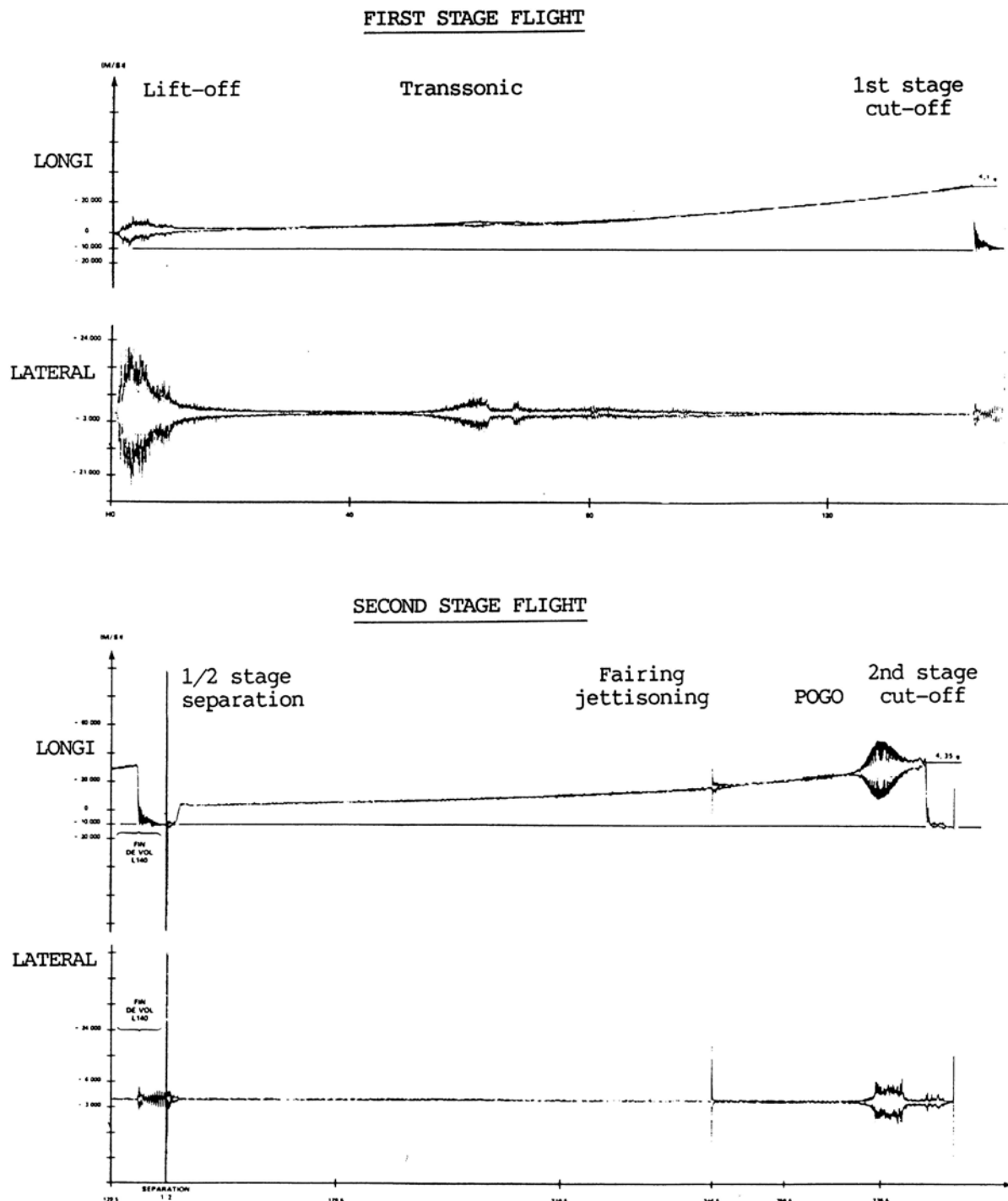


**Figure 5-2: Ariane 1 first flight - LV/SC interface acceleration**

We can distinguish the following regimes from Figure 5-2:

- Quasi-static regime – The axial acceleration which slowly increases due to fuel consumption.
- Harmonic regime – The POGO effect (Propulsion Generated Oscillations) at the end of the 2nd stage flight (see zoom in Figure 5-3) due to an interaction between the structure, the hydraulics and the propulsion. It excites the first axial mode of the launcher whose frequency slowly increases, again due to fuel consumption, resulting in a swept sine from 28 to 32 Hz over a

period of approximately ten seconds. The anti-POGO system was intentionally deactivated during this flight in order to observe this effect, making this example quite unique.

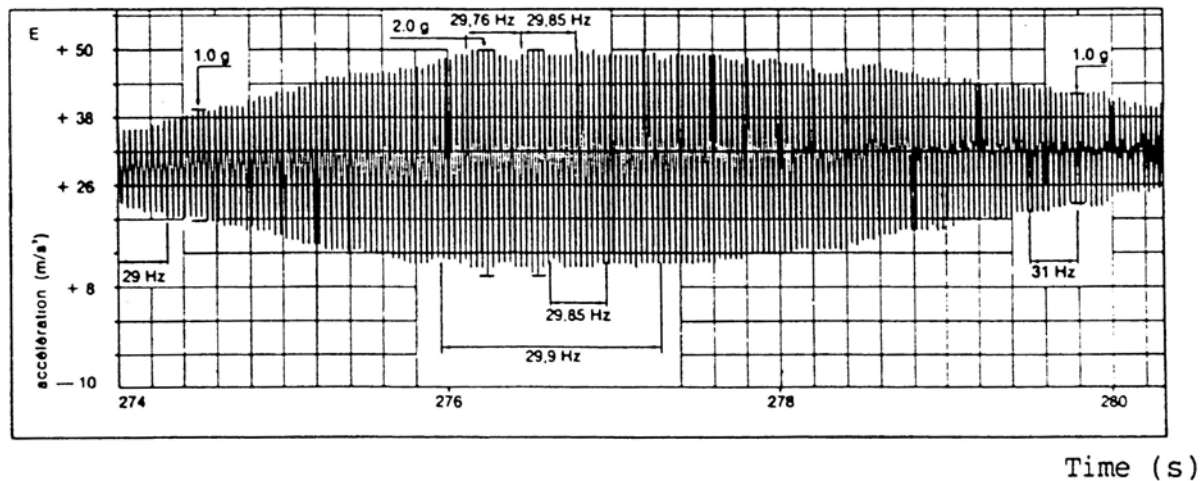


**Figure 5-3: Zoom on POGO effect**

- Transient regime – Comprising the thrust transients lasting several tenths of seconds (the most severe occurring at engine burn-out) and the separation shocks (stages and fairing) lasting several milliseconds.
- Random regime – At lift-off and transonic flight lasting between 10 and 20 seconds. With a frequency content of up to 2000 Hz, this corresponds to tens of thousands of (non-reproducible) oscillations, therefore precluding a deterministic analysis.

These events illustrate very well the different types of environment encountered during the course of launch and whose characterisation is presented hereafter.

## 5.2.3 Sine environment

### 5.2.3.1 Characterisation

A pure sine of circular frequency  $\omega = 2\pi f$  is defined by the following function of time:

$$x(t) = X \sin(\omega t + \varphi) \quad [5-1]$$

with amplitude  $X$  and phase  $\varphi$  relative to an arbitrary reference (necessary when considering several harmonics). For a phase equal to zero, the sine is defined simply by its frequency  $f$  and amplitude  $X$ .

If over the course of time the frequency of the sine changes, and sufficiently slowly such that the motion remains quasi-stationary (steady-state) at each instant, the analysis can be performed assuming a pure sine at each instant of time. This time variation, often monotonic, can sweep over a more or less wide frequency band – called swept sine or sine sweep. The POGO effect is a good example in terms of a real (true) environment. The sine sweep is commonly used in vibration tests in order to envelope the effects of the real environment in a given frequency range.

In this case the circular frequency  $\omega$  is a monotonic function of time  $\omega(t)=d(\omega t)/dt$ , along with the amplitude  $X(t)$  implying therefore  $X(\omega)$ . For sine testing, the function  $\omega(t)$  is most often exponential because of its properties with respect to the 1-DOF system. The sweep rate  $d\omega/dt$  is in this case expressed in octaves/minute and has little importance as long as the steady-state assumption is respected. This assumption is further discussed in Section 5.2.3.3.

### 5.2.3.2 Response of the 1-DOF system

The response of the 1-DOF system of Figure 5-1 due to a harmonic excitation at frequency  $\omega$  can be expressed as follows:

$$\begin{bmatrix} \ddot{u}_i(\omega) \\ F_j(\omega) \end{bmatrix} = \begin{bmatrix} -\omega^2 G_{ii}(\omega) & T_{ij}(\omega) \\ -T_{ji}(\omega) & M_{jj}(\omega) \end{bmatrix} \begin{bmatrix} F_i(\omega) \\ \ddot{u}_j(\omega) \end{bmatrix} \quad [5-2]$$

revealing the three fundamental FRF:

$G_{ii}(\omega)$  dynamic flexibility (displacement/force)

$T_{ij}(\omega) = T_{ji}(\omega)$  dynamic transmissibility for forces and displacements (identical according to reciprocity theory)

$M_{jj}(\omega)$  dynamic mass (force/acceleration)

The solution of the equations of motion leads to:

$$G_{ii}(\omega) = H_k(\omega) \frac{1}{k} \quad [5-3]$$

$$T_{ij}(\omega) = T_{ji}(\omega) = T_k(\omega) 1 \quad [5-4]$$

$$M_{jj}(\omega) = T_k(\omega) m \quad [5-5]$$

where the subscript  $k$ , in anticipation of the general case, designates the mode of the 1-DOF system. We see that each FRF is the product of two terms:

- a static term – static flexibility  $\frac{1}{k}$ , static transmissibility 1, and static mass  $m$ .
- a dimensionless complex-valued dynamic amplification which is a function of the circular natural frequency  $\omega_k = \sqrt{\frac{k}{m}}$  and the damping ratio  $\zeta_k = \frac{c}{2\sqrt{k m}}$ :

$$H_k(\omega) = \frac{1}{1 - \left( \frac{\omega}{\omega_k} \right)^2 + i 2\zeta_k \frac{\omega}{\omega_k}} \quad \text{dynamic amplification} \quad [5-6]$$

$$T_k(\omega) = \frac{1 + i 2\zeta_k \frac{\omega}{\omega_k}}{1 - \left( \frac{\omega}{\omega_k} \right)^2 + i 2\zeta_k \frac{\omega}{\omega_k}} \quad \text{dynamic transmissibility} \quad [5-7]$$

The dynamic amplification functions  $H_k(\omega)$  and  $T_k(\omega)$  are equal to 1 at  $\omega=0$  (static case) and equal to  $\frac{1}{2\zeta_k} = Q_k$  at  $f = f_k$  (resonance). The shape of their amplitude forms a peak at the resonance whose sharpness (acuity) is directly related to the damping. This peak can therefore be used to directly identify the two parameters of the system or mode (Single DOF or SDOF identification):

- natural frequency  $f_k$  – approximately equal to the frequency of the maximum.

- damping ratio  $\zeta_k$  – approximately equal to  $Q_k = \frac{1}{2\zeta_k} = \frac{f_k}{\Delta f_k}$  with  $\Delta f_k$  the half-power frequency interval defined using the frequencies at the amplitude equal to the maximum divided by  $\sqrt{2}$ .

These approximations can be refined by use of a suitable method.

### 5.2.3.3 Influence of the sweep rate

If the sweep rate is not sufficiently slow, the response is no longer stationary (steady-state) at each instant of time, resulting in a modification of the response envelope due to transient behaviour [3].

In the following we consider exponential sweeps expressed in octaves/minute, where  $R$  octaves/minute indicates that after each minute the excitation frequency is multiplied by  $2^R$ . The advantage of the exponential sweep is that all modes (with the same damping) are excited for the same duration regardless of their frequencies.

As an example, response profiles of a 1-DOF system with  $f_k = 20$  Hz and  $Q_k = 25$  are plotted in Figure 5-4 for two different exponential sweep rates ( $R = \pm 1$  and  $\pm 4$  octaves/minute) and compared to the steady-state response ( $R = 0$ ).

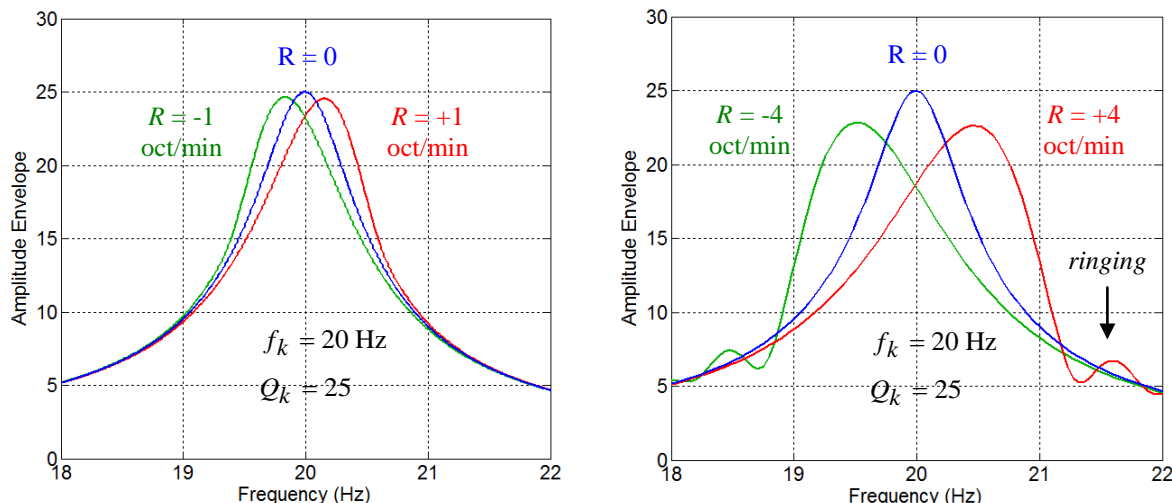


**Figure 5-4: Effect of sweep rate on response profile**

We see that the shape and position of the resonant peak are altered as a function of the sweep rate and direction. Moreover a beat pattern or "ringing" following the peak may also appear. This ringing is a result of the system responding at two frequencies of nearly the same value comprising the free response at the natural frequency  $f_k$  and the forced response at the swept excitation frequency.

These two phenomena, peak alteration and ringing, depend not only on the sweep rate and direction, but also on the natural frequency  $f_k$  and damping  $\zeta_k$  of the peak. These dependencies are described below.

- A frequency sweep *decreases* the amplitude of the peak, *shifts* the position of the peak along the direction of the sweep, *broadens* the peak width and *distorts* the shape of the peak (loss of symmetry). The higher the sweep rate, the more these effects are pronounced.
- These effects are *proportional* to the sweep rate,  $R$ , and *inversely proportional* to the natural frequency  $f_k$  and (approximately) to the square of the damping  $\zeta_k^2$ . Therefore low-frequency

and lightly damped modes are most sensitive to sweep rate effects. The dimensionless parameter  $\eta = \frac{R \ln(2) / 60}{f_k \zeta_k^2}$  is often used to quantify sweep rate effects via formulas, tables and plots.

- The direction of the frequency sweep affects mainly the direction of the peak shift and has little influence on the amplitude attenuation and ringing.

The effect of the sweep rate can be expressed in terms of the modal parameters associated with the peak: natural frequency  $f_k$ , damping  $\zeta_k$  and effective parameter  $\tilde{T}_k$  (see Section 5.3.2.2 for details). These three modal parameters may be determined as follows.

- The natural frequency  $f_k$  is estimated by using the frequency of the maximum peak amplitude  $A_k$ . This approximation is perfectly valid for typical values of damping ( $\zeta_k < 0.1$ ).
- The damping factor  $\zeta_k$  is estimated by the half-power method. The maximum peak amplitude  $A_k$  is used to determine the half-power level  $A_k / \sqrt{2}$  and corresponding frequency interval  $\Delta f_k$ . The damping factor is given by  $\zeta_k = \frac{\Delta f_k}{2f_k}$ .
- The modal effective parameter  $\tilde{T}_k$  is obtained from the maximum amplitude  $A_k$  and damping  $\zeta_k$  using the relation  $\tilde{T}_k = 2\zeta_k A_k$ . For the steady-state response ( $R=0$ ) we have  $\tilde{T}_k = 1$  (unit transmissibility).

Numerical simulation was used to determine the effect of an exponential sweep rate on the amplitude, natural frequency, damping and effective parameter of a 1-DOF system (structural mode) using the modal identification techniques described above. Both increasing and decreasing sweep directions were considered.

The results are presented in the four graphs of Figure 5-5 with each graph pertaining to a modal parameter. The relative error (in percent) of the modal parameter is plotted for four different values of damping ( $Q = 10, 25, 50, 100$ ) as a function of the frequency (Hz) divided by the sweep rate (oct/min). For a sweep rate of  $R = 1$  oct/min, the x-axis directly provides the frequencies. For other sweep rates the values on the x-axis can be simply multiplied by  $R$  to obtain the corresponding frequency values.

The results for both positive (+) and negative (-) sweep rates are provided using solid and dashed lines respectively. The differences between the two are small and often negligible especially with light damping.

From Figure 5-5 we see that the damping (peak width) is much more affected by the sweep rate than the frequency – although frequency shifts may be considered more critical. For example with a sweep rate of 1 oct/min, a mode at 10 Hz with  $Q = 50$  has 2 % error in frequency but over 70 % error in damping.

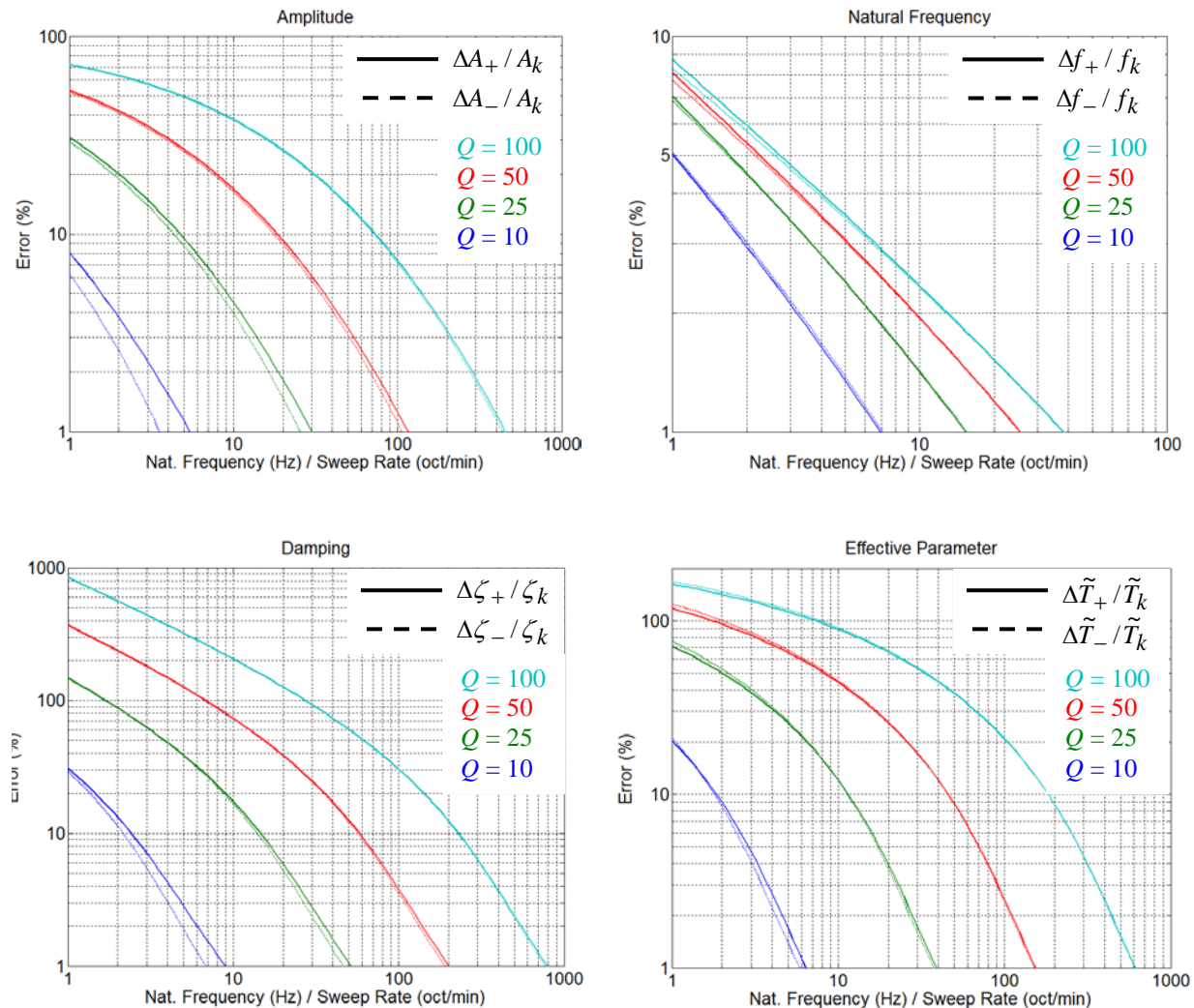


**Figure 5-5: Effect of sweep rate on modal parameters**

As another example, consider a mode at  $f_k = 20$  Hz with damping  $Q_k = 50$  and two different sweep rates of 1 and 2 oct/min. From Figure 5-5 we obtain the errors shown in Table 5-1 associated with the modal parameters:

**Table 5-1: Example of sweep rate induced errors**

Sweep Rate (oct/min)	Relative Error in Modal Parameters			
	$\Delta A_+ / A_k$	$\Delta f_+ / f_k$	$\Delta \zeta_+ / \zeta_k$	$\Delta \tilde{T}_+ / \tilde{T}_k$
1	~ 9 %	~ 1 %	~ 39 %	~ 26 %
2	~ 16 %	~ 2 %	~ 72 %	~ 45 %

## 5.2.4 Transient environment

### 5.2.4.1 Characterisation

The frequency characterisation of a transient signal is performed naturally by the Fourier transform which expresses the decomposition of a periodic signal by a sum of continuous sine functions in the form of an amplitude and phase as a function of frequency. This transformation is reversible – therefore providing a two-way passage between the time and frequency domains.

### 5.2.4.2 Response of the 1-DOF system

The response of a structure to a transient excitation can be determined by expressing the excitation as an infinite sum of impulse functions. This leads to Duhamel's integral – the convolution of the excitation with the response of the structure to a unit impulse. This response to a unit impulse, called the impulse response or impulse response function (IRF), is equivalent to the FRF in the frequency domain. That is, the FRF is none other than the Fourier transform of the IRF (impulse response).

For the 1-DOF system of Figure 5-1, the IRF are damped sine functions corresponding to the inverse Fourier transform of the FRF seen in Section 5.2.3.2. In particular, the inverse Fourier transform of the dynamic amplifications  $H_k(\omega)$  and  $T_k(\omega)$  results in:

$$h_k(t) = \omega_k e^{-\zeta_k \omega_k t} \frac{1}{\sqrt{1-\zeta_k^2}} \sin\left(\omega_k \sqrt{1-\zeta_k^2} t\right) \quad [5-8]$$

$$t_k(t) = -\ddot{h}_k(t) / \omega_k^2 \quad [5-9]$$

As for the FRF peaks, these damped sine functions allow direct identification of the two parameters of the 1-DOF system (or isolated mode) using the SDOF identification in the time domain:

- natural frequency  $f_k$  – approximately equal to the damped natural frequency  $f_d = f_k \sqrt{1-\zeta_k^2}$
- damping ratio  $\zeta_k$  – deduced from the exponential decay of the function leading to the logarithmic decrement (logarithm of the ratio between two successive maxima)  $\Delta_k$  from which  $\zeta_k$  is obtained using  $\Delta_k = \frac{2\pi \zeta_k}{\sqrt{1-\zeta_k^2}} \approx 2\pi \zeta_k$ .

### 5.2.4.3 Shock response spectra

As mentioned earlier in Section 5.2.1, the Fourier transform with its amplitude and phase spectra, does not contain directly the notion of severity required to elaborate specifications. The solution generally adopted is the shock spectrum or shock response spectrum (SRS) which is by definition the maximum response of a 1-DOF system as a function of its natural frequency and for a given damping ratio, as illustrated in Figure 5-6.

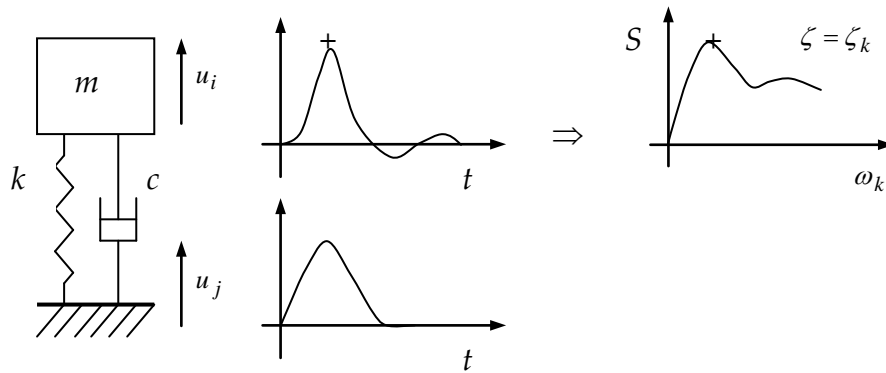


**Figure 5-6: Principle of the SRS**

For example, if we consider an imposed acceleration at the base of the 1-DOF system, its acceleration response in the frequency domain is obtained using the dynamic transmissibility  $T_k(\omega)$  which depends on the two parameters  $f_k$  and  $\zeta_k$ . The damping ratio  $\zeta_k$  must therefore be prescribed in order to obtain a function of  $f_k$  alone. If the actual damping of the structure in question is unknown, then a default or estimated value for  $\zeta_k$  must be specified. In practice it is common to specify the factor  $Q = 1 / (2\zeta)$ , for example  $Q = 10$  (i.e.  $\zeta = 5\%$ ) often used in various fields of study.

Among the different possible response types of the 1-DOF system (displacement/velocity/acceleration, relative/absolute motion, minima/maxima, primary/residual) along with their variants, the most interesting in the present context is the absolute acceleration (minima or maxima if the distinction is warranted) and in particular its use with the effective mass models examined in Section 5.3.3.

As an example, Figure 5-7 illustrates the SRS of a half-sine transient often used in various fields because of its simple shape, ease of use and representativity in certain classes of shock.

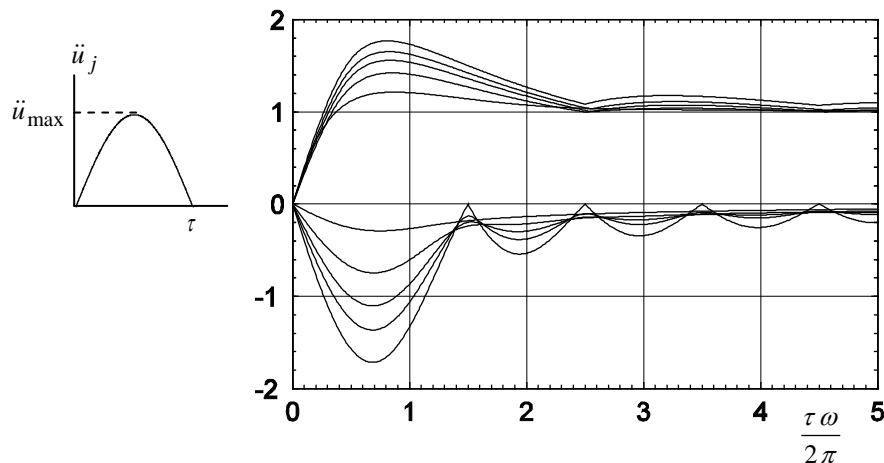


**Figure 5-7: SRS of a half-sine acceleration**

The use of the maximum response corresponds perfectly to the notion of severity, and therefore justifies the use of the SRS for the characterisation of transients and the subsequent elaboration of specifications. However, this approach does have certain drawbacks:

- The SRS is mathematically very complex and highly nonlinear, thus requiring special attention when being used.

- Above all, the SRS is irreversible. That is, a time history relates to a unique SRS, however a SRS does not relate to a unique time history, but rather to an infinite number of time histories. This is due to the fact that the SRS provides only amplitude whereas the Fourier transform provides both amplitude and phase. We have therefore lost the information contained in the phase which can be interpreted here by the notion of duration.

To illustrate this last point, notice that any SRS can be obtained by an equivalent (steady-state) sine sweep whose amplitude is given by the SRS divided by the factor  $Q$ . In this way we can replace a half-sine of several milliseconds by an equivalent sine sweep (in terms of the SRS) lasting several minutes!

This intentionally exaggerated example clearly demonstrates the potential danger of using the SRS without precaution. Replacing one environment by another whose nature is completely different, always involves risks related to the assumptions used to define the equivalence.

Moreover, the SRS is valid only for a 1-DOF system with a given damping ratio, which can therefore lead to several problems when used in conjunction with the actual structure:

- The structure can be represented by its normal modes which behave as 1-DOF systems, each mode having its maximum response according to the SRS. However, the mode superposition technique used to combine the modal contributions cannot be strictly applied, resulting in an approximate combined response with the risk of obtaining significant differences in amplitude (see Section 5.3.3.2).
- The damping in the structure can be very different from the damping ( $Q$  factors) used to compute the SRS. Here again the risk of error can be high.

Literature on the SRS and its use is abundant. We can cite [4] as an overview with historical information, Vol. 2 of [2] as a technical reference and [5] in particular for use in the context of LV/SC coupled analysis.

The risks mentioned above can be tempered by complementing the SRS with additional information about the environment in order to limit the degree of irreversibility, using durations for example. Developments in this field can be found in [6], [7]. In the present context, one simple idea is to consider two values of  $Q$ . The two corresponding SRS have the same amount of information contained in the amplitude and phase of the Fourier transform. It should therefore be possible to derive a nearly reversible transformation based on two  $Q$  values in order to obtain a more representative transient with respect to the actual environment.

Any SRS, with or without complementary information, can be used in the following ways:

- Structural analysis – The computation of responses for any given structure using SRS is addressed in Section 5.4 in terms of coupled analysis.
- Shock synthesis – The elaboration of a time history for testing in order to qualify the structure. This inverse problem can be solved more or less accurately by several techniques. The most widely used is the wavelet technique based on the combination of waveforms (wavelets) to represent a given spectrum.

In conclusion, the SRS satisfies the need to characterise the severity of an environment for specification purposes. However it should be used with caution due to the loss of information in the initial transform. Nonetheless this loss offers a certain leeway consistent with the uncertainty (irreproducibility) of the actual environment, which can be taken advantage of, within certain limits.

## 5.2.5 Random environment

### 5.2.5.1 Random process

The basics of random processes and random vibrations are discussed in detail in Crandall [8], Papoulis [9], Lin [10], Thomson [11], Lin [12], Wirsching [13], Gatti [14], Sun [15] and Wijker [16] (special focus on spacecraft structures design).

A process  $x$  is considered random, as opposed to deterministic, if it is irregular and non-repetitive. Its analysis from an ensemble of records  $x_i(t)$  can be performed in one of two ways as schematized in Figure 5-8:

- Time averaging – The analysis is performed over a time sample for a given record  $i$  leading to a random function  $x_i(t)$ .
- Ensemble averaging – The analysis is performed over all records at a given instant of time  $t_j$  leading to a random variable  $x(t_j)$ .

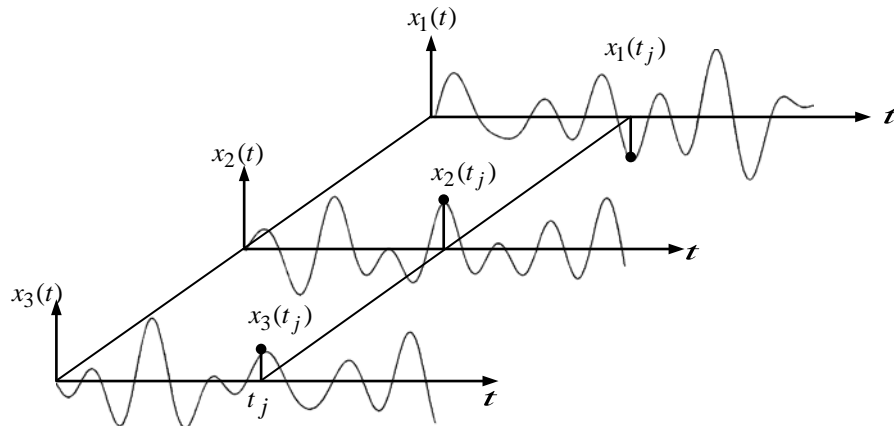


**Figure 5-8: Random process**

Time analysis on the function  $x(t)$  over a time interval  $T$ , as illustrated in Figure 5-9 provides the following values:

- the mean value  $\bar{x}$ :

$$\bar{x} = \frac{1}{T} \int_0^T x(t) dt \quad [5-10]$$

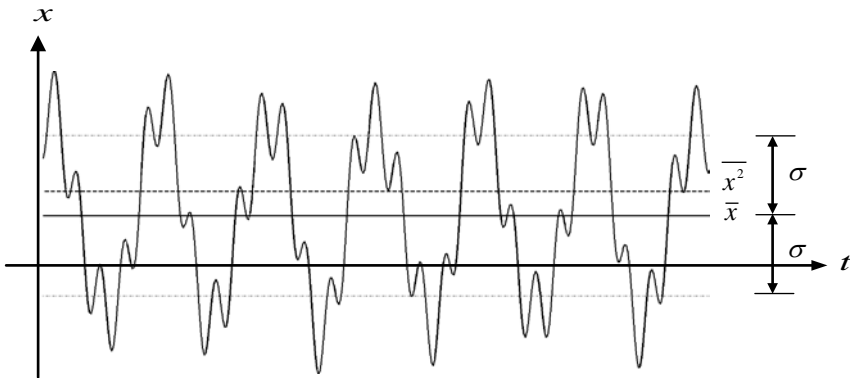
- the mean square value  $\overline{x^2}$  and the root mean square or rms value:

$$\overline{x^2} = \frac{1}{T} \int_0^T x^2(t) dt \quad x_{RMS} = \sqrt{\overline{x^2}} \quad [5-11]$$

- the variance  $\sigma_x^2$  and the standard deviation  $\sigma_x$ :

$$\sigma_x^2 = \frac{1}{T} \int_0^T [x(t) - \bar{x}]^2 dt = \overline{x^2} - \bar{x}^2 \quad [5-12]$$

where  $\sigma_x$  represents the mean deviation, in the quadratic sense, between  $x(t)$  and its mean.

**Figure 5-9: Mean value and standard deviation**

If these properties are independent of the considered time interval  $T$ , the process is said to be stationary as assumed in what follows.

If we consider the mean of the product  $x(t)x(t+\tau)$ , for a given delay  $\tau$ , we obtain a function of  $\tau$  called the autocorrelation of  $x$ :

$$R_{xx}(\tau) = \frac{1}{T} \int_0^T x(t) x(t+\tau) dt \quad [5-13]$$

where  $R_{xx}(\tau)$  is even and:

$$R_{xx}(0) = \bar{x}^2 \quad [5-14]$$

For two processes  $x(t)$  and  $y(t)$ , the average of the product  $x(t)y(t+\tau)$  is the cross correlation between  $x$  and  $y$ :

$$R_{xy}(\tau) = \frac{1}{T} \int_0^T x(t) y(t+\tau) dt \quad [5-15]$$

where  $R_{xy}(\tau)$  is generally not even.

Statistical analysis on the random variable  $x$  with values  $x_i$  produces the same types of properties using a probability density function  $p(x)$  defined by:

$$p(x) = \frac{dP(x)}{dx} \quad [5-16]$$

where  $P(x)$  is the probability of  $x_i$  having a value less than a given value  $x$ . As an example, the mean value is given by:

$$\bar{x} = \int_{-\infty}^{+\infty} x p(x) dx \quad [5-17]$$

If the statistical properties are the same as those obtained from time averaging, the process is said to be ergodic. In this case a single record is sufficient to completely represent the process. This is assumed in the following.

To complete the information about  $p(x)$ , we can note that many random processes have a tendency to follow a normal or Gaussian distribution where  $p(x)$  depends only on the mean value  $\bar{x}$  and the standard deviation  $\sigma_x$ :

$$p(x) = \frac{1}{\sigma_x \sqrt{2\pi}} e^{-\frac{(x-\bar{x})^2}{2\sigma_x^2}} \quad [5-18]$$

In practice, we often retain the  $n\sigma$  probabilities listed in Table 5-2 for  $n = 1, 2$  and  $3$ .

**Table 5-2: Normal distribution probabilities**

$n$	$P(x \leq \bar{x} + n\sigma_x)$	$P( x - \bar{x}  \leq n\sigma_x)$
1	84.13 %	68.27 %
2	97.72 %	95.45 %
3	99.87 %	99.73 %

Another interesting case is the Rayleigh distribution which is the distribution of the peaks of a narrow band signal (response of a 1-DOF system to noise), with:

$$p(x) = \frac{1}{\sigma_x^2} x e^{-\frac{(x-\bar{x})^2}{2\sigma_x^2}} \quad [5-19]$$

giving the probabilities listed in Table 5-3.

**Table 5-3: Rayleigh distribution probabilities**

$n$	$P(x \geq \bar{x} + n\sigma_x)$
1	60.65 %
2	13.53 %
3	1.11 %

### 5.2.5.2 Frequency characterisation

The frequency characterisation of an ergodic random process can be performed by the Fourier transform of the correlation functions defined in the time domain as the average of the products of the process at two different instants of time. This leads to the notion of spectral density functions which fall into two categories:

- Auto Spectral Density  $W_{xx}$  – Also called Power Spectral Density (PSD), this function is obtained by the Fourier Transform of the autocorrelation  $R_{xx}$  of the process  $x$  (Wiener-Khinchin theorem). The function  $W_{xx}$  is real and positive, and represents the distribution of the mean square (or square of the rms) of the signal  $x(t)$ ,  $\overline{x^2} = (x_{rms})^2$ , as a function of the frequency, therefore characterising the frequency content of the signal. Inversely, we have:

$$\overline{x^2} = \int_0^\infty W_{xx}(f) df \quad [5-20]$$

- Cross Spectral Density  $W_{xy}$  – This function is obtained by the Fourier Transform of the cross-correlation between two processes  $x$  and  $y$ . The function  $W_{xy}$  is complex-valued ( $W_{yx} = W_{xy}^*$ ) and represents the distribution of the mean  $\overline{xy}$  as a function of the frequency.

With the auto and cross spectral density functions, the coherence function  $\gamma_{xy}$  between two processes  $x$  and  $y$  can be defined as shown below. This dimensionless function with values between 0 and 1 represents the degree of dependence between  $x$  and  $y$  (0 for independent processes, 1 for completely dependent processes). This notion is particularly useful in an experimental context.

$$\gamma_{xy}^2(f) = \frac{|W_{xy}(f)|^2}{W_{xx}(f)W_{yy}(f)} \quad [5-21]$$

An environment described by a single random excitation,  $x$ , is characterised by its auto spectral density function  $W_{xx}$ . In the case of two sources of excitation  $x$  and  $y$ , the environment is characterised not only by the auto spectral functions  $W_{xx}$  and  $W_{yy}$ , but also by the cross spectral density,  $W_{xy}$ . In the general case with several excitation sources, the environment is characterised by a matrix of spectral density functions with auto densities on the diagonal and cross densities in the off-diagonal terms (zero for independent excitations).

In the case of an acoustic excitation, the associated pressure field is represented by random forces acting on each exposed (wetted) DOF of the structure with their auto and cross density functions. The auto spectral densities may be deduced from the pressure spectrum acting on each element of the exposed surface. The cross spectral densities are obtained from the coherence between points in the pressure field, which in turn depends on the nature of the field (diffuse, turbulent boundary layer, etc.).

Note that according to Eq. [5-20] the rms value of a signal is given by the integral of its PSD  $W_{xx}$ . If  $x$  is an excitation, the rms value is a global indicator of its severity. However the PSD, i.e. the frequency content, provides a complete characterisation and therefore allowing the determination of the response to the excitation.

A particular case of PSD is white noise corresponding to a constant value over all frequencies. For random testing, in the common case of an imposed acceleration,  $W_{xx}$  is generally expressed in  $\text{g}^2/\text{Hz}$ , with constant levels by bands, separated by slopes expressed in dB per octave, as illustrated in Figure 5-10.

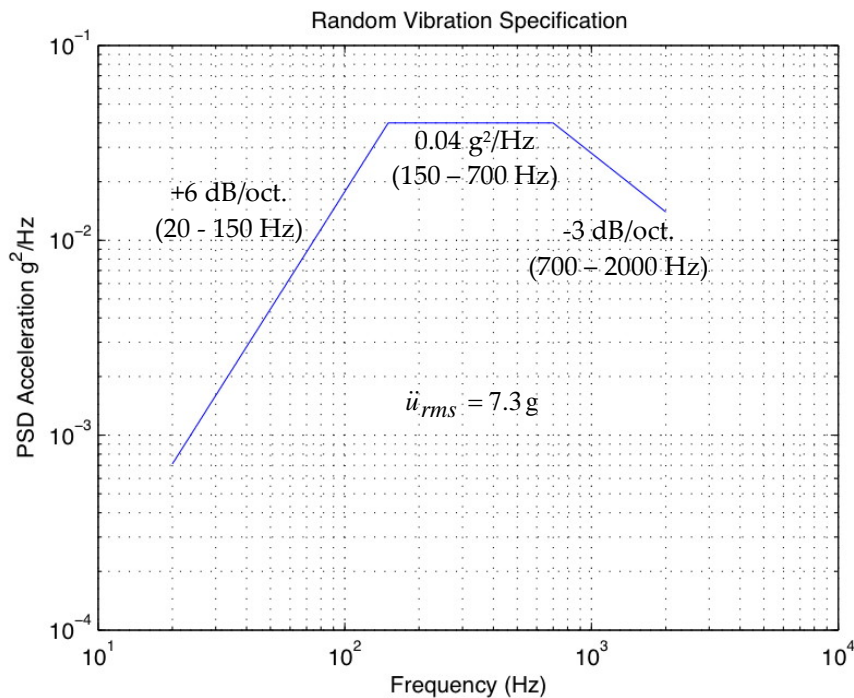


**Figure 5-10 Example of acceleration PSD specification**

Given that an octave corresponds to a ratio of 2 in frequency, and 3 dB a factor of 2 in PSD level, a slope of  $n$  dB/octave has a variation of  $f^{n/3}$ . Using this, the mean square value of the PSD of Figure 5-10 is given by Eq. [5-22].

$$\overline{\ddot{u}^2} = (\ddot{u}_{rms})^2 = \int_{20}^{2000} W(f) df = 0.04 \text{ g}^2 / \text{Hz} \left[ \int_{20}^{150} \left( \frac{f}{150} \right)^2 df + (700 - 150) + \int_{700}^{2000} \left( \frac{700}{f} \right) df \right] \approx (7.3 \text{ g})^2 \quad [5-22]$$

The notion of dB used above to specify the slopes of the PSD and encountered in numerous scientific and engineering contexts, has its origins in acoustics to express a level of sound pressure according to the following definition:

$$N \text{ dB} = 10 \log_{10} \left( \frac{p^2}{p_{ref}^2} \right) = 20 \log_{10} \left( \frac{p}{p_{ref}} \right) \quad [5-23]$$

where  $p$  is the acoustic pressure and  $p_{ref}$  a reference value fixed at  $2.0 \times 10^{-5}$  Pa corresponding to the threshold of perception of the average human ear at 1000 Hz. As an example,  $N = 139$  dB corresponds to an acoustic pressure of 178 Pa.

In a more general manner, the dB can be used to express a ratio of values in a logarithmic scale based on Eq. [5-23]. A coefficient of 10 is used for power quantities (sound intensity, energy, power, etc.) and a coefficient of 20 for field quantities (pressure, acceleration, force, etc.). In the example of slopes of the PSD, the suitable coefficient is therefore 10, leading to a ratio of 2 for 3 dB. On the other hand, for the rms value, the coefficient is 20 with 3 dB corresponding to a ratio of  $\sqrt{2}$ .

### 5.2.5.3 Response of the 1-DOF system

In general, if  $H_{yx}$  is the FRF between the excitation  $x$  and the response  $y$ , the response PSD,  $W_{yy}$  can be obtained from the excitation PSD,  $W_{xx}$  according to:

$$W_{yy}(f) = |H_{yx}(f)|^2 W_{xx}(f) \quad [5-24]$$

Using the FRF of Eq. [5-3] [5-4] [5-5] along with Eq. [5-20], we can compute the rms values for the responses of the 1-DOF system excited by white noise – that is, a constant excitation PSD  $W_{xx} = W$ . For example, in the case of the dynamic transmissibility  $T_k(\omega)$ , it is necessary to integrate the function  $|T_k(f)|^2$  which can be done with the help of the following formula from Crandall [8]:

$$\int_{-\infty}^{+\infty} \left| \frac{i\omega B_1 + B_0}{-\omega^2 A_2 + i\omega A_1 + A_0} \right|^2 d\omega = \pi \frac{(B_0^2/A_0) A_2 + B_1^2}{A_1 A_2} \quad [5-25]$$

Assuming weak damping, we obtain the following simplified expression known as Miles' Equation:

$$y_{rms} \approx \sqrt{\frac{\pi}{2} f_k Q_k W(f_k)} \quad [5-26]$$

Note that the amplification here is proportional to  $\sqrt{Q_k}$ , instead of  $Q_k$  in the sine regime.

Since most of the integral comes from the resonance, we can assume that the PSD  $W(f)$  varies only slightly and therefore use  $W(f_k)$  in [5-26]. Note also that integration using  $H_k(\omega)$  instead of  $T_k(\omega)$  gives the same result, so all FRF of Eq. [5-3] [5-4] [5-5] give formulas similar to Eq. [5-26].

Another useful property of the 1-DOF system is its rms response to an excitation defined by the response of a 1-DOF system excited by white noise. This "response to a peak" is used to deduce a

white noise  $W_0$  which is equivalent to a given acceleration PSD comprising an isolated peak similar to that of the 1-DOF system. This problem is illustrated in Figure 5-11 where the unknown factor  $\alpha$  is the ratio between the amplitude of the peak and the amplitude of the equivalent white noise.

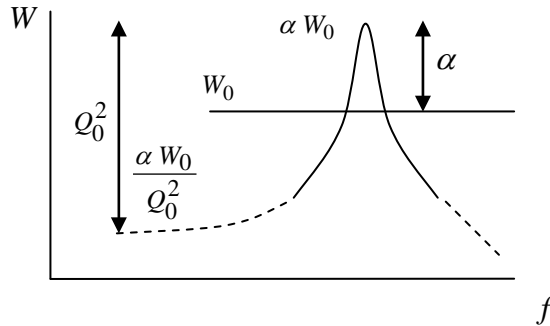


**Figure 5-11: White noise equivalent to an isolated peak**

We wish to determine  $\alpha$  such that both the peak and the equivalent white noise produce the same rms response in the 1-DOF system of frequency  $f_0 = f_k$  and damping  $Q_0 = Q_k$ . This requires integration which can be done using the following formula from Crandall [8]:

$$\pi \frac{\int_{-\infty}^{+\infty} \left| \frac{-i\omega^3 B_3 - \omega^2 B_2 + i\omega B_1 + B_0}{\omega^4 A_4 - i\omega^3 A_3 - \omega^2 A_2 + i\omega A_1 + A_0} \right|^2 d\omega}{(B_0^2 / A_0)(A_2 A_3 - A_1 A_4) + A_3 (B_1^2 - 2 B_0 B_2) + A_1 (B_2^2 - 2 B_1 B_3) + (B_3^2 / A_4)(A_1 A_2 - A_0 A_3)} = \frac{(B_0^2 / A_0)(A_2 A_3 - A_1 A_4) + A_3 (B_1^2 - 2 B_0 B_2) + A_1 (B_2^2 - 2 B_1 B_3) + (B_3^2 / A_4)(A_1 A_2 - A_0 A_3)}{A_1 (A_2 A_3 - A_1 A_4) - A_0 A_3^2} \quad [5-27]$$

Assuming weak damping, we obtain:

$$\overline{y^2} \approx \frac{\pi}{4} f_0 Q_0^3 \frac{\alpha W_0}{Q_0^2} = \frac{\pi}{4} \alpha f_0 Q_0 W_0 \quad [5-28]$$

Comparing Eq. [5-28] with Eq. [5-26] we see that  $\alpha = 2$ . This factor 2 corresponds to the "half-power" amplitude of the peak such that the energy within the half-power frequency band is equal to the energy outside of this band.

Using this equivalence criterion we can therefore "clip" any peak representing the amplification of a 1-DOF system (or mode) by a factor of 2. The levels close to the peak that are clipped are compensated by those outside of the half-power band that are amplified. This can be summarized as follows: to represent the effects of an excitation defined by a PSD with well isolated (individual) peaks associated with modes of the exciting structure, an equivalent white noise can be used locally whose amplitudes are half of those of the peaks.

This factor of 2 is an approximation based on several assumptions. If these assumptions are not satisfied (e.g. strong damping or  $Q_0 \neq Q_k$ ), a corrected value for  $\alpha$  can be obtained by going back to Eq. [5-25] and [5-27].

As for the sine regime, an SDOF identification can be performed on the response peak, either using Eq. [5-24] which provides  $|H_{yx}(f)|^2$  knowing  $W_{xx}$  and  $W_{yy}$ , or using the following expression which provides directly the FRF:

$$W_{yx}(f) = H_{yx}^* W_{xx}(f) \quad [5-29]$$

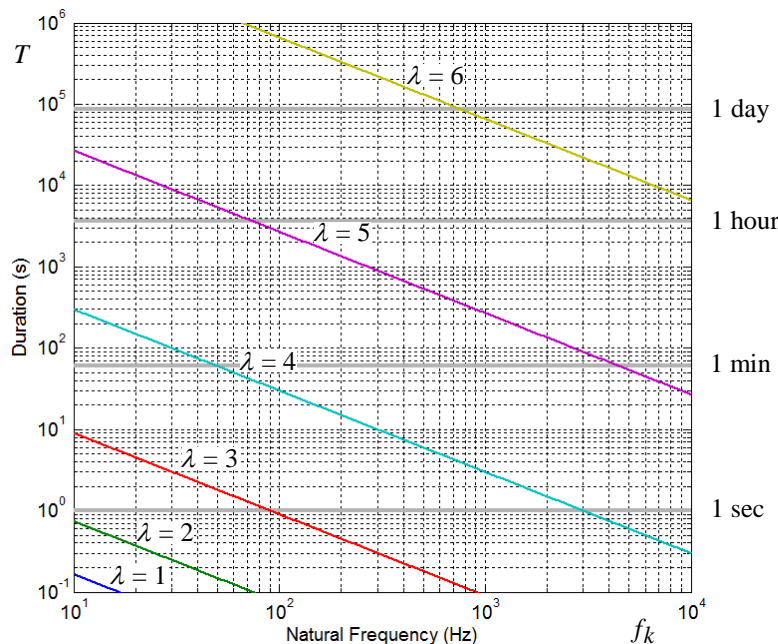
### 5.2.5.4 Shock response spectra for random environments

The notion of SRS seen in Section 5.2.4.3 can be applied to the random regime in which case we wish to estimate the average maximum response of a 1-DOF system as a function of its natural frequency for a given damping ratio. An approximate expression relating the maximum response to the rms response for a zero-mean signal is given by:

$$y_{max} \approx y_{rms} \sqrt{2 \ln(f_k T)} \quad [5-30]$$

where  $T$  is the duration of the excitation. The product represents the number of oscillations with each cycle contributing to the statistical analysis. The longer the duration, the higher the maximum response is, unless the statistical distribution is non-Gaussian – for example during testing where the peaks can be limited to a specific value for safety reasons. Details can be found in Vol.3 of [2].

This approach offers better accuracy compared to the use of a simple coefficient  $\lambda$  instead of  $\sqrt{2 \ln(f_k T)}$ , for example the often-used value of  $\lambda = 3$  (the well-known "3 $\sigma$ " approach) which corresponds to a 0.13 % probability of exceeding  $3x_{rms}$  for a Gaussian distribution. By inspection of Eq. [5-30] we see that the value of 3 can be overly optimistic. For example with  $f_k = 100$  Hz, the corresponding duration  $T$  is only 0.9 s. For a duration of 2 minutes, typical for an equipment qualification test, the corresponding value is 4.3. Values obtained from Eq. [5-30] are displayed below in Figure 5-12 for a wide range of frequencies and durations.



$f_k$	10 Hz	100 Hz	1000 Hz	10000 Hz
$T = 1$ s	2.1	3.0	3.7	4.3
$T = 1$ min	3.6	4.2	4.7	5.2
$T = 1$ hour	4.6	5.1	5.5	5.9
$T = 1$ day	5.2	5.7	6.0	6.4

Figure 5-12: Values for  $\lambda = y_{max} / y_{rms} \approx \sqrt{2 \ln(f_k T)}$

The SRS initially conceived for the transient regime can also be applied to random and sine regimes according to the following rules.

- Transient: The SRS is obtained according to its definition.
- Sine: The SRS is obtained by multiplying the amplitude by the Q factor.
- Random: The SRS is obtained by multiplying the RRS (see below) by the factor  $\lambda = y_{max} / y_{rms}$ .

The SRS is a useful criterion for comparing environments of different nature and in particular for obtaining equivalent environments in that two environments are considered equivalent if they have the same SRS. However this criterion for equivalence is to be used with precaution for the same reasons discussed in Section 5.2.4.3, and in particular the influence of the Q factor whose value is often difficult to establish. Sine amplitudes are proportional to  $Q$  whereas random amplitudes are proportional to  $\sqrt{Q}$ . As for transients, their relation to  $Q$  can vary greatly and depends on the degree of oscillation in the signal (weak for a half-sine shown in Figure 5-7).

The rms value can also be used instead of the maximum value to elaborate a response spectrum similar to the SRS. In this case the maximum response is replaced by the rms response leading to the Random Response Spectrum (RRS). The RRS is defined as the rms response of a 1-DOF system as a function of its natural frequency for a given damping ratio. Unlike the SRS, the RRS has no loss of information and can be used directly to compute structural responses assuming that the modes are sufficiently uncoupled.

As an example, consider the PSD and corresponding RRS shown in Figure 5-13 for three types of random excitation: a unit white noise, a unit resonant response with  $f_0 = 1$  and  $Q_0 = 10$ , and a general response. The RRS are plotted over the same frequency range as the PSD and for 3 values of damping. For the case of white noise excitation we see that the RRS values are consistent with Eq. [5-26] using  $W_{xx} = 1$ . For the case of resonant excitation, we can verify the RRS value at the resonant frequency ( $f_k = 1$ ) for  $Q_k = 10$  by use of an equivalent white noise equal to the peak PSD level divided by two. Using the value of  $W_{xx} = 100 / 2 = 50$  in Eq. [5-26] results in an rms value of 28 consistent with the RRS plot. For the general response, we see that the RRS provides a smoother profile compared to the PSD.

Finally, the RRS can also be used to construct spectral envelopes for specifications – similar to the approach used for SRS. Compared to PSD, the RRS provide smoother curves which are better adapted to elaborating specifications by conversion of the RRS envelope to a PSD using Eq. [5-26]. Note that the same factor of 2 mentioned above should be found in the PSD near the principal resonances. This strategy was used in the 80's and 90's to elaborate the very first equipment specifications in the random regime based on a statistical analysis of the results of the system-level acoustic test [17].

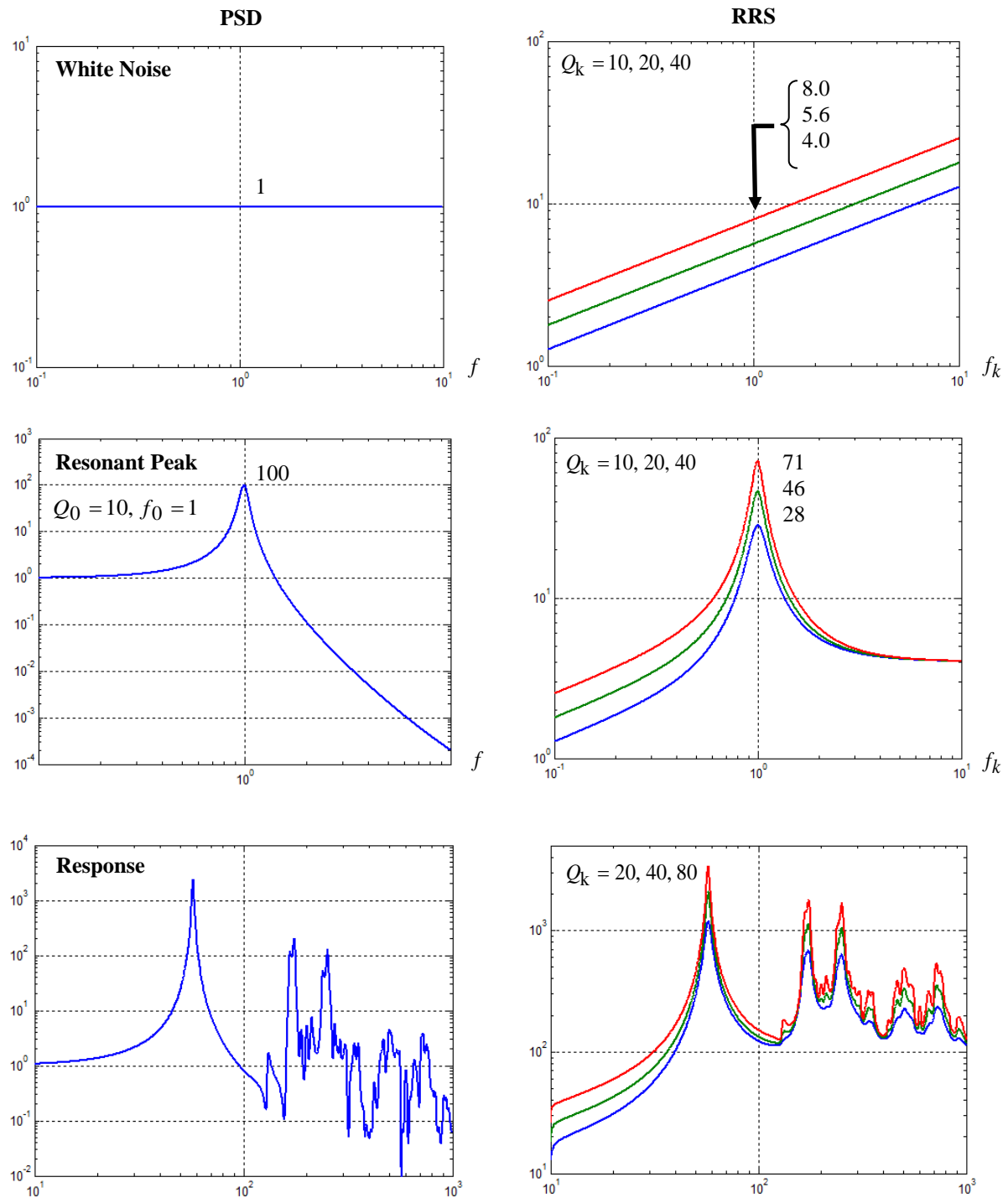


Figure 5-13: PSD and RRS for various excitation types

## 5.2.6 Sine-equivalent dynamics

### 5.2.6.1 Introduction

When addressing the equivalence of different types of vibrational loading, e.g. transient loads, sinusoidal loads, or random loads, the equivalence with respect to critical damage processes of each particular loading is usually understood. However, equivalence principles might be also used to perform tests that are intended to adequately simulate the conditions of the service (operational) vibration [38].

This section illustrates how to establish the equivalence between a low frequency transient load in the time domain and a harmonic excitation in the frequency domain, the so-called “sine-equivalent level” or “equivalent sine input”. The “equivalent sine input” circumvents the shortcomings of current vibration test facilities where the transient flight load cases cannot be easily simulated on the electro-dynamic shaker. Performing tests with an equivalent harmonic excitation is the only practical alternative.

As a result, the philosophy behind and the mathematical procedures of the equivalent sine calculation has a practical importance since decisions can be taken whether a sine test notched profile is acceptable also on the basis of the equivalent sine input (ESI) level of the acceleration predicted at the spacecraft/launcher interface. Remarks and limitations of the approach are also addressed.

### 5.2.6.2 Sine-equivalent level

Let us consider a SDOF system having a natural frequency  $f_k$  and being excited at the base with a transient acceleration  $\ddot{u}(t)$ . The equivalent sine input  $ESI(f^*)$  at a generic frequency  $f^*$ , of  $\ddot{u}(t)$ , can be defined as the amplitude of the sinusoidal acceleration at the base, with an excitation frequency equal to  $f^*$ , which makes the SDOF system with natural frequency  $f_k = f^*$  reach, at steady-state condition, the acceleration amplitude  $SRS(f^*)$  which is the shock response spectrum of  $\ddot{u}(t)$  at the frequency  $f^*$ . The value  $SRS(f^*)$  is, by its definition, equal to the maximum that would be reached by applying  $\ddot{u}(t)$  at the base of the SDOF system. In this way an equivalence can be established between the structural response due to a transient acceleration input  $\ddot{u}(t)$ , for example at the LV/SC interface, and a sinusoidal acceleration input given by  $ESI(f^*)$ . Note that this equivalence is established in terms of maximum response of a SDOF system to the transient acceleration and steady-state response of a SDOF system with enforced base motion by sine acceleration.

The ESI level is normally calculated as:

$$ESI(f) = SRS(f)/Q \quad [5-31]$$

where  $Q$  is the dynamic amplification factor which has been assumed for the generation of the SRS. The exact expression for the ESI can be obtained by imposing harmonic motion to the base of the SDOF. It can be shown that (e.g. [39]):

$$ESI(f) = SRS(f)/\sqrt{Q^2 + 1} \quad [5-32]$$

For small damping ratios Eq. [5-32] is numerically equivalent to Eq. [5-31].

From Eq. [5-31] it appears that the ESI curve has a similar shape as the SRS curve since obtained by the latter applying the scaling factor  $Q$ . From the analysis of the SDOF system mass-base relative motion and by the processing of the LV/SC CLA typical interface accelerations, the following important points can be noted.

- For very low frequencies the SRS and the ESI level are close to zero (if the quasi-static component of the acceleration is neglected or filtered out from the time signal). In fact, the inertia of the mass keeps it from moving much, so that the relative motion consists primarily of the base moving relative to the mass.
- In the “high” frequency range of the spectrum, e.g. above 80 Hz, there could be little relative motion between the mass and the base, that is, the mass moves with the base, and consequently the SRS value is close to the maximum value reached by the transient signal.
- In the middle of the frequency spectrum, the SRS and the ESI level show a number of peaks (in general not to be confused with resonances). It means that there is a significant relative motion between the mass of the SDOF system and its base, due to the significant frequency content of the transient signal.

Note: The SRS (and ESI) is conceptually and substantially different from a frequency response function as well as from a Fourier spectrum (e.g. the SRS presents non-zero values even in case there is no frequency content of the signal at that frequency [39]).

The calculation of sine-equivalent levels at the base of the spacecraft encompasses the following main steps:

1. Recovery of the LV/SC interface accelerations from the CLA transient analysis, for all load cases (e.g. “lift-off”, “engines cut-off”, “booster pressure oscillations”).
2. Calculation of the acceleration SRS from the translational interface accelerations assuming different damping levels (usually  $Q = 20$  and  $Q = 50$ , respectively), for all load cases.

Note: SRS calculation is not necessary for CLA load cases calculated in the frequency domain, e.g. the booster pressure oscillation load cases for Ariane 5 (see the example given in Figure 5-14).

3. Calculation of the ESI levels from the SRS curves, by Eq. [5-31], for all load cases.
4. Envelope of the ESI curves performed separately for each of the three coordinate axes and the assumed damping levels, respectively (considering all load cases). If applicable, the sine levels for the CLA load cases calculated in the frequency domain are directly taken into account for the enveloping.
5. Application of relevant factors to the ESI curves (e.g. qualification factor).

As the final result three ESI curves are obtained for each assumed damping. For the purpose of notching assessment, for each axis and assumed damping, the envelope of the ESI curves pertaining to all CLA load cases is normally considered.

The equivalent sine calculation procedure for Ariane 5, which considers the combination of time domain and frequency domain load cases, is reported in Figure 5-14.

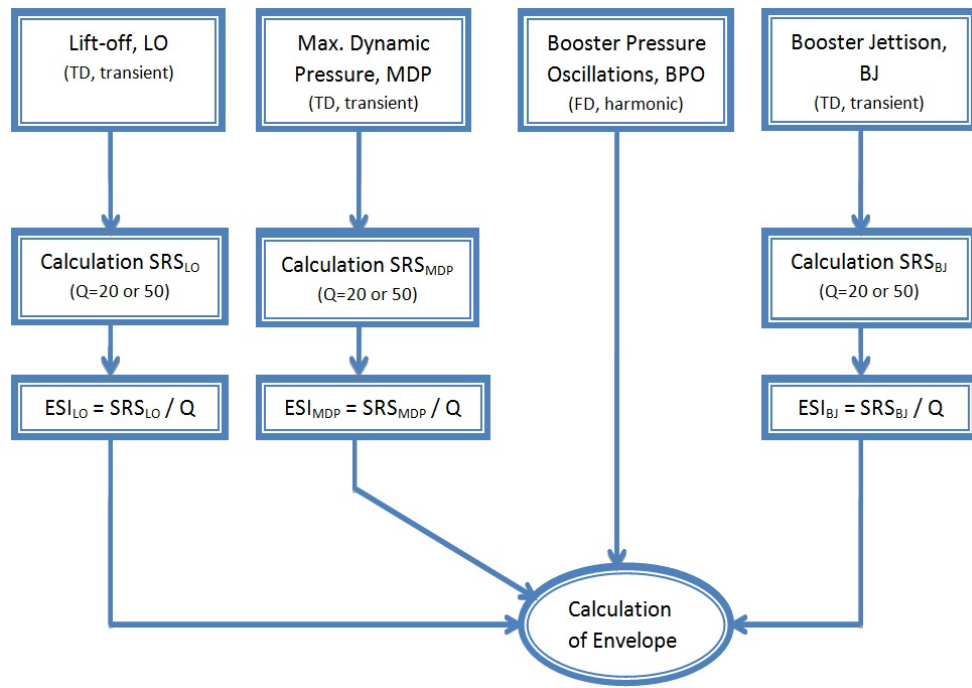


**Figure 5-14: Equivalent sine calculation procedure for Ariane 5 (combination of time domain, TD, and frequency domain, FD, load cases)**

### 5.2.6.3 Influence of damping

In accordance with the range of damping values usually found in spacecraft structures the derivation of the SRS from the CLA transient load cases is usually based on two different values of damping:  $Q = 20$  ( $\zeta = 0.025$ , fraction of critical damping) and  $Q = 50$  ( $\zeta = 0.01$ ), respectively. Contrary to the normal experience, namely that the lower the damping in a structure the larger (more conservative) the structural responses, the ESI levels from the interface transient accelerations are lower for larger assumed values for  $Q$  of the SDOF system. As a result, these ESI levels are also less conservative (i.e. lower), e.g. for the purpose of assessing the notching in the sine test. An explanation of this effect is provided hereafter.

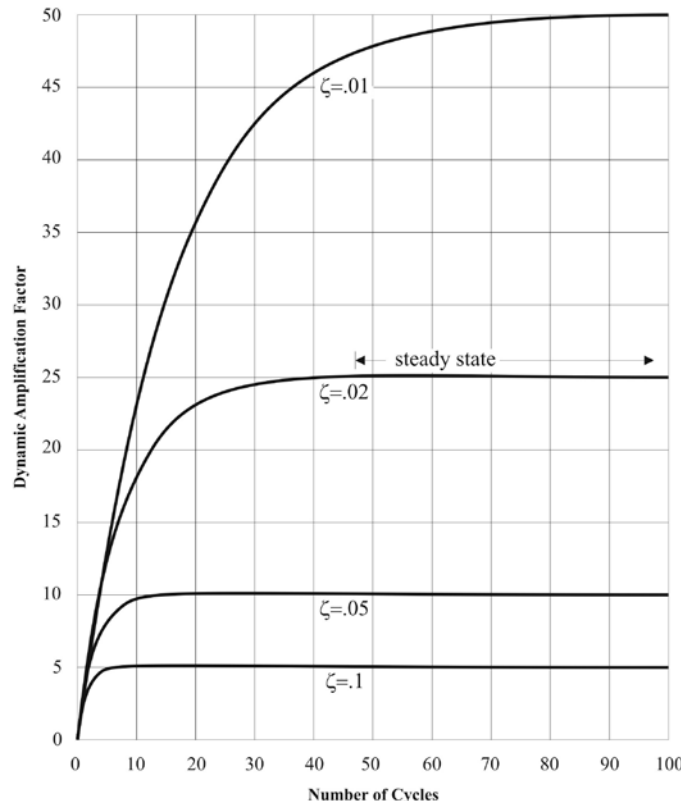


**Figure 5-15: Dynamic amplification factors vs. number of excitation cycles**

From Figure 5-15 it can be seen that a certain number of relevant excitation cycles is required to reach a steady-state condition in the SDOF response, i.e. the dynamic amplification factor does not change anymore with additional cycles. The number of cycles required to reach the steady-state condition increases with larger  $Q$  factors (or smaller percentages of critical damping, respectively). For the steady-state condition it is noted that the ratio of the dynamic amplification factors is in accordance with the ratio of the respective damping factor, e.g. the dynamic amplification for  $Q = 50$  is twice of that for  $Q = 25$ . Consequently, when considering the damping in terms of percentage of the critical damping the opposite is true: the dynamic amplification for  $\zeta = 0.02$  is half of that for  $\zeta = 0.01$ .

When the number of excitation cycles is below the one required to obtain a steady-state condition then the ratio of the “effective” dynamic amplification is no longer in line with the corresponding  $Q$  factor used. It can be also seen from Figure 5-15 that the “effective” dynamic amplification curves for different  $Q$  factors become very much the same for a very low number of excitation cycles. In typical CLA transient acceleration load cases, e.g. those for engine cut-off and stage separation, the number of significant excitation cycles is well below the minimum number of cycles needed to reach a steady-state condition in the response amplification. As a result, the ratio of the SRS values at relevant excitation frequencies is not in line with the ratio of the corresponding  $Q$  factors used for the derivation of the SRS. This can be seen in Figure 5-16 where the ratio of the SRS peaks at about 14 Hz (for  $Q = 50$  and  $Q = 20$ , respectively) is only about 1.6 (= 80/50) whereas it could be expected to be about 2.5 for a steady-state condition. Mathematically,  $SRS(f)$  is found for transient load cases to be in general less than linearly proportional to  $Q$  and consequently the derivation of the ESI levels according to Eq. [5-31] shows that the ESI for  $Q = 50$  is less than the one for  $Q = 20$ .

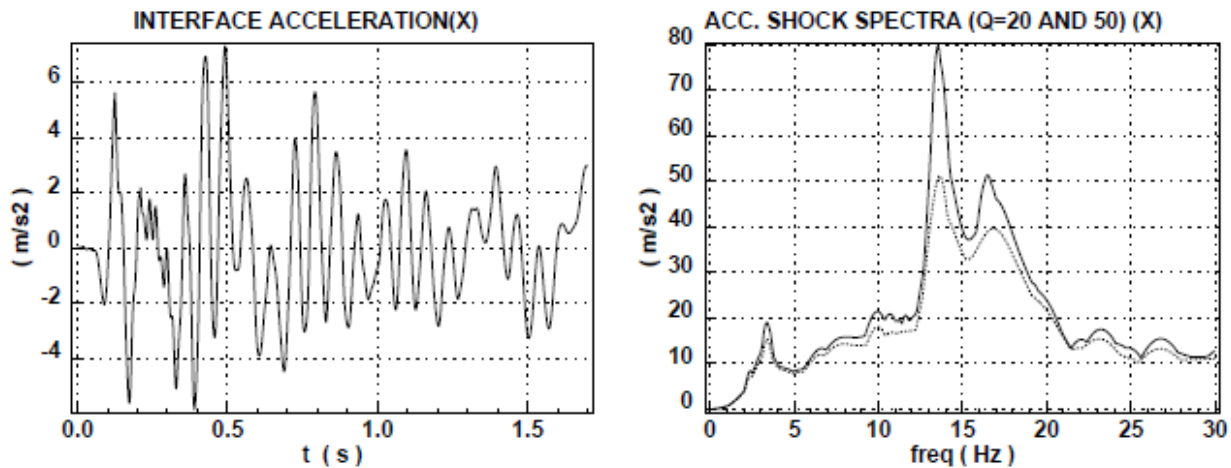


**Figure 5-16: Ariane 5 Lift-off - Booster synchronous ignition (acceleration time history and corresponding SRS for Q=20 and Q=50)**

In principle the ESI used for defining the minimum sine input required for a satellite test or for justifying notching during vibration testing, i.e. where the notched input level is still above the respective ESI level, should have been computed using a damping ratio that is very similar to the anticipated damping ratio of the "test item". However, in general this is not practical. To circumvent the problem the SRS and subsequently ESI is usually calculated from the CLA time histories with two different values of damping:  $Q = 20$  and  $Q = 50$ , respectively.

An example applicable to Ariane 5 CLA is shown in Figure 5-16. As already said above, these damping values are supposed to adequately cover the range of the applicable spacecraft damping. To define the applicable ESI level for any damping deviating from these values a linear interpolation or extrapolation might be performed in the relevant frequency range. This is considered adequate in most cases.

#### 5.2.6.4 Impact of "non-dynamic" effects on SRS calculation

##### 5.2.6.4.1 Introduction

In general the ESI levels are derived for the purpose to perform dynamic testing in the frequency domain that properly simulates the loading effects of the transient events. In this case only the dynamics of the transients should be included. However, it can be seen that the acceleration time histories of many CLA load cases also include non-dynamic effects or produce non-physical (unrealistic) effects in the SRS, and in particular:

- non-zero initial conditions; and
- quasi-static components.

These effects can be simultaneously present in the same event (e.g. "engine cut-off") and can significantly influence the shape and maximum levels of the corresponding SRS and therefore the ESI.

##### 5.2.6.4.2 Non-zero initial conditions

In some load cases (typically when the quasi-static component of the acceleration is retained) the initial condition of the acceleration time history is non-zero. In these cases specific procedures should be applied in order to overcome the issue of this "non-physical" step function at the time  $t_0 = 0$  s [5]. The application of such procedures and the resulting effects on the shock response spectrum (and therefore on the ESI level) is discussed hereafter.

In Figure 5-17 a) a typical acceleration time history (in the longitudinal thrust direction) is presented for an “engines cut-off” load case usually received from the launcher authority as part of the CLA results. The frequency content of the signal shown is practically limited to a single excitation frequency at about 22 Hz. The response of a SDOF system ( $f_0 = 22 \text{ Hz}$ ;  $\zeta = 0.025$ ), when being excited by this signal with non-zero initial conditions, i.e.  $\ddot{u}(t_0) \neq 0$ , shows in the very beginning the expected overshoot by about twice the step size of 7 g (overshoot factor applicable to very small system damping). However, the oscillations resulting from the initial step appear to be damped out relatively quickly or might be also counteracted by the opposite step occurring at about  $t = 0.1 \text{ s}$  when the excitation suddenly drops from about 7 g to 0 g due to the engine distinction. In fact the vibration pattern and in particular the response amplitudes are found to be very similar to the response of the same SDOF system when being excited by a signal with only the dynamic content as shown in Figure 5-17 c). The SRS for the signal with non-zero initial conditions is characterized by an almost constant plateau value across the complete spectrum with only the response around the single excitation frequency emerging from the cloud. It should be noted that the plateau value of about 14 g is equal to about twice the initial step size and is due to the fact that the SDOF response for all frequencies outside the range of the excitation frequency is dominated by the initial overshoot effect.

Furthermore, the maximum response amplitude seen provides a clear evidence for the validity of the estimation of the dynamic amplification factor from the number of relevant excitation cycles as shown in Figure 5-15. Investigating the excitation signal e.g. for the time window  $t = 0.1$  to  $0.5 \text{ s}$  the number of relevant excitation cycles can be estimated to be about 8 with an amplitude of roughly 1 g. From Figure 5-15 the expected dynamic amplification factor for  $Q = 20$  and 8 excitation cycles should be about 14 to 15. This is very much consistent with the maximum response amplitudes seen in particular for the excitation signal with only the dynamic content as presented in Figure 5-17 c).

A simple procedure to remove the non-zero initial conditions could be e.g. to subtract from the acceleration time history the value  $\ddot{u}(t_0)$  as shown in the left graph of Figure 5-17 b) where we have now zero initial conditions with  $\ddot{u}(t_0) = 0$ . However, the SDOF system response is now showing an overshoot in the negative direction resulting from the sharp drop of the excitation at about  $t = 0.1 \text{ s}$ . Again the overshoot is about twice the step size, i.e. we can see a response value of about -14 g immediately following the drop from 0 g to -7 g. As compared to the excitation case with non-zero initial conditions there is no possibly counteracting step in the opposite direction for this zero initial condition case. As a result, the responses in negative direction are further amplified due to being in resonance with the excitation frequency and the maximum negative response acceleration is significantly exceeding the corresponding positive counterpart for case a). Therefore the SRS, representing the maximum absolute values found in the response time history, is also showing a significantly higher peak value at the main excitation frequency.

An example for the removal of quasi-static components from the excitation signal prior to the SRS processing is shown in Figure 5-17 c). However, this subject is particularly dealt with in Section 5.2.6.4.3.

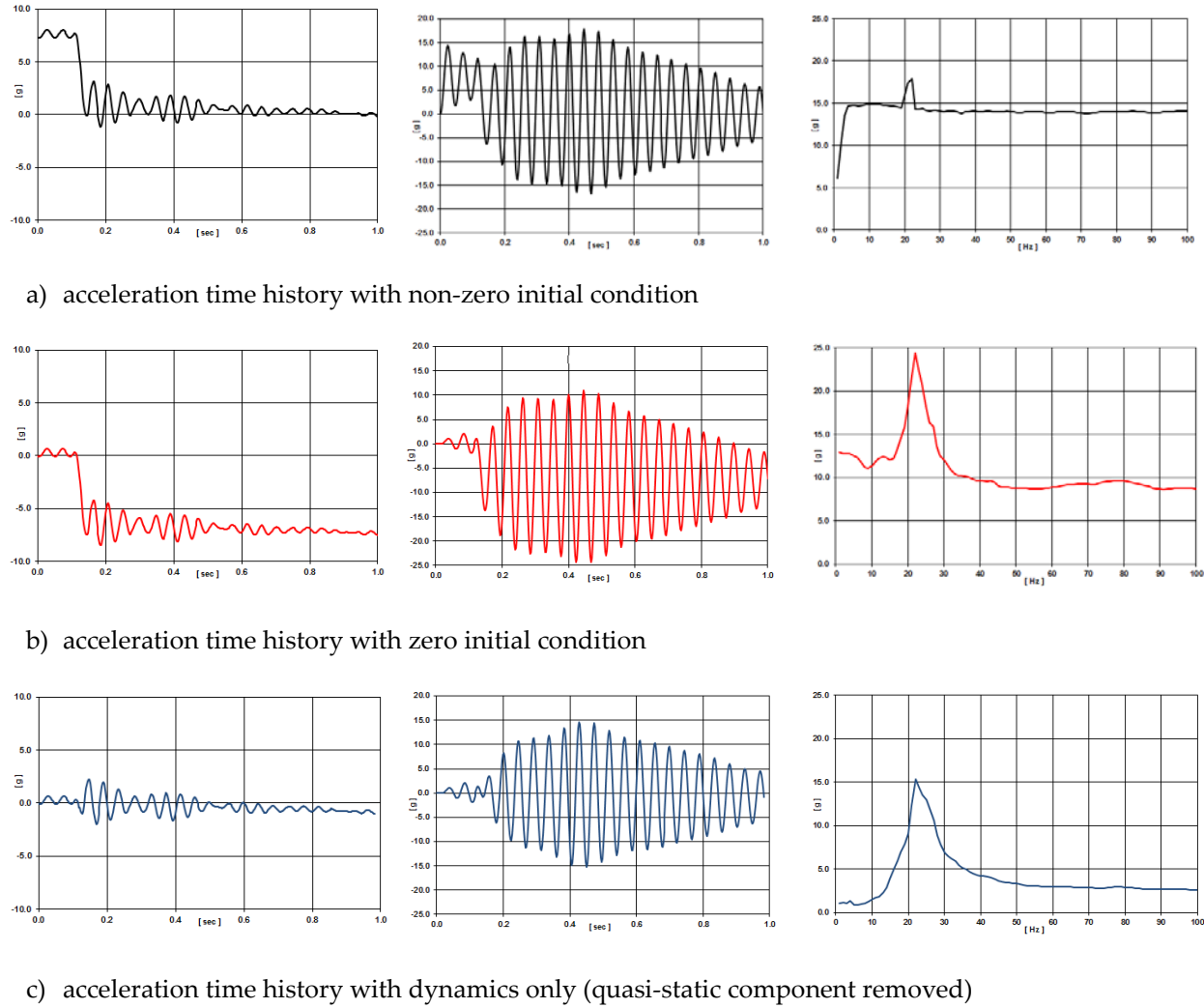


**Figure 5-17: LV/SC interface acceleration (Rockot, thrust axis, Engine Cut-off): excitation signal (left), SDOF response for  $f_0=22$  Hz and  $Q=20$  (centre), and SRS for  $Q=20$  (right)**

A slightly different and more rigorous procedure to derive the SRS and subsequently the ESI from an acceleration time history with non-zero initial conditions is reported in [5], which involves the following steps (in practice step 3 is added with respect to the previous procedure):

1. The initial acceleration  $\ddot{u}(t_0)$  is subtracted from the initial time history
2. The dynamic response (acceleration) of the SDOF system with natural frequency  $f_k = f^*$  is calculated
3. The acceleration  $\ddot{u}(t_0)$  is added to the dynamic response of the SDOF
4. The max response of the SDOF system, i.e.  $SRS(f^*)$ , is identified and  $ESI(f^*)$  is calculated
5. The calculation is repeated for all the relevant natural frequencies of the SDOF system.

Figure 5-18 shows on the left hand side an example of acceleration very similar to the one in Figure 5-17 (note that different units are used). On the right hand side the ESI curves related to the original signal, containing non-zero initial conditions (green line) and to the signal with zero initial conditions and processed as per the mentioned procedure (blue line), are reported.

The inconsistency in the response peak disappears. Moreover, it should be noted that the procedure substantially processes the full time history of the acceleration, i.e. both quasi static and dynamic components are represented in the ESI level. With reference to the example reported in Figure 5-18, it is implicitly assumed that the quasi static acceleration of the LV/SC system is equal to  $\ddot{u}(t_0)$ , that is about 7.5 g. In other words, the initial value of the acceleration is assumed as the static load associated to steady-state conditions before engines cut-off.

From a physical point of view, this procedure is equivalent to introducing a very slow rise in the acceleration from zero to  $\ddot{u}(t_0)$ , as a way of handling the non-zero initial condition.

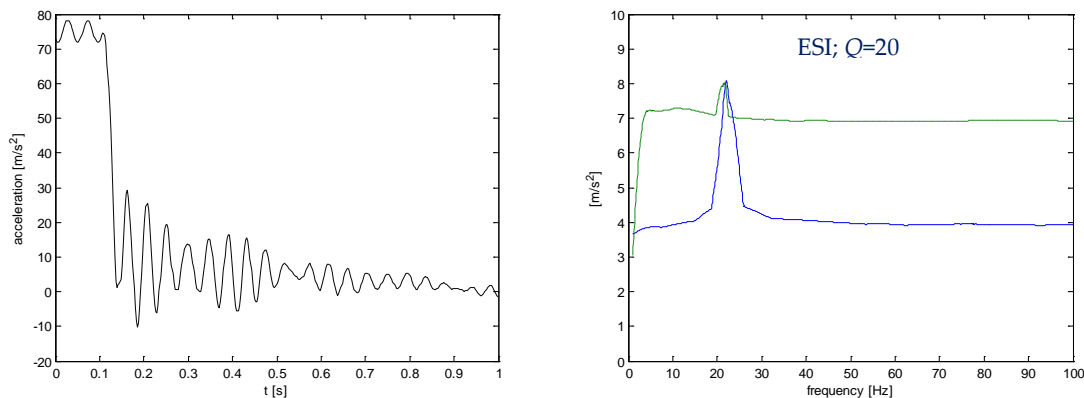


**Figure 5-18: LV/SC interface acceleration with non-zero initial condition in acceleration time history and related ESI for Q=20 (blue line) [5]**

#### 5.2.6.4.3 Quasi-static components

Quasi-static components can be identified by visual inspection of the excitation time history and their presence is seen from the fact that the mean value of the oscillations during one period is not equal to zero. Quasi-static components can be either constant values in the complete time window of the acceleration time history  $\ddot{u}(t)$  or their value might change in the excitation function either rather smoothly or in a very sharp manner e.g. by step-like acceleration increases or decreases, respectively.

Typical CLA transient load cases frequently containing a step in the excitation time history for the thrust direction are the "lift-off" and "engine cut-off" cases, see the examples shown in Figure 5-18 and Figure 5-19. These steps result from the fact that the thrust applied by the launcher significantly changes during the relevant time window. They are particularly pronounced for the "engine cut-off" load cases (due to sharp drop of thrust) but might also occur in a smoother way for the lift-off case when the launcher leaves the launch pad and the longitudinal acceleration increases from 1 g to about 1.7 g (common value found for many expendable launchers).

It should be noted that quasi-static components of the acceleration in thrust direction are not included in the CLA results provided by some launch authorities (e.g. Ariane 5) and also for the evaluation of the ESI levels. This can be considered justified on the basis of considerations given both to the timing of the loading events and to the conservativeness of the approach.

For acceleration time histories  $\ddot{u}(t)$  containing quasi-static and dynamic components it can be found that in general the maximum total acceleration is not reached by the "fictitious" SDOF system if the

quasi-static component has been removed prior to the SRS calculation. However, the effect should be small in the relevant frequency range where peak levels in the SRS occur.

In order to remove the quasi-static components from the acceleration time history  $\ddot{u}(t)$  the following methods could be used:

1. Application of a high-pass filter to the original time signal. As a rough guideline, the filter should remove the contribution from all frequencies below 2 Hz to 3 Hz.
2. Calculation of a moving average value which is then subtracted from the original time signal in order to get the “centred” time signal containing in principle only the dynamic components.

Note:

The (simple) moving average of a time series  $\ddot{u}(t_i)$  is the unweighted mean of the last  $N$  data points in  $\ddot{u}(t_i)$  and is given by the following expression:

$$\ddot{u}_{MA}(t_i) = \frac{1}{N} \sum_{k=0}^{N-1} \ddot{u}(t_{i-k})$$

Although the original acceleration time history was manually changed in this case, the Figure 5-17 c) provides in principle an example of the effects seen when applying a high-pass filter to remove the quasi-static component from the excitation signal, which in this case is the signal shown in the left graph of Figure 5-17 b). The peak SRS value is comparable to the one found for the excitation signal with non-zero initial conditions, i.e. when maintaining the quasi-static component in the signal used for the SRS processing.

Figure 5-19 provides an example where a moving average is calculated for the original acceleration time history  $\ddot{u}(t)$  and where the moving average values are subsequently subtracted from  $\ddot{u}(t)$  to constitute the signal used for the SRS processing. The particular issue with this method could be that the definition of the proper width of the sliding time window (e.g. short or long moving average, respectively) depends on the characteristics of the excitation signal as e.g. the main frequency of the oscillations to be smoothed. In general some iterations might be necessary to find the optimum width for the sliding time window.

However, for the practical case shown in Figure 5-19 the width of the sliding time window appears to be not critical for the calculation of the peak SRS values. Both the short (time window according to 1 period of the main oscillation at about 13 Hz) and the long moving average (4 periods) result to approximately the same peak SRS values although some significant differences between both averages can be noted between about 0.7 and 1.0 seconds affecting also the maximum amplitudes of the “centred” signal (the signal containing only the dynamic components).

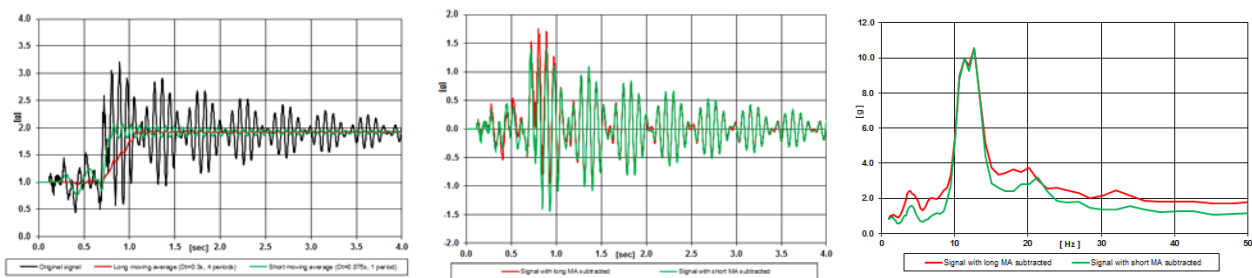


**Figure 5-19: LV/SC interface acceleration (Rockot, thrust axis, Lift-off): removal of quasi-static component by means of moving average (long and short time window, respectively) and impact on SRS calculation**

Due to possibly significantly affecting the corresponding SRS and therefore ESI level, in particular for the case of step-like changes of the excitation function value, the acceptability of removing the quasi-static components from the original time signal should be clarified with the launcher authority. This might be particularly important if such manipulations might have a significant impact on the compatibility of any notchings, applied during the satellite sine testing, with ESI levels when being considered by the launcher authority to constitute minimum input levels.

### 5.2.6.5 Remarks and limitations

The logic of swept-sine excitations to simulate transient events should be to select the magnitude and sweep rate for the resulting vibration to cause the hardware response to be similar to the response predicted for the transient. This would include, at least approximately, the same number of vibration cycles at each frequency that is anticipated due to the transient being simulated. However, this is extremely difficult if not impossible to achieve in practice.

A goal of the combined CLA-ESI approach could be to find the equivalent sinusoidal input (i.e. enforced acceleration suitable for the shaker) to make the tested satellite reach, at all locations, the maximum responses reached during the launcher-spacecraft transient analyses, plus an adequate margin. Indeed, enforcing the base of a SDOF system with the ESI level, simulating a SDOF sine test, the steady-state solution at its resonance frequency would show the same value of the SRS, calculated by processing the transient acceleration. This fact "would justify" that the ESI level is often considered as minimum threshold for the notching.

However, it can be easily understood that the combined CLA-ESI approach is rigorous (in terms of response level, not in terms of duration and vibration cycles) only in the case of sine test of SDOF systems. The extension to multiple-degree-of-freedom (MDOF) systems can be valid with a large approximation and therefore be questionable [39]. In fact, enforcing the base of a MDOF system with the ESI level, the steady-state vibration maximum accelerations reached are different from the ones reached by enforcing the base with the transient acceleration and, above all, also the internal forces are different [39]. Thus the ESI is not directly comparable with the flight load cases. With respect to the CLA events, some structural locations could be over tested and some other under tested.

Another effect that "disturbs" the equivalence between the transient time history and the ESI level is the effect of the sine sweep rate on the structural response. Even for the ideal case of the SDOF system, the sine sweep rates which are typically used for testing space hardware do not allow in general the steady-state vibration to be reached. The maximum dynamic response is function of the damping and the number of excitation cycles. For example this is illustrated in Figure 5-15 for a SDOF system.

Finally it should be noted, in theoretical terms, that comparing the ESI curve to the nominal or specified sine vibration test level is intrinsically inconsistent since the latter is substantially a Fourier spectrum, which is not the case for the ESI spectrum.

In conclusion, there is a lack of consistency between CLA results and testing at the ESI level. Consequently, the ESI does not provide an accurate minimum threshold for the notching.

### 5.2.7 Combined environments

#### 5.2.7.1 Introduction

A transient environment being of short duration can be analysed independently of other environments. This, however, is not the case for harmonic and random environments which can overlap with each other and thus require a suitable combination of the dynamic loads including possible static load contributions.

### **5.2.7.2 Combination of X, Y, Z sine loads**

Since in general the sine environments along the X, Y and Z directions occur simultaneously, the responses, which are computed separately, should be combined in order to determine the design case. This combination can be performed at different levels of accuracy and associated conservatism:

- Combining for each frequency the response amplitude and phase. There is no phase information in the X, Y, Z sine input spectrum. All phase combinations of Y-excitation and Z-excitation related to X-excitation are evaluated to find the maximum. This requires a large amount of computation but provides the lowest levels.
- Combining for each frequency the response amplitudes only. To find the maximum response for each frequency a linear combination is performed. This represents a compromise.
- Combining only the maximum amplitudes independent of frequency. This is the most simple way but also the most conservative.

If there are sufficient margins, the last approach can be applied. If not, the others should be investigated.

As the probability is quite low that all axes contribute always in the worst phase combination, the direct sum of the amplitudes, called Sinus Linear (SL) combination, can be replaced by a statistical combination, called Sinus Quadratic (SQ). The SQ combination is recommended for fatigue verification.

### **5.2.7.3 Combination of sine and random loads**

As the random loads are mainly due to acoustic sources which are often treated separately, they should be combined with the sine loads.

For the combination of random load cases between them, the  $3\sigma$  values (or  $\lambda\sigma$  values, see Section 5.2.5.4) of the different excitation axes can be naturally combined statistically.

The combination of sine and random loads can be done statistically again. Depending on the combination method for the sine, two dynamic combinations of sine and random are finally possible: Dynamic Linear (L) and Dynamic Quadratic (Q).

In Figure 5-20 the dynamic combination methods are shown for the example of the component stresses  $\sigma_x$ ,  $\sigma_y$  and  $\tau_{xy}$ .

### **5.2.7.4 Combination of static and dynamic load cases**

The dynamic load cases may be combined with static load cases, for example pressure in a propellant tank (static load case K = 1) combined with a thermal load case (K = 2) and static acceleration (K = 3) as shown in Figure 5-21.

The investigated responses can include all types of parameters, e.g. local acceleration in x, y and z or interface forces and moments or stresses. If failure modes are concerned (e.g. the equivalent stress hypothesis according von Mises for metallic material or HSB criteria for composite laminate) it is recommended to evaluate all possible combinations, as shown schematically in Figure 5-21 for a 2-dimensional stress state with  $(\sigma_x, \sigma_y, \tau_{xy})$ , 8 sign combinations and 8 static stress states from 3 load cases. Even if a load is not varying during an investigated flight event, the safety factors according to the governing rules are applied (e.g. safety factor 1.1 against yield, 1.25 against rupture), which lead to a different maximum load.

### Dynamic Loads

Random (R)  
(3- $\sigma$ -Values)

$$\tilde{\sigma}_{xR} = \sqrt{\tilde{\sigma}_{xRX}^2 + \tilde{\sigma}_{xRY}^2 + \tilde{\sigma}_{xRZ}^2}$$

$$\tilde{\sigma}_{yR} = \sqrt{\tilde{\sigma}_{yRX}^2 + \tilde{\sigma}_{yRY}^2 + \tilde{\sigma}_{yRZ}^2}$$

$$\tilde{\tau}_{xyR} = \sqrt{\tilde{\tau}_{xyRX}^2 + \tilde{\tau}_{xyRY}^2 + \tilde{\tau}_{xyRZ}^2}$$

Sinus Linear (SL)

$$\tilde{\sigma}_{xSL} = \tilde{\sigma}_{xSX} + \tilde{\sigma}_{xSY} + \tilde{\sigma}_{xSZ}$$

$$\tilde{\sigma}_{ySL} = \tilde{\sigma}_{ySX} + \tilde{\sigma}_{ySY} + \tilde{\sigma}_{ySZ}$$

$$\tilde{\tau}_{xySL} = \tilde{\tau}_{xySX} + \tilde{\tau}_{xySY} + \tilde{\tau}_{xySZ}$$

Sinus Quadratic (SQ)

$$\tilde{\sigma}_{xSQ} = \sqrt{\tilde{\sigma}_{xSX}^2 + \tilde{\sigma}_{xSY}^2 + \tilde{\sigma}_{xSZ}^2}$$

$$\tilde{\sigma}_{ySQ} = \sqrt{\tilde{\sigma}_{ySX}^2 + \tilde{\sigma}_{ySY}^2 + \tilde{\sigma}_{ySZ}^2}$$

$$\tilde{\tau}_{xySQ} = \sqrt{\tilde{\tau}_{xySX}^2 + \tilde{\tau}_{xySY}^2 + \tilde{\tau}_{xySZ}^2}$$

Dynamic Linear (L)

$$\tilde{\sigma}_{xL} = \sqrt{\tilde{\sigma}_{xR}^2 + \tilde{\sigma}_{xSL}^2}$$

$$\tilde{\sigma}_{yL} = \sqrt{\tilde{\sigma}_{yR}^2 + \tilde{\sigma}_{ySL}^2}$$

$$\tilde{\tau}_{xyL} = \sqrt{\tilde{\tau}_{xyR}^2 + \tilde{\tau}_{xySL}^2}$$

Dynamic Quadratic (Q)

$$\tilde{\sigma}_{xQ} = \sqrt{\tilde{\sigma}_{xR}^2 + \tilde{\sigma}_{xSQ}^2}$$

$$\tilde{\sigma}_{yQ} = \sqrt{\tilde{\sigma}_{yR}^2 + \tilde{\sigma}_{ySQ}^2}$$

$$\tilde{\tau}_{xyQ} = \sqrt{\tilde{\tau}_{xyR}^2 + \tilde{\tau}_{xySQ}^2}$$

**Figure 5-20: Dynamic load combinations**

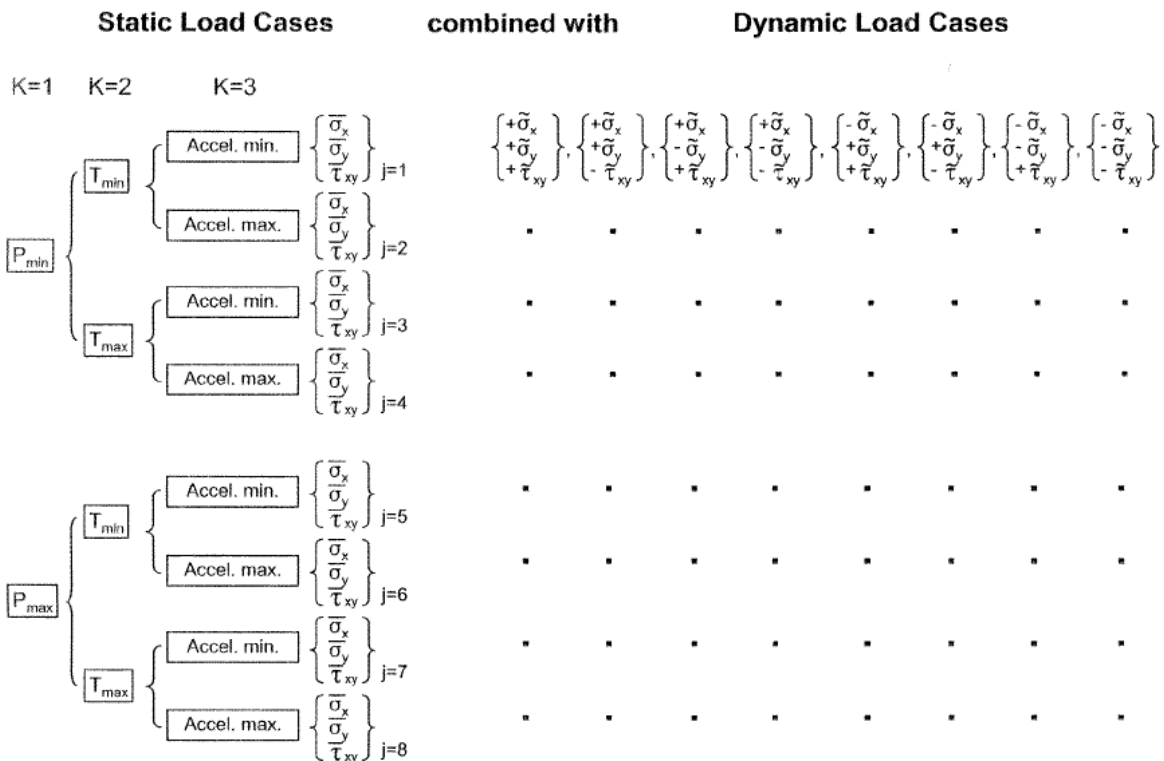


**Figure 5-21: Static and dynamic load combination**

## 5.3 Dynamic analysis

### 5.3.1 Frequency domain analysis

#### 5.3.1.1 Frequency response functions

In the frequency domain, any given function of time,  $x(t)$  can be represented by its Fourier transform  $X(\omega)$ . The relation between an excitation  $X(\omega)$  and a response  $Y(\omega)$  can be expressed by

$$Y(\omega) = H_{yx}(\omega) X(\omega) \quad [5-33]$$

where  $H_{yx}(\omega)$  is the complex-valued Frequency Response Function (FRF) between the excitation  $X(\omega)$  and the response  $Y(\omega)$ , from which the amplitude and the phase of the harmonic response can be determined at each frequency given the amplitude and phase of the harmonic excitation. Performing the analysis in the frequency domain (via the Fourier transform) has the double advantage of being better adapted to resonant behaviour and simpler to solve by the use of products instead of integration.

The derivative of the response in the time domain can be performed in the frequency domain by a simple multiplication using  $i\omega$  from which the relations between displacement, velocity and acceleration can be deduced as shown below for the sine and random regimes respectively.

$$\ddot{u}(\omega) = i\omega \dot{u}(\omega) = -\omega^2 u(\omega) \quad [5-34]$$

$$W_{\ddot{u}\ddot{u}}(\omega) = \omega^2 W_{\dot{u}\dot{u}}(\omega) = \omega^4 W_{uu}(\omega) \quad [5-35]$$

For several responses and excitations, Eq. [5-33] becomes a matrix product (see Section 5.1.4.1 for convention on matrices)

$$\mathbf{Y}_y(\omega) = \mathbf{H}_{yx}(\omega) \mathbf{X}_x(\omega) \quad [5-36]$$

where  $\mathbf{H}_{yx}(\omega)$  is a matrix of FRF with rows relative to the response DOF  $y$  and columns relative to the excitation DOF  $x$ .

#### 5.3.1.2 Responses from frequency response functions

By definition of the FRF, the responses of a structure are obtained by multiplying the FRF by the excitations. Therefore for a given excitation and response the following procedures can be used for each environment.

- Harmonic – Eq. [5-33] is used directly to obtain the amplitude and phase of the response from the amplitude and phase of the excitation and FRF.
- Transient – Eq. [5-33] can be applied with the help of the Fourier transform and then followed by an inverse Fourier transform to return to the time domain. This procedure is equivalent to computing a convolution integral directly in the time domain.
- Random – Eq. [5-33] is adapted to the PSD defined in Section 5.2.5.2 resulting in:

$$W_{yx}(\omega) = W_{xy}^*(\omega) = H_{yx}^*(\omega) W_{xx}(\omega) \quad [5-37]$$

$$W_{yy}(\omega) = |H_{yx}(\omega)|^2 W_{xx}(\omega) \quad [5-38]$$

In the case of multiple excitations and responses, Eq. [5-33] generalizes to Eq. [5-36]. For random responses, the excitations are described by the matrix of auto and cross spectral density functions,  $\mathbf{W}_{xx}(\omega)$ , and Eq. [5-37] and [5-38] become:

$$\mathbf{W}_{yx}(\omega) = [\mathbf{W}_{xy}^*(\omega)]^T = \mathbf{H}_{yx}^*(\omega) \mathbf{W}_{xx}(\omega) \quad [5-39]$$

$$\mathbf{W}_{yy}(\omega) = \mathbf{H}_{yx}^*(\omega) \mathbf{W}_{xx}(\omega) \mathbf{H}_{xy}(\omega) \quad [5-40]$$

### 5.3.1.3 Fundamental frequency response functions

All DOF of a structure can be divided into two mutually exclusive groups as described below and depicted in Figure 5-22.

- Junction DOF,  $j$ , associated with the boundary conditions or imposed motion
- Internal DOF,  $i$ , for all other DOF

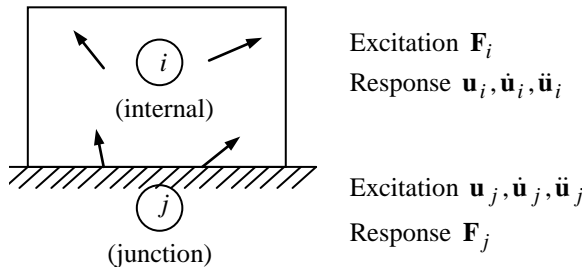


**Figure 5-22: Structural DOF**

This classification determines the nature of the excitation and response and therefore that of the FRF as described below.

- Excitation: Forces  $\mathbf{F}_i$  (possibly zero) are applied on the internal DOF  $i$ , and motion  $\mathbf{u}_j, \dot{\mathbf{u}}_j, \ddot{\mathbf{u}}_j$  (possibly zero) is imposed on the junction DOF  $j$ .
- Response: Motion  $\mathbf{u}_i, \dot{\mathbf{u}}_i, \ddot{\mathbf{u}}_i$  is obtained on the internal DOF  $i$ , and reaction forces  $\mathbf{F}_j$  on the junction DOF  $j$ .

The excitations and responses are related by the following expression

$$\begin{bmatrix} \ddot{\mathbf{u}}_i(\omega) \\ \mathbf{F}_j(\omega) \end{bmatrix} = \begin{bmatrix} -\omega^2 \mathbf{G}_{ii}(\omega) & \mathbf{T}_{ij}(\omega) \\ -\mathbf{T}_{ji}(\omega) & \mathbf{M}_{jj}(\omega) \end{bmatrix} \begin{bmatrix} \mathbf{F}_i(\omega) \\ \ddot{\mathbf{u}}_j(\omega) \end{bmatrix} \quad [5-41]$$

which is the generalization of Eq. [5-2] to an arbitrary number of DOF and comprising the following FRF:

$\mathbf{G}_{ii}(\omega)$  dynamic flexibilities (displacements/forces)

$\mathbf{T}_{ij}(\omega) = \mathbf{T}_{ji}^T(\omega)$  dynamic transmissibilities for forces or displacements

(transmissibilities in force and displacement are in general the same according to reciprocity theory)

$\mathbf{M}_{jj}(\omega)$  dynamic masses (forces/accelerations)

For the 1-DOF system the above FRF are provided in Eq. [5-3] [5-4] [5-5].

### 5.3.2 Modal approach

#### 5.3.2.1 Introduction

The modal approach uses the normal modes of a structure to solve the equations of motion. This is performed in two distinct steps:

- Resolution of the undamped equations of motion without excitation – this is the eigenvalue problem which provides the normal modes of the structure comprising for each mode an eigenvalue and associated eigenvector expressed over the internal DOF  $i$ .
- Resolution of the complete equations of motion (including damping and excitation) by summing the contribution of each mode – known as mode superposition.

From a mathematical point of view there are as many normal modes  $k$  as internal DOF  $i$ . However the modal approach is advantageous only if a small number of modes can provide the main contribution to the total response. This is the case in the "low-frequency" range where only the first few modes contribute and in particular those whose natural frequencies are located within the range of excitation frequencies. We speak of mode truncation when limiting the sum to include only these modes. However it is highly recommended to include a residual contribution representing the contribution of the neglected higher modes which can be significant.

The modal approach is equivalent to projecting the motion of the structure onto a basis of normal modes which by virtue of orthogonality uncouples the equations of motion. As a result, each normal mode behaves as a 1-DOF system whose contribution is therefore that of a 1-DOF system.

#### 5.3.2.2 Modal effective parameters

With the modal superposition approach, the FRF identified in Section 5.3.1.3 can be expressed as a sum of contributions from the  $k$  modes:

$$\mathbf{G}_{ii}(\omega) \approx \sum_{k=1}^n H_k(\omega) \tilde{\mathbf{G}}_{ii,k} + \mathbf{G}_{ii,res} \quad [5-42]$$

$$\mathbf{T}_{ij}(\omega) \approx \sum_{k=1}^n T_k(\omega) \tilde{\mathbf{T}}_{ij,k} + \mathbf{T}_{ij,res} \quad [5-43]$$

$$\mathbf{M}_{jj}(\omega) \approx \sum_{k=1}^n T_k(\omega) \tilde{\mathbf{M}}_{jj,k} + \mathbf{M}_{jj,res} + \bar{\mathbf{K}}_{jj}/(-\omega^2) \quad [5-44]$$

where the contribution of each mode is represented by the product of:

- a dimensionless dynamic amplification, function of the circular frequency  $\omega_k$  and the damping ratio  $\zeta_k$  :

$$H_k(\omega) = \frac{1}{1 - \left( \frac{\omega}{\omega_k} \right)^2 + i 2\zeta_k \frac{\omega}{\omega_k}} \quad \text{dynamic amplification} \quad [5-45]$$

$$T_k(\omega) = \frac{1 + i 2\zeta_k \frac{\omega}{\omega_k}}{1 - \left( \frac{\omega}{\omega_k} \right)^2 + i 2\zeta_k \frac{\omega}{\omega_k}} \quad \text{dynamic transmissibility} \quad [5-46]$$

- and the modal effective parameters, function of the eigenvectors  $\Phi_{ik}$  and the participation factors  $\mathbf{L}_{jk}$ , and normalized by the generalized mass  $m_k$  :

$$\tilde{\mathbf{G}}_{ii,k} = \frac{\Phi_{ik} \Phi_{ki}}{\omega_k^2 m_k} \quad \text{effective flexibilities for mode } k \quad [5-47]$$

$$\tilde{\mathbf{T}}_{ij,k} = \frac{\Phi_{ik} \mathbf{L}_{kj}}{m_k} \quad \text{effective transmissibilities for mode } k \quad [5-48]$$

$$\tilde{\mathbf{M}}_{jj,k} = \frac{\mathbf{L}_{jk} \mathbf{L}_{kj}}{m_k} \quad \text{effective masses for mode } k \quad [5-49]$$

By their presence in Eq. [5-42], [5-43] and [5-44], the modal effective parameters, physical in nature, play an important and direct role in the response analysis. Comparing Eqs. [5-42] [5-43] [5-44] with Eqs. [5-3] [5-4] [5-5] shows the equivalence between the mode and the 1-DOF system. The modal effective parameters may be interpreted as the static term associated with each mode.

Note that in the presence of modal truncation, each sum must be completed by a residual term,  $\mathbf{X}_{res}$ , in order to obtain the static properties ( $\omega = 0$ ) of flexibility, transmissibility and mass. The term  $\bar{\mathbf{K}}_{jj}$  is the stiffness matrix condensed at the junction which is null for a rigid (i.e. statically determinate) junction.

For unconstrained structures (no junction DOF  $j$ ) only dynamic flexibilities are present, and the rigid body modes ( $\omega_k = 0$ ) must be treated separately. The contribution of the rigid body modes to the dynamic flexibilities are proportional to  $1/\omega^2$  and provide the motion of the structure's centre of gravity, whereas the elastic modes provide the deformed motion relative to the centre of gravity.

If the natural frequencies are well separated, the FRF peaks can be analysed using SDOF identification (see Section 5.2.3.2) to extract the following modal terms:

- natural frequency  $f_k$  approximately equal to the frequency of the peak,
- damping ratio  $\zeta_k$  derived from the sharpness (width) of the peak,
- Effective parameter  $\tilde{X}_k$  approximately equal to the maximum of the peak divided by  $\frac{1}{2\zeta_k} = Q_k$ .

The SDOF approach neglects coupling effects between the modes which can be important and in particular for closely spaced frequencies. To account for coupling, an iterative SDOF procedure can be used or better yet by considering an MDOF identification method which can take into account several modes simultaneous by solving a coupled linear system. This is the approach behind the RTMVI method (Real Time Modal Vibration Identification) developed for performing quick identification following base excitation vibration tests [18].

Another interesting and useful property of the modal effective parameters is the relationship that exists between them. We see in Eqs. [5-47] [5-48] [5-49] that the mode shapes  $\Phi$  and participation factors  $\mathbf{L}$  are shared among the three effective parameters and common to the effective transmissibility. Following this observation, we can link the effective parameters via the effective transmissibilities, leading to the following identity. Note that certain indices are underlined indicating a fixed value (row, column or term) in order to avoid ambiguity in the expression.

$$\tilde{\mathbf{M}}_{jj,k} = \frac{\tilde{\mathbf{T}}_{ji,k} \tilde{\mathbf{T}}_{ij,k}}{\tilde{\mathbf{G}}_{ii,k} \omega_k^2} \quad [5-50]$$

Eq. [5-50] shows that the *entire* effective mass matrix  $\tilde{\mathbf{M}}_{jj,k}$  for mode  $k$  can be derived from a *single* drive-point effective flexibility  $\tilde{\mathbf{G}}_{ii,k}$  along with corresponding vector of effective transmissibilities  $\tilde{\mathbf{T}}_{ij,k}$ . From an experimental point of view, it allows obtaining the effective masses from a modal survey or phase-resonance test by the use of force measurements at each junction DOF in addition to a single acceleration measurement – without the need for base excitation.

In the particular case of phase-resonance testing, the structure is excited harmonically by a set of forces in a way to excite a single mode only. From Eq. [5-42] and [5-43] at resonance ( $\omega = \omega_k$ ), the measured accelerations  $\ddot{\mathbf{u}}_{ik}$  and reaction forces  $\mathbf{F}_{jk}$  are related to the excitation force  $\mathbf{F}_{ik}$  according to:

$$\ddot{\mathbf{u}}_{ik} = i Q_k \omega_k^2 \tilde{\mathbf{G}}_{ii,k} \mathbf{F}_{ik} \quad [5-51]$$

$$\mathbf{F}_{jk} = \tilde{\mathbf{T}}_{ji,k} (1 - i Q_k) \mathbf{F}_{ik} \quad [5-52]$$

Note that the accelerations are out of phase (purely imaginary) with respect to the excitation whereas the reaction forces have both out-of-phase and in-phase components. If we consider the out-of-phase (imaginary) components only, along with a given reference point  $i$ , the above equations can be combined to remove  $\mathbf{F}_{ik}$  leading to:

$$\mathbf{F}_{jk} = \frac{\tilde{\mathbf{T}}_{ji,k} \ddot{\mathbf{u}}_{ik}}{\omega_k^2 \tilde{\mathbf{G}}_{ii,k}} \quad [5-53]$$

Finally, introducing Eq. [5-53] into Eq. [5-50] to remove  $\tilde{\mathbf{T}}_{ji,k}$  and using Eq. [5-47], we obtain the following expression for the effective mass expressed in terms of the reaction forces  $\mathbf{F}_{jk}$  and acceleration  $\ddot{\mathbf{u}}_{ik}$ :

$$\tilde{\mathbf{M}}_{jj,k} = \frac{\mathbf{F}_{jk} \mathbf{F}_{kj}}{\ddot{\mathbf{u}}_{ik}^2} \frac{\Phi_{ik}^2}{m_k} \quad [5-54]$$

Eq. [5-54] is simply a reformulation of Eq. [5-50] but which can be used during phase-resonance testing to directly obtain the effective masses. See [19] [20] [21] for additional information.

A second identity analogous to Eq. [5-50] can be derived for the effective flexibility as shown below.

$$\tilde{\mathbf{G}}_{ii,k} = \frac{\tilde{\mathbf{T}}_{ij,k} \tilde{\mathbf{T}}_{ji,k}}{\tilde{\mathbf{M}}_{jj,k} \omega_k^2} \quad [5-55]$$

Eq. [5-55] shows that the *entire* effective flexibility matrix  $\tilde{\mathbf{G}}_{ii,k}$  for mode  $k$  can be derived from a *single* effective mass  $\tilde{\mathbf{M}}_{jj,k}$  along with corresponding vector of effective transmissibilities  $\tilde{\mathbf{T}}_{ij,k}$ . From an experimental point of view, it allows identifying the entire effective flexibility matrix from a base excitation test by the use of a *single* force measurement at the selected junction DOF in addition to the standard acceleration (transmissibility) measurements. This is case for example when using the FMD as described in Section 8.4.

### 5.3.2.3 Mode superposition

Eq. [5-42], [5-43] and [5-44] show that all FRF  $X(\omega)$  whether of type  $\mathbf{G}_{ii}(\omega)$ ,  $\mathbf{T}_{ij}(\omega)$  or  $\mathbf{M}_{jj}(\omega)$ , may be expressed using the same general form:

$$X(\omega) = \sum_k A_k(\omega) \tilde{X}_k + X_{res} \quad [5-56]$$

where  $A_k(\omega)$  is the dynamic amplification  $H_k(\omega)$  or  $T_k(\omega)$ . The other derived FRF are obtained by multiplying or dividing by  $i\omega$ .

The general form of  $X(\omega)$  (amplitude only) is plotted in Figure 5-23 using logarithmic scales. At very low frequencies the response is asymptotic to the static value equal to the sum of the modal effective parameters plus the residual term. Between two peaks there appears either an antiresonance if the modal effective parameters of the surrounding modes have the same sign, or a trough in the case of opposing signs. A driving point FRF (same excitation and response DOF) has only positive modal effective parameters and therefore contains only antiresonances.

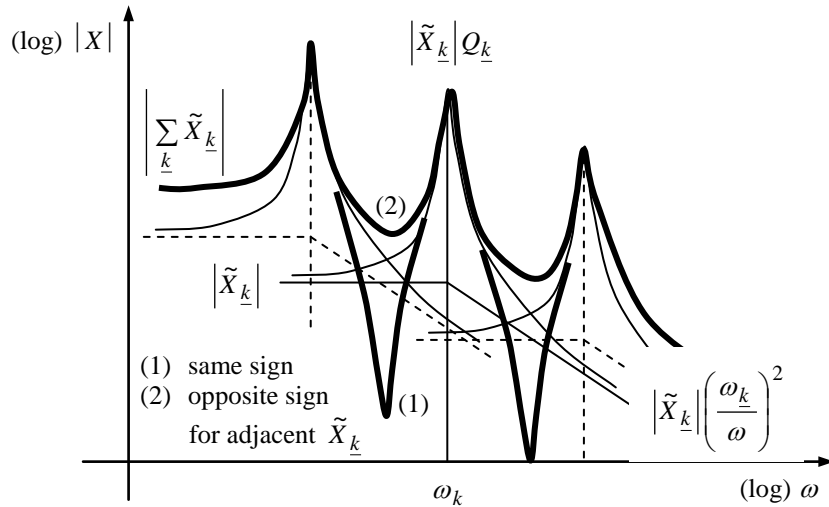


**Figure 5-23: FRF amplitude for G, T or M**

For transient responses, Eq. [5-56] can be converted to the time domain using the Fourier transform leading to the following expression for the response  $y(t)$  to the excitation  $x(t)$ :

$$y(t) = \sum_k x_k(t) \tilde{X}_{yx,k} + y_{res}(t) \quad [5-57]$$

where  $x_k(t)$  is the convolution of the excitation  $x(t)$  with the impulse response function  $h_k(t)$  or  $t_k(t)$ . Here again we see the direct role of the modal effective parameters  $\tilde{X}_{yx,k}$ .

For random responses, Eq. [5-56] is combined with Eq. [5-38] to obtain the response  $W_{yy}(\omega)$  from the excitation  $W_{xx}(\omega)$ .

Concerning the rms value, if the excitation  $W_{xx}(\omega)$  varies slowly in the vicinity of the natural frequencies, the value of  $W_{xx}(f_k)$  can be used for the contribution of each mode  $k$ . Moreover if the natural frequencies  $f_k$  are well spaced, the integral of the sum may be replaced by a sum of integrals. Combining these two assumptions leads to the following approximation for the rms value using a

quadratic sum of the modal responses – analogous to Mile's Equation [5-26] - in which we see the direct role of the modal effective parameters.

$$\overline{y^2} \approx \sum_k \left( \frac{\pi}{2} f_k Q_k \right) \tilde{X}_{yx,k}^2 W_x(f_k) + X_{yx,res}^2 \overline{x^2} \quad [5-58]$$

### 5.3.3 Effective mass models

#### 5.3.3.1 Elaboration of effective mass models

In the case of a rigid junction,  $j = r$ , the effective masses  $\tilde{M}_{rr,k}$  can be used to elaborate an equivalent model with respect to the junction. This effective mass model is illustrated in Figure 5-24 for the simple case of an axial model where each mode is represented by a 1-DOF system comprising a mass equal to the effective mass in the axial direction, a stiffness providing the natural frequency and a dashpot corresponding to the damping ratio.

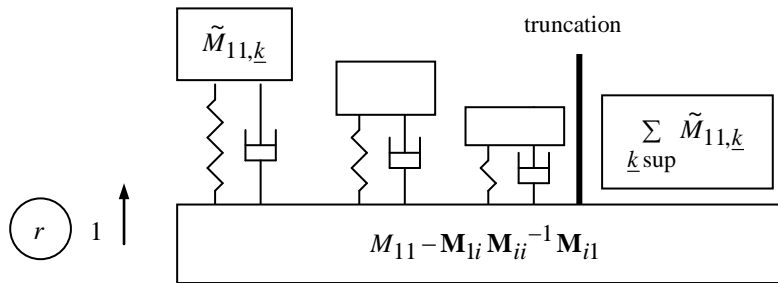


**Figure 5-24: Axial effective mass model**

In the general case of a 6 DOF junction, the 1-DOF system representing a mode is located at a specific point which is the centre of gravity of the mode, and acts along a specific direction in a combined translational and rotational motion. Unlike the arbitrary generalized mass of a mode related to its normalization, the effective mass is a physical mass (expressed in kg for translational directions) although directional (scalar mass).

The effective mass model conserves the rigid body mass properties (mass, centre of gravity and inertia) of the structure.

#### 5.3.3.2 Use of effective mass models

Effective mass models are equivalent models with respect to the junction, and therefore can be connected to adjacent structures in order to perform coupled analysis. It can be shown that the effective mass model is mathematically equivalent to the Craig-Bampton model (see Section 5.3.4).

Moreover, in transient analysis, the effective mass model can also be used to determine the maximum response of a structure via the SRS introduced in Section 5.2.4.3 for the 1-DOF system. For example, the absolute acceleration spectrum  $S_{\ddot{u}}(f)$  of a transient imposed at the base of a structure in the direction  $r$ , directly provides the maximum acceleration of each effective mass in the direction  $r$  ( $\tilde{\ddot{u}}_{r,k}$ )<sub>max</sub> =  $S_{\ddot{u}}(f_k)$  from which the following maximum responses can be deduced:

- The maximum reaction force at the junction due to each mode is obtained by multiplying  $(\tilde{\ddot{u}}_{r,k})_{max}$  by the effective mass:

$$(F_{r,k})_{max} = \tilde{M}_{rr,k} (\tilde{\ddot{u}}_{r,k})_{max} \quad [5-59]$$

- The maximum acceleration at the internal DOF  $i$  due to each mode is obtained by multiplying  $(\ddot{u}_{r,k})_{\max}$  by the effective transmissibility between the junction and the internal DOF:

$$(\ddot{u}_{i,k})_{\max} = \tilde{T}_{ir,k} (\ddot{u}_{r,k})_{\max} \quad [5-60]$$

From Eq. [5-59] and [5-60] we obtain the maximum contribution of each mode. However, as discussed in Section 5.2.4.3, the exact recombination of these maxima is impossible to perform since we do not know at which instant in time the maxima occurred. This is a direct consequence of information lost by using only the amplitudes to construct SRS. However, the modal contributions can be recombined using one of several approximate techniques by default such as:

- Direct Sum – Always conservative but can be overly pessimistic.
- Quadratic Sum – Probably more realistic but can underestimate the true levels
- Mixed Sum – Involving both direct and quadratic sums. For example the highest single contribution added directly to the quadratic sum of all other contributions. The accuracy of the results is case dependent.

## 5.3.4 Craig-Bampton models

### 5.3.4.1 Modal synthesis

The analysis of the coupled LV/SC system involves sub-structuring techniques which can be performed at different levels [1]:

- Matrix level, by direct assembly of mass, stiffness and damping matrices. Without condensation, the main disadvantage of this approach is the computation time, which can be prohibitive because of the model size.
- Modal level, by modal synthesis. Each component is represented by a basis of modes including normal modes as well as static modes. The gain in computation time is dependent on the number of retained modes and the accuracy is dependent on their representativity. This approach is particularly well adapted for linear analysis at low frequencies where the mode superposition approach is highly efficient.
- FRF level, by appropriate manipulation of the frequency response functions. It offers interesting alternatives to modal synthesis, but can be computationally intensive, especially in situations where modal synthesis applies well.

The first modal synthesis method was proposed by Hurty in 1965 [22], based on normal modes with fixed interfaces. In 1968, Craig and Bampton published a similar and numerically equivalent method that remains today one of the most popular and accurate methods used [23]. In the following decade, other approaches have been proposed using free interface normal modes (MacNeal, Rubin, Craig and Chang), loaded interface modes (Benfield and Hruda) or hybrid modes (Herting). The method proposed by Craig and Bampton combining simplicity, robustness and accuracy, is considered in the present context.

### 5.3.4.2 Craig-Bampton reduction

For each substructure with internal DOF  $i$  and connection DOF  $c = j$ , the complete equations of motion are written:

$$\begin{bmatrix} \mathbf{M}_{ii} & \mathbf{M}_{ij} \\ \mathbf{M}_{ji} & \mathbf{M}_{jj} \end{bmatrix} \begin{bmatrix} \ddot{\mathbf{u}}_i \\ \ddot{\mathbf{u}}_j \end{bmatrix} + \begin{bmatrix} \mathbf{C}_{ii} & \mathbf{C}_{ij} \\ \mathbf{C}_{ji} & \mathbf{C}_{jj} \end{bmatrix} \begin{bmatrix} \dot{\mathbf{u}}_i \\ \dot{\mathbf{u}}_j \end{bmatrix} + \begin{bmatrix} \mathbf{K}_{ii} & \mathbf{K}_{ij} \\ \mathbf{K}_{ji} & \mathbf{K}_{jj} \end{bmatrix} \begin{bmatrix} \mathbf{u}_i \\ \mathbf{u}_j \end{bmatrix} = \begin{bmatrix} \mathbf{F}_i \\ \mathbf{F}_j + \mathbf{R}_j \end{bmatrix} \quad [5-61]$$

where  $\mathbf{M}$ ,  $\mathbf{C}$  and  $\mathbf{K}$  are the physical mass, viscous damping and stiffness matrices,  $\mathbf{F}_j$  the possible external forces on junction DOF, and  $\mathbf{R}_j$  the connecting forces, cancelled after assembly.

The Craig-Bampton method assumes fixed connection DOF for each substructure. This leads to the use of a truncated set of fixed junction normal modes completed by static junction (constraint) modes, leading to the following transformation:

$$\begin{bmatrix} \mathbf{u}_i \\ \mathbf{u}_j \end{bmatrix} = \begin{bmatrix} \Phi_{ik} & \Psi_{ij} \\ \mathbf{0}_{jk} & \mathbf{I}_{jj} \end{bmatrix} \begin{bmatrix} \mathbf{q}_k \\ \mathbf{u}_j \end{bmatrix} \quad [5-62]$$

where:

- $\Phi_{ik}$  matrix of fixed junction eigenvectors  $k$ , solutions of the eigenvalue problem  $(-\omega^2 \mathbf{M}_{ii} + \mathbf{K}_{ii}) \mathbf{U}_i = \mathbf{0}_i$ ,
- $\Psi_{ij}$  matrix of static junction modes obtained by successively imposing a unit displacement at each junction DOF while blocking all the others, and defined from  $\mathbf{K}_{ii} \Psi_{ij} + \mathbf{K}_{ij} = \mathbf{0}_{ij}$  or  $\Psi_{ij} = -\mathbf{K}_{ii}^{-1} \mathbf{K}_{ij}$ .

The transformation Eq. [5-62] applied to Eq. [5-61] for each substructure provides the following mass and stiffness matrices (the damping matrix is discussed in Section 5.3.4.7):

$$\begin{bmatrix} \mathbf{m}_{kk} & \mathbf{L}_{kj} \\ \mathbf{L}_{jk} & \overline{\mathbf{M}}_{jj} \end{bmatrix} \quad \begin{bmatrix} \mathbf{k}_{kk} & \mathbf{0}_{kj} \\ \mathbf{0}_{jk} & \overline{\mathbf{K}}_{jj} \end{bmatrix} \quad [5-63]$$

where:

- $\mathbf{m}_{kk}$  and  $\mathbf{k}_{kk}$  diagonal matrices of generalized mass and stiffness
- $\mathbf{L}_{kj}$  matrix of participation factors, already seen in Eq. [5-48] and [5-49] for the modal effective parameters
- $\overline{\mathbf{M}}_{jj}$  and  $\overline{\mathbf{K}}_{jj}$  mass and stiffness matrices condensed at the junction DOF. For a statically determinate junction,  $\overline{\mathbf{M}}_{jj}$  is the rigid body mass matrix and  $\overline{\mathbf{K}}_{jj}$  is null.

These matrices can be assembled to obtain the matrices of the coupled system by imposing displacement compatibility at the junction DOF  $j$  for the two substructures. This leads to a set of equations comprising the modal (generalized) displacements  $\mathbf{q}_k$  of the two substructures and the displacements at the junction DOF  $\mathbf{u}_j$ . After solving for these displacements, it is then possible to determine the reaction forces  $\mathbf{R}_j$ .

With mode truncation, only the first  $n$  modes are retained in the transformation, which reduces drastically the size of the system to solve but also introduces errors due to neglecting the dynamic contribution of the lost higher-frequency modes, whereas the static contribution, unaffected by truncation, is provided by the junction modes  $\Psi_{ij}$ .

### 5.3.4.3 Mode displacement method

In the Mode Displacement method (MD), the physical responses  $\mathbf{u}_i$  of each substructure are simply recovered by Eq. [5-62] using displacement and acceleration OTM as follows:

$$\begin{bmatrix} \mathbf{u}_i \\ \mathbf{u}_j \end{bmatrix} = \mathbf{DTM} \begin{bmatrix} \mathbf{q}_k \\ \mathbf{u}_j \end{bmatrix} \quad \begin{bmatrix} \ddot{\mathbf{u}}_i \\ \ddot{\mathbf{u}}_j \end{bmatrix} = \mathbf{ATM} \begin{bmatrix} \ddot{\mathbf{q}}_k \\ \ddot{\mathbf{u}}_j \end{bmatrix} \quad [5-64]$$

where:

$$\mathbf{DTM} = \mathbf{ATM} = \begin{bmatrix} \Phi_{ik} & \Psi_{ij} \\ \mathbf{0}_{jk} & \mathbf{I}_{jj} \end{bmatrix} \quad [5-65]$$

In addition, displacement related data such as element stresses  $\sigma_e$  can be recovered from  $\mathbf{u}_i$  and  $\mathbf{u}_j$  using the relation:

$$\sigma_e = \mathbf{STM} \begin{bmatrix} \mathbf{q}_k \\ \mathbf{u}_j \end{bmatrix} \quad [5-66]$$

where:

$$\mathbf{STM} = [\mathbf{D}_{ei} \quad \mathbf{D}_{ej}] \begin{bmatrix} \Phi_{ik} & \Psi_{ij} \\ \mathbf{0}_{jk} & \mathbf{I}_{jj} \end{bmatrix} \quad [5-67]$$

The matrix  $\mathbf{D}$  is a differential operator resulting from the differential relations between strains and displacements and the generalized Hooke's law between stresses and strains. A similar relation exists for element forces.

### 5.3.4.4 Mode acceleration method

The Mode Acceleration method (MA) provides a second order correction to the mode displacement method by adding, during the recovery process, a static (inertia) term due to the truncated higher modes [24] [25] [26] [27].

Equation [5-61], without the damping terms for simplicity, yields:

$$\begin{bmatrix} \mathbf{u}_i \\ \mathbf{u}_j \end{bmatrix} = \begin{bmatrix} -\mathbf{K}_{ii}^{-1} \mathbf{M}_{ii} & -\mathbf{K}_{ii}^{-1} \mathbf{M}_{ij} \\ \mathbf{0}_{jk} & \mathbf{0}_{jj} \end{bmatrix} \begin{bmatrix} \ddot{\mathbf{u}}_i \\ \ddot{\mathbf{u}}_j \end{bmatrix} + \begin{bmatrix} -\mathbf{K}_{ii}^{-1} \mathbf{K}_{ij} \\ \mathbf{I}_{jj} \end{bmatrix} \mathbf{u}_j + \begin{bmatrix} \mathbf{K}_{ii}^{-1} \\ \mathbf{0}_{ji} \end{bmatrix} \mathbf{F}_i \quad [5-68]$$

Eq. [5-68] expresses the physical displacements as a function of the physical accelerations, interface displacements and internal forces, providing a static displacement correction with respect to the Mode Displacement method, associated with the truncated modes.

$$\mathbf{u}_i(MA) = \mathbf{u}_i(MD) + \Delta\mathbf{u}_i \quad [5-69]$$

where:

$$\Delta\mathbf{u}_i = \Delta\mathbf{G}_{ii} \left[ \mathbf{F}_i - (\mathbf{M}_{ij} - \mathbf{M}_{ii} \mathbf{K}_{ii}^{-1} \mathbf{K}_{ij}) \ddot{\mathbf{u}}_j \right] \quad [5-70]$$

$$\Delta\mathbf{G}_{ii} = \mathbf{K}_{ii}^{-1} - \Phi_{ik} \mathbf{k}_{kk}^{-1} \Phi_{ki} \quad [5-71]$$

The correction  $\Delta\mathbf{u}_i$  is the product of the residual flexibility matrix of the truncated modes  $\Delta\mathbf{G}_{ii}$  with the sum of the internal forces  $\mathbf{F}_i$  and the inertia forces due to  $\ddot{\mathbf{u}}_j$ .

Combining Eq. [5-62] and [5-68] leads to the following expression for the displacements:

$$\begin{bmatrix} \mathbf{u}_i \\ \mathbf{u}_j \end{bmatrix} = \mathbf{DTM}_1 \begin{bmatrix} \ddot{\mathbf{q}}_k \\ \ddot{\mathbf{u}}_j \end{bmatrix} + \mathbf{DTM}_2 \mathbf{u}_j + \mathbf{DTM}_3 \mathbf{F}_i \quad [5-72]$$

where:

$$\mathbf{DTM}_1 = \begin{bmatrix} -\mathbf{K}_{ii}^{-1} \mathbf{M}_{ii} \Phi_{ik} & -\mathbf{K}_{ii}^{-1} \mathbf{M}_{ii} \Psi_{ij} \\ \mathbf{0}_{jk} & \mathbf{0}_{jj} \end{bmatrix} \quad \mathbf{DTM}_2 = \begin{bmatrix} \Psi_{ij} \\ \mathbf{I}_{jj} \end{bmatrix} \quad \mathbf{DTM}_3 = \begin{bmatrix} \mathbf{K}_{ii}^{-1} \\ \mathbf{0}_{ji} \end{bmatrix} \quad [5-73]$$

To avoid the expensive computation of  $\mathbf{K}_{ii}^{-1}$  in  $\mathbf{DTM}_3$  we note that the applied loads  $\mathbf{F}_i$  can be written as the sum of a set of  $l$  spatial load distribution vectors ( $l \ll i$ ) times their corresponding time functions:

$$\mathbf{F}_i = \sum_l \tilde{F}_{il} \alpha_l(t) = \tilde{\mathbf{F}}_{il} \mathbf{a}_l \quad [5-74]$$

Each spatial load distribution vector  $\tilde{F}_{il}$  in Eq. [5-74] represents a set of correlated loads applied to the internal DOF. Such load vectors could be any type of forces such as lumped forces, gravity forces or pressure forces. Now Eq. [5-72] can be written as follows:

$$\begin{bmatrix} \mathbf{u}_i \\ \mathbf{u}_j \end{bmatrix} = \mathbf{DTM}_1 \begin{bmatrix} \ddot{\mathbf{q}}_k \\ \ddot{\mathbf{u}}_j \end{bmatrix} + \mathbf{DTM}_2 \mathbf{u}_j + \mathbf{DTM}_3^* \mathbf{a}_l \quad \text{with} \quad \mathbf{DTM}_3^* = \begin{bmatrix} \mathbf{0}_{jl} \\ \mathbf{K}_{ii}^{-1} \tilde{\mathbf{F}}_{il} \end{bmatrix} \quad [5-75]$$

For any displacement-related data such as element stresses or forces, the corresponding recovery equations are similar to those of Eq. [5-66]. This method is more accurate than the previous one but is also less user friendly due to more complex formulas.

### 5.3.4.5 Modal truncation augmentation method

A better recovery procedure, more accurate than the Mode Acceleration method and with the simplicity of the Mode Displacement method, is the Mode Truncation Augmentation method (MTA) [25] [26] [27] [28] [29].

Contrary to the Mode Acceleration method which corrects for the effects of mode truncation only during the data recovery process, the Modal Truncation Augmentation method corrects during the coupled analysis process by extending the modal basis with an additional set of pseudo, or residual, eigenvectors  $\Phi_{ip}$ :

$$\begin{bmatrix} \mathbf{u}_i \\ \mathbf{u}_j \end{bmatrix} = \begin{bmatrix} \Phi_{ik} & \Psi_{ij} & \Phi_{ip} \\ \mathbf{0}_{jk} & \mathbf{I}_{jj} & \mathbf{0}_{jp} \end{bmatrix} \begin{bmatrix} \mathbf{q}_k \\ \mathbf{u}_j \\ \mathbf{q}_p \end{bmatrix} \quad [5-76]$$

These residual eigenvectors are based on the correction  $\Delta \mathbf{u}_i$  given by Eq. [5-69], providing mode shapes which are transformed to satisfy the orthogonality properties with respect to  $\mathbf{M}_{ii}$  and  $\mathbf{K}_{ii}$ . Thus,  $\Phi_{ip}$  can be considered as an expansion of  $\Phi_{ik}$  and providing a correction for the dynamic contribution of the truncated modes. They can be directly used with the Mode Displacement method, and the amount of work is globally reduced compared to the Mode Acceleration method.

In Figure 5-25 a space frame FE-model is depicted. This model was subdivided into 5 substructures which were all condensed. For the outer substructures the total amount of retained modes (junction modes, normal modes and residual modes if applicable) was set to 24 for all methods (MD, MA and MTA). It is clear that the MD method does not provide a static correction whereas the two other methods do. Furthermore we can see that the MTA method outperforms the MA method at most resonance frequencies even though the number of retained normal modes is substantially less.

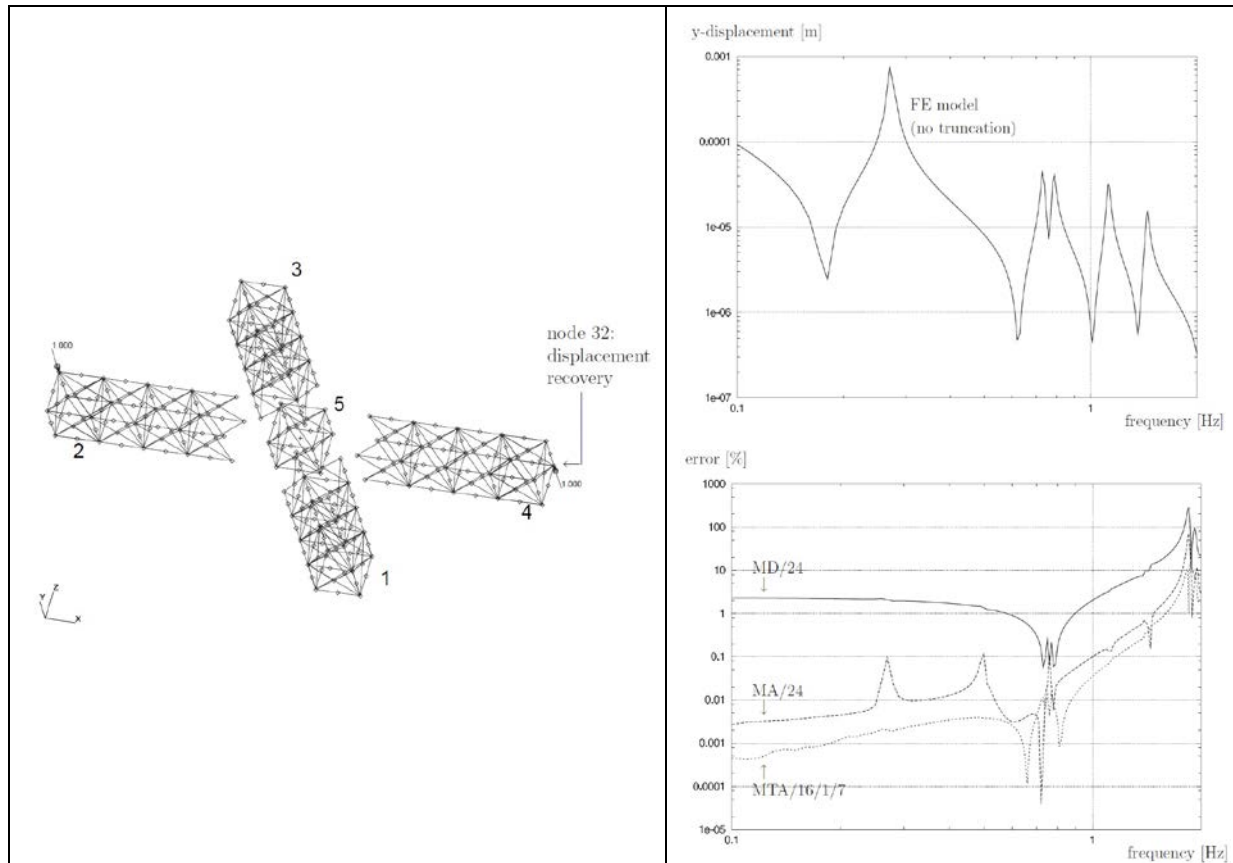


Figure 5-25: Example problem of space frame structure

#### 5.3.4.6 Interface loads and CoG accelerations

As discussed in Section 5.3.4.2, the reaction forces or interface loads  $\mathbf{R}_j$  of a substructure are recovered using Eq. [5-61] after having solved  $\mathbf{q}_k$  and  $\mathbf{u}_j$ , leading to the following Load Transformation Matrices:

$$\mathbf{R}_j = \mathbf{LTM}_1 \begin{bmatrix} \ddot{\mathbf{q}}_k \\ \ddot{\mathbf{u}}_j \end{bmatrix} + \mathbf{LTM}_2 \mathbf{u}_j + \mathbf{LTM}_3 \begin{bmatrix} \mathbf{F}_i \\ \mathbf{F}_j \end{bmatrix} \quad [5-77]$$

where:

$$\mathbf{LTM}_1 = [\mathbf{L}_{jk} \quad \bar{\mathbf{M}}_{jj}] \quad \mathbf{LTM}_2 = \bar{\mathbf{K}}_{jj} \quad \mathbf{LTM}_3 = [-\Psi_{ji} \quad -\mathbf{I}_{jj}] \quad [5-78]$$

For a statically determinate junction  $\mathbf{LTM}_2 = \bar{\mathbf{K}}_{jj} = 0$ .

The CoG accelerations are defined as the accelerations of the rigid substructure at its CoG due to the projection of all forces on the CoG including the reaction forces  $\mathbf{R}_j$  as well as applied loads  $\mathbf{F}_i$  and  $\mathbf{F}_j$  if any. The CoG acceleration vector with 6 components  $\ddot{\mathbf{u}}_r$  (CoG) is given by:

$$\ddot{\mathbf{u}}_r(\text{CoG}) = \bar{\mathbf{M}}_{rr}^{-1} \Phi_{rj} (\mathbf{R}_j + \mathbf{F}_j + \Psi_{ji} \mathbf{F}_i) \quad [5-79]$$

where  $\Phi_{rj}$  is the rigid body modes associated with the  $j$  DOF and  $\mathbf{M}_{rr} = \Phi_{rj} \bar{\mathbf{M}}_{jj} \Phi_{jr}$  the corresponding rigid body mass matrix.

Combining Eq. [5-77] and [5-79] leads to the expression for the CoG acceleration:

$$\ddot{\mathbf{u}}_r(\text{CoG}) = \mathbf{CTM} \begin{bmatrix} \ddot{\mathbf{q}}_k \\ \ddot{\mathbf{u}}_j \end{bmatrix} \quad \text{with} \quad \mathbf{CTM} = \overline{\mathbf{M}}_{rr}^{-1} \Phi_{rj} \mathbf{LTM}_1 \quad [5-80]$$

The 6 components of  $\ddot{\mathbf{u}}_r(\text{CoG})$  provide the 3 translational and the 3 angular accelerations of the CoG. In order to simplify the results in the case of slender structures, two components are often used: the longitudinal acceleration derived from the longitudinal force  $F_{long}$ , and the lateral acceleration derived from the bending moment  $M_{lat}$  (and not from the shear force) according to the following expressions with  $m$  the spacecraft mass and  $h$  the height of the CoG.

$$\ddot{u}_{long}(\text{CoG}) = F_{long} / m \quad [5-81]$$

$$\ddot{u}_{lat}(\text{CoG}) = M_{lat} / (m h) \quad [5-82]$$

Eq. [5-81] and [5-82] should be interpreted with care because of the underlying assumptions used in deriving them, and in particular that the longitudinal and lateral directions are assumed perfectly uncoupled (in terms of the rigid body mass matrix). As a result, Eq. [5-81] is strictly valid only if the CoG lies on the longitudinal axis. Otherwise, Eq. [5-81] should be interpreted as an *equivalent* CoG acceleration which, when acting alone, produces the interface force  $F_{long}$ , but approximate values for the interface moments. However, for slender structures, the interface moments induced by the longitudinal force are small.

Concerning Eq. [5-82], both translational *and* rotational CoG accelerations are, in theory, required to reproduce the corresponding shear force and bending moment at the interface. However, for slender structures we can assume that the bending moment is more critical than the shear force in terms of the dimensioning loads. Therefore Eq. [5-82] can be used to define an *equivalent* CoG lateral acceleration which, when acting alone, produces the interface bending moment,  $M_{lat}$ , but an approximate value for the shear force. The error in the shear force induced by Eq. [5-82] is examined in the beam example presented below.

The CoG is not to be confused with a physical point of the substructure located at the same point. The CoG is a fictitious point located at the average location of all points of the substructure weighted by their respective masses. It can be thought of as a point whose motion represents the average (i.e. rigid-body) motion of the entire substructure. For many substructures, the CoG may not even be located on or within the structure.

To illustrate the distinction between CoG and physical motion, consider the clamped-free bending beam of length  $L$  and mass  $m$  shown in Figure 5-26. In this 2-D example the CoG is located on the beam at  $\bar{x} = L/2$  with its motion defined by the translational and rotational accelerations  $\ddot{v}$  and  $\ddot{\theta}$ .

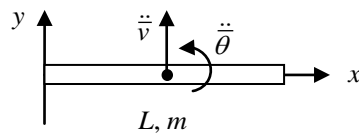


**Figure 5-26: CoG of uniform bending beam**

Let's consider the six different acceleration responses associated with the two rigid-body constraint modes and the first four normal modes. The physical responses  $\ddot{v}(x)$  are plotted below in Figure 5-27 along with the corresponding COG accelerations  $\ddot{v}$  and  $\ddot{\theta}$  depicted by a point and a line segment to illustrate the rotation. The numerical values are tabulated in Figure 5-28.

For the two rigid-body constraint modes, we see that the CoG and physical accelerations at  $x = L/2$  are the same as expected. For the first normal mode, the translational CoG acceleration exceeds the physical acceleration because of the shape of the mode and the fact that all components are in phase. In contrast, for all other normal modes, the mode shapes have both positive and negative components which cancel each other out resulting in a smaller CoG acceleration.

For each successive mode, the CoG accelerations decrease monotonically towards zero, resulting in decreasing interface forces and corresponding effective masses.

Finally, it is interesting to examine the error in the interface shear force  $F_{lat}$  when using  $\ddot{u}_{lat}(\text{CoG})$  of Eq. [5-82]. For a uniform bending beam we obtain the following expression for  $F_{lat}/m$  with the term  $\frac{L}{6}\ddot{\theta}$  representing the error introduced by the CoG angular acceleration.

$$F_{lat}/m = \ddot{u}_{lat}(\text{CoG}) = (m\ddot{v}\frac{L}{2} + \frac{mL^2}{12}\ddot{\theta})/(mL/2) = \ddot{v} + \frac{L}{6}\ddot{\theta} \quad [5-83]$$

The values given by Eq. [5-83] are provided in Figure 5-28. From Eq. [5-83] we see that if the CoG rotation  $\ddot{\theta}$  is zero, then the shear force is strictly equal to  $m\ddot{v}$ . This is the case for the first constraint mode  $\Psi_1$ . If  $\ddot{v}$  and  $\ddot{\theta}$  have the same sign, then Eq. [5-83] provides a conservative or over-estimated value for  $F_{lat}$ . This is the case for the second constraint mode  $\Psi_2$  and the first normal mode  $\Phi_1$  which result in an overestimation of  $F_{lat}$  by 33 % and 45 % respectively. On the other hand, if  $\ddot{v}$  and  $\ddot{\theta}$  have opposing signs, then Eq. [5-83] under-estimates the true shear force. This is the case for all normal modes other than the first. Fortunately, for the higher modes, the shear force amplitudes become smaller and smaller.

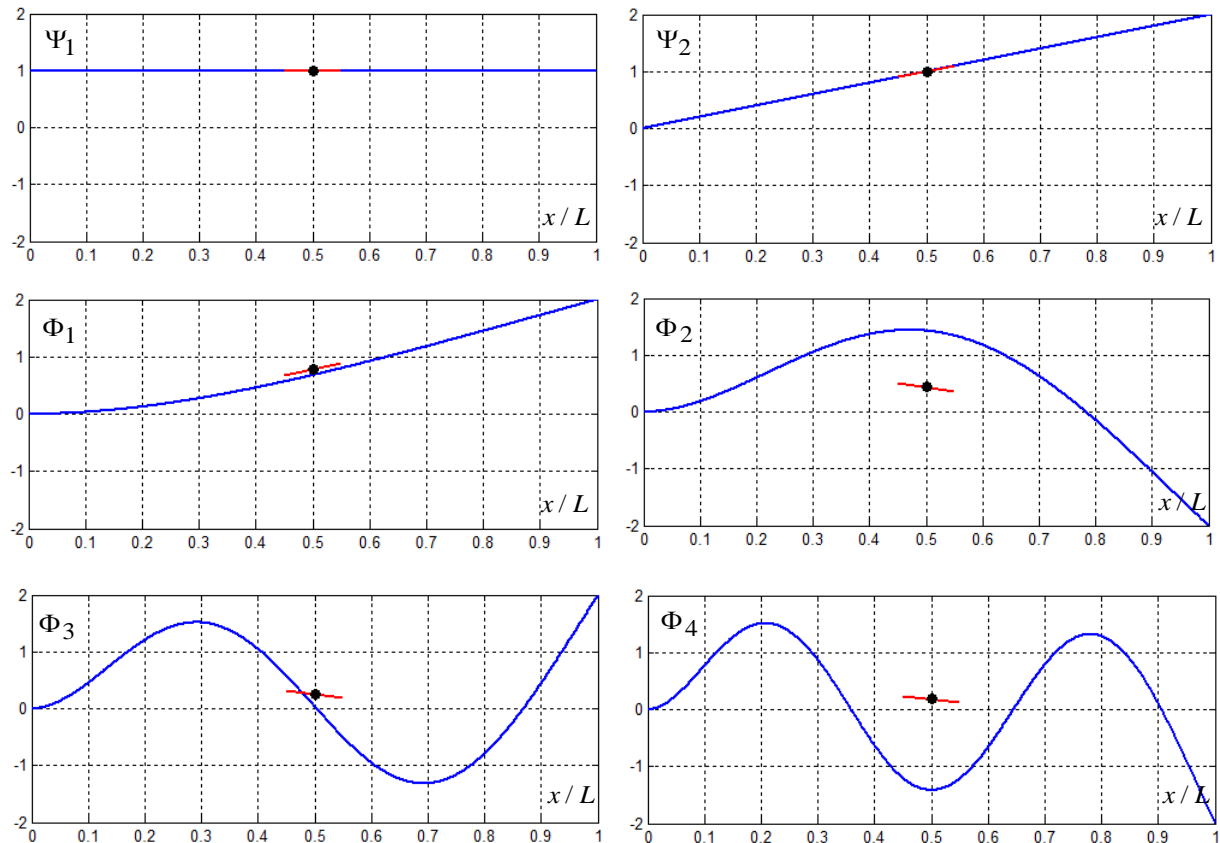


**Figure 5-27: CoG and physical acceleration of bending beam**

Mode	$\ddot{v}(L/2)$	$\ddot{\bar{v}}$	$\ddot{\theta}(L/2)$	$\ddot{\bar{\theta}}$	$\ddot{\bar{v}} + \frac{L}{6} \ddot{\theta}$	$\frac{\ddot{\bar{v}} + \frac{L}{6} \ddot{\theta}}{\ddot{\bar{v}}}$
$\Psi_1$	1.0000	1.0000	0.0000	0.0000	1.0000	1.0000
$\Psi_2$	1.0000	1.0000	2.0000	2.0000	1.3333	1.3333
$\Phi_1$	0.6790	0.7830	2.3260	2.1289	1.1378	1.4532
$\Phi_2$	1.4273	0.4339	-0.9061	-1.5144	0.1815	0.4183
$\Phi_3$	0.0392	0.2544	-11.1044	-1.1375	0.0648	0.2548
$\Phi_4$	-1.4142	0.1819	-0.0865	-0.8929	0.0331	0.1819

**Figure 5-28: CoG and physical acceleration values**

### 5.3.4.7 Damping

Damping can be introduced in physical model of each substructure by two ways:

- Viscous damping ratio  $\zeta_k$  for each mode  $k$ , as assumed in Section 5.3.2.
- Structural damping  $\eta_e$  associated with the element stiffness matrices  $\mathbf{K}_e$ , leading to complex element stiffness matrices  $\mathbf{K}_e(1+i\eta_e)$ . These matrices can be assembled in the usual way to provide a global structural damping matrix  $i(\eta_g \mathbf{K} + \sum \eta_e \mathbf{K}_e)$  including the global structural damping  $\eta_g$ .

In case of modal viscous damping along with structural damping  $\eta_j$  related to a redundant junction, the transformation of Eq. [5-62] applied to the damping matrix of Eq. [5-61] for each substructure provides the following damping matrix in addition to the mass and stiffness matrices given in Eq. [5-63].

$$\begin{bmatrix} \mathbf{c}_{kk} & \mathbf{0}_{kj} \\ \mathbf{0}_{jk} & \frac{\eta_j}{\omega^*} \bar{\mathbf{K}}_{jj} \end{bmatrix} \quad [5-84]$$

where:

- $\mathbf{c}_{kk}$  diagonal matrix of the generalized damping values :  $c_k = 2 \zeta_k m_k \omega_k$ ,
- $\omega^*$  main excitation frequency. In case of small interface deformations, i.e. a relatively stiff interface, this term could be discarded.

The best way to define the modal damping  $\zeta_k$  of a substructure is to identify its modal parameters from experimental modal analysis.

If test data are missing – as in the early phases of spacecraft and launcher design – a damping profile can be estimated by different ways:

- constant values within frequency bands. For spacecraft structures one usually chooses a low damping ratio, i.e. 1% or 2%, to be conservative on the predicted loads. However, this can overestimate loads, as shown in [30] where the modal damping of several spacecraft was found to vary between 3% and 7%,

- from statistical data. However, such an approach could easily lead to either under or overestimation of the loads,
- progressively increasing factor towards higher frequencies. This avoids strong oscillations from unrealistic high frequency modes. An example of a modal damping profile on such basis is given in Figure 5-29,

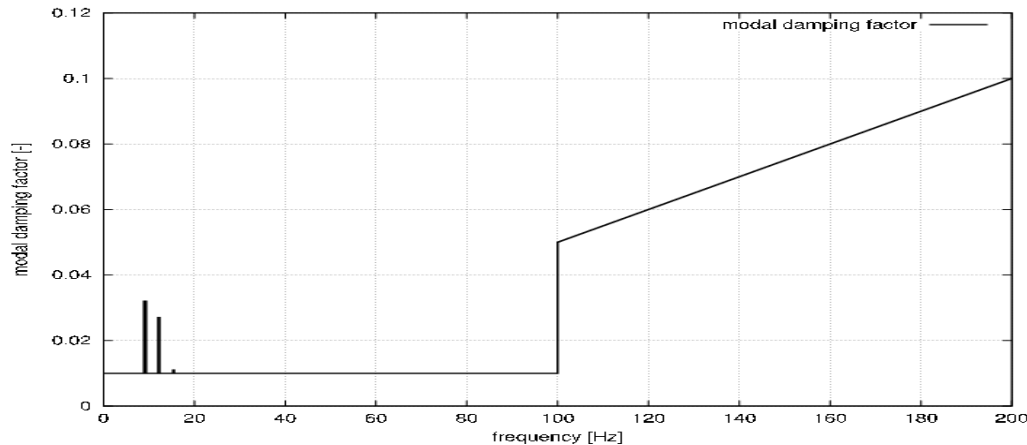


**Figure 5-29: Modal damping profile**

- from the FE model using structural damping in order to be more representative of materials with substantially different structural damping levels. For example, ceramic components have relatively low damping compared to the main structure, or a launch vehicle booster with solid propellant which has high structural damping compared to the case structure.

The last case can be directly used for harmonic response, but for transient analysis the structural damping has to be converted to viscous damping because the phase provided by the complex stiffness has no meaning. This conversion can be performed by the equivalent modal damping method [31] [32] [33] [34].

For a substructure with a structural damping  $\eta_e$  attributed to the elements  $e$ , a modal structural damping  $\eta_k$  can be deduced from the following formula [1]:

$$\eta_k = \sum_e \eta_e \tau_{ek} \quad \text{with} \quad \tau_{ek} = \frac{(\Phi_{ki} K_{ii} \Phi_{ik})_e}{k_k} \quad [5-85]$$

with  $\tau_{ek}$  representing the fraction of strain energy in the element  $e$  for the mode  $k$ . Knowing  $\eta_k$ , the equivalent viscous damping is given by  $2\zeta_k = \eta_k$ , providing the same amplification at resonance:

$$Q_k = \frac{1}{2\zeta_k} = \frac{1}{\eta_k}.$$

As an example of this approach, the equivalent modal damping of a solid rocket motor is shown in Figure 5-30.

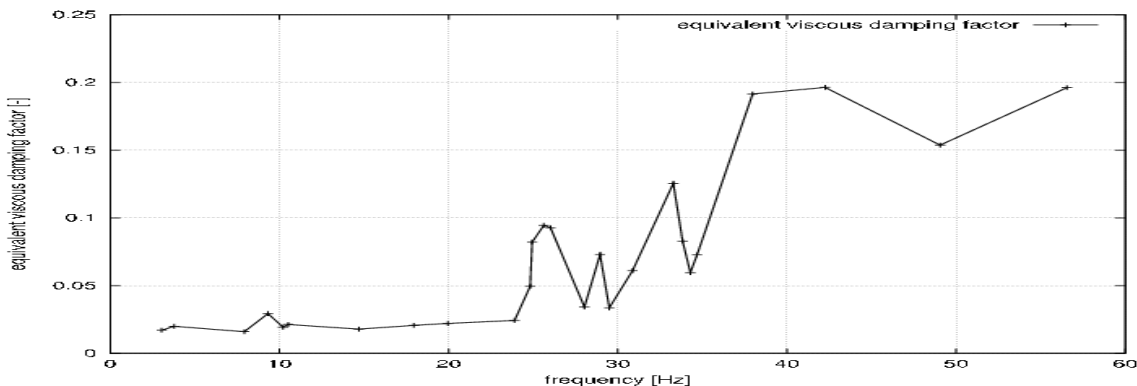


**Figure 5-30: Equivalent modal damping computed for a solid rocket motor**

#### 5.3.4.8 Equivalent damping methods

Traditionally the damping is introduced on subsystem level as modal viscous damping. Experience shows, that coupled dynamic response analysis often reveals strange behaviour. This problem can be overcome, if damping is introduced as an Equivalent Structural Damping (ESD) on substructure level.

The substructure damping is derived from subsystem tests under test boundary conditions and complies with the corresponding component modes of the test configuration. The test boundary conditions are often different from the boundary conditions of the subsystem, when integrated into the complete space transportation system. For use in coupled dynamic analysis, the subsystem mathematical models are condensed with boundary conditions in compliance with those of the integrated substructure. The corresponding component modes differ from those of the test configuration. That is the reason why the damping derived under test boundary conditions should be re-computed in order to comply with the component modes used for the condensation of the mass and stiffness matrix for use in the coupled dynamic analysis. In order to re-compute the modal damping values, the modal damping matrix of the test configuration is transformed into an uncondensed physical structural damping matrix. This is done by the Inflated Damping Matrix (IDM) process. In the following the inflated damping matrix can be condensed by the same transformation as applied on the mass and stiffness matrix. Moreover, at this point the analyst is free to modify the boundary conditions as required for the integration to the complete system.

Dynamic test set-ups generally consist not only of the substructure of interest, but also of test adapters and dummy structures. The question is how to separate the damping properties of substructures of interest from the damping matrix of the complete test assembly. A procedure has been developed, which allows the Separation of this Component Damping (SCD).

The Equivalent Structural Damping (ESD), the Inflated Damping Matrix (IDM) process as well as the Separation of Component Damping (SCD) yield a consistent damping treatment in coupled dynamic analysis and test [33].

To illustrate this point consider the coupling of two SDOF substructures with a natural frequency of 20 Hz shown below in Figure 5-31. One system is modelled using viscous damping ( $\zeta = 0.01$ ) for both substructures whereas the other is modelled with an equivalent structural damping ( $\eta = 2\zeta = 0.02$  for both substructures).

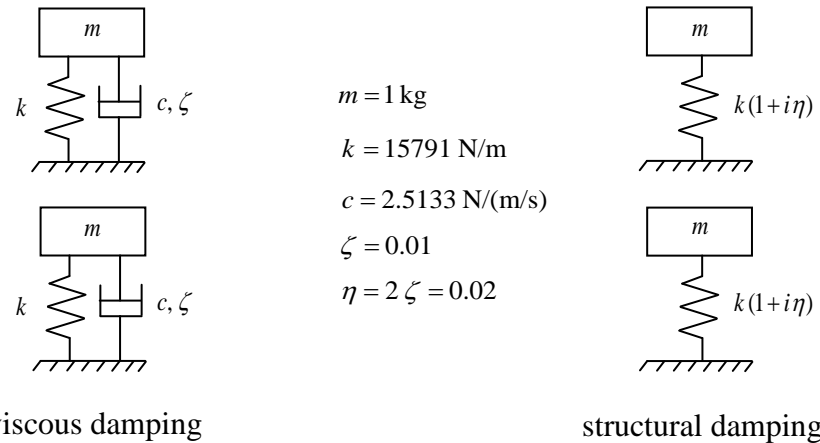


Figure 5-31: Coupling of SDOF systems using viscous and structural damping

The coupled system produces two modes with natural frequencies at 12.36 Hz and 32.36 Hz. When coupling with viscous damping, the following modal damping ratios are obtained for the two modes:

$$\zeta_1 = 0.0062 \quad \zeta_2 = 0.0162 \quad [5-86]$$

Note that coupled damping ratios are different than the value attributed to the substructures ( $\zeta = 0.01$ ). The first mode has a lower damping ratio and inversely, the second mode has a higher value.

This often undesirable behaviour can be avoided by coupling with structural damping in which case the uncoupled modal damping factor  $\eta = 2\zeta = 0.02$  is preserved in the coupled modes:

$$\eta_1 = 0.02 \quad \eta_2 = 0.02 \quad [5-87]$$

The effect of using viscous damping instead of structural damping on the frequency responses is illustrated below in Figure 5-32 for the driving point flexibility at the bottom mass (normalised by the static flexibility). Note that the differences in amplitude are proportional to the differences in modal damping.

On substructure level, it is therefore preferable to introduce the damping as equivalent structural damping (ESD). Otherwise the coupling process leads to an unphysical dynamic behaviour of the coupled system as illustrated above. However, after the coupling process a transformation from a complex formulation of the equation of motion to a real formulation remains possible. In this case, the structural damping matrix of the coupled system can be converted into an equivalent viscous damping matrix [33] [34] which can be used in transient analysis of the coupled systems.

Both [33] and [34] provide equations to convert the structural damping matrix of the system to a modal damping matrix associated to the system modes. The structural damping matrix of the system is assembled from the substructure structural damping matrices. Through a back-transformation process the modal damping matrix of the system (dimension =  $m$  modes  $\times$   $m$  modes) can be expanded to obtain the equivalent viscous damping matrix of the system (dimension =  $n$  DOF  $\times$   $n$  DOF). In [34] a new method is proposed which does not neglect the off-diagonal terms in the modal damping matrix associated to the system modes. If this method is employed, the accuracy of the obtained equivalent viscous matrix of the system is greatly improved.

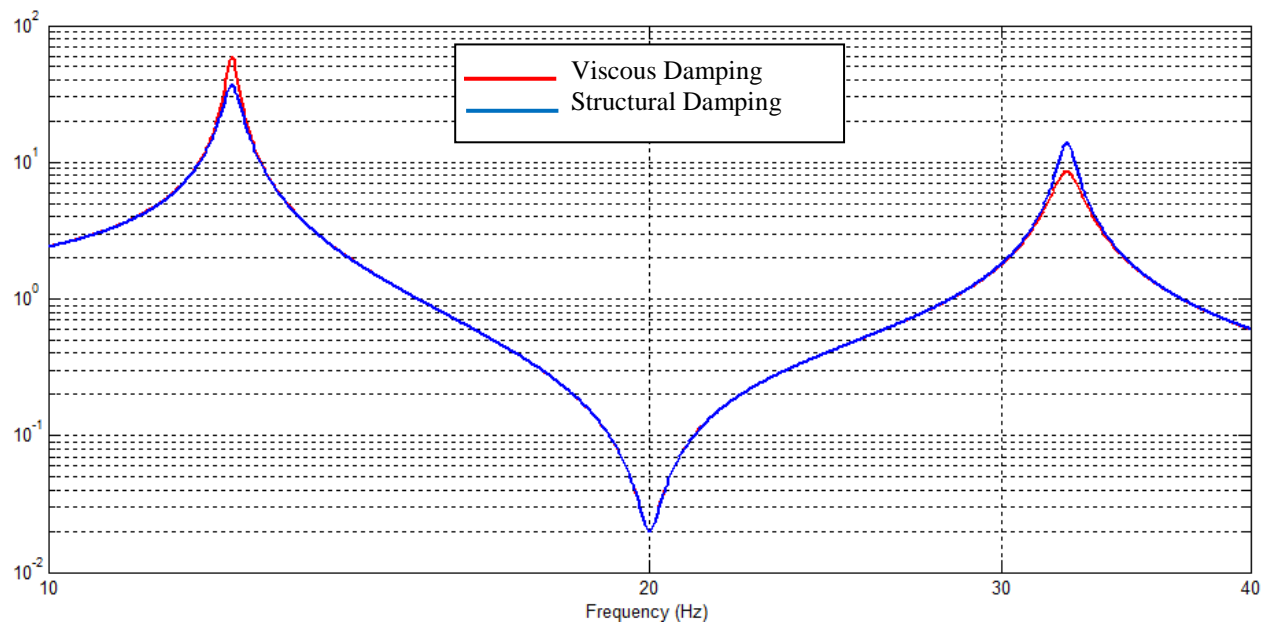


**Figure 5-32: Response of coupled system using viscous and structural damping**

### 5.3.4.9 Static and dynamic contributions

#### 5.3.4.9.1 Filtered forcing functions without quasi-static component

In order to compute the equivalent sine spectrum of a dynamic acceleration signal one should remove any quasi-static component in the signal. Such quasi-static components may be included in the acceleration signal if the launcher forcing function contains for instance a quasi-static thrust build-up from motor ignitions. One way to remove quasi-static components in the acceleration signal is to use a high-pass filter with a filter frequency of 5 Hz for instance. A disadvantage of this method is the potential introduction of the filter frequency in the response signal.

#### 5.3.4.9.2 Modal transient analyses

Another way to exclude the effects of quasi-static components in the forcing function is to exclude the rigid body modes from the computed set of modes. Hence the selected mode set contains elastic modes. A disadvantage of this method is the potential introduction of truncation effects into the modal equations of motion of the assembled CB-system. In addition it is not possible to directly use the substructure damping matrices which may have been computed on the basis of an equivalent modal damping procedure (refer to Section 5.3.4.7).

#### 5.3.4.9.3 Explicit rigid degrees of freedom

A third way to exclude the effects of quasi-static components in the forcing function is to include the geometric rigid body modes explicitly in the condensation process of each substructure. This method, proposed by Hurty [22] uses a modal base containing geometric rigid body modes, static modes and elastic normal modes as depicted in Figure 5-33 and formulated by Eq. [5-88].

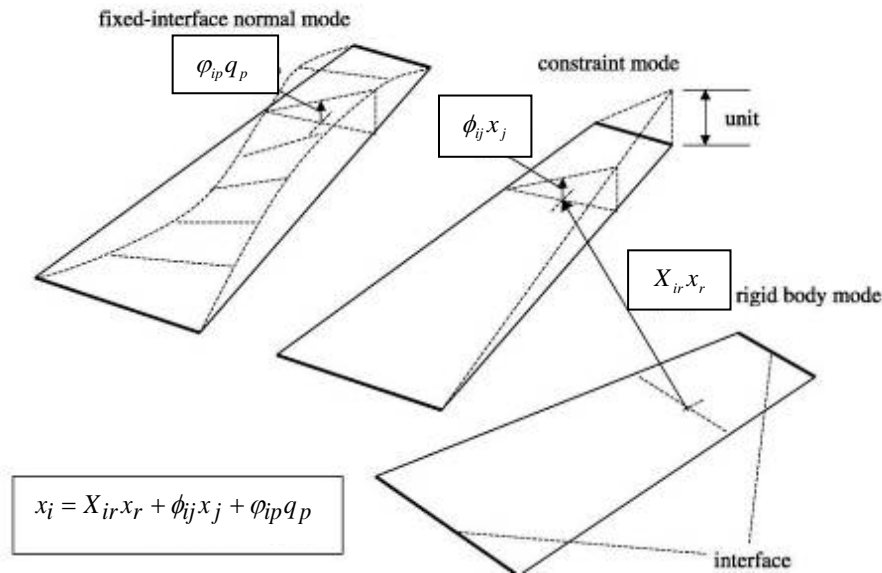


**Figure 5-33: Modes used by the Hurty method**

$$\begin{pmatrix} x_r \\ x_j \\ x_i \\ q_p \end{pmatrix} = \psi \cdot \begin{pmatrix} x_r \\ x_j \\ x_i \\ q_p \end{pmatrix} = \begin{bmatrix} I_{rr} & 0_{rj} & 0_{rp} \\ X_{jr} & I_{jj} & 0_{jp} \\ X_{ir} & \phi_{ij} & \phi_{ip} \end{bmatrix} \cdot \begin{pmatrix} x_r \\ x_j \\ q_p \end{pmatrix} \quad [5-88]$$

This yields condensed models very similar to Craig-Bampton models. In this case the equations of motion of the system of condensed models can be solved by direct integration using for example the Newmark method. The advantage is that substructure damping matrices can be used as is. The solution of the explicit rigid DOF  $x_r$  then describes the rigid body motion. Elastic motion can be computed from the interface and modal displacements  $x_j$  and  $q_p$ . In that case  $x_r$  is set to zero. Note that for a statically determinate interface (no elastic constraint modes) the Hurty and Craig-Bampton methods are identical. A disadvantage of this method is its complexity and the fact that the geometric rigid body modes are not orthogonal to the elastic normal modes. In addition the method is not implemented in any standard FE package. More information may be found in [22] and [29].

### 5.3.4.10 Sensitivity Analysis

Global stiffness and mass modifications can be parameterised directly in the Craig-Bampton model without the need for recalculating any of the associated matrices. We can define parametric stiffness and mass matrices by introducing the positive scale factors  $\alpha$  and  $\beta$  as follows:

$$\mathbf{K}(\alpha) = \alpha \begin{bmatrix} \mathbf{K}_{ii} & \mathbf{K}_{ij} \\ \mathbf{K}_{ji} & \mathbf{K}_{jj} \end{bmatrix} = \begin{bmatrix} \alpha \mathbf{K}_{ii} & \alpha \mathbf{K}_{ij} \\ \alpha \mathbf{K}_{ji} & \alpha \mathbf{K}_{jj} \end{bmatrix} \quad [5-89]$$

$$\mathbf{M}(\beta) = \beta \begin{bmatrix} \mathbf{M}_{ii} & \mathbf{M}_{ij} \\ \mathbf{M}_{ji} & \mathbf{M}_{jj} \end{bmatrix} = \begin{bmatrix} \beta \mathbf{M}_{ii} & \beta \mathbf{M}_{ij} \\ \beta \mathbf{M}_{ji} & \beta \mathbf{M}_{jj} \end{bmatrix} \quad [5-90]$$

It can be easily demonstrated that the above global stiffness and mass modifications have no effect on the eigenvectors  $\Phi_{ik}$  or the static junction modes  $\Psi_{ij}$ . Therefore, the Craig-Bampton mass and stiffness matrices from Eq. [5-63] can be parameterised in the same way as the physical matrices:

$$\begin{bmatrix} \beta \mathbf{m}_{kk} & \beta \mathbf{L}_{kj} \\ \beta \mathbf{L}_{jk} & \beta \bar{\mathbf{M}}_{jj} \end{bmatrix} \quad \begin{bmatrix} \alpha \mathbf{k}_{kk} & \mathbf{0}_{kj} \\ \mathbf{0}_{jk} & \alpha \bar{\mathbf{K}}_{jj} \end{bmatrix} \quad [5-91]$$

Note that Eq. [5-91] implies that the natural frequencies are modified according to:

$$f_k(\alpha, \beta) = \frac{1}{2\pi} \sqrt{\frac{\alpha k_k}{\beta m_k}} = \sqrt{\frac{\alpha}{\beta}} f_k \quad [5-92]$$

Concerning the OTM, the influence of the scale factors depends on the nature of each OTM. For example, using the mode acceleration method, the displacement OTM of Eq. [5-72] becomes:

$$\begin{bmatrix} \mathbf{u}_i \\ \mathbf{u}_j \end{bmatrix} = \frac{\beta}{\alpha} \mathbf{DTM}_1 \begin{bmatrix} \ddot{\mathbf{q}}_k \\ \ddot{\mathbf{u}}_j \end{bmatrix} + \mathbf{DTM}_2 \mathbf{u}_j + \frac{1}{\alpha} \mathbf{DTM}_3 \mathbf{F}_i \quad [5-93]$$

whereas the load transformation matrices of Eq. [5-77] takes on the following form:

$$\mathbf{R}_j = \beta \mathbf{LTM}_1 \begin{bmatrix} \ddot{\mathbf{q}}_k \\ \ddot{\mathbf{u}}_j \end{bmatrix} + \alpha \mathbf{LTM}_2 \mathbf{u}_j + \mathbf{LTM}_3 \begin{bmatrix} \mathbf{F}_i \\ \mathbf{F}_j \end{bmatrix} \quad [5-94]$$

Other OTM such as for stresses, accelerations and internal forces can be expressed in a similar fashion by applying the scale factors  $\alpha$  and  $\beta$  appropriately.

In the context of CLA, the above approach can be used to perform parametric analyses to define the variation of design loads of a structure due to modifications in mass and stiffness without repeating an entire coupled analysis. Details are available in [37].

### 5.3.4.11 Assembly of condensed models

The reduced substructures can be integrated with other reduced substructures to form a system of CB-models, as shown in Figure 5-34. The corresponding equations take the following form in case damping is omitted:

$$\begin{bmatrix} m_{kk}^{(5)} & 0 & 0 & 0 & L_{kb}^{(5)} \\ m_{kk}^{(4)} & 0 & 0 & 0 & L_{kb}^{(4)} \\ m_{kk}^{(3)} & 0 & 0 & L_{kb}^{(3)} \\ m_{kk}^{(2)} & 0 & L_{kb}^{(2)} \\ m_{kk}^{(1)} & L_{kb}^{(1)} \\ \text{sym} & M_{bb} \end{bmatrix} \begin{bmatrix} \ddot{q}_k^{(5)} \\ \ddot{q}_k^{(4)} \\ \ddot{q}_k^{(3)} \\ \ddot{q}_k^{(2)} \\ \ddot{q}_k^{(1)} \\ \ddot{x}_b \end{bmatrix} + \begin{bmatrix} k_{kk}^{(5)} & 0 & 0 & 0 & 0 \\ k_{kk}^{(4)} & 0 & 0 & 0 & 0 \\ k_{kk}^{(3)} & 0 & 0 & 0 & 0 \\ k_{kk}^{(2)} & 0 & 0 & 0 & 0 \\ k_{kk}^{(1)} & 0 & 0 & 0 & 0 \\ \text{sym} & \bar{K}_{bb} \end{bmatrix} \begin{bmatrix} q_k^{(5)} \\ q_k^{(4)} \\ q_k^{(3)} \\ q_k^{(2)} \\ q_k^{(1)} \\ x_b \end{bmatrix} = \begin{bmatrix} f_k^{(5)} \\ f_k^{(4)} \\ f_k^{(3)} \\ f_k^{(2)} \\ f_k^{(1)} \\ F_b \end{bmatrix} \quad [5-95]$$

where  $x_b \supset x_j^{(S)}$ ,  $S = 1 \dots 5$

Solving the corresponding set of equations gives the generalized solution in terms of interface DOF and modal DOF for the entire CB-system and hence also for each substructure in the system. For each substructure the recovery of internal displacements, accelerations etc. can be accomplished by either the mode displacement method (Section 5.3.4.3), the mode acceleration method (Section 5.3.4.4) or the modal truncation augmentation method (Section 5.3.4.5) in case the substructure's modal basis was enriched with residual vectors.

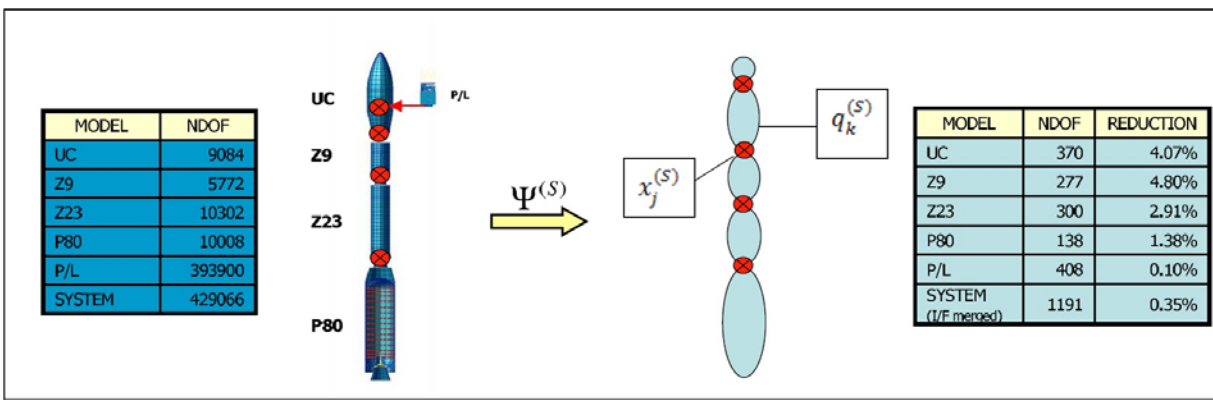


Figure 5-34: Assembly of condensed substructure models

## 5.4 Coupled analysis and notching in sine tests

### 5.4.1 FRF coupling

FRF coupling is a substructuring technique based on the direct use of FRF. It is considered here for LV/SC coupling in order to better understand the underlying behaviour.

FRF coupling at the interface of the launcher and spacecraft identified by a set of connection DOF,  $c$ , involves the following FRF:

- The launcher  $L$  considered separately is excited by its own excitation forces  $\mathbf{F}_e^L$  at the excitation DOF,  $e$ , as well as by the forces coming from the spacecraft  $S$  at the connection DOF,  $c$ . The relevant FRF are therefore  $\mathbf{X}_{ce}^L$  and  $\mathbf{X}_{cc}^L$ .
- The spacecraft  $S$  considered separately is excited only by the forces coming from the launcher  $L$  at the connection DOF,  $c$ . The relevant FRF are therefore  $\mathbf{X}_{cc}^S$ .

The nature of  $\mathbf{X}$  depends on the boundary conditions imposed at the connection DOF for each substructure considered separately - which in most cases are chosen either free or fixed.

- For the spacecraft  $S$ , substructure analysis is usually performed using fixed connection DOF leading to the FRF  $\mathbf{M}_{cc}^S$ .
- For the launcher  $L$ , substructure analysis is usually performed using free connection DOF given its significant mass compared to that of the spacecraft. However for the sake of physical interpretation let us consider fixed connection DOF for the launcher leading to the FRF  $\mathbf{T}_{ce}^L$  and  $\mathbf{M}_{cc}^L$ . In this case the coupled analysis leads to:

$$\ddot{\mathbf{u}}_c(\omega) = \left( \mathbf{M}_{cc}^L(\omega) + \mathbf{M}_{cc}^S(\omega) \right)^{-1} \mathbf{T}_{ce}^L(\omega) \mathbf{F}_e(\omega) \quad [5-96]$$

Equation [5-96] expresses Newton's Second Law with the sum of the dynamic masses of the launcher and spacecraft excited by the forces  $\mathbf{T}_{ce}^L(\omega) \mathbf{F}_e(\omega)$ . These forces can be interpreted as the reaction or blocking forces  $\mathbf{F}_c^L(\omega)$  at the connection DOF considered fixed due to the excitation forces,  $\mathbf{F}_e$ .

We see from Eq. [5-96] that the effect of the spacecraft is located exclusively in the dynamic masses  $\mathbf{M}_{cc}^S(\omega)$  whose influence depends on the dynamic masses of the launcher,  $\mathbf{M}_{cc}^L(\omega)$ . In spite of the

large difference in static mass between the launcher and spacecraft, and depending on the frequency, a highly amplified dynamic mass of the spacecraft associated with an attenuated dynamic mass of the launcher can have a significant influence on the responses at the interface. This is the justification for performing notching at the natural frequencies of the spacecraft which is demonstrated hereafter using mode superposition theory.

### 5.4.2 Modal approach

Consider Eq. [5-44] expressed for the case of a rigid (statically determinate) junction  $j = r$ . There is no loss of generality in this simpler case since the type of junction has little bearing on what follows.

$$\mathbf{M}_{rr}(\omega) \approx \sum_{k=1}^n T_k(\omega) \tilde{\mathbf{M}}_{rr,k} + \mathbf{M}_{rr,res} \quad [5-97]$$

Using the effective mass model of Figure 5-24, the launcher and spacecraft may be coupled according to the schema presented in Figure 5-35.

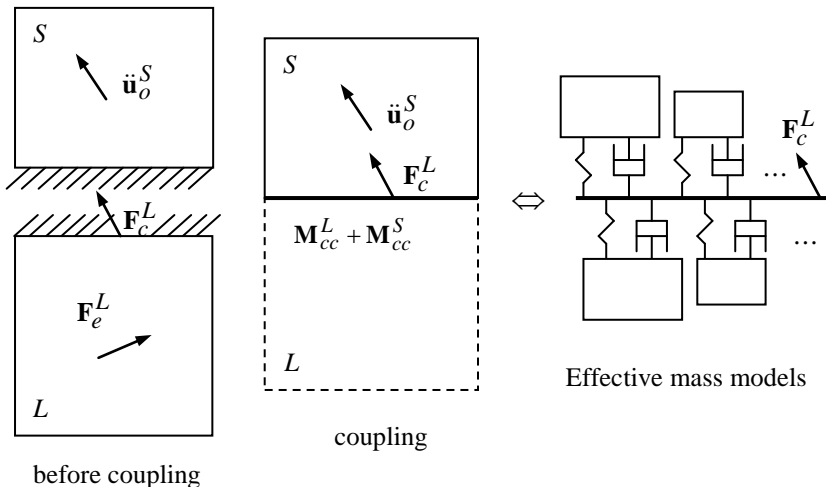


**Figure 5-35: Coupled analysis with effective mass models**

In this schema we can see that:

- for the spacecraft  $S$ , modes with large effective masses  $\tilde{\mathbf{M}}_{rr,k}^S$ , (often the first modes along each axis) produce large dynamic masses at the spacecraft's resonances equal to  $Q_k^S \tilde{\mathbf{M}}_{rr,k}^S$ .
- for the launcher  $L$ , at the frequencies of the first spacecraft modes:
  - the first modes with very large effective masses, but at much lower frequencies, produce relatively small dynamic masses because of the frequency filtering effect.
  - the following modes, closer in frequency to the spacecraft modes, have much smaller effective masses and therefore a limited contribution to the dynamic mass.

As a result, at the resonant frequencies of the spacecraft, its dynamic masses may be substantially greater than those of the launcher and therefore significantly attenuate the motion at the interface according to Eq. [5-96] thus justifying the use of notching.

In more qualitative terms, each mode of the spacecraft produces both a resonance and an antiresonance in the coupled FRF of Eq. [5-96]. The resonance is located at the natural frequency of the

coupled system closest to the mode whereas the antiresonance is located directly at the frequency of the spacecraft mode. The depth of the antiresonance is comparable to the sharpness of the resonance. Moreover, this depth increases with increasing effective mass of the spacecraft and decreasing dynamic mass of the launcher at the given frequency. The purpose of notching is therefore to simulate this antiresonance during the sine test via prescribed levels associated with accelerometers and derived from coupled analysis.

The modal parameters involving the spacecraft are therefore limited exclusively to the effective masses (along with their amplification at resonance). The large effective masses of the spacecraft producing large reaction forces on the launcher are responsible for the use of primary notching - i.e. the notching imposed by the dynamics of the coupled LV/SC system.

### 5.4.3 Simple example

To illustrate the concept of notching, consider the simple model presented in Figure 5-36, designed to representing the overall orders of magnitude of the various physical parameters (masses and frequencies) involved in the analysis.

- $M_1$  order of magnitude of the launcher mass excluding the mass at the spacecraft interface
- $M_2$  order of magnitude of the launcher mass at the spacecraft interface + the spacecraft residual mass
- $M_3$  order of magnitude of the effective mass of the spacecraft's first mode
- $K_1$  stiffness of the free-free system at 20 Hz with infinite  $K_2$ , ( $K_1 = 1.56 \times 10^8$  N/m)
- $K_2$  stiffness for the first spacecraft mode at 40 Hz, ( $K_2 = 6.32 \times 10^7$  N/m)

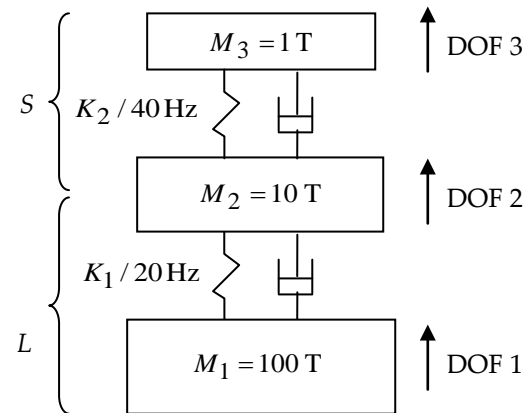


**Figure 5-36: Simple model for coupled analysis with launcher/spaceship (L/S)**

The model in Figure 5-36 can be interpreted as an effective mass model with respect to the connection DOF 2, comprising one launcher mode and one spacecraft mode. The fixed-interface launcher mode has a frequency of 6.3 Hz - much lower than the fixed-interface spacecraft mode - and therefore significantly filtered.

Let's consider a harmonic force excitation at DOF 1 of constant amplitude and determine the acceleration responses at DOF 2 and 3 while focusing our attention at the frequencies near 40 Hz.

The two elastic modes of the coupled system have the following characteristics:

- mode 1 :  $f_1 = 19.7 \text{ Hz}$   $\Phi_{i1} = \begin{bmatrix} -0.1132 \\ 1 \\ 1.32 \end{bmatrix}$   $\tilde{G}_{i1} = -5.67 \cdot 10^{-10} \begin{bmatrix} -0.1132 \\ 1 \\ 1.32 \end{bmatrix}$
- mode 2 :  $f_2 = 42.5 \text{ Hz}$   $\Phi_{i2} = \begin{bmatrix} -0.0223 \\ 1 \\ -7.77 \end{bmatrix}$   $\tilde{G}_{i2} = -4.44 \cdot 10^{-12} \begin{bmatrix} -0.0223 \\ 1 \\ -7.77 \end{bmatrix}$

Using an amplification factor of  $Q_k = 25$  and a force excitation amplitude of 100 T ( $g = 10 \text{ m/s}^2$ ), we obtain the coupled responses displayed in Figure 5-37.

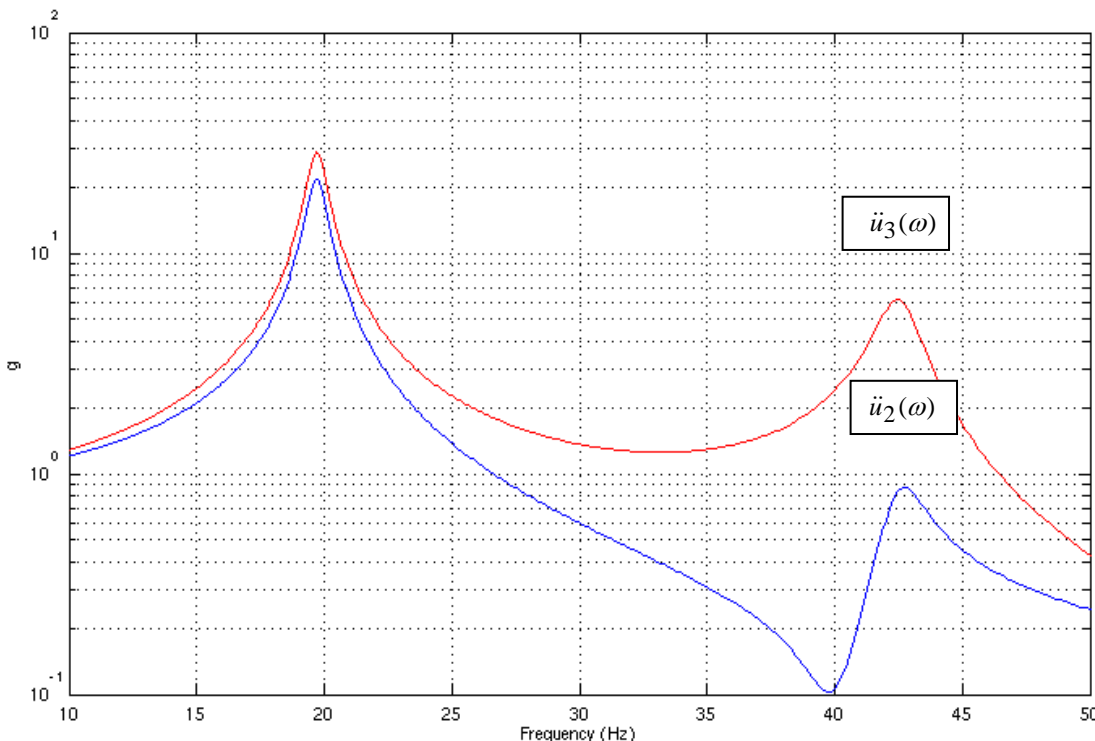


**Figure 5-37: Coupled responses of the simple model**

A test specification based on the envelope of the response levels near these frequencies (0.86 g at the interface), should therefore be notched based on the level at the antiresonance (0.10 g), resulting in a notching factor of approximately 9 in order to account for the reaction of the spacecraft at its resonance.

These results can also be obtained using the model excited by the blocking force at DOF 2  $F_2 = F_1 T_{21}(f)$  with  $T_{21}$  the force transmissibility of the launcher from DOF 1 to DOF 2 which is highly filtered near 40 Hz - a frequency well above the launcher mode at 20 Hz.

By examining the role of each mass at 40 Hz, the resonance of the spacecraft, we can interpret their influence on the coupled response:

- mass  $M_1$  of 100 T, representing essentially the total mass of the launcher, is nearly entirely filtered,
- mass  $M_2$  of 10 T, representing the residual mass of the launcher and spacecraft, is directly excited by the blocking force,

- mass  $M_3$ , of 1 T, representing the effective mass of the spacecraft, is amplified by the resonance to 25 T.

Mass  $M_1$  has a very small influence on the displacements at DOF 2 and 3, and therefore nearly the same results would be obtained by removing DOF 1 from the model and exciting with the blocking force at DOF 2. Mass  $M_3$  of the spacecraft at its resonance is sufficient to counter the excitation coming from the launcher, which with only a mass of  $M_2$  does not have enough dynamic mass to impose a response level comparable to those at the neighbouring frequencies.

This example therefore clearly illustrates the reason and need for notching by analysis of the relevant FRF and the associated modal effective parameters.

## 5.4.4 Use of the shock response spectrum

### 5.4.4.1 Introduction

Coupled analysis is used to predict maximum response levels at the LV/SC interface and at critical points within the spacecraft. Typically the coupled analysis is performed using a modal approach with each structure represented by the normal modes of its FE model along with associated modal damping factors.

Following coupled analysis, base-excitation sine sweep tests are performed on the spacecraft to qualify the structure by comparison of the measured response levels with respect to the required levels derived from the coupled analysis predictions.

The measured FRF (dynamic transmissibilities) can be compared with the predicted FRF obtained from the Spacecraft FE model. This comparison may reveal differences at the resonant peaks due to differences between the FE modes and actual modes of the Spacecraft in terms of natural frequencies, modal effective parameters and damping factors.

The question that naturally arises is what is the effect of these differences on the maximum response levels of the coupled analysis, and how can the response levels be adjusted without having to redo coupled analysis? The adjusted levels are then used to assess the qualification of the spacecraft structure.

### 5.4.4.2 Methodology

The coupled analysis maximum response levels can be adjusted using the FE and measured modes of the Spacecraft along with the SRS of the interface accelerations used for coupled analysis. However this methodology assumes the following:

- Each resonant peak in question is dominated by a single mode. This allows a simple 1-DOF approach to adjusting the maximum response levels.
- The mode in question has a small influence on the interface motion and therefore a negligible effect on the SRS of the interface accelerations, thus avoiding the need to redo coupled analysis.

Based on the above assumptions we can characterise each peak by its natural frequency,  $f_k$ , modal effective transmissibility,  $\tilde{T}_k$ , and dynamic amplification,  $Q_k$  (SDOF approach, Section 5.2.3.2). The dynamic amplification,  $Q_k$ , can be easily obtained from the sharpness of the peak (e.g. using the half-power method) after which the effective transmissibility,  $\tilde{T}_k$ , can be immediately deduced from the amplitude of the peak,  $A_k$ , using the simple relation:

$$A_k = \tilde{T}_k Q_k \quad [5-98]$$

Moreover, Eq. [5-98] can be expressed in terms of either the measured,  $m$ , or FE-predicted,  $p$ , modal terms according to:

$$A_k^m = \tilde{T}_k^m Q_k^m \quad [5-99]$$

$$A_k^p = \tilde{T}_k^p Q_k^p \quad [5-100]$$

Next, we assume that the maximum response level from CLA,  $\ddot{u}_{\max}$ , can be approximated by considering only the contribution of mode  $k$  according to:

$$\ddot{u}_{\max} \approx \tilde{T}_k S_a(f_k, Q_k) \quad [5-101]$$

where  $S_a(f_k, Q_k)$  is the acceleration SRS at the LV/SC interface.

From Eq. [5-101] along with the test and predicted modal terms of Eq. [5-99] and [5-100] we can derive a simple expression for the adjusted or *corrected* maximum response level,  $\ddot{u}_{c\max}$

$$\ddot{u}_{c\max} = c \ddot{u}_{\max} \quad [5-102]$$

where the dimensionless correction coefficient,  $c$ , is defined by:

$$c = \frac{\tilde{T}_k^m}{\tilde{T}_k^p} \frac{S_a(f_k, Q_k^m)}{S_a(f_k, Q_k^p)} = \frac{A_k^m}{A_k^p} \frac{Q_k^p}{Q_k^m} \frac{S_a(f_k, Q_k^m)}{S_a(f_k, Q_k^p)} \quad [5-103]$$

The following observations can be made about  $c$  with respect to its modal terms:

- For identical measured and predicted peaks,  $c$  is equal to 1.
- For peaks with equal damping,  $c$  is equal to the ratio of the amplitudes.
- For peaks with equal effective transmissibility,  $c$  is equal to the ratio of the SRS.
- For peaks with equal amplitude and different damping,  $c$  is not equal to 1.

#### 5.4.4.3 Simple example

Consider the LV/SC interface acceleration SRS shown in Figure 5-38 for two values of damping,  $Q_k = 20$  and  $Q_k = 40$ . Note that variation between the two SRS at 40 Hz is not proportional to the variation in damping ( $12g/10g \neq 40/20$ ). Proportionality occurs only in the particular case where the input excitation is harmonic.

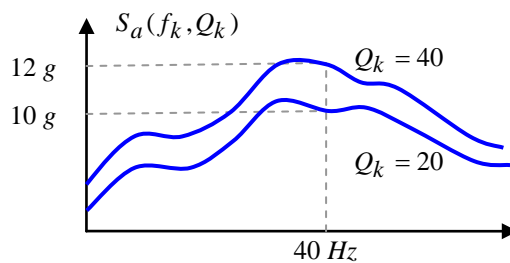


**Figure 5-38: LV/SC I/F SRS**

The measured and predicted FRF (dynamic transmissibilities) are plotted in Figure 5-39 for a peak at 40 Hz using various modal values. The correction coefficient,  $c$ , is shown for each case from which the following remarks can be made:

- Case 1 (same  $Q_k$ ) - the correction is proportional to the amplitudes,  $A_k$ , since the error is in  $\tilde{T}_k$ .

- Case 2 (same  $\tilde{T}_k$ ) - the correction is proportional to the SRS amplitudes,  $S_a$ , since the error is in  $Q_k$ .
- Case 3 (same  $A_k$ ) - a correction is necessary even though the amplitudes,  $A_k$ , are the same, because of the differences in  $\tilde{T}_k$  and  $Q_k$ .
- Case 4 ( $c=1$ ) - no correction is necessary even though the amplitudes,  $A_k$ , are different, because of the particular values of  $\tilde{T}_k$  and  $Q_k$ .

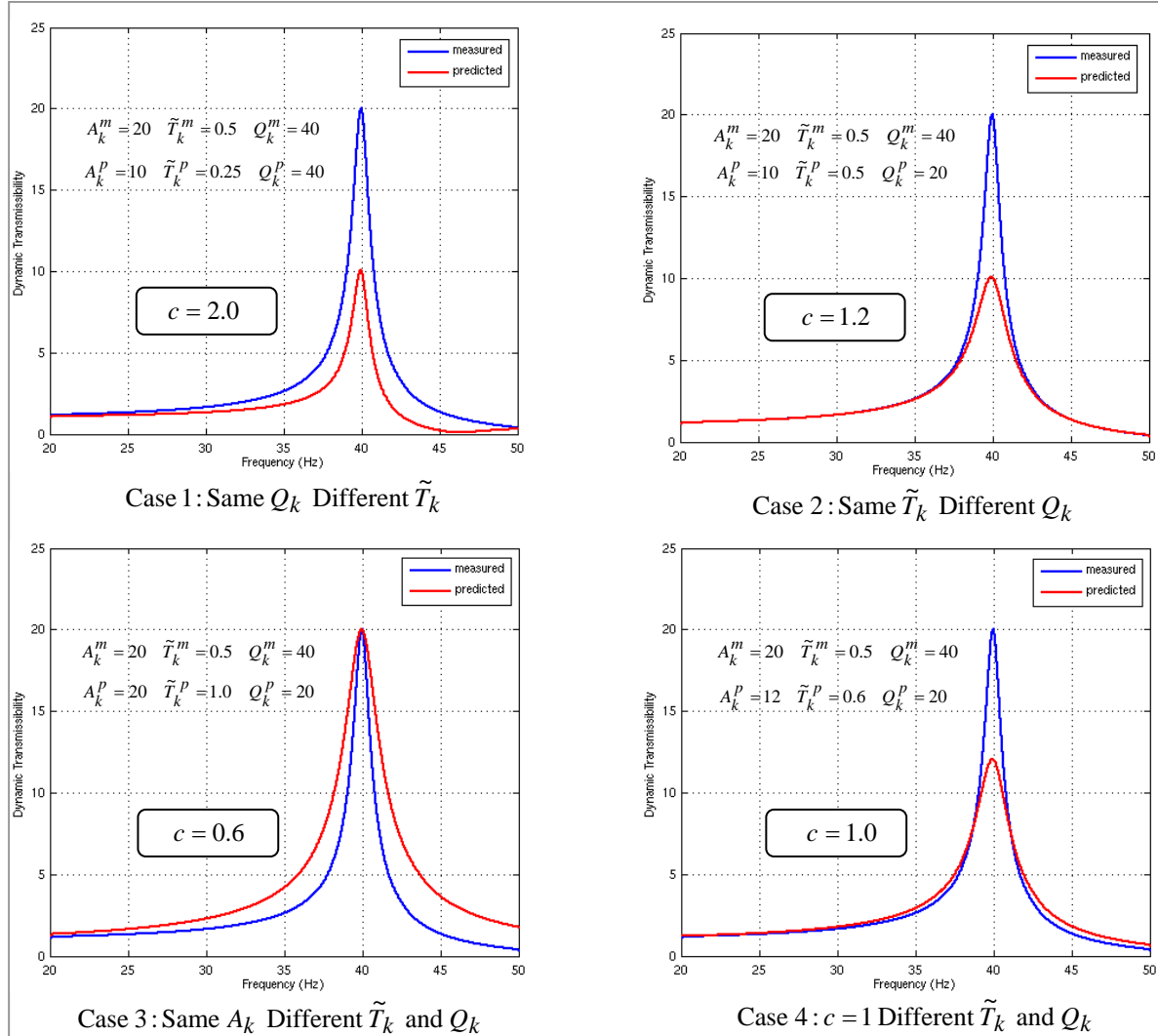
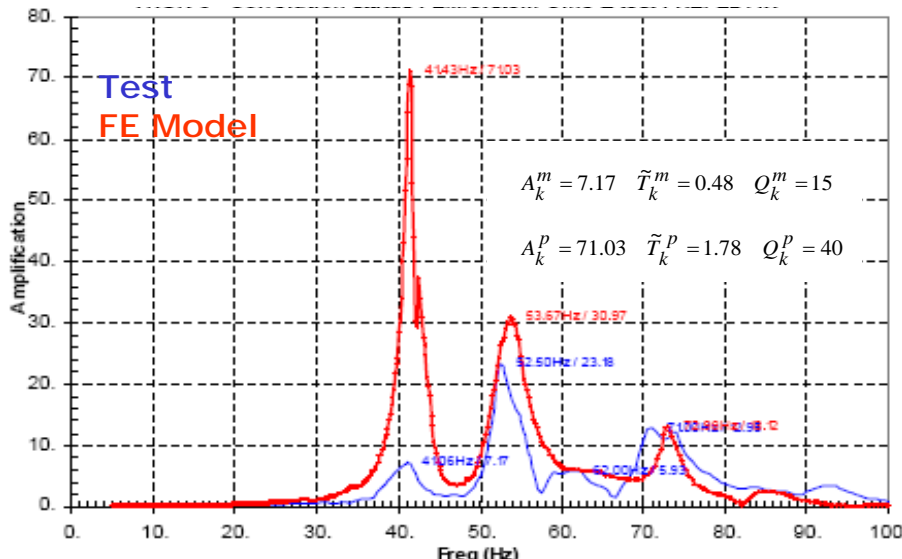


Figure 5-39: FRF test/prediction comparison and correction coefficients

#### 5.4.4.4 LV/SC example

Consider the spacecraft and launch vehicle example presented in more detail in Section 6.5.3.4. In this example the maximum coupled analysis response of a particular spacecraft component is  $\ddot{u}_{\max} = 50 \text{ g}$  at 40 Hz. However, during the sine-sweep test of the spacecraft a maximum response level of only 10 g was produced.

In order to determine if the test is compliant with the CLA with respect to this component, we can compare the measured and predicted FRF plotted in Figure 5-40.



**Figure 5-40: FRF test/prediction comparison for LV/SC example**

The modal terms  $Q_k$  and  $\tilde{T}_k$  for the peak at 40 Hz are identified approximately using the half-power method for both measured and predicted responses. The values (displayed in Figure 5-40) indicate that the measured and predicted modes differ significantly in both effective transmissibilities ( $(\tilde{T}_k^m/\tilde{T}_k^p \approx 0.27)$ ) and damping ( $Q_k^m/Q_k^p \approx 0.375$ ).

The correction coefficient,  $c$ , is calculated for a range of  $S_a$  ratios to illustrate their effect on the corrected CLA response,  $\ddot{u}_{cmax}$ . The results are tabulated below in Figure 5-41.

$\frac{\tilde{T}_k^m}{\tilde{T}_k^p}$	$\frac{S_a(f_k, Q_k^m)}{S_a(f_k, Q_k^p)}$	$c$	$\ddot{u}_{cmax} = c \ddot{u}_{max}$
0.27	0.375	0.10	5.0 g
	0.525	0.14	7.1 g
	0.750	0.20	10.0 g
	0.850	0.23	11.5 g

**Figure 5-41: Corrected coupled response levels for LV/SC example**

The following observations can be made concerning the above results:

- In the most conservative case ( $S_a$  ratio =  $Q_k$  ratio = 0.375), the maximum CLA response is reduced by a factor 10 resulting in a corrected CLA response level (5 g) equal to half of the tested level (10 g). In this case the test may be considered compliant.
- However for  $S_a$  ratios > 0.75, the corrected CLA response remains greater than the tested level of 10 g resulting in a non-compliant test.

## 5.5 Primary and secondary notching

### 5.5.1 Modes concerned by primary notching

We saw above that the degree of notching is directly related to the magnitude of the effective masses. Given the large difference in static mass between the launcher and spacecraft, only the largest effective masses of the spacecraft are likely to justify what is called primary notching.

It should be mentioned that so-called global modes of the spacecraft which correspond to a global movement, do not necessarily have large effective masses - nor inversely. It is in fact quite easy to have a global mode with negligible effective mass due to the presence of opposing motion in the mode. This antagonistic motion becomes more prevalent with increasing mode number. Inversely, a local mode associated with a large mass (tank, battery, etc.) could very well have a relatively large effective mass. Therefore care should be taken to reason exclusively in terms of effective mass rather than global modes in the context of notching.

For modes with small effective mass, the influence on the interface motion is greatly diminished along with the justification for notching. The cut-off point is case-dependent - however the following indications based on a launcher of several hundred tons may be helpful:

- effective mass of roughly 1 ton most likely justifies a primary notching - except for pathological cases,
- an effective mass of roughly 100 kg could possibly justify a primary notching - but the risk of refusal by the Launch Authority is high,
- an effective mass of roughly 10 kg has no chance of justifying a primary notching.

### 5.5.2 Secondary notching

If the effective mass of a mode cannot justify a primary notching, it may nonetheless justify another type of notching based on the response level at one or several critical components of the spacecraft rather than on the reaction forces at its interface with the launcher. This is called the secondary notching, aimed at preserving spacecraft critical components. Secondary notching can only be justified by examination of the coupled analysis responses at the critical components. Unlike primary notching, there are numerous independent factors related to the mode in question which can influence these responses - making the secondary notching verdict difficult to pronounce.

Starting from the responses at the interface derived previously from coupled analysis, recovery of the responses within the spacecraft at some observation DOF,  $o$ , requires only the FRF between the connection and observation DOF  $\mathbf{X}_{oc}^S$ . In the case of a spacecraft analysed with fixed-interface boundary conditions, the recovery is achieved using the dynamic transmissibilities  $\mathbf{T}_{oc}^S$  leading to:

$$\ddot{\mathbf{u}}_o(\omega) = \mathbf{T}_{oc}^S(\omega) \ddot{\mathbf{u}}_c(\omega) \quad [5-104]$$

where, according to Eq. [5-43]:

$$\mathbf{T}_{oc}^S(\omega) \approx \sum_{k=1}^n T_k^S(\omega) \tilde{\mathbf{T}}_{oc,k}^S + \mathbf{T}_{oc,res}^S \quad [5-105]$$

We see that what is important here, are the effective transmissibilities of the modes between the interface and the critical observation DOF. In other words, the effective transmissibilities play the same role in secondary notching that the effective masses play in primary notching.

During the computational analysis of the mathematical models for notching, the verifications performed on the effective masses for primary notching are therefore complemented by verifications performed on the effective transmissibilities for the secondary notching.

### 5.5.3 Simple example

To illustrate the notion of secondary notching in relation to primary notching, consider the simple model in Figure 5-42, derived from the model of Figure 5-36.

- $M_1$  represents a large subsystem of 1000 kg within the spacecraft (e.g. telecom platform) producing a single mode at 40 Hz, leading to  $K_1 = 6.32 \times 10^7$  N/m.
- $M_2$  represents a component of 10 kg attached to the subsystem (e.g. antenna reflector) producing a single mode at 80 Hz, leading to  $K_2 = 2.53 \times 10^6$  N/m.
- $M_{res}$  represents the rest of the spacecraft considered rigid for simplification, and therefore without influence.

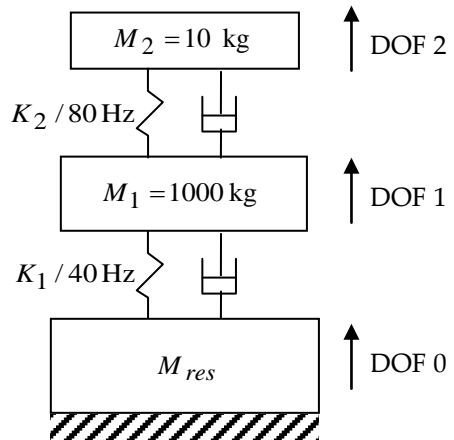


**Figure 5-42: Simple model for illustrating primary and secondary notching**

The two modes of the model have the following characteristics:

- mode 1:  $f_1 = 39.74$  Hz  $\approx 40$  Hz       $\Phi_{i1} = \begin{bmatrix} 1 \\ 1.3275 \end{bmatrix}$        $\tilde{M}_{00,1} = 1008.9$  kg       $\tilde{T}_{20,1} = 1.3219$
- mode 2:  $f_2 = 80.53$  Hz  $\approx 80$  Hz       $\Phi_{i2} = \begin{bmatrix} -0.0133 \\ 1 \end{bmatrix}$        $\tilde{M}_{00,2} = 1.1$  kg       $\tilde{T}_{20,2} = -0.3219$

The 10 kg of  $M_2$  have been largely absorbed by the effective mass of mode 1 which can justify a primary notching as illustrated previously. On the other hand the effective mass of mode 2 is much smaller due to the opposing motion between  $M_1$  and  $M_2$  and therefore cannot be a candidate for primary notching.

The dynamic mass and dynamic transmissibility (between DOF 0 and 2) are plotted in Figure 5-43 for an amplification factor of  $Q_k = 25$ .

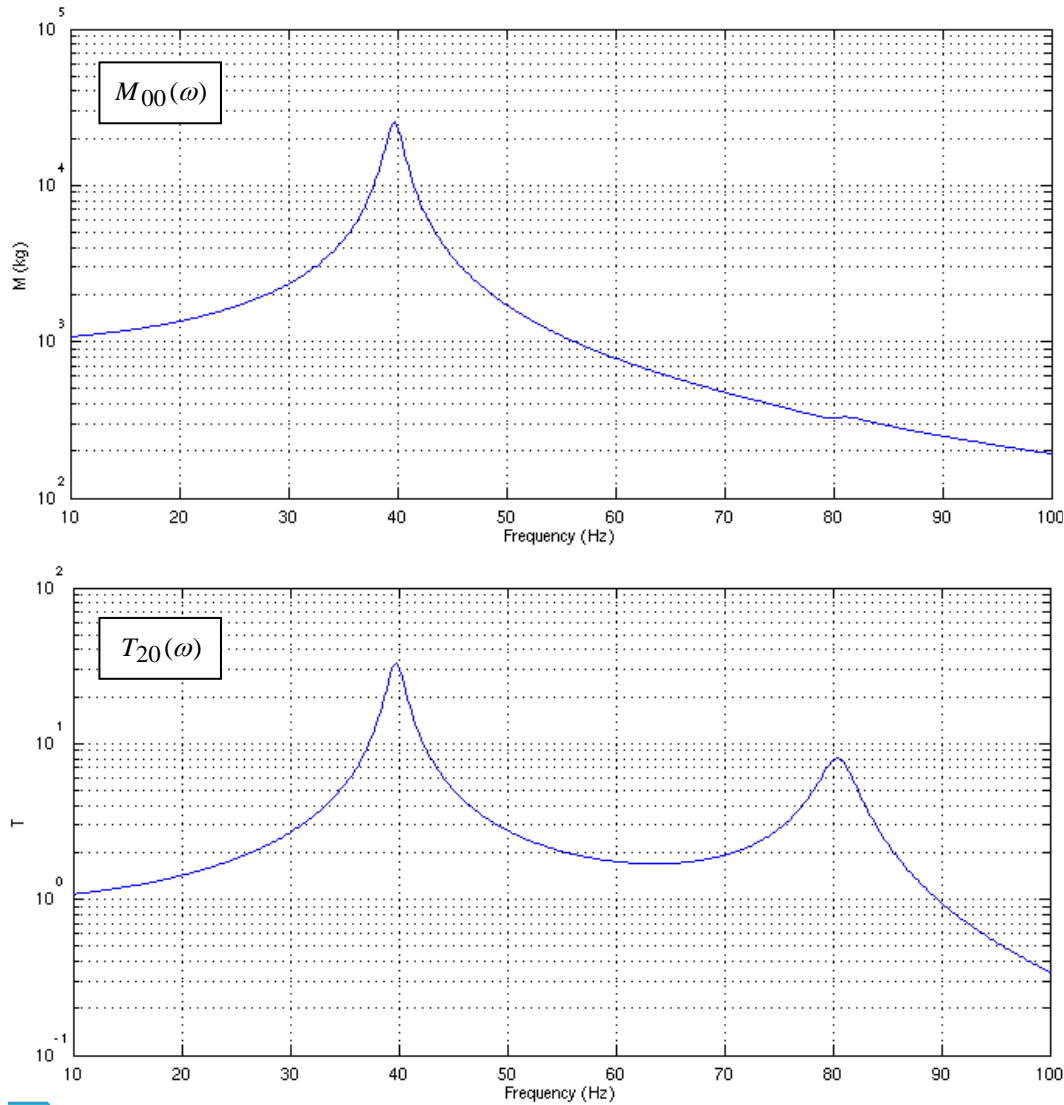


**Figure 5-43: Responses of the simple model**

We see that the dynamic mass reaches a maximum of 25000 kg near 40 Hz while providing only 330 kg near 80 Hz - with nearly no contribution from mode 2. Moreover, the resonance and antiresonance of mode 2 are masked by the contribution of mode 1 because of its very small effective mass.

By contrast the dynamic transmissibility with respect to DOF 2 has a maximum value of 33 near 40 Hz but also a value of 8 near 80 Hz where the contribution of mode 2 dominates because of its non-negligible effective transmissibility. In consequence:

- mode 1 near 40 Hz generates a strong reaction at the interface likely to require primary notching which significantly reduces the displacements at the interface and as a result protect the component. This notching should be justifiable by coupled analysis. The relevant modal parameter in this case is the effective mass,
- mode 2 near 80 Hz has very little influence at the interface, yet yields relatively high response levels at the component (e.g. 8 g at the component for 1 g of excitation). A secondary notching is therefore necessary if the response level risks damaging the component. This notching may or may not be justifiable by coupled analysis, depending on the response levels near this frequency. The relevant modal parameter in this case is the effective transmissibility.

This example clearly illustrates the distinction between primary and secondary notching by analysis of the relevant modal parameters.

## 5.5.4 Conclusions on notching in sine tests

Primary notching can be justified in the presence of spacecraft modes with large effective masses capable of producing strong reaction forces at the interface. Notching results from the simulation of flight events, inherently transient, by an equivalent sine sweep whose enveloped levels neglect the reactions of the spacecraft.

Secondary notching can be considered in the case of critical components which are unprotected by the primary notching. The relevant modal parameters in this case are the effective transmissibilities between the interface and the components. Although less well-known than the effective masses, the effective transmissibilities are used in the same way for FRF analysis and can be analysed at the same time in the mathematical models.

## 5.6 Random tests

### 5.6.1 Issues on random tests

Sine tests with notching verified by coupled analysis are used to qualify a structure with respect to its low-frequency environment where the number of normal modes remains limited and therefore a modal approach can be used for analysis. For a spacecraft during the launch phase as described in Section 5.2.2, this covers thrust transients and particular phenomena such as gusts or the POGO effect. However the other remaining events involve a much wider range of frequencies:

- Pyrotechnic shocks, due to the different separation events, are generally simulated using dedicated test apparatus in order to reproduce as well as possible the various types of propagation throughout the structure.
- Vibro-acoustic environment experienced at lift-off or during transonic flight where the spacecraft is excited simultaneously at its base and by the surfaces exposed to the acoustic field under the fairing. The simulation of the vibro-acoustic environment is covered in this section.

Ideally one would like to simulate both mechanical and acoustic excitations simultaneously but the required test setup consisting of a shaker table in an acoustic chamber would be too complex and costly, especially since one of the excitation sources often dominates the other as described below:

- For compact structures, i.e. small physical dimensions with respect to the mass, the mechanical excitation concentrated within a reduced volume dominates over the acoustic field which acts on relatively small surfaces.
- For extended structures, i.e. large dimensions with a limited structural mass, the mechanical excitation propagates ineffectively along the various structural paths whereas the acoustic excitation acts efficiently on the large surfaces.

The first case (compact structures) corresponds to equipment or small subsystems – especially those which are not in direct contact with exposed surfaces. This case can also apply to small compact spacecraft. Here, mechanical tests are preferable.

The second case (extended structures) corresponds to large spacecraft with walls and platforms of significant surface area. It also includes light subsystems with large exposed surfaces such as solar panels or antenna reflectors which are particularly sensitive to the acoustic field. Here, acoustic tests are preferable, although one should be cautious with the parts of the structure near the base where the mechanical excitation is directly injected.

Unlike low-frequency sine tests, these wide-band tests are more difficult to simulate numerically for response predictions or coupled analysis. This difficulty is accentuated as the frequency range

increases in that the phenomena become more and more localized and affect smaller structures. This in turn requires a more highly refined FE mesh with a large number of excited DOF in the case of an acoustic field, and a greater number of modes to be considered. Other methods such as SEA can be of help but at the cost of simplifying assumptions.

As for the mechanical qualification of equipment, in the absence of reliable analysis techniques we can consider an approach by extrapolation of response levels obtained from previous system level acoustic tests and compiled into a data base. This technique has been used since the 1980's [17] but requires constant data base updating due to evolutions in launcher and spacecraft design.

We could also consider equivalent sine tests using the SRS as an equivalence criterion as mentioned in Section 5.2.5.4. However this is not without risk since the equivalence is based entirely on the behaviour of a 1-DOF system and an assumption on the value of the Q factor which could result in highly different excitation levels and profiles. This approach should therefore be avoided.

Finally, we could consider a base excitation random vibration test instead of an acoustic test in a reverberant chamber. Although both are random in nature, the distribution of the excitation is very different leading to large differences in the responses as illustrated in the following paragraph using a simple example. Here again we conclude that it's better to remain as close as possible to the actual environment.

## 5.6.2 Mechanical equivalence example

Testing a structure on a mechanical vibrator in order to simulate an acoustic environment requires replacing a distributed force excitation (due to the acoustic pressure) by a mechanical excitation at the base of the structure. The acoustic forces are more or less correlated depending on the frequency and the distance between them whereas the vibrator imposes a global motion at the base. These two types of excitation are therefore quite different making it difficult to establish an equivalence between them. The following example illustrates this point.

Consider the 2-DOF system of mass  $M$  shown in Figure 5-44 representing in a very simplified manner a structure with a uniformly distributed mass excited by uniformly distributed acoustic forces.

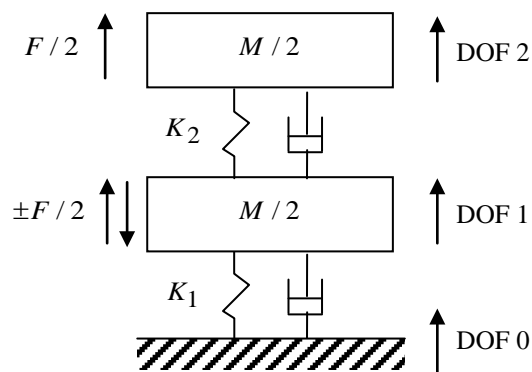


**Figure 5-44: Simple model for mechanical equivalence**

For a given mode  $k$  with an eigenvector of  $\Phi_{ik} = \begin{bmatrix} \Phi_{1k} \\ \Phi_{2k} \end{bmatrix}$  excited at its natural circular frequency  $\omega_k$  we wish to determine the base acceleration  $\ddot{u}_0$  equivalent to the two acoustic pressure forces. Starting with the modal effective parameters and leading to the modal terms we obtain the following expression.

$$\ddot{u}_0(\omega) = \frac{\omega_k^2 (\tilde{G}_{21,k} \pm \tilde{G}_{11,k})}{\tilde{T}_{10,k}} \frac{F(\omega)}{2} = \frac{\omega_k^2 (\tilde{G}_{22,k} \pm \tilde{G}_{12,k})}{\tilde{T}_{20,k}} \frac{F(\omega)}{2} = \frac{\Phi_{2k} \pm \Phi_{1k}}{\Phi_{1k} + \Phi_{2k}} \frac{F(\omega)}{M} \quad [5-106]$$

From the above expression we can derive the numerical results displayed below in Figure 5-45.

Case	$\Phi_{1k}$	$\Phi_{2k}$	$\frac{M \ddot{u}_0(\omega)}{F(\omega)} = \frac{\Phi_{2k} \pm \Phi_{1k}}{\Phi_{1k} + \Phi_{2k}}$						
Forces in phase : $F/2 + F/2$	any		1						
Opposing Forces : $F/2 - F/2$									
$K_1 \approx K_2$	<ul style="list-style-type: none"> <li>• Mode 1</li> <li>• Mode 2</li> </ul>	<table style="margin-left: auto; margin-right: auto;"> <tr> <td style="text-align: center;">1</td> <td style="text-align: center;">2</td> <td style="text-align: right;">1/3</td> </tr> <tr> <td style="text-align: center;">-2</td> <td style="text-align: center;">1</td> <td style="text-align: right;">3</td> </tr> </table>	1	2	1/3	-2	1	3	
1	2	1/3							
-2	1	3							
$K_1 \ll K_2$	<ul style="list-style-type: none"> <li>• Mode 1</li> <li>• Mode 2</li> </ul>	<table style="margin-left: auto; margin-right: auto;"> <tr> <td style="text-align: center;">1</td> <td style="text-align: center;">1.1</td> <td style="text-align: right;">0.05</td> </tr> <tr> <td style="text-align: center;">-1.1</td> <td style="text-align: center;">1</td> <td style="text-align: right;">21</td> </tr> </table>	1	1.1	0.05	-1.1	1	21	
1	1.1	0.05							
-1.1	1	21							

**Figure 5-45: Mechanical equivalence results for simple model**

For the case of forces in phase the equivalent acceleration is given by  $F/M$  regardless of the mode shape, and therefore the two types of excitation have similar effects.

For the case of opposing forces the equivalence is more complex as described below:

- The equivalent acceleration is less than  $F/M$  for the first mode since the two mode shape components are in phase (same sign). This is because the mode is more excitable by the base than by the acoustic forces whose combined effect is antagonistic. A reduced base excitation level would therefore be required – similar to a notching.
- The equivalent acceleration is greater than  $F/M$  for the second mode since the two mode shape components have opposing phases (different signs). This is because the mode is less excitable by the base than by the opposing acoustic forces which have a cumulative effect. An increase in the base excitation level is therefore necessary – the opposite of a notching.
- When the base stiffness is relatively low ( $K_1 \ll K_2$ ) as in the case of a suspension, the above effects are amplified. The first mode or suspension mode is highly excitable by the base thus requiring a significantly reduced base excitation level. The second mode (internal mode) is nearly unexcitable by the base yet extremely excitable by the opposed acoustic forces.

We see that the results vary greatly depending on the shape of the mode and the phases (signs). This is due to the considerable difference between the excitation types – global motion imposed at the base instead of pressure forces distributed over the structure. The elaboration of an equivalence strategy is therefore case dependent and can only be achieved by a thorough knowledge of the structure and the excitation.

### 5.6.3 Notching in random vibration tests

Notching for random vibration testing is analogous to notching for sine testing in that they both seek to reduce response levels at the principal resonances to avoid overtesting. Newton's second law of motion expressed by Eq. [5-96] is always applicable between the excited structure ( $S$ ) and the exciting structure ( $L$ ) - for all types of excitation. It can therefore be applied at all levels of analysis - for the instrument of the satellite as well as for the equipment item of the instrument. The key factor is the relationship between the dynamic masses in question. Notching is justified by a large dynamic mass of the excited structure opposed to a small dynamic mass of the exciting structure resulting from a filtering effect of its modes (see Section 5.4).

The difference between the LV/SC level and more local levels (equipment/unit) resides in the knowledge of the excitation forces. In the case of LV/SC analysis, the excitation is well known due to the use of detailed models of the launch vehicle with well-defined load cases, leading to a reliable coupled analysis in the useful frequency range. On the other hand, when considering more local phenomena intrinsic to smaller structures, the excitation is more complex with a higher range of frequencies. This precludes the use of deterministic analysis in favour of random vibration tests.

In the absence of sufficiently detailed models of the exciting structure and its excitation, statistical analyses have been performed on system-level (satellite) acoustic tests. They provide specifications in terms of acceleration PSD at the base of the equipment items as a function of the governing parameters such as their mass or position within the satellite [17] [35].

This approach assumes that the items are rigid, such that their dynamic mass can be represented simply by their static mass. However, this assumption does not likely hold for large instruments and equipment items in which case it is valid to resort to notching in order to adapt the specifications as justified above.

Since the coupled analysis involves the dynamic masses, the notching is based on the interface forces which need to be estimated from tests using one of several techniques. Ideally the interface forces should be measured directly via load cells. Although load cells may require the use of a special fixture at the specimen/shaker table interface whose presence should not modify the overall dynamic behaviour, they provide an accurate and reliable measurement.

If force measurement is not possible, then the interface forces can be estimated by combining the measured internal accelerations with an analytically derived mass operator according to Newton's second law (see Section 8.4.3.7.2). However this mixed approach has its share of difficulties such as the representativity of the internal motion by the accelerometers, taking into account the phase from cross-correlations and the validity of the model used to derive the mass operator.

In the case of an equipment item located within an instrument to be tested, and susceptible to require notching, the direct measurement of reaction forces at the equipment/instrument interface is in general not possible. However, they can be estimated in one of several ways depending on available data - with a preference for experimental data for the best representativity. By measuring the accelerations at the equipment interface, we only need the dynamic masses in order to estimate the reaction forces by Newton's second law. The force PSD is obtained using Eq. [5-38] where  $W_{xx}(\omega)$  is the acceleration PSD and  $H_{yx}(\omega)$  the dynamic mass. The dynamic masses can be estimated by one of several techniques:

- By the use of a dedicated sine or random test performed directly on the equipment in question from which the dynamic masses can be obtained. As mentioned previously, the use of load cells, simpler at the equipment level, is preferable to the use of internal acceleration measurements combined with a mass operator.

- In the absence of a dedicated test, the acceleration measurements on the equipment (if available!) can be combined with a mass operator to estimate the reaction forces. In practice, the number of accelerometers on the equipment is very limited, and therefore does not allow representing the motion beyond the first modes. In this case a model of the equipment could be used instead to estimate the dynamic mass - assuming however that it is sufficiently representative. In any event, the idea is to make the best use of all available analytic and experimental data.

Similar to the LV/SC coupled analysis case, if the exciting structure has its first significant modes located well below those of the excited structure, then these modes naturally filter the excitation and improve the ratio of the dynamic masses at the resonances of the excited structure - thus favouring the presence of notching. As illustrated in the example of Figure 5-37 a frequency ratio of 2 between the principal modes is already sufficient for two structures with an order of magnitude difference in mass.

For example, an instrument of approximately 100 kg in a satellite of several tons could justify a notching for a first mode near 100 Hz. Or at a more local level, an equipment item of approximately 10 kg in the above mentioned instrument could also justify a notching for a mode around 200 Hz as illustrated below in Figure 5-46.

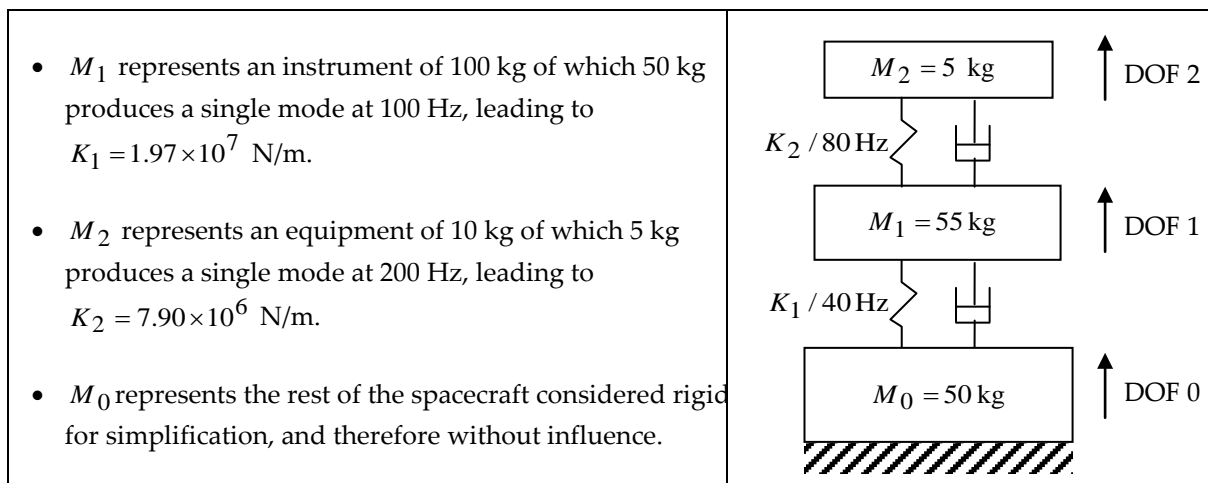


**Figure 5-46: Simple instrument/equipment model for random notching**

The two modes of the model have the following characteristics:

- mode 1 :  $f_1 = 90.2$  Hz  $\approx 100$  Hz  $\Phi_{i1} = \begin{bmatrix} 1 \\ 1.2555 \end{bmatrix}$   $\tilde{M}_{00,1} = 59.7$  kg  $\tilde{T}_{20,1} = 1.2234$
- mode 2 :  $f_2 = 211.1$  Hz  $\approx 200$  Hz  $\Phi_{i2} = \begin{bmatrix} -0.1141 \\ 1 \end{bmatrix}$   $\tilde{M}_{00,2} = 0.3$  kg  $\tilde{T}_{20,2} = -0.2234$

The dynamic mass and dynamic transmissibility (between DOF 0 and 2) are plotted in Figure 5-47 using an amplification factor of  $Q_k = 25$ .

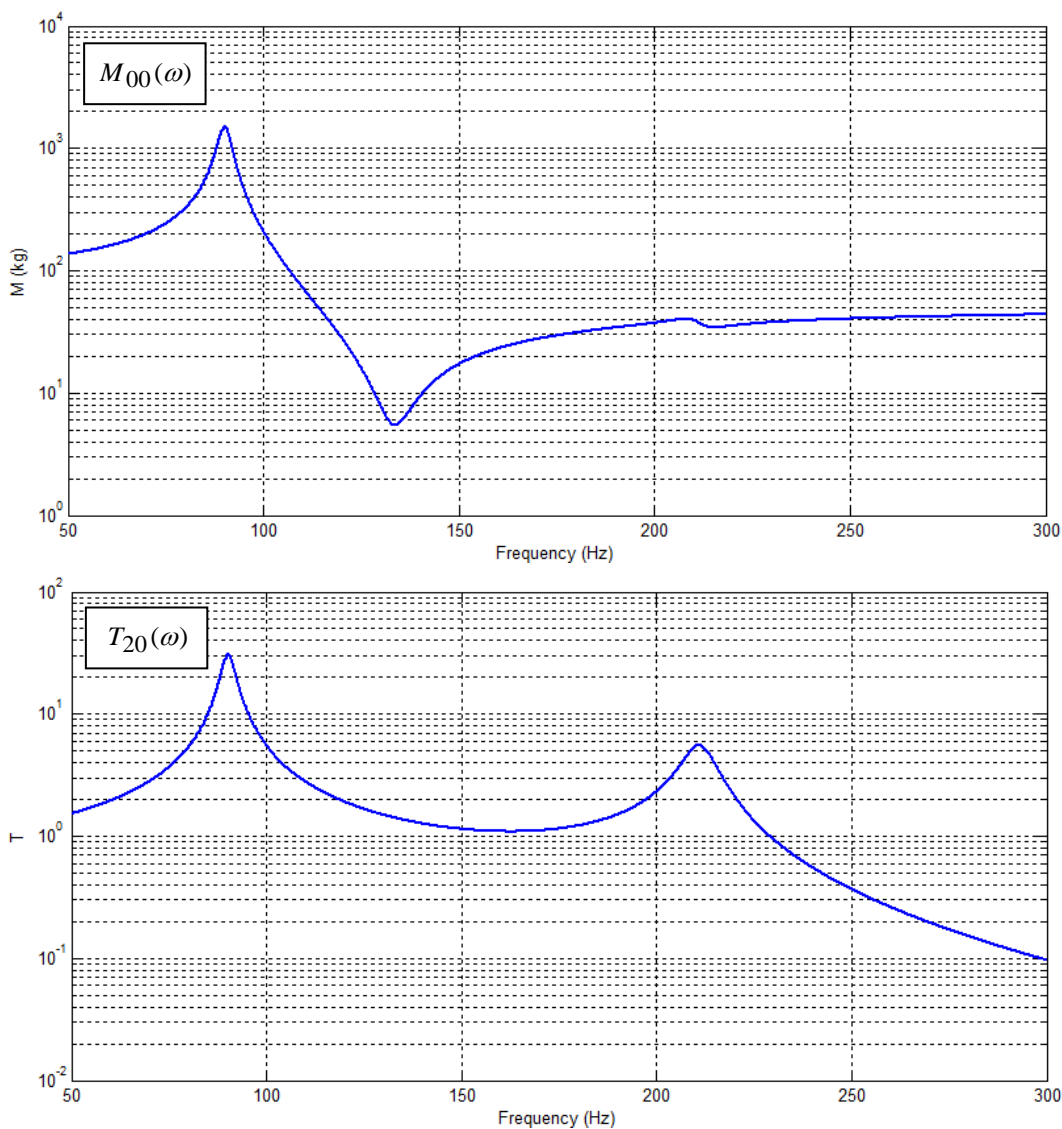


**Figure 5-47: Responses of the instrument/equipment model**

With respect to the instrument, the notching at 100 Hz is primary (although it would be secondary with respect to the satellite), whereas the notching at 200 Hz is secondary. Note that the distinction between primary and secondary notching is relative to the level at which the analysis is being performed.

However, what this simple example fails to show is that in practice, a secondary mode of the exciting structure may coincide more or less with a principal mode of the excited structure. In this case the ratio of the dynamic masses decreases and as a result the notching is no longer justified. This condition should be verified by coupled analysis using available models.

In general, as the level of analysis becomes more local, the number of modes increases, leading to more complex behaviour involving the combined effects of amplification and filtering, and increased difficulty in terms of understanding and prediction.

During random testing, the input acceleration PSD is reduced or notched so as to keep the interface force equal to or below a specified limit. The specification may be expressed as a PSD spectrum or as an RMS value derived from the quasi-static CoG acceleration (see Section 5.3.4.6). Additional information on this topic can be found in [36].

If the specification is given as a force PSD,  $S_{ff}^*(\omega)$ , then the notching can be determined by comparing the specification to the predicted or measured force PSD,  $S_{ff}(\omega)$  obtained using the un-notched input acceleration  $S_{aa}(\omega)$ . The notched input  $\hat{S}_{aa}(\omega)$  is obtained simply by multiplying the input acceleration PSD by the notching coefficient  $C_n(\omega)$  according to:

$$\hat{S}_{aa}(\omega) = S_{aa}(\omega) C_n(\omega) \quad \text{with} \quad C_n(\omega) = \min\left(1, \frac{S_{ff}^*(\omega)}{S_{ff}(\omega)}\right) \quad [5-107]$$

If, on the other hand, the specification is given as an RMS value, many different notching coefficients  $C_n(\omega)$  satisfying the specification can be constructed. The simplest case is when the structure has a single mode with large effective mass producing a dominant peak in the force PSD  $S_{ff}(\omega)$ . In this case the peak can be simply clipped in order to obtain the specified RMS value. The width of the clipped region can be defined manually or automatically using criteria such as half-octave, half-power and trough-to-trough.

If several modes have important contributions then there exists a greater degree of flexibility in the choice of notching. For example each peak could be clipped proportionally to its contribution, or treated individually in order to introduce a desired amount of conservatism.

## 5.7 Practical aspects of modal effective masses

In the preceding sections the role of the dynamic mass of the spacecraft has been shown to be of particular importance in the context of coupled analysis with the launch vehicle. Indeed, the motion at the LV/SC interface is solely a function of the dynamic mass as illustrated in Eq. [5-96] via Newton's Second Law.

Using mode superposition, the dynamic mass can be expressed in terms of the effective masses according to Eq. [5-97]. These same effective masses play a fundamental role in primary notching as illustrated throughout Section 5.4, and therefore require a practical as well as theoretical understanding.

Effective masses can be derived from base excitation sine and random vibration tests under certain conditions. First, they require force measurements in addition to the acceleration measurements since they are obtained from the ratio force/acceleration. Table 5-4 summarizes the different techniques available for force measurement along with their advantages and drawbacks. Further details can be found in Section 8.4.

Table 5-4: Force measurement techniques

Method	Advantages	Drawbacks
Load Cells (FMD)	- Accuracy	- Added mass and flexibility of test fixture at interface - Limited availability
Strain Gages	- Simple setup	- Difficulties with calibration and sensitivity
Coil Current (electrodynamic shaker)	- No test fixture required	- Single force measurement along excitation direction - Influence of mobile mass of shaker - Limited accuracy
Mass Operator	- Requires only acceleration measurements	- Finite element model required - Accuracy depends on quality of FE model

The above techniques allow determining the 6 reaction components (3 forces and 3 moments) at the base of the spacecraft assuming a statically determinate (rigid) interface. The one exception is the coil current technique which provides only a single force component along the excitation direction, yet which can be easily used as a cross check for the other techniques.

A run along a given direction  $\underline{r}$  therefore allows determining the 6 components  $\mathbf{M}_{r\underline{r}}(f)$  (column  $\underline{r}$ ) of the dynamic mass matrix  $\mathbf{M}_{rr}(f)$  as a function of frequency  $f$ . Analysis of these 6 components allows identifying the effective masses as well as certain terms of the rigid body mass matrix.

The six effective masses  $\tilde{\mathbf{M}}_{r\underline{r},k}$  for each mode  $k$  are identified using modal identification methods as indicated in Section 5.3.2.2. From these values, the entire 6x6 effective mass matrix  $\tilde{\mathbf{M}}_{r\underline{r},k}$  matrix can then be deduced via the participation factors  $\mathbf{L}_{r\underline{k}}$  of Eq. [5-49].

The six terms (column  $\underline{r}$ ) of the rigid body mass matrix  $\overline{\mathbf{M}}_{rr}$  of Eq. [5-108] are obtained by extrapolating the six dynamic mass components to their static ( $f = 0$ ) values  $\overline{\mathbf{M}}_{r\underline{r}} = \mathbf{M}_{r\underline{r}}(0)$ .

$$\overline{\mathbf{M}}_{rr} = \begin{bmatrix} M & 0 & 0 & 0 & M z_G & -M y_G \\ 0 & M & 0 & -M z_G & 0 & M x_G \\ 0 & 0 & M & M y_G & -M x_G & 0 \\ 0 & -M z_G & M y_G & I_{xx} & -I_{xy} & -I_{xz} \\ M z_G & 0 & -M x_G & -I_{xy} & I_{yy} & -I_{yz} \\ -M y_G & M x_G & 0 & -I_{xz} & -I_{yz} & I_{zz} \end{bmatrix} \quad [5-108]$$

$M, (x, y, z)_G, I_{xx} \dots$  mass, centre of gravity and inertias with respect to interface

From a single run (column 1, 2 or 3), the mass  $M$  and two of the centre of gravity coordinates can be determined. A second run is therefore necessary in order to deduce the third centre of gravity coordinate. As for the inertia values, they cannot be obtained since the excitation is restricted to translational directions only. However, they can be estimated by the summing the identified effective inertias according to the following summation rule resulting in a truncation error equal to the residual term  $\mathbf{M}_{rr,res}$ .

$$\bar{\mathbf{M}}_{rr} = \sum_k \tilde{\mathbf{M}}_{rr,k} + \mathbf{M}_{rr,res} \quad [5-109]$$

The above identification of effective and static masses provides a nearly complete characterisation of the dynamic mass matrix and which can be used to update and validate the FE model for subsequent coupled analysis and primary notching predictions.

Finally, in the case of a modal survey test with applied force excitation as mentioned in Section 5.3.2.2, the same effective and static masses can be identified from force measurements at the interface using Eqs. [5-50] to [5-54], even with only a single excitation point.

## 5.8 Conclusions

Examination of the various flight events affecting the spacecraft illustrates the importance of the dynamic loads and justifies the need for detailed analysis depending on the specific environment – harmonic, transient and random.

The state of the art methods in numerical analysis were first presented and illustrated using several examples for a better understanding of the physical phenomena. These methods were then applied to the coupled LV/SC system to examine the qualification of structures by sine, random and acoustic tests. Several topics covered only partially in the literature have been treated more thoroughly and include in particular:

- Influence of the sine sweep rate on the structural responses (see Section 5.2.3.3)
- Use of the shock response spectrum (SRS) in coupled analysis to compensate for differences between test measurements and predictions (see Section 5.4.4)

Performing sine tests to qualify primary structures in the low-frequency environment, which is essentially transient, requires the use of notching to avoid overtesting near the principal resonances. The equivalent sine excitation levels are deduced from the SRS – a step which should be performed with precaution because of the various underlying assumptions. Several possible improvements to this current practice have been suggested in Section 5.2.4.

Qualification of structures in the random environment raises several specific problems such as difficulties in numerical analysis for test prediction due to the extended frequency range, and the choice between mechanical base-excitation and acoustic excitation – given that both exist in reality and depend on the type of structure. The problem should be handled case by case with the help of experience acquired from previous projects.

## 5.9 References

- [1] Girard A., Roy N., Structural Dynamics in Industry, John Wiley & Sons, ISBN 978-1-84281-004-2, 2008.
- [2] Lalanne C., Mechanical Vibration & Shock Analysis, John Wiley & Sons, 2nd Ed., 2009, Vol 1: Sinusoidal vibration, Vol 2: Mechanical Shock, Vol 3: Random Vibration, Vol 4: Fatigue Damage, Vol 5: Specification Development.
- [3] Roy N., Girard A., Revisiting the Effect of Sine Sweep Rate on Modal Identification, European Conference on Spacecraft Structures, Materials & Environmental Testing, Noordwijk, The Netherlands, 20-23 March 2012.

- [4] Alexander J. E., The Shock Response Spectrum – A Primer, Proceedings, IMAC-XXVII, Orlando, Florida, Feb 9-12, 2009.
- [5] Calvi A., Nali P. – Some Remarks on the Reduction of Overtesting during Base-Drive Sine Vibration Tests of Spacecraft – Proc. of the ECCOMAS Conf. on Computational Methods in Structural Dynamics and Earthquake Engineering - Rethymno, Crete, Greece, June 2007.
- [6] Girard A., Finkler O., Shock characterization by amplitude/duration spectrum, 1st European Conference on Launcher Technology, Toulouse, 14-16 December 1999, Proceedings 471-477.
- [7] Girard A., Lucas T., Bugeat L-P., Shock synthesis from amplitude/duration spectrum, Proceedings (CD-Rom) of 19th AIAA International Communications Satellite Systems Conference, Toulouse, 17-20 april 2001.
- [8] Crandall S.H., Mark W.D., Random vibration in mechanical systems, Academic Press, 1963.
- [9] Papoulis A., Probability, Random Variables, and Stochastic Processes, 1965, McGraw-Hill Kogakusha Ltd.
- [10] Lin Y.K., Probabilistic Theory of Structural Dynamics, 1976, Robert E. Krieger Publishing Company, ISBN 0-88275-377-0.
- [11] Thomson W.T., Dahleh M.D., Theory of Vibration with Applications, 1998, 5<sup>th</sup> edition, Prentice Hall, ISBN 0-13-651068-X.
- [12] Lin Y.K., Cai G.Q., Probabilistic Structural Dynamics, 1995, McGraw\_Hill, ISBN 0-07-038038-4.
- [13] Wirsching P.H., Paez T.L., Ortiz H., Random Vibrations, Theory and Practice, 1995, John Wiley and Sons, ISBN 0-471-58579.
- [14] Gatti P.L., Probability Theory and Mathematical Statistics for Engineers, 2005, Spon Press, ISBN 0-41525172-9.
- [15] Sun J.Q., Stochastic Dynamics and Control, Monograph Series on Nonlinear Science and Complexity, Volume 4, 2006, Elsevier, ISBN 0-444-52230-1.
- [16] Wijker J.J., Random Vibrations in Spacecraft Structures Design, Theory and Applications, Springer, ISBN 978-90-481-2727-6, 2009.
- [17] Girard A., Moreau D., Derivation of Satellite Equipment Test Specifications from Vibration and Acoustic Test Data, ESA Journal, Vol. 10, 1986/3.
- [18] Lefevre Y.M., Bonetti J.C., Girard A., Roy N., Calvi A., Real-Time Modal Identification Techniques for Improved Satellite Vibration Testing, European Conference on Spacecraft Structures, Material and Mechanical Testing, Toulouse, 11-13 December 2002.
- [19] SPACEHAB STA Modal Survey Test Report, IABG Report B-TR 0777/22, Ottobrunn, Germany, June 1992.
- [20] Calvi A., Notarnicola M., Fleming P. – Experimental Verification of SPACEHAB Dynamic Mathematical Model – Proc. of the International Conference on Structural Dynamics Modelling, Milton Keynes, U.K., pp. 239-257, July 1993.
- [21] Calvi A., Finite Element Model Updating in Structural Dynamics Using Design Sensitivity and Optimisation, Ph.D. Thesis, College of Aeronautics, Cranfield University, Cranfield, UK, October 1998.
- [22] Hurty W.C., Dynamic Analysis of Structural Systems Using Component Mode Synthesis, AIAA Journal, Vol.3, No.4, 1965, pp. 678-685.
- [23] Craig R. R., Bampton M. C. C., Coupling of Substructures for Dynamic Analysis, AIAA Journal, Vol. 6, No. 7, 1968, pp. 1313–1319.

- [24] Craig R.R., Structural Dynamics – An Introduction to Computer Methods, Wiley, New York, 1981, pp. 350, 351, 478-480.
- [25] Rixen D.J., Generalized Mode Acceleration Methods and Modal Truncation Augmentation Methods, AIAA paper 2001-1300, April 2001.
- [26] Fransen S.H.J.A., An Overview and Comparison of OTM formulations on the Basis of the Mode Displacement Method and Mode Acceleration Method, Wordwide Aerospace Conf. and Technology Showcase, MSC.Software Corp., Paper 17, 2002.
- [27] Fransen S.H.J.A., Data Recovery Methodologies for Reduced Dynamic Substructure Models with Internal Loads, AIAA Journal, Vol. 42, No. 10, October 2004.
- [28] Dickens J.M., Nakagawa J.M., Wittbrodt M.J., A Critique of Mode Acceleration and Modal Truncation Augmentation Methods for Modal Response Analysis, Computers and Structures, Vol.62, No.6, 1997, pp.985-998.
- [29] Dickens J.M., and Stroeve A., Modal Truncation Vectors for Reduced Dynamic Substructure Models, AIAA paper 2000-1578, April 2000.
- [30] Carrington H. and Ottens H., A Survey of Data on Damping in Spacecraft Structures, Technical Report ESRO CR-539, ESTEC contract No. 2142173, Fokker Space and NLR, Noordwijk, The Netherlands, 1975.
- [31] Fransen S.H.J.A., et al., Damping Methodology for Condensed Solid Rocket Motor Structural Models, IMAC paper 62, Jacksonville, Feb. 2010.
- [32] Rittweger A., et al., Coupled Dynamic Load Analysis with Different Component Damping of the Substructures, 59th International Astronautical Congress, Glasgow, UK, 2008.
- [33] Albus J., Dieker S., Beuchel W., A Consistent Approach of Damping Treatment in Coupled Dynamic Analysis and Test, 62nd International Astronautical Congress, Cape Town, SA, 2011.
- [34] Vaquer Araujo X., Fransen S., Germès S., Thiry, N., Validation of Equivalent Viscous Damping Methodologies, 12<sup>th</sup> European Conference on Spacecraft Structures, Materials & Environmental Testing, Noordwijk, The Netherlands, 20-23 March 2012.
- [35] Girard A., Dupuis P.E., Imbert J.F., Moreau D., Updating of European Satellite Equipment Test Specifications from Vibro-Acoustic Test Data, 46<sup>th</sup> International Astronautical Congress, Oslo, October 2-6, 1995.
- [36] Girard A., Newerla A., Methodology for Notching in Random Vibrations, 4<sup>th</sup> International Symposium on Environmental Testing for Space Programmes, Liège, June 12-14, 2001.
- [37] Bellini M., Paron A., Tizzani L., Design of an integrated Stowage Platform, new structure for Modules of International Space Station: Application of a new approximated methodology to define the design loads, 11th European Conference on Spacecraft Structures, Materials & Mechanical Testing, September 2009.
- [38] Fackler W., Equivalence techniques for vibration testing, Shock & Vibration Information Center, 1972.
- [39] Nali P., An investigation on the spacecraft design loads cycles and sine vibration test, Stage Final Report TEC-MCS/2006/1362/In/AC, ESA, Noordwijk, The Netherlands, March 2006.

# 6

# Launcher / spacecraft coupled loads analysis

## 6.1 Introduction

### 6.1.1 General aspects

The launcher/spacecraft coupled loads analysis (CLA) is the process of calculating the loads caused by launch transients. The term “loads” refers to the set of internal forces, displacements and accelerations that characterise the structural response to the applied forces.

The CLA is a key task of the loads cycle process. The main goal is to produce a bounding set of loads for design or verification. It is performed to check that a spacecraft design is compliant with the overall mechanical environment generated by a launcher during all flight phases and to ensure that the launcher mission can be achieved.

The launch service can be provided with a vehicle under development, subjected to a partial qualification or facing flight or production issues. Therefore, coupled loads analyses may also be necessary from the launcher point of view, as predictions should demonstrate that the launcher specifications are not exceeded.

In practice the CLA consists of a number of transient or harmonic dynamic analyses performed by using the mathematical models of the payloads and launcher, coupled together, and by applying the forcing functions for the different launch events. The excitation may be of aerodynamic origin (wind, gust, buffeting at transonic velocity) or may be induced by the propulsion system (e.g. thrust build up or tail-off transient, acoustic loads in the combustion chambers). The low frequency domain typically ranges from 0 to up 100 Hz and corresponds to the frequency content of the forcing functions used in the CLA.

The dynamic response of the spacecraft determines launch loads within the spacecraft. Of primary interest are the spacecraft interface accelerations and interface forces. The interface accelerations can be used to derive an equivalent sine spectrum at the spacecraft interface. The interface forces can be used to calculate the “equivalent accelerations” at the spacecraft centre of gravity (quasi-static accelerations). Also of large interest is the recovery of the internal responses which are used to verify the structural integrity of the spacecraft and its components. In the test verification phase of the spacecraft, the equivalent sine spectrum computed by means of CLA is used to locally reduce the prescribed level from the launcher user’s manual at specific resonant frequencies (“notching”). This might be required to avoid possible damage to the spacecraft structure itself or its components (e.g. solar arrays, booms).

The spacecraft structural design is then evaluated for these loads. In practice the CLA results define the limit loads for the spacecraft (subsystems and units) and show compatibility with the launch vehicle for all critical phases of the mission.

Coupled loads analyses may be performed by launcher and/or spacecraft authorities depending on the project maturity, the flight worthiness assessment philosophy and the industrial organization between prime- and sub-contractors for instance. On one hand, a spacecraft authority may be interested in conducting preliminary coupled loads analyses and to process a very large amount of data in order to assess the design of its system in details. On the other hand, the launcher authority usually performs the final verification cycle to conclude on the vehicle operability and to cross-check spacecraft predictions. Attention should be paid to the functional organization between commercial or governmental spacecraft operators, governmental agencies, spacecraft and launcher industries, private and national laboratories as the CLA is a major contributor to the spacecraft design and qualification process efficiency. Indeed, the expected amount of interactions may be limited by commercial issues (proprietary data) and regulation issues (e.g. ITAR controlled projects) for instance.

### **6.1.2 Launch loads and terminology used in the CLA process**

A spacecraft structure is normally subjected to high mechanical loads during launch. A spacecraft is subjected to launch loads through two paths: accelerations transmitted through the launch vehicle interface and direct acoustic noise through the shroud. Acceleration through the interface consists of steady state, low frequency transient and random vibrations. The acoustic noise also generates random vibrations in the spacecraft. The LV/SC CLA covers the low frequency mechanical environment of the launch phase. Launch starts when the booster engines ignite (lift-off) and ends with the separation of the propulsion device that puts the spacecraft in its orbit.

Figure 6-1 shows the steady state (or “static”) longitudinal acceleration for an Ariane 5 launch vehicle versus time. During the stage burns, the acceleration gradually increases because of the decreasing mass of propellant. In the context of the CLA the static acceleration is normally understood as CoG “mean acceleration” of the LV/SC system assumed as rigid body. The mean acceleration does not include the dynamic response, or vibration, to transient short-duration forces. Since the mean acceleration is equivalent, by definition, to the quasi-static component of the acceleration, this would justify the term “quasi-static acceleration” used as synonymous of “static acceleration”.

Furthermore it should be also noted that a “static acceleration” is by definition an acceleration of constant magnitude and direction with respect to the structure. This definition cannot be rigorously applied to the full launch phase as depicted for example in Figure 6-1 since the acceleration does not have constant magnitude. This could further justify the fact the LV/SC system “static acceleration” is also indicated as “quasi-static acceleration”. In practical cases, however, it is always possible to identify a “static” (i.e. constant magnitude and direction) acceleration for a specific time or limited period.

In general the steady state acceleration should not be identified as the acceleration associated to a quasi-static event, i.e. an event generated by external forces which change slowly with time so that the dynamic response of the structure is not significant. In fact, even if a large part of the launch phase can be considered as quasi-static, a number of events are transients. For example Figure 6-2 reports a case of axial acceleration at LV/SC I/F for the engine cut-off event. Nevertheless it should be noted that in some contexts the term “quasi-static acceleration” indicates the acceleration associated to quasi-static events.

Moreover in general the steady state acceleration should not be identified as the acceleration associated to the rigid body modes in the structural dynamic response analysis performed by a mode superposition scheme. Within that scheme the total response of the system can be split into “rigid” and “elastic”, making reference to the modal DOF which are involved. In order to clarify the above concept let us consider a zero-mean “high frequency” oscillation of the engine thrust. It would produce a rigid body motion acceleration of the system without changing its static acceleration, i.e. without changing the quasi-static component of the acceleration.

Finally it should be noted that the structural response calculated in the launcher-spacecraft CLA can be considered as the sum of “static” and “dynamic”(see Section 5.3.4.9) or “rigid” and “elastic” contributions, the two approaches, as mentioned, not being mathematically equivalent. The practical importance of separating the contributions relies on the fact that major uncertainties are assumed to be in the dynamic (or elastic) response and uncertainty factors are normally used for calculating the spacecraft limit loads.

In conclusion and summarizing, the launch loads environment is made up of a combination of steady-state, low-frequency transient and higher-frequency vibro-acoustic loads. The LV/SC CLA covers the low frequency mechanical environment of the launch phase. To determine the combined loads for any phase of the launch, low- and high-frequency dynamic components are superimposed upon the steady-state component. In practice when determining the limit loads, consideration are given to the timing of the loading events; the maximum steady state and dynamic events can occur at different times in the launch and may provide too conservative estimate if combined. Also, the frequency band of the vibro-acoustic energy to be combined is evaluated on a case-by-case basis.

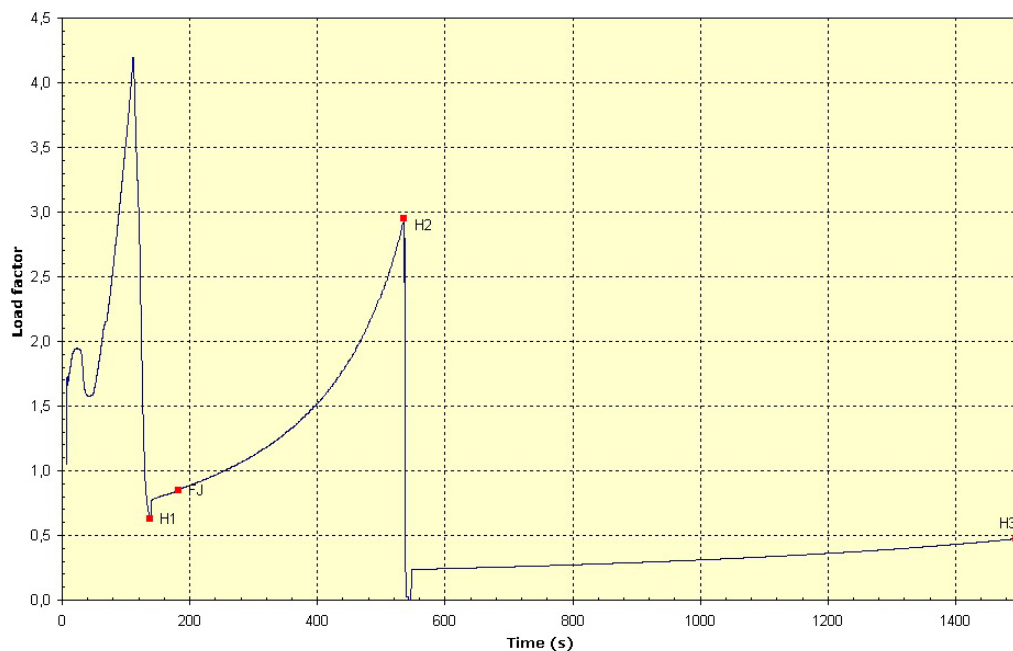


**Figure 6-1: Ariane 5 typical longitudinal static acceleration**

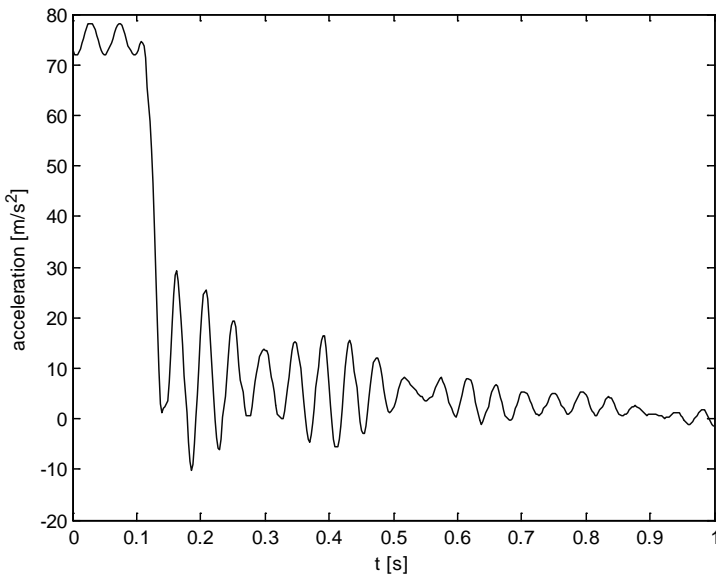


**Figure 6-2: Example of axial acceleration at LV/SC I/F for engine cut-off**

### 6.1.3 The role of the CLA within the loads cycle

Loads cycles, introduced in Section 4.2, are the iterative processes of predicting and assessing structural loads. Since the CLA allows the calculation of loads caused by the launch transients, it is then clear the key role played by the CLA within any loads cycle process.

In principle coupled loads analyses can be performed anytime in the development process of a new spacecraft, depending on the spacecraft project mission and maturity. Coupled loads analyses may be considered as:

- *a single (and normally mandatory) indicator of compliance* between the overall environment specified by the launcher at the interface with the spacecraft and the strength of the spacecraft structure
- *an integrated tool in the design process* of a spacecraft structure

In the first case the compliance is assessed by comparing flight-like FEM predictions to overall spacecraft measurements from the most representative vibration tests possible plus static tests on the primary structure. The launcher specifications are checked to be consistent with its required performance. They are defined as the envelope of the worst environments resulting from parametric predictions associated with a whole domain of flight worthy spacecraft. As a result and as a first approximation, one spacecraft may have to demonstrate its compliance with completely different spacecraft behaviours, since it has to withstand overall specifications. However, notching specifications are usually allowed by the launcher authority to relax the approach robustness. This is a “winning” process since no major flight qualification issue should be raised as long as the spacecraft behaviour remains close to the specifications. There are also industrial and commercial advantages of specifying overall environments. The verification cycle from predicting CLA loads to analysing sine tests results may be unique and very fast. The spacecraft development is separated from specific launcher requirements. The worst flight environment may be another argument for selecting a launch service. This is the Ariane 5 philosophy.

In the latter case CLA predictions are used as a major input to the spacecraft structure definition rather than as a single verification step in a spacecraft flight qualification process. Many runs may be performed to converge on a satisfactory architecture. There is no specification to withstand at the

common interface with the launcher. Spacecraft modal survey tests results are used for the purpose of validating the entire FEM only. As a result, there is no consideration on notching at system level. This is a refined approach which yields an efficient but sufficient design at worst, as it may be tuned to the specific need of a single launcher. This is a NASA philosophy which is applied to the Space Shuttle programme for instance.

## 6.2 The phases of the CLA process

### 6.2.1 Introduction

The main phases of the CLA process according to [1] are:

- Development of FE models of the launcher and spacecraft, here generically referenced as “substructures”
- Identification of the loads parameters, i.e. selection of important response parameters for the definition of the Output Transformation Matrices (OTMs) for design evaluation and structural verification
- FE models reduction, normally in Craig-Bampton format
- Generation of OTMs for the substructure models
- Modal coupling of the models to generate a system model
- Application of forcing functions for the different launch events and calculation of the generalized responses at “small” time increments over the duration of the event
- Calculation of responses by OTMs
- Calculation of maximum and minimum values for each load parameter
- Concomitant CLA load cases combination

Other specific activities performed within the CLA process are the following:

- Mathematical model verification and databases integration
- Damping synthesis
- Post-processing
- Uncertainty management
- Results review, verification and validation
- Reporting

The CLA duration may vary significantly depending on the spacecraft mission and characteristics, the launcher life phase and the amount of desired outputs. Although computational resources are often available, evaluating whether raw predictions are relevant or not remains an important engineering operation. Considering that a reasonable budget is also a key indicator to the project success, one can understand that mission analysis cycles on a proven launcher may vary from several weeks for recurrent commercial spacecraft to several months for uncommon scientific payloads.

## 6.2.2 Parameters driving the CLA process

The quality of the coupled loads analysis results is as important as the relevance of the tests selected for spacecraft qualification. The main factors for accurate and efficient predictions are:

- The launcher and the spacecraft dynamic FE model accuracy in terms of natural frequencies, mode shapes and damping. CLA load cases may be computed in the frequency domain where any missed sub-structures coupling and/or any missed excitation interaction may result in highly underestimated predictions.
- The spacecraft damping assumptions used in the coupled system mathematical model on the launcher side (refer to Sections 5.3.4.7 and 5.3.4.8). Inappropriate diagonal damping assumptions may produce numerical aberrations.
- The modelling of the physical load cases on the launcher side, especially concerning the excitation profile definition (Section 6.4.3 for instance). Non predictive excitation schemes may be corrected by coefficients for simplicity, however their use can interfere with the CLA output post processing.
- The OTM computation scheme (Section 5.3.4) and the output selection relevance (Section 6.3.4). The output computation method should be consistent with the obtained output parameters for best accuracy.
- These parameters are discussed in details in the following sections.

## 6.2.3 Mathematical model verification and database integration

Coupled loads analyses may be performed using commercial (NASTRAN by MSC or PERMAS by Intes for instance) and/or homemade solvers and post-processing toolkits. The conversion (e.g. from NASTRAN to PERMAS) of the spacecraft (or launcher) mathematical model provided by the relevant authority and its integration to the software database constitute a major step in the coupled loads analysis. Although it may be required to first assess the compliance of the FEM with some specified software capabilities (OTM formulations, matrices sizes, damping schemes, etc.), it may also be important to perform cross-check tests with respect to the selected choice of modelling. The purpose is to guarantee:

- the correct mathematical formulation of the expected spacecraft outputs (rigid body characteristics, effective masses, internal harmonic responses, etc.). Those parameters are systematically compared before and after the conversion and the integration for the Ariane 5 CLA for instance, using the data sets from both launchers and spacecraft authorities.
- the proper understanding of the spacecraft FEM dynamic behaviour (e.g. transfer functions) since it is a main factor of CLA output validation.

## 6.2.4 Finite element model reduction

Once the quality of the mathematical model has been verified, the generation of the reduced model and corresponding Output Transformation Matrices (OTM) can be performed. Model reduction is particularly beneficial when the number of DOF following reduction is small compared to the initial number of DOF. The basic theory of commonly used reduction techniques (Craig-Bampton, Mode Acceleration and Mode Displacement methods and Mode Truncation Augmentation) is presented in Section 5.3.4.

## 6.2.5 Checks on the Craig-Bampton matrices and OTM

Once generated, the Craig-Bampton matrices and the OTM are checked. The reduced model should satisfy the verification criteria described in Section 16.6. A comparison with the initial FEM demonstrates that the dynamic characteristics are the same. To verify the OTM, a sine excitation can be applied to both the initial and reduced models to verify that the responses are similar. The check should be performed for all types of recovered output.

## 6.2.6 Frequency cut-off for computed modes

The coupled system normal modes are computed up to a frequency which is consistent with the excitation frequencies of the physical phenomenon to be predicted. A practical assumption is  $\sqrt{2} \times f$ , where  $f$  is the upper bound of the frequency content of the excitation, such that the dynamic amplification of the nearest truncated mode is small. As an example, modes for the Ariane 5 2<sup>nd</sup> acoustic mode load case are computed up to 80 Hz for an excitation varying from 33 to 53 Hz (refer to Section 6.4.5.5). Both launcher and spacecraft models may also be reduced to allow efficient coupled loads analysis. A 70 Hz cut-off frequency is used for coupled analysis with the Space Shuttle. Reducing the launcher model may also be required for proprietary considerations when the coupled loads analysis is not performed by the launcher authority.

## 6.2.7 Coupling of the launcher and spacecraft models

The coupling of the launcher and spacecraft models is performed considering the applicable launcher requirements. For example, the interface points should have the same coordinates and the same output coordinate systems. The quality of the assembled model should be also checked in accordance with Section 16.6.

## 6.2.8 Calculation of the generalized responses

Generalized coordinates may be computed in the time domain, the frequency domain or by a random analysis depending on the load case assumptions, as idealized from the physical phenomenon (Section 6.4.3). Moreover, the quasi-static acceleration of the launcher may not be included in the CLA forcing function, resulting in additional post-processing to be performed when evaluating CLA results. This is a major CLA assumption to be verified prior to comparing QSL, interface and OTM outputs parameters with spacecraft design and/or spacecraft tests results.

## 6.2.9 Determination of the physical responses

Once the generalized coordinates are determined, the spacecraft physical responses (accelerations, displacements and interface forces) are computed by mode superposition. QSL and internal responses may be then directly deduced from these responses. It is worth mentioning that responses can also be computed from direct integration as an alternative to the modal approach.

## 6.2.10 Post-processing

The launcher / spacecraft interface loads are converted into QSL (e.g. equivalent accelerations at the spacecraft CoG). The QSL are combined between all concomitant load cases and for all types of environments (refer to Section 6.4.4). Interface accelerations from transient and random load cases are converted into equivalent sine responses from a shock spectra treatment (see Section 5.2.4.3).

Load cases may be defined as the envelope of several sub-load cases of the same nature. For instance, for the Ariane 5 launcher, 290 possible configurations of the Mach and angle-of attack of the launcher are computed to conclude on the rear part buffeting environment. Depending on the parameter, limit responses may be defined as the envelope of all sub-load cases or as the worst value from each sub-load case. For instance, for the Ariane 5 rear part buffeting presented in Section 6.4.5.3, the spacecraft QSL is equal to the worst prediction among the 290 sub-load cases whereas the spacecraft interface equivalent sine level is defined as the envelope of 290 SRS.

The CLA predictions normally include all uncertainties from the launcher side. CLA predictions are limit-level predictions.

### 6.2.11 Uncertainty factors

The uncertainties associated with the models and forcing functions used in the launcher-spacecraft coupled loads analysis are accounted for when the results are delivered to the spacecraft developer. Hence a model factor is introduced that covers those uncertainties. In case a launcher is still under development or has been launched only very few times, uncertainties associated with the validation of the launcher FEM and forcing functions are covered as well. This is done by the development factor.

In order to account for those uncertainties two factors are usually used:

- models and loads factor  $K_M$
- development factor  $K_D$

The product of these uncertainty factors yields the global uncertainty factor that is normally applied to the dynamic part of the CLA responses. The dynamic results produced by the launcher authority include this factor unless specified otherwise. It should be noted that some launcher authorities also apply this factor to the static part of the response. An example of uncertainty factors applied to VEGA CLA results at the time that the vehicle was still under development is given in Table 6-1. Once the launcher structural model and forcing functions are fully correlated component-wise as well as from flight, the development factor is reduced to 1.0.

**Table 6-1: Example of uncertainty factors used in Coupled Loads Analysis**

	P80 Ignition	P80 Pressure oscillations	Standard gust 4.5 m/s		Solid motor ignition  Z23
			MACH1	$Q_{MAX}$	
<b>Model factor (KM)</b>	1.20	1.20	1.20	1.20	1.20
<b>Development factor (KD)</b>	1.25	1.25	1.25	1.25	1.25
<b>Global factor (KM)*(KD)</b>	1.50	1.50	1.50	1.50	1.50

## 6.3 CLA output and results evaluation

### 6.3.1 Overview

Coupled loads analyses are usually performed to produce accelerations and loads at the interface with the launcher and inside the spacecraft. Displacements within the spacecraft, at spacecraft interface or in the fairing may also be computed. This output is used to verify the spacecraft design and conclude on its flight worthiness.

*Launcher/Spacecraft interface loads* are converted into QSL and compared with the launcher specifications. If a specification is exceeded and a discussion on the conservatism of the prediction and/or loads is out of the question, QSL should be converted into interface mechanical fluxes and compared with equivalent static tests results (refer to Section 6.4.5) including the applicable factors of safety. These QSL are defined as the combination of all concomitant events (refer to Section 5.2.7).

*Launcher/Spacecraft interface accelerations* are defined as the envelope of all limit predictions per spacecraft axis, including fixed values for non-simulated load cases. This envelope is upgraded to a qualification level and compared to the sine tests results at the same excitation level (refer to Section 6.5.3). Non-simulated load cases may correspond to load cases which have been computed during the launcher development, for which the whole domain of investigated spacecraft remains qualified (e.g. under the launcher specification) or for which the environment remains "reasonable" (e.g. much lower than the specification), meaning that no specific computation is required for the CLA. Non-simulated load cases may also correspond to some phenomena which are identified during flight but for which no simulation can be performed (because the phenomenon is not understood) or for which a simulation is useless given the poor level of response. Whatever the reason, non-simulated load cases are covered by a fixed value of QSL and interface acceleration (see straight lines in Figure 6-8) to which the spacecraft has to demonstrate compliance by test.

*Spacecraft OTM predictions* should be corrected first by the adequate spacecraft FEM uncertainty factor (refer to Section 6.2.11). CLA predictions usually include any modelling uncertainty coming from the launch system, from its FEM to the load case simulation assumptions. The spacecraft FEM correction may vary from one OTM parameter to another and may be applicable to a limited number of load cases. It should be consistent with the correlation results between the modal and/or vibration tests FEM predictions and the associated ground test results. Internal accelerations should be defined as the envelope of all limit predictions. Internal loads and CoG accelerations should be combined together for all the concomitant events predicted. Non-simulated load cases may be evaluated inside the spacecraft by transposing its associated interface fixed value. Internal acceleration should be at last upgraded to a qualification level and compared to consistent sine tests results whereas internal loads and CoG accelerations should demonstrate the adequate safety margin with respect to each subsystem design load.

Interface results might also be provided at the spacecraft interface to allow post-CLA base excitation analyses. This is a useful approach for spacecraft secondary structures and equipment items which may not have been included in the OTM and which may need a more thorough analysis following the vibration tests (refer to Section 6.5.3). Acceleration and loads may also be extracted from coupled loads analyses at some launcher interface locations for mission qualification purposes.

Predictions should be computed inside the spacecraft at a reasonable number of meaningful locations. The selection of outputs should be performed with care to guarantee the most efficient CLA post-processing taking into account available computational resources and technical testing limitations (Section 6.3.2). Extended CLA may be performed to generate additional output provided that the additional OTM is consistent with both stiffness and mass matrices of the spacecraft reduced model.

### 6.3.2 Guidelines to response parameter selection

The list of parameters should be discussed in the context of each program to correctly identify the most interesting parameters for design and to minimize the time necessary to perform the CLA. This includes in particular, the CoG accelerations of the spacecraft, the main parts of the structure and the main equipment items. Interface forces and, if necessary, stress of some elements, can be requested. Displacements of some locations to verify the clearance with respect to the launcher (i.e. fairing or cargo bay), and relative displacements between points in the spacecraft, where possible problems of clearance can occur, are examples of parameters that should be considered.

### 6.3.3 Equivalent sine input

From the SRS of the acceleration at the LV/SC interface it is possible to calculate the Equivalent Sine Input (ESI) [2]. The ESI plot is usually considered as the minimum threshold for the notching, after having included the applicable qualification factor. The ESI produces the same peak response level as the transient input in a SDOF system. It is obtained by dividing the SRS by the dynamic amplification  $Q$ . Considerations about the use are reported in [2]. See Section 5.2.6 for theory and limitations.

### 6.3.4 Computation of static components from OTM

In general, the forcing functions for CLA are defined without static components resulting in the dynamic responses only. If the forcing function includes the static part, techniques are used to remove its contribution from the computed responses (see Section 5.3.4.9) in order to obtain only the dynamic responses. Following this procedure, the uncertainty factors can be applied to the dynamic part of the response and the equivalent sine spectra can be computed without static contributions. For the dimensioning of the spacecraft, the spacecraft developer is interested in the responses that take into account the effect of static acceleration of the launcher for the dimensioning flight events. To obtain the QSL one can simply add the dynamic and static accelerations as follows:

$$QSL = K_M \ K_D \ddot{u}_{CoG_{dynamic}} + \ddot{u}_{CoG_{static}} \quad [6-1]$$

To obtain the total displacements (or element forces or stresses) consisting of dynamic and static components the data recovery procedure can be extended as follows:

$$\begin{aligned} \begin{Bmatrix} x_j \\ x_i \end{Bmatrix} &= K_M \ K_D \cdot \left( DTM_1 \begin{Bmatrix} \ddot{x}_{j_{dynamic}} \\ \ddot{q}_p \end{Bmatrix} + DTM_2 x_{j_{dynamic}} \right) + DTM_1 \begin{Bmatrix} \ddot{x}_{j_{static}} \\ 0 \end{Bmatrix} + DTM_2 x_{j_{static}} = \\ K_M \ K_D \begin{Bmatrix} x_j \\ x_i \end{Bmatrix}_{\text{dynamic}} &+ \begin{Bmatrix} x_j \\ x_i \end{Bmatrix}_{\text{static}} \end{aligned} \quad [6-2]$$

In Eq. [6-2] we assumed that the mode acceleration method was used to compute the OTMs of the spacecraft (See Section 5.3.4). The static acceleration vector of the spacecraft interface  $\ddot{x}_{j_{static}}$  can be constructed easily from the static launcher axial acceleration for the flight event considered. The static interface deformation  $x_{j_{static}}$  is computed from a static analysis of the CB-model of the spacecraft mounted on the payload adapter and loaded by the applicable gravitational field (launcher axial acceleration in opposite direction). Obviously the static contribution can also be obtained directly by static gravitational analysis of the spacecraft FEM mounted on the payload adapter. In case of the application of mode displacement method or residual vector method this is even required since the static modal displacements due to gravitational loads cannot be obtained from static analysis with the CB-model.

### 6.3.5 Relative displacements

Sometimes the clearance between the spacecraft and launcher fairing is very limited. Under specific circumstances it may even occur that the spacecraft slightly exceeds the allowable payload volume defined in the launcher user manual. Under these circumstances the clearance between fairing and spacecraft under flight loads is investigated. This can be done by computing the relative displacements between points on the spacecraft FEM that are closest to the fairing as illustrated in Figure 6-3.

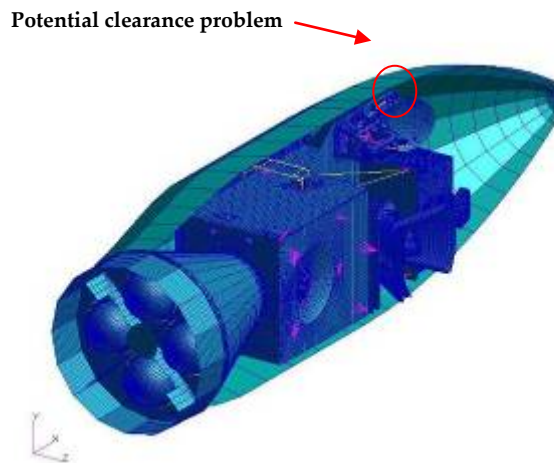


Figure 6-3: Example of spacecraft with potential clearance problem

### 6.3.6 Interface mechanical fluxes and overfluxes

#### 6.3.6.1 Introduction

The QSL at the SC CoG calculated in the CLA (or reported in the launcher user manual) can be processed in order to verify the design of the structural components securing the SC to the LV. A clamp band is usually employed for securing the SC and LV adapters through appropriate preloading. The LV adapter typically has a conical shape. LV core structures are mostly cylindrical and thus they are efficient only if no local effects are introduced along the adapter [1]. Such local effects can be caused by structural discontinuities (e.g. stringers and cut-outs) which lead to significant non-uniform load paths [3], SC CoG eccentricity and more in general by non-cylindrical structures. Some simple formulae can be used in order to calculate the corresponding theoretical fluxes (or *line loads*) from QSL (see Section 6.3.6.2). In the general case, the actual fluxes are different from the theoretical ones. The so-called overfluxes (or *line loads peak*) represent such differences and typically vary along the interface perimeter. Overfluxes can be predicted by FE analyses (see Figure 6-5 for an example) or quantified experimentally by tests. The actual values of overfluxes should stay within a range specified by the launch authority. Some launch authorities furnish some predetermined constant values of additional fluxes (each one pertaining to a specific flight event) in order to envelop the distribution of overfluxes with confident margin [4].

The maximum value of the LV/SC interface tensile axial flux is the input for the assessment of the clamp band tension. In fact, a specific clamp band tension is necessary to safely keep the SC attached to the LV during the launch phase until the scheduled separation, or during ground testing. Section 6.3.6.3 illustrates how to perform such evaluation while Section 6.3.6.4 provides a numerical example.

### 6.3.6.2 Theoretical interface fluxes and overfluxes

In this section the formulae for calculating the theoretical interface line loads from the QSL at CoG are discussed. A thin walled cylindrical structure is assumed.

The longitudinal force  $N$  can be calculated as:

$$N = M_{SC} \ QSL_{Longitudinal} \quad [6-3]$$

Where  $M_{SC}$  is the spacecraft mass.

The bending moment  $M_{Lat}$  at the LV/SC interface can be obtained as:

$$M_{Lat} = M_{SC} \ QSL_{Lateral} \ h_{CoG} \quad [6-4]$$

where  $h_{CoG}$  is the longitudinal coordinate of the static CoG with respect to the LV/SC interface. Eqs. [6-3] and [6-4] are used again in Section 6.4.6.

Figure 6-4 illustrates the I/F axial fluxes  $f^N$  and  $f^{M_{Lat}}$  along the adapter's ring, which are generated by  $N$  and  $M_{Lat}$  respectively. Furthermore, given  $R_{IF}$  the radius of the adapter's ring and  $\theta$  the angle defined in Figure 6-4, the following formulae can be written.

$$N = f^N 2\pi R_{IF} \Rightarrow f^N = \frac{N}{2\pi R_{IF}}. \quad [6-5]$$

The flux generated by  $M_{Lat}$  is harmonic function of  $\theta$ :

$$f^{M_{Lat}} = f_{max}^{M_{Lat}} \cos(\theta) \quad [6-6]$$

This lead to:

$$M_{Lat} = \int_0^{2\pi} (f_{max}^{M_{Lat}} \cos^2(\theta) R_{IF}^2) d\theta \Rightarrow f_{max}^{M_{Lat}} = \frac{M_{Lat}}{\pi R_{IF}^2}. \quad [6-7]$$

Compressive forces and fluxes are expressed here using a *positive* sign in accordance with the convection used in the Rockot User's Guide [3]. This is in contrast to the Ariane 5 User's Manual which uses a *negative* sign for compressive forces and fluxes.

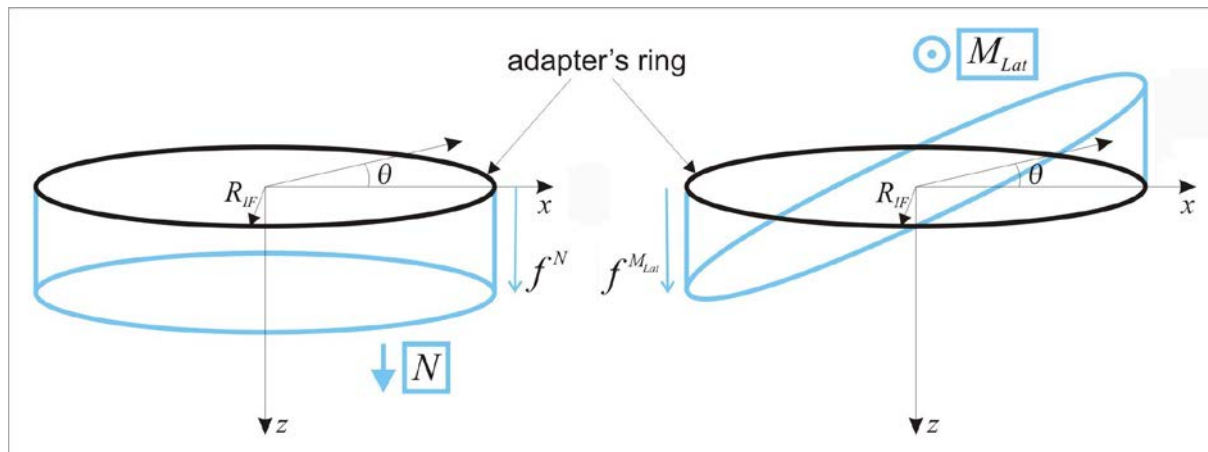


**Figure 6-4: Theoretical load distribution of axial fluxes along the adapter's ring in the case of axial force (left) and bending moment (right)**

In accordance with the superposition principle for linear systems, and assuming that axial force and bending moment act simultaneously, it follows that  $f_{1,2}$  are the maximum and minimum values of the I/F axial flux:

$$f_{1,2} = f^N \pm f_{\max}^{M_{Lat}} = \frac{N}{\pi D} \pm \frac{4M_{Lat}}{\pi D^2} \quad [6-8]$$

with  $D = 2R_{IF}$ .

The equivalent axial forces  $A_{1,2}$  which are produced by considering  $f_{1,2}$  constant along the interface adapter's ring can be obtained from Eq. [6-9]. These forces might be used for clamp band verification test purposes, for example by applying these loads during a static load or sine burst test, respectively.

$$A_{1,2} = f_{1,2} \pi D = N \pm \frac{4M_{Lat}}{D} \quad [6-9]$$

The theoretical quantities calculated above are typically different from the real ones. A more realistic flux distribution can be obtained through FE analysis and by using a detailed FE model of the spacecraft. An example of it is provided in Figure 6-5, which refers to a specific load case of Sentinel 3 satellite ( $QSL_{Longitudinal} = 2.08g$ ,  $QSL_{Lateral} = 2.34g$ ). In the figure, the theoretical axial flux is compared with the axial flux calculated by FE analysis, which is indicated as "Actual". The difference between the two curves gives the distribution of the axial overflux (line loads peak). An *overflux factor* can be defined as.

$$\text{overflux factor} = \frac{\max(|actual\ flux|)}{\max(|theoretical\ flux|)} \quad [6-10]$$

For the purpose of the SC I/F verification,  $f_{1,2}$  and  $A_{1,2}$  should be multiplied by the *overflux factor* and by the appropriate design factor  $K_D$ , leading to the maximum and minimum Design Limit Load value of the I/F axial flux and force:

$$f_{1,2}^{DLL} = f_{1,2} \cdot \text{overflux factor} \cdot K_D \quad [6-11]$$

$$A_{1,2}^{DLL} = A_{1,2} \cdot \text{overflux factor} \cdot K_D \quad [6-12]$$

As additional remark, the mean value of the curves in Figure 6-5 is positive and this reveals the constant compressive contribution of  $f^N$ .

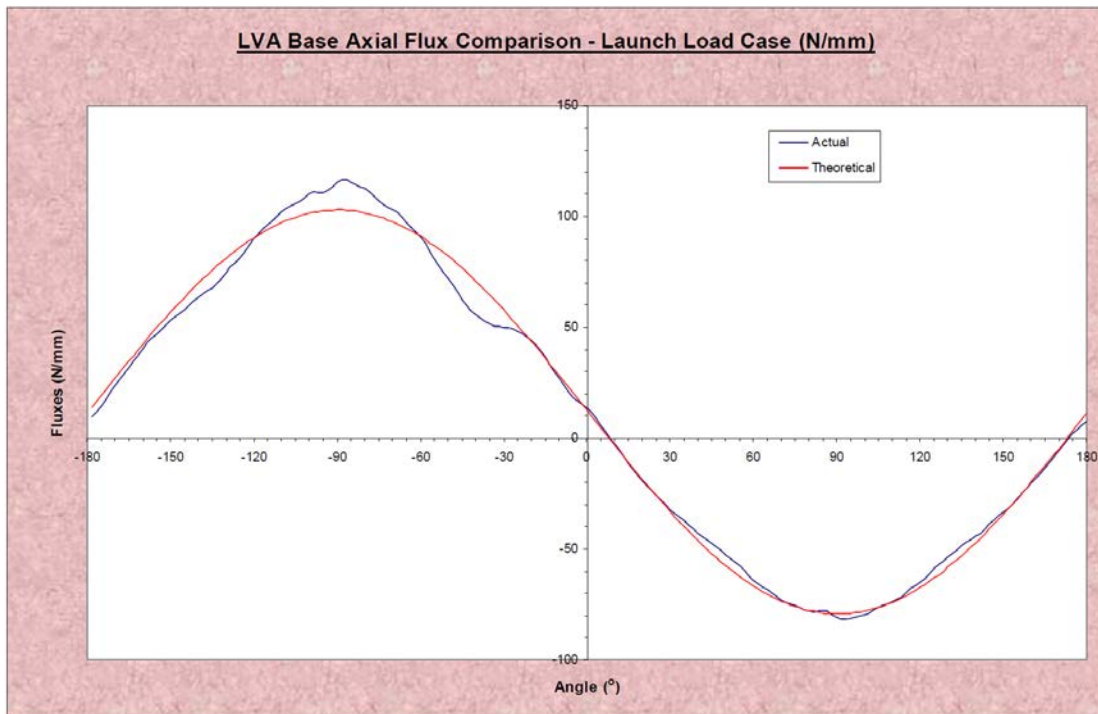


**Figure 6-5: A comparison between theoretical and FEM-predicted axial flux (courtesy of RUAG Schweiz AG)**

### 6.3.6.3 Clamp band tension assessment

Compressive loading is normally not critical for safely maintaining the attachment of the SC to the LV by means of the clamp band. Differently, an assessment is performed for tensional loading, which could cause the separation of the SC from the LV adapter. Adequate clamp band tension is applied in order to avoid this. The steps for verifying the value of the clamp band tension are illustrated and discussed in the following.

According to Figure 6-6, assuming the total flux orthogonal to the surface of contact, the design maximum radial flux  $f_{\max}^{\text{radial}}$  on the clamp band is given by [5] :

$$f_{\max}^{\text{radial}} = 2|f_2^{\text{DLL}}| \frac{\tan(\alpha) - \mu_{cl}}{1 + \mu_{cl} \tan(\alpha)} \quad [6-13]$$

where  $\alpha$  is the angle between the clamp band bearing surface and the ring-plane and  $\mu_{cl}$  the friction coefficient between the clamp and the flanges. When neglecting the effect of friction ( $\mu_{cl} = 0$ ), the above equation reverts to a simpler form:

$$f_{\max}^{\text{radial}} = 2|f_2^{\text{DLL}}| \tan(\alpha) \quad [6-14]$$

The absolute value in Eqs. [6-13] and [6-14] takes into account that  $f_2^{\text{DLL}}$  is a tensile flux.

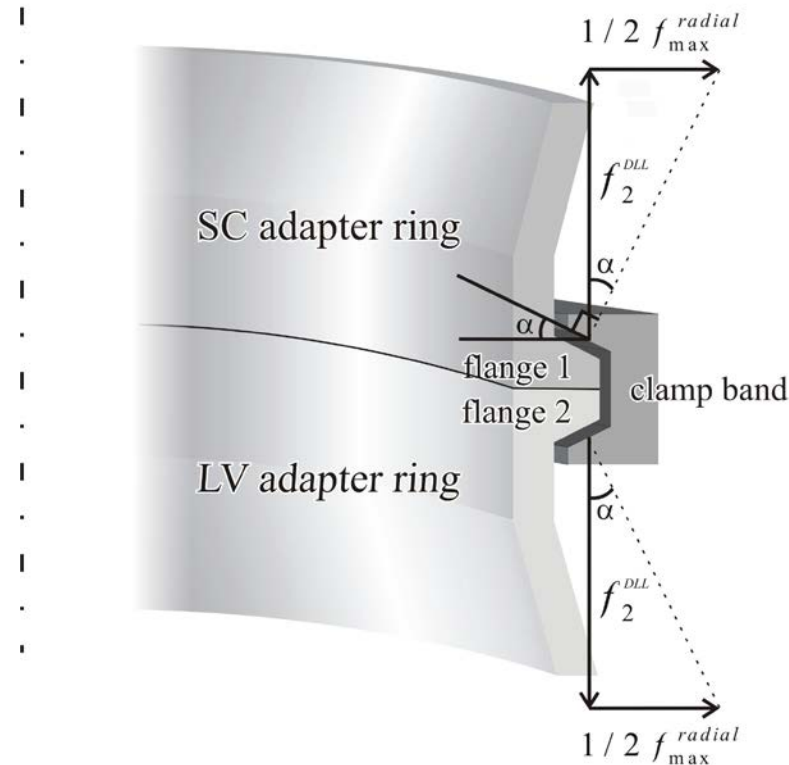


**Figure 6-6: Axial and radial flux components along the clamp band perimeter**

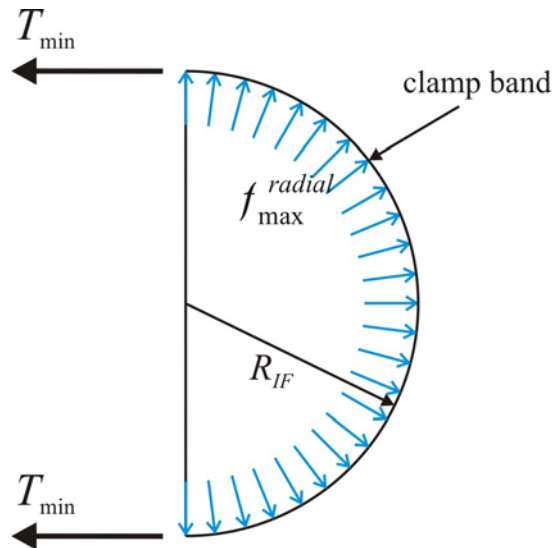


**Figure 6-7: Minimum clamp band tension equilibrating  $f_{\max}^{\text{radial}}$**

The vector decomposition described in Figure 6-6 for a specific section of the LV/SC interface involves the whole clamp band perimeter, as illustrated in Figure 6-7.  $T_{\min}$  is the minimum clamp band tension necessary to avoid the SC separation under the design maximum tensile load. Assuming conservatively that  $f_{\max}^{\text{radial}}$  acts along the whole perimeter, the equilibrium of the clamp band shows that:

$$T_{\min} = f_{\max}^{\text{radial}} \frac{D}{2} \quad [6-15]$$

In practice, additional effects like the temperature variation, assembly related influences or tension relaxation should be taken into account, leading to a resulting clamp band tension higher than  $T_{\min}$ . However, taking into account the friction between the clamps and the interface flanges results in a lower clamp band tension as can be seen from Eq. [6-13] for the maximum radial flux  $f_{\max}^{\text{radial}}$  since  $\mu_{cl}$  has a larger impact on the value of the numerator than the denominator.

### 6.3.6.4 Example of clamp band assessment

This section provides an example of clamp band assessment showing how to calculate  $T_{\min}$  in a realistic case. According to previous sections, compressive forces and fluxes are taken with positive sign.

The following initial data are considered:

$$N = 1.4 \text{ kN};$$

$$M_{Lat} = 14.2 \text{ kNm};$$

$$D = 0.937 \text{ m};$$

$$\alpha = 15^\circ;$$

$$\mu_{cl} = 0.1.$$

By using the negative sign in Eqs. [6-8] and [6-9], since the tensile flux is considered, gives:

$$f_2 = -20.12 \text{ N/mm};$$

$$A_2 = -59.22 \text{ kN}.$$

Assuming  $N$  and  $M_{Lat}$  as limit loads coming from CLA, an *overflux factor* of 1.25 and a design factor of 1.3, Eq. [6-11] leads to:

$$f_2^{DLL} = -32.7 \text{ N/mm}.$$

Using Eqs. [6-13] and [6-14] gives:

$$f_{\max}^{\text{radial}} = \begin{cases} 17.5 \text{ N/mm} & \text{for zero friction} \\ 10.7 \text{ N/mm} & \text{for non-zero friction} \end{cases}$$

Finally, from Eq. [6-15] the minimum clamp band tension is found to be:

$$T_{\min} = \begin{cases} 8.2 \text{ kN} & \text{for zero friction} \\ 5.0 \text{ kN} & \text{for non-zero friction} \end{cases}$$

In practice clamp-bands are qualified for standard tension values, and are selected depending on spacecraft characteristics and adapters.

### 6.3.7 Results review, verification and validation

This section describes how CLA results may be validated on the launcher side to guarantee the correct conditioning of the spacecraft outputs and how CLA assumptions may be updated to prevent exceeding specifications.

Validating CLA predictions should not be underestimated, particularly when the spacecraft flight worthiness is determined from the direct comparison between a single set of CLA outputs and few

runs of spacecraft system vibration tests (e.g. “the Ariane 5 philosophy” from Section 6.1.3). Performing multiple CLA predictions during the design process of a spacecraft (e.g. “the NASA philosophy” from Section 6.1.3) offers many occasions to refine the computations. Verification and validation may be performed by:

- simply redoing computations and cross-checking calculations using different solvers and/or toolboxes or other engineering teams for instance;
- verifying that the secondary structures and equipment item responses are consistent with their own dynamic behaviour and the nature of the excitation they are subjected to, as produced by the spacecraft interface acceleration (e.g. there should be spacecraft responses where the spacecraft is prone to respond, where it is subjected to launcher excitation, or both);
- performing, if possible, sensitivity analysis with respect to damping, structural coupling and excitation interactions;
- assessing the consistency of CLA output with all comparable load cases or from the experience of previous space missions with spacecraft built on similar platforms and/or equipped with the same instruments (this is essentially applicable to commercial spacecraft such as telecommunication constellations).

Reviewing CLA predictions may also be necessary in case of exceeded system specifications, irrelevant predictions, FEM updates, production issues or in-flight anomalies. CLA computation may be rerun as soon as the spacecraft FEM quality is assessed (e.g. when preliminary damping assumptions are re-evaluated). CLA outputs may be corrected by coefficients to include any excitation update or processing of a preliminary in-flight anomaly. CLA methodologies may be questioned following post-flight analyses, lead to a new CLA with updated coupled system damping and FEM assumptions.

### 6.3.8 Use of CLA results for structural verification

The use of CLA results should be consistent with the flight worthiness assessment philosophy specified by the launcher authority.

When the CLA is considered as “a single but mandatory indicator of compliance”, CLA responses are compared with the measured levels from spacecraft system qualification tests performed as close as possible to the actual flight conditions. Such tests should also be used to evaluate the representativity of the FEM. Tests results are used to determine the acceptability of CLA output. The flight qualification is pronounced from direct comparison between dynamic responses at limit load level and sine vibration tests, along with direct comparisons between combined limit loads and static tests loads using the appropriate margins. Design considerations should be raised only if no other demonstration using test/predictions comparisons is available or possible.

When the CLA is considered as “a fully integrated tool in the design process”, CLA responses are compared with the design itself.

### 6.3.9 Reporting

The CLA report should summarize the CLA major assumptions, indicate how the load case raw outputs have been post-processed (refer to Section 6.2.10) and how they may have been combined together (refer to Section 6.4.4). The CLA report should also mention how predictions may be post-processed given that it might be necessary to compare them to design specifications or qualification tests. The report should clearly mention which events have been computed and how launcher qualification studies and/or post-flight analyses may be representative of non-simulated load cases. A summary of the spacecraft mathematical model characteristics may also be included.

Examples of CLA reports are shown below in terms of QSL (Table 6-2), interface accelerations (Table 6-3 and Figure 6-8) and internal responses (Table 6-4). Values in italic correspond to fixed values of non-simulated load cases. The Ariane 5 load cases do not take into account any quasi-static contribution from the trajectory. However they are extracted from the launcher qualification studies and are taken into account when concluding on the qualification of the spacecraft from static test results, for the primary structure, and dynamic test results for the secondary structures (refer to Section 6.5). The quasi-static lateral contributions from gusts are taken into account in the computations for the transonic phase.

**Table 6-2: QSL synthesis (example)**

EVENT	LONGITUDINAL QSL			LATERAL QSL	
	STATIC	DYNAMIC		STATIC + DYNAMIC	
Lift-off	-1.8 g <i>(-1.8 g spec.)</i>	<i>± 1.5 g</i> <i>(± 1.5 g spec.)</i>		± 1.2 g <i>(± 2.0 g spec.)</i>	
Transonic	-2.2 g <i>(-2.7 g spec.)</i>	<i>± 0.25 g</i> <i>(± 0.5 g spec.)</i>		± 1.2 g <i>(± 2.0 g spec.)</i>	
SRB end of flight	-4.4 g <i>(-4.55 g spec.)</i>	<i>± 0.6 g</i> <i>(± 1.45 g spec.)</i>		± 0.65 g <i>(± 1.0 g spec.)</i>	
Boosters jettisoning	No tension	<i>(+2.5 g spec.<sup>①</sup>)</i>		± 0.3 g <i>(± 0.9 g spec.)</i>	

Minus sign with longitudinal axis indicates compression

① Tension specification (including static part) for a spacecraft which mass exceeds 2 tons

**Table 6-3: Interface acceleration synthesis (example)**

		Z AXIS LONGITUDINAL	X AXIS LATERAL	Y AXIS LATERAL	A5 UM SINE TEST SPECIFICATION	
Lift-off	Equivalent sine levels	0.16 g 0.27 g 0.60 g 0.20 g	3.4 Hz 13.4 Hz 15-20 Hz 65-100 Hz	0.60 g 0.35 g 0.40 g	14.9 Hz 15-20 Hz 60-100 Hz	
				0.39 g 0.75 g 0.40 g	14.2 Hz 15-20 Hz 60-100 Hz	
Transonic		0.16 g 0.16 g	14.2 Hz 14.2 Hz	0.20 g 0.30 g 0.13 g	12.8 Hz 15.0 Hz 18.8 Hz	Longitudinal:  1 g between [2 Hz - 50 Hz] 0.8 g between [50 Hz - 100 Hz]
				0.59 g 0.18 g	14.5 Hz 18.8 Hz	
3 <sup>rd</sup> acoustic mode	Sine levels	-		0.20 g	60-65 Hz	Lateral:  0.8 g between [2 Hz - 25 Hz] 0.6 g between [25 Hz - 100 Hz]
		0.17 g 0.26 g 0.10 g 0.16 g 0.20 g 0.15 g	20.1 Hz 22.6 Hz 26.2 Hz 33.8 Hz 35.6 Hz 37.2 Hz	0.42 g 0.60 g 0.19 g	18.3 Hz 20.3 Hz 24.7 Hz	
SRB end of flight	Sine levels			0.23 g 0.26 g 0.10 g	17.8 Hz 20.3 Hz 24.6 Hz	
		0.10 g 0.14 g 0.18 g	14.6 Hz 34.4 Hz 77.0 Hz	0.11 g 0.10 g	35.4 Hz 42.7 Hz	
Boosters jettisoning	Equivalent sine levels	<0.10 g	0-100 Hz	<0.10 g	0-100 Hz	

Since the spacecraft qualification process for the Ariane 5 is based on vibration test results, transient and harmonic responses are converted to equivalent sine responses using a shock response spectrum with an amplification factor typical of spacecraft (e.g.  $Q = 20$ ). This is the standard approach for qualifying the launcher stages and subsystems.

Values shown in italic in Table 6-3 are not computations results. They are extracted from launcher qualification studies and/or post-flight processing to include non-simulated load cases contributions or to cover in-flight anomalies. For most commercial spacecraft, no OTM response is deduced from non-simulated load cases. It is assumed acceptable since these load cases are eventually compared with notching profile from sine tests. However, OTM responses may be associated with non-simulated load cases when the Ariane 5 qualification process is not standard, as for ATV for instance which flight worthiness is based on sub-system tests results and design considerations.

An example of SC interface acceleration synthesis is presented in Figure 6-8. It refers to an upper position payload for the Ariane 5 ECA launcher. The levels associated with non-simulated load cases are also presented.

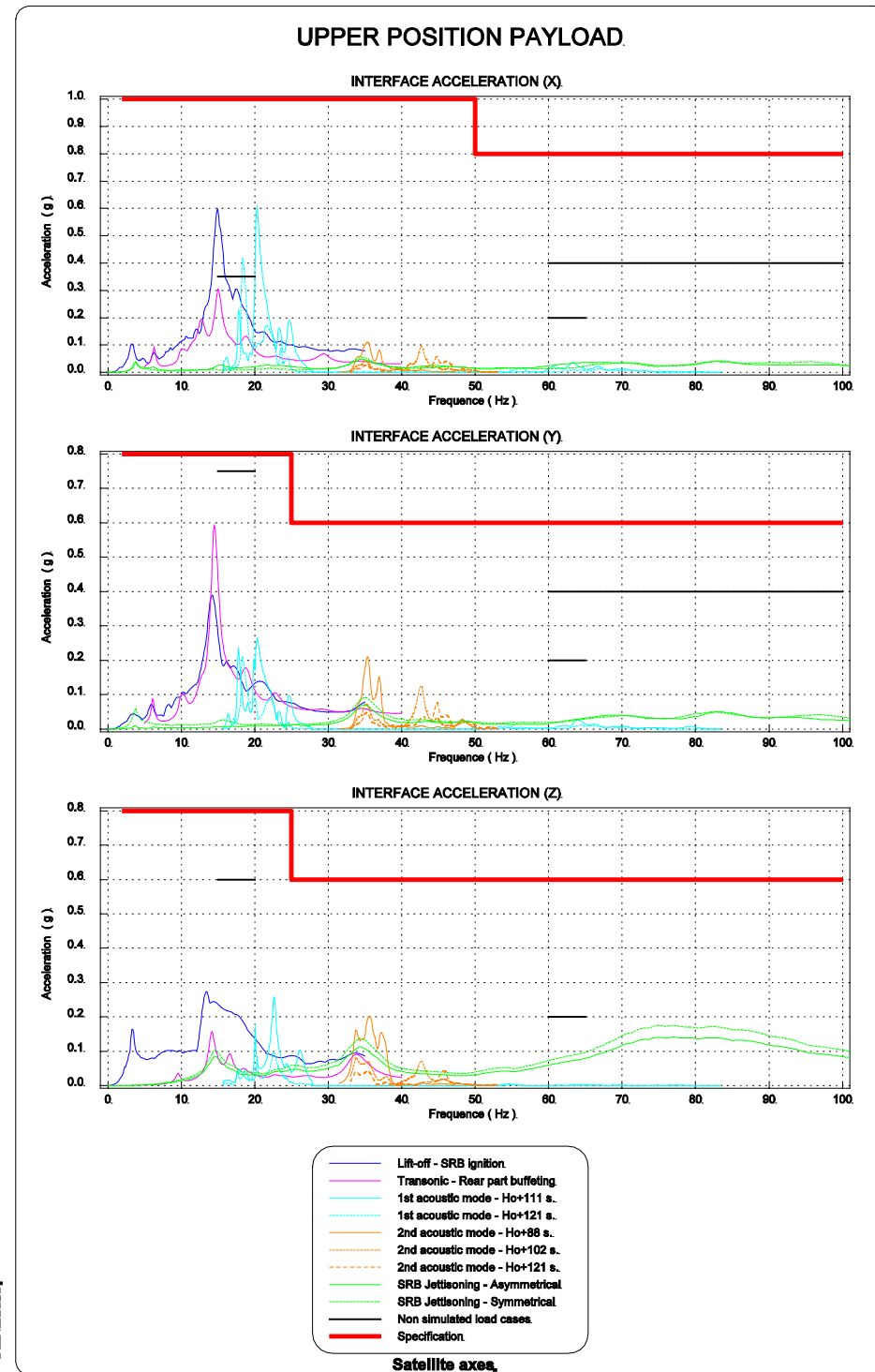


Figure 6-8: Interface acceleration synthesis (example)

**Table 6-4: Internal acceleration responses (example; min/max values in g or g/m)**

TITLE	Node	dof	dcls	bpa	op1s 111s	op1s 121s	op2s 102s	op2s 121s	sepx	seps
ATM Row #105	400911	1	3.30	5.01	0.70	0.93	0.09	0.10	0.67	1.90
			-3.35	-5.01	-0.70	-0.93	-0.09	-0.10	-0.91	-1.24
	400912	2	<b>2.96</b>	<b>2.58</b>	<b>0.82</b>	<b>0.83</b>	<b>0.11</b>	<b>0.04</b>	<b>1.25</b>	<b>0.84</b>
			-2.22	-2.58	-0.82	-0.83	-0.11	-0.04	-0.91	-1.26
	400913	3	1.08	1.91	0.54	0.53	0.16	0.08	0.78	1.08
			-1.64	-1.91	-0.54	-0.53	-0.16	-0.08	-0.83	-0.90
	400914	1	4.38	6.46	0.59	0.65	0.07	0.12	0.85	1.13
			-4.00	-6.46	-0.59	-0.65	-0.07	-0.12	-1.02	-1.51
	400915	2	<b>3.80</b>	<b>3.40</b>	<b>1.18</b>	<b>1.07</b>	<b>0.21</b>	<b>0.08</b>	<b>1.42</b>	<b>1.22</b>
			-2.91	-3.40	-1.18	-1.07	-0.21	-0.08	-1.30	-1.21
	400916	3	1.10	1.78	0.52	0.52	0.13	0.05	0.98	1.41
			-1.55	-1.78	-0.52	-0.52	-0.13	-0.05	-0.92	-1.30
	400917	1	4.43	6.02	0.41	0.47	0.08	0.12	0.73	0.91
			-3.78	-6.02	-0.41	-0.47	-0.08	-0.12	-0.84	-1.25
	400918	2	<b>3.78</b>	<b>3.40</b>	<b>1.18</b>	<b>1.08</b>	<b>0.21</b>	<b>0.08</b>	<b>1.40</b>	<b>1.13</b>
			-2.94	-3.40	-1.18	-1.08	-0.21	-0.08	-1.22	-1.14
	400919	3	1.14	1.94	0.51	0.53	0.10	0.04	0.76	1.03
			-1.51	-1.94	-0.51	-0.53	-0.10	-0.04	-0.60	-0.77

OTM responses are presented per load case, as shown in Table 6-4 for internal accelerations. They include transient, random and harmonic responses. Both min/max and averaged value are presented. The envelope of the average responses (shown in boldface) should be compared with sine tests results. Internal loads and absolute displacements may also be provided depending on the spacecraft project. However, they cannot be used as qualification criteria since no comparable qualification test results are available. Nevertheless, they may be used by the spacecraft authority to assess the design of the structure, as soon as they are properly processed (e.g. combined). Internal displacements may be used to perform specific fairing or SYLDA clearance studies.

## 6.4 Ariane 5 coupled loads analysis

### 6.4.1 Introduction to Ariane 5 CLA

In the mission analysis process [4] the standard procedure is to perform at least two coupled loads analyses for recurrent commercial spacecraft. Normally:

- Preliminary Coupled Loads Analysis (PCLA) should be planned as soon as the contract organization is set between the launch service provider and the spacecraft customer:
  - to confirm the launcher and spacecraft compliance,
  - to contribute to the spacecraft design verifications by providing a preliminary dynamic environment for the most severe load cases (refer to Section 6.4.3),
  - to provide sufficient input to review the spacecraft tests plan by identifying any specifications deviation and any possible adjustment (refer to Chapter 8).
- Final Coupled Loads Analysis (FCLA) should be performed as soon as the spacecraft mathematical model has been successfully correlated with tests results and once the launcher configuration has been frozen:
  - to provide, as a PCLA update, the final estimation of the dynamic environment the spacecraft has to withstand,
  - to conclude on a qualification status given the test measurements associated with the spacecraft test plans and notching procedures.

In both cases the computation includes:

- Computation of the spacecraft interface accelerations for all relevant load cases (simulated or non-simulated, refer to Section 6.3.9).
- Computation of the spacecraft internal responses based on the OTM matrices provided by the spacecraft authority.
- Computation of the spacecraft QSL at the CoG (used for the static environment verification, as detailed in Section 6.5.2).

PCLA results are used as a standard basis for the sine test level verification. They may not be considered as the reference for qualification, meaning that vibration test levels should not be designed to the PCLA predictions.

Production and/or in-flight issues may also occur between the PCLA and the FCLA, which means that their treatment in predictions may not be included in the PCLA set of results.

Single scientific missions may require additional runs as they cannot benefit from previous tests and flight experiences. They may also have to deal with very unusual spacecraft architectures. In such situations, less severe load cases may be added to the standard coupled analysis process to produce a higher amount of exploitable data.

The launcher authority has the full responsibility of both preliminary and final coupled loads analyses.

## 6.4.2 Mission analysis organization and management

The Ariane 5 launch service is offered by Arianespace which is, above all, a service company. Astrium Space Transportation is the industrial prime-contractor responsible for delivering the operable launch vehicle to Arianespace. As the launcher qualification authority, ESA and CNES guarantee that the load verification cycle is consistent with the specified process. For standard commercial missions, PCLA are performed by Arianespace whereas FCLA are performed by Astrium Space Transportation. However Arianespace is the single launcher interface with the spacecraft designer via the spacecraft operator which has contracted the launch service. As a result the spacecraft qualification process involving these multiple entities may not always be easy to deal with. The Ariane 5 load verification cycle is a so called “winning” approach, meaning that at best no major technical issue should be discussed between the launcher prime-contractor and the spacecraft designer.

For the Ariane 5 programme, the launcher authority is fully responsible for CLA predictions and their correct exploitation in the framework of the spacecraft qualification. However, it is not responsible for the design of the spacecraft.

Major milestones are fulfilled in the mission analysis management process. Examples of Ariane 5 milestones include:

- *Interface Control Document* (DCI) edition: it results from Arianespace negotiations with its customer. The DCI documents interfaces, relations and activities between the Ariane launch system and the client.
- *Preliminary Mission Analysis Review* (RAMP): it is a technical key point where Arianespace presents the preliminary expected environments. It is a support to the test plans. It is held under the joint responsibility of Arianespace and its client.
- *Final Mission Analysis Specification* (SAMF) edition: it freezes the launch vehicle flight configuration and details all assumptions used in analyses (thermal, dynamic and trajectory analyses). FCLA may start as soon as an agreement has been reached between Arianespace, Astrium Space Transportation and ESA/CNES.

- *Final Mission Analysis Review* (RAMF): it is a technical key point where Arianespace concludes on the final expected environments. It is a major step of the spacecraft qualification process as tests results may be then exploited to conclude on the flight worthiness. It is held under the joint responsibility of Arianespace and its client. Arianespace may ask for the support of its launcher prime contractor.
- *Combined Operations Plan* (POC) readiness review: it outlines all activities involving the spacecraft and the launch vehicle simultaneously. Spacecraft waivers should be cleared here (e.g. the spacecraft qualification should be already pronounced). The POC is prepared by Arianespace and submitted to the customer's approval.
- *Flight Worthiness Review* (RAV): a synthesis of all the technical events is performed at this time of the launch campaign. It summarizes all the mission analyses conclusions as an extract from the RAMF but it also concludes on the acceptability of any waiver on the launcher side. The launcher should be cleared for flight then.
- *Launch Worthiness Review* (RAL): it closes the launch campaign. Arianespace authorizes the launcher transfer from its final assembly building to the launch pad. The final sequence of operations in preparation for the final count-down may start then.

### 6.4.3 CLA events and load cases

#### 6.4.3.1 Overview

The most common events and physical load cases analysed by coupled loads analyses are:

- *Stage(s) ignition* and the following *lift-off*. These events may result in transient loads on the engines and their stage due to pressurisation effects, stage(s) thrust transient, shocks induced by any environmental nozzle breakdown, or instantaneous release of launcher/pad interface forces [6]. Some excitations are of a wide band transient nature (some of them are specifically described hereunder).
- *Blast waves* which hit the launcher right after engine ignition and then the lift-off. The acoustic field around the launcher results from the interaction between the engine jets and the launch pad. The excitation is of a medium band transient nature (e.g. [0-40] Hz), applied to the whole launcher body [6] and it interacts with the primary modes of the vehicle. Loads can be significant on the spacecraft primary structure in both axial and transverse directions as waves are reflecting on the pad in the axial direction and coming from the jets exhaust ducts in the lateral direction. The spacecraft qualification may be jeopardized by predictions from this load case as the spacecraft primary modes may be coupled with the launcher ones, e.g. coupling the spacecraft with the launcher's fairing would result in high quasi-static loads (in the lateral direction mostly). Additional information on handling this load case in the Ariane 5 context is found in Section 6.4.3.2.
- *Gust* which hits the launcher during the atmospheric flight. The excitation is of a medium band transient nature and the load case stakes are of the same nature as for the blast waves (interaction with the primary modes and substructures coupling). Loads are usually insignificant in the longitudinal direction. Gusts and buffeting may occur simultaneously for instance and resulting loads are combined together if computed separately (refer to Section 6.4.4).
- *Buffeting* phenomenon. Buffeting results from an unsteady air flow around the launcher. The excitation is of a wide band random nature and occurs during the atmospheric flight at any significant break of shape of the vehicle (e.g. around a fairing or a nozzle for instance). Its severity depends on the overall body form, the cruising Mach number and the angle-of attack of

the launcher [6]. Loads on the spacecraft primary and secondary structures may be high, particularly in the transverse direction given the frequency range involved ([10-40] Hz) and the wide range of Mach and angle of attack values for the launcher.

- *Boosters pressure oscillations.* This load case results from a harmonic coupling between combustion instabilities inside the engine chamber and acoustic modes of the cavity. Several excitation blasts may occur [6]. Coupling phenomena between substructures at frequencies close to those of the acoustic modes may also happen and turn the event into a very severe load case for both launcher and payload, especially on the secondary structures and its equipment given the frequency range involved (e.g. around 40 Hz for Ariane 5 for instance, where smaller items are prone to respond). Additional information on handling this load case in the Ariane 5 context is found in Section 6.4.3.3.
- *Engine(s) cut-off(s)* or the *chugging* phenomenon. This event results in a wide band transient excitation applied to the whole engine [6]. The phenomenon also happens when igniting the engine. The spacecraft mechanical environment is among the lowest.
- *Stage(s) separation.* This load case results from the instantaneous release of both static and dynamic loads at the interface between the stages. The excitation is of a transient nature, with a wide band step-like function [6]. Its severity depends on the sequence of actions for separating the stages (e.g. igniting separation rockets before cutting attachments would result in higher loads than igniting separation rockets while cutting attachments). The low frequency environment is reproducible from one mission analysis to another and the higher frequency responses may be only significant for spacecraft items of equipment (responses are located around 80 Hz).

Load cases associated with the stage ignition, the lift-off, the blast waves and boosters pressures oscillation are typically the most severe load cases. Some other load cases are mentioned here for the information purpose mostly as the associated environment is usually less severe and finally not specifically computed:

- *Nozzle jet separation*, transient or permanent, that may occur at the engine ignition (or in case of launch abort) and in the early atmospheric flight phase respectively. The transient jet separation phenomenon occurs when (de)pressurising the combustion chamber in the atmosphere. The transient excitation is applied to the nozzle. The permanent phenomenon may occur at a steady state of the engine, where the jet sticks to the nozzle. The excitation is then of a wide band random nature [6].
- *Screech phenomenon* at the engine ignition or in case of launch abort. This phenomenon may be hard to characterise [6]. The excitation is of an acoustic nature as traduced by spectral lines which severity depends on the engine.
- *Nozzle swivelling* during the whole flight. For multi-body launchers like Ariane 5, the boosters' end of flight phase may be a critical phase since thrust is no longer "perfectly" symmetric between both boosters and since nozzles are set to a zero angle with respect to the thrust axis before stage separation. At lift-off, swivelling may be critical due to control commands occurring immediately after the vehicle has left the launch pad [6].

Specific predictions may be provided exceptionally for some additional load cases, depending on the project maturity and the spacecraft sensitivity in the related frequency range. Simulation may not be possible for some load cases where the excitation has not been characterised. Their influence on the spacecraft dynamic environment may be taken into account through uncertainty factors (refer to Section 6.2.11) or through fixed values of interface accelerations and/or QSL. Some load cases cannot be simulated or taken into account through uncertainties factors or fixed values. In this case, launcher qualification studies should demonstrate that the associated dynamic environment is sufficiently covered by other load cases.

### 6.4.3.2 Blast waves - Ariane 5 example

#### 6.4.3.2.1 Characterisation

The acoustic field around the launcher results from the interaction between the engines jets and the launch pad and generates a complex gas dynamics problem to be solved.

Experimental investigations or post-flight analyses may be used to characterise those excitations. A reliable process to obtain the acoustic field characteristics consists of carrying out experimental investigations using subscale models of the launch vehicle and its pad in association with complete simulations of the gas dynamics problem and the thermodynamic parameters of the engine jets. Such an approach has been used for the Ariane 5 launcher to design the water injection system that reduces noise at lift-off for instance.

The pressure field is dependent on the launch pad architecture and the propulsion characteristics of the rocket motors. It may be evaluated from in-flight measurements as long as those parameters remain the same from one launch to another. It may be then a major input to the excitation definition for the system's predictions. The so-called 'inverse method' uses an optimal control method which is based on direct and adjoined equations with a time-domain boundary integral approach [8]. Identifying acoustic sources is however a major difficulty as mentioned in [9].

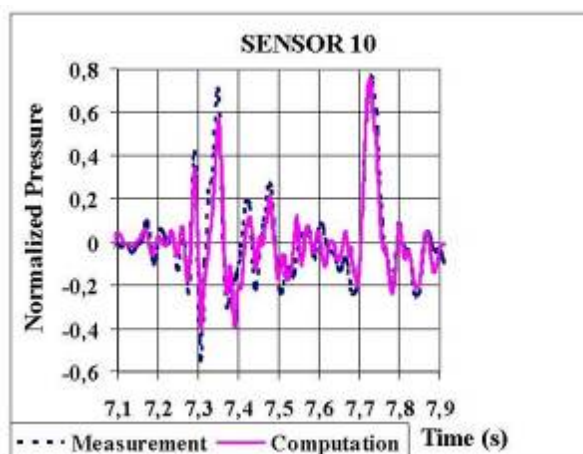


**Figure 6-9: Comparison between prediction and measurement (fairing sensor)**

Applying this approach to the Ariane 5 launcher has yielded good correlation levels between predicted and measured pressures for a given fairing sensor for instance (Figure 6-9) where a part of the excitation is distributed on. In practise, once the pressure field has been rebuilt from flight measurements, pressures may be evaluated at any point of the launch vehicle skin. Integrating those pressures on given surfaces results in loads that can be used as an excitation input.

#### 6.4.3.2.2 Nature

As far as the Ariane 5 launcher is concerned, the most severe loads result from overpressures and the following acoustic phase.

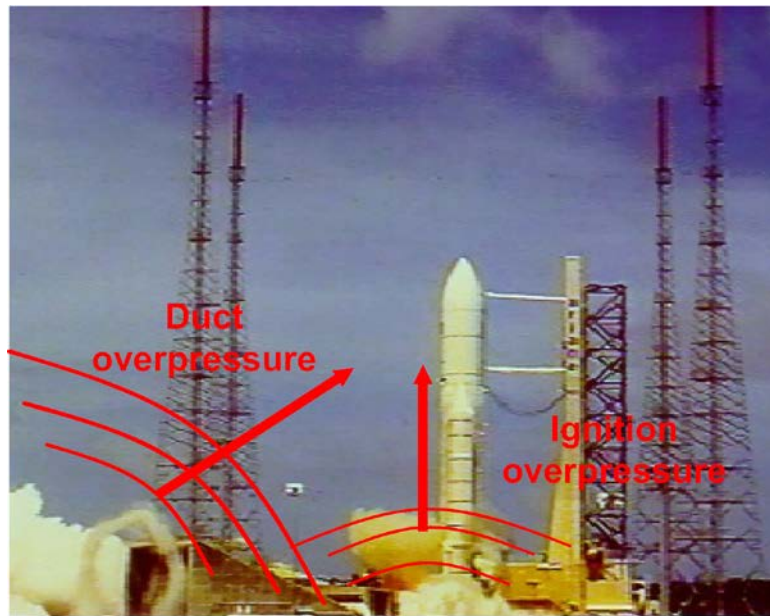


Figure 6-10: Ariane 5 IOP and DOP

Overpressures are generated by engine(s) jets which reflect on the pad or propagate from the launch pad exhaust ducts. It is a deterministic phenomenon which is analysed in the time domain. Most of the overpressures come from the EAP ignition, the contribution from the Vulcain ignition being weak. Two types of overpressures occur (Figure 6-10):

- The *ignition overpressure* (designated as "IOP") which results from a compression wave going up from the bottom of the launch pad directly; it generates longitudinal responses.
- The *duct overpressure* (designated as "DOP") which results from the propagating wave coming from the launch pad exhaust ducts and which hits the launcher right after its lift-off; it generates lateral responses.

Fluctuating turbulences in the mixing region of the rocket exhaust flow generate most of the acoustic field that the launcher has to withstand. The associated loads are random and broadband and they are analysed in the frequency domain.

### 6.4.3.3 Boosters pressure oscillations - Ariane 5 example

#### 6.4.3.3.1 Introduction

Booster pressure oscillations may be very critical for the mechanical environment on the launcher and its payload, particularly because boosters usually provide most of the thrust in the early flight phase. Pressure oscillations appear in the boosters because acoustic modes are excited by vortex shedding in the combustion channel. Coupling phenomena between substructures at frequencies close to those of the acoustic modes can amplify significantly the dynamic responses on the vehicle and the spacecraft [10].

#### 6.4.3.3.2 Origin

The impact of booster pressure oscillations has been quickly taken into account in the Ariane 5 development process. They appear when firing the solid rocket boosters (designed as EAP). They are due to the complex coupling between the combustion and the internal aerodynamics in the boosters' combustion chamber. In the Ariane 5 case, acoustic modes are excited by vortex shedding (Figure 6-11) that can mainly correspond to:

- the *parietal vortex shedding*, which results from a coupling between the main flow and the flow produced by the propellant flame front;
- the *obstacle vortex shedding*, which results from obstacles in the flow, such as the powder segment thermal face protections.

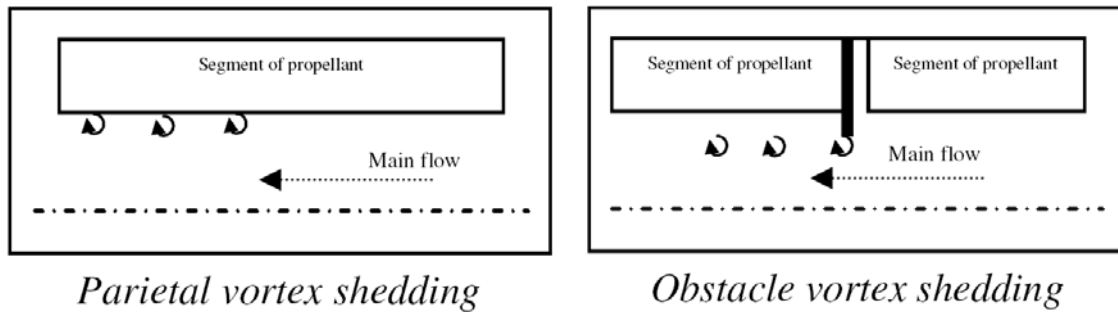


**Figure 6-11: Parietal and obstacle vortex phenomena**

Vortex shedding frequencies follow the hydrodynamic characteristics and vary given the burning grain surface (geometrical and speed evolution). The different frequency lines, designed as Strouhal lines, correspond to the variation of the cardinal number of vortices emitted from the segment thermal face protection:

$$f = \frac{Str \times U}{L} \quad [6-16]$$

where  $f$  corresponds to the vortices frequency emission,  $Str$  is a Strouhal number,  $U$  is the flow speed near the obstacle and  $L$  is the distance between the emission source and the impact point.

As far as the Ariane 5 launcher is concerned, four main pressure oscillations peaks are observed, each one being associated to a frequency drop. This cascading organisation is due to the coincidence between the vortex shedding frequency and the acoustic frequency of the EAP cavity. The four blasts (designated as B1, B2, B3 and B4) are distinguished by the frequency step that occurs when the acoustic mode frequency jumps from one Strouhal line to another (Figure 6-12). The strongest levels of pressure oscillations are obtained when the acoustic frequency crosses the vortex shedding frequency.

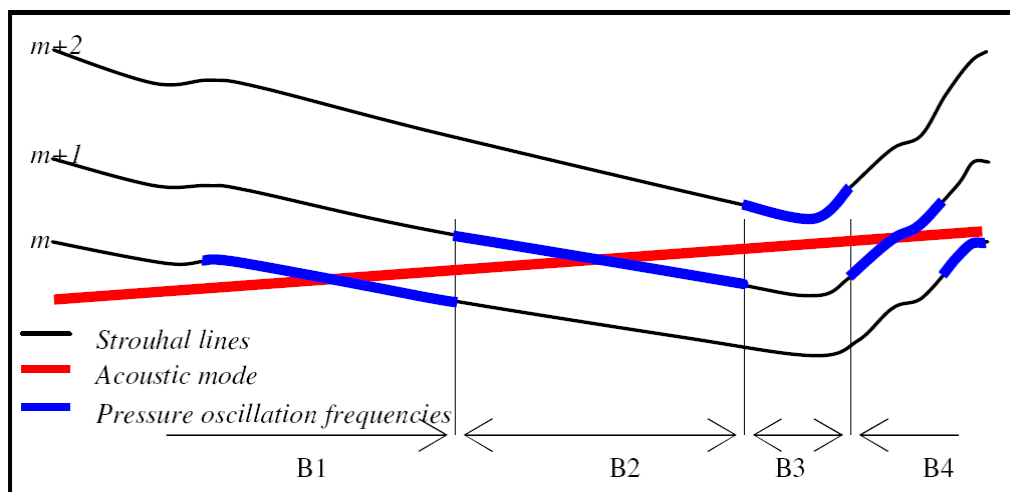


**Figure 6-12: Vortex shedding frequency and acoustic mode interaction**

The acoustic frequencies of the EAP chamber result from the reflection of pressure waves on the extreme end surfaces of the EAP cavity. They are particularly reproducible when firing an EAP or another given that they are linked to the engine geometry and the gases characteristics:

$$f_a = n \frac{V}{2L_c} \quad [6-17]$$

where  $f_a$  corresponds to the acoustic frequency,  $n$  is the acoustic mode number,  $V$  is the speed of sound of the combustion gases and  $L_c$  is the combustion chamber length.

The oscillatory behaviour begins at one characteristic instant of combustion, starting from the second half of the EAP firing, and it is mainly observed on the three first acoustic modes. The first two generate the worst dynamic environment on the launcher.

#### 6.4.3.3.3 Pressure oscillation characteristics

The maximum pressure oscillation levels are obtained on the front and rear bulkheads of the EAP. This results in a longitudinal translational mode and a breathing mode for the first and second acoustic modes respectively, as those bulkheads are opposed surfaces. For the first acoustic mode, pressure oscillations lead to thrust oscillations, given the loads distribution (Figure 6-13).

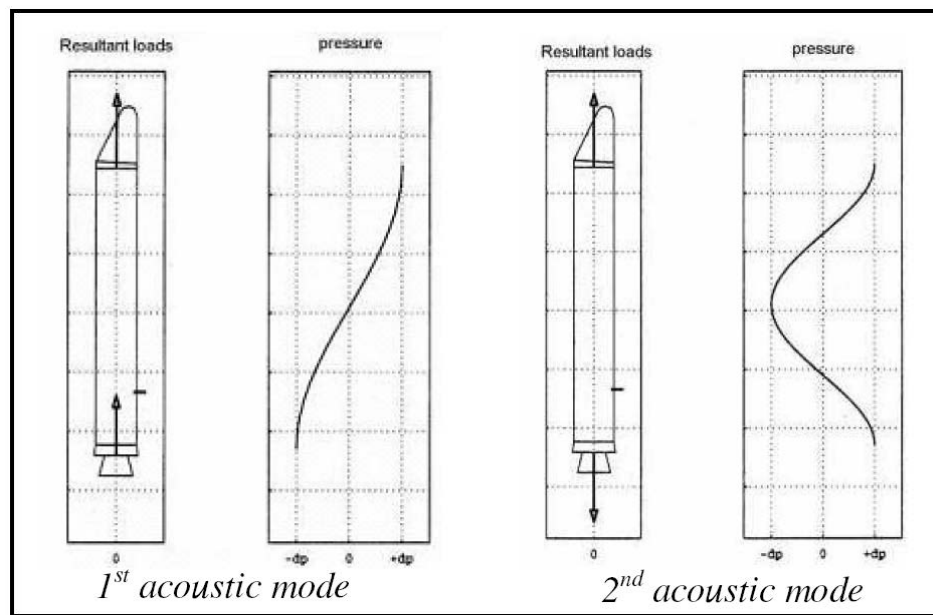


**Figure 6-13: Pressure acoustic modes profiles**

Figure 6-14 illustrates the four peaks of pressure oscillations measured by pressure transducers on the EAP during flight. This type of sensor plus vibration sensors are systematically exploited after an Ariane 5 mission to quantify the excitation and its impact on the launcher. They are also used in ground tests measurements to define the statistic limit excitation profiles for the CLA predictions.

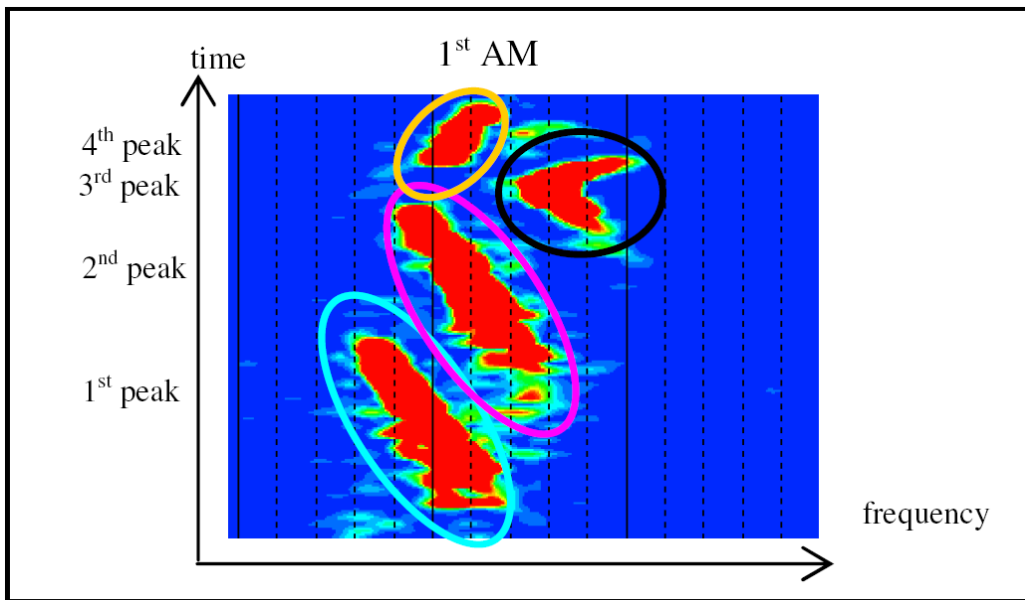


**Figure 6-14: Pressure oscillations associated with the first acoustic mode (PSD amplitudes vs. time and frequency)**

Those peaks are characterised by a slow frequency variation during the combustion phase and are associated with a single frequency at a given time. The frequency and the time of occurrence of each peak are reproducible from one EAP to another. The frequency step between each blast in Figure 6-14 is consistent with the behaviour described in Figure 6-12.

#### 6.4.3.3.4 Vibrations characteristics

Pressure oscillations lead to vibration on the EAP stages. Figure 6-15 presents the pressure oscillations and vibration profiles as a function of time and frequency for both first and second acoustic modes.

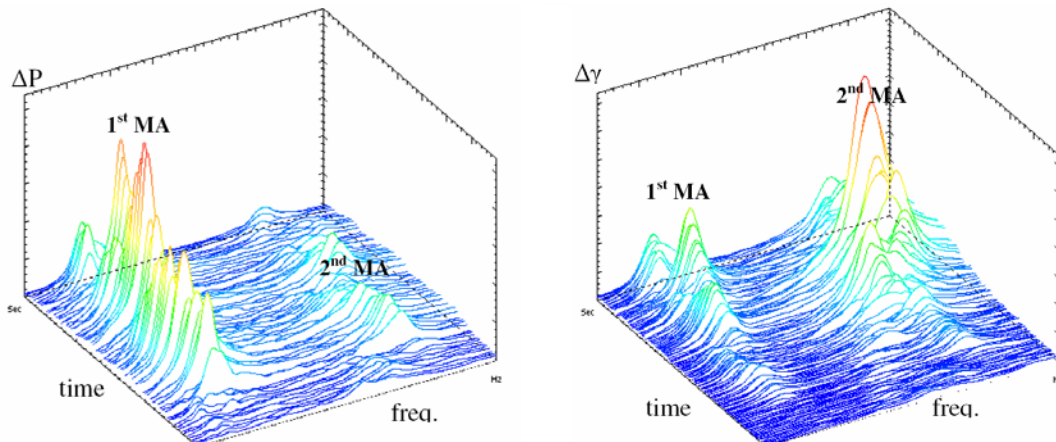


**Figure 6-15: Pressure oscillations (left) and vibrations (right) PSD**

#### 6.4.3.3.5 Potential impact on the launcher

The mechanical environment on both EAP stages is transmitted to the Ariane 5 central body through DIAS (longitudinal and lateral loads) and DAAR (lateral loads only) connections (Figure 6-16).

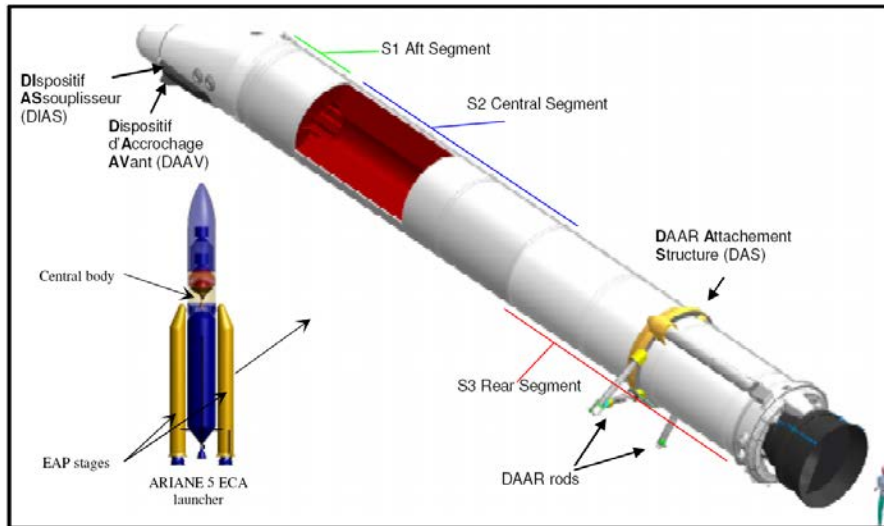


**Figure 6-16: Ariane 5 and EAP stage**

The potential severity of the mechanical environment on the EAP stage is mainly due to:

- the excitation level, in terms of pressure oscillations amplitude,
- a coupling phenomenon between the excitation frequency and the EAP structural modes,
- a coupling phenomenon between this combined excitation and structural modes of the central body.

**Table 6-5: Load cases impacts on the EAP stages and the central body**

Load case	Excitation level	$\Delta P$ mode / EAP stage mode	$\Delta P$ mode / Central body mode
1st acoustic mode	High	No	Yes
2nd acoustic mode	Low	Yes	Yes

The highest pressure oscillations levels are obtained for the first acoustic mode (Table 6-5). Moreover, the vibrations induced on the EAP may lead to a coupling phenomenon with the central body at frequencies close to those of the first acoustic mode. The pressure oscillations levels are usually low for the second acoustic mode. However, the EAP first longitudinal structural mode crosses the second acoustic mode frequencies. Its frequency shift is indeed quick in flight. The spectral coincidence may lead to high dynamic responses on the stage and on the central body of the launcher.

#### 6.4.3.3.6 Attenuation devices

During the Ariane 5 development phase, some simulations emphasized the risk of high dynamic responses on the launcher, particularly on the central body. Correction devices have been developed to reduce levels. The first one was introduced at the interface between the EAP and the central body. This device (Figure 6-17), designed as the DIAS, adds flexibility which reduces the transmitted loads at the frequency of the excitation, working as a low pass filter. It is made up as a sandwich of metallic and rubber shearing plates. Its design results from a compromise between efficiency and sufficient stiffness to maintain the launcher's controllability.

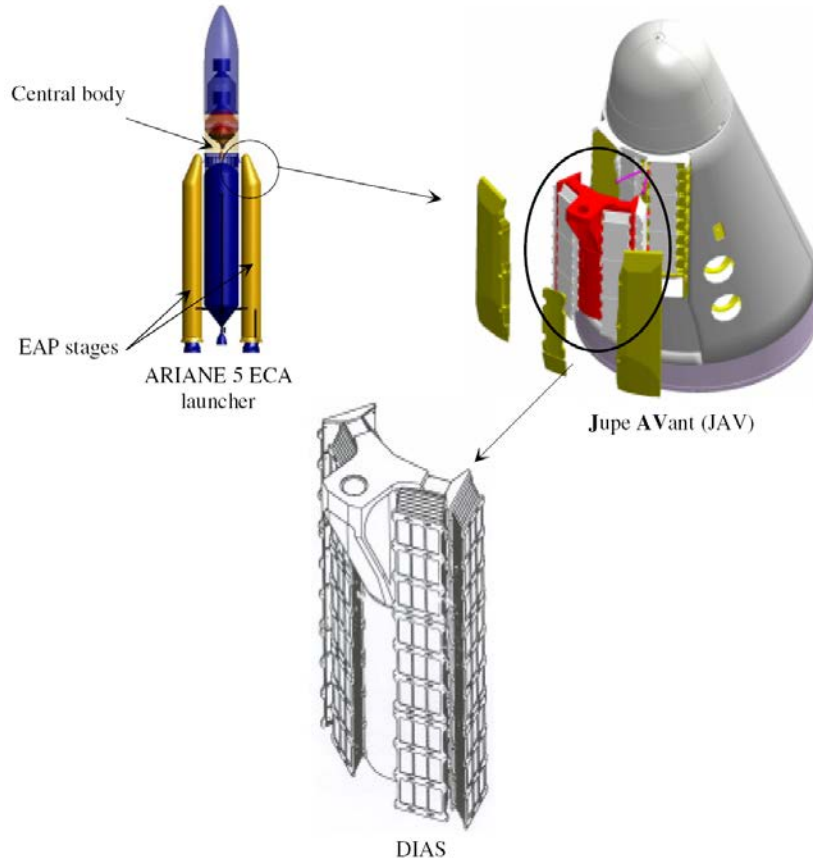


**Figure 6-17: DIAS system**

For the first acoustic mode load case, the oxygen tank of the ESC-A upper stage is sensitive to lateral motions and prone to payloads coupling, inducing then high payloads lateral responses. Damping struts have been introduced in the stage between the top of the oxygen tank and the bottom of hydrogen one to limit the oxygen tank motion. This so-called SARO (Figure 6-18) turned the ESC-A stage excitability into an advantage by damping its responses and significantly improving the payloads comfort. The oxygen tank turns into a dynamic damping device that activates itself from a given threshold level, given the nonlinear behaviour of the SARO system.

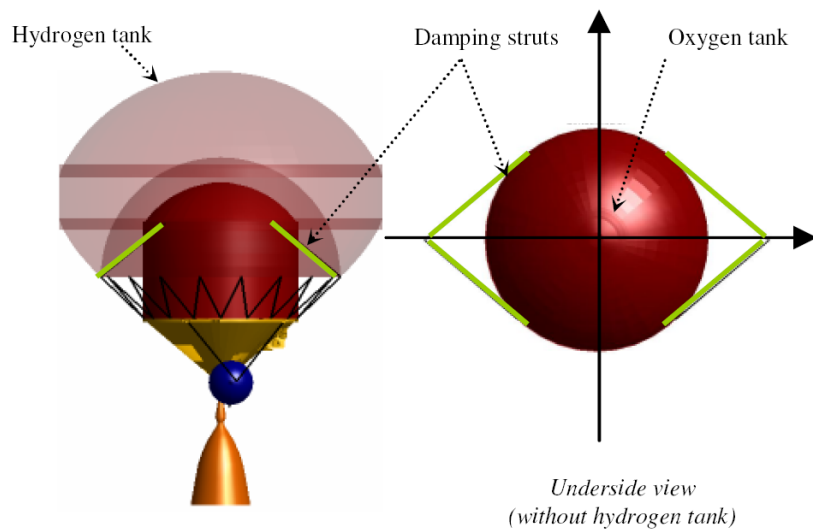


**Figure 6-18: ESC-A damping struts (SARO system)**

#### 6.4.4 Concomitant events and load cases combination

Ariane 5 physical load cases have been elaborated considering each source of excitation separately. Therefore, concomitant events are combined together when applicable (e.g. when comparing CLA predictions to static tests results). In practise, both pressures oscillations associated to the 1st and 2nd acoustic mode may occur on the same flight phase (e.g. from around H0+70s to H0+120s). However, the 1st acoustic mode load case is computed separately from that of the 2nd acoustic mode. Summations rules have been defined to combine both sets of results (on spacecraft QSL only however), depending on the severity of the load cases, the nature of the phenomenon and the knowledge of the system. Moreover, the quasi-static acceleration may not be included in the CLA forcing functions.

As a result, several combinations are often performed when comparing CLA predictions to static tests results or design specifications. Concomitant load cases of the same nature should be combined together first. Those combined loads may then be summed up with other environmental loads. These "all-included" loads may then be integrated in the appropriate qualification or design margin.

As far as the Ariane 5 launcher is concerned, no combination is performed on OTM responses since the qualification statement is based on the comparison between accelerations measurements from sine tests and OTM accelerations responses from the CLA. Only the spacecraft QSL are combined together and converted into interface fluxes to conclude on the flight worthiness by comparison with static tests results on the primary structure. The QSL may be combined together using, from [7]:

- a statistic formulation, used for the lift-off flight phase:

$$\begin{aligned} QSL_{Combined}^{Limit} &= QSL_{Lift-Off}^{Average} + QSL_{NozzleSwivelling}^{Average} \\ &+ 2.33 \sqrt{QSL_{Lift-Off}^{\sigma}^2 + QSL_{NozzleSwivelling}^{\sigma}^2} + QSL_{NozzleSeparation}^{Limit} \end{aligned} \quad [6-18]$$

$$\text{where } QSL^{Average} = \frac{QSL^{Limit}}{1.25} \text{ and } QSL^{\sigma} = \frac{QSL^{Limit} - QSL^{Average}}{2.33}$$

- a pseudo root-sum-squaring (RSS) rule, used for the transonic flight phase:

$$\begin{aligned} QSL_{Combined}^{Limit} &= QSL_{Wind}^{Limit} \\ &+ \sqrt{QSL_{Gust}^{Limit}^2 + QSL_{UpperPartBuffeting}^{Limit}^2 + QSL_{LowerPartBuffeting}^{Limit}^2 + QSL_{NozzleSwivelling}^{Limit}^2} \end{aligned} \quad [6-19]$$

- an arithmetic rule, used for the EAP end of flight phase (the worst case):

$$\begin{aligned} QSL_{MaxAcceleration}^{Limit} &= QSL_{1MA-H0+111s}^{Limit} + MAX(QSL_{2MA-H0+102s}^{Limit}; QSL_{2MA-H0+121s}^{Limit}) \\ &+ QSL_{Static}^{Limit} + QSL_{NozzleSwivelling}^{Limit} \end{aligned} \quad [6-20]$$

$$QSL_{EAPEndOfFlight}^{Limit} = QSL_{1MA-H0+121s}^{Limit} + QSL_{2MA-H0+121s}^{Limit} + QSL_{(Statique+NozzleSwivelling)}^{Limit} \quad [6-21]$$

$$QSL_{Combined}^{Limit} = MAX(QSL_{MaxAcceleration}^{Limit}; QSL_{EAPEndOfFlight}^{Limit}) \quad [6-22]$$

## 6.4.5 Flight phases and CLA standard load cases

### 6.4.5.1 Introduction

This section explains how the physical load cases presented in Section 6.4.3 are converted into practical numerical load cases to be computed by CLA. For the Ariane 5 launcher, the flight is divided into 5 different phases (also called “flight events”) depicted in Figure 6-19 for which all concomitant load cases are combined together (see Section 6.4.4): SRB ignition / Lift-off, Transonic, SRB 3rd acoustic mode, SRB end of flight and SRB jettisoning. For each standard phase, there is one or more load cases, each one of these load cases possibly being the envelope of several sub-load cases. For instance, the third phase “SRB 3rd acoustic mode” is made of one single “relevant” event which is the booster pressure oscillations of the 3rd acoustic mode (hence the name). On the contrary, “Transonic” combines “gusts” plus “buffeting” and buffeting here corresponds to the envelop of 290 possible situations of buffeting for the launcher (see Section 6.4.3) whereas “gust” is the envelope of 2 simulations only.

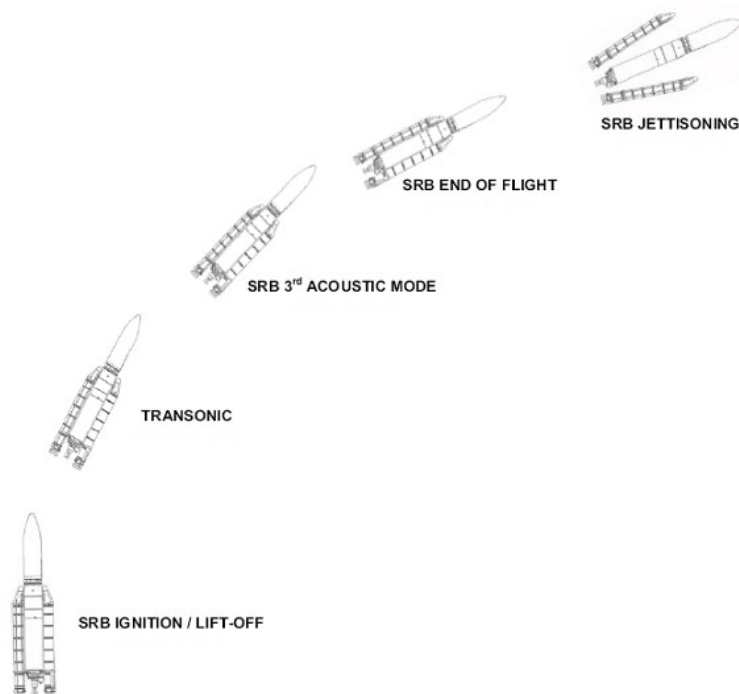


**Figure 6-19: Ariane 5 flight phases and CLA standard load cases**

As shown by qualification studies and flight processing, these load cases are the most dimensioning ones in terms of low frequency dynamic environment.

### 6.4.5.2 SRB ignition – Lift-off

This event occurs at H0+7s. The major contributors to the payload dynamic environment are the blast waves induced by the SRB jets (Figure 6-10): reflecting on the exhaust ducts entrance (ignition overpressure) and coming from the exhaust ducts (duct overpressure).

Some other effects also occurring during this phase:

- thrust transient of the SRB;
- shock induced by the break-down of nozzle diaphragms;
- launcher / launch pad hyperstatic force release at lift-off;

- Vulcain nozzle flow separation;
- gimbaling effects due to sensor noises.

A synthetic excitation that contains all these contributors is applied to the Ariane 5 launcher. It covers a time delay between the two boosters ignition varying from 0 ms to the limit value of 25 ms.

The modal base is computed up to 50 Hz and the modal damping is equal to 1% for all modes. Interface and internal responses are computed in the time domain.

Also, some other contributions, that concern the Vulcain or SRB ignition and that are not simulated, may lead to significant interface acceleration levels.

#### 6.4.5.3 Transonic

This phase occurs around H0+50s. Many load cases that occur during the entire atmospheric flight reach their maxima during this phase. The most important ones are due to aerodynamic effects, such as gust and buffeting on the upper or rear part of the launcher. Some gimbaling due to sensor noises may also occur, as well as quasi-static loads due to wind and trajectory.

For the rear part buffeting, a specific computation is performed. Random excitations are applied on the Vulcain nozzle and thermal protection to characterise the unsteady pressure field around the engine. PSD functions of pressure come from wind tunnel tests measurements on a small-scale mock-up of the launcher and flight exploitations. They are consistent with dimensioning winds occurring all along the year and the angle-of-attack range specified for the launcher.

The modal base is computed up to 65 Hz. As for the modal damping, a synthesis is performed. The launcher damping behaviour is based on dynamic tests performed on the launcher substructures. Interface and internal responses are obtained by means of a random analysis.

For the other dynamic contributors (quasi-static, gust, buffeting on the upper part and gimbaling), dimensioning values resulting either from Ariane 5 qualification studies or from parametric studies are considered.

#### 6.4.5.4 Third acoustic mode event

This event occurs around H0+60s. It corresponds to the boosters' internal pressure oscillations associated with the 3rd acoustic mode as shown below (Figure 6-20).

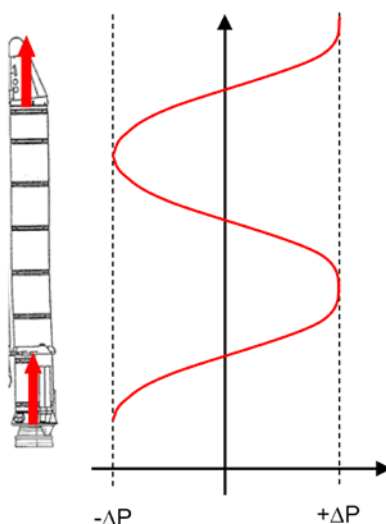


Figure 6-20: Third acoustic mode on Ariane 5

No specific computation is performed. Nevertheless, a value that comes from the Ariane 5 qualification studies is presented in the frequency range [60-65 Hz] for the lateral acceleration sine levels. It covers levels induced by this phenomenon and should be considered for the spacecraft qualification tests.

#### 6.4.5.5 SRB end of flight

This phase takes place between H0+70s and the SRB jettisoning. Combined to the important static longitudinal acceleration that reaches its maximum during this phase, some dynamic contributors occur as booster pressure oscillations (1st and 2nd acoustic modes) and gimbaling (due to sensor noises or thrust variation of the boosters). The static lateral levels are not significant, except during the SRB thrust tail-off.

For the 1st acoustic mode (Figure 6-21), two flight times that give the maximum pressure oscillations are studied: H0+111s and H0+121s. The first one is close to maximum longitudinal acceleration seen during the SRB flight and the second one corresponds to middle of the SRB thrust tail-off.

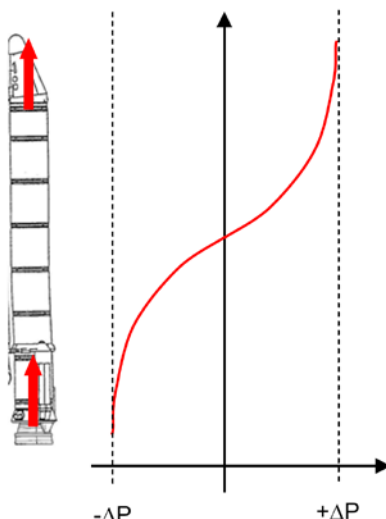


**Figure 6-21: First acoustic mode on Ariane 5**

These load cases concern the [17.5-25.3 Hz] frequency range (extended to [15.8-27.8 Hz] in the computation to cover some model discrepancies). A frequency dependent force function is associated to each flight time concerned. The limit excitation levels come from a statistic including flight and ground firing tests. The resulting forces of the pressure oscillations are applied to both front and rear domes of the boosters as shown on Figure 6-21. The phase between the excitation of the two boosters is maximized for each result presented in the following.

The modal bases are computed up to 80 Hz. As for the modal damping, a synthesis is performed. The launcher damping behaviour is based on dynamic tests performed on the launcher substructures. Interface and internal responses are computed in frequency domain.

For the 2nd acoustic mode (Figure 6-22), two flight times are also studied. They correspond to the maximum peaks of the excitation, when coupling between the SRB longitudinal mode (which frequency depends on the burning mass flow rate) and pressure oscillations are obtained. They occur at approximately H0+102s and H0+121s.

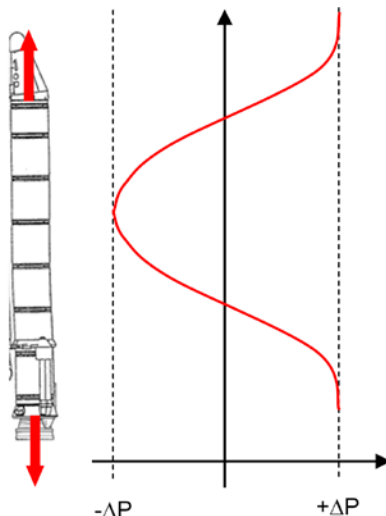


**Figure 6-22: Second acoustic mode on Ariane 5**

The frequency range concerned by the 2nd acoustic mode is [37-48 Hz] (extended to [33-53 Hz] to take into account model discrepancies). As for the 1st acoustic mode, the limit excitation levels come from flight and ground firing tests statistics. A constant value is applied on the frequency range associated to each flight time studied.

The modal bases are computed up to 80 Hz with 1% modal damping for all modes except the boosters' first longitudinal modes. Interface and internal responses are computed in the frequency domain.

The other contribution to this flight phase (gimballing) has effects only in terms of launcher / spacecraft interface bending moment. That is why a limit value is summed up with the ones obtained for the computed load cases and why it is not considered for the interface accelerations and internal responses.

Two summations are performed on the load factors: one for the maximum longitudinal acceleration event and one for the SRB thrust tail-off phase. The envelope of these two summations is presented.

#### 6.4.5.6 SRB jettisoning

This event occurs around H0+140s. This load case consists of the instantaneous release of the SRB / EPC interface forces on DAAV and DAAR. The SRB thrust asymmetry and zero gimballing reset of the nozzles (EPC and SRB) is also taken into account in these interfaces forces. Two different cases are studied:

- “symmetrical” that maximizes the sum of the longitudinal forces on DAAV;
- “asymmetrical” that maximizes the difference of the longitudinal forces on DAAV.

The modal base (without SRB) is computed up to 100 Hz. The modal damping used is equal to 1% for all modes, except for the longitudinal mode of the EPC hydrogen tank. For this one a synthesis is performed. Interface and internal responses are computed in the time domain.

#### 6.4.6 Aspects of the Ariane 5 CLA methodology

After having coupled the spacecraft mathematical model to the launcher model, the normal modes of the composite are computed for each flight event studied. A complete three-dimensional model with compressible fluids is used. It contains more than 100 000 DOF.

The responses are then computed by mode superposition. The analysis type used is transient, random or harmonic depending on the load case. The nonlinear behaviour of the SARO (friction damping system used to reduce the pendulum effect of the oxygen tank of the ESC-A stage) is taken into account for the lift-off and the first acoustic mode of the boosters. For the other load cases, it can be modelled as a rod. Concerning the modal damping used in the computations, a constant value is considered (1% for most of the case), except for load cases which are highly sensitive to this parameter (as the rear part buffeting and the EAP acoustic modes). For internal responses, the real spacecraft damping is taken into account for high frequency responses load cases. When several load cases occur during a flight event, they are combined by summation on their QSL. The static part associated to the load cases presented in the following is only taken into account for the calculation of QSL and interface mechanical fluxes.

All CLA results normally correspond to limit values. No additional coefficients are needed, but the qualification factor (see the Ariane 5 User's Manual) is considered before comparing CLA results to qualification test results. The QSL are normally obtained using the following expressions analogous to Eqs. [5-81] and [5-82]:

$$QSL_{Longitudinal} = \frac{N}{M_{SC}} \quad QSL_{Lateral} = \frac{M_{Lat}}{M_{SC} h_{CoG}} \quad [6-23]$$

with:  
 $N$  longitudinal force at the spacecraft / launch vehicle interface,  
 $M_{Lat}$  bending moment at the spacecraft / launch vehicle interface,  
 $M_{SC}$  spacecraft mass,  
 $h_{CoG}$  height of the spacecraft CoG relative to the spacecraft / launch vehicle interface.

If some QSL exceed the specification of the Ariane 5 User's Manual [4], the interface mechanical fluxes are computed by the following formulations using the convention of negative values for compression and positive values for tension.

$$f_{Compression} = \left( \frac{N_{Static} - N_{Dynamic}}{2 \pi R_{IF}} \right) - \left( \frac{M_{Lat}}{\pi R_{IF}^2} \right) \quad [6-24]$$

$$f_{Tension} = \left( \frac{N_{Static} + N_{Dynamic}}{2 \pi R_{IF}} \right) + \left( \frac{M_{Lat}}{\pi R_{IF}^2} \right) \quad [6-25]$$

where:  
 $N_{Static}$  Longitudinal static force (negative)  
 $N_{Dynamic}$  Longitudinal dynamic force amplitude (positive)  
 $M_{Lat}$  Lateral bending moment amplitude (positive)  
 $R_{IF}$  Interface radius

## 6.5 The ArianeSpace spacecraft qualification process

### 6.5.1 Introduction

All spacecraft flying on the Ariane 5 launcher are subjected to the qualification process here reported. Specifications are associated with each type of environment and the compliance with each excitation demonstrated by spacecraft system tests:

- A *static test* is performed on the primary structure equipped with its main components (STM-like) to demonstrate that the Spacecraft is compliant with the static plus dynamic overall quasi-static loads specified in the Ariane 5 User's Manual plus the line-load peaking induced by the boosters thrust (all parameters include the qualification factor). By default, the spacecraft static qualification is pronounced by comparison with the launcher specification. However, CLA outputs may be used in case of non-compliance. The comparison is performed at a qualification level, e.g. including a 1.25 qualification factor on top of the CLA raw static plus dynamic limit level predictions. For spacecraft series, the static test may be performed once as long as it covers the specification including the qualification factor.
- A *sine vibration test* is performed at spacecraft system level in the flight configuration mostly to conclude on the equipment flight worthiness once integrated on the spacecraft in a flight configuration. The CLA raw limit level dynamic predictions are summed up with the steady state acceleration of the launcher (mainly longitudinal) and increased by a 1.25 qualification coefficient before comparison with test measurements. The comparison is made:
  - at the interface in terms of equivalent sine level, in order to conclude on the acceptance of non-simulated flight events (e.g. plateaus associated with dimensioning values resulting from the launcher qualifications studies and/or post-flight detailed analyses);
  - at *each OTM location* corresponding to a transducer in the sine vibration test. Transfer functions from the spacecraft interface to the OTM location are corrected by the adequate coefficient (as deduced from the test prediction vs. test measurement analysis). In practice, the worst under predictive response axis correction is applied to all the axes given that the CLA responses are obtained from multi-degree of freedom excitations. As mentioned in Section 6.5.3.3, summing the steady-state acceleration to the OTM dynamic response is a very conservative approach when the success criterion to conclude on the qualification status of the spacecraft is based on a dynamic test rather than on a static test.

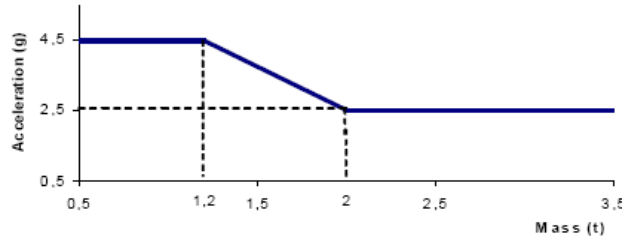
Both comparisons are made at the qualification level by increasing the CLA raw limit level static plus dynamic predictions by a 1.25 qualification coefficient. Attention should be paid to primary notching only if dynamic accelerations predictions are much higher than the launcher specifications. This may happen if the simulations assumptions of the launcher qualification studies have been updated for considering in-flight and/or on-ground issues a posteriori. Otherwise, the qualification status with respect to primary notching should be directly deduced from static tests results.

## 6.5.2 Quasi-static loads

The spacecraft authority should perform a static test at qualification level in an STM-like configuration at least.

Acceleration (g)	Longitudinal		Lateral	Additional line load (N/mm)
	Static	Dynamic	Static + Dynamic	
Critical flight events				
Lift-off	- 1.8	$\pm$ 1.5	$\pm$ 2	26
Aerodynamic phase	- 2.7	$\pm$ 0.5	$\pm$ 2	23
Pressure oscillations / SRB end of flight	- 4.40	$\pm$ 1.6	$\pm$ 1	37
SRB jettisoning *	-0.7	$\pm$ 3.2	$\pm$ 0.9	0

\* This flight phase leads to a 2.5 g tension case, except for a spacecraft with first longitudinal frequency above 40 Hz where the tension value is the following:



*The minus sign with longitudinal axis values indicates compression.  
Lateral loads may act in any direction simultaneously with longitudinal loads.  
The Quasi-Static Loads (QSL) apply on payload CoG.  
The gravity load is included.*

**Figure 6-23: Ariane 5 QSL and boosters line loads specifications**

Sets of forces and moment should be applied to the structure in order to cover the QSL specifications from the MUA5 (see Figure 6-23).

Table 6-6 provides a comparison example (the “QSL S/C” column corresponds to QSL deduced from static tests whereas the “QSL MUA 5” column refer to the total loads to be demonstrated, both without line loads).

**Table 6-6: Static test – Test vs. MUA5 specification QSL (example)**

<b>Flight event</b>	<b>QSL MUA 5 (g)</b>		<b>QSL S/C (g)</b>	
	Longi.	Latéral	Longi.	Latéral
Lift-off	-3.2	$\pm$ /- 2.0	-3.87 *	$\pm$ /-2.42 *
Max. dynamic pres.	-3.2	$\pm$ /- 2.0	-4.00 **	$\pm$ /-2.5 **
SRB end of flight	-6.0	$\pm$ /- 1.0	-8.80 *	
SRB jettisoning	+2.5	$\pm$ /- 0.9		
				$\pm$ /-2.5 **

\* Specific test on the primary structure of the spacecraft only (e.g. the spacecraft “platform”)

\*\* STM generic test

The QSL from tests should be then converted into interface mechanical compression and tension fluxes in order to add the additional line-loads peaking from Figure 6-23. Line loads are due to the boosters thrust which induce sinusoidal deformation of the central cylindrical body up to the spacecraft base. As these line load peakings are directly linked to the boosters thrust, they depend on the flight phase. The resulting interface fluxes should be then compared with the ones deduced from the limit level QSL of the MUA5 specification (also including line loads peaking), flight phase by flight phase, as shown in Table 6-7. A qualification factor of 1.25 (e.g. the “factor column” hereunder) should be eventually demonstrated.

**Table 6-7: Static test – Test vs. MUA5 specification fluxes (example)**

	<b>MUA 5</b>					<b>S/C Test</b>		<b>Facteur</b>
	<b>QSL MUA (g)</b>			<b>Flux (N/mm)*</b>		<b>Flux (N/mm)</b>		
<b>Flight event</b>	Longi.	Latéral	Surflux	Comp.	Tens.	Comp.	Tens.	
Lift-off	-1.8±1.5	+/- 2.0	26N/mm	-198.81	154.79	377.3	301.0	<b>1.90 / 1.94</b>
Max. dynamic pres.	-2.7±0.5	+/- 2.0	23N/mm	-194.59	128.56			
SRB end of flight	-4.55±1.45	+/- 1.0	37N/mm	-176.59	65.33			
Booster jettisoning	+2.5	+/- 0.9			90.17			

\* Flux (line loads) are computed according to the following expressions using the convention of negative values for compression and positive values for tension.

$$f_{Compression} = \frac{N}{\pi D} - \frac{M_{Lat}}{\pi D^2 / 4} - surflux \quad f_{Tension} = \frac{N}{\pi D} + \frac{M_{Lat}}{\pi D^2 / 4} + surflux \quad [6-26]$$

where  $N$  Longitudinal force (negative)

$M_{Lat}$  Lateral bending moment amplitude (positive)

$surflux$  Overflux (line loads peaking) amplitude

$D$  Diameter of SC interface

In this example, the spacecraft static qualification is directly demonstrated by test.

As already mentioned the CLA predictions may exceed the launcher specifications, even though they are not supposed to. Therefore, the spacecraft static test results plus line loads should be also compared with the ones deduced from the coupled loads analysis, as shown in Table 6-8.

**Table 6-8: Static test – Test vs. FCLA fluxes (example)**

	<b>CLA</b>					<b>S/C</b>		<b>Facteur</b>
	<b>QSL CLA (g)</b>			<b>Flux (N/mm)*</b>		<b>Flux (N/mm)</b>		
<b>Flight event</b>	Longi.	Latéral	Surflux	Comp.	Tens.	Comp.	Tens.	
SRB end of flight	-4.55±2.10	+/- 0.7	20N/mm	126.20	57.70	221.67** 246.1***	130.32** 196.8***	1.76/2.27 1.95/3.41

\*\* Specific test on the primary structure of the spacecraft only (e.g. the spacecraft “platform”)

\*\*\* STM generic test

In this example, the dynamic longitudinal load factor associated with the SRB end of flight phase is above the MUA5 specification by 0.50 g ( $\pm 2.10$  g in FCLA vs.  $\pm 1.60$  specified in Figure 6-23), the static longitudinal is also above by 0.15g (4.55 in CLA vs. 4.40 specified in Figure 6-23). However, the exceedance is acceptable once all QSL are converted into interface mechanical fluxes and compared with the sets of results from tests. Interface mechanical fluxes are mostly driven by lateral loads. Therefore exceeding the longitudinal specification is not usually a major issue for qualifying spacecraft.

## 6.5.3 Dynamic environment

### 6.5.3.1 Overview of the dynamic environment qualification process

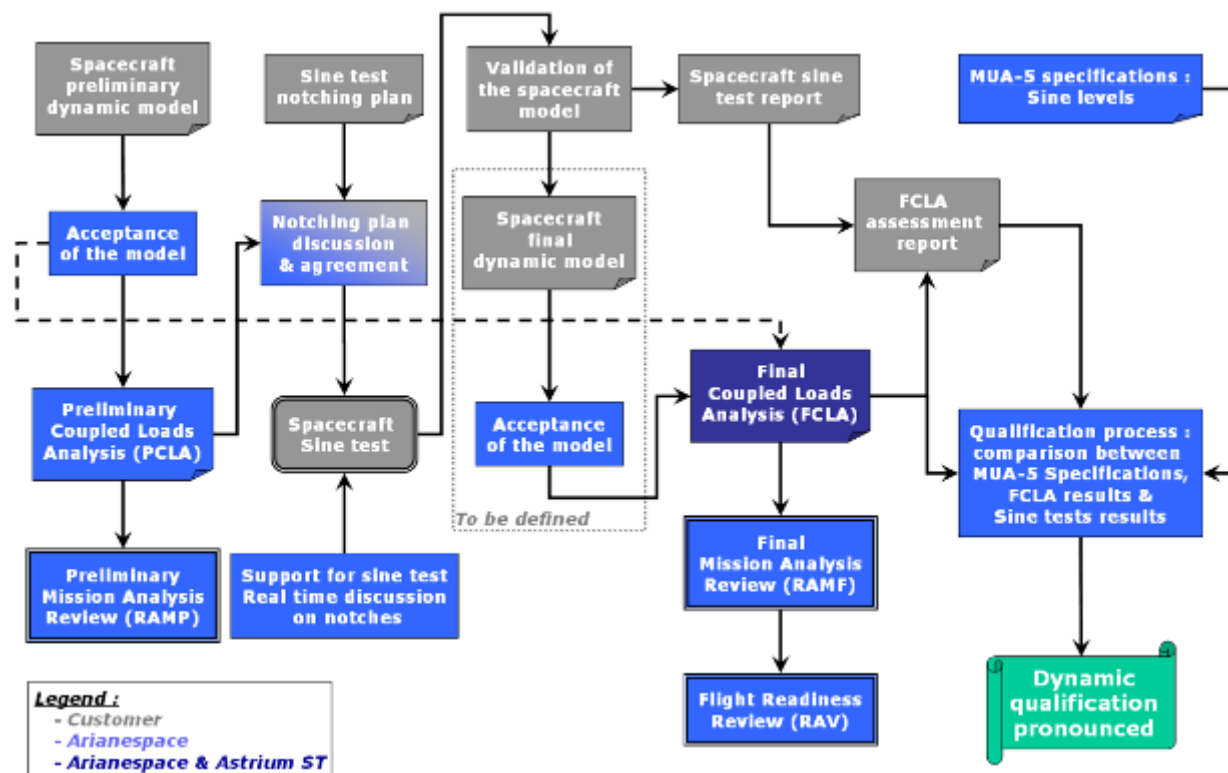
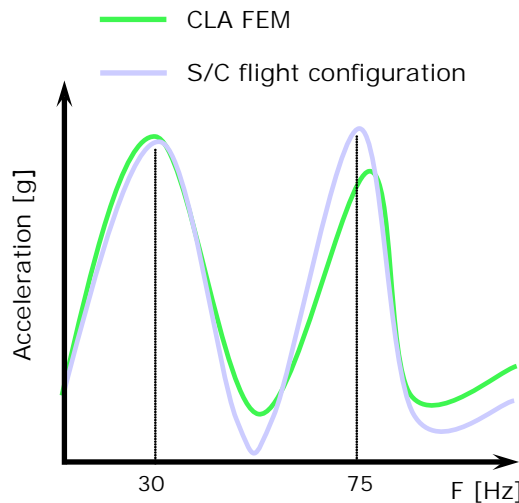


Figure 6-24: Arianespace dynamic overall qualification process

A first spacecraft “Preliminary Dynamic FEM” is modelled by the spacecraft authority. An acceptance loop is done by Arianespace with this model to verify its compliance with the Ariane 5 General Specification [21], as done by Astrium Space Transportation for the FCLA later on (refer to Section 6.4.1). Then, this model is used for a PCLA. Results are presented during the Preliminary Mission Analysis Review (RAMP). In parallel, a sine test notching plan is proposed by the spacecraft authority and discussed with Arianespace. PCLA predictions are used as a support to evaluate if notches can be accepted: the proposed interface excitation levels should at least cover PCLA interface accelerations in terms of equivalent sine dynamics levels. However, the sine test excitation profile should be based on the maximum acceptable level for each item of equipment: The sine test profile should be based on spacecraft limits and then compared to the CLA. CLA should not be the guideline for defining the sine profile.

Once sine tests are achieved, the correlation between test measurements and FEM predictions is checked (e.g. comparison of frequencies and magnitude of each mode). The Ariane 5 General Specification [21] mentions that “the comparison between test and prediction should indicate less than 5% shift in frequency for primary modes, and less than 10% for the main secondary structures” for instance. A 20% discrepancy is also allowed on transfer functions.



**Figure 6-25: FRF comparison of test and prediction**

For each equipment item a comparison between actual spacecraft in flight configuration and CLA model transfer functions is performed as illustrated in Figure 6-25. If the model is not accurate enough, a new dynamic model designated as the “Final Dynamic FEM” should be generated by the spacecraft manufacturer and cross-checked by Arianespace. This final correlated model is then used to perform the FCLA. Results are presented during both Final Mission Analysis Review (RAMF) and Flight Readiness Review (RAV), as explained in Section 6.4.2. The results of the FCLA are the input data for the dynamic qualification assessment process. This qualification process includes a comparison between the Ariane 5 User’s Manual specifications, the FCLA results and the sine test results. The following sections detail this process.

### 6.5.3.2 Spacecraft sine tests

The spacecraft qualification levels are Ariane 5 User’s Manual sine levels specification multiplied by a qualification factor of 1.25 [4]. The Ariane 5 standard qualification procedure assumes a prototypical model subjected to prototypical levels.

These qualification levels are presented in Table 6-9, Figure 6-26 and Figure 6-27 hereafter.

**Table 6-9: Ariane 5 sinusoidal vibration tests levels**

Sine	Frequency range (Hz)	Qualification levels (0-peak)	Protoflight levels (0-peak)	Acceptance levels (0-peak)
Longitudinal	2-5* 5-50 50-100	12.4 mm 1.25 g 1 g	12.4 mm 1.25 g 1 g	9.9 mm 1 g 0.8 g
Lateral	2-5 5-25 25-100	9.9 mm 1 g 0.8 g	9.9 mm 1 g 0.8 g	8.0 mm 0.8 g 0.6 g
Sweep rate		2 oct./min	4 oct./min	4 oct./min

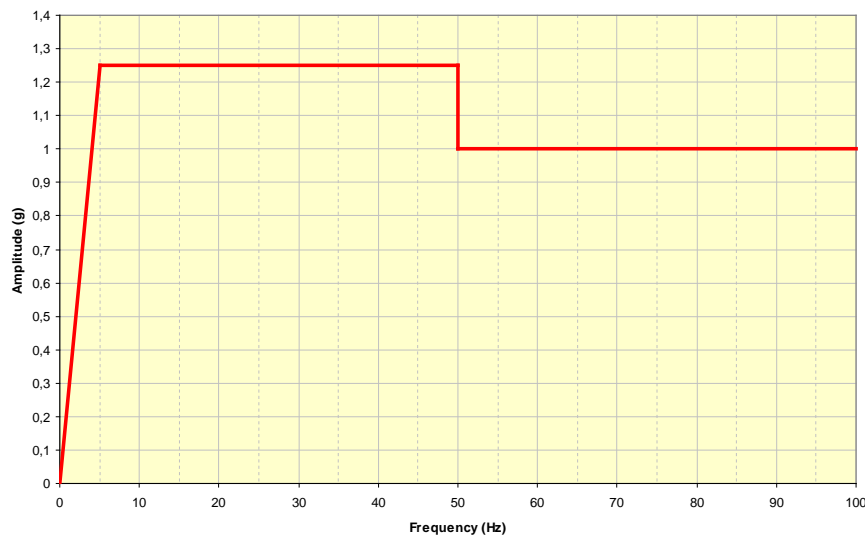


**Figure 6-26: Ariane 5 longitudinal sine test specification**

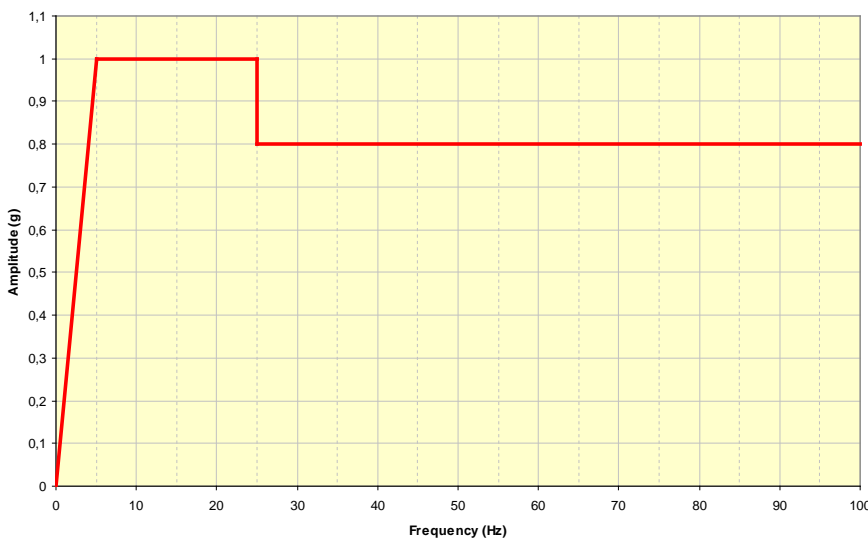


**Figure 6-27: Ariane 5 lateral sine test specification**

As a reference, the Ariane 5 User's Manual mentions that "the objective of the sine vibration tests is to verify the spacecraft secondary structure dimensioning under the flight limit loads multiplied by the appropriate safety factors. The spacecraft qualification test consists of one sweep through the specified frequency range and along each axis. Flight limit amplitudes are presented in Table 6-9 and applied successively on each axis. The tolerance on sine amplitude applied during the test is  $\pm 10\%$ . A notching procedure may be agreed on the basis of the latest coupled loads analysis (CLA) available at the time of the tests to prevent excessive loading of the spacecraft structure or equipment. However, it should not jeopardize the tests objective to demonstrate positive margins of safety with respect to the flight loads. Sweep rates may be increased on a case-by-case basis depending on the actual damping of the spacecraft structure. This is done while maintaining the objective of the sine vibration tests."

The Ariane 5 test factors, rates and durations are presented in Table 6-10:

**Table 6-10: Ariane 5 test factors, rates and durations**

<b>S/C tests</b>	<b>Qualification</b>		<b>Protoflight</b>		<b>Acceptance</b>	
	Factors	Duration/Rate	Factors	Duration/Rate	Factors	Duration/Rate
Static (QSL)	1,25 ultimate 1,1 yield	N/A	1,25 ultimate 1,1 yield	N/A	N/A	N/A
Sine vibrations	1,25	2 oct/min	1,25	4 oct/min	1.0	4 oct/min
Acoustics	1.41 (or +3 dB)	120 s	1.41 (or +3 dB)	60 s	1.0	60 s
Shock	1.41 (or +3 dB)	N/A	1.41 (or +3 dB)	N/A	N/A	N/A

On the launcher authority side, the objectives of spacecraft sine test are:

- Characterisation of the spacecraft dynamic behaviour
- Validation of the spacecraft mathematical model used for CLA
- Solicitation of the Spacecraft to its maximum acceptable capability
- Assessment of the need to perform complementary static test on main fundamental spacecraft modes (high axial loads and bending moments can be achieved)

As much as possible, the spacecraft is tested fully integrated in flight configuration. If for specific reasons flight hardware cannot be mounted, it is replaced by an equivalent mass and inertia simulator. If not, a detailed justification is delivered (e.g. as for empty tanks configuration). Moreover, the following general rules are fulfilled:

- The impact related to test configuration on the notching profile is addressed (e.g. empty vs. full tanks)
- Excluding test configuration discrepancies, the mathematical model used for sine test predictions along with the CLA model are supposed to be fully consistent. If not, it should be clearly addressed and detailed
- The notch frequencies and depth should be minimized. Broad-band and manual notching should be avoided when possible

Moreover, the excitation should achieve the following levels:

- For primary structure (fundamental spacecraft modes) : CLA base force (moment)  $\times 1.25$  (not including static contribution if the Spacecraft static qualification is well demonstrated),
- For secondary structures (appendages/units responses) : 80% of the equipment capability (subsystem qualification levels or even design limit if acceptable).

### 6.5.3.3 FCLA predictions versus sine test results

Following the FCLA delivery, the spacecraft authority makes a formal assessment by comparison with sine test results:

- The FCLA results at qualification level (including a 1.25 factor) should be covered by sine test results. If not, a comparison with sub-system test results is performed. If sub-system test results are not available or not sufficient, this verification should be done with the equipment structural capability value (design value: analytical limit). In that case, FCLA results should be covered by a factor of 2.0 instead of 1.25. In other words, a 1.25 qualification factor is requested if the verification is done by test, a qualification factor of 2 is requested if the verification is performed by analysis.
- If the mathematical model validation process has produced some under conservatism in the transfer functions of specific locations, an appropriate factor should be applied on the related CLA results.

It is worth mentioning again that the quasi-static contribution (e.g. the steady state acceleration of the launcher) should be summed up with dynamic responses when comparing CLA total responses with sine vibration test measurement. The qualification factor should be applied to the total CLA response deduced alike. In practice, only the longitudinal quasi-static load should be added to OTM responses as the single major contribution in the transverse direction (e.g. during the transonic phase of the atmospheric flight) is already included in the recovered responses (see Section 5.3.4.9). Note that comparing static plus dynamic CLA responses to sine vibration test measurements is conservative since the static value specified in the User's Manual does not necessarily occur simultaneously with the maximum dynamic values. The standard sine test is not designed for covering such an environment. However, it is the only possible way in which Arianespace can assess the spacecraft qualification without discussing the entire design of the spacecraft - as done in the NASA approach. Of course, such a conservative approach can be relaxed on a case-by-case analysis since it may not always be justified to roughly sum the longitudinal quasi-static acceleration to OTM responses, and since the design may sometimes be the only reference for eventually concluding.

### 6.5.3.4 Examples

The profile shown in Figure 6-28 is an example of a typical profile for a longitudinal axis. This profile is given at the interface between the spacecraft and the launch vehicle.

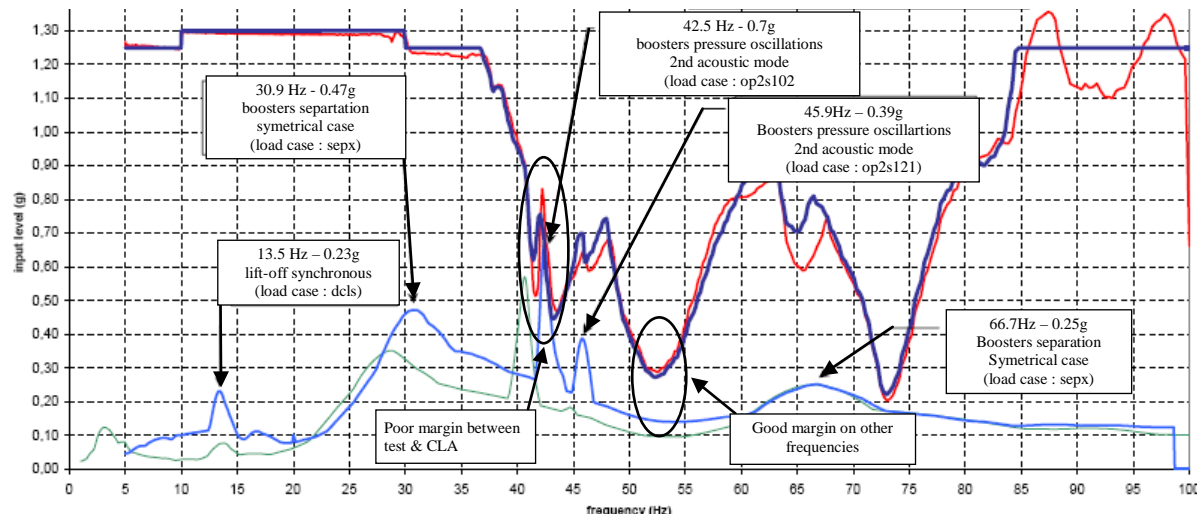


Figure 6-28: Ariane 5 LV/SC longitudinal acceleration profiles

The red curve is the actual profile of the sine test. This curve follows closely the blue curve which represents the theoretical level assuming a perfect control of the shaker. It is possible to see some "over-shooting" and "under-shooting" due to shaker control inaccuracy. These profiles (blue and red) are compared with the PCLA results (equivalent sine level in green) and the FCLA results (in light blue). CLA equivalent sine levels are computed considering a conventional Q-factor of 20, equivalent to a damping factor of 2.5%.

In this example, there is a poor margin between 40 and 45 Hz (in the SRB 2nd acoustic mode zone). In the other frequency ranges, a good margin is obtained. This does not necessarily mean that the spacecraft is not qualified in the [40- 45 Hz] frequency band and qualified elsewhere. To determine this, an analysis should be performed for each equipment item on the entire frequency range to determine if the unit modelling is conservative or not.

- First case: unit modelling is too conservative in the CLA model. Considering a specific sensitive unit 'A' response around 40 Hz, and a unit 'A' first assessment giving a CLA result (transient load case with qualification factor included) at 50g. The sine test results indicate an attained level of 10 g during the sine sweep. In this case, before conclude a non-compliance, one needs to check the Unit 'A' transfer function predicted by the CLA dynamic model and the one measured during the sine test (Figure 6-29).

The red curve is the predicted transfer function. The blue curve is the measured one. A factor of 10 appears between the predicted amplification of the Unit A at 40 Hz and the actual Unit A behaviour. In other words the CLA model was very conservative in this frequency band by a factor 10. Consequently, the correlated CLA level is in fact  $50\text{g}/10 = 5\text{g}$ . In this case, the "scaled" ratio between test and CLA result is now  $10\text{g}/5\text{g} = 2 > 1$ . We can therefore conclude this equipment item is compliant.

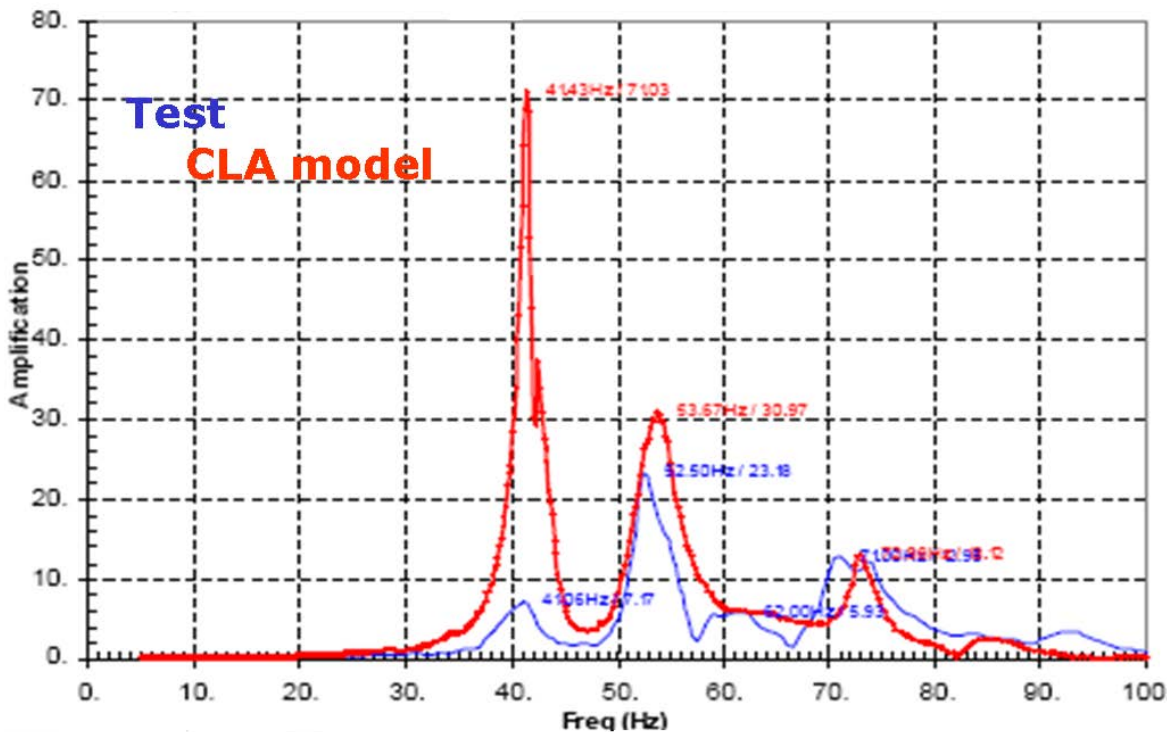


Figure 6-29: FRF Test/Prediction Comparison for the first case

- Second case: under conservative unit in the CLA model. In this case we consider a specific sensitive unit 'B' response around 50 Hz, and a unit 'B' first assessment giving a CLA result of 10g (transient load case with qualification factor included). The sine test result shows an attained level of 20 g. In this case, we could conclude that the equipment item is compliant with a comfortable margin, but the Unit 'B' transfer function has to be analysed in detail to validate this conclusion (Figure 6-30).

Indeed, a major under-conservatism of the CLA model appears at 52 Hz. A factor of 1.4 can be seen between the unit 'B' actual amplification (blue) and the CLA prediction (red). Consequently, the scaled CLA level is in fact  $10\text{g} \times 1.4 = 14\text{g}$ . In this case, the ratio between test and CLA result is  $20\text{g}/14\text{g} = 1.42 > 1$ . Therefore, we can confirm that this equipment is compliant.

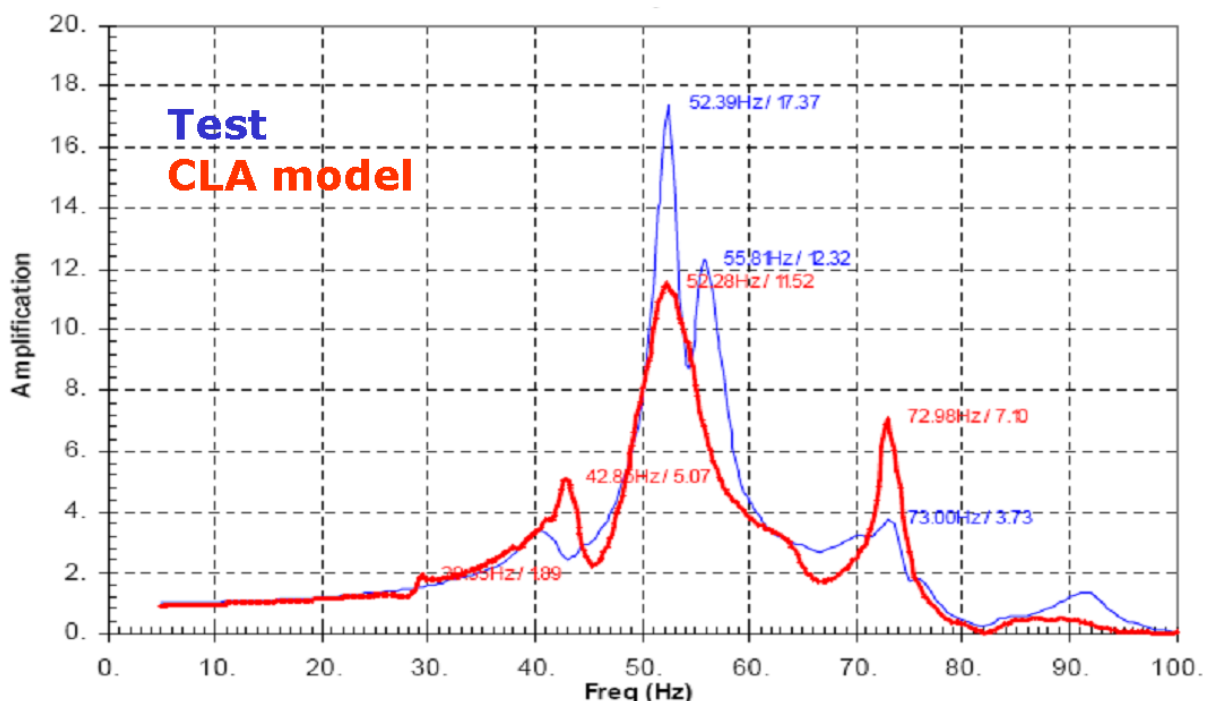


Figure 6-30: FRF Test/Prediction Comparison for the second case

## 6.6 Space Shuttle coupled loads analysis

### 6.6.1 Overview

The Space Shuttle Program requires performing coupled loads analyses during the different phases of the project.

Prior to flight on the Space Shuttle, all payload structures are demonstrated safe for flight and meeting all requirements for structure and safety from so-called *Design Coupled Loads Analyses* (DCLA). For all these CLA, the updated model of the cargo and the most current Space Shuttle Vehicle models and forcing functions are used. All these analyses provide a better loads estimate which can be used at the beginning of the project in lieu of the generic load criteria, established as initial design load criteria and with the progress of the project, values always more reliable to be compared with the design loads.

The *Verification Loads Analysis* (VLA) is the final official cargo system coupled dynamic and quasi-static structural analysis that is conducted prior to launch. Thus the VLA is the final structural mission risk assessment tool [11].

The launcher authority has the full responsibility of the VLA. DCLA can be performed by certified partners.

Several coupled loads analyses are foreseen in the frame of the Space Shuttle program. Coupled loads analyses are performed at each step of the design process by the Cargo Element (CE) developer [12]. The CE is designated as the entity that is installed in the Orbiter cargo bay and retained with latch assemblies or attached to side walls. Also additional load cycle analyses may be required during the design process to evaluate the effects of changes in either Cargo Element or Space Shuttle criteria. In the first step of the design process, the dynamic loads analysis results provide a better loads estimate and can be used when available in lieu of the generic load criteria, for establishing the initial design load criteria for design studies. A minimum dynamic uncertainty factor of 1.5 is used to multiply the elastic portion of the dynamic responses. The value of the uncertainty factor decreases to 1.1 when the Cargo Element is updated to reflect the results of appropriate tests and modal surveys. If the model correlation or validation is very good then the uncertainty factor can be removed. The results of the analysis are compared with the design load criteria and with load allowable previously established by strength analysis and proof or qualification tests. The final loads analysis cycle is conducted by the Space Shuttle Program prior to each Space Shuttle launch.

## 6.6.2 CLA load events

The load events analysed in the Space Shuttle CLA process are [12] [13]:

- Quasi-Static Flight Events,
- Transient Flight Events,
- On-orbit Loads Events.

The “quasi-static flight events” correspond to conditions for which the externally applied forces change slowly with respect to time and produce relatively small dynamic responses. Consequently, coupled transient dynamic analyses are not requested. For cargo elements having a statically indeterminate Orbiter interface, a coupled static analysis is used for determining mission specific Orbiter/Cargo Element deflections and interface forces. These events occur during Space Shuttle ascent and descent.

The transient flight events, typically lift-off and landing, correspond to conditions for which the external forces are highly transient in nature and significant elastic response occurs. The Space Shuttle Program is responsible for generating the Space Shuttle lift-off, landing and quasi-static models. These models are generated from detailed finite element of the Space Shuttle components. Models that are generated in response to a request from the CE developer contain a unique set of Cargo Element location.

Forcing functions and quasi-static deflections, for events associated with the launch vehicle, are developed by the launch vehicle organization. In general, launch vehicle organizations provide forcing function that envelope flight experience and are intended to yield load responses which are not exceeded with respect to a 99.87 percent probability.

Concerning the landing event, it should be noted that the Cargo Element can be distinguished in returnable and non-returnable cargo. The returnable cargo element is planned for return from orbit by the Space Shuttle, whether it is on the mission on which it is launched or on subsequent missions. Non-returnable CE is a cargo which is not intended to ever be returned by the Space Shuttle. The landing events can be divided in abort, contingency and nominal landings. The nominal landing

corresponds to the landing which is planned to occur after the completion of a successful mission. The contingency landing corresponds to the cases where a cargo element malfunctions or where an Orbiter on-orbit failure occurs. A return of the vehicle is requested with a cargo bay manifest which is neither the launch nor the planned landing manifest. The abort landing results from a Space Shuttle vehicle problem. The abort landing case utilizes the launch cargo bay manifest and contingency landings occur. Non-returnable cargo elements are designed to and compatible with abort landing requirements (refer to [12] and [13]).

## 6.6.3 Elements of the design and verification process for Space Shuttle payloads

### 6.6.3.1 Coupled loads analysis and load cycles

The preliminary spacecraft design is performed using loads provided by the Launcher Authority. These loads are given according to the weight of the payload. They correspond to the total externally applied force and moment on the Cargo Element and they are consistent with external forces generated by e.g. thrust, aerodynamics, wind shear, prelaunch constraints, entry manoeuvres, landing gear impact. They are valid for any location inside the Orbiter cargo bay and they can be linearly interpolated for intermediate weights. The lift-off limit load factor and angular accelerations proposed for a preliminary CE design are presented in Table 6-11 (as an extract from [14]):

**Table 6-11: Lift-off CE Limit Load Factors/Angular Accelerations for Preliminary Design**

	ZERO POUNDS	5,000 POUNDS	20,000 POUNDS	50,000 POUNDS	65,000 POUNDS
$N_x$ (G's)	+3.1 -6.0	+3.1 -6.0	+0.3 -3.2	+0.3 -3.2	+0.3 -3.2
$N_y$ (G's)	+3.5 -3.0	+3.5 -3.0	+1.6 -1.6	+0.4 -0.4	+0.4 -0.4
$N_z$ (G's)	+6.4 -6.4	+6.4 -6.4	+3.5 -3.5	+1.5 -1.5	+1.5 -1.5
$\phi$ (RAD/SEC <sup>2</sup> )	+10.0 -10.0	+10.0 -10.0	+8.0 -8.0	+3.0 -3.0	+3.0 -3.0
$\theta$ (RAD/SEC <sup>2</sup> )	+35.0 -35.0	+35.0 -35.0	+8.0 -8.0	+6.0 -6.0	+6.0 -6.0
$\Psi$ (RAD/SEC <sup>2</sup> )	+12.0 -12.0	+12.0 -12.0	+5.0 -5.0	+2.5 -2.5	+2.5 -2.5

In a similar way, loads factors for secondary structures are indicated by the launcher authority.

As indicated in the NSTS 14046 [15], the payload developer is encouraged then to perform multiple cycles of loads analysis, coupling both launcher and payload mathematical models and applying the forcing functions as delivered by the Launcher Authority. The analysis results using the preliminary design load factors should be superseded by theses CLA results. Then, a possible optimization of the design may be evaluated in order to increase the operational mass of the payload. As soon as the design is frozen, the modelling of the payload is also frozen and a CLA can be performed in the frame of the Critical Design Review (CDR). Eventually, the payload validated FEM in the defined flight configuration is delivered to the Launcher Authority to predict the flight loads and deflections during the Verification Loads Analysis (VLA). During all these CLA an uncertainty factor is applied to the dynamic response of the structure, as required by the Launcher Authority. The assessment status of the payload FEM is a criterion to refine this uncertainty factor.

### 6.6.3.2 Cargo Element FEM validation process

NASA recommends modal survey tests for correlating frequencies, mode shapes and damping assumptions (while Arianespace suggests exploiting sine vibration tests measurements for correlating transfer functions directly). The system FE model (primary structure plus secondary structure) in the flight configuration is studied to select a set of modes ("target modes") able to properly describe the dynamic behaviour of the spacecraft. The target modes are normally selected upon a number of criteria and from a visual inspection of the preliminary predicted mode shapes. The selection criteria usually are:

- the modal effective mass;
- the *strain energy distribution* over a number of logically chosen element groups;
- the modal contribution to the design driver parameters under the worst possible flight conditions.

The "design driver" parameters (e.g. the global net accelerations, the Space Shuttle / CE primary structure interface forces, the primary structure / secondary structure interface forces) are selected because they constitute the main load path of the primary structure. The modal contribution to these parameters is computed from a dedicated coupled loads analysis which is limited to a restricted number of critical cases. A modal survey test configuration is defined on the basis of that. The definition of the test configuration takes into account:

- the limited number of accelerometers and excitors,
- the accessibility for the instrumentation,
- the need to use a stiff test-stand which is able to support the CE primary structure, assuring an adequate decoupling between the test-stand alone and the primary structure.

The test configuration should have a significant advantage over the flight configuration: the reduced modal density. In this way, the acquisition of the modal parameters is simpler and more accurate. However the adequacy of the test performed using the selected test configuration should be demonstrated. For example, the same target modes as defined for the flight configuration should be identifiable. This can be demonstrated by "Modal Assurance Criterion" (MAC) and "Cross-Orthogonality Factor" (COF) using a set of degrees of freedom corresponding to the instrumentation plan, already demonstrated adequate for the identification of the modes [17] [18] [19] [20]. An example of adequate test condition is presented on Figure 6-31 and Figure 6-32, which reports the specific suspension elements designed to carry the trunnion of the test article with a high mounting stiffness in the restraints degrees of freedom and a low stiffness in the free degrees of freedom.

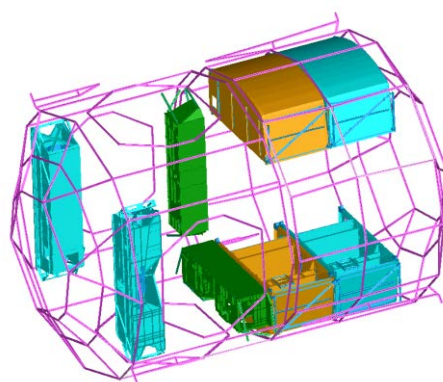
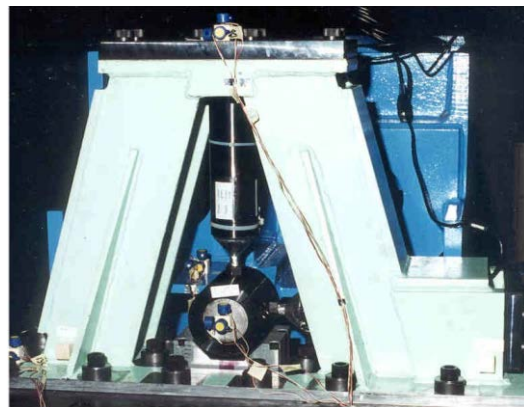


Figure 6-31: "NODE 2" test configuration

**Figure 6-32: Simulating the flight conditions**

The validation of the mathematical models of the CE secondary structures can be performed using the data collected during dedicated modal survey tests in flight-like configuration. For this reason the secondary structure absence during the modal survey test at the system level can be accepted. Also in this case, the test is finalised to the acquisition of a set of target modes. The update of the secondary structure FEM should be performed before performing predictions in view of modal survey test at the system level. Consequently, the second update activity at the system level and following its testing is related to the primary structure and to the interface between primary and secondary structures.

The update of the both primary and secondary structures FEM is carried out following the criteria reported in the NSTS 14046 [15]. This same document reports the assessment requirements.

### 6.6.3.3 Load combination

The Space Shuttle Program requires load combination for certain cases such as quasi-static loads. The following Table reports the environments which are applicable for the different mission phases.

**Table 6-12: Applicable environments for each mission phase [16]**

PHASE	ENVIRONMENT						
	LOW FREQUENCY	RANDOM	ACOUSTIC	CREW/EVR INDUCED	THERMAL	PRESSURE	SHOCK
Ground Transportation	X	X			X		X
Lift-off/Ascent	X	X	X			X	
On-Orbit (Orbiter)	X*			X	X	X	
On-Orbit (ISS) (US Element only)	X*	X*		X	X	X	X
Descent	X*				X	X	
Landing (Nominal)	X				X	X	
Landing (Emergency)	X				X	X	
Landing (Contingency De-orbit)	X				X	X	

The design loads factors for lift-off are derived by root-sum-squaring the random load factors with the low frequency transient load factors. The random loads factors are combined, in the appropriate translational direction, one axis at a time. After combining the appropriate translational low frequency and random load factors, the set of loads factors in each translational and rotational direction are then applied simultaneously. Random loads are not present at the landing. The random vibration loads acting on payload flight equipment result from the resonant structural response of the equipment to the random environment during launch. The random loads do not apply to large mass items since they do not respond to random vibrations. Random loads are calculated for items under 100 lbs (45.4 kg) [16].

## 6.7 References

- [1] Sarafin T.P. (editor), *Spacecraft Structures and Mechanisms-from Concept to Launch*, Kluwer Academic Publishers, Dordrecht, The Netherlands, 1995.
- [2] Calvi A., Nali P., "Some Remarks on the Reduction of Overtesting during Base-Drive Sine Vibration Test of Spacecraft", ECCOMAS Thematic conference on computational methods in structural Dynamics and Earthquake Engineering, Crete, Greece, June 2007.
- [3] Rockot User's Guide, Issue 05, August 2011.
- [4] ArianeSpace, "Ariane 5 User's Manual", Issue 5 – Revision 1, July 2011.
- [5] NASA Guideline No. GD-ED-2214, "Marman Clamp System Design Guidelines".
- [6] Astrium Space Transportation A5-DF-1-X-23-ASAI, "Description des excitations dynamiques basses fréquences et des amortissements pris en compte pour les études Système des lanceurs Ariane 5", to be issued.
- [7] Astrium Space Transportation A5-ST-1-X-19-ASAI, "Spécification technique relative à la réalisation des analyses couplées dynamiques finales", May 2007.
- [8] Alestra, Terrasse and Troclet, "Inverse Method for Identification of Acoustic Sources at Launch Vehicle Lift-off", AIAA journal, Vol. 41, No. 10, pp. 1980-1987, October 2003.
- [9] Schott, Troclet and Vanpeperstraete, "Caractérisation expérimentale du bruit au décollage du lanceur Ariane 5", Journal of Physics No. IV, Colloque C5, Supplement to the Journal of Physics No. III, Vol. 4, May 1994.
- [10] Bleton N., Brévière F. "Solid Rocket Boosters Thrust Oscillations Management at Launcher Level", AAAF Conference, Heraklion, May 2008.
- [11] MSC-HDBK-1974, "Guidelines for Loads Analysis and Dynamic Model Verification of Shuttle Cargo Elements", 1991.
- [12] NSTS 37329 "Structural Integration Analyses Responsibility Definition for Space Shuttle Vehicle and Cargo Element Developers".
- [13] NASA 21000-IDD-ISS, International Space Station Interface Document.
- [14] NSTS 21000, "Shuttle Orbiter / International Space Station Cargo Standard Interfaces", September 2008.
- [15] NSTS 14046, Rev. E, "Payload Verification Requirements", Space Shuttle Program, March 2000.
- [16] NASA – SSP52005, "Payload Flight Equipment Requirements and Guidelines for Safety-Critical Structures", Revision D, March 2008.
- [17] Calvi A., Fleming P., Notarnicola M., Evans E., "A Study to Define the Modal Survey Test Configuration of MPLM based on Loads Analyses Due to Transient Flight Events", Proc. of the Int. Conference on Spacecraft Structures and Mechanical Testing, Paris, France, June 1994.
- [18] Bellini M., Fleming P., "Definition of the Mini Pressurized Logistics Module (MPLM) Test Analytical Model (TAM) to Better the Chances of Conducting an Adequate Modal Survey Test", Proceedings of the Eleventh Symposium on Structural Dynamics and Control, Blacksburg, Virginia, USA, May 1997.
- [19] Bellini M., Quagliotti F., Spinello D., "COLUMBUS Modal Survey Test for the on-orbit Mathematical Model Validation", Proceedings of the Fourth International Symposium on Environmental Testing for Space Programmes, Liege, Belgium, June 2001.
- [20] Bellini M., "MPLM, COLUMBUS and NODE2 Modal Survey Tests and Mathematical Model Validation", Proceedings of 6th Cranfield Conference on Dynamics and Control of Systems and Structures in Space, Riomaggiore, Italy, July 2004.
- [21] ArianeSpace, A5-SG-0-01 Issue 4, "General specification for payload dynamic models", March 2001

# 7

# Static loads

## 7.1 Introduction

A static load is by definition a load of constant magnitude and direction with respect to the structure. Typical examples are the loads caused by joint preloads, pressure of stored propellant and the weight of supported components during spacecraft integration. Some loads are interpreted by the designer as static loads, however they are “equivalent” static loads, derived as combination of static and dynamic loading conditions. These loads are called “quasi-static”.

This chapter addresses the specification of the quasi-static loads and the verification of static loads by analysis or test. The reference document [1] provides requirements for static analyses and tests, with notes and suggestions related both to the analysis and test.

The next section specifically addresses the quasi-static loads. The rest of the chapter is focused on static tests.

## 7.2 Quasi-static loads

### 7.2.1 General aspects

In general the quasi-static load is defined as the combination of static and dynamic loads into an equivalent static load specified for design purposes. The quasi-static loads (QSL) are equivalent to, or interpreted by the designer as, static loads, typically expressed as equivalent accelerations at the CoG, also known as “CoG net accelerations”. In practical cases, the QSL are basically maximum and minimum values of the CoG net accelerations.

When the QSL are expressed in terms of load factors, attention should be paid to the sign convention, since the sign of a load factor is opposite that of the acceleration.

QSL are directly related to the (conservative) maximum load transfer capability requested to be available at the interface of two systems. QSL are normally specified as the more severe combinations of accelerations that can be encountered at any instant of the mission (ground and flight operations). The following points should be noted.

- In some cases the QSL are intended to cover only steady-state accelerations and the effects of low-frequency transient (e.g. this is usually the case for the QSL reported in the launcher user’s manual). In this situation the QSL normally are not high enough to envelope the effects of transient on secondary and tertiary structures.
- The QSL provided by the launcher user’s manual may not be fully adequate for the design of primary structures. This can happen for dynamic loading which cannot be properly represented by quasi-static loads, for example in presence of out-of-phase motion or fundamental local

modes. In fact QSL implies a “quasi-rigid” behaviour which is not far from the first global mode in each direction, but the quasi-rigid behaviour is quite different with respect to the other modes, i.e. upper global modes and local modes. In practice additional quasi-static load cases can be derived from dynamic analyses accounting for global accelerations and local accelerations due to out-of-phase local modes.

- The QSL can be verified by analysis and test. Simultaneous multi axes verification can be obtained by static analysis and static test. In case of vibration tests such as sine sweep or sine burst, the target loads are normally reached on one specific axis at the time, therefore the additional verification by analysis of the QSL should be anyhow performed.
- The “equivalence” between a dynamic loading condition and the equivalent accelerations at the CoG has some limitations due to the assumptions which are normally involved for the QSL calculation and use.

This last point is further detailed in the next section.

### 7.2.2 Equivalence between dynamic conditions and CoG net accelerations

The CoG net accelerations are calculated by means of the equivalent force at the CoG, which is the projection of all nodal forces in the rigid vector modal base, being the rigid vectors defined with respect to the CoG. An equivalence can be established between the (equivalent) force at the CoG and the CoG net accelerations, in terms of 3 translational and 3 angular CoG accelerations (see Section 5.3.4.6).

The above mentioned process establishes the equivalence in terms of resultant of the inertia forces (and external loads, if any) and allows the quasi-static loading conditions to reproduce the same resultant of interface forces with respect to the dynamic load case. As a consequence, the quasi-static loading conditions reproduce the “correct” interface forces and a conservative loading condition with respect to the interface loads, only if the structure has isostatic boundary conditions or the structure interface is rigid.

For statically indeterminate structures, specific procedures are established and implemented to account for the over-constraints effects, which can originate stresses in the structure considered massless (and therefore unloaded by its own inertia forces). These effects are usually named and accounted as “warpage” effects [2].

Note: the warpage in a statically indeterminate structure is defined as the interface displacements of a selected set of redundant degrees of freedom that produce, fixing all the other interface displacements to zero, interface forces equal to those of the actual flexible interface for a particular load environment [3].

In most of practical cases the angular accelerations are not considered and the “equivalent” QSL, expressed only in terms of translational accelerations, are determined with specific procedures which are, or should be, anyhow “conservative”. In this context it should be noted that lateral QSL for a satellite, in terms of “equivalent” CoG net accelerations, can be determined either by the maximum bending moment at the launcher interface or by the maximum shear force at the same interface. However the QSL calculated by the bending moment is often more conservative and more widely used. Refer to Section 5.3.4.6 for more details.

A final important remark is the following (e.g. [7] [8]). It has been mentioned that the quasi-static design of aerospace components is often based on a specified acceleration of the CoG of the component. However, the CoG of a flexible body is a virtual (not a real) point and its acceleration cannot be, in principle, neither accurately measured with an accelerometer in a vibration test nor

directly recovered as a local acceleration in a finite element analysis, particularly at frequencies above the fundamental resonance. For example, only well below the first resonance of the test structure, so that the structure might be assumed to move as a rigid body, the input acceleration is approximately equal to the CoG acceleration. Moreover it should be noted that once a body begins to flex under vibration, the CoG moves away from the static CoG and it is not anymore a point fixed relative to the structure (see Section 5.3.4.6). The CoG location depends on the mode shape and therefore on frequency, and is generally not located on the structure.

The conclusion is that the evaluation (both by structural analysis and test measurements) of the CoG net acceleration of the component is properly performed by means of the external forces. For example, for a pure translation, by Newton's second law, the CoG net acceleration is simply equal to the measured external force divided by the total mass.

Attempts to measure the CoG acceleration with an accelerometer usually overestimate the CoG response at resonances, so limiting these measurements to the CoG criterion (notching in a vibration test) results in an undertest [7].

### 7.2.3 Quasi-static loads specification

The launch loads environment is made up of a combination of steady-state, low-frequency transient and higher-frequency vibro-acoustic loads. In principle all vibrations which cause structural loads are considered for the calculation of the quasi-static loads, that is, the vibrations due to transient events, including steady-state acceleration and the random vibrations both transmitted through mechanical interfaces and caused by direct acoustic loading on the surface of the structure.

Often the loads due to various sources are computed separately and combination methods are used to derive the combined load. For primary structure, the steady-state and transient loads typically dominate the vibro-acoustic loads, and the latter are often ignored in practice. For secondary structure, however, the vibro-acoustic loads can be comparable to, or larger than, the steady-state and transient loads. Because the transient and vibro-acoustic loads can be of comparable magnitude, and both can be present simultaneously e.g. at lift-off, it can be unconservative to design the structure to the transient and vibro-acoustic loads separately. In this case peak loads from the various sources may be combined by a root-sum-square (RSS) approach.

Note: when determining the limit loads, consideration should be given to the timing of the loading events. For example the maximum steady state and dynamic events can occur at different times in the launch and may provide too conservative an estimate if combined. Also, the frequency band of the vibro-acoustic energy to be combined should be evaluated on a case-by-case basis.

Since the quasi-static loads are interpreted by the designer as static loads, these quasi-static accelerations are multiplied by the total mass of the item to obtain the applied loads used for preliminary design.

Preliminary sizing of spacecraft primary structure is based on quasi-static loads (or load factors) provided by the launcher user's manual or furnished by the launch vehicle organization. These load factors are applied at the spacecraft CoG and are based on design load databases, analyses of similar spacecraft, and flight data.

The preliminary design of spacecraft hardware or equipment items commonly utilize load factors obtained from semi-empirical curves developed for different launch vehicles and spacecraft configurations, the so called mass-acceleration curves (MAC) [9]. A typical mass acceleration curve is shown in Figure 7-1 [10]. In essence, it has been observed that the acceleration of physical masses of a payload is bounded by a curve. The MAC recognizes the fact that the lighter the mass, the higher the corresponding acceleration. This observation is true for both transient and random vibration analyses. The curves are usually based on a combination of prior flight and test data, analysis, and experience [9].

The MAC is an upper bound acceleration level for all components of a given mass, regardless of location, orientation, or frequency. Applicability is typically limited to appendage masses up to 500 kg, with frequencies up to approximately 100 Hz [10]. Such curves normally include the effects of both transient and random vibration, i.e. the load predicted by the curve is already a combination of transient and random vibration. It should be mentioned that MAC can be configuration sensitive.

Later in the program the quasi-static loads used for design and for analytical verification of the designs are refined by analysis. Mathematical models are then developed to initiate the load cycle process in order to ensure structural integrity and minimize weight. At low frequencies, the mathematical model of the spacecraft is almost always a FE model, whereas at somewhat higher frequencies, statistical energy analysis (SEA) or a boundary element method (BEM) model is often added.

The spacecraft loads are determined from a coupled spacecraft and launch vehicle model, and later the equipment loads are determined from a coupled equipment and spacecraft model. Obviously the validity of the FEM models depends on the skill of the modeller and upon the accuracy of the information used to develop the model. More sophisticated models are used as the programs mature. For example, in preliminary analyses of a spacecraft, much of the equipment may be modelled as a lumped masses at the equipment CoG. In this case, the calculated forces at the spacecraft and equipment interfaces are only valid at frequencies below the first resonance frequency of the equipment. Later in the program, the equipment may be represented by complex FEM's. But even these models are usually valid only in the frequency regime encompassing the first few modes of the equipment in each axis. One objective of coupled loads analyses is to maximize the upper frequency limit of the model. The validity of the models is often verified and extended to higher frequencies by refining the models with modal test data [7].

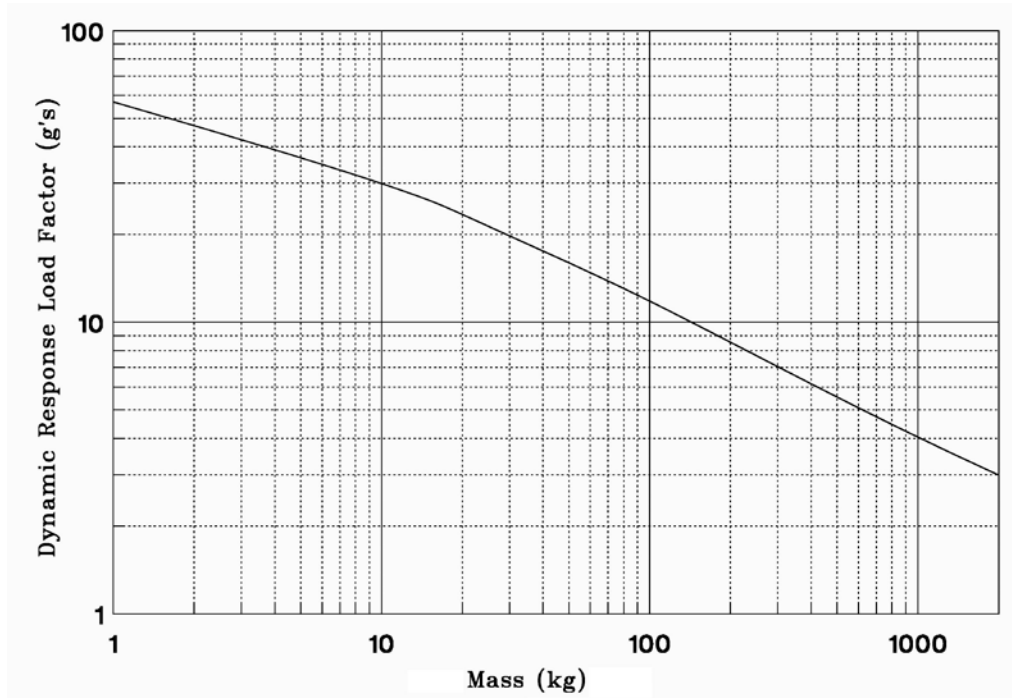


Figure 7-1: Typical Mass Acceleration Curve [10]

### 7.2.4 Prediction of QSL and mechanical environment by base-drive analysis

The quasi-static loads, and more in general the mechanical environment at lower level of assembly, can be predicted by base-drive analysis. In particular loads analysis in the frequency domain for sine vibration and random vibration are used. For example, using the spacecraft sine test specification provided by the launcher authority, the QSL for the instruments and units can be predicted by a spacecraft frequency response analysis. The recovery of the equivalent CoG acceleration of the components is properly performed by means of the interface forces. The prediction of QSL by base-drive analysis has the advantage of avoiding the execution of the relevant coupled analysis, e.g. in the time domain, however it can be very conservative with respect to the flight environment for a number of reasons. For example, considering the frequency response analysis performed by loading the spacecraft FE model with the specified acceleration spectra at the base and solving for the steady state vibration in the frequency domain, the following points should be noted:

- The sine test vibration specification is generally a conservative envelope of the launch transients.
- In general the base-drive analysis does not account for the relevant impedance effects. These effects can be very significant for the modes with large effective mass. In order to limit these effects, a primary notching strategy is normally applied. For example, the preliminary QSL of an instrument could be recovered by applying the sine input spectrum at the base of the spacecraft, notched at spacecraft fundamental modes.
- An incorrect estimation of the damping can result in significant “errors”. Considering the influence of the damping on the results, the maxima are proportional to  $Q_k$  for sine excitation and variable for transient excitation.
- The effect of the sine sweep rate is normally not taken into account in the analytical predictions of the structural response to the base-drive sine vibration test.

Similar considerations can be done for the base drive random vibration analysis, with the following specific remarks:

- Considering the influence of the damping on the results, the maxima are proportional to  $\sqrt{Q_k}$  for random excitation.
- The computational effort can be significant for large-size FE model and high modal density.
- The high frequency response can be questionable or unreliable.

In conclusion, the definition of QLS and mechanical environment of lower levels of assembly by base drive analysis has the main advantage of avoiding the relevant coupled loads analysis, however the limitations of the approach should be considered.

## 7.3 Static test philosophy and objectives

The static tests can be:

- Development,
- Qualification, and
- Acceptance tests.

Moreover, static tests can be performed on the whole structure, on a major structure assembly/component or on a single mechanical part.

Tests on scaled models are practically avoided in space engineering, and usually the static tests are performed on full-scale hardware.

For static development tests dedicated test articles are employed. For static qualification tests dedicated test articles are used in the verification prototype approach, whereas in the protoflight approach the qualification tests are performed on flight units. Static acceptance tests should be required for all the flight hardware (e.g. the proof pressure tests for pressurized hardware).

On the basis of above categorization, in accord with ECSS standards (see for example [1], Section 4.6.3), the static test objectives can be distinguished as hereinafter.

The static development tests are performed usually for mechanical parts and structure major assembly/component, rarely on the whole structure, in order to:

- evaluate design choices and concepts,
- verify analysis methods and mathematical models,
- determine failure modes and allowable loads,
- support the subsequent test campaign (e.g. the definition of static qualification tests).

The static qualification tests are performed for mechanical parts, major assembly/component or the whole structure in order to:

- verify that structure design and manufacturing techniques fulfil the specification requirements, by accounting for
- the worst hardware characteristics, which can be present in the flight unit but are not present in the test unit (e.g. by means of dedicated correction factors).

The static acceptance tests are performed on flight hardware to demonstrate that no workmanship defect prevents a structure item to fulfil the specification requirements. Typical static acceptance tests are:

- proof pressure tests of pressurized hardware
- proof tests of sandwich inserts
- acceptance tests of composite structures
- proof tests on central tube

## 7.4 Definition of static test configuration and load cases

### 7.4.1 Introduction

The following aspects are of primary importance in static tests definition and specification:

- the boundary conditions
- the load application
- the load cases
- the measurement instrumentation

## 7.4.2 Boundary conditions

The test article boundary conditions are one of the most critical subjects, especially in the case of a structure sub-assembly, but also for the test of the whole structure. The main load paths can be affected significantly by boundary conditions, which are then a fundamental parameter to judge that the test covers the flight conditions. There are two possible choices:

- use a “very stiff” fixture to fix the test article at the boundary interfaces , or
- use a test fixture with calibrated stiffness representative as much as possible of the true flight interface.

The first approach requires demonstrating that the test condition is more severe than the flight; the second approach needs design provision of a proper fixture representative of flight interface. In any case the stiffness of the boundary conditions is always well characterised and test measurements recover displacement and reaction forces at constrained interfaces. The stiffness measurements clearly require a separate experimental step, which should account for hysteresis phenomena whenever relevant.

The issue of the boundary conditions is particularly difficult for sub-assembly of the whole structure. Generally such a sub-assembly (e.g. secondary structure supporting payloads) has statically indeterminate constraints to the rest of the structure, which only approximately can be reproduced with calibrated stiffness of a test fixture. On the other hand, static tests on such sub-assembly could give better possibility of reproducing more accurately the loads acting on the sub-assembly, due to the lower complexity of the test configuration: this can be a good reason to prefer test on a subassembly (see also [1], Section 4.6.4, “Verification of composite structure”).

## 7.4.3 Loading systems

Sometimes the load application is a very simple matter, as for example for internal pressure in pressurized structure. In other cases it is very difficult to have a testing load condition representative of the flight situation. For example, in pressurized modules carrying payloads supported by secondary structures, the inertia launch loads are due to an acceleration field highly non-uniform, due to transient dynamic responses of the secondary structures.

The complexity of testing loads could influence the choice between possible test methods:

- traditional static test (with application of static loads)
- centrifuge test (with application of unidirectional linearly varying acceleration field)
- sine test on dynamic shaker (with application of quasi-static loads)

The centrifuge and sine tests sometimes are preferred because cheaper and shorter in schedule, but they have some limitations:

- for centrifuge test:
  - the centrifuge implies acceleration fields varying linearly with the radius, not always compatible with the required test loading, and then imposing a first limitation to test article size
  - the test facility capability could impose an additional limitation to the size of the test article
- for sine test:
  - it cannot be used if the control of the loading duration time is mandatory
  - the shaker powers allow only a certain mass/acceleration range of applications
  - additional instrumentation (e.g. accelerometers) is required

- for both centrifuge and sine tests:
  - they are unidirectional and require that the linear combination of the results can be applied (which could be difficult, due to e.g. common contact problems in the joints)
  - the combination with other load types (e.g. pressure and temperature) could be difficult

In traditional static tests the load application tools are usually jacks or weights, in conjunction with a proper levers system to introduce forces on attachment points or pressure on surface pads. Alternative systems as air-bags can be used to represent localized pressure loads. The most important point to design such loading fixture is however the decision of using dummies to represent payloads and reduce the number of testing forces. The drawback in this case is, again, to assess the dummy stiffness relevancy, and to evaluate if dummies with correct stiffness can be replaced by "rigid" dummies.

It is important to emphasize that everytime concentrated forces in the tests represent forces which are more "distributed" in real life conditions (e.g. body forces produced by launcher accelerations), different local load paths should be accounted carefully, with proper predictions, measurements and evaluations.

#### 7.4.4 Load cases

The definition of the test load cases includes two major points:

- The selection of the test load sets
- The level of the test loads

Each load set can include several types of loads (e.g. pressure, forces and thermal loads): minimization of the number of load sets and included load constituents is a compromise between cost reduction and test significance. As a consequence, a test load condition is not always coincident with a specific design load case, but frequently enveloping test load sets are defined to cover with the same test case, as far as possible, the maximum number of the structural items. Nevertheless this is not always achievable and it is possible that some items are not covered by defined test load conditions. In this case, examination of acquired measurements and applicability of extrapolation can suffice to cover the required demonstration by test (e.g. structure qualification). "Local" load cases can be considered, in addition to "global" test load cases on a whole structure test article, to test important aspects (e.g. load carrying capability of some interfaces).

The level of test loads depends from the type of the test, e.g. if development, acceptance or qualification test, and – for qualification - if protoflight or prototype approach is used. For development test the load level is strictly related to structure requirements and design loads, but is not defined directly by normative standards, depending from the needs of the investigation and from the engineering judgement (e.g. unitary "explorative" loads can be used to investigate structure behaviours). For acceptance and qualification tests, the load levels are defined by normative standards [5] which indicates test-coefficient KA (acceptance test factor) and KQ (qualification test factor) to be applied to the limit load in case of satellites and to the design limit load in the other cases. The basic distinction to be underlined is however between protoflight and prototype approach. In the case of protoflight approach, the test loads are part of the loads experienced by the flight hardware, and then are included in the limit loads and, for this reason, the design limit loads (which are equal or higher than the limit loads) are also higher than the qualification loads. In the case of prototype approach, the test is used to demonstrate structural adequacy to the design loads, and therefore the qualification loads are driven by the design loads.

Regarding KQ, the common practice for the static tests is to define more than a single level of qualification loads, depending from the requirements to be verified. Typically a first qualification level (e.g. equal to the limit or design limit load) is defined to verify functional requirements, a second

qualification level (e.g. equal to the design yield load) is established to verify no permanent deformation, and (in the prototype approach) a third qualification level (e.g. equal to the design ultimate load) is reached to verify no rupture requirements.

Less frequently, other qualification levels could need and are defined. For example, for pressurized overwrapped tanks the following qualification levels could be required: pressure at autofrettage, at maximum expected operating pressure (MEOP) and/or at maximum design pressure (MDP), at yield pressure (little higher than the acceptance proof pressure), at design burst pressure (ultimate level) and finally up to burst pressure (failure level) (see also [4]).

Finally, the test load level should account for any possible worst situation which can arise in flight model, but is not present in the tested hardware (e.g. lower thickness, boundary effects of adjacent structures, effects related to temperature, material properties scattering). These effects can be accounted by increasing the level of test loads, as indicated in Annex A of [5], where is explained the KQ correcting factors method as usually applied in European launch vehicle programs.

#### **7.4.5 Instrumentation**

In static tests traditionally the following instrumentation is commonly used to obtain direct measurements for quantities of interest:

- Transducers for displacements,
- Gauges (mono-, bi-, and tri-axial) for strains
- Load-cell for forces

Usually the stresses are not directly measured but are evaluated from strain measurements by applying a proper material constitutive law (e.g. the Hooke's elasticity law, the nonlinear material curve).

Figure 7-2 to Figure 7-8 refer to static qualification test campaign of the Automated Transfer Vehicle (ATV) Cargo Carrier, performed by TAS-I in Turin on 2002: it is a representative example of traditional arrangement of fixture, loading and instrumentation systems traditionally used in static tests. Typical measurements and prediction for this test are reported in Figure 7-9 and Figure 7-10.

Also other instruments and resources are now available, as pressure films for local contact pressure (e.g. pressure under bags, seals or bolted joints), photo-elastic paints, photo/video-cameras, etc. Direct measurements can be used to derive more complex quantities (e.g. several strain-gauges measurements to derive internal load path in a structural item or an interface force), and software packages can be provided to elaborate several measurements to monitor in real time some structural response quantities (e.g. a set of measured displacements to compute rigid body motion components). Properly instrumented and calibrated structural items or devices can convert direct measurements in a quantity to be monitored (e.g. a set of strain gauges on a bracket can be calibrated to recover force component on the bracket).

### **7.5 Static test evaluation**

Three levels of evaluations apply to a static test:

- Test execution correctness
- Test objectives successful demonstration
- Test significance evaluation

The test execution correctness relates to test facility quality assurance aspects. The following are examples of typical criteria:

- Test load are applied within specified tolerances
- No less than a minimum of instrumentation readings is reliable
- Test completion without test abort
- Data recordings are correctly provided

All these criteria are preliminarily checked by dedicated pre-test, before final test execution.

The successful demonstration of the test objectives is defined by specific “test success criteria”. Examples of typical success criteria are:

- No permanent deformation occurs at a specified test load (e.g. qualification yield level, or acceptance proof level)
- No rupture occurs at a specified test load (e.g. qualification ultimate load)
- Specified maximum displacement values are not exceeded at tested limit load

The evaluation of static test significance includes the examination of the following aspects related to test loading adequacy:

- Specified values of applied load components and resultants
- Values of external restraint reaction components and resultants
- Comparison of predicted and tested internal load paths
- Correlation of predicted and measured stress/strain and displacements

The loading systems directly control the applied load components (e.g. the hydraulic jack system allows the control of single force components). Therefore also the resultants of the applied forces can be evaluated and monitored.

Whenever possible, also the resultants of the restraint forces should be monitored for comparison. However, if this is difficult - due for example to continuously distributed boundary constraints – the restraint forces (or fluxes) at some location should be measured and correlated with predictions, in order to use test verified models to cover the comparison of applied and restraint force systems.

The internal loads path is an important aspect to be monitored. In fact a static test typically aims:

1. to verify that each structure component is able to sustain a certain design load, or
2. to experiment how “external” loads applied to the structure are distributed into the structure, in order to confirm the predicted stiffness of structural items and joints. Strain gauge measurements can be properly processed to derive the internal load paths.

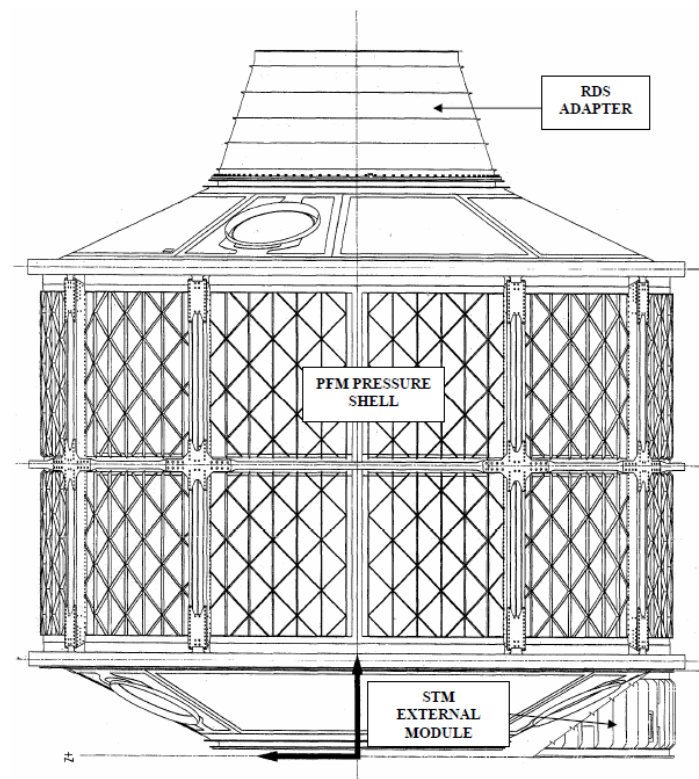
The stress analysis predicts displacements and stresses (or strains) expected in the test conditions, in order to demonstrate that the experimental behaviours are in line with the theoretical predictions and to judge the tests significance and adequacy. Moreover, based on test results, some analysis margins should be revised, due to important differences between predicted and measured quantities. Finally, a test verified static model should be available, to be used for additional not-testable conditions or to extrapolate test results (especially in the cases where nonlinear behaviours are presents, which do not allow simply linear extrapolation of test results, but require extrapolation based on test verified model).

The following correlation criteria, provided in [6], give an example of possible required correlation figures (however it is only an example and proper figures are established case by case by Programme applicable specifications):

- Model predictions for critical deflections are demonstrated within 10% of the test data.
- Model predictions for critical stresses are demonstrated within 20% of the test data.
- If the model predictions are outside the above stated correlation criteria, the model is updated until it meets the criteria and the analysis rerun.
- If the model predictions are within the correlation criteria but under-predict the test data, the stress analysis for flight load conditions is updated to reflect structural margins based on stresses that are adjusted according to the correlation results.

## 7.6 References

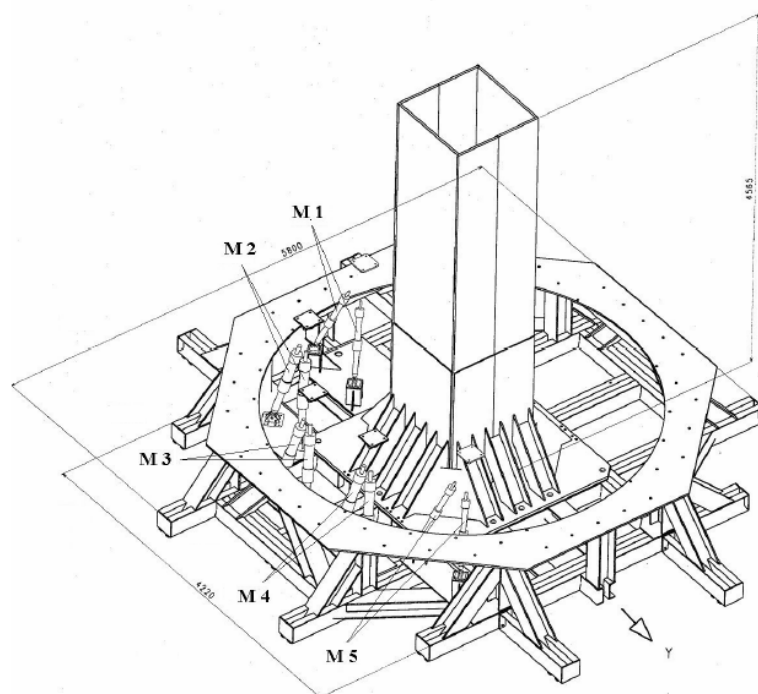
- [1] ECSS-E-ST-32C Rev.1, Space engineering - Structural general requirements, Noordwijk, The Netherlands, November 2008
- [2] Esclar D. - Derivation of 'warpage' figures for the APM payload racks. ESA Technical Note TOS-MCS/2000/171/Ln, Issue 1, 20 October 2000
- [3] Esclar D. – Biolab rack: post processing of Columbus module design coupled loads analysis. Guidelines and recovered data for Biolab payload verification - ESA Technical Note TOS-MCS/2002/704/LN/DE, Rev. 2, 23-01-2003
- [4] ECSS-E-ST-32-02C Rev.1, Space engineering – Structural design and verification of pressurized hardware, Noordwijk, The Netherlands, November 2008
- [5] ECSS-E-ST-32-10C Rev.1, Space engineering - Structural factors of safety for spaceflight hardware, Noordwijk, The Netherlands, March 2009
- [6] NSTS 14046, Rev. E, "Payload Verification Requirements", Space Shuttle Program, March 2000
- [7] Scharton T. D. - Force Limited Vibration Testing Monograph - NASA Reference Publication RP-1403, May 1997
- [8] NASA-HDBK-7004B – Force Limited Vibration Testing – January 2003
- [9] Trubert M., "Mass Acceleration Curve for Spacecraft Structural Design", NASA Jet Propulsion Laboratory, JPL D-5882, Nov. 1, 1989.
- [10] Combination Methods for Deriving Structural Design Loads - NASA-JPL Practice No. PD-ED-1211, <http://engineer.jpl.nasa.gov/practices/1211.pdf>
- [11] NASA-HDBK-7005 – Dynamic Environmental Criteria – March 2001



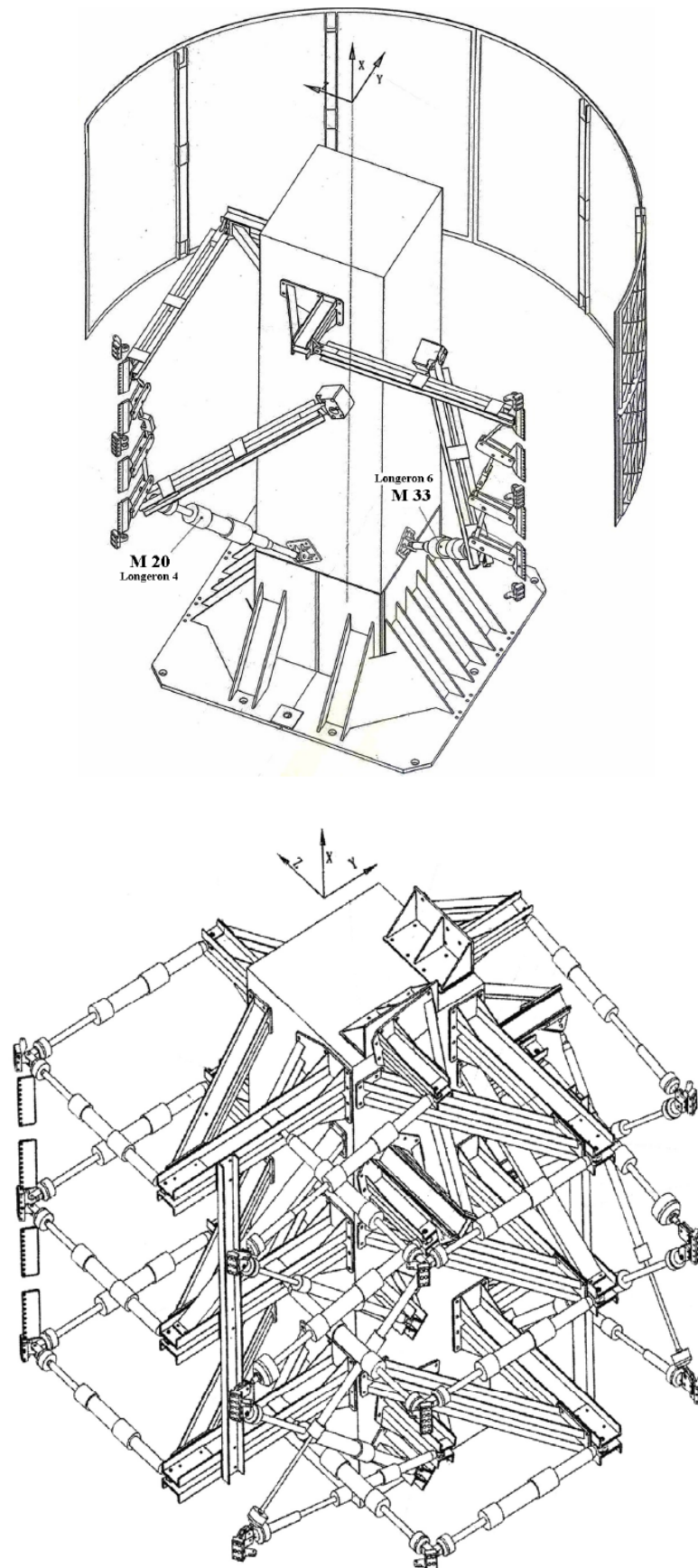
**Figure 7-2: Automated Transfer Vehicle (ATV) primary structure test article**



Figure 7-3: Setting of ATV primary structure static test



**Figure 7-4: ATV static test fixtures: “Base” to constrain the test article and “Tower” to support the internal jacks**



**Figure 7-5: ATV static test: internal loading jacks arrangement**

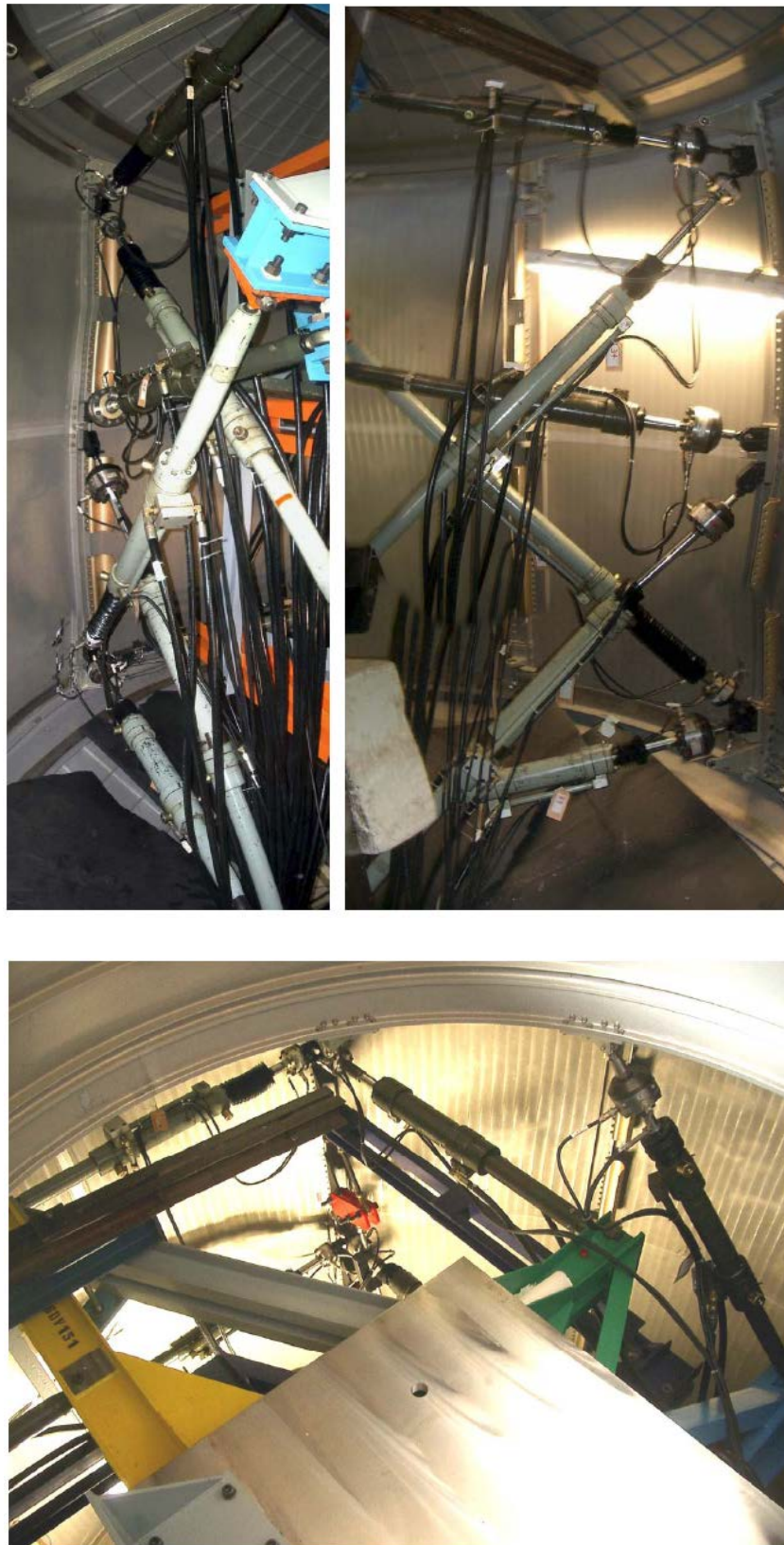


**Figure 7-6: ATV static test: internal loading jacks details**

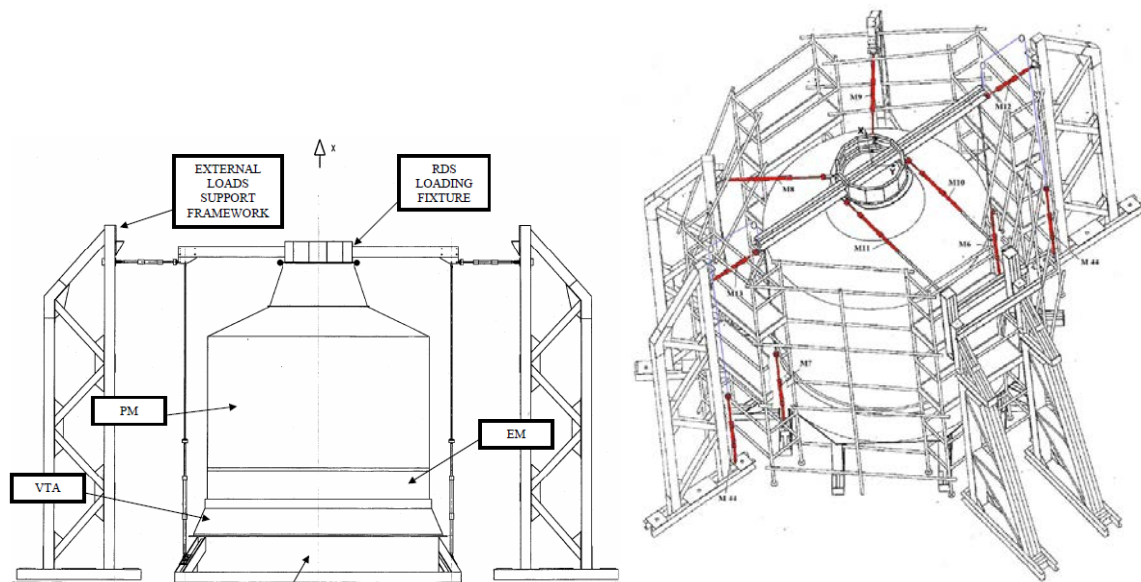
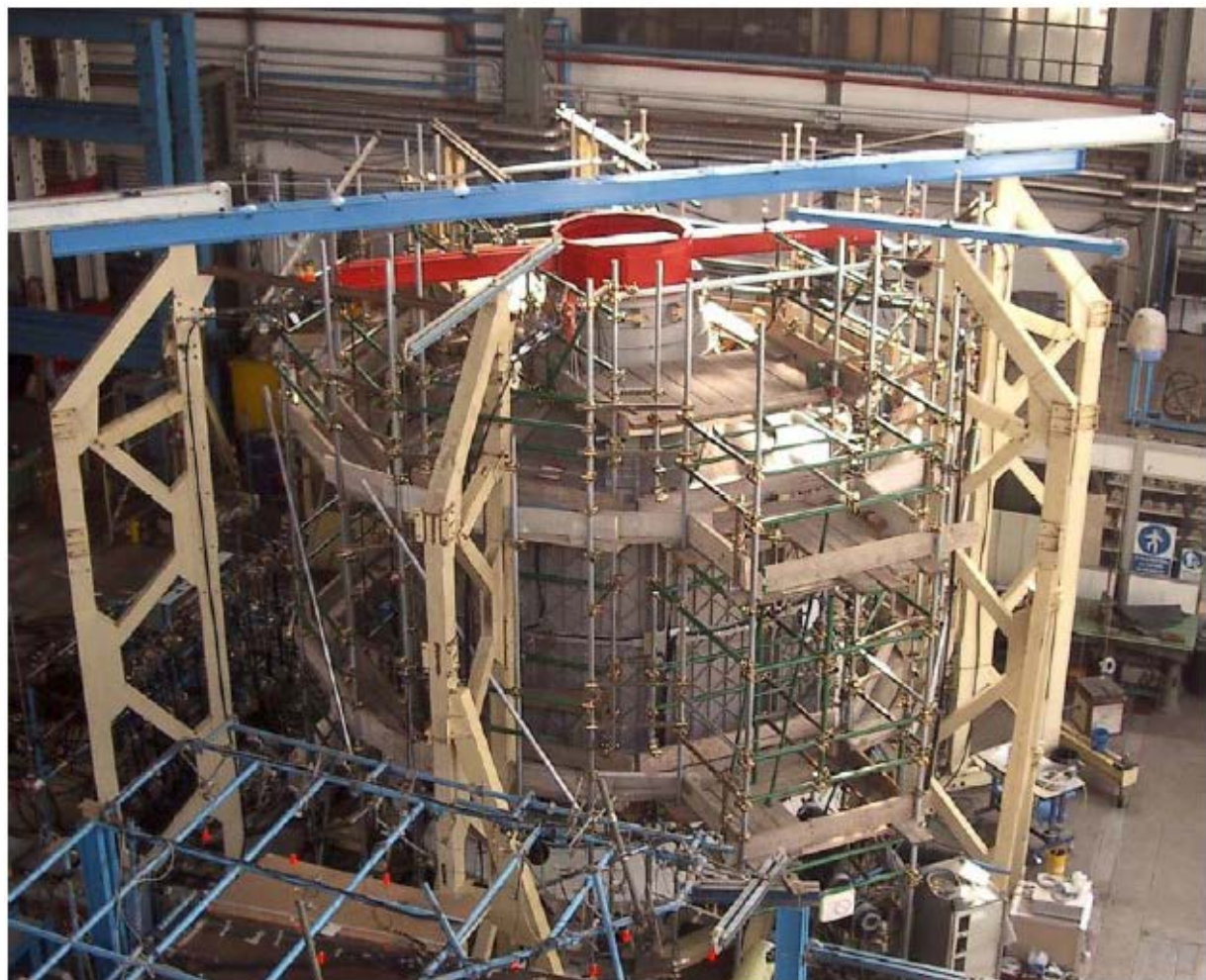
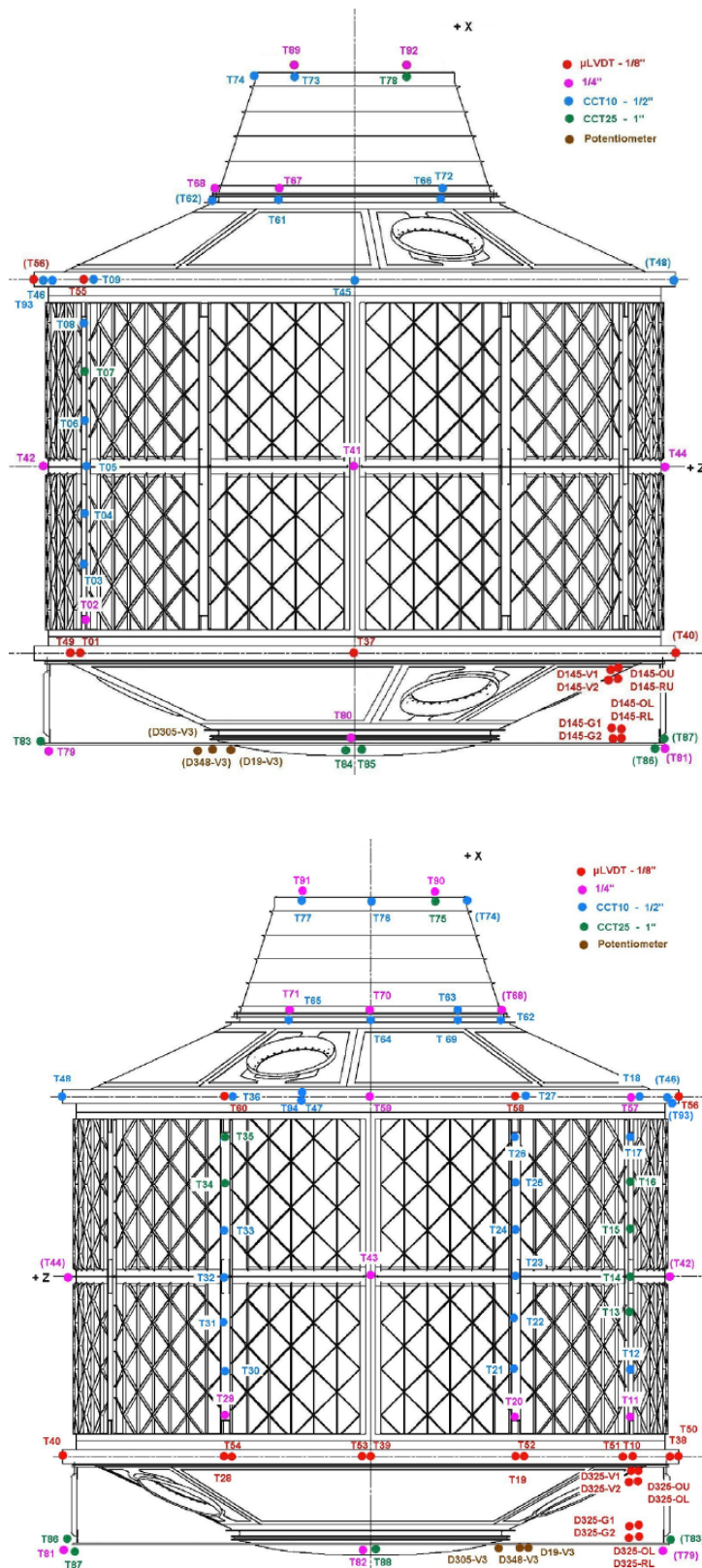
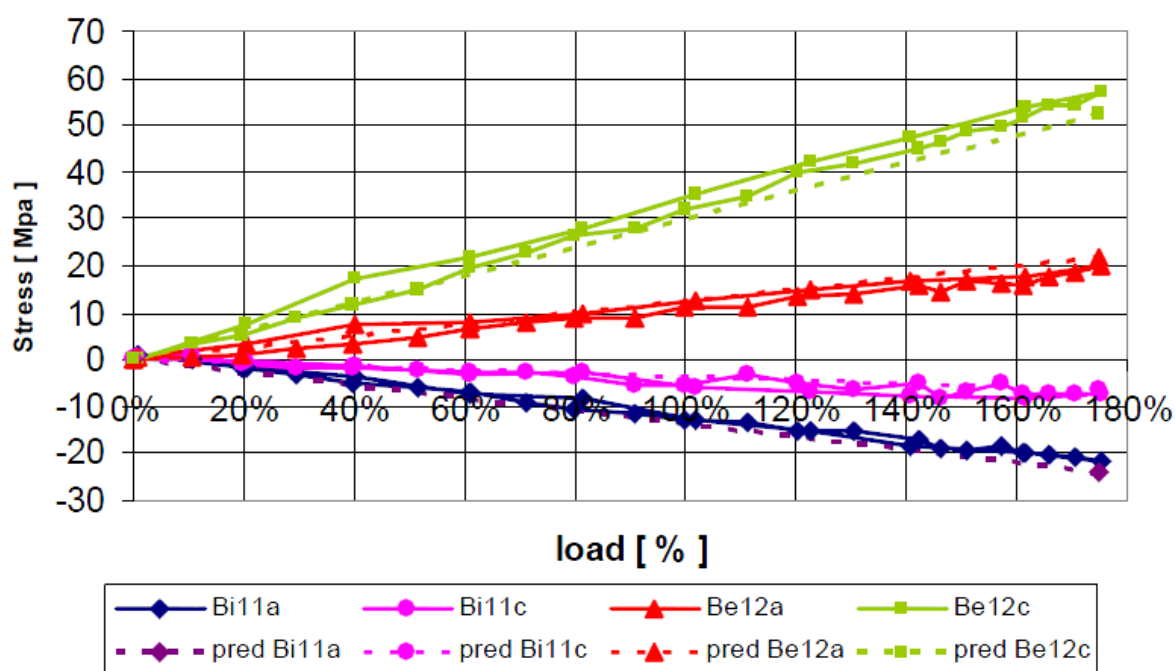
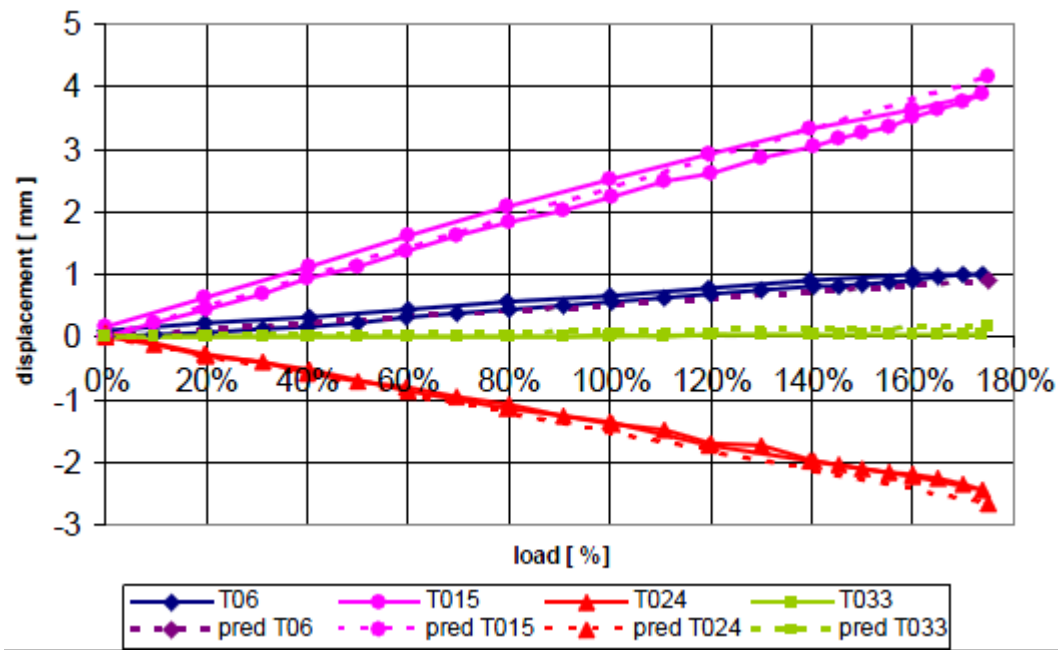


Figure 7-7: ATV static test: external view and external loading jacks



**Figure 7-8: ATV static test: layout of the displacement transducers**



## 8

# Sine vibration

## 8.1 Introduction

Sinusoidal excitations in the low frequency range up to 100 Hz affect the launch vehicle during its powered flight. The spacecraft is also submitted to those excitations because of the dynamic coupling between the structures.

The launcher induces vibration loads at the unit interfaces. The levels of these dynamic excitations depend on both the launcher type and the dynamic couplings between the launcher, the satellite and/or instrument/lower level sub-assemblies on which the units are mounted.

There is a low frequency qualification process to verify the ability of the spacecraft to bear the sine vibration loads without any damage or degradation. Thus the goals of this process are to demonstrate:

- The global qualification of the spacecraft to low frequency environment
- The qualification of all spacecraft secondary structures and appendages to sine environment
- The qualification of the payload and all spacecraft equipment to sine vibration if the stiffness of the item is low (usually: first natural frequency below 140 Hz)
- The verification of stiffness requirements (usually first fundamental frequencies)

Sine testing is a fundamental step in the spacecraft qualification process. It follows specific rules in terms of input profile, especially for notching criteria, and test duration governed by the sweep rate.

## 8.2 Sine vibration levels specification

### 8.2.1 Sine loads for spacecraft

The sine vibration environment for spacecraft is usually defined by the user's manual of the selected launcher. As an example, Figure 8-1 shows the envelope of the sinusoidal (or sine-equivalent) vibration levels at the spacecraft base as given in the Ariane 5 User's Manual [1]. In general, the definition of the launcher sine vibration environment is based on measurements during flight.

Direction	Frequency band (Hz)	Sine amplitude (g)
Longitudinal	2 - 50	1.0
	50 - 100	0.8
Lateral	2 - 25	0.8
	25 - 100	0.6

Figure 8-1: Ariane 5 sine vibration environment definition

## 8.2.2 Sine loads for payload and equipment

Equipment for space applications are designed and qualified for typical sine loads, not only for one specific mission but for the accommodation on several spacecrafts. In the majority of cases the definition of sine loads for equipment focuses on the available equipment. One philosophy is therefore to define the sine loads for equipment as shown below in Figure 8-2 and Figure 8-3 , based on a few parameters. The challenge is to design a spacecraft which provides the specified loads for the equipment.

As soon as detailed mechanical mathematical models are available the sine load specifications can be verified by simulating the relevant sine vibration tests. According to the above described philosophy the spacecraft is re-designed (or at least the equipment is re-accommodated) if the simulation shows a discrepancy to the specified sine loads. If this is not possible the specification needs to be updated and the affected equipment needs to be re-qualified. This case is clearly the exception rather than the rule.

The sine environment for payload and equipment is usually defined in the:

- General Design and Interface Requirements (GDIR) and/or
- Environment and Test Requirements Specification

These documents are normally created in early design phases when mechanical mathematical models are generally coarse or even not existing. Therefore the approaches for defining the sine levels are often based on experience and engineering judgement.

Typical parameters for the sine loads specification for payload or equipment (units) are

- unit mass
- location of the unit (internal / external)
- excitation direction (in-plane / out-of-plane)

A typical example for the definition of the sinusoidal environment for units less than 100 kg is shown below in Figure 8-2. Units mounted on the spacecraft are designed to withstand without degradation the sinusoidal environment as defined below.

Axis	Frequency (Hz)	Qualification	Acceptance
Out of plane	5 - 20	15 mm	9.9 mm
	20 - 100	24 g	16 g
In plane	5 - 20	9.9 mm	6.6 mm
	20 - 100	16 g	10.7 g
Sweep rate		2 Oct/min 1 sweep up	4 Oct/min 1 sweep up

**Figure 8-2: Sinusoidal environment for Units less than 100 Kg (example)**

A typical example for the definition of the sinusoidal environment for units greater than 100 kg is shown below in Figure 8-3. These units are designed to withstand without degradation the sinusoidal environment applied at the unit to SC interface as defined below.

Axis	Frequency (Hz)	Qualification	Acceptance
Out of plane	5 - 20	9.3 mm	7.5 mm
	20 - 60	15 g	12 g
	60 - 100	5 g	4 g
In plane	5 - 20	7.8 mm	6.6 mm
	20 - 60	12.5 g	10 g
	60 - 100	5 g	4 g
Sweep rate		2 Oct/min 1 sweep up	4 Oct/min 1 sweep up

Figure 8-3: Sinusoidal environment for Units greater than 100 Kg (example)

## 8.3 Simulation / test prediction

### 8.3.1 Introduction

Usually a spacecraft is designed for the qualification test, since the corresponding test loads should be more severe than the loads during the actual launch of the spacecraft. Therefore the simulation of the sine test plays an important role in the development cycle of a spacecraft.

The test simulation is normally based on a finite element model of the entire spacecraft. The level of detail increases during the development stage of the spacecraft. Thus the accuracy of the test prediction should increase accordingly.

The goals of the sine vibration test simulation are:

- Prediction of the global integrity of the spacecraft when exposed to sine vibration
- Prediction of the loads at the spacecraft/launcher I/F
- Prediction of the loads at the payload and equipment I/F and corresponding accelerations
- Verification of the sine load specifications for payload and equipment
- Notch assessment: identification of areas (spatial and frequency range) for potential notching

The numerical simulation is a sine response analysis performed with the finite element model of the spacecraft. In a first step a modal analysis is performed. The modal representation of the physical model builds the basis for the sine response analysis, where the applied load case is an excitation at the spacecraft I/F (base excitation). The excitation is a frequency dependent acceleration applied separately in three spatial directions.

### 8.3.2 Boundary conditions

The dynamic behaviour of a structure depends on its boundary conditions, i.e. the mechanical support at the structure I/F. Therefore the specified stiffness requirements and the dynamic loads are always in conjunction with specific boundary conditions. Typical spacecraft boundary conditions for a sine test and the corresponding simulation are *hard mounted* or *simply supported* for each interface degree of freedom. For typical spacecraft with clampband interface, the impact of boundary conditions on predictions is largely limited to the first modes. The *free-free* boundary conditions are often used for modal survey tests.

In this context the following definition is given regarding the I/F grid points:

- Hard mounted: all 6 DOF are fixed (constrained).
- Simply supported: only the 3 translational DOF are fixed. The 3 rotational DOF remain free. This is applicable only for I/F modelled with multiple grids.
- Free-free: all 6 DOF are free.

One should be aware that boundary conditions in the simulation are taken into account in an ideal way. In reality, boundary conditions are not perfect and may therefore differ from those of the model. This should be taken into account when comparing simulation results with measurement data as well as for the definition of test loads under idealized conditions.

### **8.3.3 Damping**

The damping of a structural vibration is typically described by the critical damping ratio  $\zeta$  or the Quality Factor  $Q$ , where the Quality Factor is the amplification of a single degree-of-freedom system at resonance, equal to the reciprocal of twice the critical damping ratio (see Section 5.2.3.2).

$$Q = 1/(2 \zeta)$$

The damping ratio or Quality Factor scales the responses and is therefore an important parameter for predicting the accelerations and corresponding loads. For a new structure the damping ratio is usually not known before the test and should therefore be pre-estimated. This estimation is typically based on experience and engineering judgement and depends on parameters like materials, joints, equipment, harness, excitation levels, etc.

Typical values for the critical damping ratio are:

- Low damping:  $0.1\% \leq \zeta \leq 0.5\%$
- Medium damping:  $1\% \leq \zeta \leq 2\%$
- High damping  $2\% \leq \zeta \leq 5\%$

### **8.3.4 Notch assessment**

For the basics of notching and definitions of primary and secondary notching see Section 5.5.

The notch assessment relies on the existing finite element model and depends on the damping assumption. Nevertheless it provides an important input even in early development stages. It gives an indication of necessary notching in terms of modes (i.e. frequency ranges) and expected notch depth. Expected conflicts between minimum loads (e.g. for qualification) and maximum allowable loads can be identified early enough to be solved prior to the test.

The uncertainty concerning damping affects mainly the depth of notching. Frequency shifts due to damping usually can be neglected. What is much more important for a good notch assessment is the quality of the finite element model. A prerequisite is a sufficient accuracy of the predicted modal parameters (natural frequencies and mode shapes). If the calculated and measured modal parameters are different, then the notch assessment is not valid.

## 8.4 Sine vibration test

### 8.4.1 Objectives

Sine vibration tests are usually performed on single-axis electro-dynamic shakers. The test item is vibrated in three spatial directions separately, where the excitation frequency sweeps from a lower limit to an upper limit (sweep up) or vice versa (sweep down). The sweep rate is expressed in octaves per minute (oct/min). Refer to Section 5.2.3.3 for a discussion on the influence of the sweep rate.

The sine vibration test is usually performed with the following objectives:

- To demonstrate that the spacecraft structure (including flexible appendages) can withstand the low frequency dynamic environment (qualification or acceptance loads) without failure or structural degradation
- To characterise the spacecraft dynamic behaviour (resonance search) in order to validate the spacecraft dynamic model used for CLA
- To confirm the equipment level mechanical environmental specifications
- To detect workmanship errors, if any
- To validate the spacecraft mathematical model, if relevant

Spacecraft qualification/acceptance tests are completed by electrical good health tests and alignment measurements.

The process of sine test management is summarized on Figure 8-4.

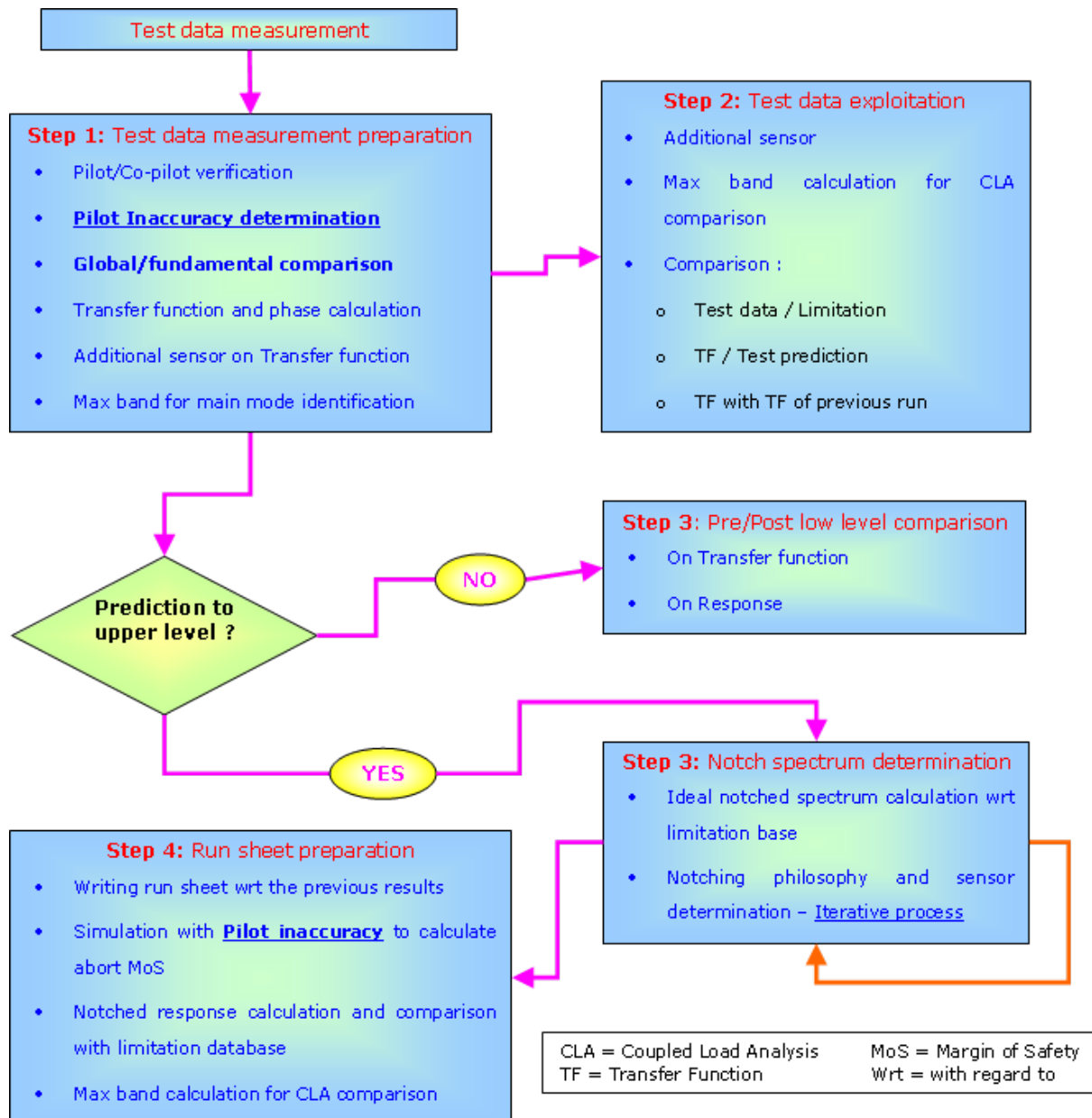


**Figure 8-4: Test management process overview**

#### 8.4.2 Notching process

In this section the practical aspects of notching are discussed. For the definition and theoretical aspects of primary and secondary notching see Section 5.5.

Each test run prior to the full level run (qualification or acceptance level) is used to adjust the notching. The starting point is the notch assessment based on analysis results. Typically the following procedure is applied during a sine vibration test for each axis separately:

- Perform the low level run (resonance search)
- Scale the results of the low level run to qualification level
- Compare this prediction with the allowable limits - check exceedances

- Make the selection for the channels / measurement points used for primary notching and secondary notching (if needed)
- Define the notch profiles including automatic and manual notches. Automatic notches are controlled by measured response (forces, accelerations) whereas manual notches are explicitly defined reductions of the input levels (accelerations).
- Make a new prediction from low level to qualification level, this time with the planned notch profile (including automatic and manual notches) and check the prediction results against the allowable limits.
- Perform the intermediate level run and follow the same steps as above.

Primary notching during spacecraft sine tests is based on the loads (forces and moments) at the I/F between launcher and spacecraft. The following methods for the measurement or derivation of I/F loads are usually applied:

- **Force Measurement Device (FMD):** The most accurate way to measure the I/F loads is the use of a FMD. Either the resulting I/F loads or individual loads at each I/F can be directly measured. For details see Section 8.4.3.7.2.
- **Strain gauges:** The I/F forces are indirectly determined by measuring strains nearby the spacecraft I/F. The knowledge of the relationship between strains and I/F forces is a prerequisite of this method. Due to the limited accuracy and liability of strain gauges this method is less accurate than the FMD measurement. In addition there is a significant effort for post-processing.
- **Coil current:** See Section 8.4.3.7.2
- **Mass Operator:** See Section 8.4.3.7.2
- **Accelerations:** This method is only applicable if the mathematical model (FEM) used for the test prediction simulates the dynamic behaviour of the test item with sufficient accuracy. It is based on the relationship between measured accelerations and spacecraft I/F loads. The relationship itself is determined by simulating the test, i.e. performing frequency response analysis with the FEM.

The challenge is to find the right measurement points where the corresponding accelerations are suitable to predict the spacecraft I/F loads. For the selection of measurement points the calculated loads as a function of frequency can be compared with the calculated response acceleration curves. If the curve characteristics of force and acceleration fit in the frequency range of interest the corresponding measurement channel could serve as a pilot for notching. A pure frequency shift between analysis and test can be mastered and normally is not a big problem. In case of a wrong damping assumption the correlation between loads and accelerations can be easily adjusted by simple scaling.

Figure 8-5 shows an example of primary and secondary notching. The grey curve shows the nominal sine input level without any notching. The frequency of the first lateral spacecraft mode is at about 16 Hz. The I/F loads in this frequency range would exceed the allowable limits. Therefore a **primary notch** is defined there.

The red curve shows a manually defined notch. The purpose of the manual notch is to avoid any damage of the test item if the automatic notch fails. A manual notch is also recommended if the shaker control is not agile enough to follow the defined input. The manual notch should be less deep than the expected automatic notch. Thus, finally the sine input levels (blue curve) are controlled by the I/F loads.

In order to reduce the risk of automatic notching, more than one response channel (pilot) should be used for controlling the shaker. The control strategy can use either the maximum or average pilot responses, where the maximum is more conservative in the sense that it reduces the risk of overtesting. In the example case an **overshoot** due to the limits of the shaker control at about 18 Hz could not be avoided.

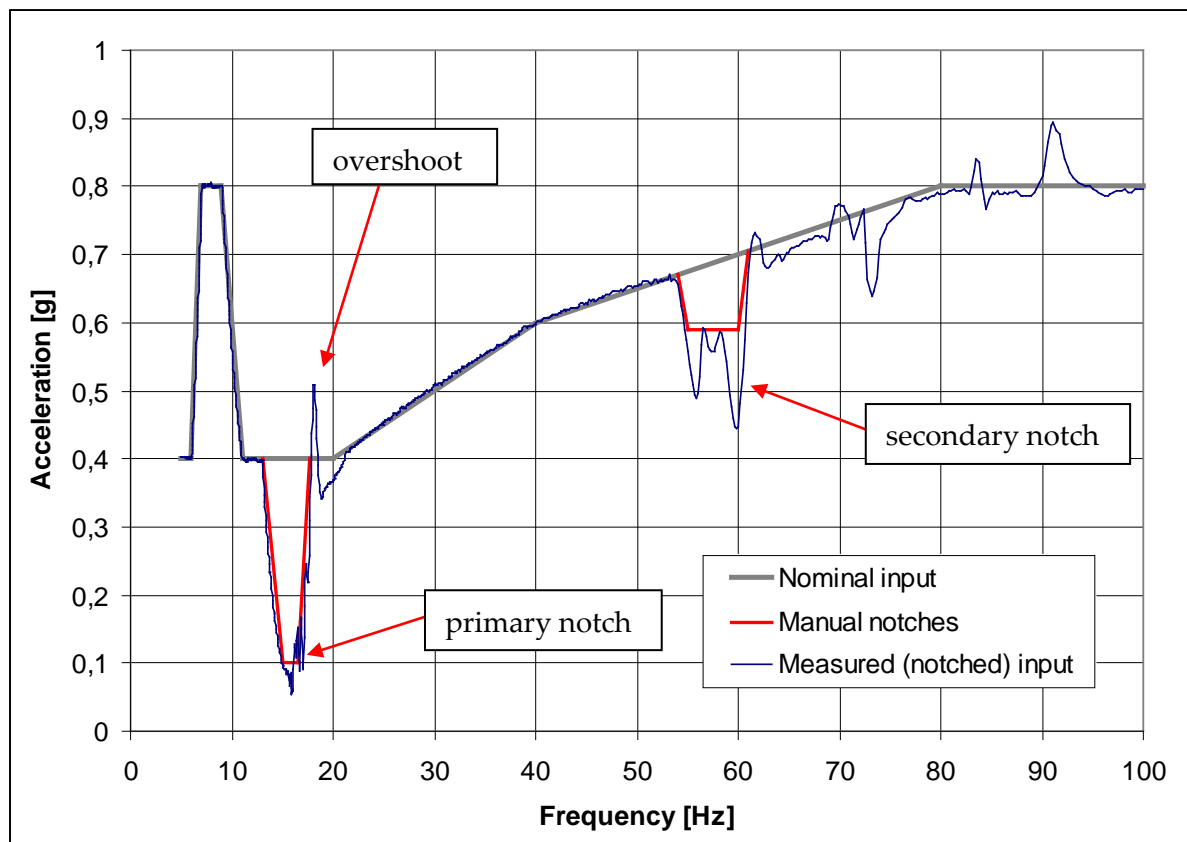


**Figure 8-5: Example of primary and secondary notching**

In Figure 8-5 a **secondary notch** is shown in the frequency range between 54 Hz and 61 Hz. This notch is justified by the maximum allowable accelerations of the propellant tank. It is controlled by the measured accelerations at the tank I/F and on the tank itself. Again a manual notch is defined to reduce the risk associated with an automatic notching.

In general CLA results should be used to verify that the notching requested for equipment protection is compatible with the flight environment. The number, width and depth of notches should be minimized, avoiding broad-band and manual notching as much as possible.

## 8.4.3 Test preparation

### 8.4.3.1 Introduction

The objectives of the test preparation procedures are to provide, based on the test prediction and test preparation aspects conclusions, some general guidelines summarizing all procedures and best practices to apply before a test:

- to anticipate possible difficulties during the test,

- to secure the dynamic test progress and improve the performance during the test thanks to enhanced predictions,
- to have the best test inputs with respect to the test objectives.

### 8.4.3.2 Test configuration

In general a spacecraft should be tested in launch configuration. For several reasons (e.g. programmatic constraints, schedule or costs) some discrepancies from this ideal configuration might be acceptable (and are often necessary) for the test configuration. The effect of these discrepancies should be assessed.

The test configuration depends whether the test is performed with a Structural Model (SM) or a Flight Model (FM or PFM).

For a SM usually employed in qualification test campaign the structure (including flexible appendages) should be flight-representative whereas equipment and instrument units might be replaced by mass dummies.

The unit attachment hardware (brackets, cabling, tubing, etc.) should be included in the tests (to a reasonable extent) to achieve dynamic similarity of the unit to actual installation. Cabling, tubing etc. should be attached to the unit as required for operating or monitoring functions; but fixed in such a way to the fixture or auxiliary supports that no higher loads are generated than in launch configuration.

For a FM or PFM the spacecraft should be tested in a fully integrated and flight-representative configuration.

Discrepancies with respect to launch configuration should be specified in the test specification and procedure and addressed during the Test Readiness Review.

The Mechanical Ground Support Equipment (MGSE) which is used for performing the spacecraft vibration test should not influence the dynamic behaviour (i.e. the modal parameters) of the test item. This is an ideal case which cannot be perfectly achieved. If the influence of the MGSE is not negligible it should be taken into account for the simulation of the vibration test.

Typical MGSE are the test adapter including head expander for mounting the spacecraft to the shaker or a Force Measurement Device (FMD).

#### Testing with dry or wet Tank

In general propellant storage tanks should be filled and pressurized to flight conditions during SC structural qualification testing. The recommendation is testing with wet tank or equivalent mass dummy. Since a wet tank has a deep impact on the programmatic constraints, schedule, risk and costs, sometimes vibration tests are performed with dry tanks or less pressure. Tests with dry tank may be proposed for sine and acoustic testing at spacecraft level when structure qualification is not required (PFM or FM test) - for acceptance testing.

The following conditions should be fulfilled for testing with dry tanks or less pressure:

- Tanks are qualified in empty configuration
- Spacecraft test predictions are performed in both dry and wet condition
- Environments on equipment are not jeopardized
- Notching approach is agreed upon with launcher authority

Due to safety reasons normally the propellant is replaced by a simulant medium, e.g. water or Isopropyl Alcohol (IPA). But there are also other approaches to be in line with the safety requirements of the test facility. For example, for a mission with three identical spacecraft:

- 1 spacecraft loaded with water during vibration test. Mass of water = 95% of nominal launch propellant mass.
- 2 spacecraft (PFM, FM) loaded with nominal propellant during vibration test, but with reduced pressure up to safety limits of test facility. Actual test propellant mass = 22% of nominal launch propellant mass.

#### Spacecraft ON / OFF configuration

The general recommendation for the ON/OFF configuration of the spacecraft during test is:

- If the spacecraft is ON during launch, the spacecraft should be ON during test
- If the spacecraft is OFF during launch, the spacecraft should be OFF during test

Note: OFF spacecraft allows separating mechanical testing from electrical testing.

#### **8.4.3.3 Test sequence**

A typical sine test sequence consists of the following test runs for each axis:

- Low level run (resonance search)
- Intermediate level run
- Full level run (qualification or acceptance level)
- Low level run (resonance search for purpose of structural integrity check)
- Following activities (random vibration test, functional test, visual inspection)

**Low level** test runs are conducted in order to:

- Identify the test item resonance frequencies and correlate results with FEM predictions,
- Estimate the Q-factors or damping factors associated to the main modes,
- Establish a basis for resonance frequencies comparison between test runs and allow eventual interface settling anomaly evaluation,
- Establish first notch prediction for the intermediate and full level run and compare this prediction with the notch assessment based on FE analyses.
- Verify the structural integrity after the full level run.

In particular, the knowledge of the results of the main unit frequencies and the associated amplification or transmissibility measured during the first resonance search test along each axis is of primary importance to support the proper performance of the higher level tests.

Resonance search tests are conducted along each of the three mutually perpendicular axes one at a time at least prior to and after performing the tests. In order to allow better Q-factor estimation, the resonance search test level is adjusted in order to avoid notching on the fundamental modes.

**Intermediate level** test runs are conducted in order to adjust the initial prediction of the full level test run with respect to the following aspects:

- resonance frequencies
- damping
- expected response levels
- notching
- nonlinearities

Before applying full levels, a test at intermediate level should be performed. For qualification testing, the intermediate levels can be set at the acceptance (flight limit) levels. For acceptance testing, the intermediate levels are often the acceptance levels divided by 2.

**Full level** test runs are conducted in order to:

- Demonstrate that the test objectives have been achieved with respect to structure qualification or acceptance
- Identify the dynamic characteristics at flight-representative load levels in case of significant structural nonlinearities.

#### 8.4.3.4 Test success criteria

The test is considered successful if all measurements are in accordance with the design requirements as stated in the particular unit design and performance specification, and expressed as test criteria in the test specification.

#### 8.4.3.5 Instrumentation improvement procedures

In general, spacecraft instrumentation is designed:

- to measure during the test some parameters like force, acceleration and strain in some specific spacecraft location
- to control some notching
- to pilot the test

Thus the spacecraft instrumentation is essentially oriented and defined to protect and/or qualify during the test equipment and subsystems to avoid exceeding allowable levels - and not to identify as well as possible the mode shapes.

Consequently, during the test preparation process, the sensor location selection is generally driven by project needs in order to control equipment or subsystem acceleration (or force or strain) on particular point or close to its interface. It may not be possible for these reasons to position sensors at locations where it could be useful to have a measurement for mode shape observation.

Nevertheless, even if most of the sensors locations are not modifiable (for the previous exposed reasons), there is generally a dual instrumentation (e.g. redundant or spare sensors, additional sensors) not always acquired during the run. For these sensors it is interesting to apply the mode observability process [2] [3].

However, most of the time, the levels at equipment locations are due to global and local mode amplification, and therefore the mode observability is generally more or less guaranteed (especially for the main modes to control notching).

It is recommended to define the sensor location jointly with the spacecraft (or sub-system) mechanical architect to determine:

- The sensors for which it is not possible to change their location. These sensors take into account the project instrumentation needs with respect to the test objectives (qualification and/or protection of the system or sub systems, identical instrumentation from previous sub-system tests for comparison purposes, etc.).
- The sensors for which location is not precisely defined with respect to project needs. These sensors can be redundant, spare sensors or additional sensors which aim to have additional measurement information or replace a prime sensor with a doubting response. These sensors form a basis for sensor positioning improvement for mode shape observability and distinguishability.
- The locations where other additional sensors could be added (and the areas where it is not possible to instrument). The aim is to identify regions where the mechanical analyst could suggest additional sensor for mode shape observability and distinguishability.

In preparation of the next step aimed at improving the instrumentation, it is necessary to select the most important modes in terms of test objectives in order to:

- verify that the instrumentation can fulfil the objectives
- apply the stochastic analysis intelligently and efficiently

The recommendation is to choose a relatively reduced set of modes per axis based on different criteria (e.g. large effective mass involved, important or critical modes to identify).

Once the modes are selected the analyst can proceed with improving the instrumentation. The objectives are to improve the distinguishability and observability of the mode shapes by iterating on the sensor locations. The analyst is normally allowed to modify the locations of certain sensors while using additional sensors in the available locations as described below.

This procedure results in a consolidated set of sensor locations providing better observability and distinguishability for the selected test modes. It provides trends while avoiding large errors.

The distinguishability and observability are defined as follows:

- The distinguishability is expressed as an auto-MAC matrix (see Section 16.7.4.3 for more details) using the optimized set of sensor DOF. For the auto-MAC the diagonal terms are always equal to 1 and the off-diagonal terms should be as small as possible.
- The observability criterion gives for each mode the ratio between the maximum mode shape component reduced to the optimized DOF and the maximum component of the mode shape reduced to all the candidate DOF. This ratio should be as close as possible to 1.

This function can be used in every test context, however:

- It is not crucial for spacecraft sine base qualification tests. In fact the sensor locations are defined with respect to the project needs (test piloting or equipment protection) and not for mode observability.
- The use of this function is very important for modal survey tests or micro-vibration performance or characterisation tests. In fact such tests are used to identify the mode shapes at

frequencies that could be high. In such a context, the instrumentation accuracy is very important to ensure that the modes are correctly measured and to distinguish the modes from each other.

From this analysis, it is important to identify sensors that produce a large dispersion in the distinguishability and observability with changes (error) in their in-plane location and/or orientation.

This leads to the following recommendations and warnings:

- In the mechanical instrumentation plan by including tolerances for the identified sensors:
  - in such location with a precision of  $n$  mm
  - with no more than  $m$  degrees from a given direction
- As a check list for the analysis team in case of differences between the predictions and the test in order to:
  - identify possible causes explaining a deviated behaviour
  - highlight the effect of the instrumentation error on the test measurement

#### 8.4.3.6 Shaker selection

Vibration shakers are available for a wide range of applications. The main differentiating parameter is the force a shaker can apply for the excitation of a test item.

The shaker capabilities can be expressed in terms of limitation in:

- **Acceleration:** this is linked to the total mobile mass (total mobile mass of the shaker + mass of the specimen) and to the force available. The maximum acceleration is the ratio between the maximum force available and the total mobile mass.
- **Velocity** (given by the shaker manufacturer): it can be checked particularly at low frequencies that the specified acceleration divided by the circular frequency ( $2\pi f$ ) is lower than the maximum acceptable velocity.
- **Displacement** (given by the manufacturer): as for the velocity, the displacement (particularly at low frequencies) can be computed as the ratio between the specified acceleration and the square of the circular frequency.
- **Position of the centre of gravity:** the position of the centre of gravity induces a bending moment that cannot exceed the maximum bending moment. This bending moment can be computed as the specified acceleration multiplied by the dynamic mass in the considered direction and by the offset of the centre of gravity. Additionally in the case of a vertical excitation, an imperfect guidance might induce lateral accelerations that can lead to significant moment values due to a high position of the centre of gravity and important mass involved.

Table 8-1 presents as an example the characteristics of the Intespace Multi-Vibration System (MVS) shaker for system testing:

**Table 8-1: Performances of the Intespace MVS shaker for system testing**

Force along longitudinal axis	320 kN (sine mode) 220 kN (random mode)
Force along lateral axis	320 kN (sine mode) 220 kN (random mode)
Frequency range	5 Hz – 2000 Hz
Total load compensation (vertical)	10000 kg
Admissible load	8000 kg
Mobile coil mass	130.2 kg
Mobile mass along vertical axis:	
- standard configuration	1884 kg
- extended configuration	3415 kg
- light configuration	1790 kg
Mobile mass along horizontal axis	1948 kg
maximum velocity	1.35 m/s (*)
maximum displacement	50.8 mm (random and shocks mode) 38 mm peak-peak (sine mode) (*)
maximum acceleration (empty)	16.7 g (horizontal) 17.3 g (vertical) 9.5 g (vertical) 18.2 g (vertical)
maximum overturning moment	600 kN.m (horizontal) 160 kN.m (vertical – standard & extended config.) 4 kN.m (vertical – light configuration)
(*) : limitation function of the load and the frequency band	

#### 8.4.3.7 Test preparation procedures

##### 8.4.3.7.1 Limitation database constitution

The limitation database aims to protect the spacecraft as far as possible from over testing and failure of any spacecraft parts during the mechanical test.

The limitation database building is mainly dependant of the spacecraft context (e.g. telecom spacecraft, observation spacecraft, platform family experience, and sub-system behaviour experience).

However it is not possible to give a detailed approach for strategy building.

Nevertheless, we can present hereafter the key points enabling the limitation database building:

- The sub-systems limitations are mainly based on the levels achieved on sub-system qualification tests. These levels may be the one seen or shaped as templates.
- The limitation may take advantage of other programs mechanical test levels to provide additional admissible levels.
- The load levels at sub-system interface or the constraints inside materials are not generally accessible at test level. Consequently, to protect equipment from failure it is generally used to:
  - Determine available accelerations having the same amplification shape as the load or constraint to limit

- Notch proportionally to the acceleration level locally around the frequency band of interest in order to not exceed the sub-system maximum admissible load or constraint.

This last step is generally taken into account in an overall prediction process including all the limitations. The final objective is to obtain a limitation database only containing measurable data in test (generally only accelerations are measurable and sometimes strain gauges whereas interface loads are not accessible).

#### 8.4.3.7.2 Base load recovery

One of the main objectives of the base excitation sine test is to cover the base force and moment predicted by the coupled loads analysis. The same base loads can be used to determine effective mass. It is therefore very important to measure the base forces and moments during the sine tests. For that purpose, various methods are available, based directly on measurement or with the help of a mathematical model:

- The Force Measurement Device (FMD) is the best solution to directly measure the complete base forces and moments - but such devices are not available in every test facility centre.
- The measurement of the coil current injected during the test to recover the SC base force along the direction of excitation. However the base moment cannot be recovered.
- The manual Mass Operator estimation using a reduced set of sensors whose responses are associated with equivalent local masses optimised on the finite element model.
- The static condensation of a mathematical model on a more complete set of sensors enables also the determination of the base load and constitute a more robust Mass Operator.

#### Force Measurement Device

The force measurement device is a general term naming a device able to measure, between two interface planes, the complete load tensor. Its generic design is composed of two rigid interfaces separated by load cells.

Thus force measurement devices can be designed for different specimen types and interfaces.

For example the main characteristics of an FMD available at ESTEC were [4]:

Frequency measurement range:	up to 100 Hz at high level,	up to ~300 Hz at low level
Measurement range:	up to 800 kN axially,	up to 200 kN laterally
Moment measurement range:	up to 260 kNm in bending,	up to 130 kNm in torsion
Axial/bending stiffness:	$9.55 \times 10^9$ N/m	/ $2.73 \times 10^9$ Nm/rad
Overall mass / height:	494 kg	/ 40 cm

The FMD is the best way to determine the base loads since:

- It provides the direct measurement of the complete interface loads with high accuracy which can be used for direct automatic notching.
- It validates immediately the qualification level achieved on the main mode, regardless of the FEM quality and thus provides useful data for the FEM correlation.
- It offers a high stiffness resulting in a limited frequency shift, a good linearity and low cross talk.

- The integration in the test set-up is simple and can be adapted to every interface diameter thanks to the modular concept.

However some particular points should be mentioned with respect to its use:

- In general an extra load spreader is required between the slip table and the FMD, which increases the over turning moment on the slip table due to the additional FMD mass and a higher CoG.
- It may not always be available and its use requires additional time and money.
- It generates a low frequency shift on the most important mode depending on its effective mass.

### Coil current coefficient estimation

The base load force from the coil current is calculated thanks to the coils intensity conversion coefficient. This coefficient is determined by the proof tests performed by the test facility centre before the sine tests to calibrate and demonstrate the shaker capability to correctly pilot the runs. Such test provides pilot acceleration measurements on the shaker table as well as the measured coil currents. Since no shaker modes are expected within the spacecraft's first mode frequency bandwidth, this provides a frequency dependant correlation factor between Force and Ampere current in the coils.

This standard test result provides only one force component, which is sufficient for order of magnitude correlation with more accurate techniques.

An example of coil current coefficient is shown in Figure 8-6. It has been calculated based on test results obtained on the Intespace MVS lateral shaker and is different for other test facilities.

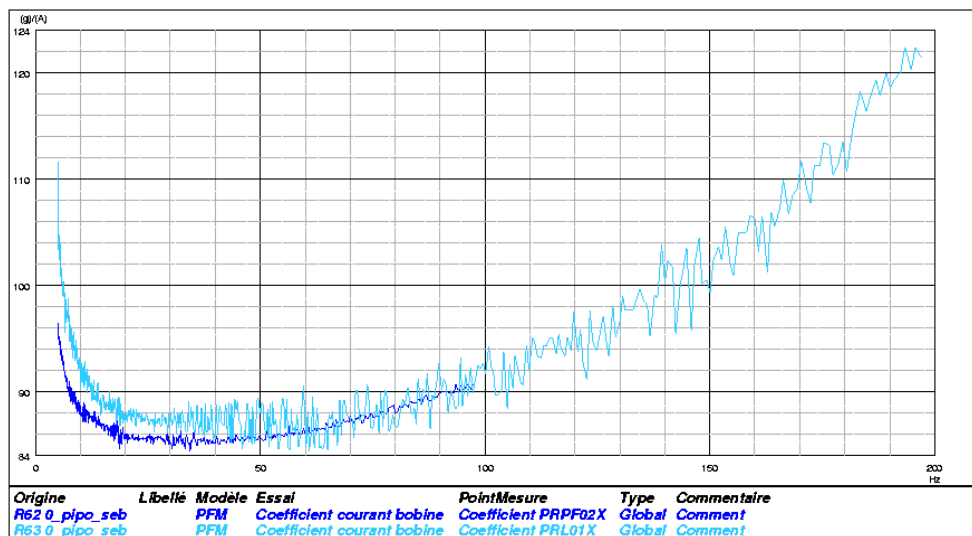


**Figure 8-6: Example coil current coefficient**

It can be noted on this figure that this highly nonlinear coefficient is function of:

- The shaker itself; the moving part slides along bearing guides which generates viscous friction.
- The frequency and the input level.
- The mass on the shaker table; it slightly modifies the coil impedance.

The coil current coefficient value is chosen near the frequency of the mode of interest and using the input level as close as possible to the test conditions.

To recover the load force in the excitation direction at the spacecraft base, it is necessary to convert the coil intensity into force and remove the contribution of the rigid shaker moving parts (coil mobile parts, shaker table mobile part, spacecraft adaptor, harness on the spacecraft).

The coil current coefficient is given by Eq. [8-1] for an acceleration imposed by the shaker *without* the spacecraft.

$$F_{\text{coils current}} = \text{Coefficient} \times \sum_{i=1}^{n^{\circ} \text{ coils}} I_{\text{coil } i} = (m_{\text{coils}} + m_{\text{shaker table}} + m_{\text{adaptor}} + m_{\text{harness}}) \times \ddot{u}_{\text{base}} \quad [8-1]$$

And then for the test with the spacecraft, assuming the coils, the shaker and the adapter are rigid, the spacecraft interface force can be easily deduced by Eq. [8-2]:

$$F_{S/C \text{ base}} = \text{Coefficient} \times \sum_{i=1}^{n^{\circ} \text{ coils}} I_{\text{coil } i} - (m_{\text{coils}} + m_{\text{shaker table}} + m_{\text{adaptor}} + m_{\text{harness}}) \times \ddot{u}_{\text{base}} \quad [8-2]$$

The coil current force calculation is not very accurate due to acceleration measurement error (about 9.8% at  $2\sigma$ ) and low Ampere-meter resolution (less than 5% at high frequency but about 20% at low frequency) whose discrepancy increases inversely with the mode's effective mass. However, it provides an order of magnitude value at low frequency (corresponding to the main spacecraft mode) to give confidence in the mass operator calculation results obtained by other techniques.

### Manual Mass Operator

In this approach, depicted in Figure 8-7, the finite element model is used to determine a set of equivalent masses at the measurement points which reproduce the same base force and moment as the model for the modes in question.

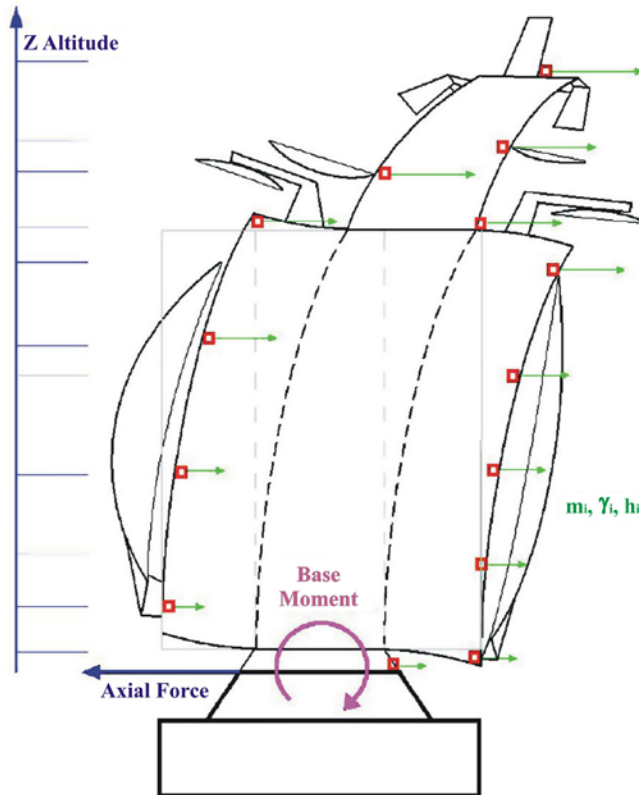


**Figure 8-7: Determination of base load and moment using Mass Operator**

With these equivalent masses, the test base force and moment can be estimated using the measured accelerations according to Eq. [8-3] and [8-4] with  $N$  the number of sensors used for the mass operator:

$$F_{\text{axial force}} = \sum_{i=1}^N m_i \times \ddot{u}_i \quad [8-3]$$

$$M_{\text{base moment}} = \sum_{i=1}^N m_i \times \ddot{u}_i \times h_i \quad [8-4]$$

#### Mass Operator using static reduction

Another way to estimate the base forces and moments is to build a Mass Operator using a static (Guyan) reduction of the FEM mass matrix on the chosen set of sensors.

The idea is based on the fact that a static condensation of the FEM on the mass operator sensors (instrumented DOF) projects on each DOF the appropriate local FEM mass properties.

Once the FEM is condensed on the sensors, the interface base loads are recovered by multiplying the condensed mass matrix by the rigid body motion vector and the measured accelerations according to:

$$\Phi_{\text{Rigid}}^T \cdot \mathbf{M}_{\text{condensed}} \cdot \ddot{u}_{\text{sensors}}(\omega) = \mathbf{F}_{\text{base}}(\omega) \quad [8-5]$$

The static FEM reduction leads to the following main conclusions:

- The condensation on the complete SC instrumentation leads to very good loads recovery on the whole frequency range (not only on the peaks). In fact the larger the number of sensor, the better the base loads recovery.
- The base loads recovery is generally better along the lateral axis than along longitudinal axis.
- Reducing the number of sensors reduces the quality of the recovered loads. The degradation is more important in longitudinal force recovery than in lateral (force and bending moment) recovery.
- Keeping all the sensors for the base loads recovery improves the robustness of the recovery even if it requires additional measured data verification during the test.

To recover the contribution of a sub-system to the global loads (and then the quasi-static load), the static condensation on the whole spacecraft instrumentation can be performed using only the mass of the sub-system. Although it is not possible to recover precisely the loads at the sub-system I/F (in the case of a statically redundant connection) this remains a good method to recover QSL from tests.

#### 8.4.3.7.3 Sensitivity analysis with stochastic notching

The objectives of stochastic notching in term of test preparation are twofold [5].

First it takes into consideration that the spacecraft FEM is not completely representative of the real behaviour in that:

- the dynamic behaviour differences between the FEM and the test specimen for each sub-systems,
- the test uncertainties identified in Section 8.4.3.5, can be taken into account before the test in analysis to determine their effect at test level,
- the test facilities shaker is not ideal and piloting introduces on the spacecraft base cross coupling effects which can be relatively important with respect to the excitation axis levels,
- the damping at system level is often considered constant whereas in real life, each sub-system has its own damping which can vary substantially from one sub-system to another one.

All these uncertainties on the real spacecraft prototype and test can be taken into account in stochastic analysis to derive all the identified error sources to provide their effects on the notched profiles.

Secondly, stochastic notching aims at anticipating the notched input profile differences between the one predicted before the test campaign (and presented to the launcher authorities and customer and agreed by them), with the one calculated using test data. This allows:

- Saving long negotiation time. In fact, in the testing process, the base input notching profile is agreed upon before the test by the customer and launcher authorities. If during the test, this notching profile is more or less different from the one presented and agreed before the test, it should be justified if the input levels are lower. Whereas if the notching profile is presented as an envelope taking into account a wide variety of uncertainties with different occurrence probability and agreed by the launcher authorities and the customer, this permits to verify during that the test notching profile is always higher than the minimum agreed envelope.
- Giving confidence in the notching prediction robustness thank to the probability associated to each mode.
- Improving efficiency and spacecraft knowledge as this highlights before the test the system level causes of problem and their reasons. Moreover, analyst has more time to investigate the problems with more tools than during the test campaign.

It is recommended to extract the stochastic notching profile for the following kinds of error sources studied to build the stochastic notching profile [5]:

- Study 1: study on subsystem modal and mass parameters; first frequencies and rigid mass of each subsystem are the parameters of this stochastic analysis.
- Study 2: test uncertainty parameters effect are added to Study 1 parameters.
- Study 3: cross-coupling effects are added to Study 2 parameters.
- Study 4: damping estimation errors are added to Study 3 parameters.

Since this requires time and large amount of calculation, the probability density of the notching envelope diagram should be provided only if critical notchings are expected to:

- Estimate prediction robustness
- Facilitate negotiation with the customer and launcher authorities

#### 8.4.3.7.4 Sweep rate selection

With a base driven sine test, the sweep rate should be sufficiently small in order to reach the steady-state response levels at the measurement points. If the sweep rate is too high, the responses are affected by a reduction in the peak amplitudes, a broadening (including loss of symmetry) of the peak profiles and a shift in the peak frequencies in the same direction as the sweep (see Figure 8-8).

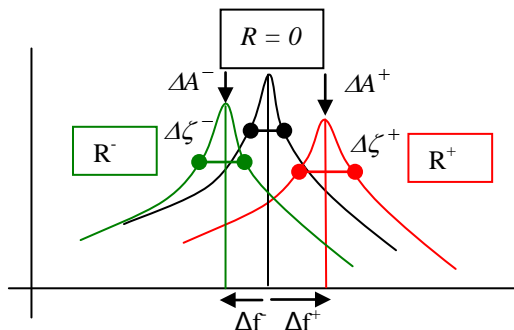


**Figure 8-8: Effects of the sine sweep rate**

The influence of an exponential (logarithmic) sweep rate on the response of a 1-DOF system is presented in Section 5.2.3.3. It is shown that the above effects are *proportional* to the sweep rate,  $R$ , and *inversely proportional* to the natural frequency  $f_k$  and (approximately) to the square of the damping factor  $\zeta_k^2$ . Therefore low-frequency and lightly damped modes are more sensitive to sweep rate effects.

Moreover, changes in the peak's shape (amplitude and width) are more pronounced than changes in the peak's frequency. Consequently the underlying modal damping and effective parameter are affected by the sweep rate more than the natural frequency.

To mitigate these effects, a stepped sine sweep can be used instead of the continuous sweep mentioned above. With a stepped sine sweep, the structure is excited only at a number of specific frequencies usually spaced linearly or exponentially over the frequency band. The number of frequency points is generally limited by the need to achieve a near steady state response at each excitation frequency, which in turn depends on the overall sweep rate as well as the damping and closeness of modes. Stepped sine testing is also well suited to measuring the responses of nonlinear structures.

As an example of stepped sine sweeps, two responses from a spacecraft sine test in the lateral direction using a PFM in qualification test conditions are plotted below in Figure 8-9. Both responses are from the same sensor located at the top of the spacecraft and oriented along the lateral excitation direction. The blue curve is from a low level run using a 1 octave/minute sweep rate, whereas the red curve is from a qualification level run using a 3 octave/minute sweep rate. Both responses have been divided by the excitation level in order to compare them directly as dynamic transmissibilities.

At the resonance of the main spacecraft lateral mode near 13 Hz, we see no effect of the sweep rate on the frequency and very little effect on the amplitude (32g vs. 35g) which is more likely due modifications in the notch depth and pilot consistency on this first mode between both runs.

This illustrates that the use of a stepped sine sweep instead of a continuous sweep can reduce the errors in the modal parameters induced by the sweep rate.

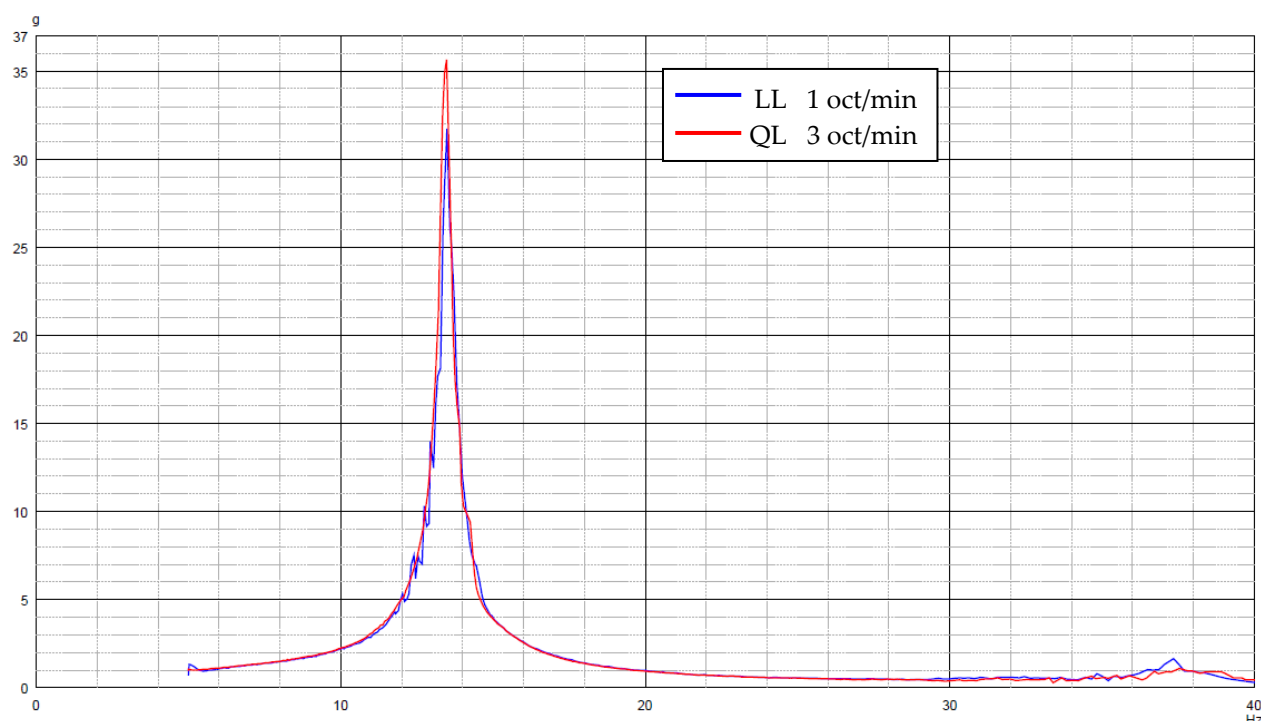


Figure 8-9: Stepped sine responses using 1 and 3 octave/min sweep rates

## 8.4.4 Sine test campaign

### 8.4.4.1 Pre-test tasks

Before the start of the sine test, the following information is prepared and clearly identified:

- Identification of test control (pilot) accelerometers. The identification number, the orientation and the position of the sensors used to pilot the test should be clearly identified. There should be several sensors in excitation direction (typically four) and a few sensors in cross-axis direction in case of failure of one or two sensors during the test and to assess whether or not the excitation is mono-axial (perfectly guided). These sensors are typically located close to shaker adaptor.
- Control strategy. To pilot the test, it should be specified if the control is made on the maximum or on the average response of the pilot sensors. It should be also specified whether piloting is performed on the global response (that is to say without low pass filter, ensuring that maximum

peak-peak acceleration is not exceeded) or on the filtered response (or fundamental response, that is to say with a filter at excitation frequency, ensuring that excitation level is well reached at this frequency)

- Selection of frequency bands and sweep rate. The objective is to define in accordance with the modal density (based on FEM sine analysis) the frequency bands to be used along with the sweep rate in octave/min in order to minimize the sweep rate effects on modal identification.
- Implementation of the run sheet. The run sheet implementation aims to prepare the run sheet parameters for test data assessment including the above frequency bands and sweep rate, the input spectrum with shaker parameters selection and a list of sensors with limitation values and abort margins to control the automatic notchings.

#### 8.4.4.2 Test data assessment

When the sine run is performed, a series of specific data processing should be done in order to validate the measurement made during sine run.

The first processing consists in calculating the test transfer function for further exploitation and extrapolation to a higher level, it involves dividing all measured responses by what is considered to be the input spectra. This calculation depends on:

- The test strategy, whether the assessment is made on global or filtered data
- The control strategy, whether the control is performed on the maximum or on the average of the control (pilot) sensors

The pilot inaccuracy factor should also be calculated: it is the ratio between the theoretical input spectrum (with theoretical automatic notching) specified to the shaker controller and the one effectively measured during the test. An example of pilot inaccuracy is shown in Figure 8-10. The upper plot (blue curve) shows the pilot inaccuracy factor derived from an intermediate level test. The predicted input level for the qualification test is illustrated in the bottom plot with and without the pilot inaccuracy (red and green curves respectively).

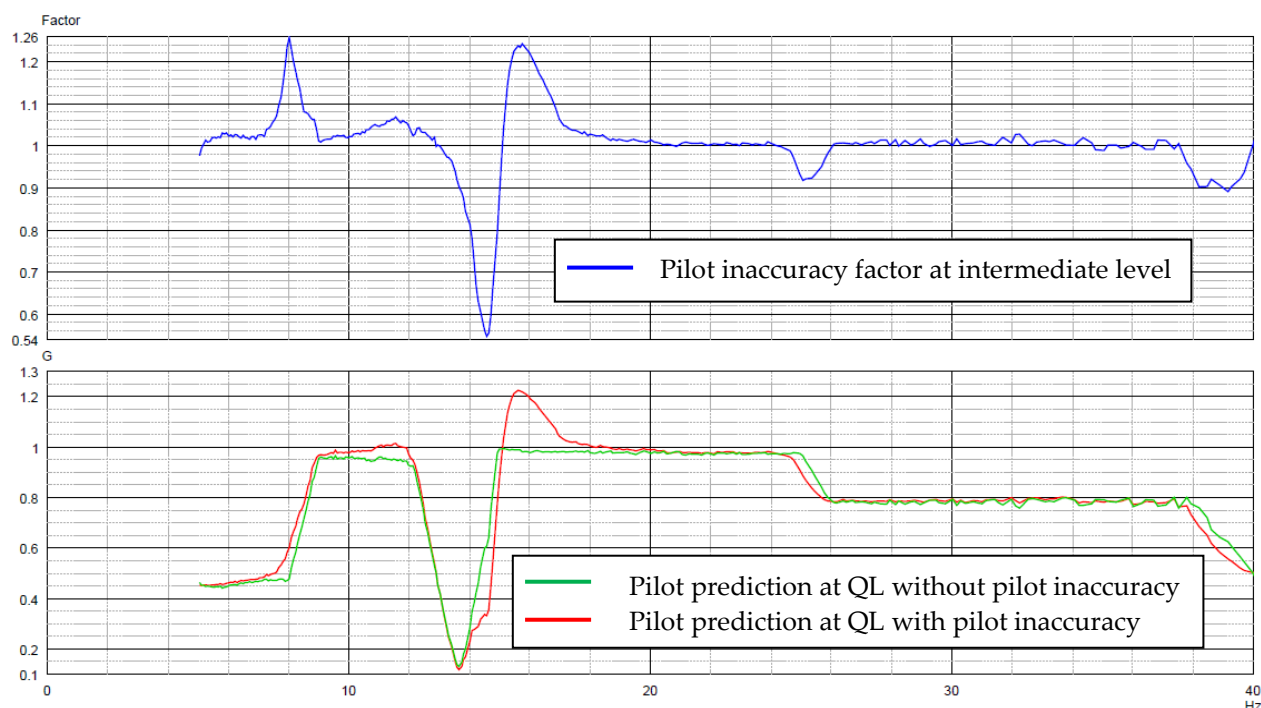


Figure 8-10: Example of pilot inaccuracy

Then a series of measurement quality assessment should be performed for all acquired data:

- **Global/fundamental comparison:** the objective is to identify potential unusual behaviour in the spacecraft dynamics; if global response is different to filtered response, it means that nonlinear effects are recorded: local/global shocks (e.g. sensor wire shocking, contact/gaps in structure, and noise introduced by the facilities). When a difference occurs, it should be identified whether it is on the whole frequency range or localized on a specific frequency bandwidth. With this comparison it is also necessary to identify dead sensors (very bad responses or sensors instrumented in the excitation axis with no response) or suspicious sensors (sensors with unusual responses or where it is not clear if responses are correct or not)
- **Static term evaluation:** the objective is to complete the transfer function database with the FRF extrapolation to the very low frequencies by both parabolic and pseudo-mode methods [6].
- **Sensor orientation verification:** the objective is to assess the sensor orientation and sign with respect to instrumentation plan and prediction. For this check, the low frequency (or extrapolated static) responses are used. Low frequency meaning the frequency band far below the natural frequency of the first elastic mode, where the specimen can be considered as rigid.

Thus:

- the ratio between the response accelerations and excitation acceleration is constant and depends only on the sensor orientation (the problem of parasitic motions is not considered here because assumed negligible at low frequencies): equal to 1 for accelerometers in the excitation direction, 0 for accelerometers perpendicular to excitation direction, and  $\cos(\alpha)$  in the general case of an accelerometer oriented at the angle  $\alpha$  with the excitation direction
- the ratio between the base reaction forces (if measured) and the excitation acceleration provides the mass  $M$  in the excitation direction. Dividing the base moments by the excitation acceleration and the mass  $M$  provides the two coordinates of the centre of gravity with respect to the centre of the test I/F in the directions perpendicular to the excitation.

These constant values represent the static properties of the system and should be identified with care as the low frequency responses are more or less influenced by the first elastic modes.

This detailed assessment is necessary to perform a representative correlation with prediction and a correct estimation of the Mass Operator. This verification is used to build the largest set of valid sensors: the sensors presenting inconsistencies should be either corrected (e.g. sign inversion, and axis correction) or disabled for the specific detailed assessments mentioned previously. This check should be executed at least once per axis. It is not necessary to repeat operation for every run except if the instrumented sensors have been modified since the previous run.

- **Estimation of parasitic motion:** Shaker tables are sometimes not sufficiently rigid and therefore deformation of the shaker table can occur at certain frequencies which in turn produces warping and ovalization at the test specimen I/F. This occurred for example during ESC-A Upper Stage vibration test (specimen diameter: 5.4m specimen weight >20 tonnes). This test specimen size and weight is close to the capacities of existing vibration test facilities. In order to solve this issue, the actual motion of the shaker table can be measured (including cross-talk and elastic deformation). The knowledge of the actual base motion of the test specimen induced by the shaker table is important for correlation of the mathematical model. This is especially necessary for large test specimens, for which the shaker table is not sufficiently rigid in the frequency range to be tested and for which no alternative test facility is available.

The needed number of sensors is defined on basis of vibration test simulations, which include the specimen and the vibration test facility.

In case it is not possible to measure the base deformation, some indicators can be computed to have an estimation of the parasitic motions, as it is detailed in the next sections.

During base-drive vibration tests, the interface between the specimen and the shaker may be considered rigid if the excitation frequency is below the natural frequencies of the loaded shaker table. In this case, the specimen is excited at its base in a given direction without parasitic motion. In practice, unwanted (parasitic) motions can be superimposed to the nominal motion, which can be decomposed in two categories:

1. A rigid body motion (average motion) with 5 components, the 2 non nominal translations and 3 rotations, which can be attributed to the imperfections of the guidance system (shaker cross-talk). It depends mainly on the specimen dissymmetries and can concern relatively low frequencies, well below 100 Hz, depending on the specimen mass properties.
2. A deformation around the previous motion due to the base flexibility (test rig effect, concerning the shaker and the adapter), for example with a so-called "horse saddle" shape. It depends to a certain extent on the dimensions of the interface and on the stiffness provided by the specimen, and concerns relatively high frequencies, a priori well above 100 Hz.

Significant parasitic motions may strongly perturb the dynamic responses and corresponding modes of the specimen, thus representing a major problem to be addressed. They should be detected, measured and their effect on the specimen estimated if possible.

The actual base motion can be measured using accelerometers located on the interface plane, generally 4 triaxials at 90°, from which the 6 rigid body components and the deformation can be derived. In the considered frequency band, the deformation, which can be compared to the rigid body motion, is generally not very significant. In this case, only the 5 parasitic motion components should be considered.

A first estimation of the influence of parasitic motion on specimen dynamics can be provided by a simple computation of the rigid body contribution of the base to the internal responses. However, this estimation gives only a trend. A correct approach should take into account the shaker/specimen dynamic coupling. A description of this method is found in [6].

- **Selection of condensation set for Mass Operator:** The objective of this task is to build the largest set of valid sensors. This set is used for mass operator condensation. It is necessary to remove from this set the non-valid sensors identified previously (e.g. important difference global/fundamental, and dead sensors). Inverted sensors should not be removed; however their sign should be taken as negative.

#### 8.4.4.3 Transfer functions and test data exploitation

When the validation of the raw test data has been performed, the detailed exploitation can be initiated with a series of:

- **Base load recovery:** The objective of this task is to calculate the base loads thanks to the mass operator. This method is based on the static condensation of the FEM which leads to a faster and more robust preparation of the operator before the test as well as a faster and more robust loads recovery during testing. The output is the recovery of the complete base loads (6 components). This can be applied on the spacecraft as well as on the subsystems. The specimen base load estimation using the Mass operator technique can be compared with the other methods defined in 8.4.3.7.2 (coil current or FMD).

- **Max band level per frequency range:** The objective of this task is to calculate the maximum level per frequency range of each sensor. The frequency ranges are selected with respect to the specimen sine behaviour in a given excitation direction to catch the different modes separately and identify the amplifications on the different sensor. The task output are a synthesis table and should be performed on:
  - Raw test data: this table should be compared to upper system level achieved everywhere in the spacecraft with respect to associated limitations and follow the evolution with respect to the different increasing input levels in the test process. This task is executed for the raw test data of every run.
  - Transfer functions: this table should be compared to the other runs transfer functions table in order to monitor evolutions of amplification factors and frequency shift with respect to specimen base input level.
- **Test correlation with FEM predictions:** The objective of this task is to provide a quick modal extraction and correlation between the FEM and the tested specimen thank to visual indicator. The final objective is to verify the correlation quality between the FEM and the tested specimen behaviour which depend directly the base limitation validity as well as the coupled loads analysis results. It is possible to perform a comparison directly on the corresponding transfer function (necessity to go through all sensors) or to perform a Fast Modal Extraction (FMEC described in [6]) which extracts two visual indicators, FrImAC and the ImMAC, to compare major modes extracted from two sine runs.
  - **FrImAC** (Frequency Imaginary Assurance Criteria). The objective is to calculate the MAC matrix between two runs over all frequencies according to:
 
$$Fr\text{ImAC}(i) = \frac{\left( \sum_{k=1}^{\text{common sensors}} \varphi_k^{\text{test } A}(i) \bullet M \bullet \varphi_k^{\text{test } B}(i) \right)^2}{\left( \sum_{k=1}^{\text{common sensors}} \varphi_k^{\text{test } A}(i) \bullet M \bullet \varphi_k^{\text{test } A}(i) \right) \bullet \left( \sum_{k=1}^{\text{common sensors}} \varphi_k^{\text{test } B}(i) \bullet M \bullet \varphi_k^{\text{test } B}(i) \right)} \quad [8-6]$$
  - **ImMAC** (Imaginary Modal Assurance Criteria). The objective is to calculate the MAC matrix for the modes extracted by the fast modal extraction methodology:
 
$$\text{ImMAC}(\varphi_i, \varphi_j) = \frac{\|\text{Im}(\varphi_i) \bullet M \bullet \text{Im}(\varphi_j)\|^2}{\|\text{Im}(\varphi_i) \bullet M \bullet \text{Im}(\varphi_i)\| \bullet \|\text{Im}(\varphi_j) \bullet M \bullet \text{Im}(\varphi_j)\|} \quad [8-7]$$

The Dynamited methodologies [6] have been developed to fit in the actual test campaign context which aims to validate the spacecraft structure mechanical qualification as fast as possible to reduce costs to deliver the spacecraft to the customer as quickly as possible.

It is thus necessary to perform during the test a correlation between FEM and real structure behaviour to validate the predictions for CLA or between two tests to follow behaviour evolution. Different powerful methods and tools exist to do such a modal identification and correlation, but these really effective methods call for time to apply and are not automatized which is not compatible with the test time constraints.

The need is thus to extract modal behaviour and correlate quickly the FEM/hardware or test/another test (different input levels) by an automatized method allowing dealing with large amount of data.

The Fast Modal Extraction and Correlation method [6] provides an automatic FRF correlation by:

- Identifying the peaks automatically by a new method based on an exhaustive curve scanning to detect local and global maxima and a quick mode extraction by maximum number of curve peaks for a given thin frequency band.
- Providing different visual indicators to assess quicker and efficiently the correlation.
- Keeping the same software environment (DynaWorks) to avoid time loss.

This method is an additional piece of information compared to standard modal approach.

- **Test correlation with previous run:** The objective of this task is to provide a quick modal extraction and correlation between the previous run and the actual run thank to visual indicator. The final objective is to verify the tested specimen evolution between the two runs and check that no major problem is met. This could also be made with transfer functions comparisons or with FMEC methodology.
- **Test data comparison with respect to limitation:** The objective of this task is to evaluate the achieved test responses with respect to the corresponding allowable by curve comparison. It is necessary during this operation to confirm (or identify missed): dead sensors, suspicious sensors, exceeding of the allowable. This task should be performed on the raw test data of every run with the exception of the low level control run.
- **Mode shape extraction:** It has been proven through the studies Dynamited [6] and RTMVI (Real Time Modal Vibration Identification) [7] [8] [9] that (“quasi-real-time”) modal identification is possible during a satellite qualification campaign through swept sine tests. This presents the advantage of obtaining relevant modal information without a dedicated modal survey test (generally not performed for time and cost reasons). Furthermore the boundary conditions and the excitation (at the satellite base) are similar to flight conditions.

The RTMVI method for modal identification is thus possible for base driven tests with nearly on-line use, which improves and simplifies test procedures such as validation of notching levels.

#### — **Test checks**

Typical activities for checking the measurements are:

- Check of the instrumentation response: It consists of visualising the transfer function curves to detect erroneous responses, accelerometers out of order or removed. It could be checked in particular that low frequency responses on accelerometers match 1 for the accelerometers in the excitation direction and 0 in the perpendicular directions.
- Comparison of global/fundamental signals to detect noise in specimen responses or potential nonlinearity problems.
- Check of the cross coupling: It consists of checking that the acceleration input at the spacecraft interface is a pure rigid body motion. It is done by multiplying the  $n$  measured accelerations at the spacecraft interface by the pseudo-inverse of the  $[n \times 6]$  matrix related to the accelerometer locations with respect to the interface centre.
- Determination of the rigid body mass matrix by low frequency behaviour analysis and comparison to the specimen mass and centre of gravity and inertia.
- Check of the spacecraft pilot signal quality: the control of the shaker can be disturbed by strong resonances with high Q factors and high specimen interface loads or by two closely-spaced main modes. This may result in perturbed FRFs, which then become too noisy for modal identification. The reduction of the sweep rate and the compression speed, or a decreasing frequency sweep improves the quality of the piloting.

— **Modes to be identified**

The mopides to be identified are mainly:

- The modes on which the loads at the spacecraft interface are important (i.e. modes with large effective mass  $\tilde{M}_{rn,k}$ ).
- The global spacecraft modes (for instance the second lateral SC mode) where significant responses occur at all accelerometer locations.
- For each appendage, the main modes (typically 2 or 3).

The notching predictions are used to complete the identification of modes on which notching is performed.

— **Modal identification process**

Information related to modal parameters can be derived in real time from the previous controlled data. For a given set of FRFs, the MIF (Mode Indicator Function) criterion enables to detect the presence of modes :

$$MIF(f) = \frac{\sum_i |\Re(\text{FRF}_i(f))| |\text{FRF}_i(f)|}{\sum_i |\text{FRF}_i(f)|^2} \quad [8-8]$$

This function has a maximum value of unity and its minima are good indicators for the presence of modes at the corresponding frequencies.

Then, basic identification can be performed directly with the peaks of the imaginary parts of the FRFs, the modes being detected directly from visual display of FRF real/imaginary parts. For each peak of the imaginary parts related to a mode  $k$ , the following parameters can be derived:

- Natural frequency  $f_k$  : common frequency of the peaks.
- Modal damping  $\zeta_k$  : estimated from the peak sharpness by least square fit using the values in the vicinity of the maximum which are proportional to  $\Im(T_k(f))$  with:

$$T_k(f) = \frac{1 + i2\zeta_k \frac{f}{f_k}}{1 - \left(\frac{f}{f_k}\right)^2 + i2\zeta_k \frac{f}{f_k}} \quad [8-9]$$

- Modal effective parameters  $\tilde{\mathbf{T}}_{in,k}$  and  $\tilde{\mathbf{M}}_{rn,k}$ : derived from the dynamic transmissibilities  $\mathbf{T}_{in}(f)$  and masses  $\mathbf{M}_{rn}(f)$  respectively:

$$\begin{aligned} \Im(\mathbf{T}_{in}(f)) &= \sum_k \Im(T_k(f)) \tilde{\mathbf{T}}_{in,k} \\ \Im(\mathbf{M}_{rn}(f)) &= \sum_k \Im(T_k(f)) \tilde{\mathbf{M}}_{rn,k} \end{aligned} \quad [8-10]$$

- Finally, a set of identified modal parameters  $(f, \zeta, \tilde{\mathbf{T}}_{in}, \tilde{\mathbf{M}}_{rn})_k$  may be obtained. Concerning the effective parameters:
- The modal effective transmissibilities  $\tilde{\mathbf{T}}_{in,k}$  are proportional to the mode shape components  $\Phi_{ik}$ :

$$\tilde{\mathbf{T}}_{in,k} = \Phi_{ik} \frac{L_{kn}}{m_k} \quad [8-11]$$

Therefore, they can be used for modal display with the wire model.

- o The modal effective masses  $\tilde{\mathbf{M}}_{rn,k}$  allow to recover the whole effective mass matrix  $\tilde{\mathbf{M}}_{rr,k}$  since

$$\tilde{\mathbf{M}}_{rr,k} = \frac{\mathbf{L}_{rk} \mathbf{L}_{kn}}{m_k} = \frac{\tilde{\mathbf{M}}_{rn,k} \tilde{\mathbf{M}}_{nr,k}}{\tilde{M}_{nn,k}} \quad [8-12]$$

The residual terms can be obtained by subtracting the sum of the modal effective parameters from the static terms.

#### 8.4.4.4 Higher level prediction

The objective of this part of the process is to determine the ideal notched input spectrum taking into account all limitations applicable to the SC and to identify a reduced set of sensors (leading generally to the deepest notch) which covers all the notching to build the next level run sheet.

Three philosophies can be considered for higher level prediction:

- predict to qualification input level whatever the true prediction input level and use as limitation the maximum allowable value. The true prediction input levels are then recovered by applying to the input spectrum, allowable values and abort values, the coefficient between the true input level and the qualification input level (dotted blue line in Figure 8-11)
- predict to the true prediction input level and use as limitation the maximum allowable value. This leads to keeping the same shaker behaviour approaching each mode but with the maximum possible limitation on the equipment (dotted green line in Figure 8-11)
- predict to the true prediction input level and use as limitation the ratio between the input level and the qualification level. This is equivalent to the first philosophy but always working with the true input level and simulation (dotted blue line in Figure 8-11)

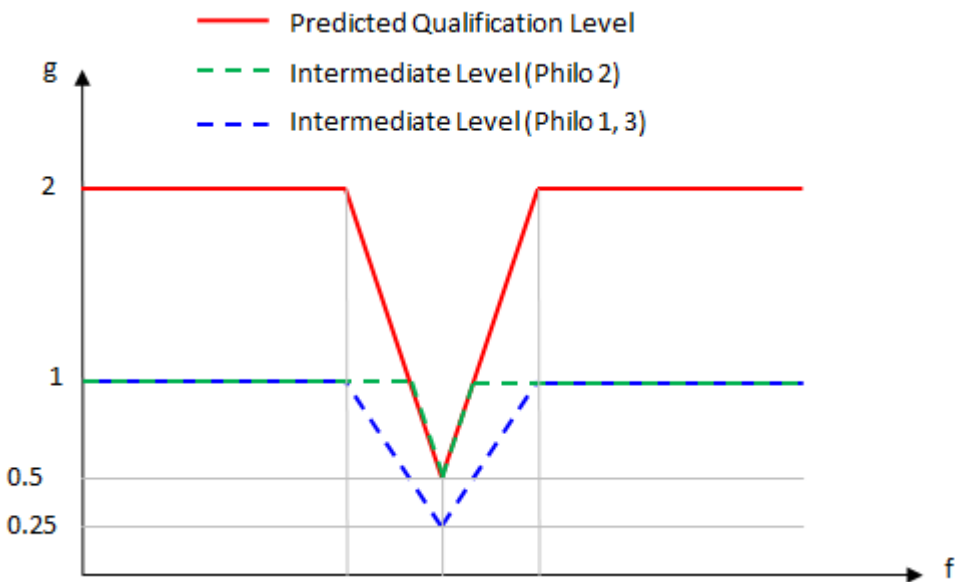


**Figure 8-11: Illustration of high-level prediction philosophies**

The same overall process is applied regardless of the philosophy:

1. First of all, the notched spectrum is calculated using the target input spectrum objective and the complete limitation base using the transfer function of all restitutions points calculated on previous runs.
2. The objective is then to identify on the obtained input spectrum the covering contributors for each notching, which means the restitution points which, with their respective associated limitation value, induce the deepest notching. The next-to-deepest notching should also be taken into consideration to anticipate potential amplification factors evolution with the increase of the input spectrum. This allows creating a reduced set of restitutions which is used to pilot the higher level run.
3. Finally, some iterative notched input calculations are performed with this reduced set of restitutions and with associated limitation adjustment. Some manual notching of the input spectrum can also be introduced during these iterations. At each iteration the induced input notching spectrum is superimposed with the initial one (when the complete limitation base is used). The iteration process can be stopped when the input notched spectrum induced by this reduced set of restitution is strictly below the initial notched spectrum.
4. The resulting notched input spectrum is then multiplied by the transfer function of each sensor in order to predict response level for all restitution which should be compared to all associated limitation.

#### 8.4.4.5 Run sheet consolidation

The aim of this final part is to validate every entry of the run sheet that is delivered to the test centre for higher level application.

##### Abort margins:

First the abort margin should be verified. It should be performed a prediction taking into account the final input spectrum (with manual notching), notching sensors with the proper notching criteria (output from previous iterative process) and corresponding frequency range and introducing the abort protection sensor, abort criteria and corresponding frequency range. The objective is to calculate the abort margin with the good notched input profile which should be positive.

When it has been performed on the ideal input spectrum (without taking into account overshoot and undershoot introduced by the shaker), the ideal notched input spectrum should be multiplied by the pilot inaccuracy factor if the previous run has allowed calculating it (which means that predicted notching profile is consistent with lower level input spectrum). In this case, abort margins should also be positive: if not, abort values and/or notching criteria should be adjusted, depending on test objective on each notching.

Based on the example previously considered in Figure 8-10, the predicted qualification level responses at the sensor piloting the notching on the first lateral mode is plotted in Figure 8-12 with and without the pilot inaccuracy factor (red and blue curves respectively). If the shaker were perfect, we would want to limit the acceleration on this sensor to 4.8g (blue curve). When multiplied by the pilot inaccuracy factor, it can be seen that the level is expected to reach 5.0g on the sensor (red curve). For an abort level of 5.2g a positive abort margin is produced and the run can be approved. However, for an abort limit of 5.0g, the abort margin is null due to the pilot inaccuracy and therefore the notching level should be adjusted to achieve a positive margin in order to avoid the risk of abort during the run.

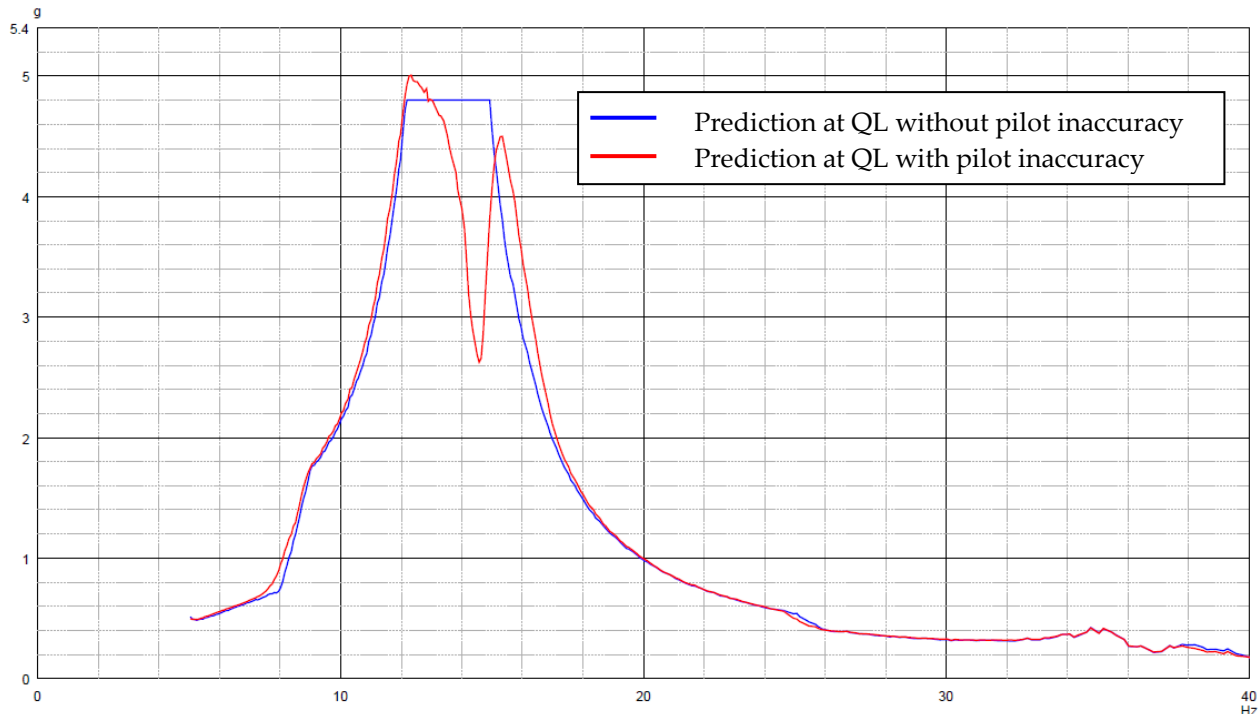


**Figure 8-12: Effect of pilot inaccuracy on abort margin**

#### Predicted test levels compared to objectives

When the abort margins are consolidated with a finalized set of notching/abort channels, all restitutions transfer functions can be multiplied by the final predicted notched input spectrum (taking into account pilot inaccuracy) to obtain the predicted response levels. These response levels should be compared to:

- Limitation base: the objective is to verify that no critical limitation is expected to be exceeded and to extract for each critical limitation the margin expected between predicted response level and limitation.
- Test target values: the objective is to verify that test target values are well predicted to be achieved for base load specified by launcher, equipment qualification values, etc.

A maximum value per frequency range table should be exported on the predicted response levels and compared to coupled loads analysis predictions with an acceptable margin factor (typically 1.25 factor).

#### Completion of the run sheet

After having performed the above mentioned verifications, the run sheet should be completed with the notching and abort values used to calculate the previous notched input spectrum.

## 8.5 References

- [1] Ariane 5 User's Manual, Issue 5, Revision 1, July 2011.
- [2] Cavro E., Capitaine A., Last Improvements in Modal Identification Methods, European Conference on Spacecraft Structures, Materials & Environmental Testing, Noordwijk, The Netherlands, 20-23 March 2012.
- [3] Girard A., Cavro E., Rodriguez F., Sensor Location for Real Time Modal Identification, Proceedings IMAC XXVII, Orlando, Florida, February 9-12 2009.
- [4] Ingemansson Force Measurement Device, Final Report V1211-B, January 28th 1998.
- [5] Laborde S., Calvi A., Spacecraft base-sine vibration test data uncertainties investigation based on stochastic scatter approach, Mechanical Systems and Signal Processing, Vol 32, October 2012.
- [6] Assessment and Improvement of Dynamic Test Data (DYNAMITED), Final Report, EADS Astrium Ref MTF.AIDT.TN.2168, ESA Contract 20307/06/NL/IA, March 3 2010.
- [7] Lefevre Y.M., Bonetti J.C., Girard A., Roy N., Calvi A., Real-Time Modal Identification Techniques for Improved Satellite Vibration Testing, European Conference on Spacecraft Structures, Material and Mechanical Testing, Toulouse, 11-13 December 2002.
- [8] Lefevre Y.M., Real-Time Modal Real Time Modal Vibration Identification for Communication Satellite Testing (RTMVI), Astrium Final Report 959.NT.YML.6908.01, ESA Contract 13772/99/NL/JG, October 2001.
- [9] Roy N., Buffe F., Improved Modal Identification from Base Excitation Vibration Tests using Modal Effective Parameters, European Conference on Spacecraft Structures, Materials & Environmental Testing, Toulouse, France, 15-17 September 2009.

**9**

# **Random vibration and vibro-acoustics**

## **9.1 Introduction**

### **9.1.1 Overview**

Acoustic pressure fluctuations under the fairing are generated by engine operation (plume impingement on the pad during lift-off) and by unsteady aerodynamic phenomena during atmospheric flight (i.e. shock waves and turbulence inside the boundary layer), which are transmitted through the upper composite structures. The sound field under the fairing is normally assumed as diffuse.

An acoustic environment is presented in terms of sound pressure level (SPL), which is the root mean square pressure within a frequency band, expressed in decibels (dB). The SPL is normally plotted at the centre frequencies of one-third (or one) octave bands, on a log scale, over the range of 20 Hz to 10 kHz.

Structures vibrate randomly in response to acoustics. The structures that respond the most are light in weight and large in surface area, such as skin panels and solar arrays. Relatively large, heavy structures have very little direct response to acoustics (vibroacoustic response), but they vibrate because of excitation from more responsive structures. This vibration is often the driving environment for a spacecraft electrical, electro-mechanical and electronic components [1].

The random vibration is characterised with a power spectral density (PSD) curve. The term “power” is a generic term that can represent e.g. acceleration, velocity, displacement, force and stress, depending on the parameter to describe.

The PSD is normally plotted on a log-log scale, typically covering the frequency range of 20 to 2000 Hz, which has been found to adequately describe random vibration for structures and electronic components.

Most of the random vibration in small payloads is transmitted through the launch vehicle interface. Not all launch vehicle users' manuals provide PSDs for this vibration, which is the sum of the launch vehicle structural response to acoustics, engine vibration, and other loads. For a large payload, especially if it has big solar arrays, the vibroacoustic response of its own lightweight structures generates most of the base random vibration for components. Thus, vibration levels at component interfaces depend on the spacecraft design, and they are predicted by analysis or test [1].

The vibro-acoustic loads are converted into random structural vibrations (accelerations). These accelerations excite mounted e.g. instruments, equipment and boxes. The generated enforced random acceleration specifications are applied to verify e.g. instruments, equipment and boxes.

Note: Usually there is no or little concern about the structural housing of components, it is the tiny structures within electronic components, the soldered joints and circuit boards, that tend to fatigue from high frequency vibration.

## 9.1.2 Random vibration loads

In [1] the following definition of random vibration is provided: “vibration (load) whose instantaneous magnitudes are specified only by probability distribution functions giving the probable fraction of the total time that the instantaneous magnitude lies within a specified range”.

The following process proposes in the following three steps the development of the random acceleration vibration specification:

1. Determine the Power Spectral Density (PSD) of the random vibration directly transmitted into the flight article through its mounts from the launch vehicle sources such as engine firing and turbo pumps). These vibration conditions at the launch vehicle-to-payload interface are often available from the launch vehicle builder.
2. Perform an analysis to predict the payload/flight article's vibration response to the launch vibro-acoustic environment. Statistical energy analysis (SEA) methods are effective predictors in the higher frequencies. If random vibration predictions are needed for the lower frequencies, finite element analysis methods are commonly used. The vibration is induced into the component both directly and indirectly.
3. Envelope the curves from 1-2 to produce a composite random vibration specification for the component. The vibro-acoustic environment is the most important source for the estimation of the random vibration specification. Further database extraction methods, build up from many acoustic tests, can be applied to generate the resultant random vibration test level.

This resultant random vibration specification, which is employed as the flight acceptance test level, covers the two primary sources of this vibration while also providing an effective process for uncovering workmanship defects, particularly for electronics. Qualification and protoflight test levels are increased typically 3dB above flight acceptance to verify that the design is not marginal.

Conventional rigid fixture vibration tests can severely overtest the hardware at resonances. It is accepted practice to response limit, or notch the input, at resonances of fragile hardware where it can be technically justified with flight or system test data, or analysis.

Note: For spacecraft components, since acoustics cause most random vibration, criteria for random vibration specification should be consistent with those for acoustic testing.

## 9.1.3 Vibro-acoustic loads

### 9.1.3.1 Acoustic loads specification

The discussion about acoustic loads is taken from [2]. Acoustic loads appear as design specifications for spacecraft and spacecraft subsystems such as solar arrays and antennae. Acoustic loads are generated during launch, or in acoustic facilities for test purposes. It is very common to specify a diffuse sound field, which means that the intensity of the sound is the same in all directions. An example of an Ariane 5 [3] acoustic load spectrum is shown in Table 9-1.

**Table 9-1: Acoustic noise spectrum under fairing (Ariane 5)**

Octave Centre Frequency (Hz)	Flight Limit Level (dB)
	(Reference 0dB = $2 \times 10^{-5}$ Pa)
31.5	128
63	131
125	136
250	133
500	129
1000	123
2000	116
OASPL (20 – 2828 Hz)	139.5

In general, the acoustic loads are described as sound pressure levels (SPL) and specified in decibels (dB). The SPL is defined by:

$$\text{SPL} = 10 \log \left( \frac{p}{p_{ref}} \right)^2, \quad [9-1]$$

where  $p$  is the rms pressure in a certain frequency band with frequency band width  $\Delta f$ , mostly one octave or one third octave band, and  $p_{ref}$  is the reference pressure  $2 \times 10^{-5}$  Pa.

The  $x$ -th octave band of two sequential frequencies  $f_{\min}$  and  $f_{\max}$  is given by :

$$\frac{f_{\max}}{f_{\min}} = 2^x, \quad [9-2]$$

Where  $x = 1$  for one-octave, and  $x = 1/3$  for the one-third-octave band. In the latter case  $f_{\max}/f_{\min} = 1.260$ .

The centre frequency  $f_c$  (Hz) is defined by :

$$f_c = \sqrt{f_{\min} f_{\max}}, \quad [9-3]$$

where  $f_{\min}$  ( $f_{\max}$ ) is the minimum (maximum) frequency (Hz).

The frequency bandwidth  $\Delta f$  (Hz) is given by :

$$\Delta f = f_{\max} - f_{\min}.$$

With  $f_{\max}/f_{\min} = 2^x$  the bandwidth  $\Delta f$  can be expressed in terms of the centre frequency  $f_c$  as follows :

$$\Delta f = \left( 2^{\frac{x}{2}} - 2^{-\frac{x}{2}} \right) f_c. \quad [9-4]$$

When

- $x = 1$ , the one octave band width is  $\Delta f = 0.7071 f_c$ ,
- $x = 1/3$ , the one-third octave band width is  $\Delta f = 0.2316 f_c$

The PSD of the pressure field  $W_p(f_c)$  (Pa<sup>2</sup>/Hz) in the frequency band with centre frequency  $f_c$ , bandwidth  $\Delta f(f_c)$  and rms pressure  $p(f_c)$  is defined as :

$$W_p(f_c) = \frac{p^2(f_c)}{\Delta f(f_c)}. \quad [9-5]$$

The mean square value  $p_{rms}^2$  of the sound pressure level is given by :

$$p_{rms}^2 = \int_0^\infty W_p(f) df = \sum_{i=1}^k W_{p,i}(f_c) \Delta f = \sum_{i=1}^k p_i^2(f_c), \quad [9-6]$$

where  $k$  is the number of one-octave or one-third octave bands.

The overall sound pressure level (OASPL) in dB is defined as :

$$\text{OASPL} = 10 \log \left( \frac{p_{rms}^2}{p_{ref}^2} \right), \quad [9-7]$$

The following relation determines the conversion of a one-third octave band to a one-octave band :

$$\text{SPL}_{1\text{-octave}} = 10 \log \left[ \sum_{k=1}^3 10^{\frac{\text{SPL}_{1/3\text{-octave}}}{10}} \right], \quad [9-8]$$

and the following relation determines the conversion of a one-octave band to a one-third octave band :

$$\text{SPL}_{1/3\text{-octave}} = \text{SPL}_{1\text{-octave}} + 10 \log \left[ \frac{\Delta f_{1/3\text{-octave}}}{\Delta f_{1\text{-octave}}} \right]. \quad [9-9]$$

### 9.1.3.2 Reverberant sound field

A clear description of a reverberant field is given in the NASA Handbook [4].

"The acoustic pressure field during the liftoff of a space vehicle propagates forward over the vehicle structure, while the aerodynamic-induced fluctuating pressure field during ascent and entry convects aft over the vehicle structure. Hence, a facility that generates a propagating pressure field excitation along the longitudinal axis of the vehicle would provide the most accurate simulation. Nevertheless, due to the complexity and high cost of large, general purpose propagating wave test facilities, most acoustic tests of space vehicles or major subsystems thereof are performed in large, high intensity acoustic reverberation rooms".

"For space vehicle structures that have a surface exposed to the atmosphere, it is understood that reverberant acoustic noise does not have the same spatial correlation characteristics as the propagating acoustic noise during liftoff or the convecting aerodynamic noise during ascent or entry through the atmosphere and, hence, for the same acoustic noise level, the response of the space vehicle structure to the reverberant acoustic noise excitation is different from the response to the liftoff and flight environments".

"Some experimental studies have indicated that this difference in structural responses may be substantial at frequencies below the first normal mode of the structure, but other studies do not reveal a significant difference. In most cases, however, the potential error due to differences in the spatial

correlation characteristics of the test and flight environments is ignored as long as an adequate margin is added to the specified 1/3 octave band levels for the test. For payloads enclosed in a fairing or payload bay, acoustic reverberation rooms provide a more accurate simulation since the payload experiences a reverberant acoustic noise excitation during flight."

## 9.2 Requirements

In the ECSS standard ECSS-E-ST-32C "Space Engineering, Structural General Requirement" [5] a number of requirements are mentioned concerning random mechanical and vibro-acoustic vibration aspects of the design and verification activities of spaceflight hardware.

In particular the following clauses contain relevant requirements: "**4.2.3 Mechanical environment**", "**4.2.7 Limit loads**", "**4.6.2.5 Dynamic response analysis**", "**4.6.2.6 Acoustics analysis**", "**4.6.3.9 Dynamic tests: sine, random, shock**", "**4.6.3.10 Acoustic test**".

How to interpret the previous stated clauses about random mechanical and acoustic loads, random and acoustic response analyses and verification is discussed in the following sections.

## 9.3 Random vibration specification

### 9.3.1 Introduction

The prediction of the vibration environment is usually required during the initial phase of a component's development to support design and procurement specifications. During the initial phase only layouts and crude structural detail are generally available. For many components acoustically driven random vibration represents the most significant vibration environment. Numerical procedures ranging from the deterministic methods as the finite element analysis, and the boundary element analysis to the non-deterministic statistical energy analysis are available. However, the use of these methods requires a reasonable accurate representation of the structure, not usually known during a system's early design phase. Some methods are discussed to define random vibration specifications in an early design phase, in particular:

1. The Spann method [6] [7] which provides a reasonable estimate of the acoustically excited component vibration environments when only the areas exposed to the acoustic environment and mass are known.
2. The method to establish specifications at unit level based on a statistical analysis performed on test data collected from random and acoustic testing at system level [8].
3. The method developed within the study "Derivation of Satellite Equipment Design and Test Specifications for Random Vibration (VibroSpec)" (e.g. [9] [10]).
4. A test-analysis extrapolation method for the determination of in-flight random responses based on acoustic test measurements.

### 9.3.2 Component vibration environment predictor, Spann method

This section describes the steps required to derive component vibration test specifications for typical spacecraft structures subjected to an acoustic environment. The theoretical basis of the prediction method is discussed. The application of this prediction method is based on two conditions:

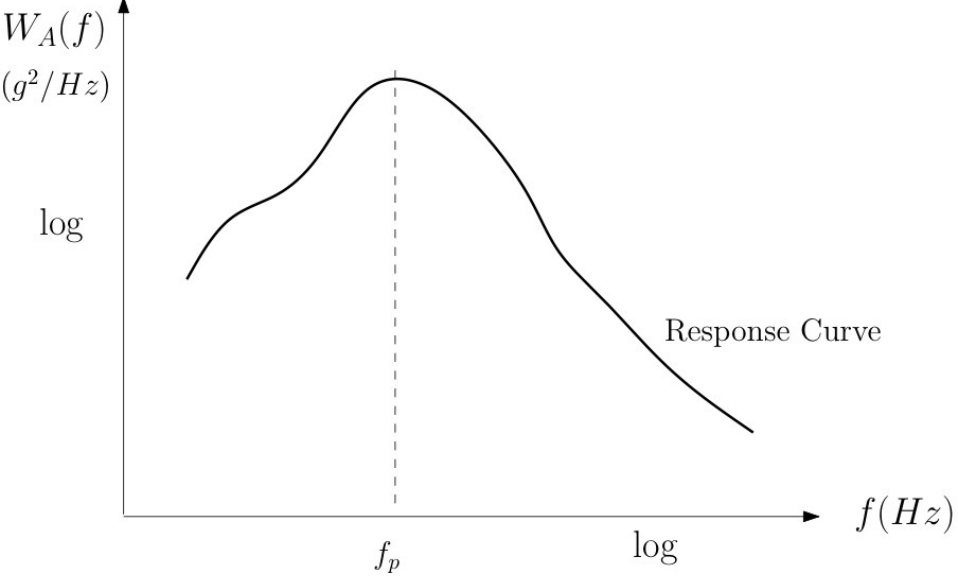
1. Definition of the acoustic environment.
2. An adequate general understanding of structure and components to obtain estimates of mass and areas exposed to acoustic excitations.

In general the procedure is applied in three axes, the same axes that are used for specifying the random vibration requirement.

Table 9-2 describes the different steps of the method.

**Table 9-2: Steps of Spann method**

Step	Task definition																																												
1	$W_P(f_c) = p_{ref}^2 \frac{\frac{SPL(f_c)}{10}}{\Delta f_c} = (2.0 \times 10^{-5})^2 \frac{\frac{SPL(f_c)}{10}}{\Delta f_c} = \frac{p_{rms}^2(f_c)}{\Delta f_c}, \quad [9-10]$ <p>Acoustic environments defined as sound pressure levels in decibels (dB) are converted into pressure spectral density. The following relationship defines the pressure power spectral density <math>W_P(f_c)</math> (<math>\text{Pa}^2/\text{Hz}</math>) in the one-third-octave band :</p> <p>where the bandwidths <math>\Delta f_c = 0.7071f_c</math> or <math>\Delta f_c = 0.2316f_c</math> are for one-octave and one-third-octave band respectively. <math>p_{rms}^2(f_c)</math> is the mean square pressure for the frequency band with centre frequency <math>f_c</math>.</p> <p><b>Example</b></p> <p>The power spectral densities <math>W_P(f_c)</math> of the pressure are calculated. The SPL values are defined in the one-octave band and are taken from [11]. The calculation results are shown below in Table 9-3.</p> <p><b>Table 9-3: Calculation of PSD function <math>W_P(f_c)</math></b></p> <table border="1"> <thead> <tr> <th>Centre frequency octave band (Hz)</th><th>SPL (dB) 0dB= 2.0E-5 Pa</th><th><math>p_{rms}^2(f_c)</math> (<math>\text{Pa}^2</math>)</th><th><math>W_P(f_c)</math> (<math>\text{Pa}^2/\text{Hz}</math>)</th></tr> </thead> <tbody> <tr> <td>31.5</td><td>130.0</td><td>4000.0</td><td>179.6</td></tr> <tr> <td>63</td><td>135.6</td><td>14523.1</td><td>326.0</td></tr> <tr> <td>125</td><td>139.0</td><td>31773.1</td><td>359.5</td></tr> <tr> <td>250</td><td>143.0</td><td>79810.5</td><td>451.5</td></tr> <tr> <td>500</td><td>138.0</td><td>25238.3</td><td>71.4</td></tr> <tr> <td>1000</td><td>132.0</td><td>6339.6</td><td>9.0</td></tr> <tr> <td>2000</td><td>128.0</td><td>2523.8</td><td>1.8</td></tr> <tr> <td>4000</td><td>124.0</td><td>1004.8</td><td>0.4</td></tr> <tr> <td>8000</td><td>120.0</td><td>400.0</td><td>0.1</td></tr> <tr> <td><b>OASPL</b></td><td><b>146.2</b></td><td></td><td></td></tr> </tbody> </table>	Centre frequency octave band (Hz)	SPL (dB) 0dB= 2.0E-5 Pa	$p_{rms}^2(f_c)$ ( $\text{Pa}^2$ )	$W_P(f_c)$ ( $\text{Pa}^2/\text{Hz}$ )	31.5	130.0	4000.0	179.6	63	135.6	14523.1	326.0	125	139.0	31773.1	359.5	250	143.0	79810.5	451.5	500	138.0	25238.3	71.4	1000	132.0	6339.6	9.0	2000	128.0	2523.8	1.8	4000	124.0	1004.8	0.4	8000	120.0	400.0	0.1	<b>OASPL</b>	<b>146.2</b>		
Centre frequency octave band (Hz)	SPL (dB) 0dB= 2.0E-5 Pa	$p_{rms}^2(f_c)$ ( $\text{Pa}^2$ )	$W_P(f_c)$ ( $\text{Pa}^2/\text{Hz}$ )																																										
31.5	130.0	4000.0	179.6																																										
63	135.6	14523.1	326.0																																										
125	139.0	31773.1	359.5																																										
250	143.0	79810.5	451.5																																										
500	138.0	25238.3	71.4																																										
1000	132.0	6339.6	9.0																																										
2000	128.0	2523.8	1.8																																										
4000	124.0	1004.8	0.4																																										
8000	120.0	400.0	0.1																																										
<b>OASPL</b>	<b>146.2</b>																																												
2	Estimate area $A$ ( $\text{m}^2$ ) of the component and spacecraft support structure supporting the component exposed to acoustic excitation.																																												
3	Calculate total mass $M$ (kg) of the component and support structure included in the above estimate in step 2.																																												
4	Calculate, at each one-third-octave band frequency, the equivalent response $W_A(f_c)$ ( $\text{g}^2/\text{Hz}$ ) using the following equation and the values of the pressure power spectral density $W_P(f_c)$ ( $\text{Pa}^2/\text{Hz}$ ), area $A$ ( $\text{m}^2$ ) and mass $M$ (kg) calculated in steps 1, 2 and 3 :																																												

Step	Task definition
	$W_A(f_c) = \beta^2 Q^2 \left( \frac{A}{gM} \right)^2 W_P(f_c) = 126.6 \left( \frac{A}{gM} \right)^2 W_P(f_c), \quad [9-11]$ <p>where the gravitational acceleration is <math>g = 9.81 \text{ m/s}^2</math>. Based on experimental test data a <math>\beta</math> factor of 2.5 and a amplification factor <math>Q = 4.5</math> is recommended [6] [7]. Construct a plot of <math>W_A(f_c)</math> versus the frequency <math>f</math> (Hz).</p>  <p style="text-align: center;"><b>Figure 9-1 : Response curve</b></p>
5	Iterate steps 2, 3 and 4, using different values of the input parameters to determine maximum $W_A(f_c)$ response curve.

### 9.3.3 Specifications derived from random and vibro-acoustic test data

#### 9.3.3.1 Introduction

A study to improve the specifications for random vibration testing at unit level has been performed in the late 80's [8].

A database was first prepared, for which nine major European satellite projects provided about 1800 response curves and associated information. For the random and acoustic test results the random response spectrum concept has been extensively used. A statistical evaluation has been made on the basis of log-normal distribution for the selection of curves using the parameters available in the database. The final equipment classification has been deduced from these results and corresponding specifications based on 95% confidence level have been provided to update the ESA standard applicable at that time. In particular, specifications for the random testing have been derived in the form of simple continuous functions of the equipment mass providing an extrapolation for heavy equipment items.

### 9.3.3.2 Unit random testing

The proposed specifications for random vibration test levels of units are given in Table 9-4 ([11]).

**Table 9-4: Proposed specification for random testing of units (95 % confidence level)**

(a) Equipment located on “external” panel (1) or with unknown location	
Vertical (2)	
Frequency (Hz)	PSD ( $\text{g}^2/\text{Hz}$ ), Mass equipment M (kg)
20-100	6dB/octave
100-400	$0.05*(M+20)/(M+1)$
400-2000	-3dB/octave
Lateral (3)	
Frequency (Hz)	PSD ( $\text{g}^2/\text{Hz}$ ), Mass unit M (kg)
20-100	6dB/octave
100-200	$0.05*(M+20)/(M+1)$
200-2000	-4dB/octave
<ul style="list-style-type: none"> <li>(1) Panel directly excited by payload acoustic environment</li> <li>(2) Equipment vertical axis is perpendicular to mounting plane</li> <li>(3) Equipment lateral axis is parallel to mounting plane</li> </ul>	
(b) Equipment not located on “external” panel	
Same as above, except that vertical levels are reduced to the lateral levels.	

These specified random vibration levels are qualification levels and, in general, the duration of the test is 120s.

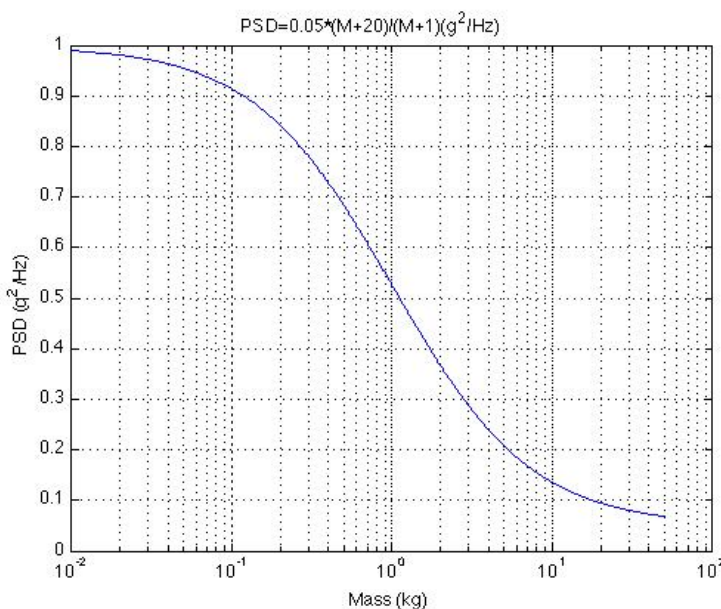


**Figure 9-2 : Proposed specifications**  $0.05 \frac{M + 20}{M + 1}$

Related to Figure 9-2, the following remarks are made [8]:

- The maximum values for very small masses, say  $M \leq 0.1 \text{ kg}$ , are close to the relatively high value  $1 \text{ g}^2/\text{Hz}$ .
- For medium masses, say between 1 and 10 kg, the specifications decrease significantly.
- Extrapolation to large masses gives a slow convergence towards the asymptotic PSD value of  $0.05 \text{ g}^2/\text{Hz}$ . For example, a mass of 30 kg gives  $0.08 \text{ g}^2/\text{Hz}$ . However, this approach is valid only if the equipment is rigid. If some very flexible parts are included in the unit, the corresponding mass should be removed,  $M$  representing the rigid part driven by the mounting. The study shows that 50 kg is an extreme limit in the present context, giving a minimum value of  $0.07 \text{ g}^2/\text{Hz}$ .

## 9.3.4 VibroSpec

### 9.3.4.1 Introduction

Experience (2005) from several ESA satellite projects shows that the approach conforming to ECSS standard ECSS-E-10-03A [11] results to requirements frequently contradicting spacecraft hardware measurements. As a result, there was a request from space industry and equipment manufacturers that the current approach for the derivation of equipment design and test load specifications needs to be reviewed and possibly improved. This was the subject of the study: "Derivation of Satellite Equipment Design and Test Specifications for Random Vibration (VibroSpec)" [10]. The objectives have been twofold:

- to derive an adequate approach for the specification of equipment quasi-static design loads and random vibration test inputs;
- to update and improve the currently applied approach derived in the 1980's [8].

The study tasks include the establishment of a relevant database containing acoustic test results from various spacecraft projects. The new approach is implemented in a user-friendly tool based on Matlab. The major goals of the study were to:

- Develop a methodology for the early specification of equipment test inputs for random environment due to acoustic loading:
  - Build a database of relevant acoustic test data.
  - Investigate the influence of more parameters
    - ECSS standard ECSS-E-10-03A: unit mass, panel location, sensor direction
    - VibroSpec: about 20 parameters e.g. equipped panel mass, launcher SPL
  - Derive an adequate approach to determine the random environment of equipment on a new platform.
  - Devote main emphasis to panel mounted units.
- Build and validate a tool to derive random test environment due to acoustic loading

### 9.3.4.2 Database statistics

Acoustic test data have been collected from in total 37 spacecraft, covering science, Earth observation as well as telecom satellites, covering spacecraft sizes from small and light to heavy and large.

In total, about 3300 valid measurements have been collected. With approximately 1970 measurements the vast majority is related to "Panel I/F".

The locations of the sensors (accelerometers) [10] are illustrated in Figure 9-3 [12].

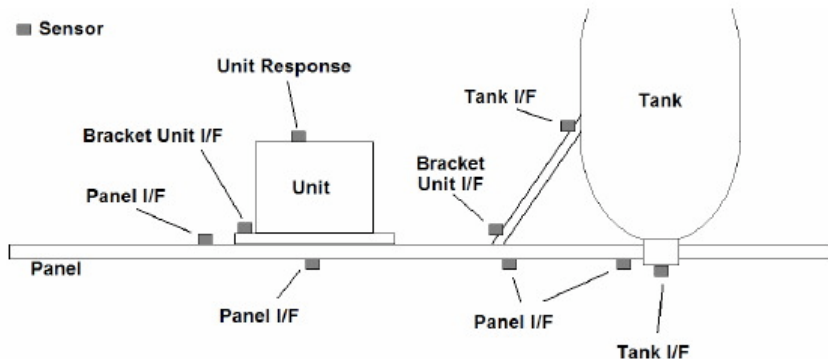


Figure 9-3 : Location of sensors (accelerometers)

### 9.3.4.3 Example

The following example (Figure 9-4) illustrates the procedure implemented in the VibroSpec software package [10]. A sensor in the database has been chosen randomly. Some parameters have been deleted to simulate a "classical" input from a user at an early stage of a project. In this case, the following 3 predictions have been performed:

- Only the mass of the unit, its location and the sensor direction are known (called 11 unknown).
- Panel dimensions, panel mass per area, number of free edges of the panel and sensor location are known additionally (named 6 unknown).
- All parameters are known (called 0 unknown).

The optimization algorithm in [10] results in predictions being significantly more accurate compared to the original measurement. The corresponding level taken from [11] has been added. It can be seen that adding new parameters allows relaxing the levels over the entire frequency range.

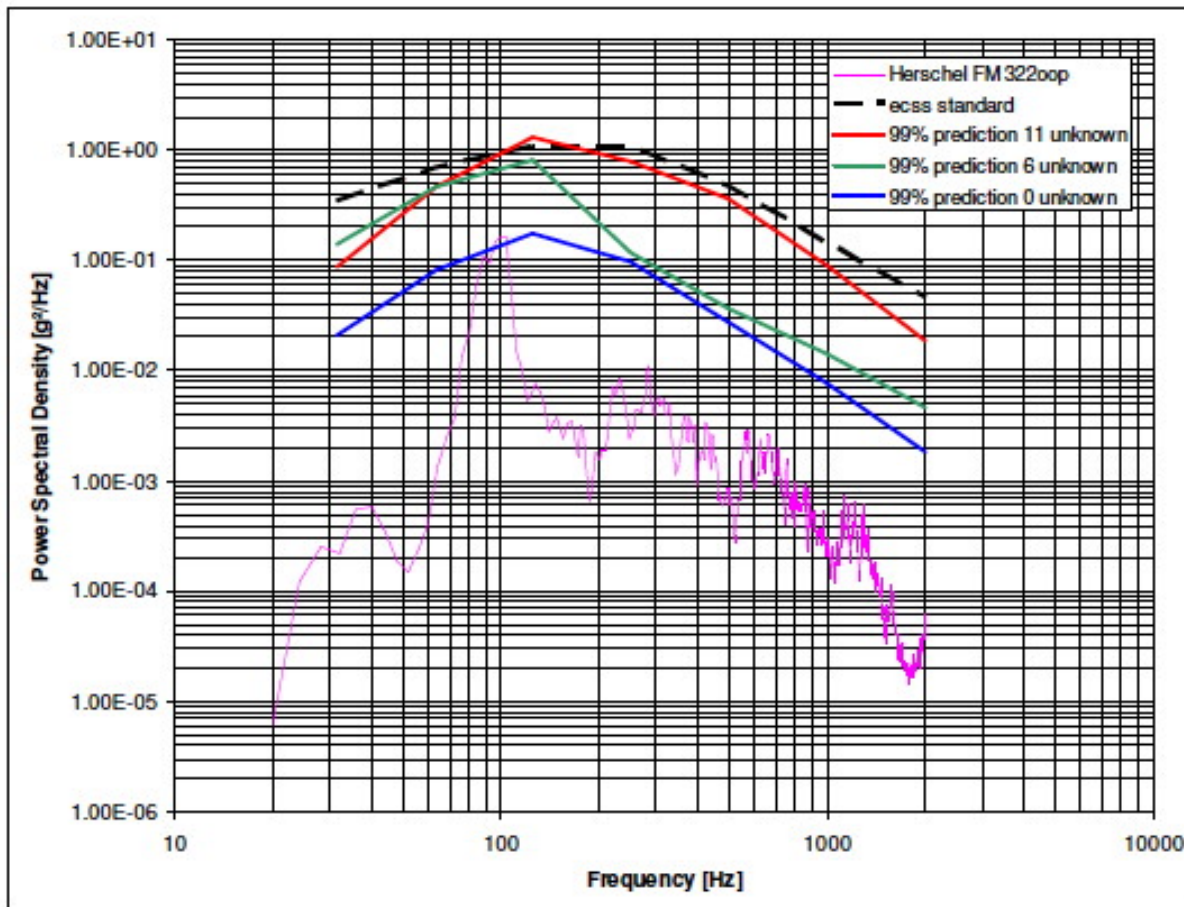


**Figure 9-4 : Prediction illustration with different number of known parameters**

### 9.3.5 Test/analysis extrapolation method

#### 9.3.5.1 Introduction

In this section a step-by-step extrapolation method for the determination of in-flight random responses based on acoustic test measurements is discussed. The method is based on procedures applied for the qualification of ESC-A Upper Stage and Ariane 5 Vehicle Equipment Bay towards the acoustic environment [3].

#### 9.3.5.2 Lift-off phase (reverberant noise):

- Step 1: Correlation of measured acceleration PSD results to analytical results from analysis model (SEA, FEM or hybrid) of the acoustic test configuration; both given in e.g. 1/3-octave bands.
- Step 2: Update of the analysis model of the acoustic test configuration to match the measured results.
- Step 3: Reconfiguration of the analysis model of the acoustic test configuration to the flight configuration. This applies for example to exciting SPL, tank filling (e.g. LOX and LH<sub>2</sub> in propellant tanks instead of water and air), and helium filling inside the cavities, structure borne noise transmitted by the adjacent structures.
- Step 4: Calculation of flight responses, e.g. given in 1/3-octave bands.

- Step 5: Determination of scaling factors between acoustic test, Step 2 results, and flight, Step 4 results, by comparison of results of the analysis models for each octave band.
- Step 6: Scaling of the measured acoustic noise test PSD results for each  $\Delta f$  value according to the scaling factor of the used octave band resolution.

### 9.3.5.3 Transonic phase (boundary layer noise):

To generate the envelope of all relevant flight load cases, an additional step needs to be performed for the transonic phase.

- Step 7: Application of acceleration PSD ratio between transonic and lift off according to vibro-acoustic analyses, to the lift off results resulting from Step 6 above. This is relevant for equipment mounted on the Launcher external shell structures.

### 9.3.5.4 Empirical random load factors

Vibro-acoustic responses for ESC-A have been compared to an empirical equation, which relates the  $3\sigma$  response to the equipment mass, the so-called mass acceleration curve (MAC).

$$n_R = 95.0M^{-0.3463} - 15(g), \quad [9-12]$$

where  $M$  (kg) is the mass of the equipment or line. Equation [9-12] could be useful as preliminary load assumptions. The enveloping curve is shown in Figure 9-5.

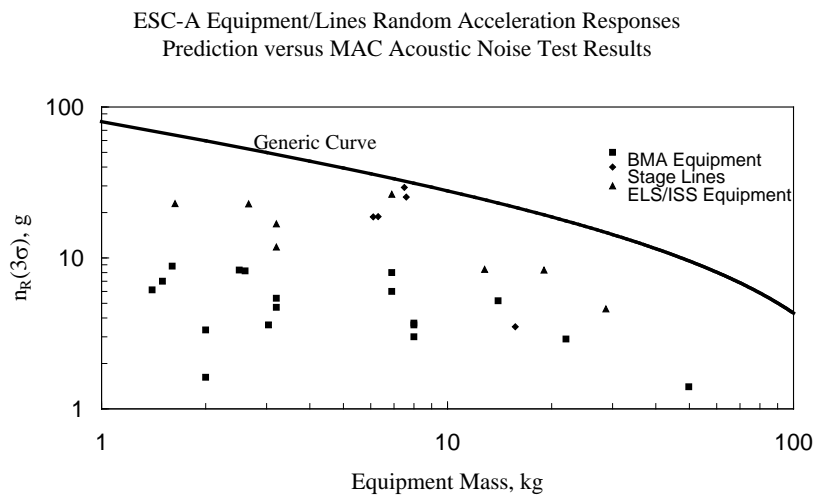


Figure 9-5 : Mass acceleration curve

## 9.4 Random vibration analysis

### 9.4.1 Finite element analysis and Miles' equation

In this section an approximate solution of the random vibration response analysis using the finite element analysis method in combination with Miles' equation is discussed. In fact the random vibration dynamic response analysis is replaced by static finite element analysis which analysis results are multiplied by appropriate Miles' representation of the random loads, both enforced acceleration and acoustic pressures.

Miles' equation assumes single degree of freedom behaviour of a structure. A limitation on the application of Miles' equation to elastic structures is that the shape of the single excited mode is supposed to approximate the profile of the structure under a static inertia load. For example, the first mode of a cantilever beam assumes the approximate shape of the beam under a transverse inertia load as illustrated in Figure 9-6 (see [13]).

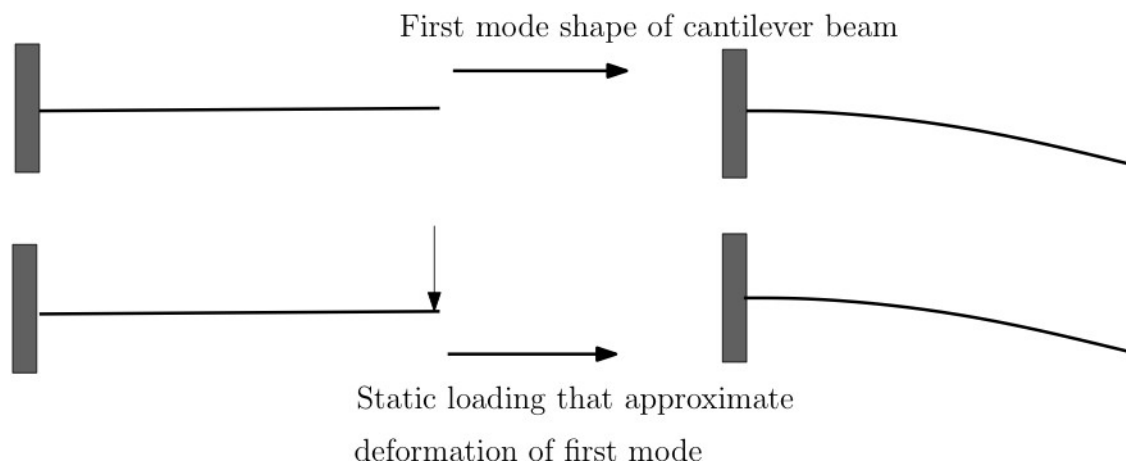


**Figure 9-6 : Static Loading for approximate first mode shape of cantilever beam**

Miles' equation is given by:

$$g_{eq} = \sqrt{\frac{\pi}{2} f_n Q_n W_{\ddot{u}}(f_n)} \quad [9-13]$$

In [9-13],  $g_{eq}$  is the approximate root mean square acceleration response, commonly used as an "equivalent static inertia load";  $f_n$  is the single natural frequency chosen for application of Miles' equation; the mode shape  $\Phi_n$  corresponding to the natural frequency  $f_n$  is selected on the basis of significant modal effective mass  $M_{eff,n}$ ;  $W_{\ddot{u}}(f_n)$  is the value of the enforced acceleration power spectral density at frequency  $f_n$ , and  $Q_n$  is the amplification factor for that mode.

The flow chart developed for this approximation is illustrated in Figure 9-7 (see [13]). The maximum root mean stresses (e.g. von Mises stress) calculated here provides a criterion for reliability, fatigue life analysis. For a traditional static analysis the  $3\sigma$  rule can be used for design verification.

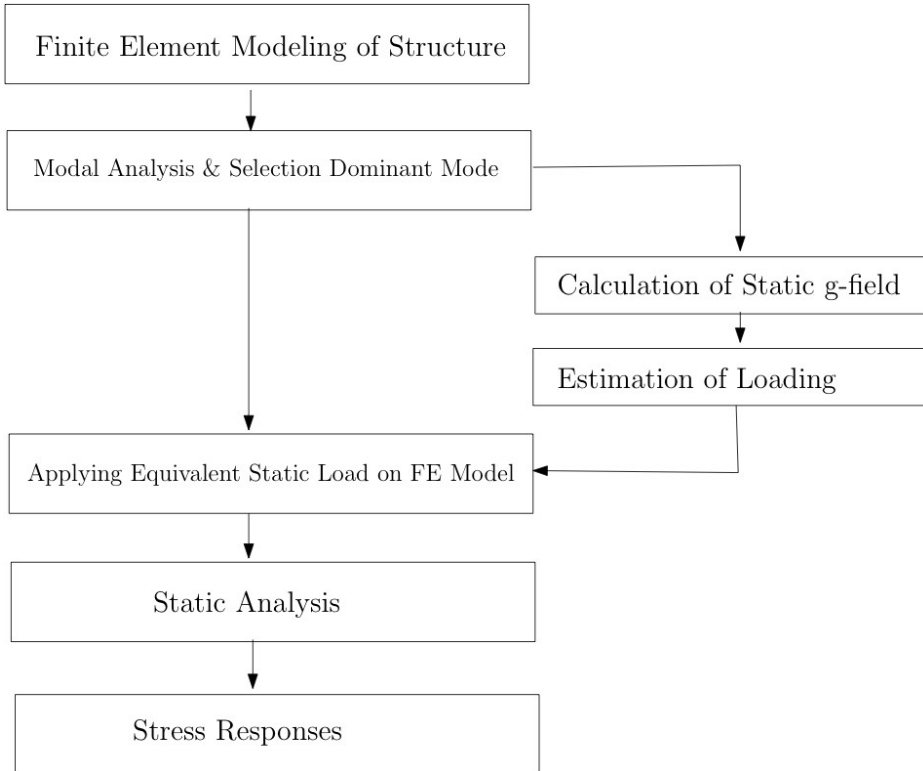


**Figure 9-7 : Design flow chart for Miles' equation**

### 9.4.2 Finite element analysis

Many textbooks and papers are written about the theory of the finite element analysis technique, e.g. [14] [15]. Hence we assume that the mass matrix  $[M]$  and stiffness matrix  $[K]$  are well defined. The damping matrix  $[C]$  is very difficult to generate. In many cases the damping is distributed over the structure and the significant contribution comes, for example, from the connections of structural element, cable harness, and fluid-structure interaction. In most cases the modal damping ratio  $\zeta_k$  (modal damping is  $2\omega_k m_k \zeta_k$ ) is applied using the modal analysis approach [16] [17].

The main purpose of the finite element analysis is the calculation of the frequency transfer function  $H(f)$  representing the load path from the applied unit forces, unit pressure, unit enforced acceleration at the point of interest, e.g. stress tensor, forces, accelerations. This is illustrated in Figure 9-8. Pressure loads are illustrated symbolically and are defined in most cases as a reverberant sound field. Figure 9-8 illustrates a simplified spacecraft with an antenna dish and solar panels on the outside exposed to vibro-acoustic loads and random enforced acceleration spectrum at the base of the spacecraft. The general (practical) specifications of the random enforced acceleration spectrum and the reverberant sound field spectrum are already discussed in previous sections. The shown points of interest are a) stresses and forces at a certain location in a structural member and b) the random vibration environment at the base of a box (instrument, equipment). The spacecraft may be easily replaced by an instrument or stage, interstage of a launch vehicle.

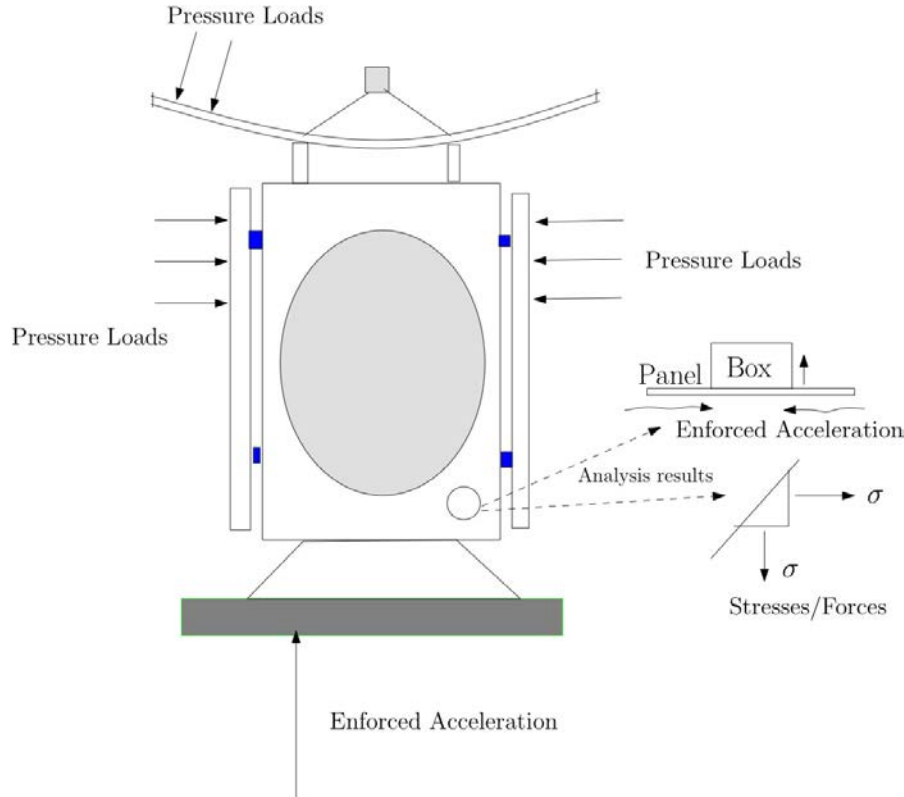


**Figure 9-8 : Spacecraft loaded by pressure loads and enforced acceleration**

The following step-by-step procedure can be followed to calculate the frequency transfer function, expressing the load path between loads and analysis results:

- Set up a finite element model (FEM) of the system (structure) of interest and assure a good mass, stiffness distribution, boundary conditions and applied loads. Check on the right rigid body mass, centre of gravity (centre of mass), zero rigid body modes, zero strain energy, etc. [1].
  - Calculate undamped natural frequencies  $f_k$  (Hz), associated vibration modes  $\{\phi_k\}$ , modal effective masses, etc. In general, the generalized masses are normalised to  $m_k = 1$ .
  - Define the modal damping ratios  $\zeta_k$ . The value of the modal damping ratio is dependent on the type of structure. The amplification factor (or quality factor) is given by  $Q_k = \frac{1}{2\zeta_k}$ .
  - Perform the modal analysis on the uncoupled equations for the generalized coordinates  $\{\eta_k\}$
- $$\ddot{\eta}_k + 2\zeta_k \omega_k \dot{\eta}_k + \omega_k^2 \eta_k = \frac{\{\phi_k\}^T(F)}{m_k}, \text{ where } \omega_k^2 \text{ is the } k^{\text{th}} \text{ eigenvalue and } (F) \text{ the applied force}$$
- (pressure, acceleration, etc.) vector, mostly defined in the frequency domain. The displacement vector  $\{x\} = [\phi_1, \phi_2, \dots, \phi_n] \eta_k$ . The number of selected vibration modes is "n". In the frequency domain the displacement vector becomes  $\{x\} = \sum_{k=1}^n \frac{\{\phi_k\} \{\phi_k\}^T}{m_k (\omega_k^2 - \omega^2 + 2j\zeta_k \omega_k \omega)} (F)$ .

If the force vector represents the unit force vectors (enforced acceleration, pressures, etc.) the vector  $\{x\}$  represents the associated frequency response functions  $H(f)$ . The latter may be

generalized for stresses, accelerations, etc. In case of static loads the displacement vector is

$$\{x\} = \sum_{k=1}^n \frac{\{\phi_k\}\{\phi_k\}^T}{m_k \omega_k^2} (F)$$

That means the inverse of the regular stiffness matrix  $[K]^{-1} = [G] = \sum_{k=1}^n \frac{\{\phi_k\}\{\phi_k\}^T}{m_k \omega_k^2}$ .

The displacement vector can be rewritten as

$$\{x\} = \left[ \sum_{k=1}^m \frac{\{\phi_k\}\{\phi_k\}^T}{m_k (\omega_k^2 - \omega^2 + 2j\zeta_k \omega_k \omega)} + \sum_{k=m+1}^n \frac{\{\phi_k\}\{\phi_k\}^T}{m_k \omega_k^2} \right] (F) \text{ or}$$

$$\{x\} = \left[ \sum_{k=1}^m \frac{\{\phi_k\}\{\phi_k\}^T}{m_k (\omega_k^2 - \omega^2 + 2j\zeta_k \omega_k \omega)} + [G_{res}] \right] (F),$$

$$\text{where } [G_{res}] = [G] - \sum_{k=1}^m \frac{\{\phi_k\}\{\phi_k\}^T}{m_k \omega_k^2}.$$

The ignored modes are taken into account statically (mode-acceleration) [18].

- When the general frequency response functions  $H_{ij}(f)$  are calculated, the output response power spectral densities (for stress, force, acceleration, etc.) can be obtained using the following equation :

$$W_{out}(f) = \sum_i \sum_j H_{ij}(f) W_{ij}(f). \quad [9-14]$$

where  $H_{ij}(f) = H_{ji}^*(f)$ . In general, the cross power spectral density function  $W_{ij}(f), i \neq j$  (e.g. between pressure and enforced accelerations, etc.) are difficult to establish and most times ignored. Previous expression becomes:

$$W_{out}(f) = \sum_j |H_{ii}(f)|^2 W_{ij}(f). \quad [9-15]$$

- The rms value of the output is calculated by integrating the PSD  $W_{out}(f)$  over the frequency range of interest.

#### 9.4.3 Guidelines for FE random vibration response analysis

Many textbooks provide guidelines and background theory for FE subsystems in mechanical random vibrations and vibro-acoustics. The following provides some brief modelling guidelines when using FE structural subsystems. These guidelines were presented in [19].

Ideally, when choosing the most appropriate FE subsystem representation for a given component, the user should:

- Use a sufficient number of elements to describe the expected response of an FE subsystem. A good rule of thumb is to use between 6 and 10 linear elements per propagating wavelength within an FE subsystem. In addition, you should try to ensure that you can capture the local evanescent fields surrounding any discontinuities or

junctions. Additional mesh density criteria also apply when resolving curved components using linear elements.

2. Use a sufficient number of global modes to get a converged response (try increasing the number of global modes used in your analysis and see if it affects your response predictions).
3. Avoid using too fine a mesh or too many degrees of freedom in your model. The more elements you use, the more expensive subsequent calculations are. One of the key things to building a good finite element model is to get a feel for the limitations on computational resources you have and then try to gauge how large a model you need for a given problem (don't overmesh if you don't need to).
4. Try to capture the overall distribution of mass, stiffness and damping for a given subsystem through your choice of elements and properties. Non-structural mass and attachments can often have a significant influence on the response of a subsystem and should be accounted for in your model.
5. Pay attention to the expected boundary conditions in a model. The narrowband discrete frequency response of an FE subsystem can be very sensitive to assumptions you make about the boundary conditions. Try investigating the effects of different boundary conditions to see how sensitive the response is to such assumptions.
6. Always consider how accurate a given prediction or model needs to be and try to keep this in mind when considering the precision of input properties (and response predictions). Try to avoid spending time and making predictions (and models) more accurate than they need to be. A lot of time can be spent refining and updating the input properties of an FE model to precisely match narrowband data. While this is very important for many problems, it is often possible to answer many vibro-acoustic design questions using simplified models and band (and space) average response predictions. The use of band averaging (as a post-processing operation when viewing the results) is therefore recommended.
7. The detailed spatial response of an FE subsystem is often sensitive to assumptions regarding the precise properties of an FE subsystem. In many problems, the use of spatial average response data is more useful for understanding the overall response of an FE subsystem. Narrowband point-to-point frequency response functions (FRFs) are of limited use at mid and high frequencies.
8. Be careful not to frequency alias the response of lightly damped FE subsystems.
9. Ideally you should initially solve for the narrowband response (using approximately 3 points per modal bandwidth).
10. Avoid using FE subsystems to describe the response of components with a large number of local modes – an SEA representation of such components is often more appropriate (and more computationally efficient).

## 9.5 Random vibration testing

### 9.5.1 Introduction

The purpose of random vibration testing is to verify strength and structural life by introducing random vibration through the mechanical interface.

Random vibration testing has two principal objectives [20]:

- To verify the test item design's capability, with some margin, to withstand the launch vibro-acoustic environment.
- To screen the workmanship integrity of the flight equipment.

Typical applications are electrical components and small spacecraft for which acoustic testing is ineffective.

In a random vibration test, an electromechanical shaker introduces vibration typically up to 2000 Hz in three single-axis tests.

The signal processing bandwidth is a common source of misunderstanding in random vibration testing [1]. In the space industry today, an enormous number of samples of random vibration data are taken with many different measurement techniques and processed in many different ways. In particular with the popularity of digital signal processing, the frequency bandwidth can be very narrow and PSD curves often show very high and sharp peaks. These phenomena sometimes create "problems", specifically when comparing PSD curves. Two typical situations are:

- When controlling, within specified tolerances, the test environment at the base of the item with respect to the specified ("target") PSD
- when processing data from system level acoustic test to arrive at PSDs for comparison with those used to test components

These "problems" in some cases can be irrelevant since created by the high resolution processing. To be consistent the processing resolution in the vibration test should match the one used to establish test conditions or the processing resolution of the test data should be converted with that used to derive the specified environment.

In conclusion, it is important to specify the processing bandwidth. For a typical spectrum of 20-2000 Hz, [1] recommends a bandwidth of 10 Hz to define and control the random vibration environment.

### 9.5.2 Notching

#### 9.5.2.1 Introduction

The need to limit input acceleration levels during the random vibration tests is often necessary not to overpass the qualification of equipment or a satellite. There are automatic procedures, which are based on interface forces and/or acceleration measurements [8]. However, even today, we use manual methods so as to not overstress the equipment.

Three examples are supplied in following sections, showing various approaches through experience feedback from projects [21].

### 9.5.2.2 Notching of random test levels based on quasi-static design loads

As for the case of sine vibrations, we perform primary and secondary notching. The primary notching is based on reduction of structure loads to quasi-static loads. The secondary notching applies to protect equipment from overtesting. There is no commonly accepted methodology to define a notched spectrum for the test. The following 3 examples allow having an approach to establish notching profiles.

#### 9.5.2.2.1 Example 1

This first example concerns lightweight equipment ( $\approx 1\text{kg}$ ) mounted at the top of a mast. The excitation at the basis of this equipment is limited frequency by frequency in order to not exceed the quasi-static loads on the three axes. It is typically a primary notching methodology. Other criteria have been taken into account to define the notched spectrum (see Figure 9-9):

- Minimum input at the basis of the equipment imposed by the satellite authority
- The slope is at a maximum of  $\pm 25 \text{ dB/oct}$ , due to the test facility limitations
- The notched levels in g rms are maintained with regard to the specification
- The frequency band of the notching around the mode is defined as  $\Delta f = 3f_0/Q (\text{Hz})$  with  $f_0 (\text{Hz})$  frequency of the mode and  $Q$  the amplification factor (we consider that the slope of the notching is  $\pm Q$  depending on the test shaker capability)

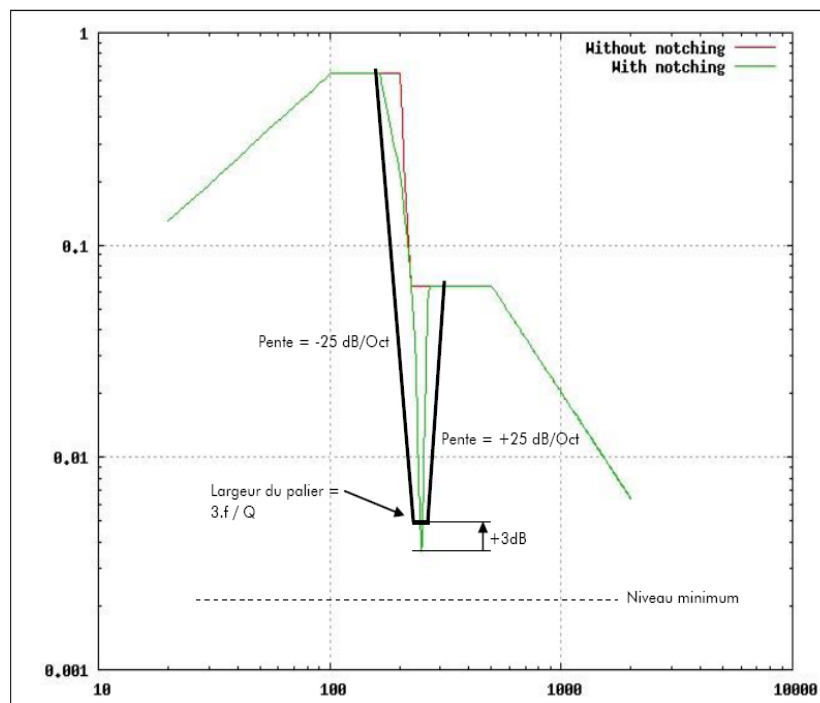
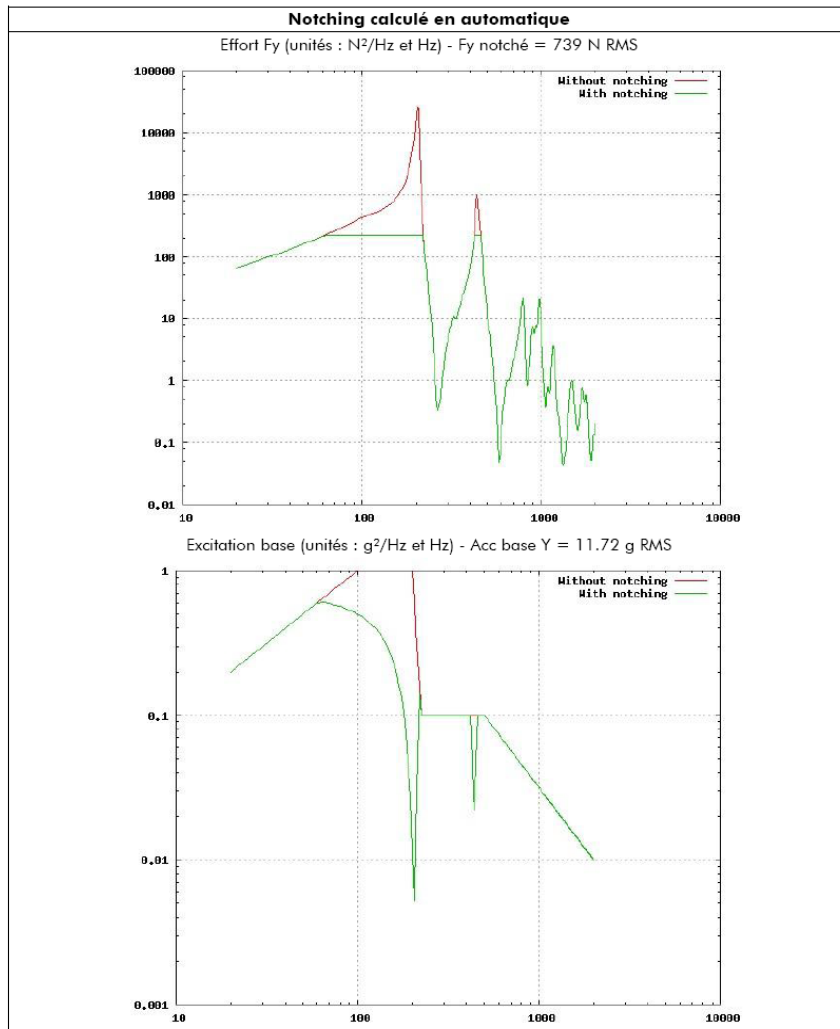


Figure 9-9 : Notched spectrum example 1

We analyse in detail the methodology on one axis (for, example, X-axis in that case), knowing that the approach is similar on the two other axes (see Figure 9-10).



**Figure 9-10 : Calculated notched PSD of enforced acceleration**

The methodology applied to define the notched spectrum is the following:

- The finite element analysis (FEA) gives the predicted, un-notched reaction force in  $N_{rms}$  (red curves)
- This reaction force is multiplied by 3 to obtain the  $3\sigma$  load,  $F_{peak}$
- The resulting force  $F_{peak}$  is compared to the QSL
- If  $F_{peak}$  is higher than the QSL, a notching can be considered.
- To define the value (green curves), we keep the PSD max and min, we take the average and we even (cut off) out all the peaks above this value. If  $F_{peak}$  is higher than  $QSL(1+\varepsilon)$  ( $\varepsilon \approx 0.05$ ), we recalculate the value by replacing the PSD max by the average PSD calculated in the previous step. On the contrary if  $F_{peak} < QSL(1-\varepsilon)$ , we recalculate the value by replacing the PSD min by the average PSD calculated in the previous step. The loop is repeated until satisfying the criterion  $QSL(1+\varepsilon) > F_{peak} > QSL(1-\varepsilon)$ .

The result of this loop is the green curve calculated through a mathematical model. Taking into account the force with notching, we can define the input level.

Nevertheless, the levels obtained are discussed with the customer. In that particular case, the final agreement for the notched spectrum has been the following: the notching has not been accepted at satellite level.

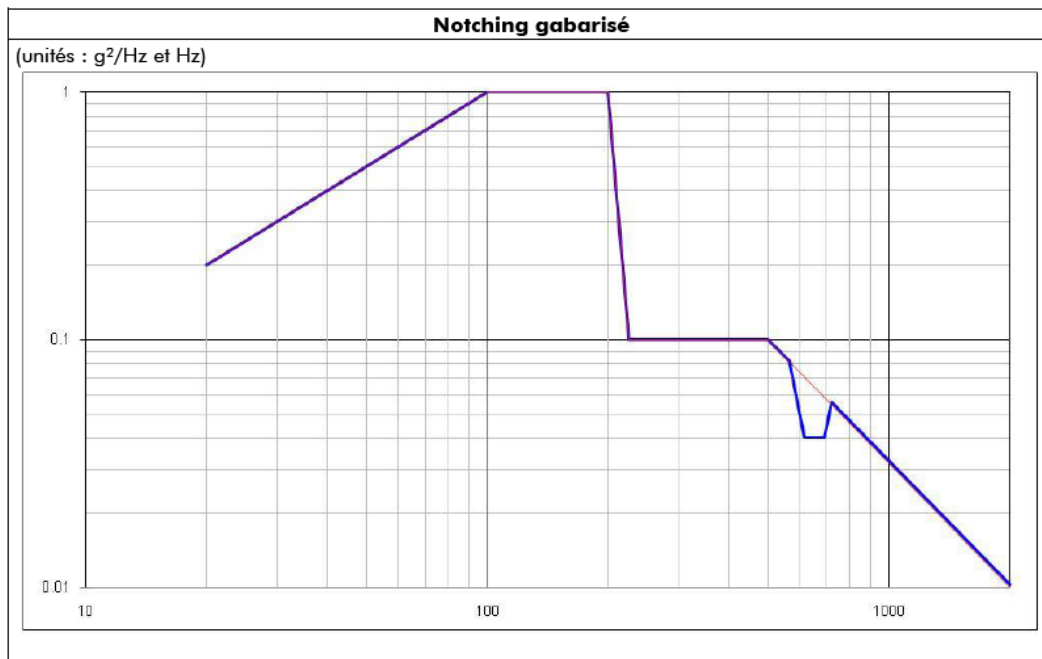


**Figure 9-11 : Final random enforced acceleration spectrum**

We can notice that only a light notch has been accepted between 600 and 700 Hz for this example. In this particular analysis, the random excitation is the dimensioning case for the structure of this equipment. Indeed, the resulting interface forces due to the random excitation are higher than the QSL in any case.

#### 9.5.2.2.2 Example 2

In this second example, we consider an equipment item with a mass of around 20 kg. The methodology applied to define the notched spectrum is rather similar to example 1. We can see on the following three figures: Figure 9-12, Figure 9-13 and Figure 9-14 (on the three axes), the input spectrum calculated using the previous methodology and the final input spectrum retained for the test after discussion at satellite level.

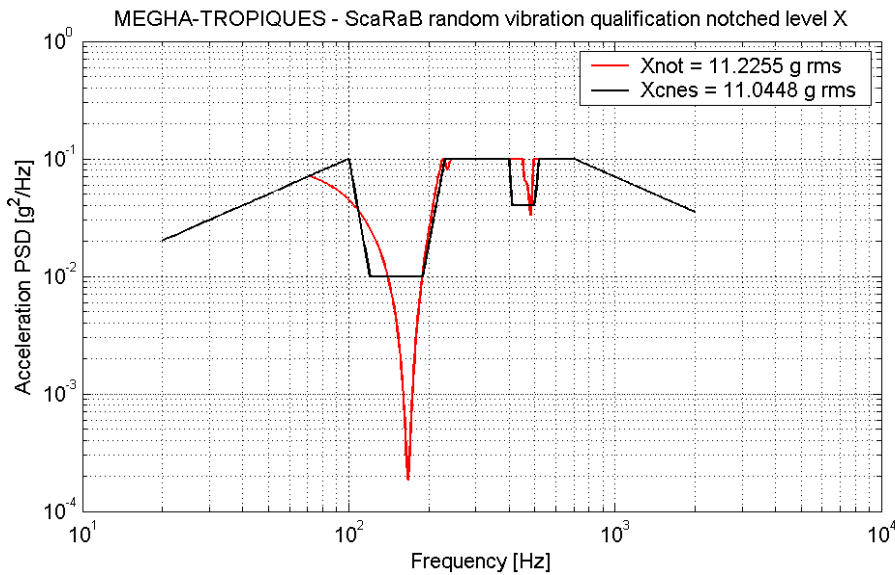


Figure 9-12 : Random vibration qualification notched level X-axis

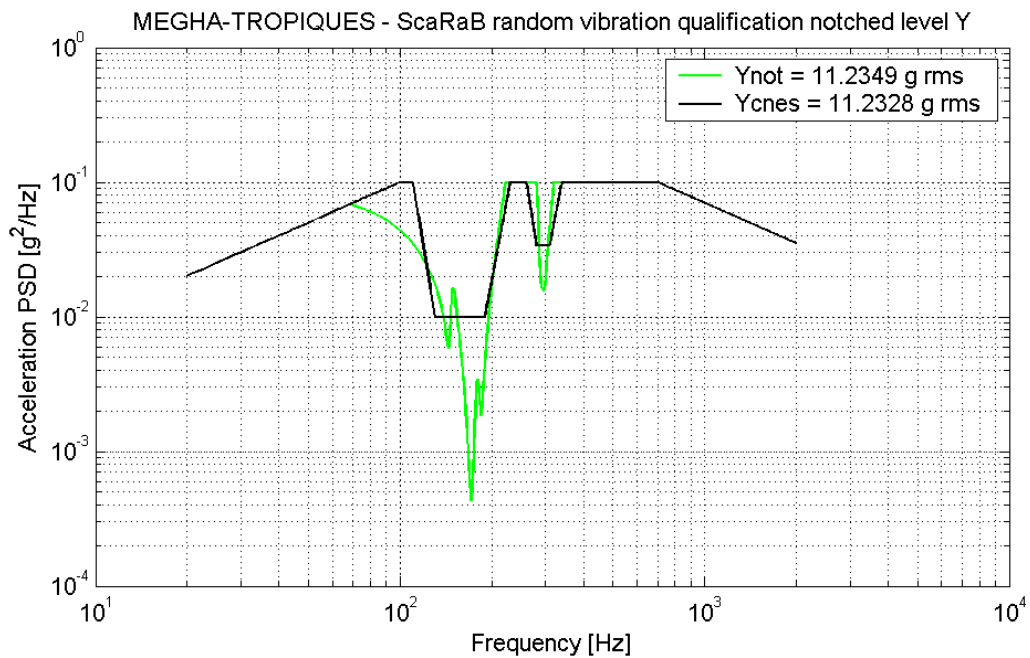
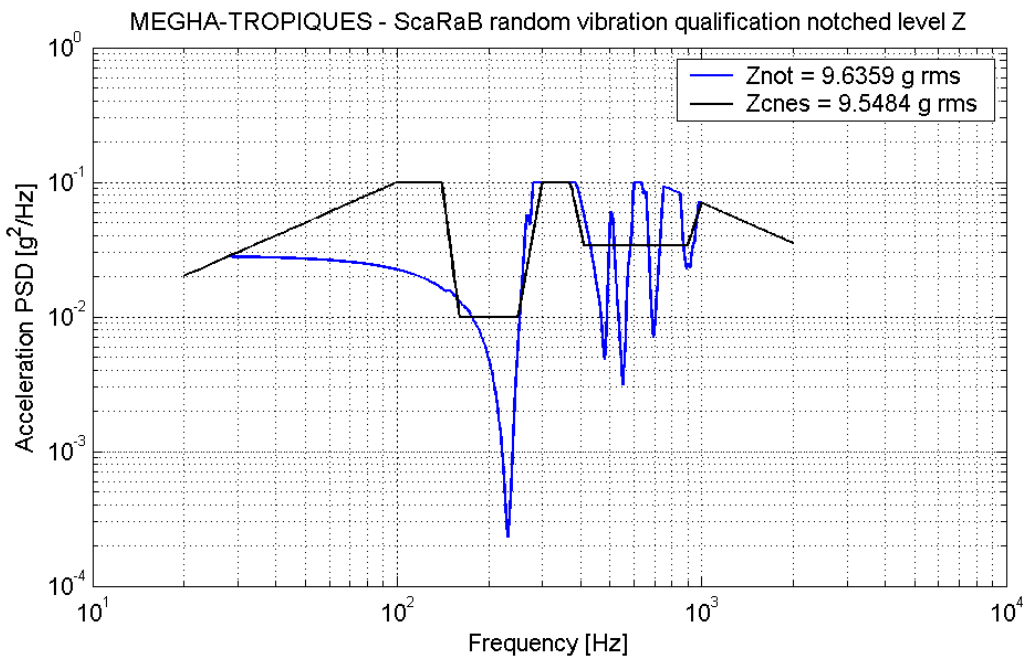


Figure 9-13 : Random vibration qualification notched level Y-axis



**Figure 9-14 : Random vibration qualification notched level Z-axis**

#### 9.5.2.2.3 Example 3: The approach at spacecraft level

In most of the cases, the spacecraft random tests are performed through acoustic test. However, for microsatellites (from 150 to 200 kg), random vibration tests can be compulsory. For example, in the case of a launch on the launcher DNEPR, it is necessary to demonstrate the qualification to the random environment by a test at spacecraft level.

In this example, the analysis has been applied in two steps. A first step at structural thermal model (STM) level where preliminary primary and secondary notching has been analysed and established, and a secondary step at flight model (FM) level where final primary notching has been done and secondary notching at equipment level has been finalized.

The prediction has been made on STM mathematical model for qualification. A factor of 1.2 has been taken into account in order to cover all the uncertainties at model and calculation levels.

The specification is defined in Figure 9-15:

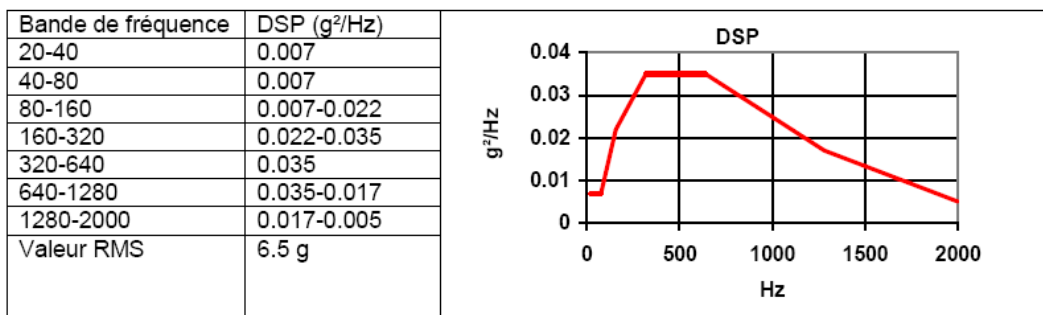


**Figure 9-15 : Random vibration specification**

After a modal analysis of the spacecraft, due to the distribution (break-down) of the modal effective masses, it was decided to apply the primary notching only on the first mode of the spacecraft based on the limitation of the QSL. The values are multiplied by a factor of 1.2<sup>2</sup> for the PSD of the enforced acceleration. The QSL are compared to the RMS value of the interface forces at  $3\sigma$  at the base of the spacecraft.

The figures below (Figure 9-16) give the input levels proposed through the random analysis in the three axes.

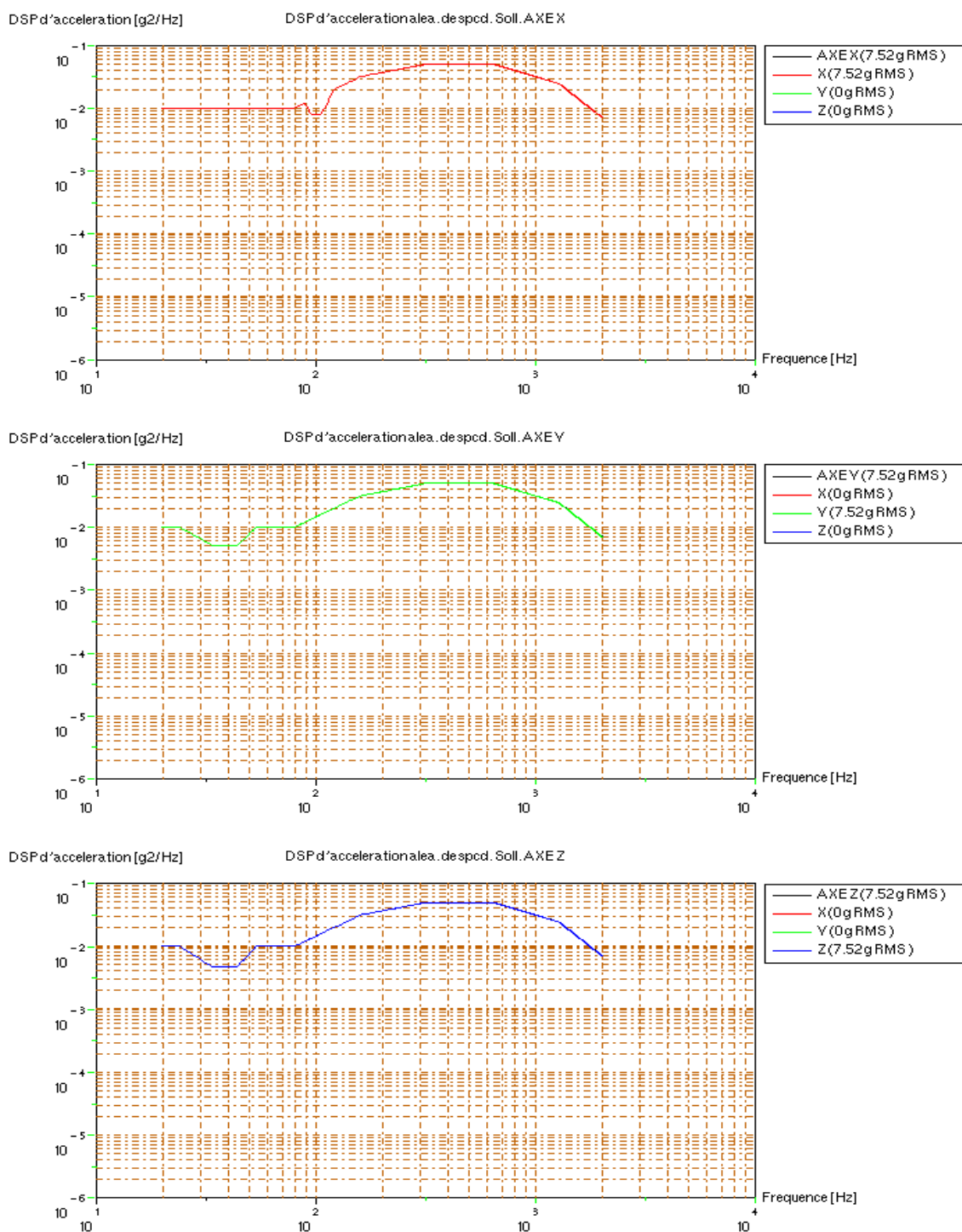
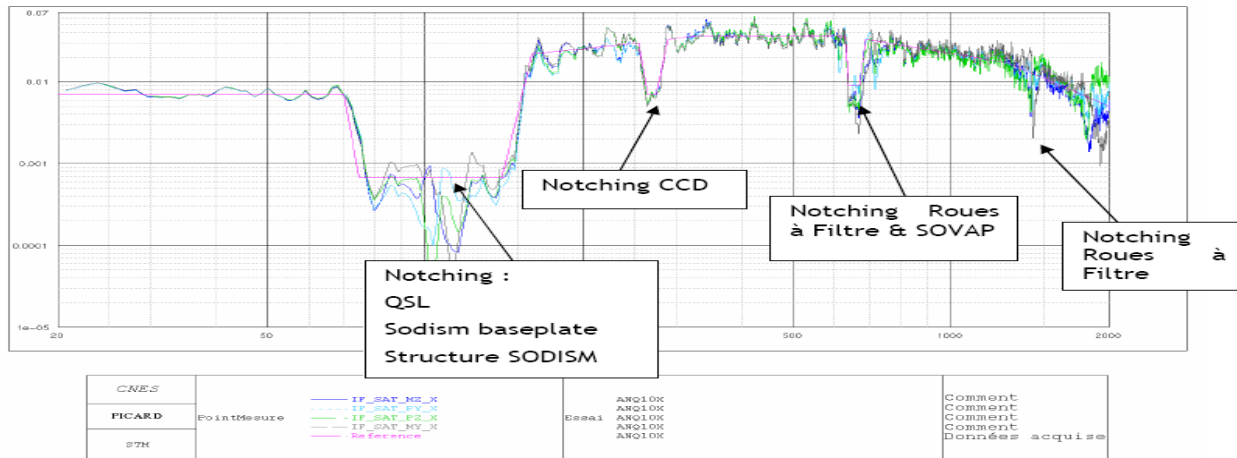


Figure 9-16 : Proposed notched random vibration spectra

Following this mathematical analysis, a qualification test has been realized to confirm the approach. The advantage in this program is the fact that we have a structural model to refine the specification.

The results are given here below in Figure 9-17 (X-axis). The results are similar for the other axes.



**Figure 9-17 : Actual notched random spectrum X-axis**

In Figure 9-17, we can notice the preliminary notching around 100 Hz corresponding to the first mode of the satellite but also covering secondary notching at equipment level. Secondary notching is applied to specific equipment taking into account the dimensioning approach used with a qualification factor of 1.5.

This qualification test has allowed adjusting the mathematical model of the satellite, to refine the specification at equipment level and to predict the input spectrum for the random test on the FM. The methodology applied for the FM is the same that for the STM but without the factor of 1.2 for the uncertainties.

### 9.5.2.3 Force limiting on ½ octave with quasi-static criterion

#### 9.5.2.3.1 Introduction

This example concerns an antenna feed mounted on a panel of a telecommunication spacecraft. The following section provides the road map used to reply to a random vibration specification as described hereinafter including a notching strategy in order to prevent an over-sizing of the equipment. First of all, the requirements are given in Table 9-5.

**Table 9-5: Extract of QS & random vibration specification**

Quasi-static load factors			
⊥ to mounting plane		// to mounting plane ( X,Y separately)	
30 g		20 g	
Random Vibration			
⊥ to mounting plane		// to mounting plane ( X,Y separately)	
Frequency range [Hz]	Level	Frequency range [Hz]	Level
20 – 100	+6 dB/oct	20 – 100	+6 dB/oct
100 – 350	1.0 g <sup>2</sup> /Hz	100 – 600	0.15g <sup>2</sup> /Hz
350 – 800	0.15 g <sup>2</sup> /Hz	600 – 2000	-6 dB/oct
800 – 2000	-6 dB/oct		
Global : 20.6 grms		Global : 12.0 grms	

The proposed notching strategy is to limit the RMS resultant interface force along the tested axis to the envelope of the quasi-static (QS) resultant interface force in the same axis taking into account the following points:

- This notching is applied on the eigen-modes with high effective masses (issued from FEM prediction or from tests measures).
- The notched frequency band is limited to the  $\frac{1}{2}$  frequency octave around the notched modes. The choice of the  $\frac{1}{2}$  octave bandwidth is a mutual agreement after discussion between the sub-system provider and spacecraft authority.  
It is a compromise between the necessity to reduce effective loads and to limit the frequency range of notching.
- The QS resultant interface force criterion is a  $3\sigma$  RMS value computed on the  $\frac{1}{2}$  frequency octave around the notched modes (criteria issued from FEM prediction or from load cells measures during test).  
Here, the compromise is between the necessity to reduce effective loads and the request to avoid too much depth notching (it can be the case if the criterion is computed on the whole frequency range).

The sizing of the equipment was performed using the next sequence for each excitation axis:

1. The random input level is notched using the Quasi-static (QS) specified criteria issued from mechanical requirements → this is the primary notching\*.
  2. I/F loads, acceleration responses and structure safety margins are computed to check the structure integrity and its dynamic responses.
  3. In the case of negative safety margins, equipment qualification level overshoot and/or acceleration level greater than heritage, an additional notching may be requested → this is the secondary notching which needs to be accepted by the spacecraft authority\*.
  4. Updated responses are computed with the combination of the primary and secondary notching to check the structure safety margins and its dynamic responses.
- \*: Even specified, the primary notching is usually treated as a waiver, so it needs to be justified and agreed with the customer.

### 9.5.2.3.2 Notching prediction during FEM random vibration analyses

The following methodology is graphically described in Figure 9-18. It explains how the notching criteria are computed (point 1) and what frequency bands are available for this notching.

- a. QS criteria definition → The QS resultant interface force criteria were computed with a equipment of 9.1 kg associated to the acceleration levels defined in QS specification:

1. Criteria on X and Y axes:  $M \times g \times \gamma = 9.1 \times 20 \times 9.81 = 1785 N$ .

This design value is compared with 3 sigma resultant load values  $Rx_{3\sigma}$  and  $Ry_{3\sigma}$  computed in specific bandwidth (see point 2) respectively with X and Y random excitation.

2. Criterion on Z axis :  $M \times g \times \gamma = 9.1 \times 30 \times 9.81 = 2678 N$ .

This design value is compared with 3 sigma resultant load value  $Rz_{3\sigma}$  computed in specific bandwidth with Z random excitation.

- b. Available notched frequency bands on Y axis (same methodology for X and Z axes) → there are 2 eigen-modes with high effective mass (see Figure 9-18) occurring at:
  - 1.  $f_1 = 181 \text{ Hz}$  leading to the  $[152 ; 215 \text{ Hz}]$   $\frac{1}{2}$  octave frequency band, obtained with
 
$$f_1 \times 2^{-(1/4)} = 181 \times 2^{-(1/4)} = 152 \text{ Hz}$$
 (1/4 octave band lower)
 
$$f_1 \times 2^{(1/4)} = 181 \times 2^{(1/4)} = 215 \text{ Hz}$$
 (1/4 octave band upper)
  - 2.  $f_2 = 286 \text{ Hz}$  leading to the  $[240 ; 340 \text{ Hz}]$  frequency band
- c. Resultant force limitation → the resultant interface force PSD is iteratively decreased in order to obtain a  $3\sigma$  value of interface force of  $1785 \text{ N}$  in each available notched frequency band.

The response without notching (dashed red curve) is compared to the notched foreseen response (blue curve).

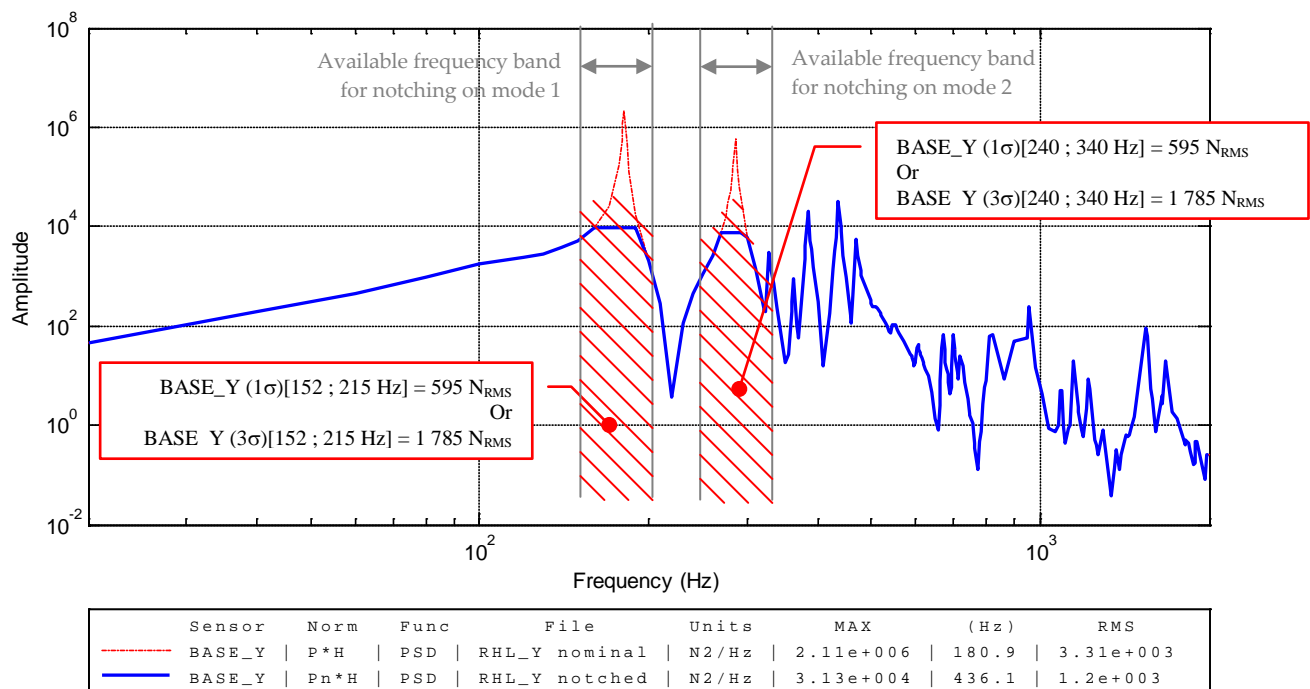


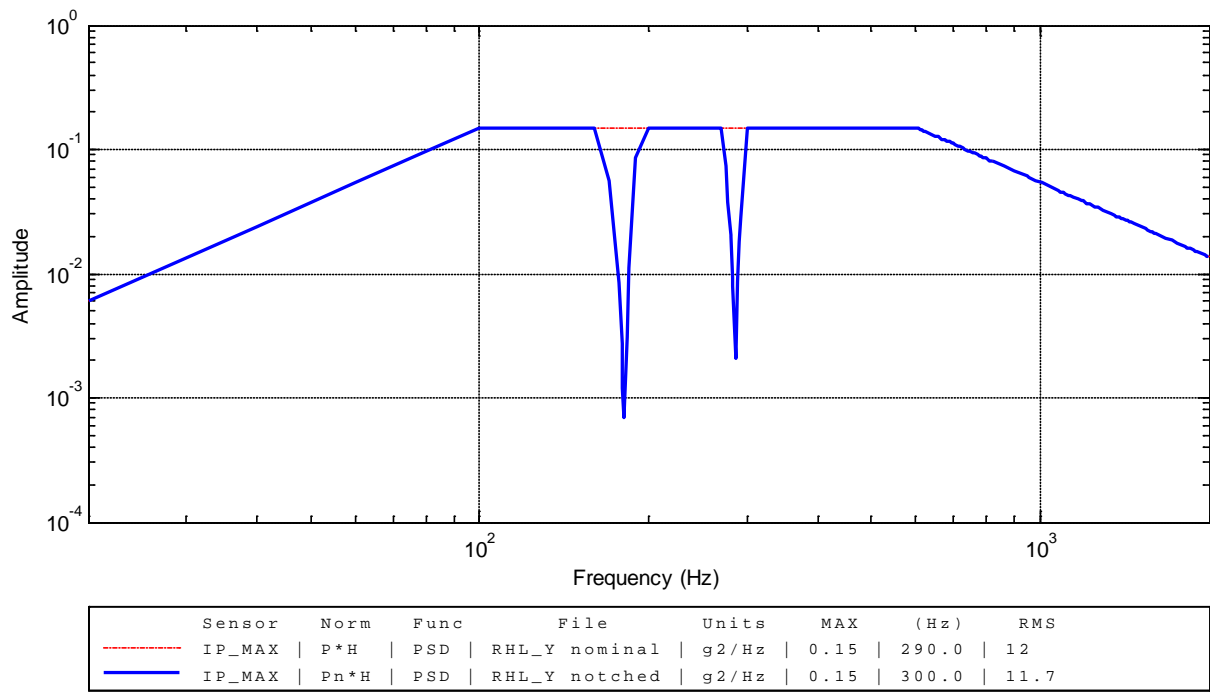
**Figure 9-18 : Resultant interface force limitation prediction - Y axis**

Thus, the  $3\sigma$  resultant interface force measured on the  $\frac{1}{2}$  octave around each notched main modes is equivalent to the QS resultant interface force of  $1785 \text{ N}$ :

- On the 1<sup>st</sup> mode, the  $3\sigma$  resultant interface force is limited to  $1785 \text{ N}_{\text{RMS}}$  compared to  $8040 \text{ N}_{\text{RMS}}$  without notching,
- On the 2<sup>nd</sup> mode, the  $3\sigma$  resultant interface force is limited to  $1785 \text{ N}_{\text{RMS}}$  compared to  $5220 \text{ N}_{\text{RMS}}$  without notching,
- The overall  $3\sigma$  resultant interface force is  $3600 \text{ N}_{\text{RMS}}$  compared to a value of  $9930 \text{ N}_{\text{RMS}}$  without notching.

The resultant interface force limitation leads to the notched random input spectra shown in Figure 9-19.

The input level without notching (dashed red curve) is compared to the notched foreseen input level (blue curve).



Frequency		Nominal level	Minimal level with notching	Active criteria
PSD	20 – 100 Hz	+6dB/oct	-	No notching
	100 – 159 Hz	0.15 g <sup>2</sup> /Hz	-	No notching
	160 - 200 Hz	0.15 g <sup>2</sup> /Hz	6.8E <sup>-4</sup> g <sup>2</sup> /Hz at 181 Hz	QS resultant on Ry (computed on ½ octave) : • Nominal → BASE_Y [152 – 215 Hz] = 8040 N <sub>RMS</sub> (3σ) • Notched → BASE_Y [152 – 215 Hz] = 1785 N <sub>RMS</sub> (3σ)
	201 – 269 Hz	0.15 g <sup>2</sup> /Hz	-	No notching
	270 - 300 Hz	0.15 g <sup>2</sup> /Hz	2.1E <sup>-3</sup> g <sup>2</sup> /Hz at 286 Hz	QS resultant on Fx (computed on ½ octave) : • Nominal → BASE_Y [240 – 340 Hz] = 5220 N <sub>RMS</sub> (3σ) • Notched → BASE_Y [240 – 340 Hz] = 1785 N <sub>RMS</sub> (3σ)
	301 – 600 Hz	0.15 g <sup>2</sup> /Hz	-	No notching
	600 – 2000 Hz	-6dB/oct	-	No notching

Figure 9-19 : Notched random input level prediction- Y-axis

Thus, the notched random input spectrum has a value of 11.7 g<sub>RMS</sub> compared to 12 g<sub>RMS</sub> at nominal level. It allows reducing resultant interface loads more than 50%.

### 9.5.2.3.3 Test configuration and instrumentation

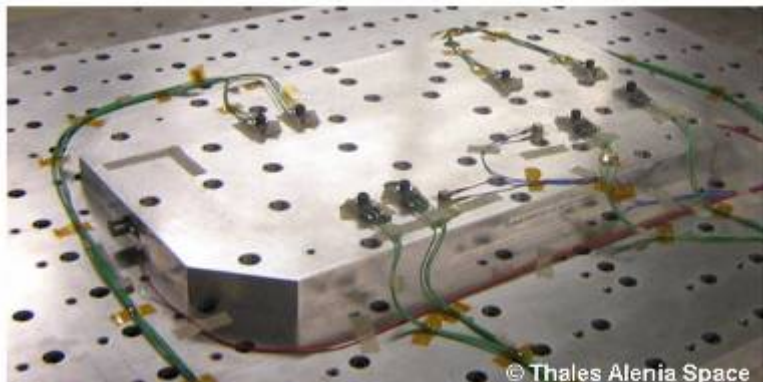
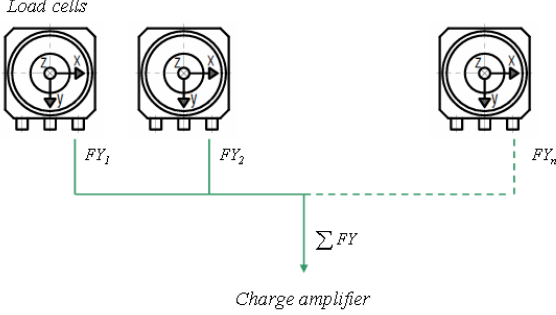
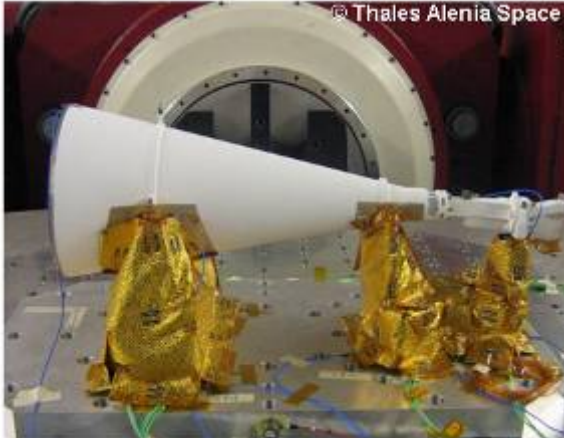
For the test implementation, load cells and summation boxes were used in order to measure the resultant interface load between the specimen and the vibration tool on the shaker (see Figure 9-20).

Load cells are piezoelectric force sensor measuring three orthogonal components of dynamic forces acting in any directions.

The output signal being non-conditioned, electric charges can be sum with T-connections → this is the principle of the summation box which provides a resultant signal from several load cells to the charge amplifier.

The channel sensitivity used for the resultant signal is the average of the sensitivity of all the load cells. Thus, it is advised to use load cells with similar sensitivity.

The use of load cells ensures that the notching is performed on modes with high effective mass. Also, the screw preload installed on interface with vibration plate tool can be controlled.

 <span style="font-size: small;">© Thales Alenia Space</span>	
<b>Load cells on vibration plate</b>	
<i>Load cells</i>  <p><math>FY_1</math></p> <p><math>FY_2</math></p> <p><math>FY_n</math></p> <p><math>\sum FY</math></p> <p><i>Charge amplifier</i></p>	 <span style="font-size: small;">© Thales Alenia Space</span>
<b>Summation box principle</b>	<b>Antenna feed on shaker</b>

**Figure 9-20 : Test configuration**

## 9.5.2.3.4 Test sequence

Figure 9-21 gives the test sequence used for the random environment qualification of the antenna feed.

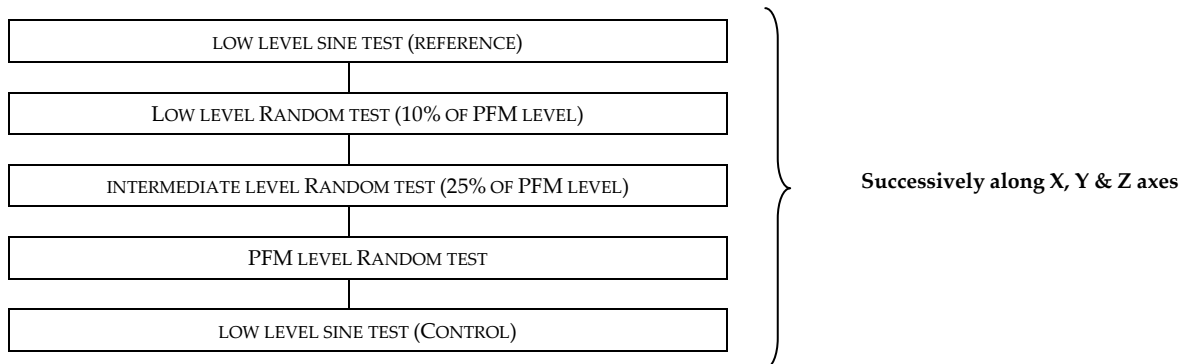


**Figure 9-21: Example of test sequence for random vibration**

- Before starting the test sequence, the specimen was weighed in order to update the QS resultant interface force criteria.
- The reference low level sine test permits to validate the instrumentation and the entire acquisition chain.

## 9.5.2.3.5 Notching definition during random vibration tests:

The following sequence was applied for each random qualification axis :

1. Perform of low level random test (10% of the nominal level during 30s).
2. In case of structure with one main mode having a strong effective mass, a notching can be applied in order to not stress the structure.
3. Use the results of the initial low level random test. Resulting interface load is extrapolated to nominal level, and a limitation of its PSD is defined in order to satisfy the notching criteria.
4. Perform the intermediate level random test (25% of nominal level during 30s) using the above values divided by 4 (16 for PSD), with an automatic control on the identified force transducers channels to limit their responses to the maximum values determined above (point 2).
5. The notching strategy is presented to the spacecraft authority, which gives its agreement to proceed.
6. Due to eventual amplification changes or overshoot on shaker control, adjustments of the maximum levels may be suggested.
7. Perform the nominal level random test, with a control strategy identical to the one used for the intermediate level test (taking into account the ratio between qualification level and intermediate level).
8. The measures of the nominal level are given to the system authority, which gives its agreement to carry on the test sequence.

Figure 9-22 shows the random input level applied for the qualification of the equipment on the 3 axes and the corresponding measured resultant interface force.

These test results (in red) are compared to the FEM predictions (in blue).

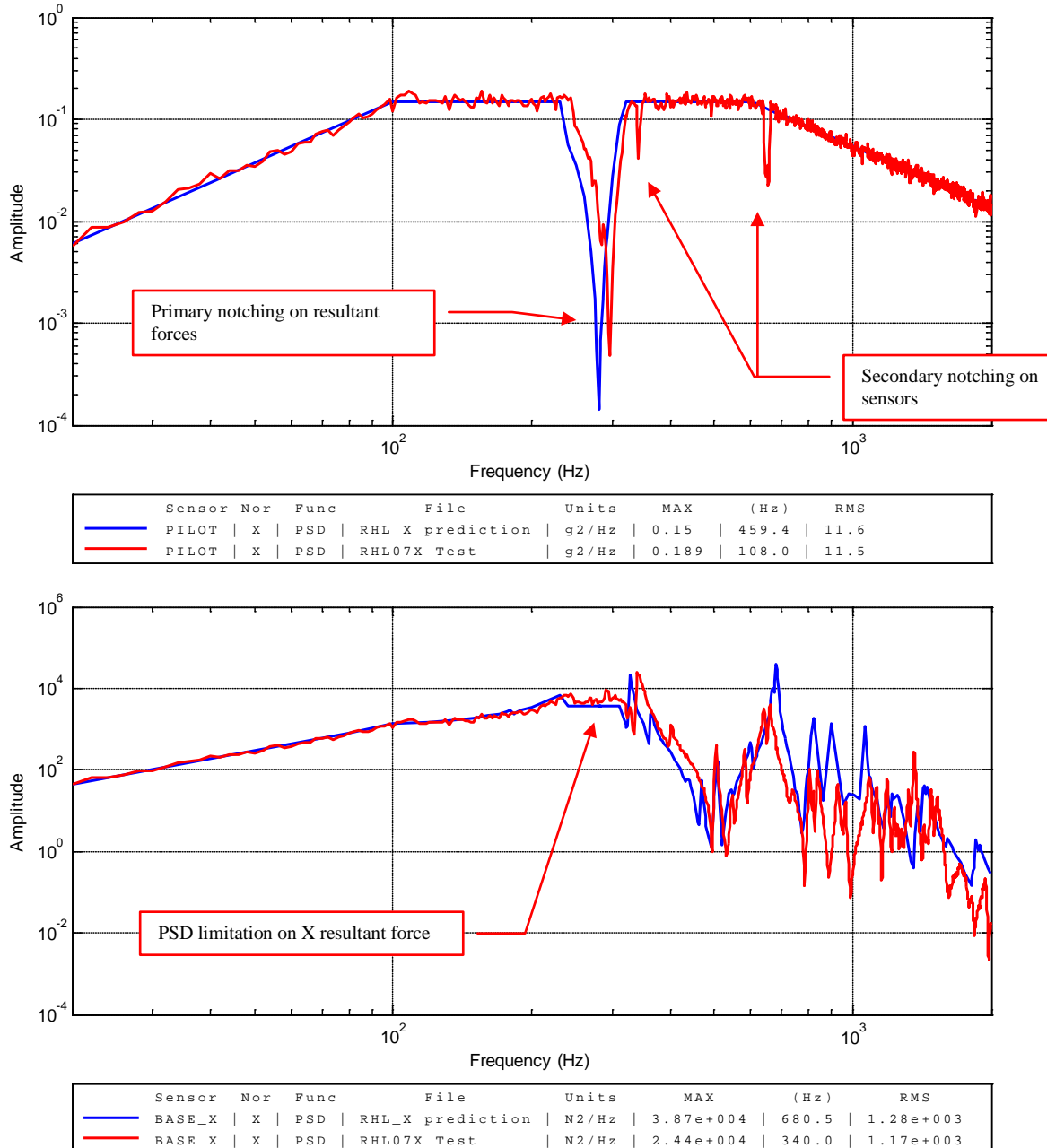


**Figure 9-22 : Random qualification - X-axis**

In X-axis, the primary notching was in line with the prediction one.

Also, two additional notching were requested in order to limit responses on some parts of the equipment and to keep positive safety margins. It was due to a lower damping than predicted on local eigen-modes.

These both secondary notching were accepted by the SC mechanical analyst on the base of heritage data on similar platform with comparable configuration and acoustic input level.

Figure 9-23 shows the random input level applied for the Y axis qualification of the equipment and the corresponding measured resultant interface force.

These test results (in red) are compared to the FEM predictions (in blue).

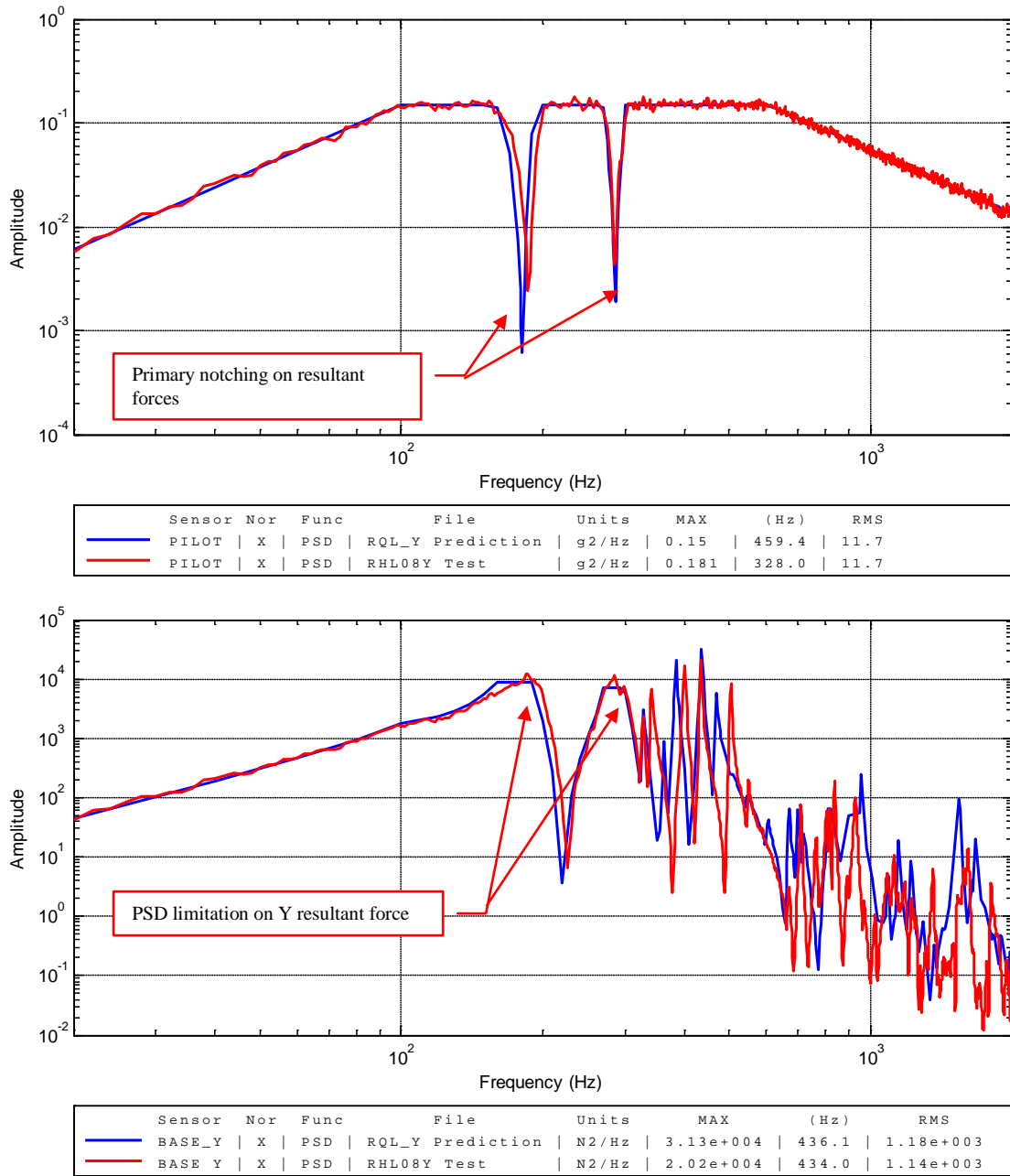


**Figure 9-23 : Random qualification - Y-axis**

Here, we see that the using of load cells associated with an automatic notching strategy ensures to reach the criteria with any evolution of damping or frequency location between different input levels (low, intermediate and qualification level).

This shaker automatic control approach is well adapted to structure with strong damping and non-linear behaviour.

Figure 9-24 shows the random input level applied for the Z axis qualification of the equipment and the corresponding measured resultant interface force.

These test results (in red) are compared to the FEM predictions (in blue).

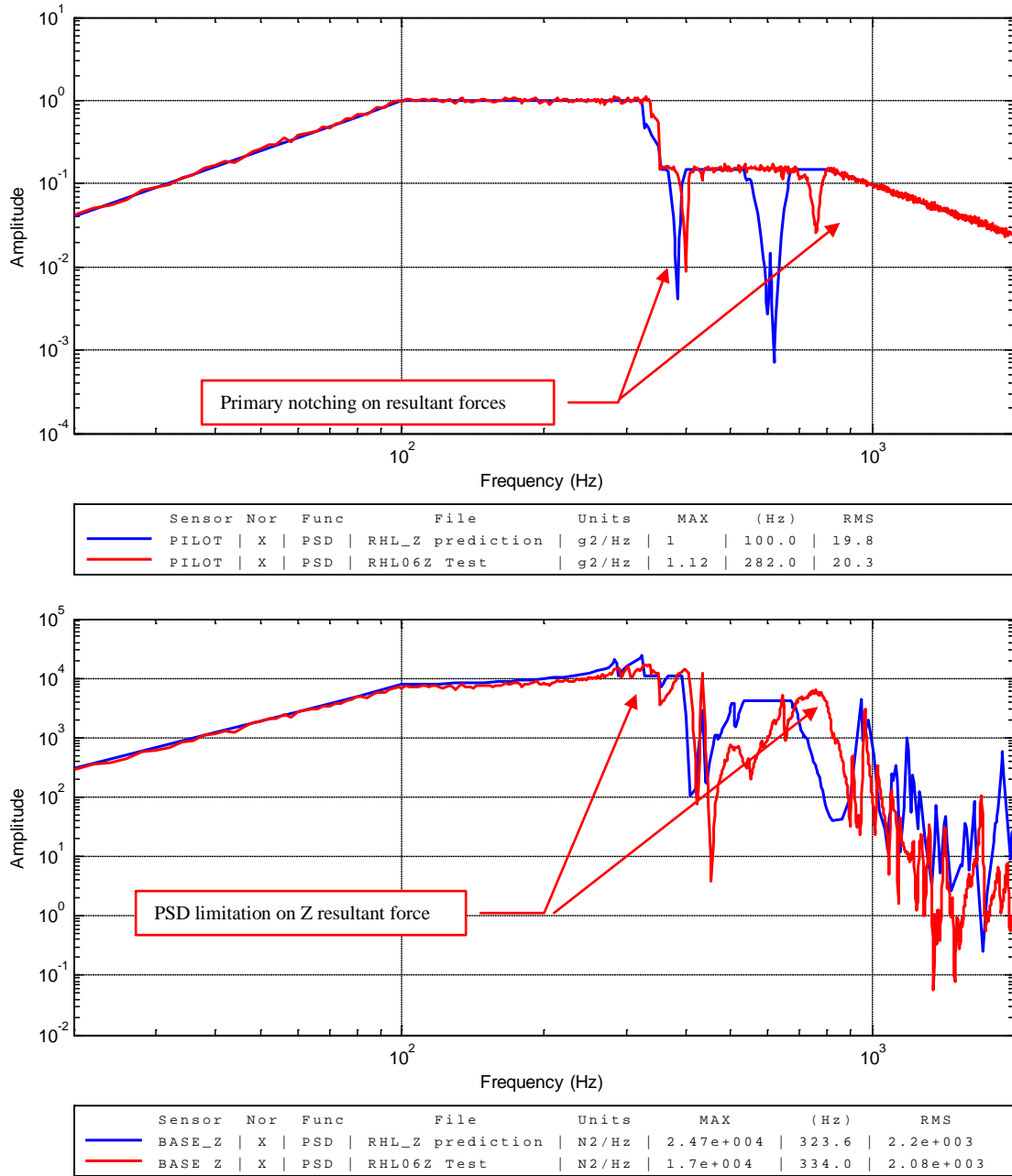


**Figure 9-24 : Random qualification - Z-axis**

On Z axis, the second main Z mode had a different shape and a higher eigen frequency than predicted.

Thanks to the load cells, the resultant interface force measures allowed ensuring that the effective mass was sufficient to reach the QS resultant interface force and to request a notching.

### 9.5.2.4 Semi-empirical force limiting specification: “Semi-empirical method”

The semi-empirical force-limit approach is a method to establish force-limits based on the extrapolation of interface force data for similar mounting structures [4] [22] [23] [24]. The following expressions between interface forces and enforced accelerations can be used:

$$W_{FF}(f) = C^2 M^2 W_{AA}(f), \quad f \leq f_o,$$

$$W_{FF}(f) = C^2 M^2 W_{AA}(f) \left( \frac{f_0}{f} \right)^2, \quad f > f_o, \quad [9-16]$$

where  $W_{FF}(f)$  is the force spectral density,  $W_{AA}(f)$  is the acceleration spectral density,  $M$  is the total mass of the test item and  $C$  is a dimensionless constant which depends on the configuration;  $f$  (Hz) is the frequency and  $f_0$  is the frequency of the primary mode with a significant modal effective mass. The natural frequency  $f_0$  may be obtained from finite element analysis and finalized from the low-level sine or random run performed just before the full-level vibration testing. In [25] recommendations for the key parameter  $C^2$  are given, however, based on limited number of flight data. One observes that in normal conditions  $C^2 = 2$  is chosen for a complete spacecraft or strut mounted heavier equipment.  $C^2 = 5$  might be considered for directly mounted lightweight test items.

The test force limits based on the above specification has been successfully used in many NASA spacecraft and flight equipment tests during the past several years.

As mentioned above the “semi-empirical method” involves the use of force sensors that limit forces transferred to the structure undergoing the vibration test. The generic test set-up is shown schematically in Figure 9-25. As shown in Figure 9-25, force sensors are used to measure forces being transferred to the test item during the test. A force sensor is inserted between the test item and the vibration fixture at each of the interface points. The summation of these force measurements is compared with the force limits and this comparison is used to augment the usual accelerometer feedback used to control the vibration test motion. As shown in Figure 9-25, the input to the shaker is modified by the force sensor feedback to maintain the forces within the force limits specified by the user in function  $W_{FF}(f)$ . This effectively results in notches or local reductions in the acceleration spectrum  $W_{AA}(f)$  experienced by the test item at its significant resonant frequencies. Notching of acceleration profiles is a traditional and accepted way of limiting test item responses. However, the use of force sensors provides direct control over the forces applied to the test item, which represent the actual hazard to the test item.

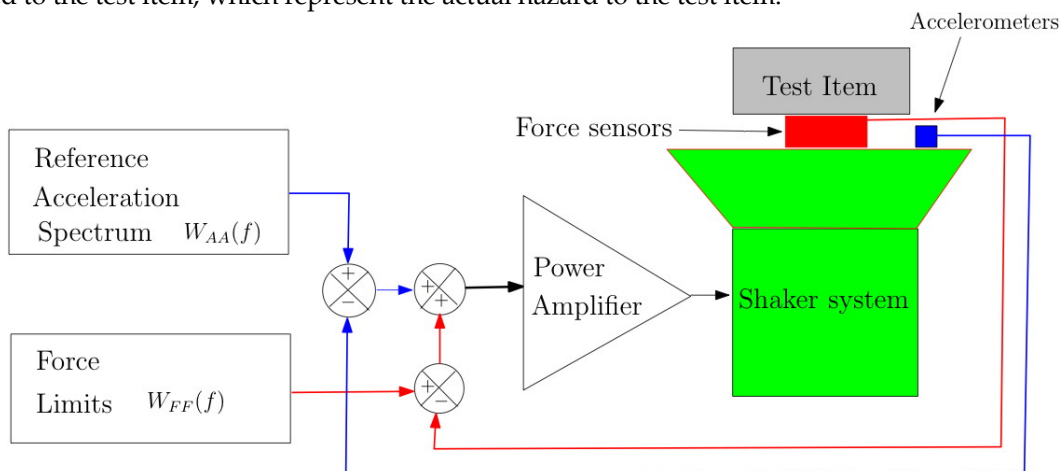


**Figure 9-25 : Force limited vibration testing [26]**

Soucy describes applications of Force Limiting Vibration Testing (FLVT) applying the “Semi-Empirical Method” in [26] [27].

## 9.6 Vibro-acoustic analysis

### 9.6.1 Introduction

Vibroacoustic response analysis is performed mainly for two reasons:

- To assess the strength and life of acoustically sensitive structures
- To predict random vibration environments for spacecraft components

Note: the most severe acoustic environment for the spacecraft is normally during the ground testing, thus, the acoustic test environments are typically assessed.

### 9.6.2 Boundary element analysis

#### 9.6.2.1 General aspects

The Boundary Element Method (boundary integral method) differs in concept from the method outlined in the previous sections (see for example [28]). The trial function approach in the finite element method is based on assuming a particular form of structural displacement and then employing Lagrange's equation or a similar approach to yield the equations of motion of the system. This approach leads to a system mass matrix and stiffness matrix from which the natural frequencies and/or the forced response can be computed. The resulting solution satisfies the governing differential equations approximately and the displacement type boundary conditions exactly.

In contrast, a solution yielded by the BEM satisfies the governing differential equations exactly and the boundary conditions approximately. The method is based on Green's Formula, which represents the displacement at some points within a structural component in terms of an integral of certain terms around the structural boundary. Formulation for the BEM, only for the acoustic field, has been included in the FEM/BEM method explanation.

The main advantage of the BEM is that only the boundary of a component needs to be discretized. In general, this leads to fewer degrees of freedom than are needed by the finite element method, particular for two and three-dimensional components. If the BEM is applied to structures then there exists a Green's function for the type of structural element, that is, a solution to differential equation for a point force.

In general, the BEM is advantageous to use as compared to the FEM only if some of the elements extend to infinity. The main disadvantages of the BEM are that the matrices tend to be fully populated rather than banded as in the FEM and the computational effort to assemble the equations can be significant. Furthermore as the BEM yields a frequency dependent stiffness matrix, the natural frequencies are normally found by a determinant search rather than by solving an eigenvalue problem as in the FEM.

The main use of the BEM in industry has been in vibro-acoustics where it has been employed to model either radiation from a structure into a semi-infinite acoustic space or free-field incidence on a structure.

In this regard, a boundary element model of the acoustic volume can be coupled to a finite element model to produce an efficient hybrid analysis scheme.

On that case, the boundary element method approach results more appropriate for the acoustic field while the finite element approach is more convenient for the structure.

The fluid field pressure distribution  $p(x, y, z, k)$  can be expressed in terms of the Green's function. The Helmholtz-Kirchhoff's integral equation reduces to:

$$p(x, y, z, k) = -\frac{1}{4\pi} \iint_{\text{Surface}} \nabla p(\xi, \eta, k) \frac{\partial}{\partial z} \frac{e^{jkr}}{r} d\xi d\eta. \quad [9-17]$$

And the pressure jump on the surface is related to the boundary condition as:

$$\rho \omega^2 w(x, y) = -\frac{1}{4\pi} \iint_{\text{Surface}} \nabla p(\xi, \eta, k) \frac{\partial}{\partial z} \frac{e^{jkr}}{r} d\xi d\eta, \quad [9-18]$$

where  $w(x, y)$  the amplitude of the normal displacement on each point on the wetted surface,  $\omega$  the angular frequency of the harmonic displacement,  $k$  is the wave number and  $\rho$  the density of the fluid (air).

Singularities are distributed along the structure-fluid interface, and, therefore, it is not necessary an infinite domain. Therefore, by formulating the structure by finite elements and the fluid domain by the boundary element method, and, including interface elements to transfer information between the two sub-domains, allows solving the problem with a reduced size of computational resources.

Solutions for the incompressible and compressible fluids exist, being each one appropriate depending on the frequency and sound speed. This method has been the most useful and adequate for the vibro-acoustic analysis in the low frequency range. Limitations due to wave number on the structure and interface elements between BEM and FEM domains on the common surface are the main sources of maximum frequency limitations.

### 9.6.2.2 Simulating a diffuse field as a superposition of a finite number of plane waves

As mentioned, a plane wave excitation is described by considering acoustic points sources located sufficiently far away from the structure. The originally spherical waves then quite fairly simulate plane waves when arriving on the structure. Typically, for a structure with overall dimension of the order of one or few meters, it is convenient to define a sphere of radius  $R = 1$  km, centred on the structure, as the site for locating the acoustic point sources.

The number of sources is defined, being obviously finite. So the source sphere is divided into  $N$  solid angles  $4\pi\alpha_i$ , with an acoustic point source of volumetric flow  $Q_1$  located at their centre.

Assuming that the chosen division is convenient, the acoustic field generated at the centre of this sphere of radius  $R$  as a superposition of  $N$  plane waves approximates a diffuse field.

### 9.6.2.3 Why the use of the boundary element method

The formulation leading to the BEM is more complex than the one leading to FEM. Nevertheless, when applied to an acoustic problem, the use of a BEM presents two important advantages in relation to the use of a FEM.

The first one is related to the number of elements required to discretize the acoustic domain. While the FEM requires a meshing for the whole acoustic space, the BEM only requires a meshing for the surfaces of the diffracting objects. There is thus less memory place required to store the data needed for the computations or the data provided by the computation. In addition, the computation runs faster.

The second advantage of the BEM formulation is when an open acoustic space is considered.

The boundary conditions to infinity (Sommerfeld's conditions), are easily integrated in the BEM formulation, using the Green function of the open space. On the other hand, satisfying this condition in FEM requires the introduction of particular elements on the boundaries of the meshed finite space.

#### 9.6.2.4 Guidelines for vibro-acoustic response analysis by BE

In general, the in vacuum undamped modal characteristics for the boundary element analysis are calculated using a finite element model. The in vacuum modal properties to be transferred are:

- Geometrical information about nodes and elements (finite element mesh to be matched with boundary element mesh).
- Natural frequencies.
- Associated vibration and stress (force) modes.

The mesh of the boundary element model may be different to the mesh of the finite element model, however, a good match between both the FEM and BEM mesh as to be made.

The mesh size in the FE model and BE mode should correspond to the minimum wavelength  $\lambda$  in the applied acoustic field. A rule of thumb is that the element dimension,  $d$ , is less than a quarter of the minimum wavelength  $\lambda$ .

Acoustic loads (e.g. plane wave, and reverberant) are defined within the frame of the boundary element analysis.

Modal damping ratios are defined within the frame of the boundary element analysis.

The coupled FEM/BEM analysis is illustrated in a flow chart in Figure 9-26.

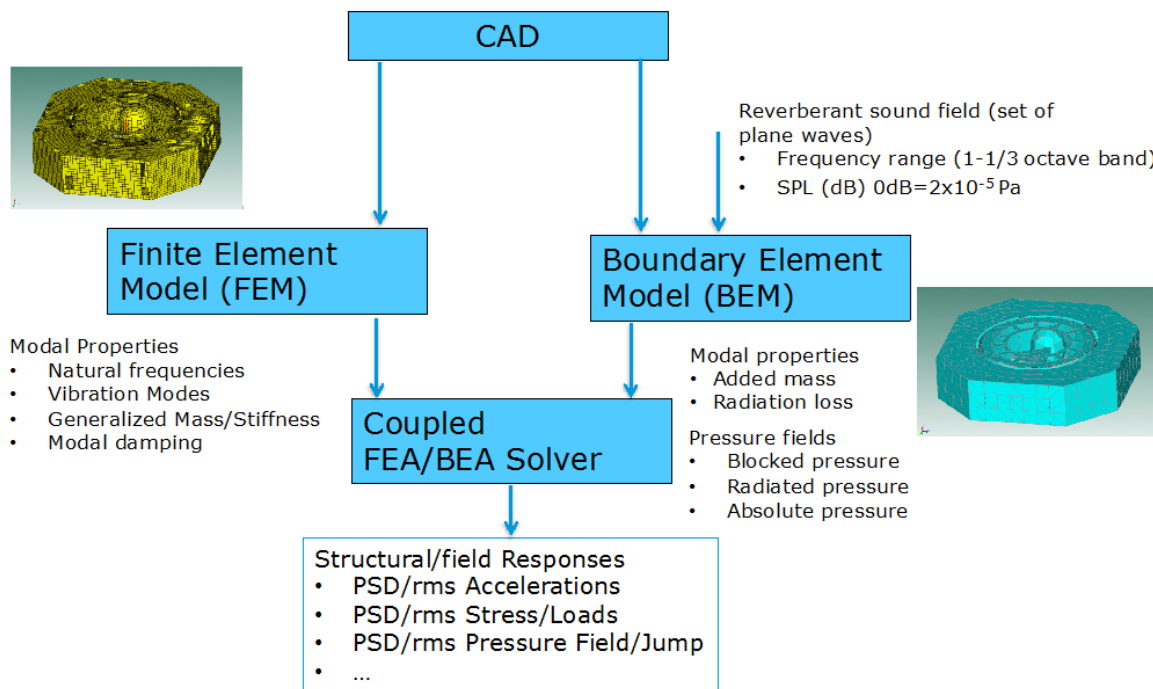
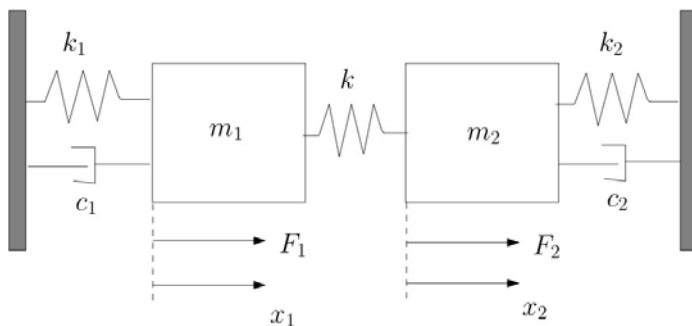


Figure 9-26: Flow chart boundary element analysis

## 9.6.3 Statistical energy analysis

### 9.6.3.1 General aspects

The basic theory about the Statistical Energy Analysis (SEA) is presented in an early paper by Lyon [29] and later in the textbooks [30] [31]. In [29] the net flow of energy transferred between the two single degree of freedom systems are calculated assuming non-correlated random forces  $F_1, F_2$  (Figure 9-27). It is shown that the transferred energy is proportional to the difference of the total energies of the individual single degree of freedom systems.



**Figure 9-27 : Two spring-coupled oscillators**

The theory of energy flow between two oscillators has been extended to groups (sets A and B) of oscillators, which is illustrated in Figure 9-28.

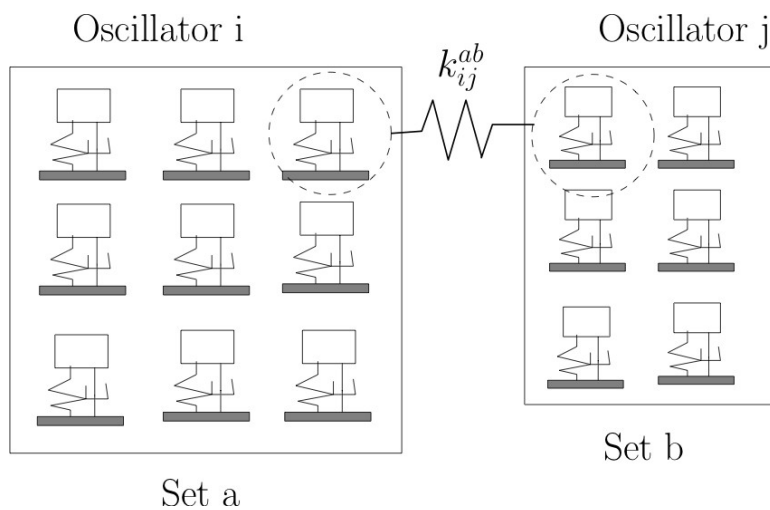


**Figure 9-28 : Two sets of spring-coupled oscillators**

SEA is applicable for predicting the average vibro-acoustic behaviour in structures in medium-to-high-frequency regions. The SEA approach is based on calculating the power between components of a complex mechanical system by analysing relatively few and low-detail subsystems, which are coupled together. The fundamental element, the subsystem, in the SEA model is a group of similar energy storage blocks  $\langle E_i \rangle$ . In Figure 9-29 a fundamental SEA model built up by two subsystems is shown. These blocks or subsystems usually are modes of the same type (e.g. flexural, torsional, and longitudinal) that exists in some section(s) of the components.

$$\Pi_1 = \omega \eta_1 \langle E_1 \rangle + \omega \eta_{12} n_1 \left( \frac{\langle E_1 \rangle}{n_1} - \frac{\langle E_2 \rangle}{n_2} \right), \quad [9-19]$$

$$\Pi_2 = \omega \eta_2 \langle E_2 \rangle + \omega \eta_{21} n_2 \left( \frac{\langle E_2 \rangle}{n_2} - \frac{\langle E_1 \rangle}{n_1} \right), \quad [9-20]$$

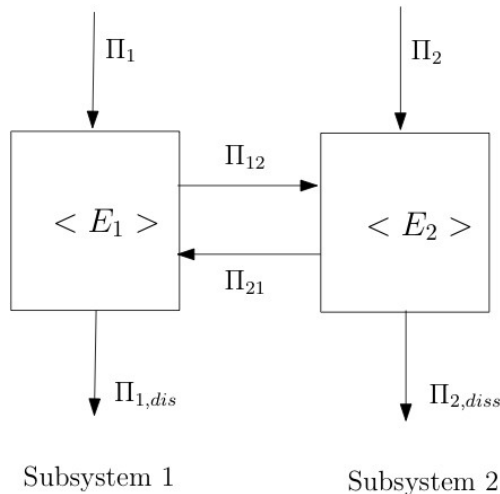


**Figure 9-29 : Fundamental SEA model built up by two subsystems**

The input power  $\Pi_1$  may result from acoustic noise or mechanical excitation. The energy in each block  $\langle E_i \rangle$  may be dissipated by damping  $\Pi_{i,dis} = \eta_i \omega \langle E_i \rangle$ , is in each block “ $i$ ” and is described by the damping loss factor (DLF)  $\eta_i$ , or transmitted to the neighbouring blocks

$\Pi_{ij} = \omega \eta_{ij} n_i \left( \frac{\langle E_i \rangle}{n_i} - \frac{\langle E_j \rangle}{n_j} \right)$  This energy transmission is proportional to the coupling loss factor (CLF)  $\eta_{ij}$ . The modal density, e.g. the average density of resonance frequencies in the frequency band

$\left[ n_i = \frac{N_{i,\Delta\omega}}{\Delta\omega} \right]$ , should be high in SEA, which can pose a problem for the finite element method (FEA).

The time average energy state is obtained by solving the energy balance equations [9-19] and [9-20]. We notice that time-average subsystem energies are the primary unknowns in SEA, not nodal displacements, which is the case in FEA. A comparison of the FEA and SEA fundamental is made in Table 9-6.

**Table 9-6: FEA and SEA fundamental comparison**

Criterion	FEA	SEA
Unknowns	Nodal displacements	Average subsystem energies
Frequency	Discrete, low	Band average, high
Spatial detail	High, discrete	Low, average
Excitation	Discrete	Average random spectrum
Procedure	Complicated, established	Quick, demanding at first
Computational effort	High	Low
Model	Large	Small

### 9.6.3.2 Guidelines statistical energy analysis models

When creating an SEA model the various transmission paths that might exist in the system should be visualized and ensure that these transmission paths are accounted for in the model by subsystems and junctions. Ideally, when choosing the most appropriate SEA subsystem representation for a given component ensures that the chosen SEA subsystem meets the following criteria [19] :

- Captures the correct energy storage capacity of each component (i.e. each SEA subsystem should have approximately the same number of modes in band, and the same propagating wavelengths, as the physical component being modelled).
- Possesses the correct mass density and average section thickness (or, for acoustic cavities, the correct characteristic impedance) so that energy of the subsystem is accurately converted to the appropriate space-averaged engineering units response.
- Is reverberant (i.e., the transmission of energy between subsystems is mainly through the reverberant field rather than being due to direct field transmission). Exceptions include the transmission loss of panel subsystems where non-resonant direct field transmission across the panel is automatically accounted for in the SEA coupling loss factors.
- Contains several local modes in each frequency band of interest (or that the component is large compared with a wavelength). The ensemble average prediction from an SEA model is then more likely to match the frequency average response of the system you are modelling.
- Correctly describes the overall level of damping in a given physical component (if you do not know the actual damping level and/or cannot measure the damping from a test article then check the sensitivity of the response to an assumed damping level; try to bound the expected levels of damping and see how this changes the response).

The junctions between subsystems should be chosen so that:

- The overall connectivity of the subsystems is similar to that of the physical system you are trying to model (ideally you should account for all transmission paths between the different subsystems in your model). Point connections are used to model structural connections that are small compared with a wavelength, line connections are used to model structural connections that are large compared with a wavelength. The line and area connections in your model should match the length and area of the connections in the physical system you are modelling.
- The impedance of the subsystems in your model at each point, line and area connection should be similar to the impedances that you would expect in the physical system you are modelling (this ensures that the transmission of energy is correctly predicted by the coupling loss factor calculations in the model).
- Any lumped masses, stiffeners or isolators at the junctions should be included in your model. The transmission of energy between subsystems depends on the local reactive and resistive impedance at a junction. Local junction details that affect the mass and stiffness of the junction often have a significant influence on the overall transmission.
- The junctions between subsystems should, ideally, be located at places where there are major impedance discontinuities between the subsystems (in order to correctly account for the scattering of energy that occurs at these junctions).

The response of an SEA model is often insensitive to many simplifying assumptions made about the subsystems in a model and to artificial sub-structuring assumptions. In the former case, conservation of energy often leads to answers that remain physically realistic. In the latter case, the subsystems often attain a state of 'equi-partition' of energy and become insensitive to assumptions made about the coupling between subsystems (exceptions to this rule of thumb include long chains of one-dimensional subsystems and radiation from panels to acoustic cavities where subdivision results in

artificial edge radiation below coincidence – this additional radiation can be corrected for in the model). Simple SEA models can therefore often be used to quickly diagnose the dominant transmission paths in a system. Once the dominant transmission paths have been obtained, more detailed modelling can often be carried out to refine the predictions for the subsystems along these paths.

This 'equi-partition' is particularly interesting in lightly damped space structures. The experimental data showed good correlation with the SEA models at frequencies that were much lower than the typical SEA rules of thumb (3 modes in band). This was most likely due to two factors:

- Equi-partition of energy in lightly damped structures, and
- Uniformity of the excitation where the acoustic pressure was applied nearly equally to most parts of the structure so that there was little need to predict the structural transfer of energy properly.

In these cases, it is likely that the structural coupling loss factors are of minimal importance in getting the response correct.

## 9.6.4 General guidelines for vibro-acoustic analyses

The following basic fundamentals are managed by the user in order to select the solution method to run a vibro-acoustic analysis [32]:

- The system to be analysed can be divided into two types of subsystems: structural subsystems and fluid subsystems (infinite fluid domain or closed fluid volume).
- The excitation sources can be classified broadly as low, medium or high frequency loads. There is no absolute frequency range associated with each of those regimes. The modal density of the structure (number of structural modes per analysis frequency band), as a whole and for different regions, is the main parameter governing the adequate analysis procedure to study the system response to a load. Hence, the vibro-acoustic problems are divided in the following categories: Low, Medium and High frequency excitation.
- The main parameters driving the structural and acoustic response of any structural system immersed in an acoustic environment are:
  - The system modal density expressed.
  - The coincidence (joint acceptance) between the incident acoustic pressure distribution and the vibration modes of every subsystem.
  - The damping loss factor of every subsystem, which controls the energy dissipation by internal damping.
  - The coupling loss factors between subsystems, which control the energy flow among them.

The following solution methods, separately or combined, can be used for modelling and analysing the response of a system under random vibro-acoustic loads; Finite Element Analysis (FEA), Boundary Element Analysis (BEA) and Statistical Energy Analysis (SEA).

- The limits on the output information required and the computational cost can be a first criterion for selection of the method:
  - When affordable, the FEM/BEM combination is appropriate to directly provide general and detailed information of common mechanical response (displacements, accelerations, strains and stresses), both as data on a particular point or as average of a region.

- When modal density is too high and the required computational resources are excessive, SEA modelling allows obtaining energy distribution by subsystem, and by post processing, mean values of mechanical magnitudes, as velocity, displacements and strains.
- Nevertheless, once the range of frequency to be analysed is established, the modal density of the whole structural subsystem defines the solution method. The solution method selection is indicated in Table 9-7.

**Table 9-7: Solution method selection**

Output required	Fluid domain	Low modal density (< 4 for all components)	Combination of components with high and low modal density	High modal density (>4 for all components)
<b>Structure</b>	-	FEA for structure BEA for fluid domain	FEA for low modal density components  SEA for high modal density components	SEA
<b>Structure &amp; fluid</b>	Infinite	FEA for structure BEA for fluid domain	FEA for low modal density components  SEA for high modal density components	SEA
	Closed	FEA for structure FEA for fluid domain	FEA for low modal density components  SEA for high modal density components	SEA

## 9.7 Acoustic testing

### 9.7.1 Introduction

The acoustic test of a complete spacecraft or components such as solar array wing and antenna dish is done to verify the load carrying capabilities of those against reverberant (diffuse) sound pressures. In practice the acoustic test verifies strength and structural life by introducing random vibration through acoustic pressure.

Typical applications are lightweight structures with large surface areas and spacecraft with acoustically sensitive structures. Acoustic tests at the spacecraft level are used to validate the random vibration environments used to qualify components.

The acoustic tests are performed in reverberant acoustic chambers which simulate the reverberant sound field (sound pressure levels). In general, the reverberant chambers have big volumes. However, the test items placed in the chamber have an influence or disturb the required reverberant sound field. Control microphones are placed around (above and below) and with a sufficient distance of the test item.

The structural responses of the test items and sound pressures can be measured using sensors, for example accelerometers, strain gages, microphones, surface microphones and flow sensors. These responses and pressure are measured in the time domain and, in general, presented as power spectral densities in the frequency range of interest (e.g. 20-2500 Hz) and with a certain frequency band (e.g. 2 Hz). The sampling frequency of the signals is dependent of the maximum frequency of interest.

The duration of the acoustic test is dependent of the specifications, in general, 120 s for the qualification and 60 s for flight loads.

In the following section some specific topics about acoustic testing are discussed.

### 9.7.2 Test plan/procedure

#### 9.7.2.1 Introduction

The verification philosophy of the design of the spacecraft assembly, subsystems, components, etc. is described in a document called the test plan. The success criteria of the acoustic test are part of this test plan.

The acoustic test plan should include:

- A summarized description of the test item; type of structure, volume, mass and position of the test item in the reverberant chamber (see Figure 9-30),
- The test sequence, associated sound pressure levels, deviations and durations, e.g. low level, intermediate level, qualification level and low level again,
- Instrumentation plan describing number and location of sensors,
- The details of presentation of the sensor measurements, resolution in time domain and frequency domain,
- Success criteria.

The test procedure is more or less a translation of the test plan in a step-by-step procedure how to perform the acoustic test.

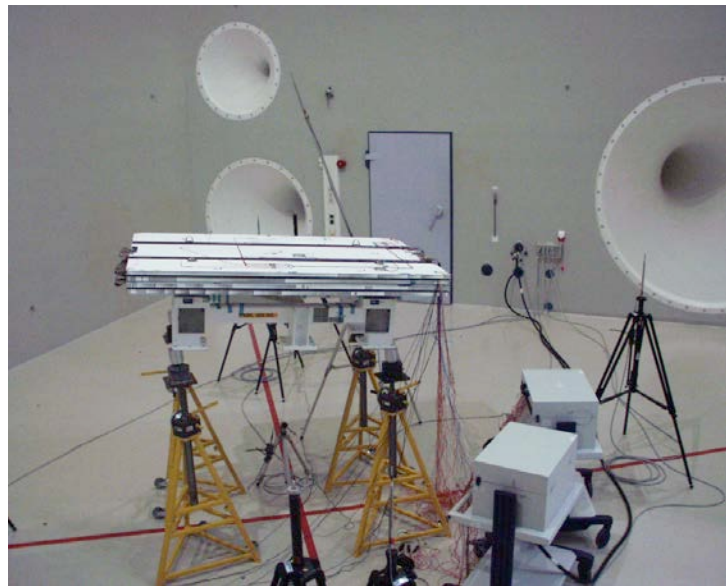


**Figure 9-30 : FRED/ATV STM-B Solar array wing in IABG reverberant chamber  
(Courtesy Dutch Space)**

#### **9.7.2.2 Test sequence**

Different levels are defined for the test and given in the test plan. The low levels are also called signature runs to be used to notice failures in the structure after test runs had been done.

#### **9.7.2.3 Test run specification**

Prior to the test of the article, empty chamber run(s) are performed (without the test article), in order to establish the settings of the control equipment and to achieve the levels as defined in the following sections.

For each run the SPL levels, allowable deviations and duration are defined. Of course these levels, deviations and time duration depend on the project; e.g. spacecraft, solar array wing.

Low-level runs would be 6dB below qualification level and as short as possible (maximum 60 seconds duration as a target) but long enough to obtain the required accuracy. The acceptance level run would be 3dB below qualification level.

#### **9.7.2.4 Input control**

Normally, six control microphones are used to control the acoustic environment. The applied input levels are defined as the mean of the 6 SPL's.

The minimum distance of the microphones from the test articles is 1 meter. The exact distances of the microphones from the test article is included in the test report.

Control microphone signals are normally analysed with both 1/3 and 1 octave bandwidth.

SPL tables of each microphone and average values of the SPL of all control microphones are provided to judge if specified SPL, OASPL and deviations do meet the specifications.

#### **9.7.2.5 Sensor data**

After each run, tables of RMS-values of the sensor measurements are supplied for all channels. Based on a review of these data, permission is given to start the next run.

## 9.8 Verification of compliance

### 9.8.1 General aspects

The assessment of the compliance of an equipment or instrument random vibration specification with system acoustic test measurements is basically performed in line with the general principles, criteria and assumptions reported in Section 4.7. In particular, with respect to the levels at the base of the unit (and assuming that relevant information from the acoustic test is only available at the unit interface), the following cases are possible:

1. The acoustic test measurements are enveloped by the unit's random specification for all frequencies. The random specification is considered adequate and no further action is needed.
2. The acoustic test measurements exceed the unit's random specification for most or all frequencies. The random specification is considered as inadequate and a "delta test" of the unit should be considered.
3. The acoustic test measurements exceed the unit's random specification only at certain frequencies. An analytical assessment of compliance should be performed before embarking on a unit delta random test.

For the analytical assessment of compliance, two cases can be identified:

Case 1: the acoustic test measurement peaks exceeding the specification are in the frequency range where unit's sine test has been performed (usually for  $f \leq 100$  Hz).

The approach consists of verifying that the severity of the excitation level applied to the unit during the sine test, at the frequency of the peak, is equivalent or larger than that found for the random environment. For example this can be done by comparing the SRS of the sine input level with the RRS of the PSD at the base of the unit, measured from the acoustic test (see Sections 4.7.2 and 5.2.5.4 for details on equivalence criteria and SRS for random environments respectively). The equivalent g-level is typically evaluated at  $3\sigma$  for comparison with the respective sine input.

Case 2: the acoustic test measurement peaks exceeding the specification for frequencies  $f > 100$  Hz. The following approaches are used:

- Peak clipping. A commonly used rule is that all narrowband spectral peaks should be clipped by 3 dB [8]. Sharp peaks or peaks with a relatively small bandwidth of exceeding the unit power spectral density specification might be clipped if the exceedance is not more than 3dB. This approach is based on the following justification. The acoustic test measurements are usually much lower than the unit power spectral density specification next to the peak. Then it can be assumed that in the relevant frequency band the random input (usually flat for a wide frequency band at left and right of the peak found) is at least equivalent to the corresponding energy input resulting from the higher peak but taking into account the significantly smaller random levels next to the peak (see Section 5.2.5.3 for the analytical discussion of the approach). However perhaps the best approach "to remove" the narrowband spectral peaks is to compute all spectra with a resolution bandwidth that is proportional to frequency (e.g., a 1/6 octave bandwidth), and then envelope all peaks without clipping [4].
- Application of random response spectrum (RRS), also called vibration response spectrum (VRS). For example Irvine [33] shows how the VRS of a typical power spectral density specification is compared with the actual peaky measurements and how it can be then demonstrated that the specification covers the measurements even if there might be large exceedances. An approximate evaluation of the VRS can be performed by applying the Miles'

equation with varying the natural frequency  $f_0$  from 20 to 2000 Hz, which is the typical random vibration frequency range. This method is illustrated in the next section.

In the above mentioned cases, and in the relevant proposed approaches, the assumption that the information from the acoustic test is only available at the unit interface has been done. However there could be the chance to compare the unit's internal responses measured during the system acoustic noise test with the ones measured during the random vibration base-drive test at unit's level.

In this case the internal responses should be checked first (see also Section 4.7.2 for more details on relevant equivalence criteria). In fact the incompatibility of the unit's random test excitation with the corresponding acoustic test measurement at the interface of the unit does not exclude a potential compatibility of the respective internal responses, which might depend much on the mounting conditions of the unit on the satellite as compared to the shaker test. In practice, if measurements of unit's internal responses are available from the acoustic test then these responses should be taken into account and, where relevant, the proposed approaches should be adapted accordingly to the comparison of the internal responses. Of course the aim is to verify that the unit's random vibration test has been performed with sufficient excitation although an incompatibility with respect to the acoustic test measurements at the unit interface was noted.

## 9.8.2 An example based on the vibration response spectrum

The method described in this example is enabling a more rigorous comparison of equipment random vibration test requirements with random responses measured at system level. It provides a rational approach dealing with the common situation, in which narrow band peaks occur in the measured system level responses above the equipment test environment. The method is less arbitrary than the common rule of thumb of drawing a line through the half-power bandwidth points. The method can be used either to define random vibration specification from measured data or to assess the compliance of random vibration specification with the system acoustic test measurements. In the first case it minimises the chance of an overtest and, hence, overall programme risk.

The example which is here reported shows how the method can be applied to define a specification. The input data for the derivation of the random vibration specification are the random vibration response measurements from an acoustic noise test (ANT). These random vibration test data are processed in order to show compliance with in-flight boundary conditions and environment.

Therefore, a mathematical model of the test configuration is set up and tuned on basis of measured test results. Afterwards the model is re-configured, reflecting in-flight boundary conditions and environment. With the re-configured analysis model a flight prediction is made. Based on the comparison of predicted vibro-acoustic responses for the test configuration and for the in-flight configuration, scaling factors e.g. per 1/3 octave band are computed. Finally, the acceleration power spectral density spectra derived from acoustic test data are scaled with the computed scaling factors. The result is the acceleration power spectral density, representative for the in-flight configuration. Such a scaled acceleration power spectral density ( $\text{g}^2/\text{Hz}$ ) is illustrated in Figure 9-31.

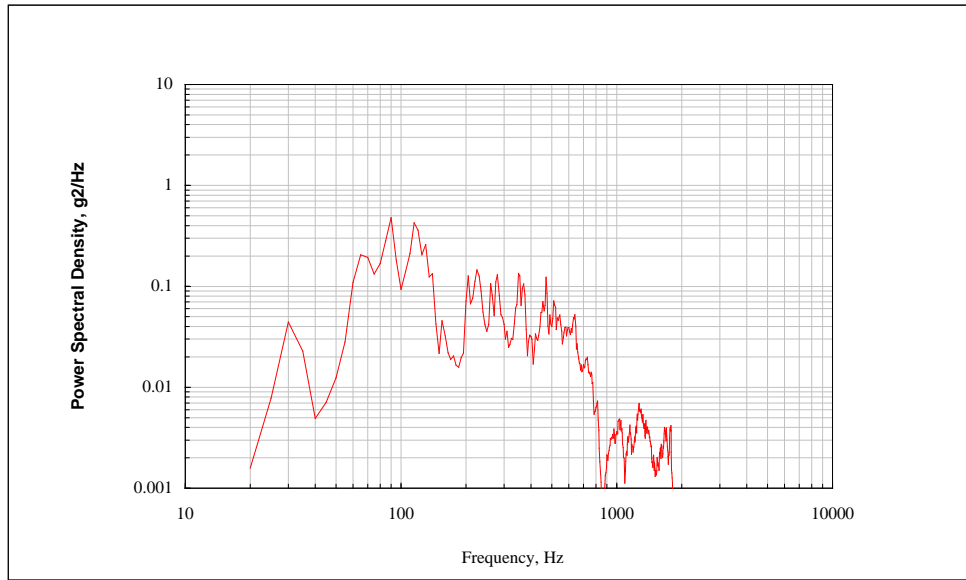


**Figure 9-31 : Scaled in-flight power spectral density response**

In this example a step-by-step procedure is shown how to generate the random vibration test specification:

1. Define a specification, which envelops the acceleration power spectral density response spectrum.
2. Compute the VRS for the power spectral density response spectrum and for the envelope specification.
3. Adapt iteratively the specification, such that the VRS is at least equal for the acceleration response curve and for the envelope acceleration specification in the frequency range of interest.

The VRS is calculated for each  $f_0$  as follows:

$$a_{\sin(3\sigma)} = 3 \sqrt{\int_{20\text{Hz}}^{2000\text{Hz}} W_{\text{ANT}}(f) \cdot T^2(f/f_0) df} \approx 3 \sqrt{\frac{\pi}{2} f_0 Q W_{\text{ANT}}(f_0)}, \quad [9-21]$$

and

$$T(\eta) = \frac{\ddot{X}}{\ddot{U}} = \frac{\sqrt{1 + (2\zeta\eta)^2}}{\sqrt{(1 - \eta^2)^2 + (2\zeta\eta)^2}}. \quad [9-22]$$

Where  $T(\eta)$  is the transfer function of the SDOF system with base excitation,  $\eta = f/f_0$ , the damping ratio is  $\zeta = 1/2Q$  and  $Q$  is the amplification factor. The enforced acceleration  $\ddot{u}$  and the absolute acceleration response  $\ddot{x}$  (see Figure 9-32) are in the frequency domain given by  $\ddot{u} = \ddot{U}e^{j\omega t}$  and  $\ddot{x} = \ddot{X}e^{j\omega t}$  respectively.

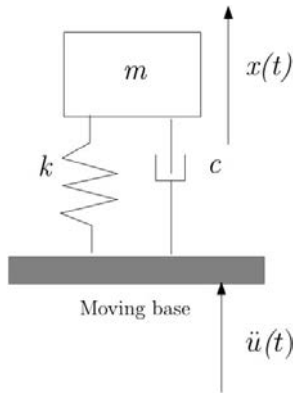


Figure 9-32 : Single degree of freedom (SDOF) system

$a_{\sin(3\sigma)}$  is the  $3\sigma$  equivalent sinusoidal acceleration response (g) of the scaled Acoustic Noise Test (ANT) acceleration response for the SDOF system with  $f_0$  and  $Q=10$ ,  $W_{g,\text{ANT}}(f)$  is the acceleration power spectral density ( $\text{g}^2/\text{Hz}$ ) from the acoustic noise test scaled to in-flight boundary conditions and environment, and  $f_0 = 1/2\pi\sqrt{k/m}$  is the natural frequency (Hz) of the SDOF system.

Repeat this computation e.g. 1980 times for  $\Delta f_0 = 1\text{ (Hz)}$  in the frequency range from 20Hz to 2000Hz.

Figure 9-33 shows an example for an envelope specification (black).

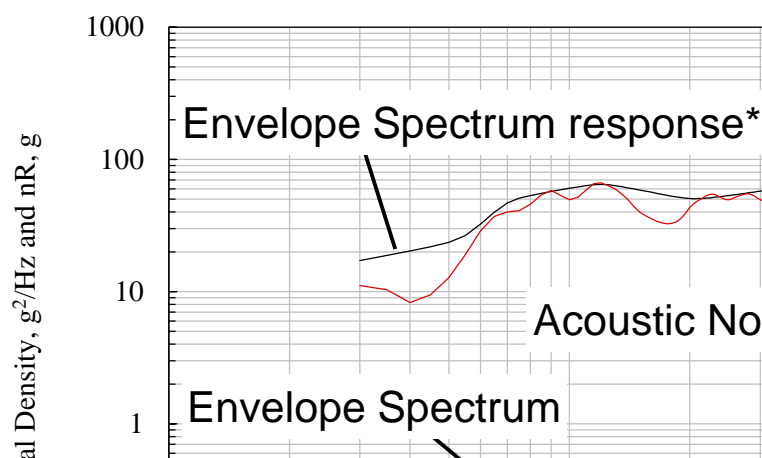


Figure 9-33 : Derived random vibration test specification

## 9.9 Special topics in random vibration

### 9.9.1 Simulation of the random time series

In [34] [35] [36] methods are discussed to simulate a stationary random process, expressed in power spectral density function  $W(f)$ , in the time domain. Time domain random processes are quite convenient and in particular for:

- The numerical analysis of dynamical response of nonlinear structures to random excitation.
- Time random analysis of the dynamic response of linear structures under random excitations in order to obtain a kind of information that is not obtainable from frequency domain analysis.

The signal  $x(t)$  can be simulated as follows:

$$x(t) = \sqrt{2} \sum_{n=0}^{N-1} \sqrt{\{W(f_n)\Delta f\}} \cos(2\pi f'_n t + \vartheta_n), \quad [9-23]$$

where  $N$  is the number of frequency intervals and is chosen large enough to simulate the random process which is approximately ergodic,  $f'_k \approx f_k + \Delta f / 20$  (Hz),  $\Delta f = f_{\max} / N$ ,  $\vartheta_k$  is a random phase angle uniformly distributed between 0 and  $2\pi$  with the probability of occurrences  $1/2\pi$  and  $f_n = n\Delta f, n = 0, 1, 2, \dots, N-1$ . It is suggested to use  $\Delta t = 1/(2f_{\max})$  (Nyquist criterion), where  $f_{\max}$  is the maximum frequency of the function  $W(f)$ .  $N$  is the number of samples. In general, the time increment  $\Delta t$  is equidistant.

Miles [36] proposed a very efficient manner to generate the series using the Fast Fourier Transform (FFT), which can be written as:

$$x_k = x(k\Delta t) = \Re \left[ \sqrt{2} \sum_{n=0}^{2N-1} a_n e^{-jnk2\pi/2N} \right], k = 0, 1, 2, \dots, 2N-1, \quad [9-24]$$

where  $a_n$  is given by:

$$\begin{aligned} a_n &= \sqrt{[W(f_n)\Delta f]} e^{-jk\vartheta_n}, n \leq N-1, \\ a_n &= 0, n \geq N. \end{aligned} \quad [9-25]$$

This is equivalent to:

$$x_k = \sqrt{2} \Re [FFT(a_n)] \quad [9-26]$$

Note that the length of the sequence  $a_n$  is  $2N$ .

The function  $W(f_n) = W(n\Delta f)$  can be reconstructed using the inverse Fast Fourier Transform (IFFT)

$$W(f_n) = W(n\Delta f) = 2 \frac{|IFFT(x_k)|^2}{\Delta f}, k = 0, 1, 2, \dots, 2N-1, n = 0, 1, 2, \dots, N-1, \quad [9-27]$$

where  $W(f)$  is the power spectral density function defined in the cyclic frequency domain and  $f$  is the cyclic frequency (Hz).

The estimated mean value of the simulated random time series  $x_k$  can be calculated using the following expression:

$$x_{mean} = \frac{1}{2N} \sum_{k=0}^{2N-1} x_k, \quad [9-28]$$

and the mean square value  $x_{rms}^2$  can be calculated:

$$x_{rms}^2 = \frac{1}{2N} \sum_{k=0}^{2N-1} x_k^2. \quad [9-29]$$

The variance can be obtained by:

$$Var(x) = \frac{1}{2N} \sum_{k=0}^{2N-1} (x_k - \bar{x})^2, \quad [9-30]$$

and the estimated standard deviation:

$$s_x = \sqrt{Var(x)}. \quad [9-31]$$

### Example

A typical random vibration specification for components ( $M \leq 22.7$  kg, e.g. equipment, and boxes) is given in [37] and shown in Table 9-8.

**Table 9-8: Component “Random Vibration levels**

Frequency [Hz]	$W(f)$ g <sup>2</sup> / Hz (enforced acceleration)
0-20	$10^{-6}$ (artificial)
20-50	6 dB/octave
50	0.16
800	0.16
800-2000	-6 dB/octave
Overall	14.12 Grms

The simulated random time series of the enforced acceleration from Table 9-8 is shown in Figure 9-34. The number of samples  $N = 500$  is taken to get a random time series, which is not too dense. The maximum time on the ordinate is  $N\Delta t = N / 2f_{max} = 0.25$  s and the maximum considered frequency  $f_{max} = 2000$  Hz.

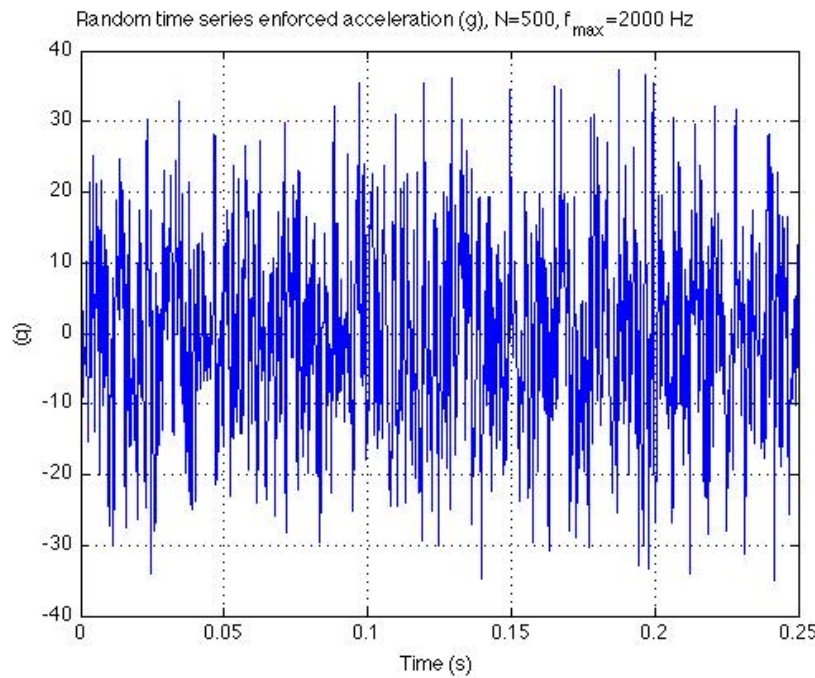


**Figure 9-34 : Simulated random time series enforced acceleration**

The reconstructed power spectral density of the enforced acceleration  $W(f)$  is shown in Figure 9-35.

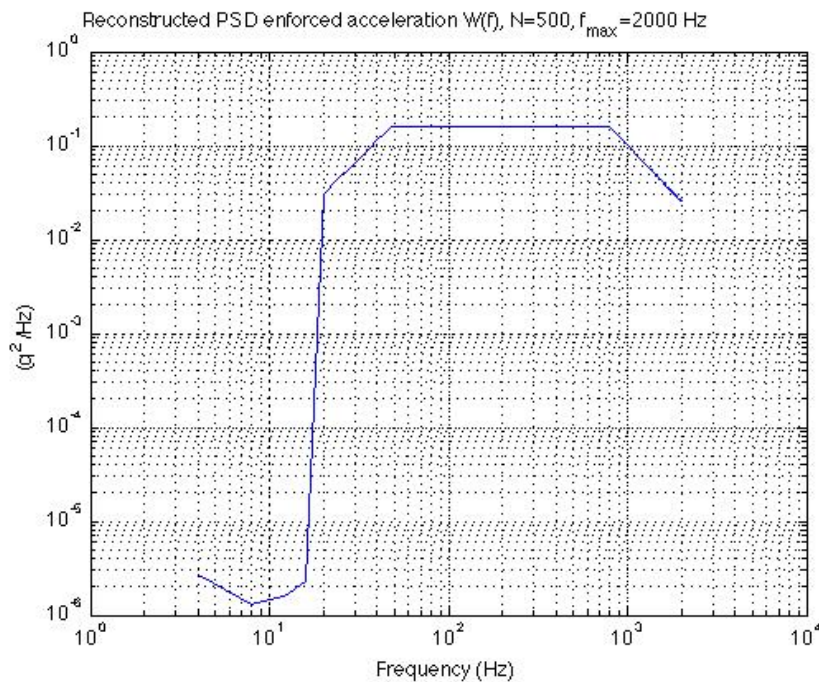


**Figure 9-35 : Reconstructed PSD enforced acceleration**

The estimated mean value and rms value of the simulated time series are 0.0027 g and 14.12 g respectively.

## 9.9.2 Prediction of random acoustic vibration of equipment mounted on panels

### 9.9.2.1 SEA Analysis satellite equipment panel (NASA Lewis Method)

In this section the response of panels with attachments (equipment) to diffuse acoustic loading with aid of the SEA are discussed. Many papers about this subject are published in the open literature, conferences and the internet ([38] [39] [40] [41] [42]). Ando and Shi discussed in their papers the development and application of the JAXA (Japan Aerospace Exploration Agency) tool for predicting random vibrations of rigid and flexible equipment mounted on honeycomb panels based on experiments and SEA mathematical models. Conlon developed in [39] a random vibration response method of complex (rigid and flexible) attachments (equipment) mounted to non-homogeneous panels. In this section we follow the work of Conlon [39] [40].

The method described here is called the “NASA Lewis Method” [41].

The loaded panel is represented by a simple SEA system shown in Figure 9-36. The panel is indicated by system 2 and the acoustic volume represents the reverberant test chamber and is indicated as system 1.

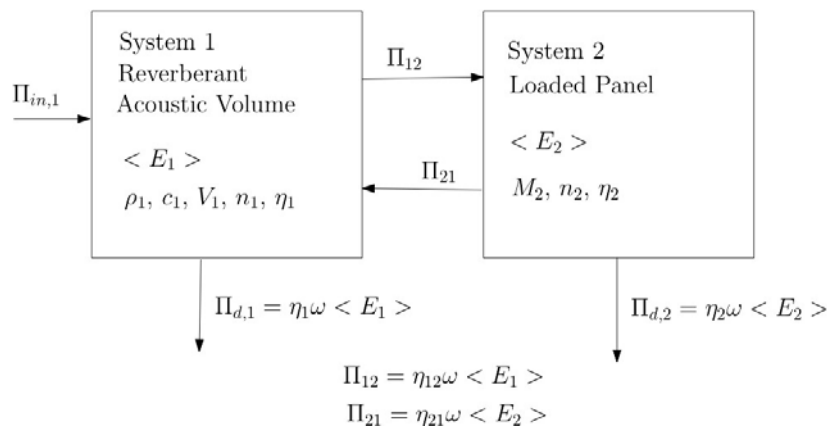


Figure 9-36 : Loaded panel SEA system model

The loaded panel is defined with the total panel mass  $M_2$  (structure plus total equipment mass),  $n_2(\omega)$  the unloaded panel (ignoring total equipment mass) modal density,  $\eta_2(\omega)$  is the damping loss factor (DLF) and the total and temporally and spatially average energy  $\langle E_2(\omega) \rangle$ . The acoustic volume is similarly defined and includes the external input, which is intrinsically included in the solution via specifying the acoustic response energy  $\langle E_1(\omega) \rangle$  (the acoustic response energy is later derived based on the average measured pressure in the volume). The power balance for the two-coupled systems 1 and 2 are:

$$\begin{aligned} \Pi_{in,1} + \eta_{21}\omega\langle E_2 \rangle - \eta_{12}\omega\langle E_1 \rangle - \eta_1\omega\langle E_1 \rangle &= 0, \\ \eta_{12}\omega\langle E_1 \rangle - \eta_{21}\omega\langle E_2 \rangle - \eta_2\omega\langle E_2 \rangle &= 0, \end{aligned} \quad [9-32]$$

where the coupling loss factor (CLF)  $\eta_{ij}(\omega)$  is frequency dependent too. Frequency dependence is implied for the SEA parameters throughout the analysis. The temporally averaged energy  $\langle E_1(\omega) \rangle$  of system 1 is known through its relationship to mean square spatial average pressure [43].

$$\langle E_1 \rangle = \frac{\langle p_1^2 \rangle V_1}{\rho_1 c_1^2}, \quad [9-33]$$

Where:

- $\langle p_1^2 \rangle$  is the acoustic volume temporally and spatially averaged mean square pressure,
- $V_1$  is the acoustic chamber volume,
- $\rho_1$  is the density of the acoustic medium,
- $c_1$  is the speed of sound in the acoustic medium.

The energy of system 2 can be expressed in terms of the energy of system 2

$$\langle E_1 \rangle = \frac{\eta_{12}}{\eta_2 + \eta_{21}} \langle E_2 \rangle. \quad [9-34]$$

Combining the consistency relationship or SEA reciprocity for coupled systems i and j

$$n_i \eta_{ij} = n_j \eta_{ji}, \quad [9-35]$$

Using [9-36] for the loaded panel

$$\langle E_1 \rangle = \left( \frac{n_2}{n_1} \right) \left( \frac{\eta_{21}}{\eta_2 + \eta_{21}} \right) \langle E_2 \rangle. \quad [9-36]$$

The load panel coupling loss factor  $\eta_{21}$  (also called radiation loss factor) is given by:

$$\eta_{21} = \frac{\rho_1 c_1 A_2}{\omega M_2} \sigma_{rad}, \quad [9-37]$$

Where  $A_2$  is the panel area and  $\sigma_{rad}$  the radiation efficiency of the unload panel.

The modal density of the acoustic volume, considering only the volume term, can be approximated by:

$$n_1 = \frac{\omega^2 V_1}{2\pi^2 c_1^2}. \quad [9-38]$$

The loaded panel mean square spatial and temporal average velocity  $\langle v_2^2 \rangle$  and acceleration  $\langle a_2^2 \rangle$  can be calculated as follows:

$$\langle v_2^2 \rangle = \frac{\langle E_2 \rangle}{M_2} = \frac{\langle a_2^2 \rangle}{\omega^2}, \quad [9-39]$$

The panel acceleration response becomes

$$\langle a_2^2 \rangle = \omega^2 \left( \frac{\eta_{21}}{\eta_2 + \eta_{21}} \right) \left( \frac{n_2}{n_1} \right) \left( \frac{V_1}{\rho_1 c_1^2} \right) \left( \frac{\langle p_1^2 \rangle}{M_2} \right), \quad [9-40]$$

where  $\langle p_1^2 \rangle$  is the octave or one-octave mean square pressure

$$\langle p_1^2(f_c) \rangle = p_{ref}^2 10^{\frac{SPL(f_c)}{10}}, \quad [9-41]$$

and  $p_{ref} = 2.0 \times 10^{-5}$  Pa and SPL(dB) is the specified sound pressure level at the octave or one-octave band centre frequency  $f_c$  (Hz).

The power spectral density of the random acceleration response  $W_A(f)$  can be obtained as follows:

$$W_A = \frac{\langle a_2^2 \rangle}{\Delta f} = \omega^2 \left( \frac{\eta_{21}}{\eta_2 + \eta_{21}} \right) \left( \frac{n_2}{n_1} \right) \left( \frac{V_1}{\rho_1 c_1^2} \right) \left( \frac{\langle p_1^2 \rangle}{\Delta f M_2} \right), \quad [9-42]$$

$$W_A = \omega^2 \left( \frac{\eta_{21}}{\eta_2 + \eta_{21}} \right) \left( \frac{n_2}{n_1} \right) \left( \frac{V_1}{\rho_1 c_1^2} \right) \left( \frac{W_p(f)}{M_2} \right),$$

where  $\Delta f$  (Hz) is the bandwidth and  $W_p(f) = \langle p_1^2 \rangle / \Delta f$  (Pa<sup>2</sup>/Hz) the power spectral density of the pressure.

The loaded panel damping loss factor  $\eta_2$  can be estimated for loaded panels with total mass panel ratios approximately [39]

$$\eta_2 = \begin{cases} 0.05, & f < 500 \text{ Hz}, \\ 0.05 \sqrt{\left(\frac{500}{f}\right)}, & f > 500 \text{ Hz}, \end{cases} \quad [9-43]$$

and for unloaded panels

$$\eta_2 = \begin{cases} 0.025, & f < 250 \text{ Hz}, \\ 0.025 \sqrt{\left(\frac{250}{f}\right)}, & f > 250 \text{ Hz}. \end{cases} \quad [9-44]$$

Ando [38] suggests an average damping loss factor, which had been measured for several loaded panels

$$\eta_2 = f^{-0.7}. \quad [9-45]$$

Conlon's damping model is used here.

In Figure 9-37 is damping loss factor for loaded panels in accordance with Ando and Conlon illustrated.

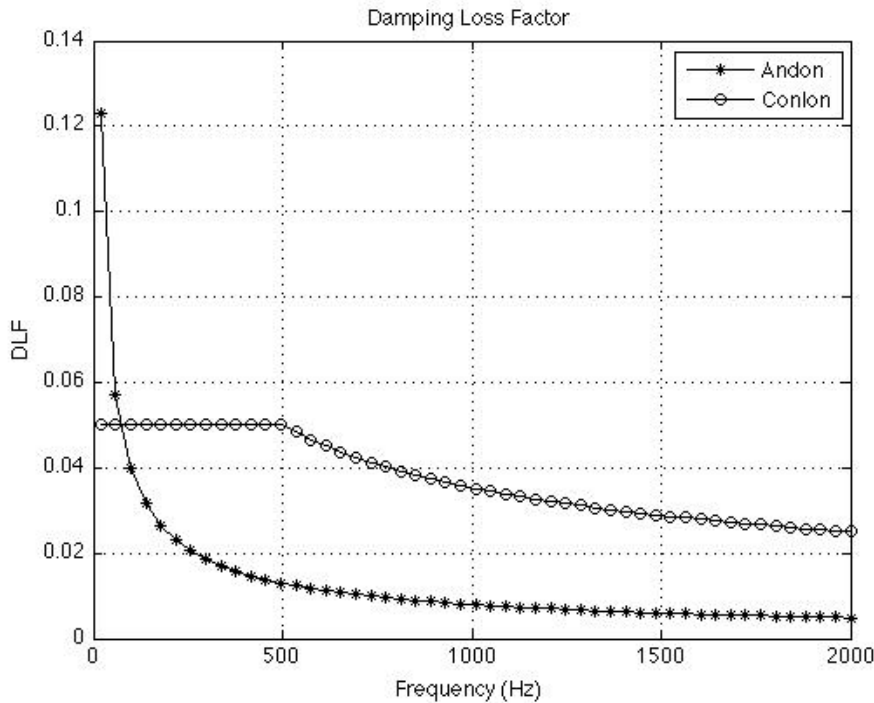


**Figure 9-37 : Damping Loss Factor loaded panel**

### 9.9.2.2 Panel wave speed, critical frequency and modal density

Two types of waves are essential for the propagation of structure-borne sound in plates: bending waves (phase speed  $c_B$ ) and shear waves (phase speed  $c_S$ ) [44]. The bending and shear wave speeds for a sandwich panel are given by:

$$c_B = \left( \frac{D}{m} \right)^{\frac{1}{4}} \sqrt{\omega}, \quad [9-46]$$

$$c_S = \left( \frac{Gh}{m} \right)^{\frac{1}{2}},$$

where  $D$  is the bending stiffness,  $h$  is the core thickness or depth and  $m$  is the mass per unit of area of the panel (pure panel mass  $M_p = mA_2$  is face sheets plus core plus bond) The equivalent shear modulus of the core is approximated by  $G = \sqrt{G_L G_W}$ , the geometric mean of the ribbon and warp direction values.

For isotropic face sheets the bending stiffness is  $D = Et_f(h+t_f)^2/2(1-\nu^2) \approx Eh^2t_f/2$  (Nm). The Young's modulus of the face sheets is indicated by  $E$  (Pa) and the thickness of the face sheet is  $t_f$  (m), The Poisson's ratio of the face sheet material is indicated by  $\nu$ .

The sandwich panel transverse or effective bending wave is [44]:

$$c_{Beff} = \frac{c_B^2}{c_S} \sqrt{-\frac{1}{2} + \frac{1}{2} \sqrt{1 + 4 \left( \frac{c_S}{c_B} \right)^4}} \approx \left( \frac{1}{c_B^3} + \frac{1}{c_S^3} \right)^{\frac{1}{3}}. \quad [9-47]$$

The approximation is accurate within  $\pm 1\%$ .

The critical frequency  $f_c = 2\pi\omega_c$  is by definition the frequency where  $c_{Beff}$  equals  $c$ , the speed of sound in air (or other medium).

The bending wave speed is dispersive and the shear wave speed is not. When the bending wave length is large compared to the thickness, then  $c_{Beff} \approx c_B$ . The critical (coincidence) frequency  $f_c$  becomes approximately:

$$f_c = \frac{c^2}{2\pi} \sqrt{\frac{m}{D}}. \quad [9-48]$$

The panel effective modal density can be written as [40] [44] :

$$n_2(f) = 2\pi n_2(\omega) = 2\pi A_2 \frac{f}{c_{Beff}^2} \left( 1 - \frac{f}{c_{Beff}} \frac{dc_{Beff}}{df} \right),$$

$$n_2(\omega) = \frac{A_2 \omega}{2\pi c_{Beff}^2} \left[ 1 - \frac{\left( \frac{1}{c_B^3} + \frac{1}{c_S^3} \right)^{-\frac{4}{3}}}{2c_{Beff} c_B^3} \right]. \quad [9-49]$$

### 9.9.2.3 Panel radiation efficiency

Following the NASA Lewis method [41] the average radiation efficiency  $\sigma_{rad}$  for baffled panels is:

$$\sigma_{rad} = \begin{cases} \left( \frac{f}{f_c} \right)^2 & f \leq f_c, \\ 1.0 & f > f_c. \end{cases} \quad [9-50]$$

One is encouraged to read more about similar prediction methods discussed in papers by Ando and Shi [38] [42] [45], which represents the prediction methods used by JAXA.

### 9.9.3 Quick way to predict fatigue life (Steinberg method)

Steinberg [46] proposed a step-by-step procedure to estimate in a quick way the fatigue life of structures exposed by random loads. A simple manner to apply random loads is illustrated in this example. The formal way to estimate fatigue characteristics are discussed in Chapter 12. The simple prediction method is based on the following theory.

Random vibrations have no repeating pattern. Rather, they are spread over a range of values from zero to  $\pm 3\sigma$  in three bands. Most of the vibrations are within band one for low-order accelerations from zero to  $\pm\sigma$ . Band two for medium-level accelerations from  $\pm\sigma$  to  $\pm 2\sigma$  contains a moderate number of vibrations. And band three for high-level accelerations from  $\pm 2\sigma$  to  $\pm 3\sigma$  contains the least number of vibration peaks. Statistically these acceleration levels  $X$  occur according to a Gaussian probability distribution curve:

$$p(x) = \frac{1}{\sqrt{2\pi}\sigma} \exp\left[ -\frac{(x-\mu)^2}{2\sigma^2} \right], \quad [9-51]$$

where, the average value is assumed to be zero  $\mu=0$  and  $\sigma$  the standard deviation. When the average value is zero the standard deviation is equal to the root mean square value of  $X$ . The number

of vibrations in each band is proportional to the areas under the curve. This is illustrated in Figure 9-38. According to the Gaussian distribution, probabilities for vibrations in the bands one, two and three are respectively.

$$\begin{aligned} P(-\sigma \leq X \leq \sigma) &= \int_{-\sigma}^{\sigma} p(x)dx = 0.683, \\ P(-2\sigma \leq X \leq -\sigma, \sigma \leq X \leq 2\sigma) &= \int_{-2\sigma}^{2\sigma} p(x)dx - \int_{-\sigma}^{\sigma} p(x)dx = 0.271, \\ P(-3\sigma \leq X \leq -2\sigma, 2\sigma \leq X \leq 2\sigma) &= \int_{-3\sigma}^{3\sigma} p(x)dx - \int_{-2\sigma}^{2\sigma} p(x)dx = 0.0433. \end{aligned} \quad [9-52]$$

These probabilities are used in to indicate the relative number of vibrations occurring in each band.

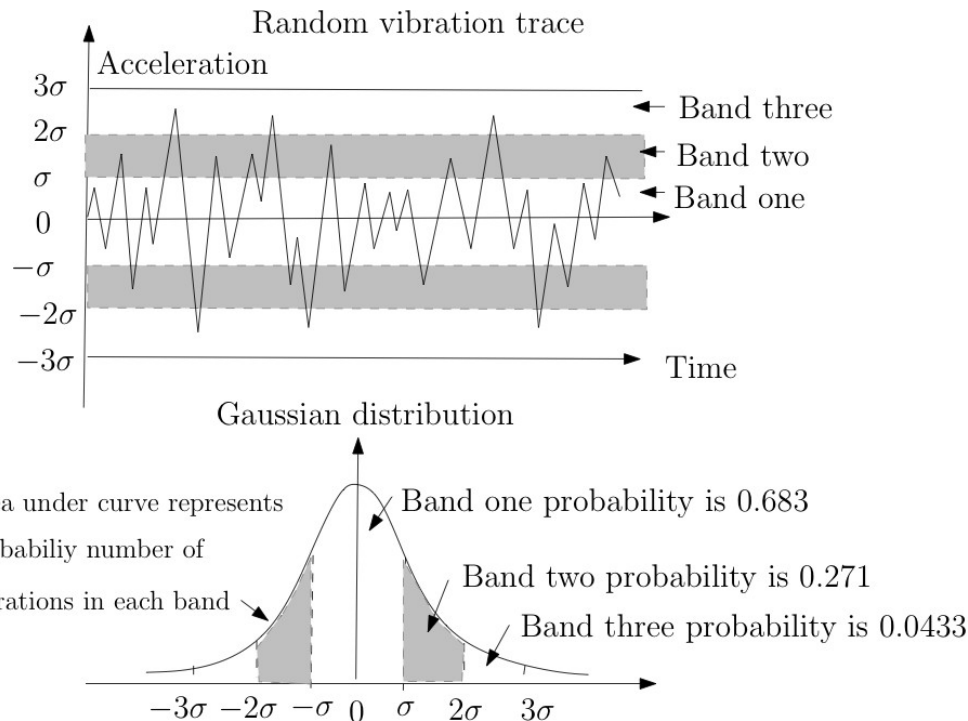


**Figure 9-38 : Random Vibration trace/distribution**

The following “three band technique”, however, is a much simpler way to predict the fatigue life of a randomly vibrating structural part. In this method, structural stress is determined from physical parameters, such as natural frequency, acceleration, and dynamic loading. These probable stress levels are then used to calculate the number of fatigue cycles required to produce failure. The nine basic steps in predicting the fatigue life of a structure in random vibration environment are described below in Table 9-9.

**Table 9-9: Steps for predicting fatigue life of a structure in random vibration environment**

Step	Task Definition
1	<p>Find the natural frequency <math>f_n</math> (Hz) of the structure. Natural frequencies of most simple structures can be calculated with standard equations and frequency tables.</p> <p>Natural frequencies may be determined empirically if a structural model of the structure cannot be made available.</p>
2	<p>Determine the amplification factor or transmissibility <math>Q</math> of the structure from testing or e.g. from [46]</p> $Q = A\sqrt{f_n}, \quad [9-53]$ <p>where <math>A</math> is usually dependent on the natural frequency <math>f_n</math> (Hz), and can be estimated for smooth plates as follows:</p> <ol style="list-style-type: none"> <li>1. <math>A = 0.5</math> for natural frequencies <math>f_n &lt; 100</math> Hz</li> <li>2. <math>A = 1.0</math> for natural frequencies <math>100 \leq f_n &lt; 400</math> Hz</li> <li>3. <math>A = 1.5</math> for natural frequencies <math>400 \leq f_n \leq 500</math> Hz</li> <li>4. <math>A = 2.0</math> for natural frequencies <math>f_n &gt; 500</math> Hz</li> </ol> <p>For simple beams supported on one or both sides, values of <math>A</math> for the same frequency ranges are twice those of the plate. For enclosed box-type of structures, the values are one-half of those listed for plates.</p> <p>In general, in instrument structure design the amplification factor is assumed as <math>Q = 10</math>.</p>
3	<p>Calculate with the aid of the Miles' equation the structure acceleration <math>\ddot{x}_{rms}</math> caused by random enforced acceleration <math>\ddot{u}</math></p> $\ddot{x}_{rms} = \sqrt{\frac{\pi}{2} f_n Q W_{\ddot{u}}(f_n)} \quad [9-54]$ <p>In this expression the power spectral density <math>W_{\ddot{u}}</math>, is the acceleration of random vibration distributed over the frequency range of the vibration.</p>
4	<p>Find dynamic (inertia) loading <math>F</math> from Newton's law</p> $F = M\ddot{x}_{rms}. \quad [9-55]$ <p>The inertia loads may be either discrete loads, or distributed as line, surface or volume loads for beams, plates and solids respectively. <math>M</math> is the total mass of the structural subsystem and the load is applied at the centre of gravity.</p>
5	Determine the critical location(s) from the geometry of the structure and the inertia loading $F$ .
6	Calculate the stresses at the critical locations. Stress concentration factors account for stresses concentrated in particularly vulnerable areas of the structure. This concentration factor is determined from the geometry of the structure. Values for most configurations are given in handbook tables by Pilkey [47].

Step	Task Definition
7	Find the number of fatigue cycles, $N_{1\sigma}$ , $N_{2\sigma}$ and $N_{3\sigma}$ , required to produce structural failure at each stress $1\sigma = rms$ , $2\sigma$ and $3\sigma$ , from the appropriate S-N fatigue diagram (Wöhler curve) for the applied material.
8	Determine the ability of the structure to withstand a life test of duration $T$ from $D = f_n T \left( \frac{0.683}{N_{1\sigma}} + \frac{0.271}{N_{2\sigma}} + \frac{0.0433}{N_{3\sigma}} \right). \quad [9-56]$ <p>If the cumulative damage <math>D</math> is less than 1.0 the design is satisfactory, and if the accumulated damage is <math>D &gt; 1.0</math>, the structure might not survive the vibration test and therefore should be redesigned.</p> <p>For more complex structure the finite element analysis method can be used to calculate in the structure, due to random loads, the root mean square responses and associated apparent or characteristic frequencies (number of positive zero crossings). The apparent frequencies may be considered as an equivalent natural frequency.</p>
9	Calculate the approximate time to failure $t$ $t \approx \frac{N_{3\sigma}}{0.0433 f_n}. \quad [9-57]$ <p>This approximate time to failure can be used to evaluate the ability of the structure to withstand particular vibration levels.</p>

## 9.10 References

- [1] Sarafin T.P. (editor), Spacecraft Structures and Mechanisms-from Concept to Launch, Kluwer Academic Publishers, Dordrecht, The Netherlands, 1995
- [2] Wijker J.J., "Random Vibrations in Spacecraft Structures Design, Theory and Applications", Springer, ISBN 978-90-481-2727-6, 2009
- [3] Ariane 5, "User's manual", ArianeSpace Issue 5, Revision 0, 2008
- [4] NASA-HDBK-7005, "Dynamic Environmental Criteria", March 13, 2001
- [5] ECSS-E-ST-32C "Space Engineering, Structural General Requirement", Rev. 1, 14 November 2008
- [6] Spann F., Patt P. (1984) "Component Vibration Environment Predictor" Journal of Environmental Sciences, pages 19-24, September/October 1984
- [7] Schaefer E.D., "Evaluating the Vibro-Acoustic Response of Honeycomb Panels", 19<sup>th</sup> Space Simulation Conference Cost Effective Testing for the 21<sup>st</sup> Century, NASA CP 3341, pages 195-204, 1996
- [8] Girard A., Imbert J.F., Moreau D. "Derivation of European Satellite Equipment Test Specifications from Vibro-Acoustic Test Data", Acta Astronautica, Vol. 19, No. 10, pages 797-803, 1989
- [9] Kasper J., Behar-Lafenêtre S., Laduree G., Laine B., Thamm H., Derivation of Satellite Equipment Design and Test Specifications from Random Vibration Environments, 11<sup>th</sup> European Conference on Spacecraft Structures, Material en Mechanical Testing, Toulouse, France, 15-17 September 2009

- [10] Kasper J., Derivation of Satellite Equipment Design and Test Specifications from Random Vibration Environments, ESA Contract No. 29502/06/NL/SFe, Title report "VibroSpec Methology & Tool" MTD.R & D.TN.2291, Issue1, 2010
- [11] ECSS-E-10-03A, "Space Engineering, Testing", European Corporation for Space Standardisation, 2002
- [12] Kasper J., Behar-Lafenêtre S., Laduree G., TRP VibroSpec-Final Presentation, Derivation of Satellite Equipment Design and Test Specifications from Random Vibration Environments, ESA Contract No. 29502/06/NL/SFe, 2010
- [13] Daneshjou K., Fakoor M., "Efficienct Algorithm for Reliability Analysis of Structures under Random Vibration", Journal of Solid Mechanics and materials Engineering, Vol. 1, No. 11, pages 1293-1304, 2007
- [14] Cook R.D., Malkus D.S., Plesha M.E., "Concepts and Applications of Finite Element Analysis", John Wiley & Sons, ISBN0-471-84788-7, Third edition, 1989
- [15] Elishakoff I., Zhu L. "Random Vibration of Structures by the Finite Element Method", Computer Methods in Applied Mechanics and Engineering, Vol. 105, pages 359-373, 1993
- [16] Craig R.R., "Structural Dynamics, An Introduction to Computer Methods", John Wiley, ISBN 0-471-87715-8, 1981
- [17] Meirowitch L. "Elements of Vibration Analysis", McGraw-Hill, ISBN 0-07-041340-1, 1975
- [18] Thomson W.T., Dahleh M.D., "Theory of Vibration with Applications", 5<sup>th</sup> edition, Prentice Hall, ISBN 0-13-651068-X, 1998
- [19] Ihle A., Grillenbeck A., Hamdi M.A., Random Vibration Environment Derivation by Vibro-Acoustic Simulation, Final Report, ESA Study Contract 20731/07/NL/SFe, VASI-HPS-RP-010, Issue 1, 2009
- [20] NASA Practice No. PT-TE-1413, "Random Vibration Testing", NASA Preferred Reliability Practices
- [21] Notching Philosophy for Random Vibration Prediction / Correlation for Acoustic Test, CNES Presentation, DCT/TV/SM - 2012 - 17983
- [22] Davis G.L., "An analysis of nonlinear damping and stiffness effects in force-limited random vibration testing", Rice University, Ph.D. Thesis, 1998
- [23] Destefanis S. "Improvement of Force Limited Vibration, Testing Method for Equipment/Instrument Unit Mechanical Verification", Final report ESTEC Contract No. 20689/07/NL/CP, SD-RP-AI-0643, July 2009
- [24] Scharton T.D., Force Limited Vibration Testing Monograph, NASA (Reference Publication) RP-1403, 1997
- [25] Soucy Y., Dharanipathi V., Sedaghati R., "Investigation of Force-Limited Vibration for Reduction of Overtesting", Journal of Spacecrft and Rockets, Vol. 43, No. 4, pages 866–876, 2006
- [26] Soucy Y., Singhal R., Lévesque D., Poirier R., Scharton T., "Force Limited Vibration Testing Applied to the Fourier Transform Spectrometer Instrument of SCISAT-1", Canadian Aeronautics and Space Journal, Vol. 50, No. 3, pages 189-197, 2004
- [27] Soucy Y., Chesser H., "Force Limited Vibration Testing Applied to the MOST Spacecraft", Canadian Aeronautics and Space Journal, Vol. 51, No. 2, pages 47-60, 2005
- [28] Kirkham S., "The boundary Element Method in Acoustics", Integrated Sound Software, ISBN 0953403106, on line [www.kirkup.info/papers/indexr.htm](http://www.kirkup.info/papers/indexr.htm) and [www.boundary-element-method.com](http://www.boundary-element-method.com), 2007
- [29] Lyon R.H., Maidanik G., "Power Flow between Linearly Coupled Oscillators", Journal of Acoustical Society of America, Vol. 35, No. 5, pages 623-639, 1962

- [30] Keane A.J., Price W.G., "Statistical Energy Analysis, An Overview with Applications in Structural Dynamics", Cambridge University Press, ISBN 0-521-55175-7, 1994
- [31] Lyon R.H. "Statistical Energy Analysis of Dynamical Systems: Theory and Applications", MIT, ISBN 0-262-12071-2, 1975
- [32] Rioboo J.L., Lopez-Diez J., Chimeno-Manguan M., Random Vibration Environment Derivation by Vibro-Acoustic Simulation (RANDERIV), Final Report, ESA Study Contract 20779/07/NL/SFe, ECE-RDR-TNO-0017, Issue 1, 2009
- [33] Irvine T. "An Introduction to the Vibration Response Spectrum", Revision D, Vibrationdata.com, 2009
- [34] Shinozuka M., "Simulation of Multivariate and Multidimensional Random", The Journal of Acoustical Society of America, 49(1), pages 357-368, 1971
- [35] Shinozuka M., Jan C.M., "Digital Simulation of Random Processes and its Applications", Journal of Sound and Vibration, 25(1), pages 111-128, 1972
- [36] Miles R.N., "Effect of Spectral Shape on Acoustic Fatigue Life Estimates", Journal of Sound and Vibration, 153(2), pages 376-386, 1992
- [37] GSFC-STD-70000, "General Environmental Verification Standard (GEVS) for GSFC Flight Programs and Projects", April 2005
- [38] Ando S., Shi Q., Nagahama K., Saitoh M., Saegusa H., "The Prediction of Random Acoustic Vibration of Equipment Mounted on Honeycomb Panel", European Conference on Spacecraft Structures, Materials & Mechanical Testing", 10-12 May, Noordwijk, Netherlands, ESA SP-581, pages 1-5, 2005
- [39] Conlon S.C., "Response of Non-Homogeneous Panels with Complex Attachments to Diffuse Acoustic", The Pennsylvania State University, The Graduate School, College of Engineering, Master of Science Report, 2000
- [40] Conlon S.C., Hambric S.A., "Predicting the Vibroacoustic Response of Satellite Equipment Panels", Journal Acoustical Society of America, Vol. 113, Nr. 3, pages 1455-1474, 2003
- [41] McNelis M.E., "A Modified VAPEPS Method for Predicting Vibroacoustic Response of Unreinforced Mass Loaded Honeycomb Panels", NASA TM-101467, 1989
- [42] Shi Q., Ando S., Tsuchihashi M., Saitoh M., "Introduction of JAXA Tool for Rando, Vibrations Prediction and its Recent Upgrading", 1<sup>st</sup> CEAS European Air and Space Conference, CEAD-2007-085, pages 2339-2343, 2007
- [43] Norton M., Karczub D., "Fundamental of Noise and Vibration Analysis for Engineers", Cambridge University Press, ISBN 0-521-49913-5, 2003
- [44] Rindel J.H., "Dispersion and Absorption of Structure-Borne Sound in Acoustically Thick Plates, Applied Acoustics, Vol. 41, pages 97-111, 1994
- [45] Ando S., Shi Q., "Prediction of Acoustically Induced Random Vibration Response of Satellite Equipments with Proposed Asymptotic Apparent Mass", Journal of Space Engineering, Vol. 1, No.1, pages 12-21, 2008
- [46] Steinberg D.S., "Quick Way to Predict Random Vibration Failures", Machine Design, pages 188-191, April 1978
- [47] Pilkey W.D., "Peterson's Stress Concentration Design factors", Wiley Interscience, ISBN 0-471-53849-3, 1997

# 10 Shock

## 10.1 Introduction

During the launch and deployment operations in the very early orbit phase the satellite is subjected to several energetic shock events: launcher stages separation, fairing jettisoning, separation of the satellite from the launcher (e.g. clampband release), and deployment of appendages such as solar arrays, antennas or scientific instruments on deployable booms. The severity of the shock, in particular the high frequency energy content, can become a source of concern for the design of particular shock sensitive equipment and instrument units. However, not only the definition of the environment but also the analysis and test verification is a complex task.

The relevant aspects of mechanical shock design and verification are discussed in detail in the "ESA Mechanical Shock Design and Verification Handbook", [1], where the current know-how on mechanical shock design and verification is documented. Only a brief summary is provided in this chapter to introduce the subject and to provide an overview of applicable methods and procedures.

## 10.2 Shock environment

Shocks are a transient mechanical loading characterised by very short duration, high frequency content and high acceleration amplitudes with rapid initial rising times. The typical processing of shock data consists of the acquisition of the related acceleration time history and the subsequent conversion of the time domain data into a shock response spectrum (SRS).

Potential damaging effects of shocks have been identified as follows:

- Impact on electronics: PCB malfunction due to failure or degradation of electronic components such as e.g. relays, quartz, transformer;
- Structural impact on materials: cracks and fractures in brittle materials (ceramics, crystals, epoxies or glass envelopes), local plastic deformation, or accelerated fatigue of materials for repeated shocks;
- Impacts on mechanisms: degradation of performances of known shock-sensitive items as bearings, gears, worm wheels and endless screws;
- Impacts on valves: unintended leakages in quantity and time and structural degradation resulting to a malfunction of the valve mechanism.

## 10.3 Shock design and verification process

The process of shock design and verification is illustrated in Figure 10-1, [1].

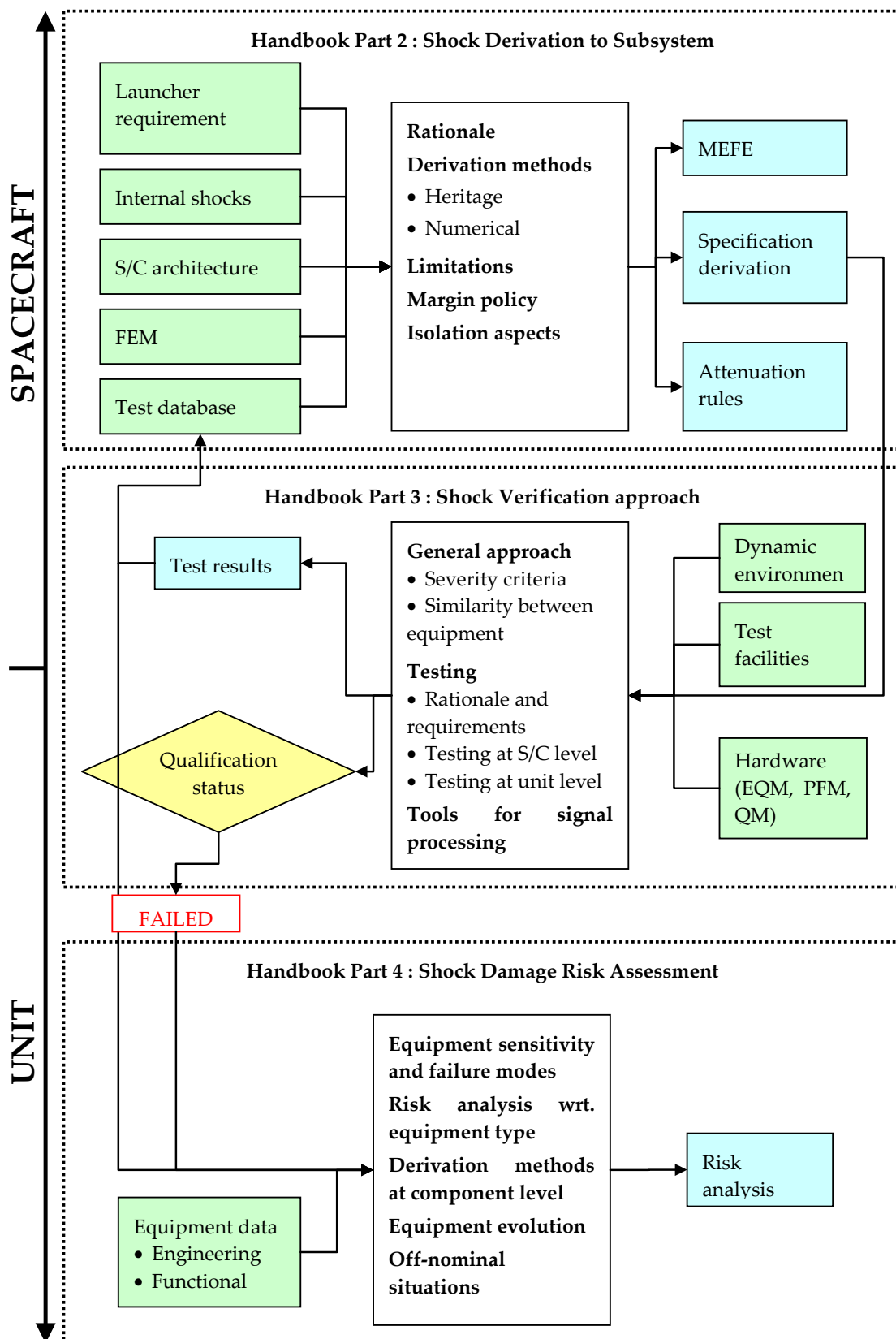


Figure 10-1: Overall logic of shock design and verification process, [1]

The shock design and verification process commences with the derivation of the spacecraft shock environment for equipment and instrument units and subsystems. The main inputs are relevant information on shock sources such as the launcher shock specification and spacecraft internal shock environments and the expected shock transmission due to the spacecraft architecture. The objective is to determine the shock environment for each unit of the spacecraft and based on this information to derive a specification using a given margin policy.

The second step of the shock design and verification process focuses on the shock verification approach. The objective is to prove that the specimen (at unit or system level) sustains the required shock environment. This may be done either by analysis or by testing. Ideally the capability of the spacecraft to withstand or, if appropriate, to operate in the induced shock environments is demonstrated after this operation and, as a consequence, the shock qualification can be considered achieved.

However, there might be cases where the required shock qualification cannot be directly achieved (i.e. the shock environment cannot be completely validated by system level and unit level testing). In general, this problem is discovered too late in the course of a space project to perform a delta qualification at unit level. As a result, a Shock Damage Risk Assessment (SDRA) might be required. This constitutes then the third step of the shock design and verification process. The SDRA focuses on assessing the consequences of shock environments on equipment and instrument units. Particular attention is given to equipment shock-sensitivity and failure modes. The main output is a risk assessment which concludes on the flight-worthiness of the concerned unit.

### 10.3.1 Shock input derivation to subsystems

The different shock events can be separated in two different categories as shown in Figure 10-2 :

- shocks during service life (launch and early on-orbit phase);
- shocks related to testing at subsystem/equipment and system level.

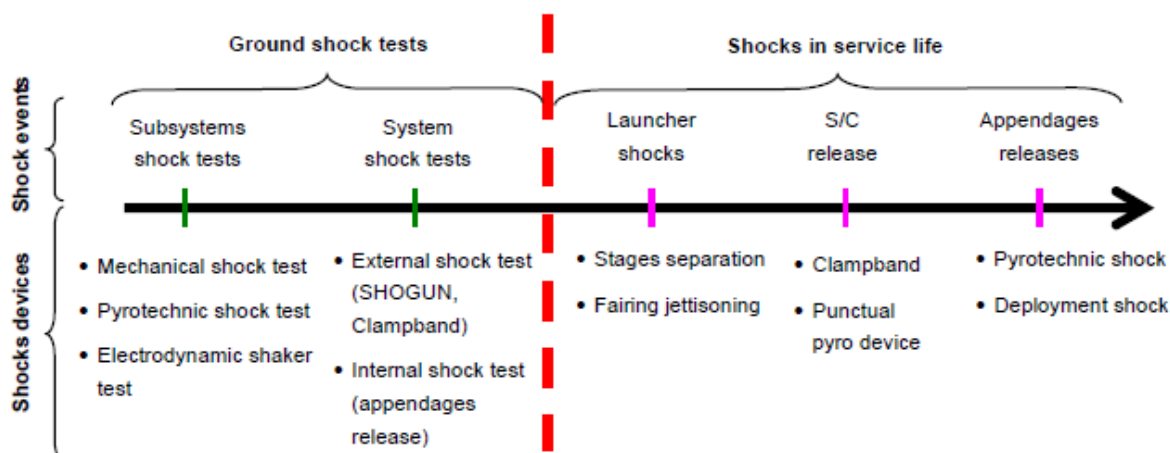


Figure 10-2: Shock events encountered by the spacecraft during its life, [1]

Although the state of the art for shock environment predictions in spacecraft has not yet reached the same level of maturity as for other mechanical disciplines, in particular due to the high-frequency nature of pyro-shocks, recent advances in prediction techniques have brought more confidence and a better understanding of this environment. Nevertheless a consolidated shock environment can be derived provided a consistent approach is strictly followed. This goal can be achieved through similarity-heritage-extrapolation based on past experiences (considering already tested spacecraft

structures presenting similar architecture, design and/or configuration) and through good engineering practices in applying shock predictions by FE analysis.

These methods are more precisely defined hereafter:

- **Similarity-heritage methods** evaluate shock levels using data from different structures considered as similar for possibly different (but physically similar) shock sources. Such methods are usually used early in a programme when no data on the studied structure is available. The validity of this analysis depends strongly on the degree of similarity between the structure studied and the reference structure(s).
- **Extrapolation methods** evaluate shock levels using data for the same structure for possibly different (but physically similar) shock sources. Such methods are usually used later in a programme when some shock tests have been performed on e.g. the Structural Model or representative structures.

After the expected shock environment has been derived with sufficient confidence the shock specification for equipment or subsystems can be established. The most common way to specify a shock test is the use of the **maximax Shock Response Spectrum (SRS) with a standard Q-factor of 10**. The SRS is considered the simplest method to compare severities and damage potential between shocks.

For qualification testing purposes the derived SRS (supposed to cover the maximum predicted or expected shock environment during the operational life of the item) is usually increased by a minimum margin of 3dB. Due to significant variability of shock measurements for near and medium-field as compared to far-field shocks the qualification margin is often recommended to be even up to 6dB.

In the case the design of the equipment or instrument unit is incompatible with the shock specification then shock isolation measures need to be considered to significantly reduce the shock transmitted to the unit interface.

### 10.3.2 Shock verification approach

Part 3 of [1] provides a detailed review of the shock verification principles. The scheme presented in Figure 10-3 aims at presenting in a synthetic way the general approach of shock verification.

This scheme is based on **several questions** to be answered, represented by the *yellow diamonds* ♦ :

- **Is the equipment a new one ?** – If yes, then heritage for the considered equipment might be present.
- **Is the equipment similar ?** – In case of a heritage the degree of similarity between the considered equipment and the equipment of the same family should be evaluated.
- **Is the equipment sensitive ?** – If the equipment is a new development or the degree of similarity is insufficient then the equipment sensitivity should be determined.
- **Has the capability to withstand the qualifying shock been demonstrated ?** – The fourth question deals with the capability to withstand the qualifying shock with respect to the available data. It is independent of the qualification approach being chosen.

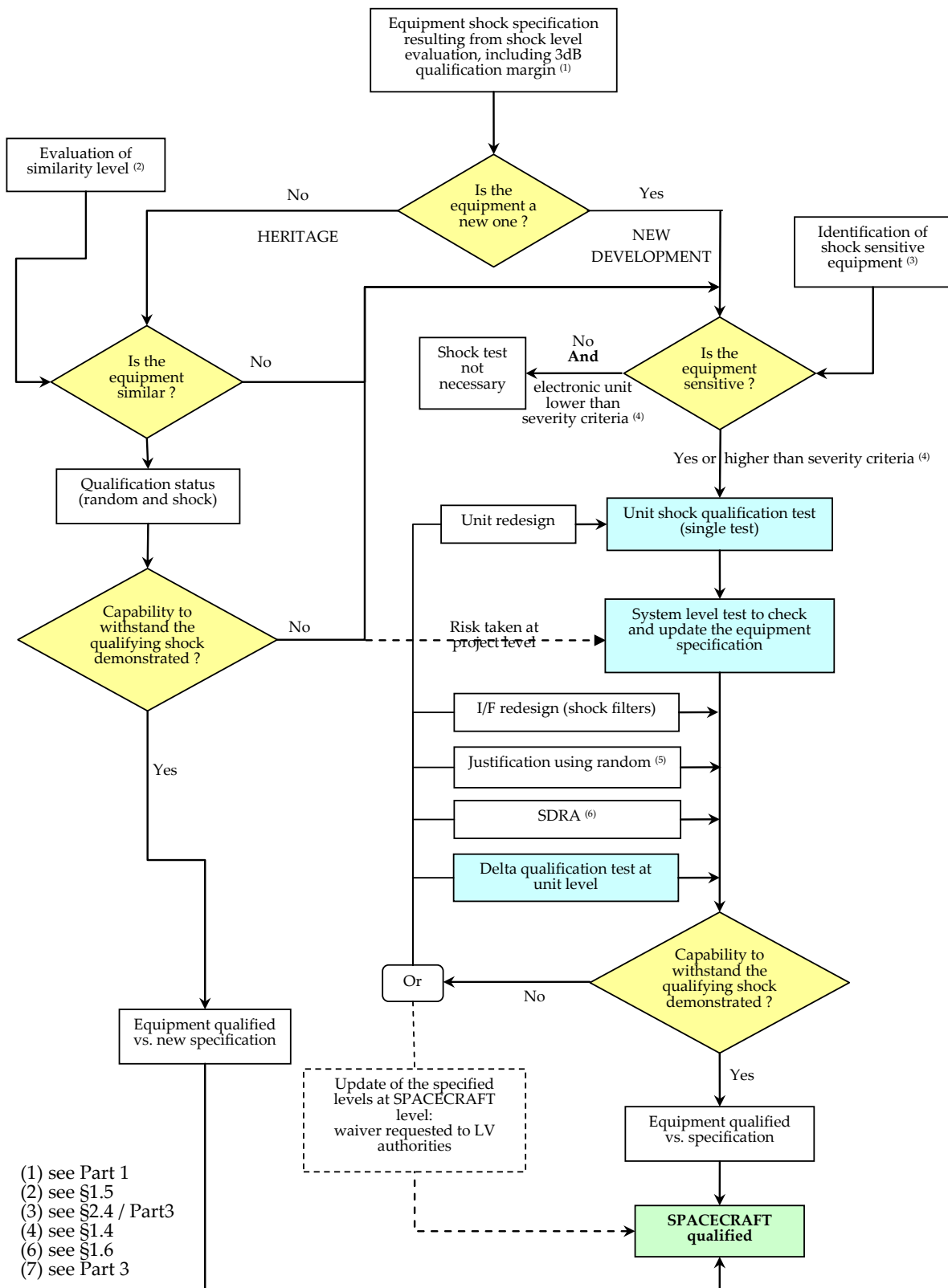


Figure 10-3: Principle of shock verification, [1]

The shock test campaigns involved in the shock verification are depicted by *blue squares* ■ :

- The unit qualification shock test aims at qualifying the considered equipment at its own qualification level.
- The system level test (generally clampband release on Structural or Flight Model or Shogun on Structural Model) aims at consolidating the different equipment shock specifications. It can also be used as an acceptance test for equipment not sufficiently verified at the unit level, with the condition that the associated risk is clearly identified or properly assessed.
- Delta qualification test at unit level might be necessary in case the capability to withstand the qualifying shock has not been demonstrated by the first qualification test. It can consist in changing test facility, test conditions or input level to meet the required levels.

In case the capability to withstand the qualifying shock has not been demonstrated, several possibilities exist:

- As previously mentioned a delta qualification test at unit level can be performed in order to reach the specified levels.
- Another way is to modify the design. This can be done either internally to the equipment or at its interface. Dedicated internal redesign can be looked at if the failure cause has been well identified. Interface redesign typically consists in adding a shock attenuation system to reduce the shock levels at the equipment base. In both cases a redesign is a difficult task especially as this design modification is decided late in the programme.
- A third way is a Shock Damage Risk Assessment (SDRA) which aims at evaluating the risk incurred by the equipment with respect to the known shock levels. Such a task is only chosen as a last resort since it bypasses the standard qualification process and represents a risk for the equipment. In this regard, the SDRA drives automatically the unit away from the qualification domain; but it either provides valuable data to ensure a successful qualification (in view of a sub-system or system level qualification test), or it provides a risk assessment on the capability of a spacecraft/equipment to withstand (or not) the required shock environment without damage.
- The three precedent ways focus on the equipment. A fourth way might be chosen by reviewing the specified levels. This is usually done by a waiver requested to launcher authorities: the aim is to reduce the specified levels at the base of the spacecraft using better knowledge of the real excitation. This is always hazardous as such waivers are seldom accepted.

The approach to be finally implemented depends on the following key issues:

- heritage for the considered equipment;
- degree of similarity between the considered equipment and the equipment of the same family in case a heritage has been identified;
- equipment sensitivity in case the equipment is a new development or the degree of similarity is insufficient to base its qualification on heritage;
- finally, independent of whichever qualification approach has been chosen the assessment on the basis of the available data whether the item is capable to withstand the qualification shock.

When reviewing the shock qualification status of equipment it is of outmost importance to assess whether the equipment is sensitive to shock. This is decisive with respect to the equipment shock verification approach. Only non-sensitive equipment may be waived to undergo shock testing provided the specified shock environment is sufficiently low. Shock sensitive equipment may be determined using the list of elements that are particularly sensible to shocks, see Table 10-1.

As a general rule all units should be demonstrated to be compatible with their shock environment. However, such a process does not always require a shock test, e.g. for the particular case of very low shock levels and non-sensitive units.

Shock severity criteria have been defined below which the unit is considered safe with respect to shock and for which no shock test is required. Unit types have been categorized in order to define such severity criteria: electronic units, structural or non-sensitive equipment and other types of equipment.

Furthermore, the unit random test specification (PSD) might be converted into an equivalent shock environment. Some difficulty might arise from the stochastic nature of the random vibrations as compared to shocks being deterministic. Ref. [1] imposes however the restriction that the approach to demonstrate coverage of a shock environment by the random environment may be only used after unsuccessful shock test at subsystem or unit level.

Shock tests are usually performed at subsystem / equipment unit level and at system level, respectively. For subsystem / equipment unit shock testing either mechanical and pyrotechnic shock machines or electro-dynamic means (shaker) may be used. The latter qualifies equipment to shocks by applying short excitation pulses, however with significant limitations in terms of level and frequency band capacities as compared to the specified shock environment. For dedicated shock tests at spacecraft system level (other than e.g. the clampband release shock test) the SHOGUN device might be used which is a specific shock generating device to represent Ariane 5 launcher shocks, especially fairing separation.

Where the capability to withstand the qualification shock environment has not been demonstrated several options exist to nevertheless declare the unit ready to fly:

- performance of a delta qualification test;
- modifications of the design followed by a qualification shock test;
- performance of a Shock Damage Risk Assessment (SDRA), see Section 10.3.3 here below;
- review of the shock specification to identify potential over-conservatisms.

### 10.3.3 Shock damage risk assessment

The Shock Damage Risk Assessment (SDRA) is required in such cases where the qualification of the equipment or instrument unit with respect to the shock specification could not be achieved by performing relevant analyses or tests. The SDRA rationale is shown in Figure 10-4.

The SDRA is built on a good knowledge of failure modes of shock sensitive equipment, on good engineering practices for the derivation of shock level at components interface, and for the identification of the qualification status of the shock sensitive equipment. It should be emphasized that a SDRA by itself cannot substitute for qualification, however it can provide an assessment whether or not the spacecraft can withstand the required shock environment without damage/degradation.

The level of confidence in a SDRA is directly and obviously related to the conservatism considered for the various analysis parameters. In particular due to the high frequency nature of pyro-shocks there are significant uncertainties associated with the analysis or simulation of the induced phenomena. This affects the credibility of derived safety margins and the estimation of relevant probability risk levels. However, the SDRA might provide either valuable data to ensure a successful qualification (in view of a sub-system or system level qualification test) or a relevant risk assessment on the capability of a spacecraft / equipment to withstand (or not) the required shock environment without damage.

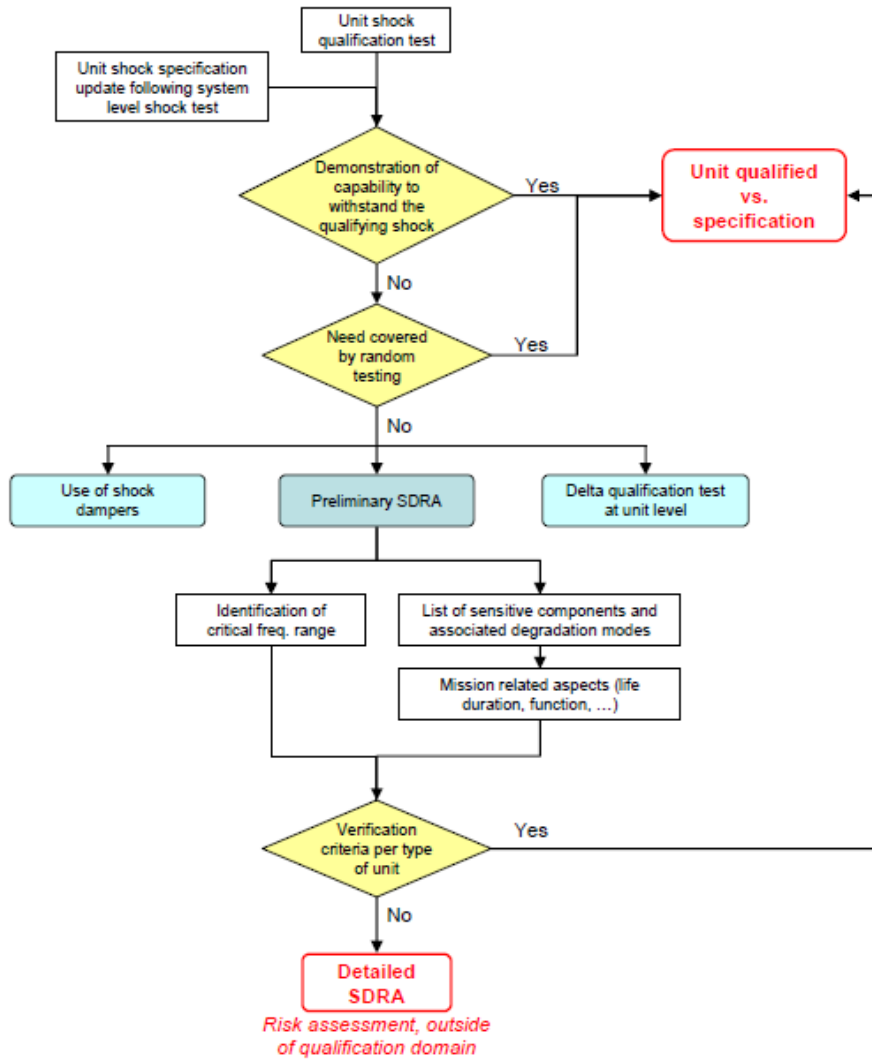


**Figure 10-4: Rationale of shock damage risk assessment, [1]**

The first step to assess the susceptibility of equipment to pyro-shocks consists in an immediate screening of equipment criticality with respect to shock, and in the identification of the associated critical frequency ranges. The evaluation of damage risk with respect to shock is built on:

- good engineering practices for the derivation of qualification shock levels at unit interface;
- the identification of the critical frequency ranges;
- good knowledge of failure modes of shock sensitive equipment;
- good engineering practices for the identification of the compatibility status of the shock sensitive equipment, based upon a set of general evaluation criteria and taking into account the type of equipment;
- the consideration of mission related aspects.

Based upon experiences gained from unit development / qualification testing, failure case histories and engineering judgment relevant rules for failure modes of shock sensitive components have been established. Shock sensitive electronic components are listed here below in Table 10-1.

Once this first step has been achieved a detailed analysis should be performed in order to quantify more precisely the damage risk with respect to shock on all the units that have been identified as

potentially sensitive. A complete evaluation of the sensitivity against shock requires the knowledge of parameters such as:

- units design via engineering drawings, unit architecture (especially for electronic boxes with detailed description of PCB, components, mounting technologies);
- geometrical data, material, mass and stiffness properties;
- dynamic behaviour as resonant frequencies, Q factors, preferably obtained from sine survey test or random test on FM units (or QM only if FM data not available) or from FEM analysis. If both are available, a test-analysis comparison is recommended in order to assess whether the FEM is correlated and trustful to derive parameters usually not measured as e.g. effective masses, effective transmissibilities, and mode shapes;
- function description, mission criticality;
- qualification data as equivalent SRS derived from random qualification levels;
- heritage shock data from similar units by subcontractor's data;
- identification of the aforementioned unit category and subsequent comparison with the foreseen qualification shock levels derived by scaling the measured levels to the flight levels and adding the required qualification margin.

**Table 10-1: Shock sensitive components [1]**

Electronic components	Damage modes			
	Mode 1	Mode 2	Mode 3	Remarks
Relay	Bouncing	Temporary or permanent transfer	Non reversible mechanical damage	
Quartz	Relief of residual stress in the quartz ⇒ frequency shift that can be temporary during the shock application or definitive	Solder overstress or adhesive crack at clip interfaces	Broken crystal	Quartz are usually mounted on a damping material
Magnetic components (RM) Transformer and self	Crack initiation in ferrite			Heavy component in general The internal part is fragile, in particular if the component is composed of ferrite or ceramic
Hybrid	Particle transfer	Rupture of small bonded parts (getters, absorbers)	Solder over stress at attachment level	Particles in hybrids are detected by a PIND test
Tantalum capacitor	Bending of the PCB leading reversible electrical peak of current due to local destruction of the dielectric	Bending of the PCB leading to internal over-stresses with non-reversible total destruction by short circuit		
Heavy component	For heavy components, overstress at the attachment due to loads e.g. capacitor, transformer			
Optical components	Fibre optic pigtail cleavage	Damaged fibre surface in connectors		
Low insertion force DIP socket	Disjunction of the component			
Semiconductors (IC) components, Hybrid components, relays, capacitors with cavities	Dislodging of mobile particle			

## 10.4 References

- [1] ESSB-HB-E-005, "ESA Mechanical Shock Design and Verification Handbook", Issue 1, April 16 2012.

# 11

## Dimensional stability

---

### 11.1 Introduction

In general highly dimensionally stable structures are needed for current and future space telescope or Earth observation missions with stringent pointing requirements. Dimensional stability is best described as the behaviour of highly accurate structures to maintain their dimensions under all kinds of conditions like mechanical loads, temperature, humidity, vacuum, irradiation and chemical environment. The dimensional changes should usually be limited to a few microns.

The "ESA Pointing Error Engineering Handbook", [1], describes the relevant engineering guidelines and procedures to establish the satellite system pointing error budget taking into account the effects of even small deviations of the structure dimensions from the nominal configuration.

Particular contributors affecting the dimensional stability of satellite structures have been identified as e.g. thermo-elastic effects, moisture release, 1g-0g environment transition, in-orbit loads, material ageing (material property changes), and material dimensional instability. As an example a list of error sources is provided in Table 11-1 affecting the GRACE satellite centre of gravity position which should be exactly at the proof mass centre location to avoid unacceptable measurement disturbances.

According to ECSS-E-ST-32C Rev.1 [2] the dimensional stability requirements address the short, medium and long term alignment stability of a space structure under the operational environment. Dimensional stability of the structure is necessary to conform to mission specified system and payload requirements, e.g. by ensuring that no loss of the alignment of the structure occurs by the action of applied loads (e.g. launch loads, deployment loads, thermal, moisture release) which might jeopardize or degrade the mission objectives.

**Table 11-1: Error sources for GRACE spacecraft centre of gravity position**

Error source	Dx [mm]	Dy [mm]	Dz [mm]
COM Measurement uncertainties	0.200	0.200	0.200
Remaining unbalanced	0.067	0.042	0.021
Accuracy Of Tank Mounting	0.076	0.076	0.076
Difference in Tank volume	0.010	---	---
1g/0g effects---gravity	0.105	0.042	0.049
1g/0g effect---temperature	0.083	0.004	0.027
Moisture Release CFRP / shrinkage	0.053	0.021	0.011
Moisture release CFRP / mass decrease	---	---	0.038
Moisture release foam / mass decrease	---	---	0.078
Shrink due to moisture release of foam	---	---	0.008
Sum of other sources (uncertainty boom position, buoyancy)	0.123	0.053	0.053
RMS value of error	0.270	0.230	0.240
Requirement	0.500	0.500	0.500

## 11.2 Dimensional stability analysis

The dimensional stability analysis (DSA) evaluates the effects of environmental as well as material changes on the stability behaviour of the structure and provides relevant stability figures for each configuration that can be encountered for the studied structural item. Environmental effects include thermo-elastic deformations and 1g-0g transition (gravity release). Geometrical changes of the satellite structure due to moisture release are a concern for in particular composite materials.

The latter effects are well predictable by relevant analyses. Only these predictable effects are further covered in this chapter together with the corresponding test verification approaches.

However, there are other causes for the satellite structure to deviate from the on-ground aligned configuration which are not easily quantifiable. These are in particular:

- potential micro-slipping for bolted joints or creep when being exposed to the launch loads;
- ageing of materials (including e.g. internal stress release or internal micro-creep of material).

The structure dimensional stability might be of a transient or permanent nature depending on the events causing the deviation from the nominal satellite configuration.

The DSA is used for the understanding of the performance status within the project development and to identify in time any potential criticality with respect to stability requirements, and it constitutes an input for the final stability budget. Assessments of the uncertainties on these figures are usually performed to define the probable range of structural deformations.

In general the DSA should provide the following information in order to demonstrate the structure compliance with the dimensional stability performance requirements:

- identification of the reported dimensional stability performance figure together with the associated requirement,

- justification of the derived value, i.e. either computed, measured (accompanied by relevant information regarding the associated test conditions), or estimated based on past experience,
- identification of the loading case (setting, micro-sliding when submitted to launch or test environment ; thermo-elastic or hygro-elastic load case), and
- identification of the reference frame used for the dimensional stability performance description.

## 11.2.1 Thermo-elastic distortion analysis

### 11.2.1.1 Introduction

Thermal loads may be defined as the internal loads in a structure caused by the expansion or the contraction (or both) of certain structural elements when being exposed to a temperature field which deviates from the one where the same structure is stress free (in general the temperature at which the structure parts have been assembled, usually being the room temperature). The resulting thermal stresses may become a serious concern for static strength verifications of the structure with respect to the applicable thermal load cases.

However, when performing thermo-elastic distortion analyses the main interest is focussed on determining the deformations of the structure due to the thermal loads rather than verifying sufficient static strength. In most cases the thermo-elastic distortion analyses are performed by means of finite element analysis where the required information is obtained from the displacements calculated at the finite element nodes.

The change of the geometrical configuration which a structure undergoes under the influence of thermal loads is expressed by the following simple relation

$$\Delta L = \alpha * \Delta T * l_0 \quad [11-1]$$

where  $\Delta L$  is the change in length which depends on the original length  $l_0$  of the structural element, the Coefficient of Thermal Expansion (CTE)  $\alpha$ , and the applied temperature change  $\Delta T$ .

The CTE is therefore a particularly critical model parameter for the thermo-elastic distortion analysis since it determines the amount of structure elongation or shrinkage, respectively, under the influence of thermal loads. It is a characteristic material property to be provided for the analytical predictions e.g. on Nastran MAT bulk data cards. CTE values are well known for metallic materials. However, in the case of composite structures the specific direction-dependent CTE values for the laminate lay-up are generally obtained from coupon and component tests in the early structure design and development phase.

The analysis boundary conditions should adequately represent the structure constraints applicable to the spacecraft configuration when the thermal load case to be analysed occurs during launch or on orbit. The most common application of the thermo-elastic distortion analysis for spacecraft structures however concerns the on-orbit configuration. In that case the boundary conditions should properly reflect the free-free situation where no displacement constraints exist to take any reaction forces. Nevertheless, constraints preventing rigid body motions are required for performing linear static analyses. So-called iso-static boundary conditions form a suitable solution.

### 11.2.1.2 Thermo-elastic model verification

The adequacy of the finite element model should be demonstrated by performing relevant model checks. The main purpose of these checks is to verify that no artificial, i.e. non-physical constraints of the thermo-elastic analysis model are present which might invalidate the analysis results.

In the past such constraints were typically generated by so-called multiple-point constraints (MPC, e.g. Nastran RBE2 elements) which are frequently applied in structural analysis to simplify the modelling of quasi-rigid structures. Only recently relevant improvements were made to these rigid body elements allowing for the definition of a CTE value and therefore for thermal expansion under thermal loads, thereby also avoiding to introduce non-physical constraints in the case that these elements had a non-zero length. Proper care should be nevertheless taken to either replace these MPC's by adequate physical elements with thermal expansion properties for the thermo-elastic analysis or to use the new rigid elements together with the activation of their specific thermo-elastic properties.

The most common model check is the "zero stress check" the purpose of which is to verify that the model to be used for the thermo-elastic analysis is well conditioned and suitable for thermo-elastic analysis. This check verifies that no residual stresses occur for the following specific model characteristics:

- the model is iso-statically constrained;
- all the materials used in the model have been replaced by fictitious homogenous and isotropic ones with the following properties:
  - Young's Modulus = 100 GPa
  - Poisson's Ratio = 0.3
  - CTE =  $10^{-5}$  m/m/°C
- all elements have the same reference temperature  $T_{ref} = 20$  °C
- uniform temperature increase of  $\Delta T=100$  °C is applied to the complete model.

Besides the verification of the model for the thermo-elastic analysis it is also important to verify the numerical integrity of the finite element model, in particular the resulting maximum stresses and rotations anywhere in the model should comply with the following values:

- maximum stresses:  $\leq 100$  Pa
- maximum rotations:  $\leq 10^{-4}$  rad

### 11.2.1.3 Specific thermo-elastic modelling aspects

In general the thermo-elastic analysis predictions at satellite level are performed with the finite element models developed for strength or dynamic analyses. However, these models are frequently not well suited for executing thermo-elastic analyses where good confidence in the results obtained is required. To compensate these deficiencies a conservative margin policy might be necessary to be applied in order to demonstrate that the thermo-elastic performances are compatible with the mission requirements.

Typical thermo-elastic model inadequacies might result e.g. from the standard practices applied to the modelling of the interfaces between equipment and payload units and their mounting structure but also from the representation of these units as commonly done for the purpose of static and dynamic analyses at satellite level.

In Figure 11-1 the typical design of spacecraft panel / equipment interfaces is shown. The attachment area involves a number of single constitutive items with (partially) quite different mechanical and thermal properties such as the bolt, the insert, the washers, the potting and the glue. As a result, the total assembly of these items composes a complex joint when subjected to thermal loads.

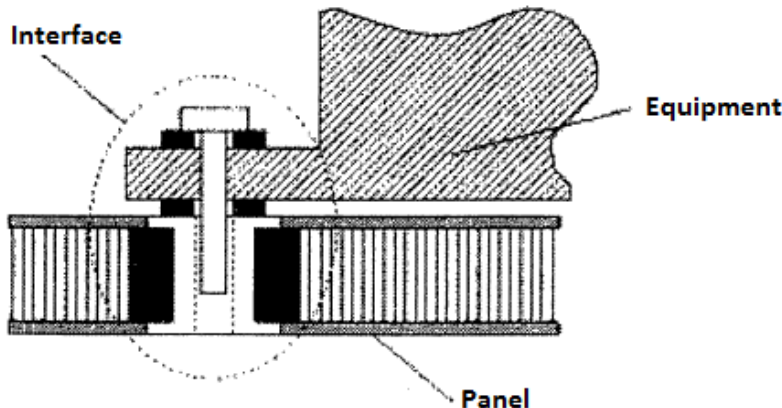


**Figure 11-1: Typical design of spacecraft panel / equipment interface, [6]**

Potential uncertainty sources are the material property dispersion and the modelling of the panel, equipment and attachment area, respectively.

The material property dispersions are in general negligible for metallic materials; however they might be significant for composite materials where the mechanical and thermal properties are depending on several parameters as e.g. the fibre orientation, the fibre mechanical and thermal characteristics and the resin volume.

The satellite panels are usually modelled with 2D plate elements rather than 3D elements in order to keep the satellite model size manageable. This can be considered adequate in most cases for the static and dynamic analyses but it might introduce significant errors into the thermo-elastic predictions for particular panel configurations. The latter applies in particular to sandwich panels where the face sheets material (e.g. CFRP) might be different from the core material (e.g. aluminium honeycomb).

Equipment and payload units with the lowest eigenfrequency being sufficiently above 100 Hz are typically represented in the satellite system FEM by lumped mass models (mass point connected by rigid links to the unit mounting interfaces). As long as the extended thermo-elastic capabilities of e.g. the Nastran rigid elements (see Section 11.2.1.2) are not used such modelling might be however inadequate for thermo-elastic analysis purposes since the unit is not able to expand under the temperature loads and, as a result, the mounting panel becomes severely constrained. Figure 11-2 shows the unit represented by a thermo-elastically equivalent model considering the important stiffness characteristics (bending, membrane) and the respective coefficient of thermal expansion, [6]. Such modelling is considered preferable as compared to keeping the lumped mass model even when a proper CTE value according to the equipment unit housing material has been defined for the rigid elements.

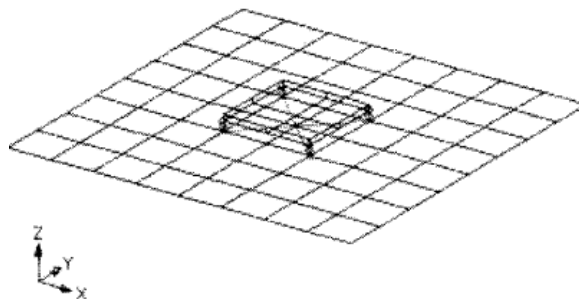


**Figure 11-2: Rough but thermo-elastically equivalent unit model, [6]**

Although the interface between the unit and the mounting panel (attachment area) is a quite complex thermo-elastic system the most important parameters have been identified from previous studies to be the junction global stiffness and the load path.

A detailed analysis of particular interfaces might be necessary to support the derivation of relevant guidelines for the modelling of these interfaces in the satellite system thermo-elastic model. The objective should be to establish a simplified but nevertheless adequate model of the structural parts concerned.

#### 11.2.1.4 Temperature mapping process

Conventional spacecraft thermal analyses are done with dedicated software packages making use of the so-called lumped parameter method (LPM). This method is based on the analogy with electrical circuits and in general it is very efficient for calculating the thermal balances and heat flows and therefore for simulating thermal control systems. The LPM is implemented in thermal analysis tools like ESATAN, [3], and SINDA, [4], which are equipped with various features to model the specific space thermal phenomena.

In general the temperature field to be used as input for the thermo-elastic analysis is generated by means of a thermal analysis performed with the above mentioned software tools. Usually the nodes of the thermal mathematical model and the structural mathematical model, respectively, are different with respect to their locations and the level of model discretisation (mesh) but most importantly due to underlying simulation method assumptions.

As a result, the temperatures predicted for the thermal nodes need to be appropriately projected onto the mesh of the structural finite element model. This “temperature mapping” is performed with the help of dedicated software tools as e.g. the SINAS software, [5]. Figure 11-3 shows as example the LISA Pathfinder Science Module (SCM) where the spacecraft thermal model has about 10000 nodes and the structural model about 400000 nodes, respectively.

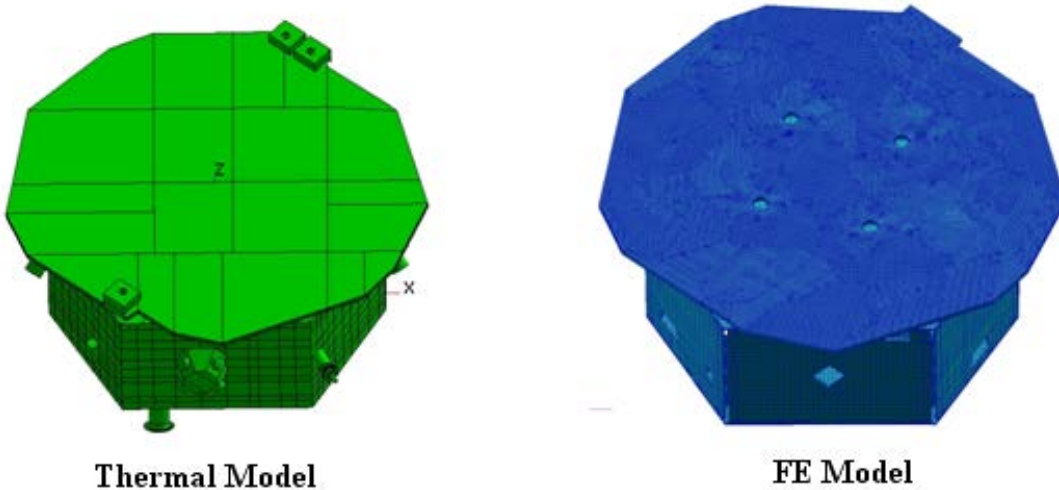


**Figure 11-3: Comparison of typical spacecraft thermal and structural model**

The temperature mapping involves an interpolation of the thermal node temperatures with respect to the corresponding entities of the structural finite element model (nodes and elements). The method implemented into SINAS is based on a conductive relation between the nodes of the finite element model and on the constraint which simulates the assumption of the LPM in the finite element model, namely that the thermal node temperature is the average temperature of the material or volume represented by the respective thermal node.

The SINAS method for the temperature mapping consists of 3 steps:

1. Building the correspondence between lumped parameter thermal nodes and the structural finite elements. The software includes an automatic overlap detection algorithm.

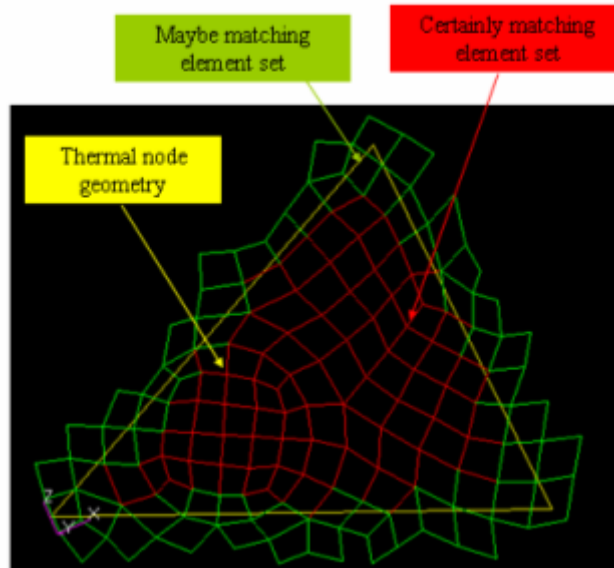


**Figure 11-4: Temperature mapping**

2. Mathematically linking the thermal nodes and the FEM nodes using the "Prescribed average temperature method" where the weighted average temperature of the nodes of FEM elements overlapping a thermal node is equal to the thermal node temperature.

First, FEM shape functions are used to obtain the weighting coefficients:

$$T_j^t = \sum_i a_i T_i^f \quad \longrightarrow \quad [T]^t = [A][T]^f \quad \text{and} \quad \sum_i a_i = 1 \quad [11-2]$$

$T_i^f$  is the FE node temperature,  $T_j^t$  is the thermal node temperature, and  $a_i$  a weighting coefficient.

Then the conduction matrix  $[C]$  can be calculated from the structural finite element model by replacing in e.g. Nastran the structural material definitions with the respective thermal ones (e.g. MAT4 replacing MAT1 bulk data cards).

3. Solving the following partitioned system of interpolation equations:

$$\begin{bmatrix} C & A^T \\ A & 0 \end{bmatrix} \begin{Bmatrix} T^f \\ q \end{Bmatrix} = \begin{Bmatrix} 0 \\ T^t \end{Bmatrix} \quad [11-3]$$

$T^t$  and  $T^f$  are the thermal and FE node temperatures, respectively, in vector form and  $q$  is a vector with Lagrangian multipliers.

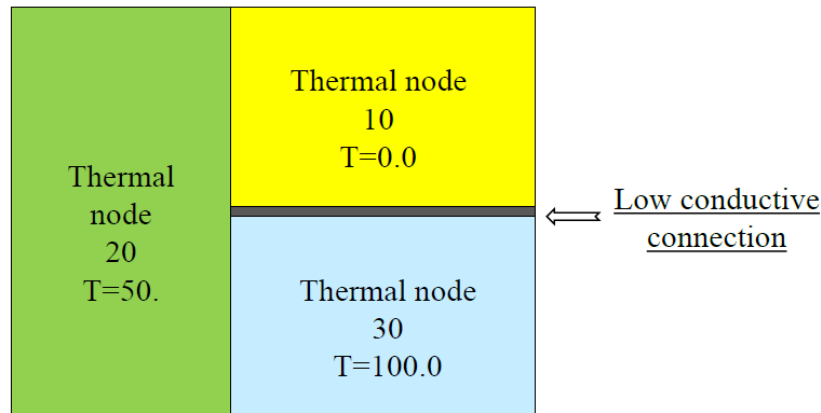
The system is then solved for the temperatures  $T^f$  at the finite element nodes.

The beneficial effect of using conductive FE model information for the temperature mapping process is demonstrated with the help of a simple thermal model that has a very coarse mesh as shown in Figure 11-5. Between the thermal nodes 10 and 30 (temperature difference:  $\Delta T = 100^\circ$ ) there is a layer with a low thermal conductivity providing good thermal isolation between these two nodes. The temperature mapping based on a purely geometrical interpolation does not take into account the

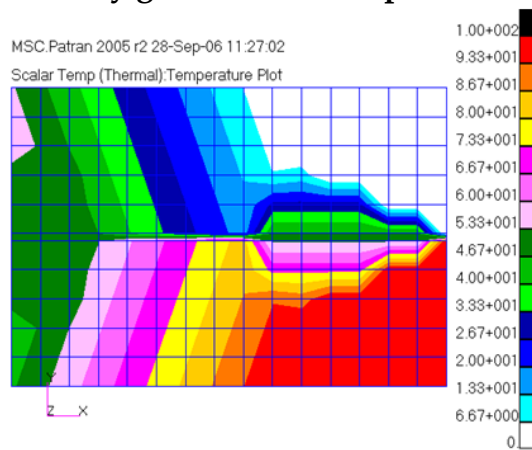
existence of this layer and the temperatures are interpolated across this layer which is not physically realistic.

However, when the conductive FE model information is taken into account as it is the case for the method implemented into the SINAS software then a temperature mapping is provided that is physically realistic. This is because the FE model topology is used to interpolate the temperatures in a way that is consistent with the actual heat transfer paths in the structure.

### Thermal analysis model with 3 thermal nodes



### Purely geometrical interpolation



### Using conductive FE model information

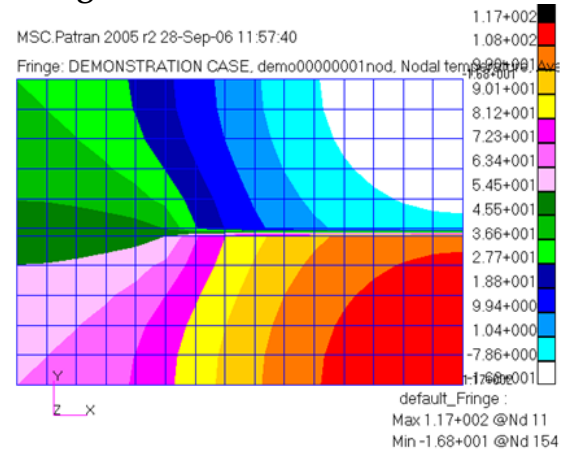


**Figure 11-5: Temperature mapping based on purely geometrical interpolation (left) and when also using conductive FE model information (right)**

#### 11.2.1.5 Thermo-elastic mathematical model correlation

In order to have good confidence in the validity of the predictions obtained a test-validated mathematical model should be in general used when performing thermo-elastic distortion analyses for potentially mission critical performance assessments. The data needed for the correlation of the hardware deformation measurements with the respective finite element model (FEM) predictions should be obtained from a thermo-elastic distortion test involving representative spacecraft hardware. Where necessary, the mathematical model should be subsequently updated to achieve the required quality.

However, it appears that no well-defined criteria exist, e.g. in the applicable ECSS standards, to demonstrate satisfactory correlation of satellite hardware performances with the predicted thermo-elastic distortion behaviour. As a result, relevant correlation criteria need to be established on a case by case basis and agreed between all parties involved.

In general the strategy for performing thermo-elastic model correlation should be based on the following steps:

1. Identification of the structural parameters expected to significantly influence the thermo-elastic distortion behaviour.
2. Performance of thermo-elastic distortion analyses in order to investigate and possibly quantify the influence of single or combined parameters on the thermo-elastic distortion behaviour.
3. Evaluation of the analysis results to determine the “best-fit” value for each parameter to obtain a satisfactory correlation.

The most important sources for differences between the thermo-elastic predictions and corresponding hardware deformation behaviour are e.g. the following:

- Incorrect material property specification in the analysis model, in particular concerning the Coefficient of Thermal Expansion (CTE), the thermal conductivity (when performing a temperature mapping based on geometrical interpolation but also using conductive FE model information, see Section 11.2.1.4 and Figure 11-5) and the representation of orthotropic material properties.
- Inaccurate temperature measurements during the test and resulting inaccuracies of the temperature field mapped onto the thermo-elastic analysis model.
- Significant deviations from the hardware design and geometry, e.g. inadequate modelling of structural joints and too coarse representation of curved surfaces by linear elements.

As described in more detail in [12] the test/analysis correlation could be performed based on a deterministic approach or a stochastic approach.

For the deterministic correlation approach the sensitivity of the performance prediction due to variations of selected parameters is evaluated. These parameter variations are usually limited to only one or a few values. The starting point (reference) for the sensitivity studies might be the nominal configuration. Depending on the number of relevant structural parameters the deterministic approach might be very time consuming by requiring a large number of analysis runs before reaching a satisfactory correlation.

The stochastic analysis aims at quantifying the influence of uncertainties on the simulation results. The influencing parameters which might include the measured or predicted temperature field are defined as stochastic variables with usually a Gauss normal distribution around the nominal value. In order to efficiently implement a Monte Carlo Simulation (MCS) for the prediction analysis the automation of the complete analysis process is necessary, in particular if several process steps as thermal analysis, thermo-elastic distortion analysis and subsequent data post processing are involved.

A flow chart for the correlation of a thermo-elastic mathematical model with tests results based on a stochastic approach is shown in Figure 11-6.

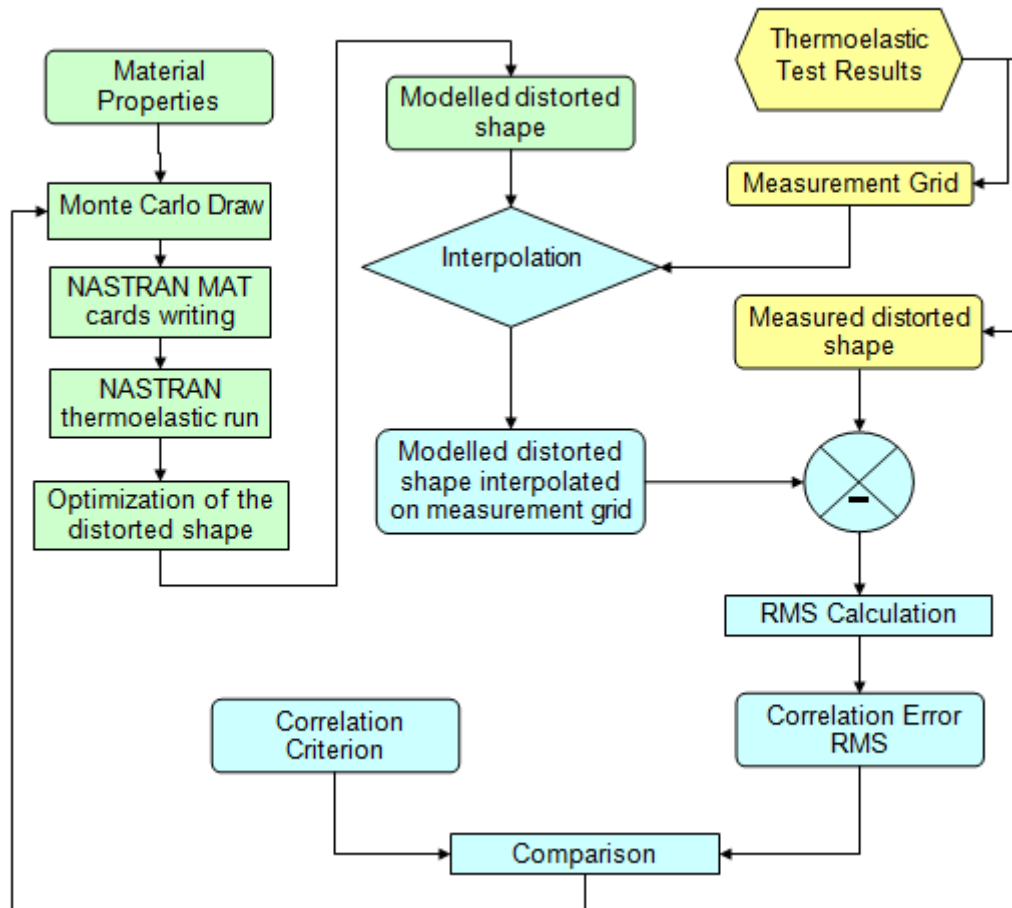


**Figure 11-6: Flow chart for thermo-elastic analysis model correlation based on stochastic approach, [12]**

### 11.2.2 1g-0g transition (gravity release)

Spacecraft are assembled on Earth under the influence of gravity loads and then alignment checks are usually performed in order to verify the relative position between parts during manufacturing, assembly and verification testing. However, once in orbit the effects of gravity are cancelled and the spacecraft structure ‘relaxes’ from the distortions occurring under the 1g environment. As a result, the on-orbit alignment of payload units with respect to the star trackers deviates from the on-ground measurement conditions. The gravity release effects on the pointing accuracy of the payload units should be assessed and considered in the overall satellite pointing budget.

The 1g-0g transition effects can be evaluated by performing a simple static loads analysis where the gravity loads are applied in a consistent manner with respect to the configuration in which the satellite is assembled on-ground. In general the gravity loads can be assumed to act only in the spacecraft longitudinal direction. As a result, the 0g environment can be represented in the analysis by the application of 1g in the longitudinal direction, usually pointing in a positive direction upwards from the launcher/spacecraft interface. The calculated deflections as shown in Figure 11-7 for the LISA Pathfinder Science Module can then be taken into account for an assessment of the on-orbit deviation from the on-ground spacecraft alignment.

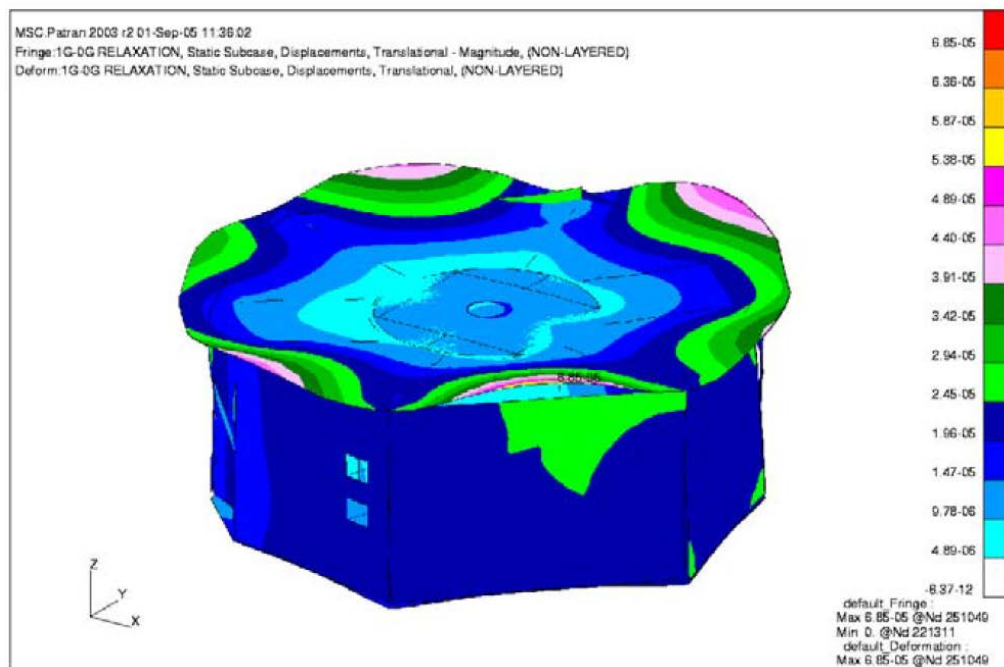


**Figure 11-7: LISA Pathfinder Science Module distortions due to gravity release in longitudinal direction**

### 11.2.3 Moisture absorption / release

Composite spacecraft structures are sensitive to humidity. Moisture is taken up on ground and is released under vacuum conditions. As a result, the structure might swell or shrink and therefore might lose its dimensional stability. The swelling / shrinkage of composite structures due to moisture absorption or release, respectively, is very small and typical Coefficient of Moisture Expansion (CME) values are in the range of less than  $5 \times 10^{-5}$ /wt%H<sub>2</sub>O in the fibre direction and about  $1 \times 10^{-3}$ /wt%H<sub>2</sub>O normal to the fibres.

Where necessary for the verification of the compatibility of the spacecraft design with the mission performance requirements dedicated hygro-elastic analyses should be performed to assess the impact of the expected moisture release on the dimensional stability of the structure when being in orbit.

The induced hygro-elastic deformations  $\varepsilon_H$  can be estimated from the following relationship

$$\varepsilon_H = \frac{\Delta l}{l_0} = \beta \frac{\Delta m}{m_0} \quad [11-4]$$

where  $\Delta L = \frac{\Delta l}{l_0}$  is the length variation (%),  $\Delta M = \frac{\Delta m}{m_0}$  is the moisture absorption (%),  $l_0$  and  $m_0$  are the initial length and mass, respectively, for e.g. the dry material, and  $\beta$  is the Coefficient of Moisture Expansion.

Consequently, the CME is defined by the ratio of the length variation to the mass variation due to moisture absorption or release:

$$\beta = \frac{\Delta l}{l_0} \left( \frac{\Delta m}{m_0} \right)^{-1} \quad [11-5]$$

The CME value depends strongly on the composite lay-up and, as  $\Delta M$  does, on the resin type and the resin volume (or fibre volume fraction, respectively). Therefore dedicated tests to determine the

relevant moisture release characteristics and the CME value might be necessary for new composite lay-ups.

Typical moisture absorption values are given in Table 11-2 where the composite moisture absorption  $M_{s,c}$  is given by the following relationship

$$M_{s,c} = M_{s,r} \frac{\rho_r(1-V_f)}{\rho_c} \quad [11-6]$$

where  $M_{s,r}$  is the resin moisture absorption (%),  $V_f$  is the fibre volume content, and  $\rho_r$  and  $\rho_c$  are the resin and composite densities, respectively.

**Table 11-2: Pure resin and composite lay-up moisture absorption characteristics at equilibrium and in 100% relative humidity environment**

	Pure resin $M_{s,r}$	CFRP ( $V_f=60\%$ ) $M_{s,c}$
FIBERITE 934	6.5 %	2.03 %
CIBA M18	2.2 %	0.66 %
YLA RS-3M	1.35 %	0.40 %

The finite element model for the moisture release analysis can be deduced from the thermal distortion analysis model by replacing the Coefficient of Thermal Expansion (CTE) values by the relevant CME values. Usually, the most important outputs from the moisture release analysis concern the evaluation of the relative deflections of AOCS equipment between each other and from the specified satellite axes orientations, respectively. Furthermore the expected pointing errors of scientific instruments due to structural shrinkage resulting from the mass loss might be of interest.

A typical result plot showing the deformations due to moisture release is presented in Figure 11-8.

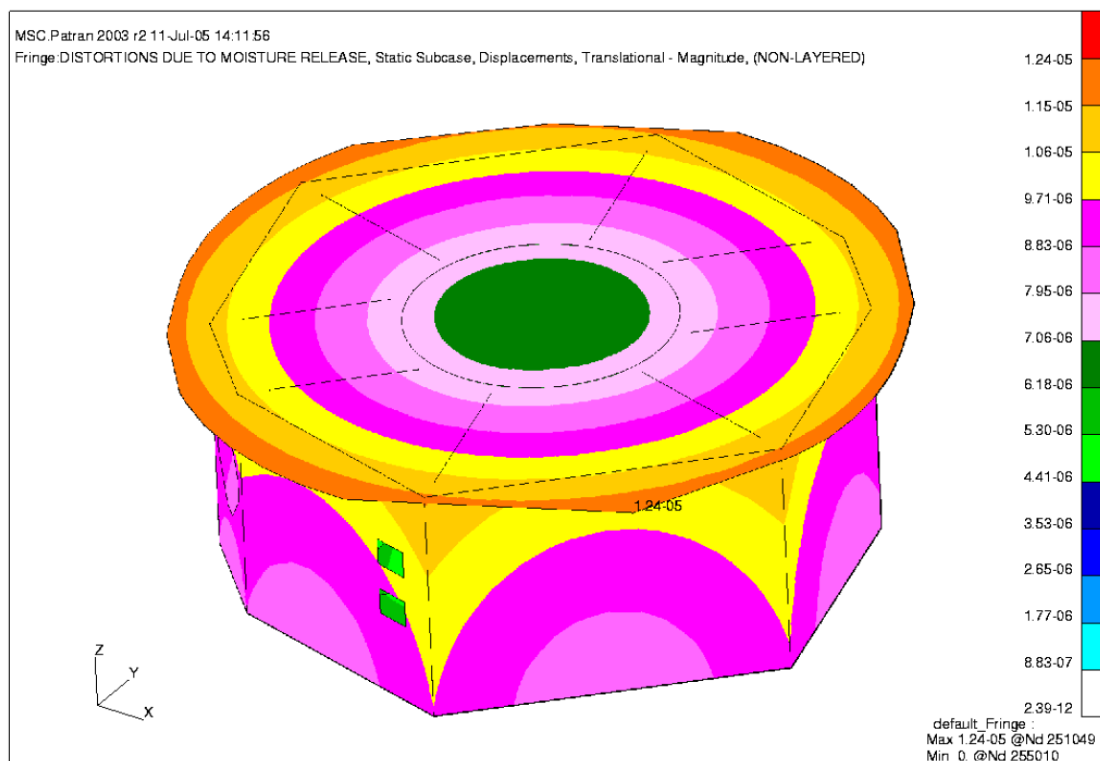


Figure 11-8: LISA Pathfinder Science Module distortions due to moisture release

## 11.3 Dimensional stability verification

### 11.3.1 Introduction

Dimensional stability tests are performed on relevant satellite hardware in order to verify that the satellite structure fulfils the mission performance requirements under all expected operational conditions. The most important tests are thermal distortion and gravity release tests.

Dedicated material characterisation tests, e.g. to determine the Coefficient of Thermal Expansion (CTE) or Coefficient of Moisture Expansion (CME) for new composite lay-ups, might be performed to provide relevant information for analytical predictions or to verify the conformance of long term changes of material properties with the specification, e.g. concerning dimensional changes due to moisture release, ageing and creep.

### 11.3.2 Thermal distortion test

#### 11.3.2.1 General

Relevant information to adequately predict the thermo-elastic behaviour of a composite structure in particular is acquired at gradually increasing complexity level during the structure design and development phase. The characteristic CTE values to be used as relevant material properties for the analytical predictions are generally obtained from coupon and component tests in the early structure development phase. Knowing adequately the thermo-elastic behaviour of the individual components is of paramount importance to the understanding of the behaviour of the assembled structure. In addition to the CTE characterisation tests thermal distortion tests at component or subassembly level

might be performed to assess the impact of e.g. local effects of individual metallic inserts in composite structures or the contributions of connections between structure panels.

Nevertheless a full scale thermal distortion test is usually needed for the final verification of the dimensional stability of the structure.

### 11.3.2.2 Test objectives

In general the thermal distortion test is performed with the following two objectives:

1. To measure the distortions of the test structure under the specified thermal load cases and thereby to contribute to the understanding of the thermo-elastic behaviour of the structure, as e.g. predicted by the thermo-elastic analysis.
2. To generate sufficient data in order to allow the correlation of the hardware measurements with the finite element model (FEM) used for the thermo-elastic distortion predictions and to subsequently validate the mathematical model.

The CTE is usually the most critical performance parameter to be identified from the thermal distortion test for correlation with the analysis model.

### 11.3.2.3 Test setup and performance

In general the thermal distortion test is performed for the on-orbit satellite configuration, i.e. the satellite configuration should be the fully deployed configuration and the structure should be allowed to expand freely under the thermal loads. In practice this is mostly achieved by kinematic support concepts, Figure 11-9.

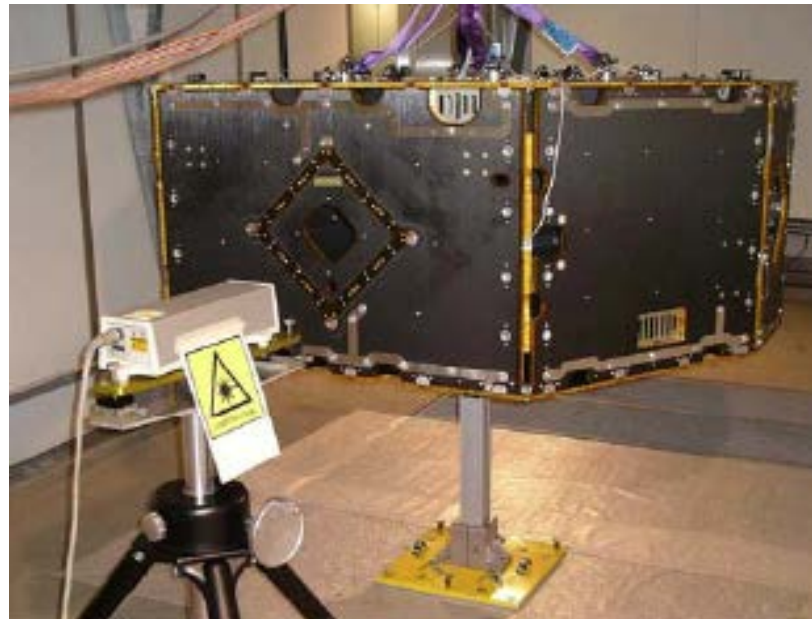


**Figure 11-9: LISA Pathfinder Science Module structure on kinematic support for thermal distortion test, [9]**

Alternatively the test structure can be freely suspended by slings. However, problems with such test setup have been experienced due to laser alignment problems caused by small movements of the structure due to circulating air in the test room.

For executing the test the assembled structure is usually placed in a climatic chamber and then subjected to the temperature variations. Several options exist to measure the structure deformations and to determine the distorted shape of the structure, e.g. laser metrology, video-grammetry, or a combination of both.

Cut-outs in the structure or removal of panels might be needed to provide the required access for the measurement devices or to ensure unobstructed line-of-sight for e.g. laser beams. However, care should be taken to ensure that these modifications do not significantly affect the thermo-elastic distortion behaviour of the test structure.

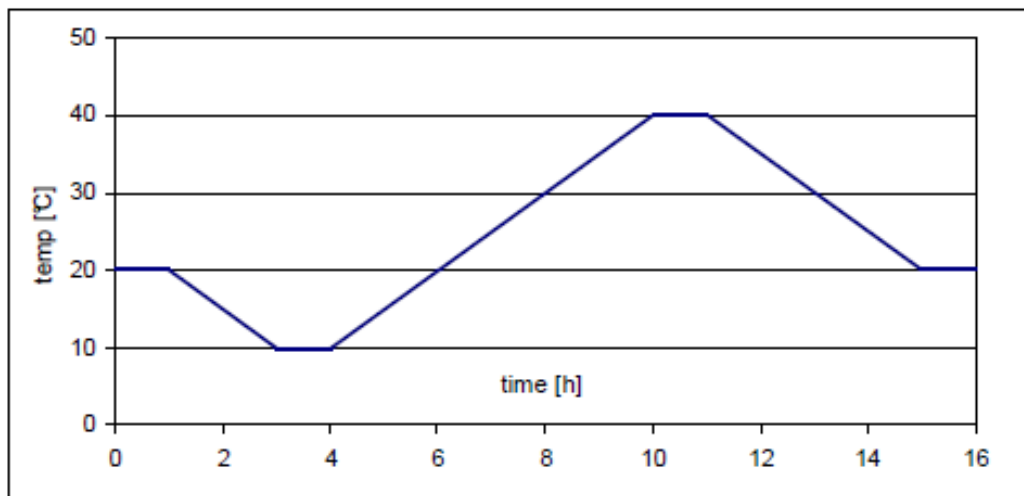


**Figure 11-10: Typical temperature profile for thermal distortion test, [9]**

The thermal distortion (or thermo-elastic) test consists of applying a uniform temperature to the test specimen and subsequently measuring the structural deformations. A typical temperature profile for thermal distortion test is shown in Figure 11-10. The distortion of the test article was measured in the temperature range from 10°C to 40°C, the heat-up and cool-down rates were 5°C/hour and the extreme temperatures of +10°C and +40°C were kept constant for 1 hour in order to equalize the temperature on the whole structure.

The relatively simple thermal distortion test case as shown in Figure 11-10 has the advantage that it can be easily conducted in a climatic chamber and has in general a good repeatability.

#### 11.3.2.4 Deformation measurements

As already mentioned above the measurement of the structure deformations can be performed e.g. by laser metrology, video-grammetry, or a combination of both.

##### 11.3.2.4.1 Laser-interferometric measurements

Laser metrology as illustrated in Figure 11-11 is considered the most accurate method to measure distortions of one micrometer or smaller. However, it is not a practical method to determine the distorted shape of a complete structure as only the change of one dimension with temperature can be measured. In addition, the method requires mounting provisions for the interferometer and mirrors and even mass compensation devices when the optical elements are connected to vertical panels.

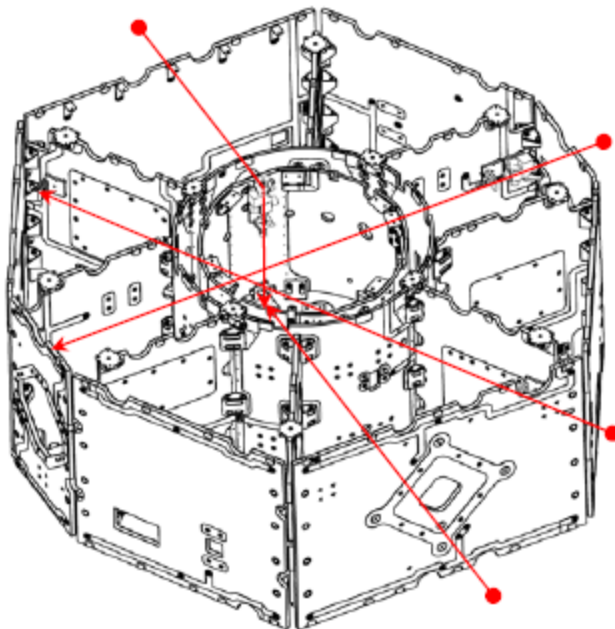


**Figure 11-11: Illustration of different courses of laser beams for LISA Pathfinder Science Module thermal distortion test, [9]**

#### 11.3.2.4.2 Videogrammetry

Digital photogrammetry, also known as video-grammetry, is a well proven method to measure 3D geometry and distortions. Video-grammetry is a measurement technology based on optical triangulation in which the three-dimensional coordinates of points (targets) on an object are determined by measurements made in two or more images taken from different angles. These can be obtained from successive images captured by the same camera with a view of the object.

To perform the video-grammetry measurements the test structure needs to be equipped with an adequate number of self-adhesive optical targets. Calibrated reference scales (yellow bars in Figure 11-12) are positioned close to the test article to provide absolute dimensions.

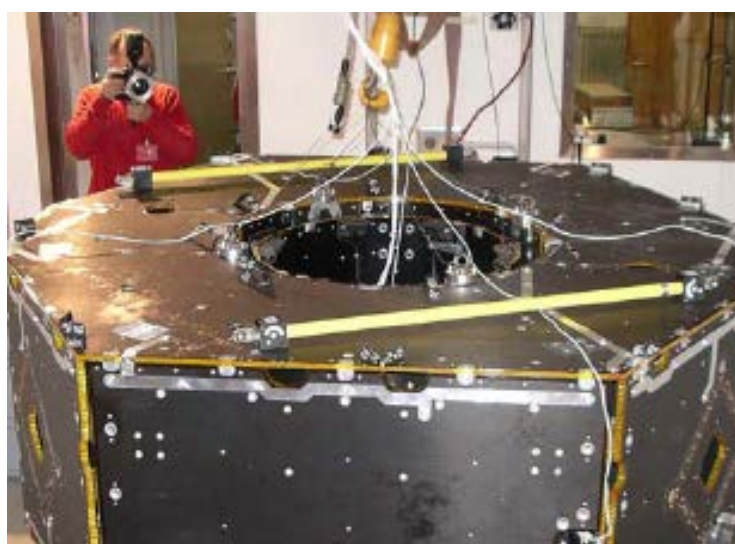


**Figure 11-12: Video-grammetry measurements during LISA Pathfinder Science Module thermal distortion test, [9]**

Practical experience shows that video-grammetry requires full visibility of the test article and that best results are achieved when the targets are seen from many different angles, see Figure 11-13. To obtain the best possible coverage, approximately 250 pictures were taken e.g. during the LISA Pathfinder Science Module thermal distortion test at the minimum and maximum temperatures, respectively (see the temperature profile shown in Figure 11-10).

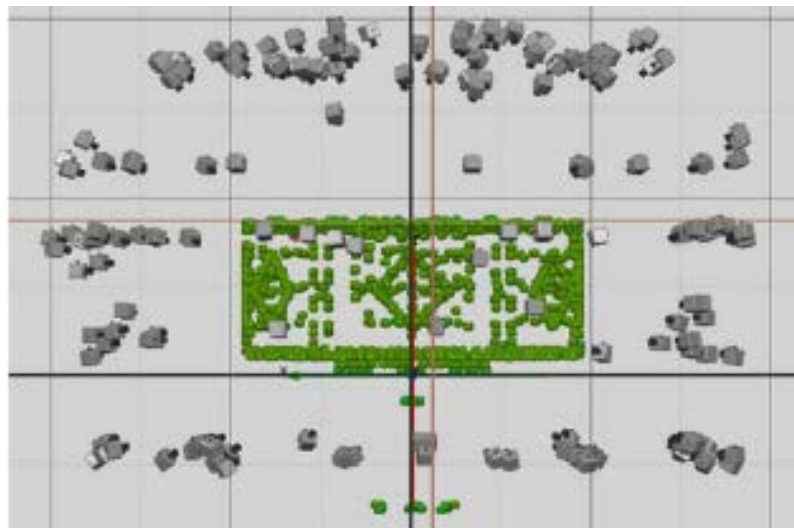


**Figure 11-13: Overview of camera positions used during LISA Pathfinder Science Module thermal distortion test to generate the images of the test article, [9]**

The accuracy of the video-grammetry is typically  $10 \mu\text{m} - 15 \mu\text{m}$  for objects of the size of the LISA Pathfinder Science Module structure (diameter of octagonal structure: about 1.8 m). Although the accuracy of the video-grammetry is at least one order of magnitude less than the accuracy of the laser metrology, it still provides useful information on the global behaviour. The distortion of the external structure caused by a uniform temperature increase of approximately  $30^\circ\text{C}$  is shown in Figure 11-14.

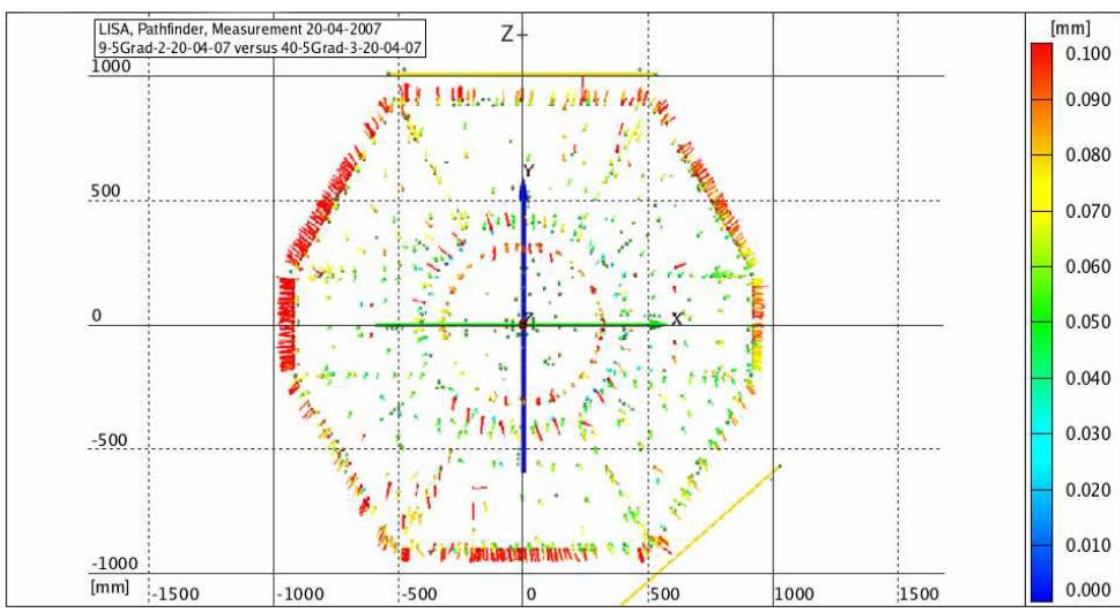
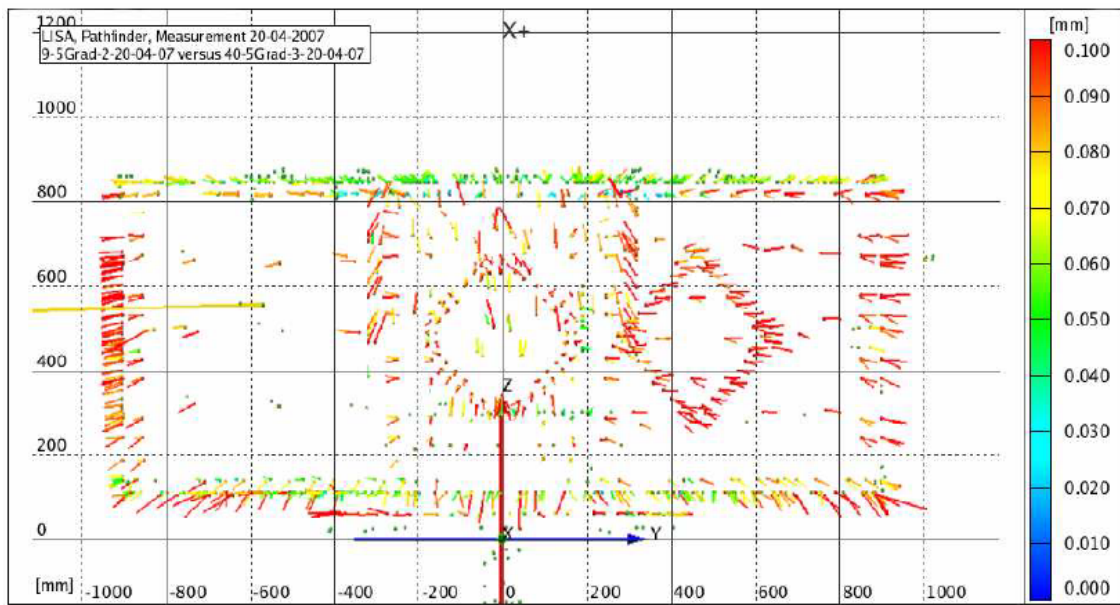


Figure 11-14: Displacement of targets mounted on LPF SCM external structure for a temperature variation from +9.5°C (reference temperature) to +40.5°C, [9]

### 11.3.2.5 Post-test activities

The main activities after the thermal distortion test are the following:

1. Engineering evaluation of the test results in order to assess the thermo-elastic behaviour of the test structure with respect to the design requirements.
2. If necessary, the application of structural design modifications to meet the performance requirements, e.g. to change the CTE characteristics of the structure by selecting a different fibre or changing the laminate lay-up in the case of composite structures.
3. To compare the recorded distortions with the analytical predictions, usually obtained from a sufficiently detailed 3D structure finite element model, and thereby to assess the thermo-elastic model quality. If necessary, to update this model to be able to adequately predict the thermo-elastic behaviour of the structure.

### 11.3.3 Gravity release test

The gravity release test has the main objective to assess the effects of the absence of gravity loads for the on-orbit configuration being in contrast with the measurement conditions on Earth during the AIT/AIV activities. Based on the results of such test, the potential defocus or decentre of an optical instrument can be quantified which occurs by the release in space of the gravity loads. Furthermore the test might provide relevant information to validate the predictions obtained from the 1g-0g transition analysis.

During the test the alignment is measured with different gravity vector orientations. However, only two integration directions are usually considered: axial and lateral, and as a consequence two loading directions are tested. The test specimen is constrained at its mounting interfaces as applied e.g. for a static test. In case the gravity release effects are applied in two opposite directions (+1g and -1g, respectively) for any integration axis then the measured quantity is 2 times the expected quantity due to gravity release.

For the test the unloaded state conforms to the natural gravity acting on the test specimen. Gravity compensation loads are then applied to the unloaded state and the deformations are measured. The loads are usually applied in several load steps as for standard static tests.

As an example the gravity-release test configuration for the NIRSpec engineering test unit (ETU) is shown in Figure 11-15.



**Figure 11-15: NIRSpec engineering test unit (ETU) during gravity-release test  
(courtesy: EADS Astrium)**

## 11.4 Material property characterisation testing

### 11.4.1 Coefficient of Thermal Expansion (CTE) characterisation

The CTE is defined as the fractional increase in strain per unit rise in temperature. It can be defined either at a precise temperature or as the average over a finite temperature range.

The measurements can be done by using a Michelson laser interferometer according to ASTM E289 standard or with a dilatometer according to ASTM E228 and D696 standards. Typical experimental setups are shown in Figure 11-16 and Figure 11-17, respectively. The application of the laser interferometer technique provides more accurate data. It is particularly advisable for materials that have a very small expected CTE and where the CTE is derived from limited temperature ranges to be applied during the characterisation test.

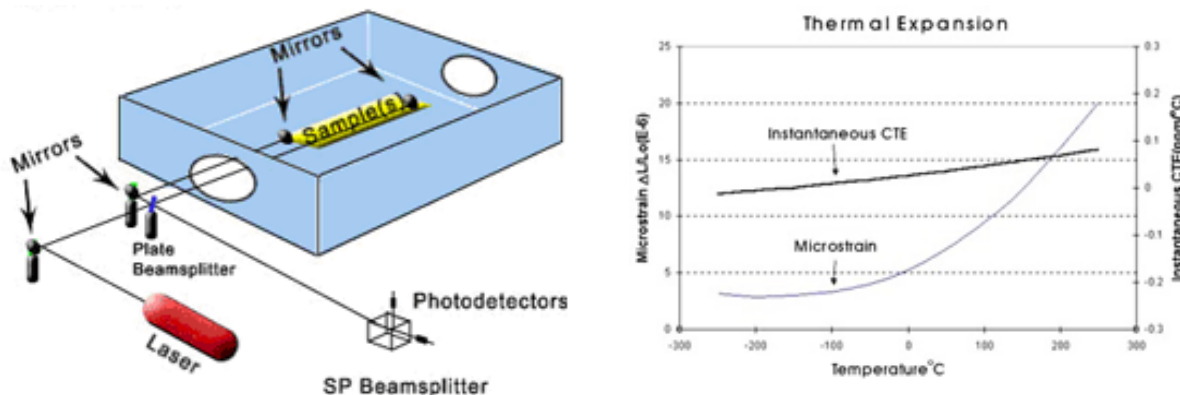


**Figure 11-16: High resolution thermal expansion measurement using Michelson laser interferometer (credit: PMIC, <http://www.pmiclab.com>)**

Continuous strain and temperature data are normally plotted as shown in the right graph of Figure 11-16. The slope of the strain/temperature curve at a given temperature is the instantaneous CTE value whereas an average CTE value can be obtained from the average slope over a finite temperature range.

Except of any limits imposed by the test facility the Michelson laser interferometer measurement technique is little restricted by the sample size or shape. For composite components or structures multi-directional strains could be determined simultaneously by using multiple interferometers.

The dilatometer measurement technique might be used with materials that have a large expected CTE and when larger temperature ranges can be applied during the test. As for the laser interferometry the use of a dilatometer usually imposes little restrictions on sample size or shape. The experimental setup might also allow testing multiple specimens at one time.

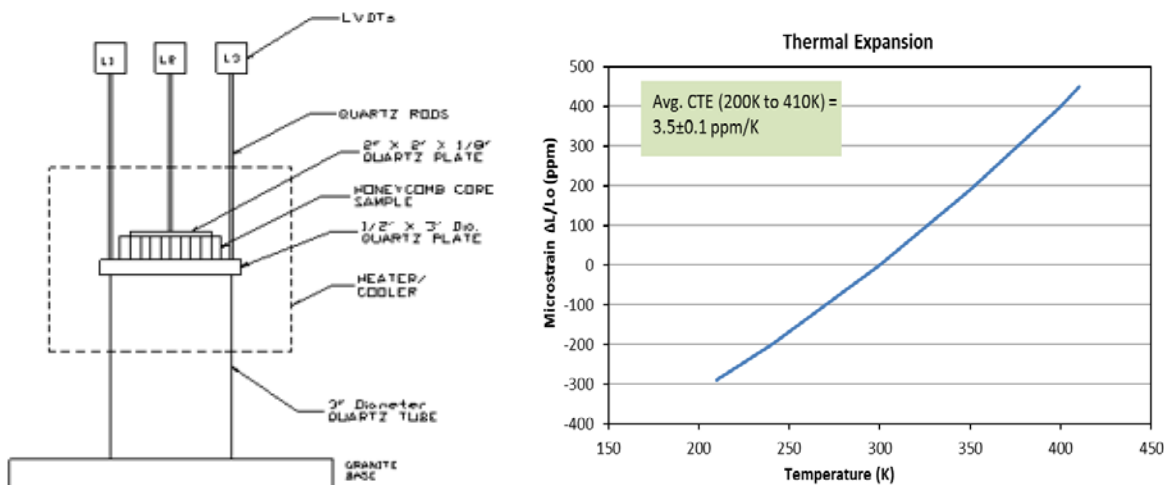


**Figure 11-17: Thermal expansion measurement using basic dilatometer configuration (credit: PMIC, <http://www.pmiclab.com>)**

#### 11.4.2 Coefficient of Moisture Expansion (CME) characterisation

As described in Section 11.2.3 the CME is defined by the ratio of the length variation to the mass variation due to moisture absorption or release:

$$\beta = \frac{\Delta l}{l_0} \left( \frac{\Delta m}{m_0} \right)^{-1} = \frac{\Delta L}{\Delta M} \quad [11-7]$$

Measuring the length change  $\Delta L$  and the mass change  $\Delta M$  between two moisture equilibrium states allows determining the respective CME value. The mass change  $\Delta M$  can be gained by directly weighing the sample before and after testing.

An assessment of available test facilities and methods for determining CME values is provided in [13]:

- Only high resolution / high accuracy measurement systems can provide the length variation data needed to experimentally determine the CME (caused by the very small swelling or shrinkage of composite structures due to moisture absorption or release, respectively).
- Conventional dilatometers cannot provide the required resolution and accuracy (typically  $\pm 1\mu\text{m}$ ) and in general the commercial facilities cannot be operated in vacuum.
- Online external interferometric measurement systems, like the one presented in [14] (where simultaneous and continuous measurements of mass and related length variations are performed within the test chamber) are very sophisticated and the measurement times are not practical.

Instead [13] proposes a methodology based on commercial laser micro-interferometers operated inside the vacuum chamber. The advantages of this methodology are an exceptional accuracy and reduced measuring times since all errors introduced by external interferometric systems (e.g. ambient temperature and pressure variations, external beam path deviations) can be eliminated. Furthermore simultaneous multi-directional measurements are feasible due to the use of multiple miniaturised interferometers.

The methodology presented in [14] claims to yield more reliable results and to reduce the measurement time considerably since online weighing during the outgassing in vacuum is carried

out. The measurement principle is similar to the one presented in Section 11.4.1 for the Michelson laser interferometer.

The following should be noted:

- CME measurements in the fibre direction were identified to be more difficult since the values are usually very small.
- The method presented in [13] cannot be easily adapted to rather extreme temperature ranges (e.g. from -200°C to 200°C) which are of interest for space relevant materials. Problems identified were due to the mirror refraction index which changes so much that there is no longer total reflection of the laser beam and due to the thermostat system for the sample operating by thermal radiation only and taking a very long time to reach stable conditions.
- The method of just weighing the samples was found not to be very accurate and often resulted in lower CME values. The online measurement of the mass change  $\Delta M$  gives the expected constant CME values and is therefore the preferred method.

## 11.5 References

- [1] ESSB-HB-E-003, ESA Pointing Error Engineering Handbook, Issue 1, July 2011
- [2] ECSS-E-ST-32C, Space engineering – Structural general requirements, Rev.1, November 2008
- [3] ESATAN-TMS r4 Release Notes, ITP Engines UK Ltd., <http://www.esatam-tms.com>, October 2011
- [4] SINDA User's Manual, C&R Technologies, Inc., <http://www.crtech..com>, October 2011
- [5] SINAS-IV Theoretical Manual, Fokker Report SINAS-IV-R-005, issue 1, April 1998
- [6] De Zotti, S., Lome, J.-M., Parquet, J.-L., Lemcke, C. "Thermo-mechanical verification techniques", European Conference on Spacecraft Structures, Materials and Mechanical Testing, Braunschweig, Germany, 1998
- [7] Helwig, G. "Highly dimensional stable composite structures", Workshop Advanced Materials for High Precision Detectors, CERN, 1994
- [8] Bailly, B., Cornu, J. L., Capdepuy, B., Leleu, F., Kornmann, M., Pradier, A. "Dimensionally Stable Structures, European Conference on Spacecraft Structures, Materials and Mechanical Testing, Noordwijk, The Netherlands", 1996
- [9] Di Carlo, A., Usinger, R. "Development of a Dimensionally Stable CFRP Structure for Supporting Optical Instruments in Laser Communication Device", CEAS European Air & Space Conference, Berlin, Germany, 2007
- [10] Gröbelbauer, HP., Heer, M. "Development of a Dimensionally Stable Lightweight Structure for LISA Pathfinder Science Module", CEAS European Air & Space Conference, Berlin, Germany, 2007
- [11] Scheulen, D. et al. "The Dimensionally Stable CFRP Camera Structure of Kompsat 3: Development, Manufacturing and Verification", European Conference on Spacecraft Structures, Materials and Mechanical Testing, Toulouse, France, 2009
- [12] Ravelli, L. "Thermal Distortion Analysis & Test Correlation for Antenna Reflectors", EADS ST Technical Note TDA – EST – TN – 3104, Issue 01, 2005
- [13] Poenninger, A., Defoort, B. "Determination of the coefficient of moisture expansion (CME)", 9<sup>th</sup> Int. Symposium on Materials in Space Environment, Noordwijk, The Netherlands, 2003
- [14] Estrada, E., Colozzi, F. "A new highly accurate CME test facility", European Conference on Spacecraft Structures, Materials and Mechanical Testing, Noordwijk, The Netherlands, 1996

# 12

## Fatigue and fracture control

### 12.1 Introduction

Fracture control and fatigue life verification of spacecraft, launchers and their payloads and experiments is of paramount importance for the safety and reliability of manned and unmanned space operations. Therefore fatigue (i.e. crack initiation) and crack growth analyses or tests are required by various ECSS standards, including ECSS-E-ST-32C [1] and ECSS-E-ST-32-01C [2]. The objective of this chapter is to discuss the various aspects involved in deriving fatigue load spectra (i.e. sequence of cyclic loads) to perform such analyses or tests, as well as providing references, guidelines and examples.

For fatigue crack initiation (or ‘fatigue’) analysis, the fatigue spectrum is used to calculate the damage for each of its lines using an S-N curve: e.g. the simple Basquin relationship or equations as used in the former MIL-HDBK-5, now MMPDS, (see Figure 12-1) and cumulating the damage of each load line using e.g. linear damage accumulation rule of Miner. The ‘MIL-HDBK-5’ formulation is implemented in the ESAFATIG module of the ESACRACK software.

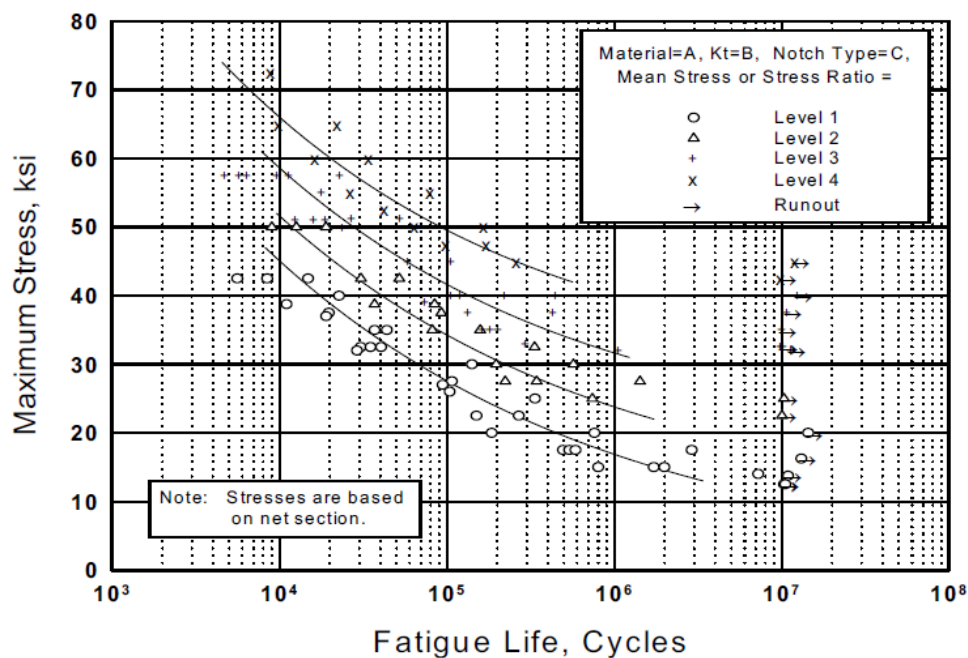
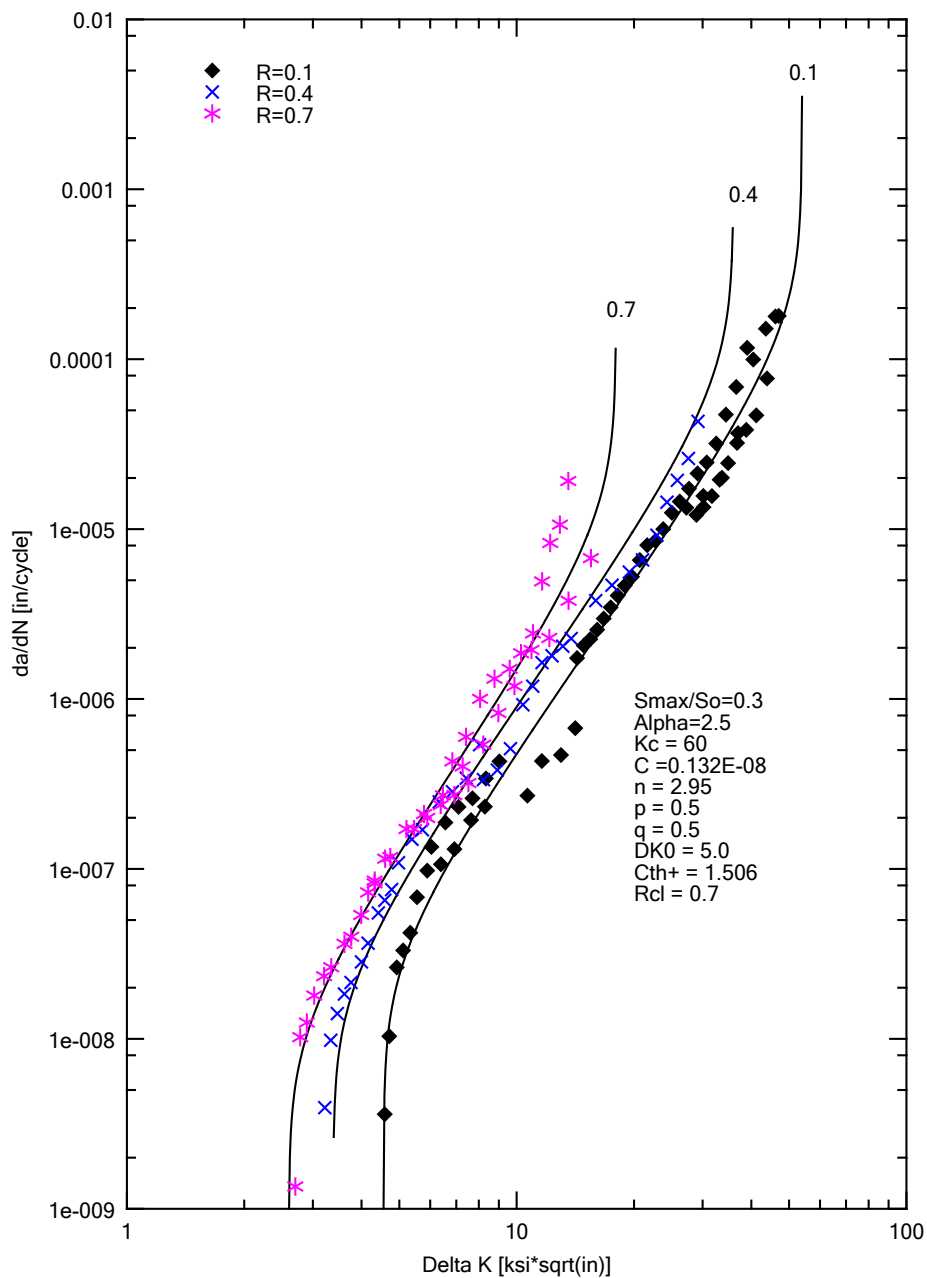


Figure 12-1: Example of an S-N curve used in fatigue crack initiation analysis

For fatigue crack growth analysis, the fatigue spectrum is used to calculate the evolution of a macroscopic crack using e.g. the simple Paris law, or the NASGRO equation (see Figure 12-2) until failure occurs when the maximum stress intensity factor, which is a function of stress and crack size, exceeds the fracture toughness, or when ductile failure of the cracked structure occurs. This means that the severity of an event for damage tolerance verification does not only depend on the number and level of cyclic loads ('fatigue content'), but also on the value of the maximum load (a single loading can cause premature failure of a cracked structure).



**Figure 12-2: Example of a fatigue crack growth rate curve used in fatigue crack growth analysis**

This chapter addresses mainly the following aspects:

- ‘normal’ fatigue (i.e. crack initiation and/or propagation due to cyclic loads), and
- residual strength (due to extreme loads in the presence of cracks or other defects).

‘Static’ fatigue phenomena, e.g. due to environmental conditions: stress-corrosion (metals, glass, ceramics, etc.), creep, etc, are not addressed in detail.

For complex loading histories, which very often occur within space projects, the manual calculation and gathering of load data can become an overwhelming task.

Very often extensive dynamic and functional testing is applied on the structure, which induces fatigue damage, which should be considered in the life verification of the structure.

In most of this section, the methodology implemented in the ESALOAD software [3] is followed. This software is developed under ESA contract since the 1980s as part of the ESACRACK fatigue and fracture mechanics analysis software package, and is designed to create a representative stress spectrum at the location of interest on a specific part of a space vehicle structure. It must be noted that the ESALOAD software was primarily based on the fracture control verification method generally applied to payloads and their subsystems. In certain cases (e.g. launchers) a modified approach may be more appropriate.

The load spectrum derivation method presented in this section is in principle independent of the type of material. However, in case spectra are truncated by omission of certain events or load types (e.g. compression) or levels (below threshold level) material dependence may be introduced. For example, delaminated composites are more sensitive to compressive loads. Also in metals, omission of the negative part of load cycles may result in underestimation of fatigue crack growth rate.

NOTE:

Some assumptions that are commonly/implicitly made throughout this section that may however not always be applicable:

- The verification applies to flight hardware. Generally qualification testing is therefore not taken into account (or in modified form, in case of protoflight hardware).
- It is assumed that the stress distribution in the item due to dynamic loads can be described with a single, uniform acceleration. The stress can be derived from the acceleration by means of the ‘unit stresses’. This is in line with the approach commonly used for verification of space structures. If this assumption is not valid, a more refined dynamic analysis/specification may be necessary, or other ad-hoc approaches may have to be adopted.
- The sequence of application of load cycles is not very important, especially within events. The sequence of events may be significant.

This assumption is normally not valid when e.g. crack-growth retardation methods (or more generally: load interaction methods) are applied in the analysis. The application of such load interaction methods is generally discouraged in [2] for analytical verification, unless an unconservative prediction may result (in case of e.g. very high compressive loads). In load spectra applied in fatigue testing, the sequence of load cycles may be significant, and include both retarding and accelerating effects.

Figure 12-3 provides an overview of the fatigue load (or stress) spectrum derivation. On the basis of a selected event history, indicating the total number of different events, and load curves for each of the individual events, a fatigue load spectrum can be generated. The resulting load spectrum, defining all loads seen by a system or subsystem during its lifetime, can be transformed into a stress spectrum using unit stresses, i.e. stresses derived from knowledge of the structural response to unit loads. The various steps are described in more detail in the remainder of this chapter.

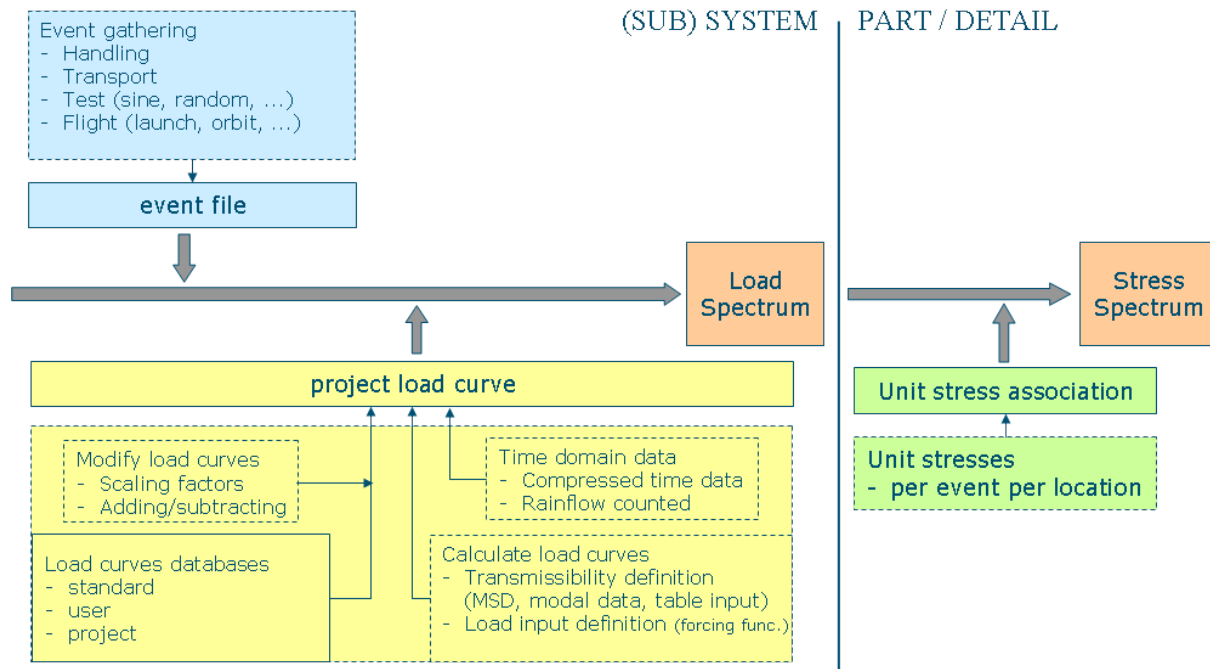


**Figure 12-3: Overview of load and stress spectrum derivation**

## 12.2 Definitions

For the purpose of this chapter, the following definitions apply:

**(load) Event:** basic building block of the life of a (sub)structure, consisting of condition, phenomenon, environment or mission phase to which the structural system is exposed and which induces loads in the structure.

**Load (exceedance) curve:** describes how the (cumulative) number of cycles experienced by the payload is distributed over the load range.

**Load spectrum:** representation of the cumulative static and dynamic loadings including load level and number of cycles anticipated for a structural element during its service life. Load spectrum is also called load history.

**Service life:** interval beginning with the manufacturing (for crack growth: the last item inspection or flaw screening proof test after manufacturing, and ending with completion of its specified life).

**Stress spectrum:** same as load spectrum but expressed in terms of stresses.

**Unit load:** a load equal to the unit used in the load curve data base (examples: 1g acceleration, 1°C temperature increase, 1 bar pressure, MDP, limit load case, temperature load case).

**Unit stress:** a stress (or, a combination of stress components), at a specific location, resulting from the application of a unit load on the structure.

## 12.3 List of events

The first step in the process of fatigue load spectrum derivation is the definition of the list of events. The complete service life of a spacecraft or payload can be described by a series of events where each event describes a certain load sequence seen by the structure.

This definition is accurate for items subjected to crack-growth analysis where the initial crack size of the analysis is based on the analysis or proof test. In other cases, like fatigue crack initiation analyses, all load events experienced in the as-manufactured condition are part of the service life (assuming that material properties used in the verification are representative of the as-manufactured condition).

The typical life of a space structure starts with the cutting of the first material. From this material, the parts are produced and combined to form subassemblies and assemblies. This is called the 'production phase'.

Then all parts are collected and assembled. This is called the 'assembly/disassembly phase' (the assembly/disassembly phase also includes the refurbishment of a spacecraft or payload after a certain number of flights). After the assembly of the structure, acceptance tests are generally performed. These tests can be performed in-house or at test facilities elsewhere.

After the assembly phase, a 'transport phase' takes place and then a 'testing phase' (acceptance or qualification), followed by additional transport. These transport and testing phases are repeated for all required vibration tests (in case of in-house testing the transport phase is omitted). After vibration testing the spacecraft is transported to the launch site, again experiencing transport loads. At the launch site the spacecraft starts the flight phase with the mating to the launcher. Sometimes the loads experienced while waiting on the launch pad can be significant.

The flight phase may consist of an Ascent phase, an on Orbit phase and a Descent phase for retrievable payloads.

After the flight phase transport, refurbishment, test and re-flight phases can follow in case the spacecraft returns to earth (for Shuttle payloads in general the possibility of abort landing and re-flight had to be accounted for).

For multi-flight payloads the above described sequence is repeated, with modifications where necessary, to complete the service life, see Figure 12-4 for an example.

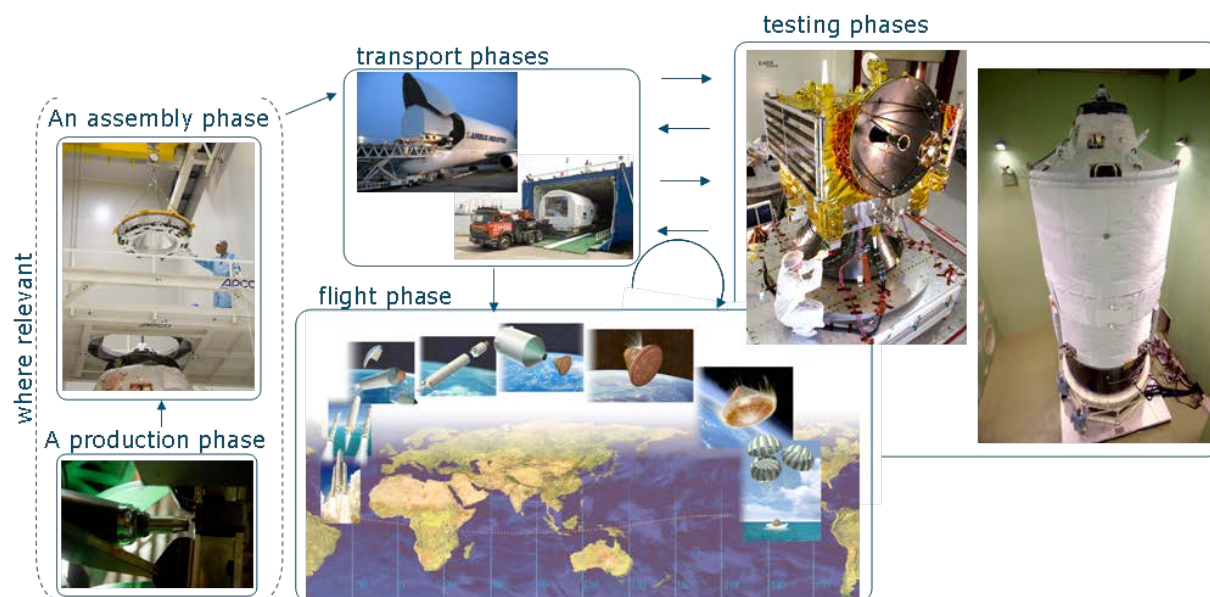


Figure 12-4: Events during service life of spacecraft or payload

For the creation of a load and stress spectrum only the load generating events are relevant. In general, only events after manufacturing are taken into account. In rare cases, however, exceptional initial defects are generated by the manufacturing process (e.g. fatigue cracks due to long grinding operations have been observed). In cases where it is not possible to prevent this, it is normally dealt with on a case by case basis (depending on criticality of failure, inspectability, etc.).

During production, before and after transport, before and after test, and, in case of multiple flights also between the flights, handling events occur. Such events can be separated into transverse (horizontal and vertical) handling, rotational handling and mating handling.

For small payloads with relatively high natural frequencies, handling events can in general be neglected (this can e.g. be justified by comparing the specified allowable accelerations with the design limit accelerations or other dimensioning loads).

The spacecraft or its subsystems can be transported over longer distances by means of:

- Land transport:

On several occasions the spacecraft or its subsystems are transported over the road or by train to test locations, assembly places, harbours, factories etc. During all these transport events the spacecraft or its subsystems are subjected to vibrations induced by the vehicle.

- Sea transport:

Sometimes it may be necessary to transport the spacecraft or its subsystems over water to its destination. During fair weather the load event is the motion of the waves (inertia loads due to rolling of the boat etc.), while in rough weather an additional slamming of the boat may occur.

- Air transport

During its trips through the air the spacecraft or its subsystems are subjected to manoeuvring loads, gust loads and landing loads. Also a continuous vibration takes place due to taxiing, take-off, climb and cruise.

In the testing phase the spacecraft or its subsystems may undergo acceptance testing (including protoflight test where applicable). This may include one or more of the following tests:

- Pressure test;
- Sinusoidal vibration test in X-, Y-, and Z-direction;
- Random vibration test in X-, Y-, and Z-direction;
- Acoustic noise test;
- Shock test in X-, Y-, and Z-direction;
- Thermal test;
- Functional test.

Each of these tests induces certain loads on the structure.

Note: in certain tests (e.g. sine, random) significant 'cross-talk' between the excited axis and transverse axes may be experienced, that may need to be accounted for in the fatigue spectrum.

The flight phase obviously depends on the launcher used for the mission. For the Space Shuttle, the flight phase can generally be split into three main sections:

### 1. Lift-off/ascent

The lift-off/ascent phase starts with the ignition of the main engines and ends with the shutdown of the main engines. In this period the Shuttle and its payload pass through the following flight stages:

- Lift-off, which lasts from main engine ignition via solid rocket booster ignition to main engine throttling;
- High-Q boost, which lasts from main engine throttling all through transonic flight up to supersonic flight;
- Max. boost, which lasts from the start of the supersonic flight to separation of the solid rocket boosters;
- Orbiter max. load, which lasts from solid rocket booster separation, after which the flight continues with main engines only, to main engines cut-off.

### 2. On Orbit

This section of the flight is mission dependent. However, the following environments may be applied to all payloads:

- Thermal cycling,
- Deployment, with the following possibilities for deploying a spacecraft or payload:
  - Spinning up and push out by springs;
  - Deployment of appendages. Note that for deployable or reconfigurable structures, the unit stresses may be different in the various configurations. In that case the configuration applicable to each event should be defined.
  - Remote manipulator handling (NSTS and ISS);
  - Items removed from launch attachment or from soft stowage used for launch, and mounted in on-orbit configuration.
- Load events occurring during the mission, e.g. pressure cycles, rotation and actuation of equipment, docking loads, exercises, AOCS and other manoeuvring loads, plume impingement, etc.

NOTE:

Due to the micro-gravity environment experienced on board of most spacecraft, most or all of the inertial load events experienced on orbit may be negligible both from fatigue and residual strength perspective. Other loads (thermal, deployment) can be quite demanding.

### 3. Descent/landing, where applicable

The descent/landing can be separated into:

- Descent in which the vehicle bumps back into the atmosphere (re-entry), and flight with many manoeuvres to decrease speed and height, including parachute deployment when relevant;
- Landing, during which the vehicle touches the ground with the main landing gear and the nose landing gear, after which the roll-out (including braking) takes place, or alternatively water/land landing with parachute and retro-rockets. These stages are indicated in Figure 12-4. A ferry flight was a typical part of the Shuttle post-landing events.

After the landing the demating takes place, where applicable.

## 12.4 Load spectra per event

### 12.4.1 General

The next step in the process of deriving a fatigue load/stress spectrum is generating load spectra for the loads occurring in each event that is present in the event list. A load spectrum, sometimes also called exceedance curve, describes the relation between a load value and the cumulative number of times this value occurs. An exceedance curve is defined for a certain physical unit, like time (e.g. hour or day), or length (e.g. km or miles) or event (e.g. mating or launch). Another format is available in ESALOAD identified as 'load curve' which lists the number of cycles instead of the cumulative number of cycles but also contains the combination of different loads. See Figure 12-5 for an example of an exceedance curve.

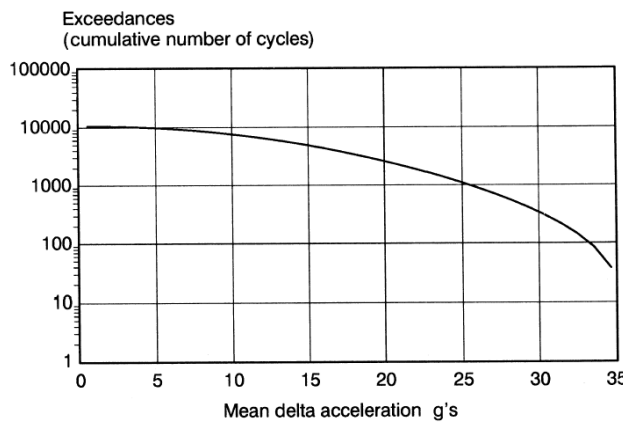


**Figure 12-5: Example of load (exceedance) curve**

A load curve contains load data e.g. in the form of (cumulative) number of cycles versus mean and/or alternating:

- acceleration values;
- pressure;
- temperature;
- other load components like hyperstatic loads (see e.g. [4]).

Load curves can be obtained from available existing load curves, by counting available (measured) load data, or from a structural response analysis. This is described in the following sections.

### 12.4.2 Existing load curves

Existing load curves, either from previous project related to identical (or conservative) events, or normalized curves from e.g. [3] and [5] can be useful when the load levels and number of cycles are not known (yet). Since the dynamic behaviour of the (sub)structure under consideration can differ from those for which the standard load curves are derived, the standard load curves may need to be changed to reflect these differences. If it is assumed that the distribution of cycles over the load range depends on the event only and not on the limit load itself, linear scaling of the cycles and accelerations of the load curves can be used without having to redistribute load values over the total load range. Furthermore, knowing that a load curve is merely a collection of load data versus cycles, scaling of the load curves can generally be split in two distinct parts:

- Scaling of number of cycles based on the fundamental (first mode) frequency
- Scaling of load values to the appropriate limit load

Appendix B of reference [3] contains normalized load curves for (careful) handling, transport, ascent and descent events. It should be noted that these curves are not symmetric in X, Y, and Z-direction, and assumptions about payload orientation are made. Gravity (+1g) is in Z-direction for all ground phases. For handling and transportation events, in general X is the direction of movement (except for e.g. hoisting and tilting). In case the orientation of the item is not fixed during these operations, or unknown, conservative assumptions can be made, e.g. by manipulating the curves. In general using conservative assumptions is not a problem as long as handling and transportation loads are small w.r.t. flight and test loads.

The handling and transport loads are typically derived for large payloads (assemblies) which are handled carefully, and transported by means of a well damped transportation system with a resonance frequency of 5 Hz.

For small payloads with relatively high natural frequencies, conservative estimates of the transport environment can be made without significant effect on fatigue and crack growth life, e.g. by scaling the standard load curve accelerations to the specified maxima for transport of these payloads, and the numbers of cycles of the standard load curve (derived for transport on a 5 Hz attenuation frame) to the frequency of the actual suspension. This approach is valid as long as no resonance frequencies are excited which would require a different approach not being covered by the standard load curves.

The ascent and descent standard load curves are worst case combinations of the load curves from various STS flights and are normalised to a limit load of 100g (or 100%). These load curves are derived for payloads with significant natural frequencies below 50 Hz and are considered conservative for payloads with significant natural frequencies below this 50 Hz. For payloads with higher significant natural frequencies, e.g. smaller payloads, the number of cycles in each load step can be considerably higher, and should therefore be scaled accordingly:

$$N_y = N_{stdbase} \cdot \frac{f [Hz]}{50 [Hz]} \quad [12-1]$$

where:  $N_y$  is the new (scaled) number of cycles;

$N_{stdbase}$  is the number of cycles in the standard data base; and

$f$  is the relevant natural frequency

For flight load curves that are all scaled to 100 g in each direction the scaling is given as:

$$P_y = P_{stdbase} \cdot \frac{LL[g]}{100[g]} \quad [12-2]$$

where:  $P_y$  is the new (scaled) load;

$P_{stdbase}$  is the load in the standard data base; and

$LL$  is the relevant limit load

Naturally, if different limit loads apply for different load directions, different scaling factors also apply.

All the standard load curves provided with ESALOAD have a mean acceleration of 1.0 g in z-direction (gravity pull) and 0.0 g in other directions (exceptions: launch and on orbit thermal cycling events). Around this mean value the alternating values are defined, depending on direction/load type. Therefore, for scaling the standard load curves, only the delta accelerations should be multiplied by the appropriate limit load ratio.

Appendix D of reference [5] gives the Goddard Space Flight Center (GSFC) equivalent spectrum for the Shuttle launch and landing events. It is applicable for primary load-carrying payload structure in the Space Shuttle Orbiter payload bay and for payloads with a fundamental frequency below 50 Hz. Payloads that have a fundamental frequency above 50 Hz may be analysed by applying the following multiplication factors to the number of cycles of the GSFC flight spectrum:

Fundamental frequency	Multiplication factor
0 – 50 Hz	1
50 – 100 Hz	2
100 – 200 Hz	4
200 – 300 Hz	6

These GSFC launch and landing curves are slightly different than the ESALOAD ascent and descent curves, especially for the descent event the ESALOAD curve in Y-direction is more severe.

Also for other vehicles and missions dedicated fatigue spectra may be available (e.g. HTV (JAXA), Dragon (SpaceX)).

### 12.4.3 Measured load curves

When standard or previously derived load curves are not available, but load time history data are available, then this information can be used to generate load curves. Since only minima and maxima are of importance in a fatigue or crack propagation analysis, the load time history can be reduced by removing intermediate points and retaining the reversal points. Then two options are available:

- Store the compressed peak-valley sequence, where a Rise-Fall filter to remove non-damaging small peak-valley cycles can be used. This option can result in very large load curves as only subsequent cycles with the same minimum and maximum values are applied together as one load line.
- Use counting methods to reduce the load time history into a load or exceedance curve. Several counting methods have been proposed (see [7] and [8]), like peak counting, level crossing counting, range counting, but the counting method most commonly used in relation to fatigue analysis is the Rainflow counting or 'range pair-range' method.
- The Rainflow or Pagoda-roof method was developed at the end of the 1960's in Japan [6]. In Europe at the same time and independently, a counting method was developed that was later called the range pair-range counting method [7]. Although the descriptions of both sources are very different, both yield the same result, that is, they extract the same range pairs and single ranges from the load.
- Using the range pair-range description, the principle of the algorithm can be simplified to three elements:
  1. Search for extremes:  
The continuous signal is searched for peaks and valleys.
  2. Full-cycle recognition:  
Employing a four-point check the time domain data is searched for full cycles that are contained within major single ranges, see Figure 12-6. A range filter of certain size can be applied to suppress the smallest ranges. The full cycle found is deleted from the 4-points sequence and a new 4-point sequence is evaluated "moving backwards" two points. If the above criterion is not met one step forward is taken, and so on. The successive full cycles found are stored in a from/to Markov matrix.

## 3. Residue handling:

After having omitted all full cycles from the sequence as depicted under 2, a "residue" of single load ranges remains that has a diverging-converging shape. As seen in Figure 12-7 the residue contains the largest load variation present within the signal. The single load ranges are stored in the from-to level Markov matrix additionally to the already existing full-cycle content by means of range-counting.

This way of storing has the advantage that all one-dimensional counting results (peak counting, level crossing counting, etc.) can be derived from the matrix directly [7].

Since the measured load time history often does not reach the limit level, it may be appropriate to apply a factor to the obtained load curves in order to represent the limit load level according to the applicable definition of limit load level.

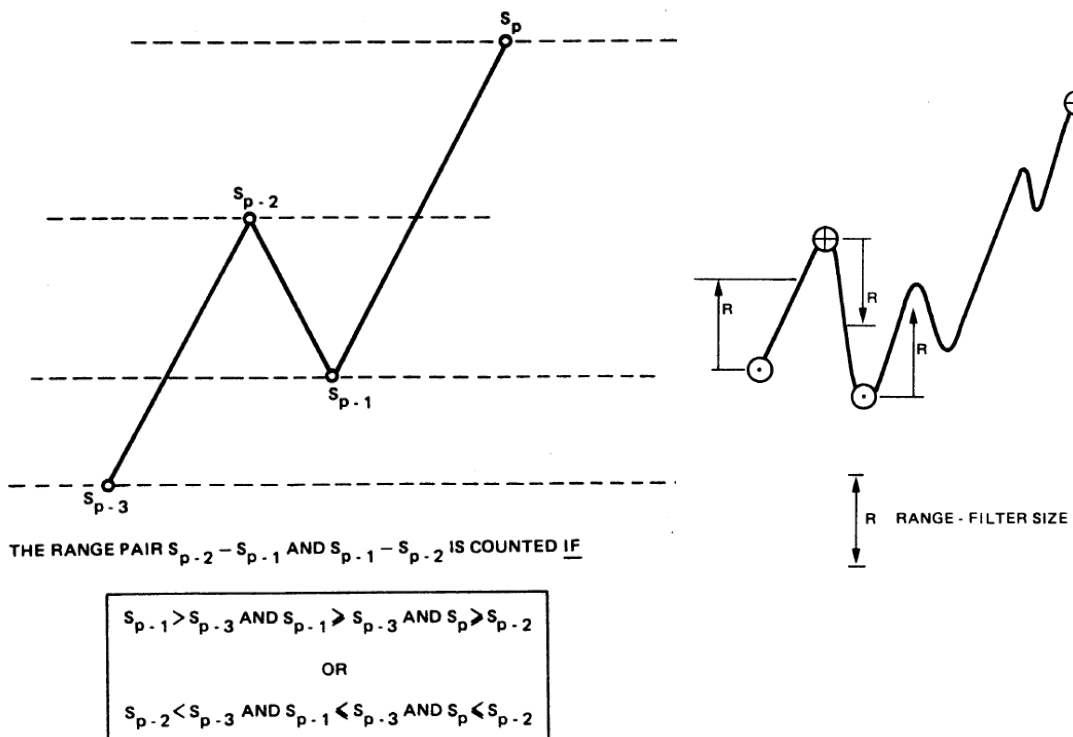


Figure 12-6: Rainflow (range pair-range) counting criterion



Figure 12-7: Typical residue shape

## 12.4.4 Calculating load curves

### 12.4.4.1 Introduction

A possible but generally relatively ‘expensive’ method for load curve generation is coupled analysis, i.e. a finite element analysis of the launcher together with the spacecraft, to obtain the behaviour and the response of the combined launcher-spacecraft system.

For dynamic load events as experienced in sine tests, random tests, acoustic tests, shock tests and certain flight events, load curves can be calculated based on the structure’s dynamic behaviour and its loads. This load curve calculation approach is based on the use of a transmissibility function. This transmissibility function relates the excitation input to the response. If the excitation input and the transmissibility function are known, the response (and thus the load curve) can be calculated.

The transmissibility function is defined as the absolute value of the dynamic transmissibility,  $T(\omega)$ , previously defined in Eq. [5-43] and which can be rewritten as:

$$T(\omega) = 1 + \sum_{k=1}^N \frac{\omega^2}{\omega^2 + 2i\zeta_k \omega_k \omega + \omega_k^2} \cdot \tilde{T}_k \quad [12-3]$$

where:  $\omega$  is the frequency

$\omega_k = 2\pi f_k$  is the natural frequency of mode  $k$ ;

$\zeta_k$  is the modal viscous damping of mode  $k$ ;

$\tilde{T}_k$  are the modal effective transmissibilities for each direction of mode  $k$ , and defined in Eq. [5-48]. They can be positive or negative, but the sum of all the effective transmissibilities is equal to one.

The transmissibility function is fully described when the above data is given for each mode. The theoretical background of the modal analysis used in ESALOAD is described in Appendix A of [3].

Modal data can be obtained from a finite element dynamic analysis.

If the structural responses are known, for instance from measured vibration test responses, the data can be given as input directly.

Before being able to create new load curves with the previously defined structural transmissibility definitions, the load input at the base or foundation of the structure needs to be defined. In general the forcing function, i.e. the input, can consist of contributions from:

- sine vibration loads;
- random mechanical loads;
- transient loads; and
- acoustic loads.

Sine vibration loads are normally given as applied acceleration levels versus excitation frequency, at a given sweep rate (in oct/min).

The random mechanical loads are given in terms of power spectral density (PSD) versus frequency.

The transient loads can be given in terms of a shock response spectrum or a Fourier transform, defining the behaviour of the structure at its natural frequencies. Sometimes forcing functions are defined directly.

Finally, the acoustic loads are normally given in terms of sound pressure levels (SPL) versus frequency, for a given duration. These sound pressure levels are converted into power spectral densities in order to make additions of loads possible.

Obviously the different load types require different mathematical treatment in order to calculate the response.

In general the total dynamic load during a flight consists of contributions from:

- random loads;
- shock/transient loads;
- acoustic loads, and
- constant loads (quasi-static).

#### 12.4.4.2 Calculating the response

In this section, the relations for calculating the response due to the different input types are given.

##### 12.4.4.2.1 Response from shock/transient input

It is assumed that the acceleration at the base of the structure  $\hat{\ddot{q}}_r$  is known as a Fourier transform. The Fourier transform of the response becomes

$$\hat{\ddot{x}} = T(\omega) \hat{\ddot{q}}_r \quad [12-4]$$

To get the time history of the acceleration response,  $\hat{\ddot{x}}$  is back-transformed according to:

$$\ddot{x}^p(t) = \frac{1}{2\pi} \int_{-\infty}^{\infty} T(\omega) \hat{\ddot{q}}_r e^{i\omega t} d\omega \quad [12-5]$$

If the damping  $\zeta_k$  is small (less than 5 %), if the frequencies are well separated and if the natural frequencies of the structure are

$$\omega_k \quad k = 1..N \quad [12-6]$$

a reasonable approximation of equation [12-5] is

$$\ddot{x}^p(t) = \sum_{k=1}^N 2\zeta_k \omega_k T^p(\omega_k) \hat{\ddot{q}}^p(\omega_k) e^{-\zeta_k \omega_k t} \sin(\omega_k t) \quad [12-7]$$

where the index  $p$  denotes the direction of the base excitation.

##### 12.4.4.2.2 Response from random input

The random input signal, given as a power spectral density load  $S_r(\omega)$ , is applied at the base. The corresponding response is also a power spectral density and is given by

$$S^p(\omega) = T(\omega) T^*(\omega) S_r(\omega) \quad [12-8]$$

where the index  $p$  denotes again the direction of the base excitation and  $T^*(\omega)$  is the complex conjugate of  $T(\omega)$ .

The root mean square of the response acceleration in the direction  $p$  is

$$\ddot{x}_{rms}^p = \sqrt{\int_0^\infty S^p(f) df} \quad [12-9]$$

The maximum acceleration is normally taken as 3 times the standard deviation for an event of limited duration.

#### 12.4.4.2.3 Response from acoustic load

In many cases random loads on subsystems, resulting from acoustic loads on the spacecraft, are directly specified and can be treated as above. In some cases the following alternative empirical approach may be suitable: A reference structure is used to predict the behaviour of a new structure, and the relation between the reference structure and the new structure, determined by experiment, is defined by the factor

$$C_r(f) \quad [12-10]$$

describing the ratio of the resulting vibration to the magnitude of the fundamental source as a function of the frequency or the bandwidth. This approach is called the frequency response method.

$C_r(f)$  values have been calculated among others, by Brust and Himmelblau [10]. In order to calculate the response of a new structure the frequency response method assumes the following relation.

$$S_r(f) = C_r(f) S_n(f) \quad [12-11]$$

where:  $S_r(f)$  is the power spectral density of the response; and

$S_n(f)$  the sound pressure level of the acoustic load.

The response at the point of interest can be calculated with the aid of the formulas given for random base excitation.

The method translates power spectral densities (actually sound pressure levels) measured above the structure into power spectral densities measured on the structure.

This method is easy to use and applicable for several types of structures if they resemble the reference structure. In this case, the reference structures were large panels on B52 and B58 aircraft. In relation to satellites (spacecraft), the use of these data is conservative.

Cases that are not covered by the above are treated on a case by case basis.

#### 12.4.4.2.4 Response from Sinusoidal Input

For a sine test, the input is given as acceleration amplitudes  $\hat{q}_r$ , which are specified at each frequency. The response amplitude can then simply be calculated from

$$\hat{x} = T(\omega) \hat{q}_r \quad [12-12]$$

Equation [12-12] thus describes the response amplitude at the point of interest as a function of the input frequency  $\omega$ .

#### 12.4.4.3 Calculating the number of cycles

In order to obtain the load curves, the number of cycles for each load level is needed. The calculation of the number of cycles is in general different for the different types of excitations and thus responses.

#### 12.4.4.3.1 Cycles for Transient Loads

The time signal is a superposition of sinusoidal motions decaying in time. The signal with the highest frequency varies most rapidly. This signal is first removed from the time signal. It corresponds to cycles with the amplitude

$$2\zeta_N \omega_N T^p(\omega_N) \hat{q}^p(\omega_N) e^{-\zeta_N \omega_N t} \quad [12-13]$$

Where index  $p$  denotes the direction of the base excitation. The amplitude decays according to

$$\ddot{x} = kst \cdot e^{-\zeta_N \omega_N t} \quad [12-14]$$

The number of cycles and the associated amplitudes can be calculated from these relations. The time for which the sine performs one cycle can be calculated from

$$\Delta t = \frac{2\pi}{\omega_k} \quad [12-15]$$

where  $\omega_k$  is the natural frequency and  $\Delta t$  the time in seconds.

The number of cycles is attached to a certain discrete load (stress) level. In ESALOAD this is accomplished by dividing the total load range into 32 load intervals.

Next the second highest frequency is considered. To remove it from the time signal we take for the amplitude of the cycles

$$\sum_{k=N-1}^N 2\zeta_k \omega_k T^p(\omega_k) \hat{q}^p(\omega_k) e^{-\zeta_k \omega_k t} \quad [12-16]$$

Again the number of cycles and the amplitude can be calculated. This is done until the lowest natural frequency is reached.

#### 12.4.4.3.2 Cycles for Random and Acoustic Loads

Suppose the random base excitation is stationary and normally distributed. Then the expected rate of upcrossings of a level  $b$ , i.e. per second, can be calculated from

$$v_b^p = v_0^p e^{\frac{-b^2}{2M_0^p}} \quad [12-17]$$

where:

$$v_0^p = \sqrt{\frac{M_2^p}{M_0^p}} \quad [12-18]$$

$$M_i^p = \int_0^\infty f^i S^p(f) df \quad [12-19]$$

Here  $v_0^p$  is the number of zero crossings per second when the base is excited in the p-direction.  $M_0^p$  is the variance of the motion in the p-direction, when the mean is assumed equal to zero.

#### 12.4.4.3.3 Cycles for Sinusoidal Loads

For the calculation of the number of cycles for a sine load the following is assumed. The frequency range is divided into a certain number of frequency ranges for which the response amplitude (acc. Eq. [12-12]) is assumed constant. If the sweep rate, i.e. the number of octaves per minute, is  $v_{oct}$  then the number of cycles, when the frequency goes from  $f_{i-1}$  to  $f_i$ , is defined by

$$cyc = \frac{60(f_i - f_{i-1})}{v_{oct} \ln(2)} \quad [12-20]$$

## 12.5 Generation of fatigue spectra

A fatigue load spectrum can be created by combining all events with their relevant load curves. The fatigue load spectrum gives the total number of cycles versus mean and alternating accelerations, pressure and temperature for all the different events. A fatigue load spectrum is typically derived for a (sub)system.

A fatigue stress spectrum is an input to the fatigue and crack growth analysis and needs to be available before performing such an analysis. Therefore, the fatigue load spectrum needs to be converted to a fatigue stress spectrum. Although this is normally not a loads analysis, it is included here for completeness.

Generally speaking, each payload has several critical items with different potentially critical locations that should all be studied in detail with respect to fatigue or crack growth. Clearly, a fatigue stress spectrum varies according to the stress-state of the individual item. Therefore a fatigue stress spectrum is needed for each component to be analysed, and possibly also for each location on the component.

The stress-state of the individual item depends on the loads on the complete payload or (sub-)system. The stress at the considered location can be determined by:

- using load cases as input for a FEM analysis, or by
- using unit stresses that relate the load information for the (sub)structure to the item's stress-state (location specific).

Unit stresses are typically derived by applying unit acceleration loads (or unit pressure/temperature) to the structure at the centre of gravity, normally derived with the use of finite element models. Unit stresses may not only vary due to the location on a part, but also due to change of configuration or boundary condition (e.g. launch vs. on-orbit configuration, test vs. flight boundary condition). In order to simulate this different unit stress definitions with load curves of different events may be needed.

According to [2], principal stresses must be used to define the fatigue spectrum. To simplify the work, in many cases von Mises stresses are employed in the analysis. However, this is not always conservative: for e.g. cylindrical pressure vessels the von Mises stress may be lower than the maximum principal stress. Conservatism of the applied approach based on von Mises stress is then verified on a case by case basis.

Figure 12-8 may be useful in understanding the situation for plane stress ( $\sigma_z = 0$ ) states, as encountered in many practical cases (e.g. near stress free surface). The minimum ratio of von Mises stress divided by the maximum absolute principal stress appears to be 0.87, i.e. up to 15% unconservatism, which can have very significant effect on the life.

In a 3D tensile stress state the unconservatism can be very large: in the limit the von Mises stress can be zero for hydrostatic stress state ( $\sigma_x = \sigma_y = \sigma_z = \sigma_1 = \sigma_2 = \sigma_3$  where 1, 2, and 3 are the principal stress directions) while the principal stress is finite.

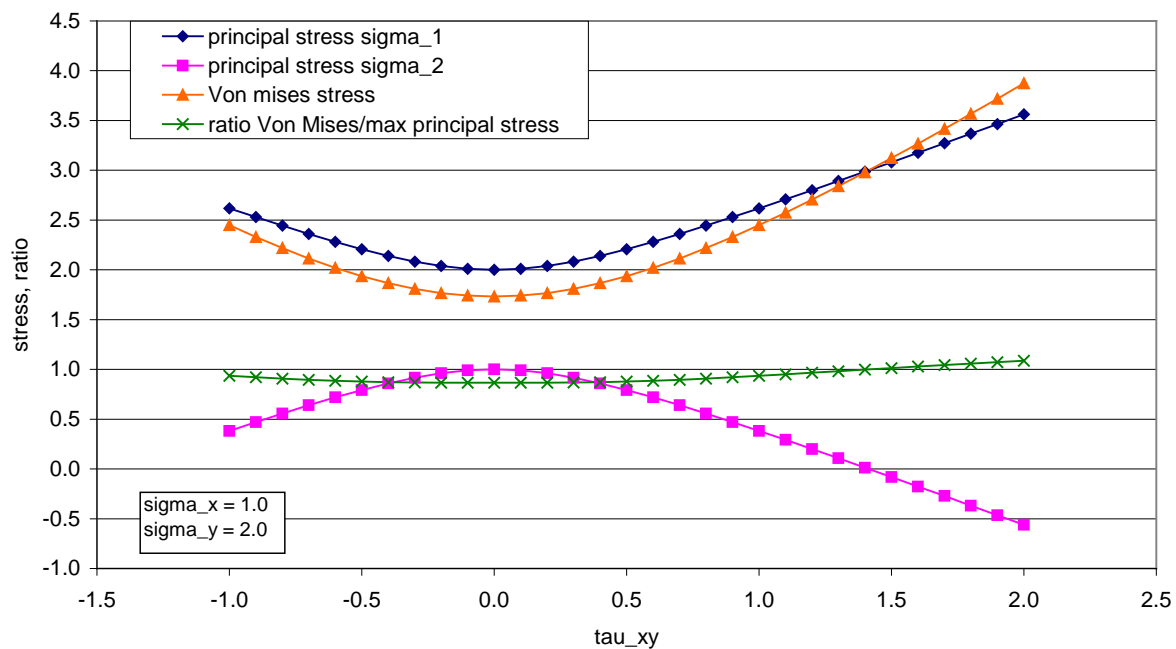


**Figure 12-8: Comparison of von Mises stresses with principal stress, example only**

Sometimes the dynamic and static behaviour of a structure is not the same in terms of mode shape and deformed shape. For instance, the static application of a unit load may result in a pure (overall) bending of the structure, while the mode shapes show bending about two axes. In such cases, it is advisable to analyse smaller parts of the structure where loads can be adequately described by (local) uniform accelerations.

The unit stresses are multiplied by the load factors in the load spectrum to obtain the stress spectrum. It is however clear that multiple loads, i.e. cycles of dynamic loads from different directions, occur at the same time, but no information about their relative phase exists. In many cases (including ESALOAD), as an assumption, alternating stress components due to acceleration components (both linear and rotational) are evaluated in all possible combinations.

## 12.6 References

- [1] ECSS-E-ST-32C, Space engineering - Structural general requirements, Rev. 1, November 2008
- [2] ECSS-E-ST-32-01C, Space engineering - Fracture control, Rev. 1, March 2009
- [3] Veul, R.P.G., Brunetti, F., Sinnema, G., Henriksen, T.K., "ESALOAD User's manual, version 4.2.1a", Annex 1 of ESACRACK Manual TEC-MCS/2006/1448/In/GS, Issue 3, July 2010.
- [4] Veul, R.P.G., "Evaluation and guidelines of the NASA STS flight load curves implemented in ESALOAD", NLR-CR-2004-511, December 2004
- [5] NASA-HDBK-5010, Fracture control implementation handbook for payloads, experiments, and similar hardware, May 2005
- [6] Matsuiski, M. and Endo, T., "Fatigue of Metals Subjected to Varying Stress" (in Japanese), Kyushu District Meeting of the Japan Society of Mechanical Engineers, No. 68-2, pp. 37-40, Fukuoka, Japan, March 1968

- [7] Jonge, J. B. de, "The analysis of load-time histories by means of counting methods", Helicopter Fatigue Design Guide, AGARDograph No. 292, pp. 89-105, Advisory Group for Aerospace Research and Development, 1983
- [8] Lalanne, C., "Fatigue damage, mechanical vibration & shock analysis", Volume 4, Hermes Penton Ltd, London, 2002
- [9] Mushung, L.J., DeFord, L.C., "Ferry Flight Loads Environment for Returnable Payloads", SMD-91-2104, Lockheed Engineering & Science Company, 1991
- [10] Himmelblau, H., Myron Fuller, C., Scharton, T., "Assessment of Space Vehicle aeroacoustic - vibration prediction, design and testing", NASA-CR-1596, 1970
- [11] Devoldere, D., Sinnema, G., Bureau Dacal, R., "Guidelines to create stress spectra for small payloads transported by Soyuz or Progress module", TEC-MCS/2004/1110/ln/DD, 2004

## 13

# Micro-gravity and micro-vibrations

## 13.1 Introduction

### 13.1.1 Background

Both micro-gravity and micro-vibration (also frequently called jitter in particular in the American technical literature) are sometimes embraced by the term micro-dynamics which describes more generally the dynamic environments that are characterised by very low acceleration levels transmitted by the spacecraft structures. Both the acceleration responses and the force levels causing these accelerations are significantly below usual structural design loads and dynamic environments encountered by the spacecraft structure during launch. As a result, they are not considered to jeopardize the structural integrity of a spacecraft.

Why then, are they a concern for space missions?

Taking into account the micro-gravity and micro-vibration environments must be considered a relevant aspect for verifying the mission performances in terms of providing a very low gravitation environment for micro-gravity experiments, e.g. on-board the space station, or for compliance with high pointing requirements of optical instruments on space telescopes.

Both the micro-gravity and micro-vibration environment assessments are concerned with the following:

- To investigate the transmission of very low vibrations by the spacecraft structure from the disturbance source to the receiver location which might be a sensitive instrument or payload, respectively;
- To identify whether the performance requirements for the instrument or payload, respectively, are fulfilled under the influence of the relevant disturbance sources;
- Where necessary, to find adequate methods to attenuate the vibrations along the transmission path.

The micro-gravity environment is characterised by the following:

- Requirements concern the provision of a low gravitation environment that is required for micro-gravity experiments. These requirements are usually defined in terms of maximum residual accelerations versus frequency (typically  $10^{-6}g$  for frequencies less than 1 Hz and up to  $10^{-3}g$  for frequencies above 100 Hz).
- In general micro-gravity environment requirements are applicable only to manned spacecraft, in particular laboratory modules where micro-gravity experiments are performed.

Note: The low gravitation environment requirements for the GOCE (Gravity field & steady-state Ocean Circulation Explorer) satellite have been an exception from this general rule due to the specific mission objectives to map the Earth gravity field in unprecedented detail.

- Continuous quiescent periods might be required up to several weeks dependent on the experiments to be performed.

On the other hand the micro-vibration environment is characterised by the following:

- Requirements concern the stability of the spacecraft platform; they are usually defined in terms of maximum allowable distortions and resulting pointing errors of the line of sight of high accuracy pointing payloads.
- In general micro-vibration environment requirements are applicable to scientific, Earth observation and telecommunication satellites.
- Requirements for continuous quiescent periods might reach from short term periods of just a few minutes up to long term periods of several months depending on the instrument operation times and related high pointing stability requirements.

Due to the complex nature of the micro-gravity and micro-vibration environment control iterative steps are usually required, in general involving disturbance characterisation tests, relevant performance predictions, end-to-end verification tests at satellite system level and finally updated performance predictions employing test validated inputs and models.

### **13.1.2 Scope**

This chapter provides an overview how to assess the effects of the micro-gravity and micro-vibration environment, respectively, and how to determine the proper design measures to achieve compliance with the specified mission performance requirements. Both subjects are first addressed in dedicated sections; then the applicable disturbance sources, to a large extent common for both environments, are identified and described with the necessary detail.

## **13.2 Micro-gravity**

One of the major goals for the future space utilization projects is to conduct activities, experiments and processes in a very low gravity environment, the so-called micro-gravity environment. Micro-gravity environments, partially with very stringent requirements, are usually required for low-earth-orbiting spacecraft systems and pressurized module compartments without interruptions over long periods of time in order to allow performing e.g. material processing, fluid physics and scientific experiments.

Consequently spacecraft systems should be designed and operated such that limit acceleration levels are not exceeded during the execution of such experiments and processes.

In the following sections the general aspects related to the micro-gravity environment (Section 13.2.1), the derivation of micro-gravity specifications (Section 13.2.2), and the verification of the micro-gravity requirements (Section 13.2.3) are illustrated and explained.

Further details concerning micro-gravity environment control methods and verification tools are provided in the final report of the ESA study "Microgravity environment dynamic disturbance study", [1] where also a computational model for the prediction of dynamic disturbance effects has been developed. In the follow-on study "Microgravity payload disturbance study", [2], relevant guidelines were established for the design and development and the requirement verification of micro-gravity environment disturbance sources / mechanisms contained in the micro-gravity mission payloads.

## 13.2.1 General aspects

The scope of this section is to describe the ranges of applicability of the micro-gravity environment, the ways in which the micro-gravity requirement can be defined and furthermore the different criteria for identifying the satellite / ISS module reference configuration and the interfaces to micro-gravity payloads.

### 13.2.1.1 Applicability

Micro-gravity environment requirements have an impact at all levels of spacecraft design, e.g. concerning orbit attitude and orientation stability, mission timeline, spacecraft configuration, on-board mechanisms, mass motions, fluid vibrations, thermally induced stick/slip in structural joints and also crew motion and handling as well as acoustic noise in manned modules.

In general the disturbance forces, torques and accelerations are transmitted from the sources to the receiver locations by the connecting structure due to accelerated rigid body motions and structural dynamic vibrations. When noise producing equipment is installed in pressurized compartments and this equipment is generating structural and airborne vibrations then a secondary transmission path, namely the vibro-acoustic coupling should be taken into account.

Usually all activities, from system level down to equipment level, which are necessary to verify that the micro-gravity environment requirements are not exceeded can be organized within a micro-gravity environment control plan document.

The relevant statements of work should make the micro-gravity environment control plan document applicable to the flight configuration of the spacecraft system and to the related sub-system and equipment sub-contractors.

Initial steps towards micro-gravity environment specification and control comprise:

- The identification of competing requirements on system/flight configuration level followed by appropriate system definition or requirement re-definition.
- A particular effort on all relevant levels yielding an identification of all micro-gravity disturbances, their determination and the definition of major emphasis areas.
- The breakdown and allocation of individual requirements to all essential disturbance sources.
- The identification and assessment of new and novel means for avoiding, attenuating or compensating micro-gravity disturbances.

After the allocation of requirements to the different levels, which should be achieved prior to starting the Phase C/D of the satellite project, a very strict design, hardware and software evaluation in the light of allocated requirements should be performed with early emphasis on major micro-gravity disturbance sources.

Early micro-gravity requirement fulfilment assurance by the design can be achieved with general/generic transfer functions and preliminary equipment test results which properly describe, and help to evaluate, the disturbance factors.

Respective tools consist of computational models based upon test databases which are suitable for the structural and vibro-acoustic transfer function evaluation for comparison with the specified ones.

The micro-gravity environment control approach generally follows, for example, the design development cycle as shown in Figure 13-1.

The preliminary design definition is used to perform an initial micro-gravity analysis resulting to the identification of design optimization needs.

The analysis should be supported by tests and experimental measurements, as early as test hardware is available, because the analytical assessment is limited and should include, to a major extent, empirical data of the units under design.

In the final performance units should be tested for verification of the specifications, with analytical corrections, if necessary.

Design optimization might become necessary with iterative steps after initial modifications, repeating the design and development cycle.

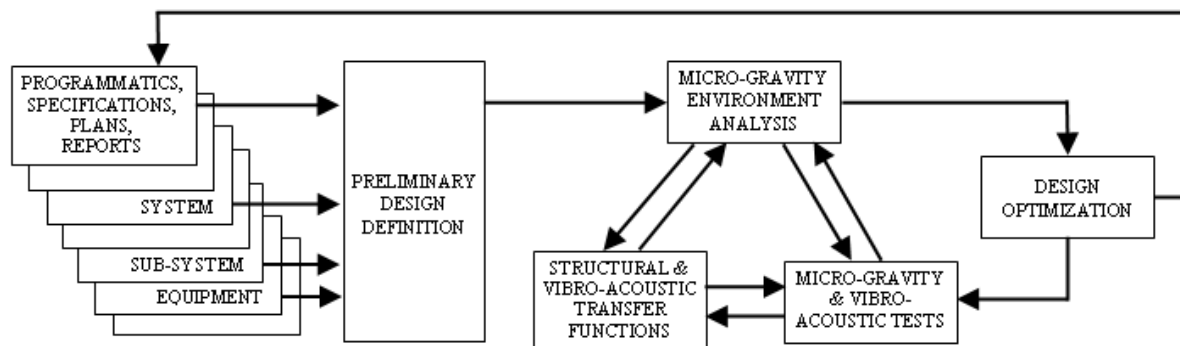


**Figure 13-1: Micro-gravity environment control approach – design and development cycle**

Design and development activities do not rely on the control of perturbations sources, only. The transmission of vibration to the micro-gravity specified interfaces, the interaction of forces and torques with the spacecraft rigid body motions and structural dynamics including fuel sloshing and flexible appendages should be controlled as well.

This includes the structure-borne transmission paths and also air-borne and fluid-borne transmission paths in case of pressurized structure.

In Figure 13-2 the interrelationship of design specification and verification responsibilities from system to equipment level, and vice-versa the basic design verification from equipment level up to system level is shown.

The flow diagram follows in principle the project schedule and the key milestones for the exchange of data are closely related to the individual design reviews:

- System/Flight configuration design reviews
- Sub-system design reviews
- Equipment design reviews
- Interface reviews

The documentation to be produced on the individual project levels for review and verification of the micro-gravity natural and induced disturbances should be:

- a. Micro-gravity environment control plan – at system configuration level
- b. Micro-gravity analysis and budget reports on system configuration, sub-system and equipment level

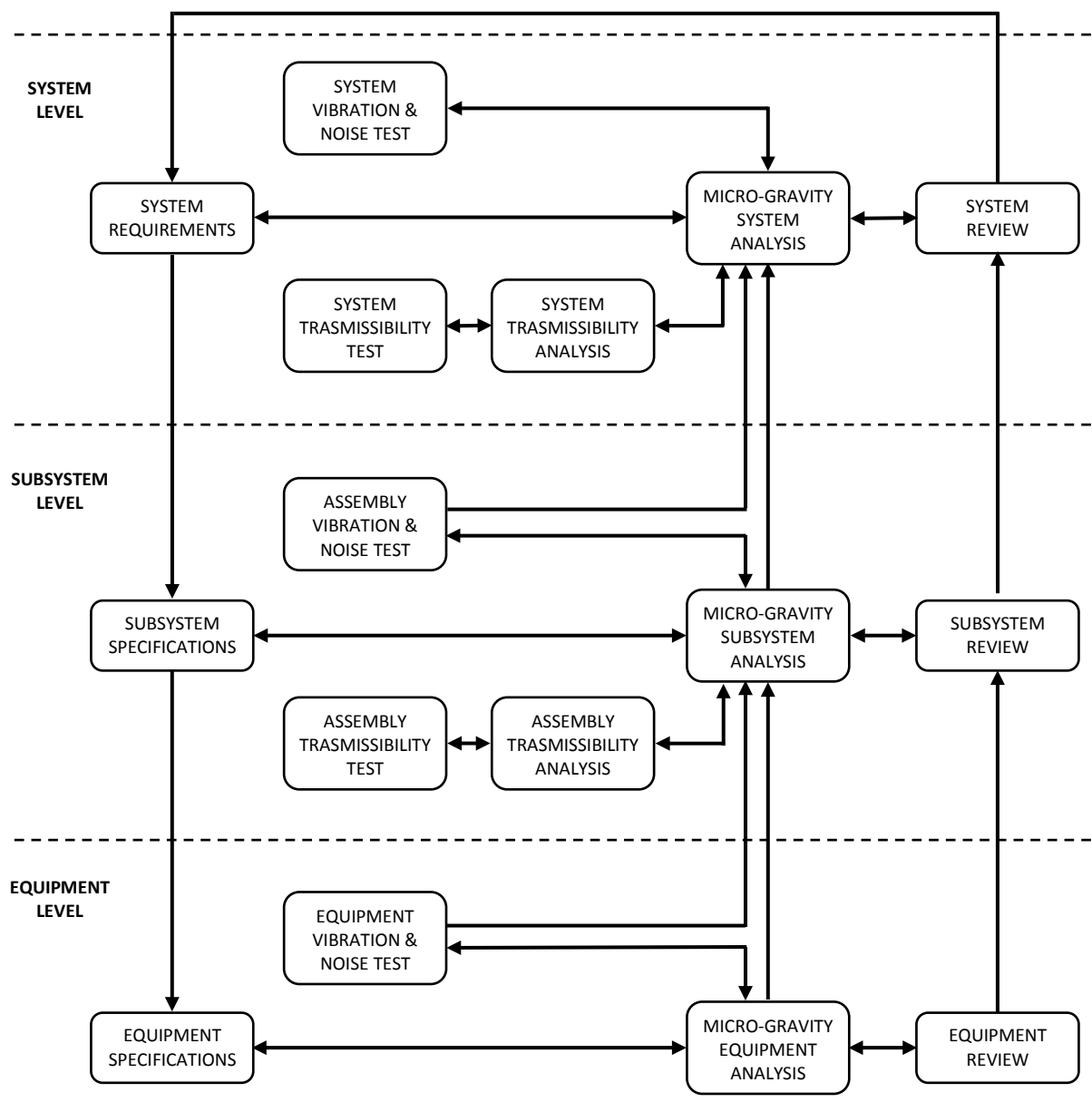


**Figure 13-2: Micro-gravity environment control approach – design, specification and verification flowchart [3]**

### 13.2.1.2 Micro-gravity system requirements definition

#### 13.2.1.2.1 Introduction

The micro-gravity environment requirements at system level are normally issued by the customer within the *System Requirements document* and implemented in the *Satellite System Specification document*. The latter document provides the micro-gravity requirements together with the indication of the verification method at system, assembly/subsystem and equipment level.

The micro-gravity system requirements are usually defined as follows:

*"The disturbances of the micro-gravity environment generated by the system and its subsystems and equipment excluding disturbances from payloads, servicing, crew activities, maintenance, reconfiguration shall not exceed certain acceleration limits characterised both in time (i.e. quasi-steady and transient categories) and frequency domain (i.e. vibratory category)."*

### 13.2.1.2.2 Time domain micro-gravity requirements

There are several ways to express the micro-gravity requirement in the time domain. The following classification can be applied:

- 1) The micro-gravity requirement is considered depending on the type of the disturbance source, so it can be referred to:
  - a. transient and impulsive sources
  - b. quasi-steady sources
- 2) The micro-gravity requirement is considered depending on the location where this requirement should be verified, hence it can be defined at:
  - c. the payload reference mechanical interface location
  - d. the disturbance source mechanical interface location
- 3) The micro-gravity requirement is considered associated to the physical quantity that must be verified; then it can be defined in terms of:
  - e. linear acceleration peaks
  - f. linear force peaks
  - g. linear impulse levels

Consequently, in the past space projects, the micro-gravity requirement in the time domain has been found described as a combination based on the above classification. The following combinations have been used in practice to specify the micro-gravity requirements:

- Combination of the points a), c) and e):
- Combination of the points a), d) and g):
- Combination of the points a), d) and f):
- Combination of the points b), d) and g):

As an example, the combination of the points a), c) and e) leads to the following definition of the micro-gravity requirement:

*"The micro-gravity requirements at the payload reference mechanical interface location, during the measurement mode, are expressed so that the induced perturbations on the micro-gravity environment over any time period caused by all transitory and impulsive sources of the satellite and its subsystem/equipment should generate any linear acceleration ( $\mu\text{g}$ ) at the micro-gravity reference mechanical interface locations with peaks not higher than certain values in a time record of certain duration".*

Usually acceleration limits are referred to the micro-gravity payload mechanical interface location, with respect to the satellite reference frame, in any of three orthogonal directions and are applicable at any instant during the on-orbit measurement period. This acceleration limit should be intended as the root-sum-square of the acceleration response from each of the three orthogonal axes.

Whereas force limits are referred to the disturbance source mechanical interface location, with respect to the satellite reference frame, in any of three orthogonal directions and are applicable at any instant during the on-orbit measurement period.

### 13.2.1.2.3 Frequency domain micro-gravity requirements

The micro-gravity requirement is habitually expressed in the frequency domain. The following classification can be applied:

- 1) The micro-gravity requirement is considered depending on the location where this requirement should be verified, hence it can be defined at:
  - a. the payload reference mechanical interface location
  - b. the disturbance source mechanical interface location
- 2) The micro-gravity requirement is considered associated to the physical quantity that must be verified, then it can be defined in terms of:
  - c. acceleration levels
  - d. force levels
- 3) The micro-gravity requirement is considered depending on the type of the function necessary to represent it, so it can be referred to:
  - e. spectrum (in third octave bands or in narrow bands)
  - f. power spectral density (PSD) curve
  - g. root mean square (rms) value
- 4) The micro-gravity requirement is expressed depending on the type of response needed to represent it, so it can be referred to:
  - h. linear
  - i. angular

Consequently, in the past space projects, the micro-gravity requirement in the frequency domain has been found described as a combination based on the above classification. The following combinations have been used in practice to specify the micro-gravity requirement:

- Combination of the points a), c), e) and h) to define the linear acceleration spectrum micro-gravity requirement.  
For example, in Figure 13-3 (left side) the Columbus micro-gravity environment disturbance specification is plotted as acceleration limit at the module to rack interfaces (for racks without Active Rack Isolation System, ARIS). This acceleration limit should be intended as the peak acceleration response along each of the three orthogonal axes.
- Combination of the points b), d), e) and h) to define the linear force spectrum micro-gravity requirement.  
For example, in Figure 13-3 (right side) the Columbus micro-gravity environment disturbance specification is plotted as force limit at the mechanical interfaces of the payload rack without ARIS. All force limits are referred to the disturbance source mechanical interface location, with respect to the satellite reference frame, in any of three orthogonal directions and are applicable at any instant during the on-orbit measurement period.
- Combination of the points a), c), f) and h) to describe the linear acceleration spectral density (ASD) micro-gravity requirement.  
For example, in Figure 13-4 (left side) the GOCE micro-vibration environment disturbance specification is plotted as linear acceleration limit at the location of each ASH accelerometer.

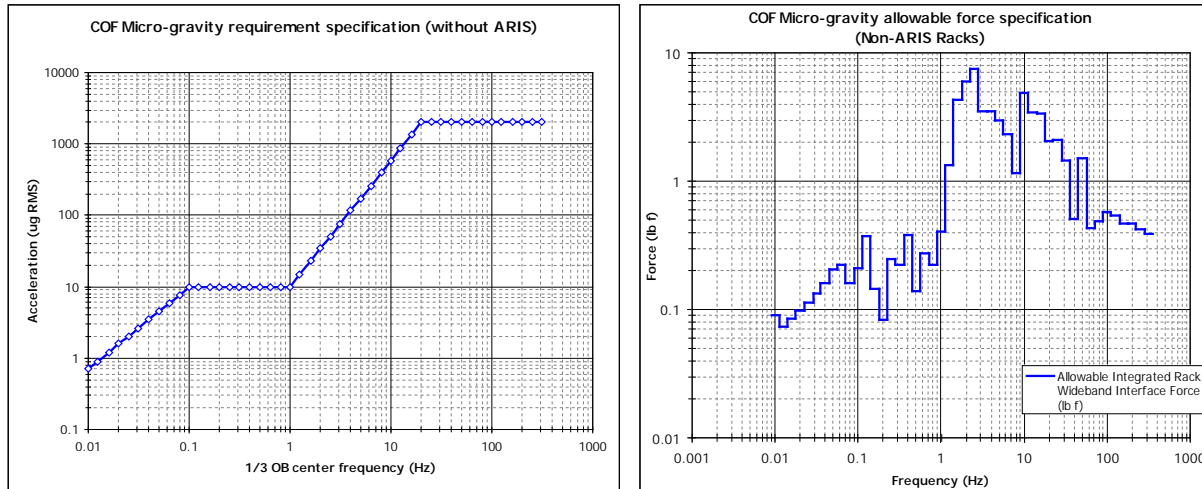


**Figure 13-3: Columbus micro-gravity environment disturbance specifications  
(left side: acceleration limit; right side: force limit)**

All acceleration limits are referred to the micro-gravity payload mechanical interface location, with respect to the satellite reference frame, in any of three orthogonal directions and are applicable at any instant during the on-orbit measurement period.

- Combination of the points a), c), g) and i) to define the micro-gravity requirement as angular acceleration rms value:

For example, according to the ARTEMIS micro-gravity environment disturbance specification specific angular acceleration rms values were applicable to the open-loop and closed-loop phase, respectively.

- Combination of the points a), c), f) and i) to define the angular acceleration spectral density (ASD) micro-gravity requirement:

For example, Figure 13-4 (right side) shows the GOCE micro-vibration environment disturbance specification given as angular acceleration limit at the satellite Centre of Mass location.

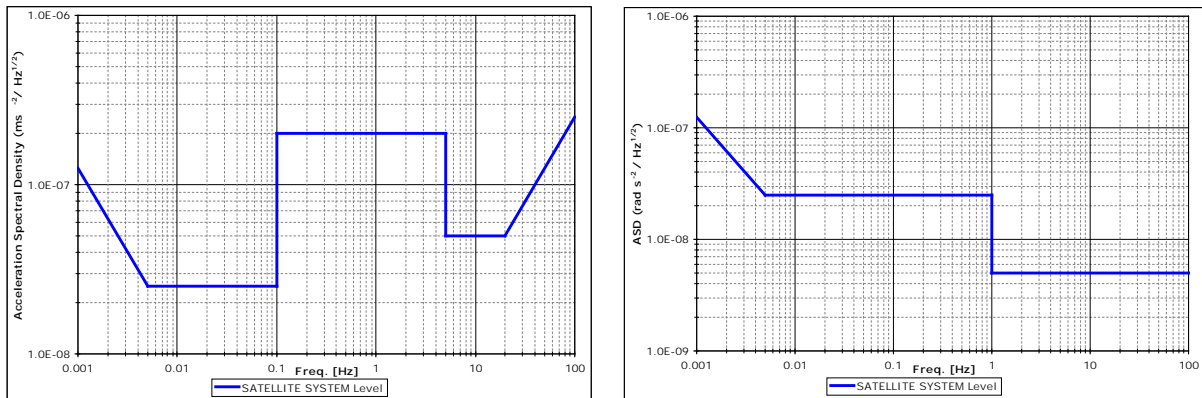


**Figure 13-4: GOCE micro-vibration requirement during measurement mode  
(left side: linear ASD profile; right side: maximum angular ASD profile) [4]**

Sometimes the micro-gravity requirement in the frequency domain is also defined in terms of **differential acceleration requirement**:

*"The micro-gravity requirements at the payload reference mechanical interface location, during the measurement mode, are expressed so that the induced perturbations on the micro-gravity environment caused by all **vibratory sources** within a certain frequency range of the satellite and its sub-system/equipment should generate any **differential acceleration** at the micro-gravity reference mechanical interface locations with levels not higher than certain **acceleration spectral density curve**".*

### 13.2.1.3 Identification of reference configuration and interfaces to micro-gravity payloads

The specified micro-gravity environment should be provided for the spacecraft during the on-orbit measurement modes, with the exception of spacecraft reconfiguration phases or during crew activities and maintenance for the pressurized spacecraft.

The on-orbit reference configuration of the spacecraft and the reference interface locations to micro-gravity payloads for the verification of the micro-gravity environment requirements are in general imposed by the customer and they are based on the fully equipped spacecraft on-orbit configuration.

For example, the Columbus micro-gravity environment specification reference locations and the GOCE specified reference locations for the micro-vibration environment verification are shown in Figure 13-5 and Figure 13-6, respectively.

The overall spacecraft system mass and inertias properties provided for the purpose of performing the micro-gravity environment verification should include:

- the origin of the reference coordinate system,
- the centre of gravity (CoG) location,
- the total mass,
- the mass moments of inertia (with respect to the CoG),
- the principal mass moments of inertia, and
- the location of the centre of the pressure (with respect to the CoG).

This data is used, as analysis reference, for accelerated rigid body motions (as limited by the time domain micro-gravity requirement) caused by forces and torques of spacecraft equipment with regard to acceleration observed at the reference interface to the micro-gravity payloads.

The geometry and dimensions of the overall spacecraft system are requested for the same purpose.

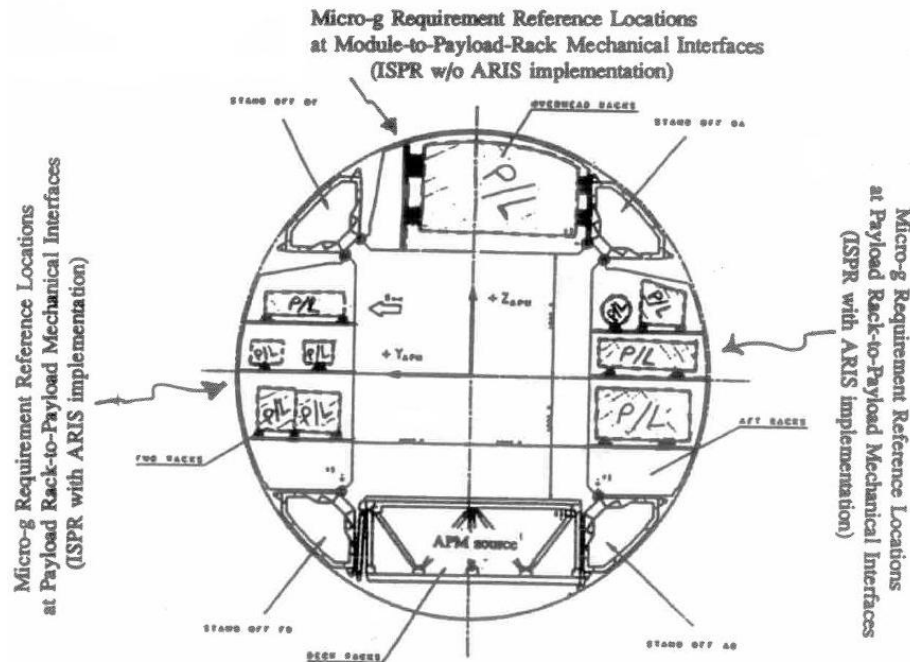


**Figure 13-5: Reference locations for COLUMBUS micro-gravity environment specification**

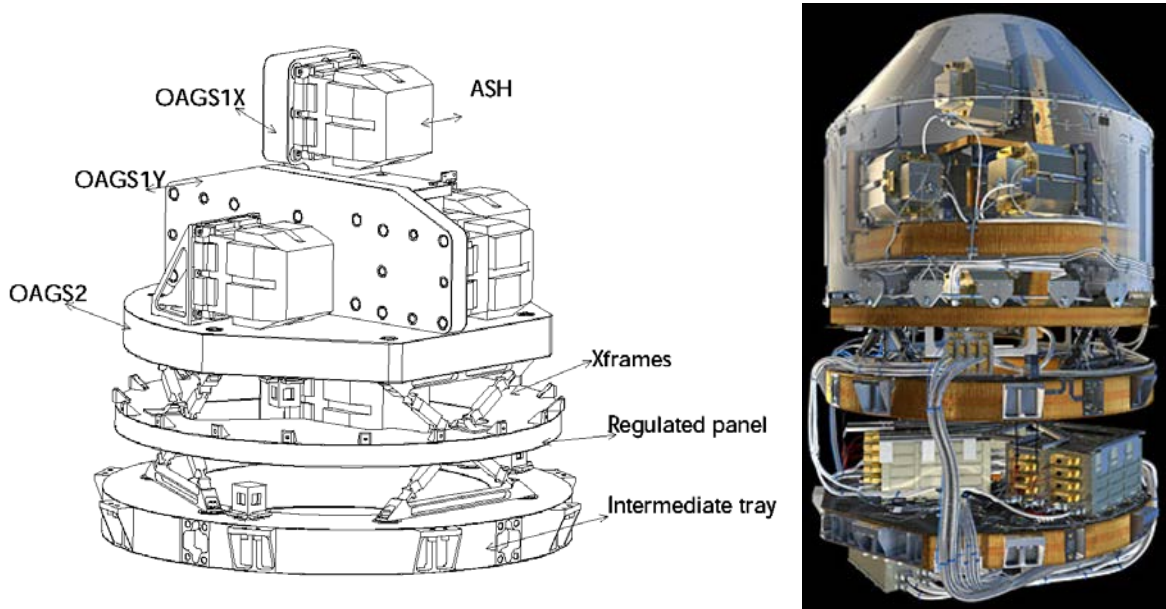


**Figure 13-6: Reference locations for GOCE Micro-vibration Environment**

#### 13.2.1.4 Micro-gravity environment control activities

In general, exhaustive spacecraft design and performance characteristics should be adopted and optimized versus the micro-gravity payload sensitivity (in terms of limit accelerations in the time and frequency domain) for given locations on-board the spacecraft and for specified mission periods.

The micro-gravity environment quality is usually impacted by several spacecraft design parameters, such as the mission scenario, the operational constraints, the mechanical configuration and general dimensions, the mass, the orbit height, the orientation, the external and internal (equipment)

disturbance forcing functions, the attitude control laws, the rigid body motions, in particular the accelerated ones, and the spacecraft low frequency and high frequency dynamics.

In order to maintain a controlled micro-gravity environment, a programmatic concept concerning the micro-gravity environment control activities should be introduced into the project flow as shown in Figure 13-7.

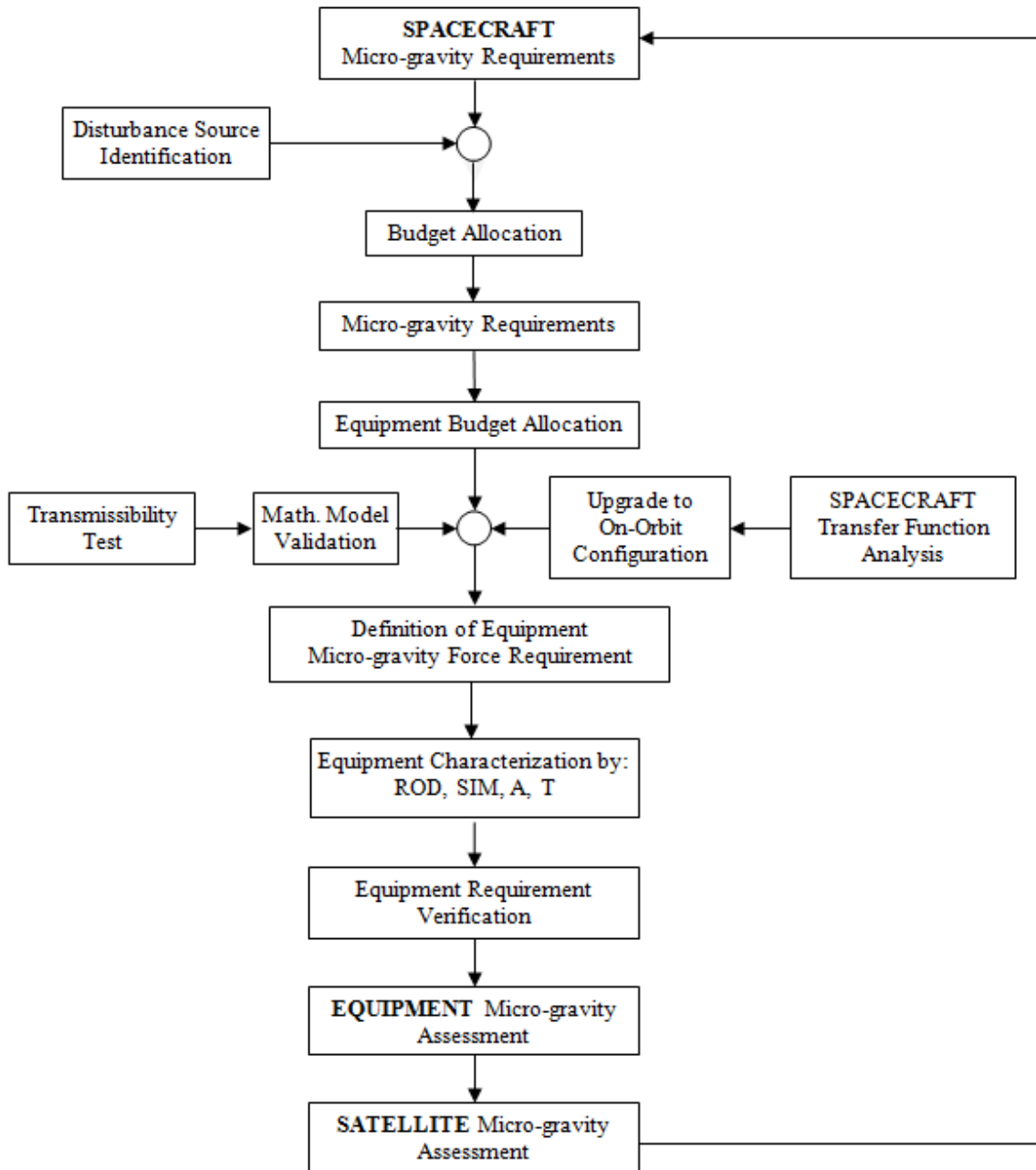


**Figure 13-7: Micro-gravity environment control activities**

The system configuration level micro-gravity requirement has been broken down into subsystem and also into equipment requirements following the budgeting rules as indicated in Section 13.2.2.3.

These sub-requirements, as budget contributions, are defined in a way to allow design optimization and verification at each stage of project level. This involves analyses and/or tests at equipment,

subsystem and spacecraft system level. Preliminary micro-gravity analysis might be performed including optional trade-offs in the areas determined by critical subsystems and equipment.

The micro-gravity environment qualification approach at each project level can be based on review of design (ROD), similarity (SIM), analysis (A, to be performed where applicable), and test (T, to be performed where necessary) or a combination of them. Tests should be always performed in case that the other verification methods do not provide reliable results.

The spacecraft micro-gravity environment analyses for design qualification comprise:

- In response to the time domain micro-gravity requirement, the assessment of the disturbance sources, which introduce quasi-static forces and torques, involves their interaction analysis with the spacecraft rigid body mass and inertia.
- In response to the frequency domain micro-gravity requirement, the low/high frequency dynamic disturbance prediction involves the overall analysis model.

Subsystem and equipment analyses of the micro-vibration disturbance environment consider the interaction of disturbance forces and torques with the spacecraft dynamics, as shown Figure 13-8.

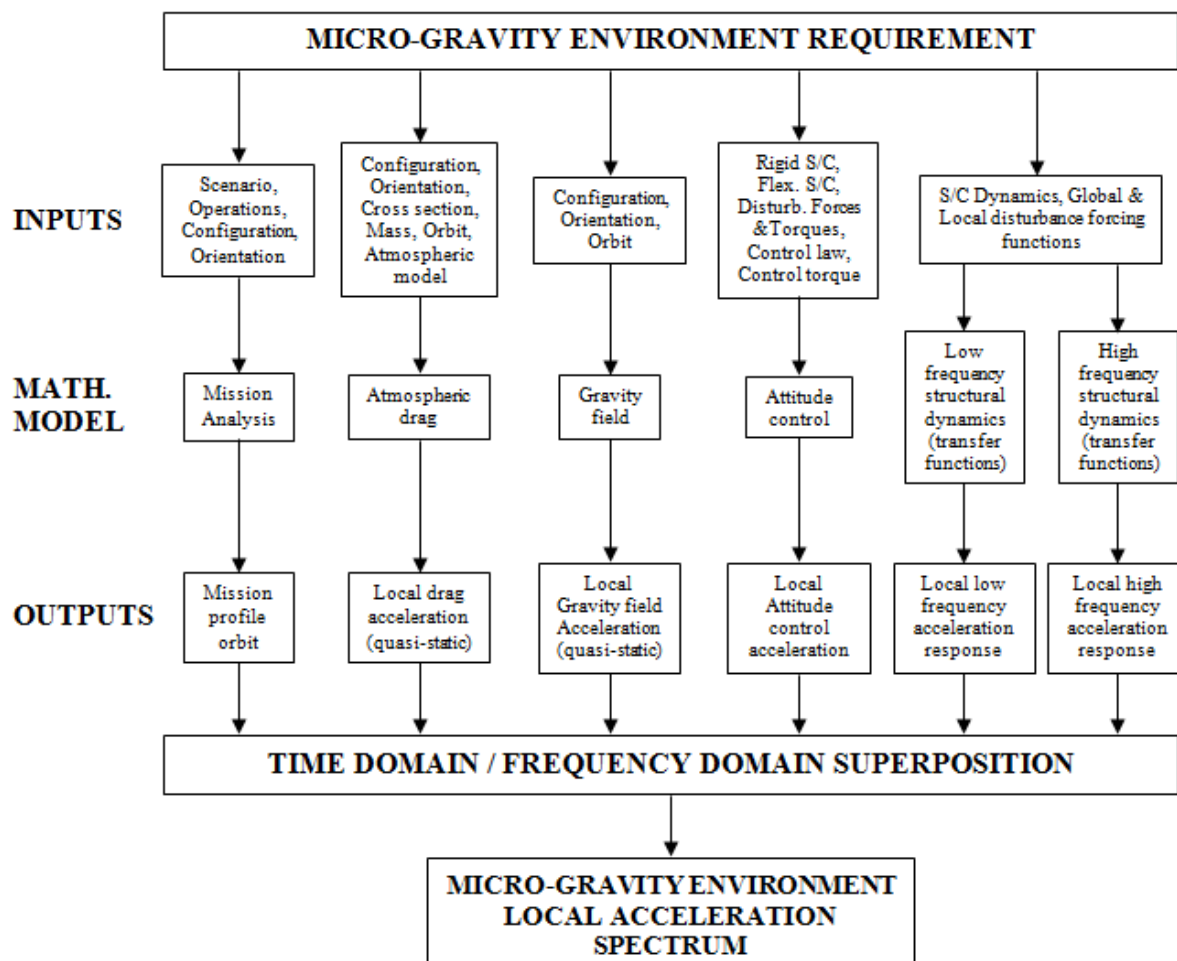


**Figure 13-8: Flight configuration micro-gravity environment analysis [3]**

The micro-gravity environment can be characterised either in the time domain or in the frequency domain on the basis of input-to-output transfer functions, as shown in Figure 13-9, covering the structural transmission paths and eventually the vibro-acoustic energy transfer between the sources and receiver locations (see Figure 13-10).

In general, these transfer functions are obtained by dedicated FEM and SEA, [5], mathematical models and/or by specific transmissibility tests as explained in Sections 13.2.2.1 and 13.2.2.2, respectively.

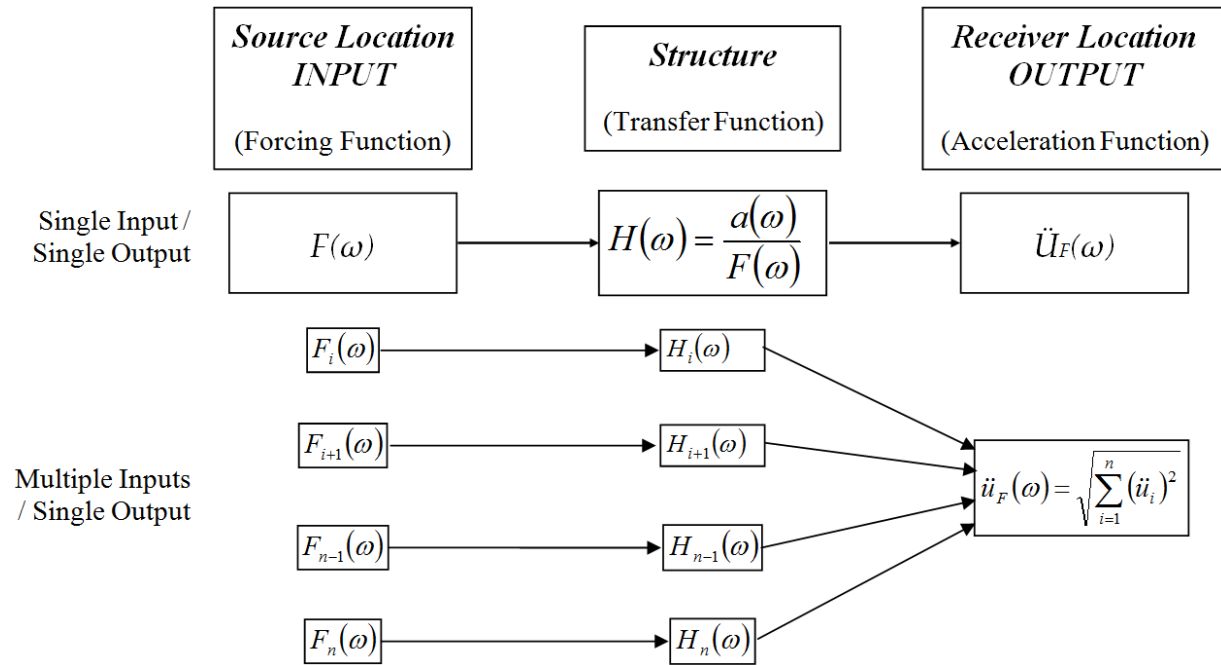


**Figure 13-9: Micro-gravity environment dynamic disturbance control (structural transmission path)**

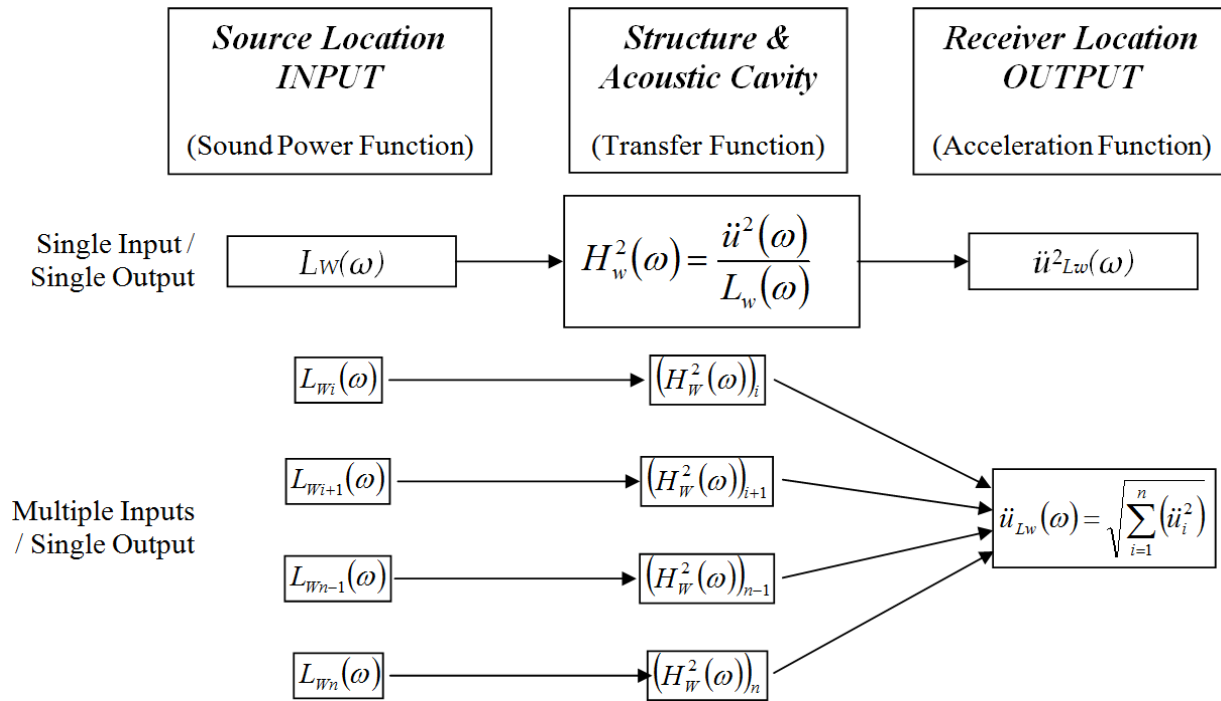


**Figure 13-10: Micro-gravity environment dynamic disturbance control (vibro-acoustic transmission path) [3]**

The following analysis procedures should be applied taking the respective models as the basis for the structural transfer function computation and for micro-gravity environment derivation:

- Low frequency structural dynamics:
  - model based on FEM techniques using commercial software packages, e.g. Nastran;
  - frequency range of interest from approximately 0.1 Hz up to 80 Hz in case of large structures like pressurized modules, or up to 150 Hz in case of small satellites.
- Optionally, a fluid/structure interaction model based on FEM/BEM techniques could be applied in case of pressurized modules to evaluate the vibro-acoustic transfer functions.
- High frequency structural dynamics:
  - model is based on SEA technique using commercial software packages, e.g. VA-One;
  - frequency range of interest from 80 Hz up to 315 Hz (in third octave bands).

This transfer function approach allows the subsystem responsible and the equipment supplier to define and verify their budget level requirements, specified at the receiver locations, and the equipment interface force limits, respectively. The transfer functions are defined as system support functions in the subsystem specifications.

Applying the transfer function approach avoids the need for distribution and handling complex simulation programs or finite element structural dynamics models at all project levels.

By utilizing the transfer function approach the equipment specifications should be subsequently verified to comply with allowable disturbance forces, which are derived via these transfer functions and acceleration response budget allocations.

Contributions by subsystem and other equipment sources are specified in terms of acceleration response budgets at the receiver location as deeply explained in Section 13.2.2.3.

If disturbances are synchronously generated by several sources and transmitted to receiver locations the multiple inputs/single output approach should be selected and, as a result, the total micro-gravity environment assessment should be based on the superposition of multiple disturbance sources:

- time domain: linear summation considering the phase, if possible,
- frequency domain: superposition based on the root-sum-square (RSS) value:

$$\ddot{u}(f) = \sqrt{\ddot{u}_F^2(f) + \ddot{u}_{Lw}^2(f)} \quad [13-1]$$

Transfer functions are given as acceleration-to-force relations for structural transmission paths and also as vibro-acoustic transfer functions for vibro-acoustic transmission paths as worst-case envelope functions between any source and any receiver locations. Micro-gravity dynamic disturbance transfer functions are defined and explained in more detailed in the Sections 13.2.2.1 and 13.2.2.2, respectively.

The transfer function derivation should be controlled at satellite system level but should be updated when either structural dynamics response calculations or measured transfer functions are available.

## 13.2.2 Derivation of micro-gravity specifications

In this section the derivation of micro-gravity specifications is explained involving:

- the characterisation of transfer functions (structural and vibro-acoustic, respectively),
- the definition of the micro-gravity environment control budget (in time and frequency domain, respectively),
- the definition of the micro-gravity force limits at the micro-gravity disturbance source locations from the allocated micro-gravity environment requirement.

### 13.2.2.1 Characterisation of the general structural micro-gravity transfer functions

#### 13.2.2.1.1 Introduction

The approach for the verification of the micro-gravity environment in the time and in the frequency domains at the reference receiver locations due to any disturbance source is based on the application of the structural transfer functions, i.e. the structural transmission of the disturbance between the equipment location and the receiver location.

As indicated by the micro-gravity environment control model in Section 13.2.1.4 the structural transfer functions are used for the micro-gravity requirements verification and budget allocation. By utilizing this technique it is possible to redefine the acceleration micro-gravity requirements specified at the receiver locations in terms of force micro-gravity requirements specified at the disturbance source locations (i.e. equipment locations).

The characterisation of the micro-gravity structural transfer functions is presented in more detail in the next sections. They can be obtained by:

- Analytical formulation,
- Numerical analyses,
- Test measurement.

#### 13.2.2.1.2 Characterisation of the micro-gravity structural transfer functions by analytical formulation

The approach for the prediction of the micro-gravity environment at the reference receiver locations due to subsystems and equipment disturbances is based on the identification of the structural transfer function assuming the following:

- In case the spacecraft is sufficiently rigid in the frequency range of the analysis or, in other words, the frequency range of the analysis is below the first main resonance frequency of the spacecraft then the following relationship can be used:

$$\left( \frac{A}{F} \right) = \left( \frac{1}{M} \right) \quad [13-2]$$

where  $A$  is the response acceleration,  $F$  the disturbance force and  $M$  the spacecraft mass.

- If the spacecraft is flexible in the frequency range of the analysis or, in other words, the first main resonance frequency of the spacecraft is within the frequency range of the analysis then the relationship related to the response of one degree-of-freedom system can be used and the obtained A/F transfer function should be enveloped at high frequency starting from the maximum peak.

#### 13.2.2.1.3 Characterisation of the micro-gravity structural transfer functions by numerical analyses

The approach for the prediction of the micro-gravity environment at the reference receiver locations due to the subsystems and equipment disturbances depends on whether it is performed in the time or frequency domain, respectively:

- Time domain:  
Identification of the Input-to-Output maximum amplitude scaling factor as shown in Figure 13-11. The way to perform this task is based on the mathematical processing of the amplitude scale factors from the disturbance source locations to the reference receiver locations that can be

carried out using the FE model of the whole satellite or ISS module, respectively, in free-free boundary condition to simulate the spacecraft in on-orbit configuration.

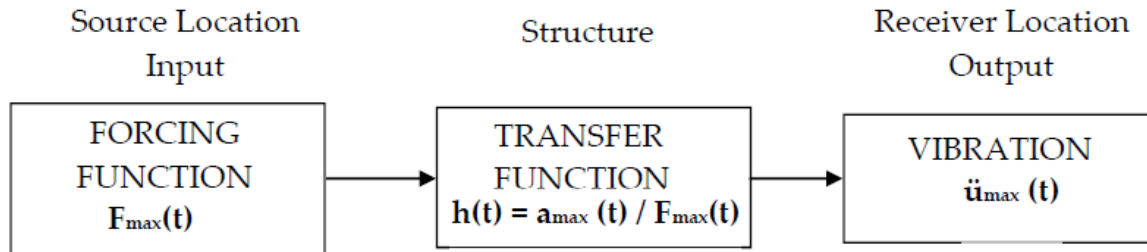


**Figure 13-11: Structural Input-to-Output maximum amplitude scaling factor method (time domain)**

A FEM transient analysis can be performed to compute the acceleration time history at the reference receiver locations induced by an excitation force applied at the considered disturbance source location. Consequently the amplitude scaling factors can be derived from the computed acceleration-to-force peak ratio.

- Frequency domain:  
Identification of the Input-to-Output structural transfer function as shown in Figure 13-9. In order to perform this prediction it is necessary to compute the structural acceleration-to-force transfer functions from the disturbance source locations to the reference receiver locations using the FE model of the whole satellite or ISS module, respectively, in the low frequency range and the corresponding SEA model at medium to high frequency range.  
The simulations should be performed in free-free boundary condition to simulate the on-orbit configuration.

#### 13.2.2.1.4 Characterisation of the micro-gravity structural transfer functions by tests

As for the characterisation of the micro-gravity structural transfer functions by numerical analyses the approach for characterisation by tests depends on whether it is performed in the time or frequency domain, respectively:

- Time domain:  
Utilization of the shock response spectra obtained by experimental measurements of the structural transmissibility or eventually by the utilization of the maximum response peaks from experimental measurements of acceleration time histories,
- Frequency domain:  
Utilization of classical frequency response functions, in the applicable frequency range, obtained by experimental measurements of the structural transmissibility.

The transfer function experimental measurements should be executed on the whole satellite or ISS module, respectively, in free-free boundary conditions to reproduce the on-orbit configuration. Such dynamically free-free boundary could be achieved by softly suspending the test article or alternatively to simply support it by its standard Mechanical Ground Support Equipment (MGSE).

The testing should be executed at Structural Model (SM), Structural/Thermal Model (STM) and/or Prototypical Model (PFM) level. A schematic test set-up for the structural transfer functions test is given in Figure 13-12.

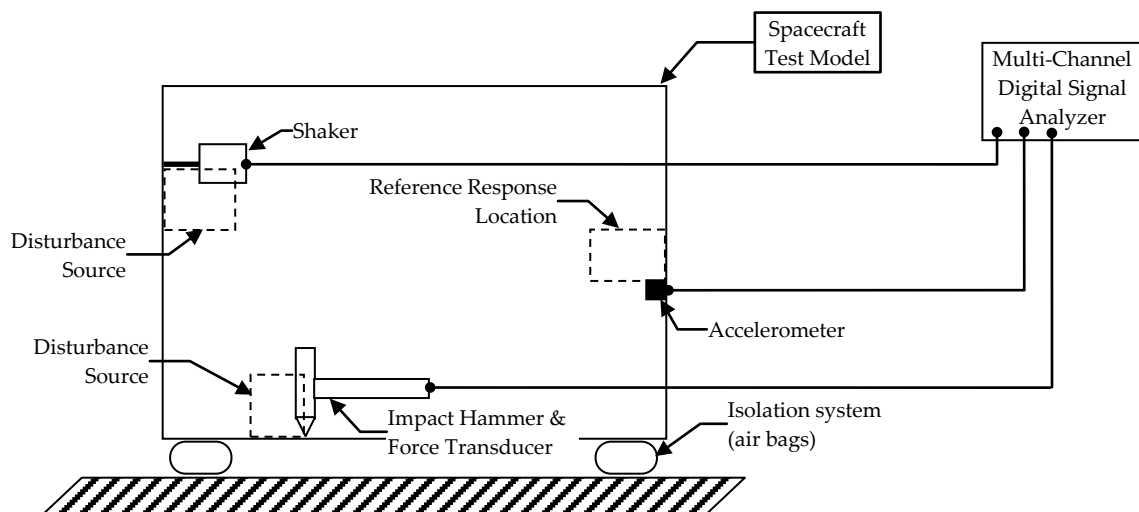


**Figure 13-12: Structural transfer function measurement set-up [3]**

The Multi-Channel Digital Signal Analyzer should measure, calculate and store the information:

- a. Input force spectrum  $F_i(\omega)$  [13-3]
- b. Acceleration response spectrum  $a_i(\omega)$  [13-4]
- c. Single point transfer function spectrum  $H_i(\omega) = \frac{a_i(\omega)}{F_i(\omega)}$  [13-5]
- d. Multiple point transfer function spectrum  $\bar{H}(\omega) = \frac{1}{n} \sum_{i=1}^n H_i(\omega)$  [13-6]
- e. Single point transfer dynamic mass spectrum  $m_i(\omega) = \frac{F_i(\omega)}{a_i(\omega)}$  [13-7]
- f. Multiple point transfer dynamic mass spectrum  $\bar{m} = \frac{1}{m} \sum_{i=1}^n m_i(\omega)$  [13-8]
- g. Input force background noise spectrum  $F_{iB}(\omega)$  [13-9]
- h. Acceleration response background noise spectrum  $a_{iB}(\omega)$  [13-10]

### 13.2.2.2 Characterisation of the general vibro-acoustic transfer functions

#### 13.2.2.2.1 Introduction

The verification of the micro-gravity environment at the reference receiver locations due to any disturbance source is performed in the frequency domain and the approach is based on the application of the vibro-acoustic transfer functions, i.e. the vibro-acoustic transmission of the disturbance between the equipment location and the receiver location, respectively.

As indicated by the micro-gravity environment control model in Section 13.2.1.4 the vibro-acoustic transfer functions are used only in the case of pressurized modules (i.e. for the ISS) for the micro-gravity requirements verification and budget allocation.

By utilizing this technique it is possible to redefine the acceleration micro-gravity requirements specified at the receiver locations in terms of force micro-gravity requirements specified at the disturbance source locations (i.e. the equipment locations).

The characterisation of the micro-gravity vibro-acoustic transfer functions can be obtained by:

- Numerical analyses
- Experimental test

More details are presented in the next sections.

### 13.2.2.2.2 Characterisation of the vibro-acoustic transfer functions by numerical analyses

The prediction of the micro-gravity environment at the reference receiver locations due to the subsystems and equipment disturbances is based on the identification of the input-to-output vibro-acoustic transfer function, as shown in Figure 13-10.

In order to perform this prediction it is necessary to compute the vibro-acoustic acceleration-to-sound power transfer functions from the disturbance source locations to the reference receiver locations using the FE model of the ISS pressurized module in the low frequency range and the corresponding SEA model in the medium to high frequency range.

The fluid/structure simulations should be performed considering the ISS pressurized module in free-free boundary condition to simulate the on-orbit configuration.

### 13.2.2.2.3 Characterisation of the vibro-acoustic transfer functions by tests

The prediction of the micro-gravity environment at the reference receiver locations due to the subsystems and equipment disturbances is based on the utilization of the acceleration-to-sound power transfer functions, in the applicable frequency range, obtained by experimental measurements of the vibro-acoustic transmissibility.

The transfer function experimental measurements should be executed on the ISS pressurized module in the free-free boundary condition reproducing the real on-orbit configuration. Such dynamically free-free boundary could be achieved by softly suspending the test article or alternatively to simply support it by its standard Mechanical Ground Support Equipment (MGSE).

The testing should be executed at Structural Model (SM), Structural/Thermal Model (STM) and/or Protoflight Model (PFM) level. A schematic test set-up for the vibro-acoustic transfer functions test is given in Figure 13-13.

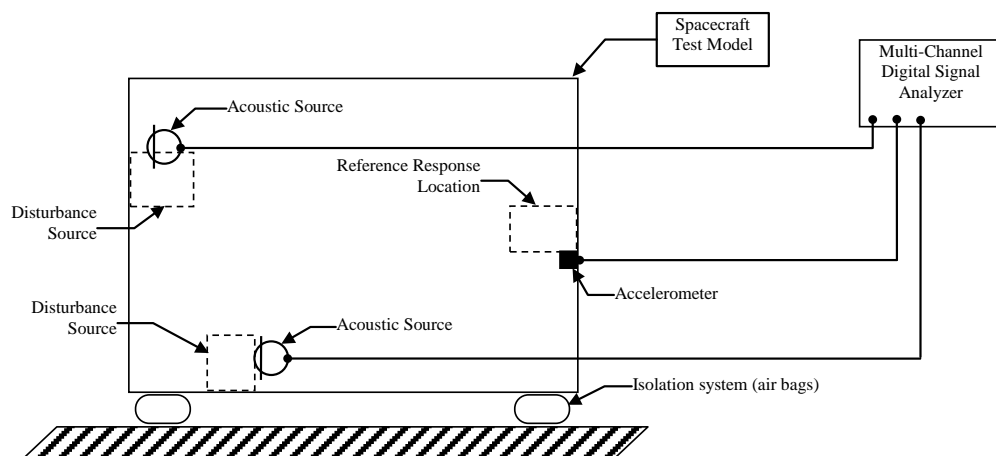


**Figure 13-13: Vibro-acoustic transfer function measurement set-up [3]**

The Multi-Channel Digital Signal Analyzer should measure, calculate and store the information:

$$a. \text{ Input sound power spectrum} \quad L_{w_i}(\omega) \quad [13-11]$$

$$b. \text{ Acceleration response spectrum} \quad a_i(\omega) \quad [13-12]$$

$$c. \text{ Single point transfer function spectrum} \quad H_{w_i}(\omega) = \frac{\ddot{a}_i(\omega)}{L_{w_i}(\omega)} \quad [13-13]$$

$$d. \text{ Multiple point transfer function spectrum} \quad \bar{H}_w(\omega) = \frac{1}{n} \sum_{i=1}^n H_{w_i}(\omega) \quad [13-14]$$

$$g. \text{ Input sound power background noise spectrum} \quad L_{w_B}(\omega) \quad [13-15]$$

$$h. \text{ Acceleration response background noise spectrum} \quad a_{i_B}(\omega) \quad [13-16]$$

### 13.2.2.3 Definition of the micro-gravity environment control budget

#### 13.2.2.3.1 Introduction

The total micro-gravity acceleration limit at the reference receiver locations should be apportioned on flight configuration level to the subsystem level for their individual micro-gravity environment control and verification activities. Consequently the allocated subsystem micro-gravity requirements should be apportioned down to their equipment levels by means of the budget rules introduced in the following sections for the time and frequency domain, respectively.

#### 13.2.2.3.2 Identification of micro-gravity environment budget criteria in time domain

Intermittent vibration sources (harmonic and/or random signals lasting less than 8 hours) can be considered according to probable timeline interaction depending on the duration of the event.

The budget level allocated to the single equipment is given as multiples (factor "n") of the corresponding time domain micro-gravity acceleration limit such that the time domain acceleration budget limit is:

$$a_i(t) = n \cdot a_{Total}(t) \quad [13-17]$$

where  $a_{Total}(t)$  corresponds to the maximum peak expected from the time domain micro-gravity acceleration requirement.

The budget factor "n" should be 1 for events with time duration  $< 10^{-4}$  seconds (i.e. non-simultaneous time events). For events within a time record of 1.0 seconds (i.e. simultaneous time events) this factor is in general less than 1 and its definition should be based e.g. on precedent system study results, manufacturer's data, electrical power consumption and previous experiences in similar systems.

The inverse application of the micro-gravity budgeting criterion, based on the linear summation of the single contributions in the time domain, is the superposition of each single budget contribution for system verification purposes such that:

$$a_{Total}(t) = \sum_i a_i(t) \quad [13-18]$$

#### 13.2.2.3.3 Identification of micro-gravity environment budget criteria in frequency domain

Micro-gravity disturbances induced by periodic and random vibration sources were considered according to their probable frequency interaction for the derivation of the micro-gravity acceleration budget levels.

The budget levels are given as factors "m" of the relating frequency domain micro-vibration acceleration limit such that the frequency domain acceleration budget limit is:

$$a_i(f) = m \cdot a_{Total}(f) \quad [13-19]$$

where  $a_{Total}(f)$  corresponds to the frequency domain micro-gravity acceleration requirement.

The definition of the budget factor "m" (in general  $m \leq 1$ ) can be based on precedent system study results, manufacturer's data, electrical power consumption and previous experiences in similar systems.

The inverse application of the micro-gravity budgeting criterion, based on the ***power level summation (root-sum-squared, RSS) of the single contribution*** in the frequency domain, is the superposition of each single budget contribution for system verification purposes such that:

$$a_{Total}(f) = \sqrt{\sum_i a_i^2(f)} \quad [13-20]$$

### 13.2.2.4 Definition of the micro-gravity force limits at micro-gravity disturbance sources location

#### 13.2.2.4.1 Introduction

Considering that the micro-gravity requirements and the budgets allocated to the corresponding subsystems are defined at the reference receiver location it could be necessary to redefine the acceleration micro-gravity allocated budget at the disturbance sources. This step is essential to specify the maximum allowable disturbance forces that equipment can induce at their interfaces with the mounting structure to not exceed the allocated acceleration micro-gravity requirement at the reference receiver locations.

The way forward to obtain the force micro-gravity requirements, allocated at the single equipment level, from the allocated acceleration micro-gravity requirement at the reference receiver locations is introduced in the following sections for a time and frequency domain method, respectively. In both cases the approach is based on a mathematical processing of the structural transmissibility from the disturbance source locations to the reference receiver locations.

So, taking into account the Input-to-Output (Source-to-Receiver) transfer function application method it is possible to compute the acceleration at the reference receiver locations, induced by an excitation force applied at the considered disturbance source location.

#### 13.2.2.4.2 Identification of micro-gravity force limits at disturbance sources location in time domain

In case of intermittent vibration sources (harmonic and/or random signals lasting less than 8 hours) the micro-gravity force limits can be defined according to the probable timeline interaction that is depending to the duration of the event as following:

- **For events with a time duration <  $10^{-4}$  seconds (i.e. non-simultaneous time events)**

Assuming that the event corresponds to an excitation frequency of 10 kHz, which is usually well above the frequency range of the analysis, and provided the frequency range of the analysis is below the first main resonance frequency of the spacecraft then it is possible to use the following relationship:

$$\left(\frac{A}{F}\right)(t) = \left(\frac{1}{M_{sc}}\right)(t) \quad [13-21]$$

where  $M_{SC}$  is the spacecraft mass.

Assuming a linear and reciprocal behaviour of the structure the following result is then obtained:

$$(F_{Max.Allowable})_{Unit}(t) = M_{SC} \cdot (A_{Req.}(t))_{Unit} \quad [13-22]$$

Thus, the maximum allowable excitation force levels that a specific micro-gravity disturbance source can generate at its interfaces to be compliant with the allocated micro-gravity requirement at the reference response location can be computed solving the previous equation.

However, if the first main resonance frequency of the spacecraft is within the frequency range of the analysis then the approach suggested hereafter might be followed.

- **Within a time record of 1.0 seconds (i.e. simultaneous time events)**

For this situation the assumption is no longer valid that the frequency range of the analysis is usually well below the frequency of the disturbance and consequently the spacecraft should be assumed as flexible. The fact that the acceleration micro-gravity environment allocated at the reference receiver locations can be generated by an unknown excitation force applied at the considered disturbance source interface location is expressed by the following relationship:

$$(A_{Req.}(f))_{Unit} = H_{SC}(f) \cdot (F_{Max.Allowable}(f))_{Unit} \quad [13-23]$$

$$(A_{Req.}(f))_{Unit} = FFT((A_{Req.}(t))_{Unit}) \quad [13-24]$$

$$(F_{Max.Allowable}(f))_{Unit} = FFT((F_{Max.Allowable}(t))_{Unit}) \quad [13-25]$$

where:

$H_{SC}(f)$  is the Source-to-Receiver structural transfer function,

$(A_{Req.}(f))_{Unit}$  the Fast Fourier Transform (FFT) of the allocated acceleration micro-gravity requirement at the reference receiver location for the specific unit, as specified following the budgeting rules,

$(F_{Max.Allowable}(f))_{Unit}$  the Fast Fourier Transform (FFT) of the maximum allowable disturbance forces limit at the excitation interface location for the specific unit.

Then assuming that the behaviour of the structure is linear and reciprocal:

$$(F_{Max.Allowable}(f))_{Unit} = \frac{1}{H_{SC}(f)} \cdot (A_{Req.}(f))_{Unit} \quad [13-26]$$

Consequently the maximum allowable excitation force level in the time domain is obtained by Inverse Fast Fourier Transform (IFFT):

$$(F_{Max.Allowable}(t))_{Unit} = IFFT(F_{Max.Allowable}(f))_{Unit} \quad [13-27]$$

Thus, the maximum allowable excitation force levels that a specific micro-gravity disturbance source can generate at its interfaces to be compliant with the allocated micro-gravity requirement at the reference response location can be computed solving the previous equation.

### 13.2.2.4.3 Identification of micro-gravity force limits at disturbance sources location in frequency domain

The deterministic approach to determine the allocated acceleration micro-gravity requirement at the reference receiver locations resulting from an unknown excitation force applied at the considered disturbance source interface location is very similar to what has been presented in Section 13.2.2.4.2 for the time record of 1.0 seconds.

Starting off from the relationship:

$$(A_{\text{Re qu.}}(f))_{\text{Unit}} = H_{\text{SC}}(f) \cdot (F_{\text{Max.Allowable}}(f))_{\text{Unit}} \quad [13-28]$$

the maximum allowable excitation force level can be obtained, again assuming a linear and reciprocal structure behaviour:

$$(F_{\text{Max.Allowable}}(f))_{\text{Unit}} = \frac{1}{H_{\text{SC}}(f)} \cdot (A_{\text{Re qu.}}(f))_{\text{Unit}} \quad [13-29]$$

The aforementioned approach can be adopted even if the micro-gravity requirement is expressed in Power Spectral Density (PSD) terms for a random excitation. In this case it is necessary to take into consideration the following relationship:

$$\left( \frac{A_{\text{Re qu.}}^2(f)}{\text{Hz}} \right)_{\text{Unit}} = H_{\text{SC}}^2(f) \cdot \left( \frac{F_{\text{Max.Allowable}}^2(F)}{\text{Hz}} \right)_{\text{Unit}} \quad [13-30]$$

where:

$\left( \frac{A_{\text{Re qu.}}^2(f)}{\text{Hz}} \right)_{\text{Unit}}$  the allocated acceleration micro-vibration requirement at the reference receiver location for the specific unit, as specified following the budgeting rules,

$H_{\text{SC}}^2(f)$  the square of the Source-to-Receiver structural transfer function,

$\left( \frac{F_{\text{Max.Allowable}}^2(f)}{\text{Hz}} \right)_{\text{Unit}}$  the maximum allowable disturbance forces limit at the excitation interface location for the specific unit.

Then assuming that the behaviour of the structure is linear and reciprocal the following result is obtained:

$$\left( \frac{F_{\text{Max.Allowable}}^2(f)}{\text{Hz}} \right)_{\text{Unit}} = \frac{1}{H_{\text{SC}}^2(f)} \cdot \left( \frac{A_{\text{Re qu.}}^2(f)}{\text{Hz}} \right)_{\text{Unit}} \quad [13-31]$$

## 13.2.3 Micro-gravity environment verification

The techniques necessary to verify by analysis and by test the micro-gravity requirements at system and at equipment level, respectively, are described in the following. The corresponding activities are performed with the following objectives:

- **Micro-gravity analysis** to compute the acceleration levels at the micro-gravity payload locations (at system level), and to compute the force levels at the disturbance source interfaces (at equipment level),
- **Micro-gravity test** to measure the acceleration levels at the micro-gravity payload locations (at system level), and to measure the acceleration and force levels, respectively, at the equipment disturbance source interfaces (at equipment level).

The micro-gravity environment verification approach defined at system and equipment level, respectively, establishes an integrated structure of analysis and test leading to the final verification.

### 13.2.3.1 System level micro-gravity environment verification

#### 13.2.3.1.1 Introduction

The system level verification activities regard the following:

- Definition of verification criteria,
- Control of lower level verification data,
- Delta verification,
- Verification of source interaction effects.

Delta verification activities are performed to close the gap between lower level configuration/verification data and the data required for full verification of the system configuration level requirements.

Regarding source interaction effects and cumulative parameters, this level verifies that respective resultant disturbances, as measured and analysed, are below the limit specified for the system level configuration.

Particular attention should be taken regard the location of counteracting measures, i.e. either within the disturbing mechanism, or at the mechanical interface of the equipment containing the mechanism, or at the interface of the assembly containing the equipment, or elsewhere.

#### 13.2.3.1.2 System level micro-gravity environment verification by analysis

The system level micro-gravity environment verification by analysis scrutinizes the sub-system and equipment design and assures that they can be developed and built within the specified requirements. This applies, in particular, to those equipment units that should be enhanced in order to comply with micro-gravity requirements.

The general compliance of sub-system and equipment micro-gravity performances with the related micro-gravity specification should be controlled as follows:

- Review all data on sub-system and equipment as designed and as built, which are necessary for the verification of micro-gravity environment requirements,
- Evaluate/approve the validity of this data,
- Evaluate/approve the adequacy/sufficiency of this data to constitute verification.

The system level configuration micro-gravity environment analysis predicts the induced acceleration level and verifies the compliance with the system level micro-gravity environment requirement. It should be performed considering:

- Mathematical models for transfer function calculations,
- Source forcing functions characterisation (derived by analysis and/or by test).

At least the following two analysis loops should be implemented for a correct design and verification process:

- A *preliminary micro-gravity analysis* should be performed in the early program phases with the main objective to provide the initial information for the allocation of the micro-gravity requirements at the equipment level.

- A *conclusive micro-gravity analysis* should be performed in the frame of the satellite Phase C/D with the main objective to provide the micro-gravity verification versus the allocated equipment micro-gravity requirements.

The *preliminary micro-gravity analysis* is based on the utilization of uncorrelated mathematical models (i.e. FE model and/or SEA model) for the derivation of the structural (acceleration-to-force) and eventually the vibro-acoustic (acceleration-to sound power) transfer functions between the excitation locations and the receiver locations and by the utilization of the analyzed or tested (if available) micro-gravity disturbance loads. This analysis permits to obtain the preliminary micro-gravity environment perturbations generated by the system level and by its sub-system and other equipment.

Based on this assessment micro-gravity budget requirements for the sub-system and the other equipment can be defined and implemented into the sub-system and other directly controlled equipment specifications.

The *conclusive micro-gravity analysis* is based on the utilization of correlated (if available) or updated mathematical models for the derivation of the structural (acceleration-to-force) and eventually the vibro-acoustic (acceleration-to sound power) transfer functions between the excitation locations and the receiver locations and by the utilization of the tested micro-gravity disturbance loads.

Equipment and sub-system micro-gravity test data should be implemented as they become available, because test data forms a vital part for the verification due to the general limitations in the analytical evaluation of the disturbance forcing functions.

Based on this assessment the micro-gravity budget requirements for the sub-systems and other equipment can be confirmed and/or updated.

### 13.2.3.1.3 System level micro-gravity environment verification by test

The philosophy for system level micro-gravity environment verification by test implies that a test should be performed to ensure the compliance of the flight configuration with the applicable requirements as specified by the corresponding specification.

Flight configuration micro-gravity environment tests should be planned and performed with the integrated flight configuration PFM. The following two possible test approaches could be applied:

- **Micro-gravity test by direct acceleration characterisation:**  
in order to measure the micro-gravity environment, acoustically and vibrationally induced, under simulated on-orbit operational conditions,
- **Micro-gravity test by transmissibility characterisation:**  
in order to measure the vibro-acoustic and structural transfer functions from the excitation sources to the receiver locations.

The final requirement verification should be provided after analytical/numerical corrections of the disturbance forcing functions and the correlation of the transmissibility measured during the ground tests with the predicted on-orbit conditions, if necessary.

The test set-up can be realized to be the same of the audible noise/human vibration tests, with the test model simply supported by its standard MGSE. Following this hard-mounted solution implies a simplification in the test management but, on the other hands, requires a re-evaluation of the test results towards the on-orbit boundary conditions.

For both types of tests a background noise measurement is required before each test measurement to determine the ambient or residual noise level. During this background noise measurement all equipment should be switched off.

### Micro-gravity test by direct acceleration characterisation

The micro-gravity environment can be measured directly on the integrated flight configuration PFM switching on separately or simultaneously all potential micro-gravity disturbance sources mounted into the spacecraft.

This approach is in general simpler than the micro-gravity test by transmissibility characterisation because it is only necessary to place accelerometer sensors in correspondence to the defined receiver locations and define a test sequence where all potential micro-gravity disturbance sources are activated in their operative modes.

The main drawback of this kind of test is that accelerometers with a very high sensitivity are needed, and they might be not capable to measure the micro-gravity acceleration levels if the latter are very low or comparable with the laboratory background noise.

### Micro-gravity test by transmissibility characterisation

The more useful solution for the verification by test of the micro-gravity environment at system level is the execution of a micro-gravity test by transmissibility characterisation.

In this case, instead of measuring directly the micro-gravity acceleration, the structural transfer function ( $\mu\text{g}/\text{N}$ ) and the vibro-acoustic transfer function ( $\mu\text{g}/\text{pW}$ ), if necessary, are measured and used for the evaluation of the micro-gravity environment.

The structural transfer functions should be acquired by applying first relevant excitations with e.g. electro-dynamic shakers and/or impact hammers at the positions where the micro-gravity disturbance sources are mounted and then measuring the induced acceleration levels at the specified receiver locations.

This approach is more complex than the micro-gravity test by means of direct acceleration characterisation because, for example, adequate test instrumentation should be available and a longer period for the test execution and the subsequent data post-processing should be expected.

However, this type of test allows acquiring an increased amount of information, because tests can be performed as follows:

- change of the excitation direction (i.e. along the three orthogonal directions),
- variation of excitation levels, such studying the linearity of the response,
- change of excitation type, delivering forcing functions for e.g. steady state and/or transient test cases.

With the transfer functions  $H_{SC}(f)$  extracted from the test data and using the forces  $F_{Unit}(f)$  measured during the micro-gravity tests at the equipment interfaces the micro-gravity acceleration levels  $A_{Unit}(f)$  can be calculated and compared with the associated requirements using the following equation:

$$A_{Unit}(f) = H_{SC}(f) \cdot F_{Unit}(f) \quad [13-32]$$

In case the forces  $F_{Unit}(f)$  are measured “hard-mounted” (see Section 13.2.3.2.3) then they cannot be simply applied to the transfer functions  $H_{SC}(f)$  but it is necessary to correct those forces taking into account the source dynamics if interfering with the frequency range of the analysis.

Alternatively it could be ensured that the transfer functions  $H_{SC}(f)$  also include the dynamic effects of the source (see Section 13.4.3.3.2).

### **13.2.3.2 Equipment level micro-gravity environment verification**

#### **13.2.3.2.1 Introduction**

The equipment design, development and verification forms a vital part of the system micro-gravity environment control because the reduction of the vibration directly at the source is the most effective one.

The equipment suppliers should perform very detailed design and development activities, based on analyses and tests, to verify their compliance with the applicable micro-gravity requirements as defined in the respective equipment specification.

Equipment micro-gravity disturbance analysis reports, micro-gravity environment compatibility (MEC) test reports and relevant design and development documentation should be produced and delivered to the system level responsible providing evidence that the disturbance micro-gravity levels produced by the equipment are compliant with the allocated micro-gravity budget.

#### **13.2.3.2.2 Equipment level micro-gravity analysis**

The equipment micro-gravity disturbance analysis and the demonstration of compliance with respect to the allocated budget should be prepared by the equipment supplier.

The equipment micro-gravity disturbance analysis predicts:

- the perturbation forces and/or the induced micro-gravity acceleration levels, and
- the equipment transmissibility functions from the internal source location to its mechanical interfaces.

In the early equipment design phase this analysis could be done by a preliminary analytical assessment of the design data and a later update could be based on a detailed numerical analysis and/or the evaluation of test data.

The analysis should evaluate the impact, at the mechanical interfaces, of all the structural disturbance sources present in the equipment in its foreseen operational condition (e.g. equipment self-induced vibration forcing function) and the impact, at the surrounding volume, of all the acoustic disturbance sources present in the equipment in its foreseen operational condition (e.g. equipment radiated sound power), where applicable.

The internal equipment structural vibration transmission and acoustic attenuation function, if any, should be evaluated.

Micro-gravity disturbance levels in term of forcing functions at the equipment mechanical interfaces should be computed by means of analytical formulations and/or numerical simulations.

Equipment micro-gravity disturbance analyses should be delivered as soon they become available or, as a minimum, together with each equipment design review data package to permit the execution of the preliminary micro-gravity analysis at system level.

#### **13.2.3.2.3 Equipment level micro-gravity test**

The equipment level verification by test should ensure that the equipment complies with the allocated requirements as specified by the equipment configuration specification.

In addition the equipment level verification by test can be used to provide the interface forcing functions information for the system level verification by analysis and for the system level verification by test based on the transmissibility characterisation.

Since the system level micro-gravity analysis and prediction is strongly depending on empirical data, the equipment micro-gravity tests provide the earliest information about the system performance. So,

equipment micro-gravity tests should be performed as early as possible in the program starting with breadboard, development and engineering units. In fact, due to the empirical nature of micro-gravity disturbance/vibration control, iterative steps should be planned for the implementation vibration and acoustic noise reduction countermeasures.

Equipment micro-gravity tests are required to determine mainly the structure-borne and, if applicable, the air-borne/fluid-borne vibration generated by the source.

Final equipment micro-gravity environment tests should be planned and performed on the flight standard or on PFM's. The following two tests approaches could be applied (under simulated on-orbit operational conditions):

- **Micro-gravity test by direct force characterisation:**  
to measure directly, with load sensors, the forcing functions at the equipment mechanical interfaces,
- **Micro-gravity test by indirect force characterisation:**  
to measure indirectly, with accelerometers, the induced forcing functions at the equipment mechanical interfaces.

The micro-gravity test should produce, at least, the output in term of interface forcing functions and radiated sound power, if requested.

For both types of tests the background noise should be measured before each test measurement to determine the ambient or residual noise level. During this background noise measurement all equipment should be switched off.

#### Micro-gravity test by direct force characterisation

This test approach allows measuring the micro-gravity forcing functions at the equipment mechanical interfaces directly on the equipment model, switching on separately or simultaneously all the potential micro-gravity disturbance sources mounted inside.

This approach is simpler than the micro-gravity test by indirect force characterisation because it is only necessary to place force sensors in correspondence to the equipment mechanical interfaces and to define a test sequence where all potential equipment micro-gravity disturbance sources are activated at their operative modes.

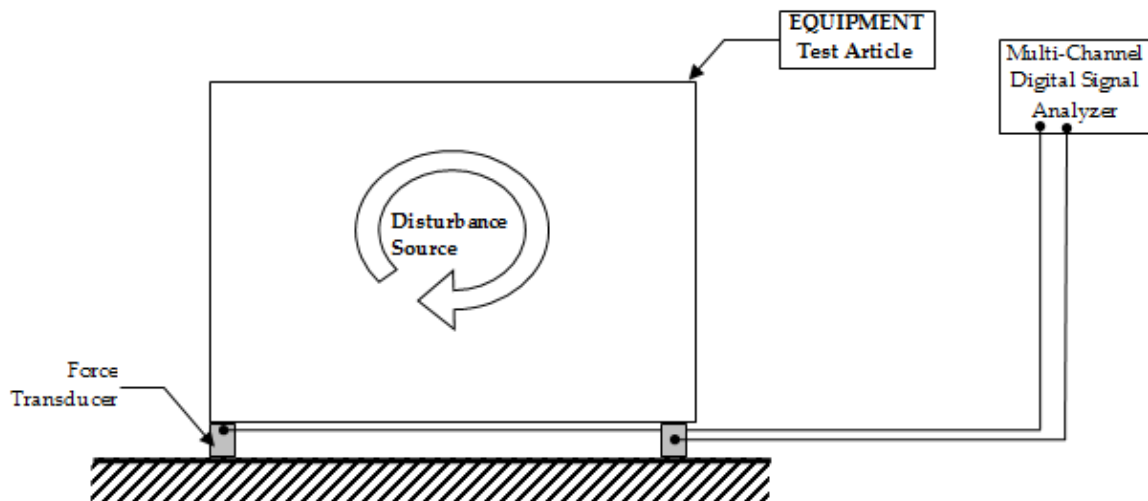


Figure 13-14: Micro-gravity measurement test, direct force characterisation [6]

The main drawback of this kind of test is that it is necessary to use force sensors with a very high sensitivity, and they might not be capable to measure the micro-gravity force levels if the expected micro-gravity disturbances are very low or comparable with the laboratory background noise. Consequently, for this kind of test, it appears necessary to mount the equipment under test on a seismic mass to isolate as much as possible the disturbances coming from the external environment.

A schematic test set-up for the micro-gravity test by direct force characterisation is given in Figure 13-14. The equipment under test model should be hard-mounted through the force transducers to the equipment mechanical interfaces.

#### Micro-gravity test by indirect force characterisation

By this test approach the micro-gravity forcing functions at the equipment mechanical interfaces cannot be measured directly on the equipment model but they can be obtained by the following two experimental measurements:

1. Acceleration-to-force transfer function measurement,
2. Self-induced acceleration spectrum measurement, switching on separately or simultaneously all the potential micro-gravity disturbance sources mounted inside the equipment.

The **transfer function experimental measurements** should be executed acquiring the acceleration-to-force spectra from each equipment mechanical interface to the same interface and to all others, respectively.

The **self-induced acceleration spectrum measurements** should be executed acquiring the acceleration spectra at all equipment mechanical interfaces for each foreseen equipment operational condition. Figure 13-15 shows a schematic test set-up for the micro-gravity test by indirect force characterisation.

The equipment under test should be hard-mounted to a reference test structure via its mechanical interfaces and the reference test structure softly suspended to allow a dynamically free-free boundary to filter the mechanical vibration coming from the external environment.

This approach is more complex than the micro-gravity test by direct force characterisation because, for example, adequate test instrumentation (for example instrumented impact hammer or mini-shakers), should be available and a longer period for the test execution and the subsequent post-processing should be expected.

However, this type of test requires a simpler test set-up because the seismic mass can be replaced by a reference test structure softly suspended capable to isolate the equipment under test from the laboratory noise. In addition the use of high-sensitive accelerometer sensors allows measuring extremely low acceleration levels.

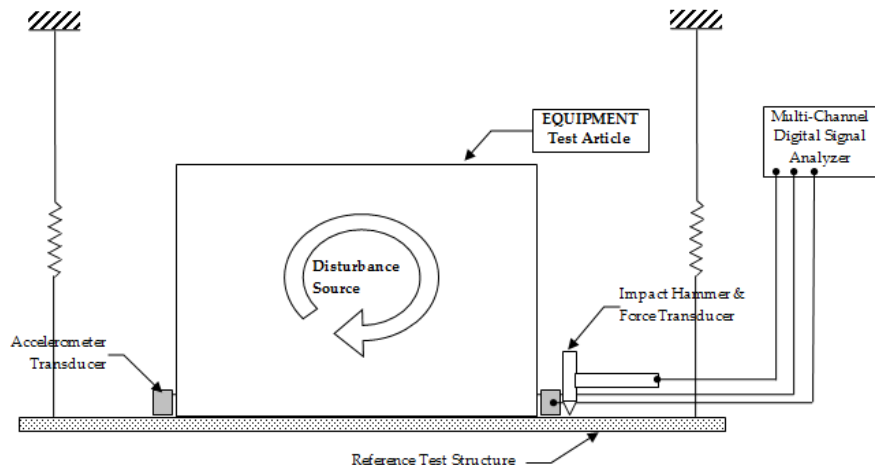


**Figure 13-15: Micro-gravity measurement test, indirect force characterisation [6]**

## 13.3 Micro-vibration

### 13.3.1 General aspects

Micro-vibrations are the low-level vibrations occurring during on-orbit operations of mobile or vibratory parts. These perturbations are in general amplified by the satellite structure when being transmitted to sensitive payload units on e.g. Earth observation satellites or space telescopes. As a result, micro-vibrations might cause severe disturbances of instrument pointing performances. This is well demonstrated in Figure 13-16 where the line-of-sight (LoS) pointing as function of time is shown in the left graph. The right picture compares the images taken when significant micro-vibration perturbations were present, when some corrective measures had been applied afterwards and when the imager LoS was undisturbed during the picture-taking.

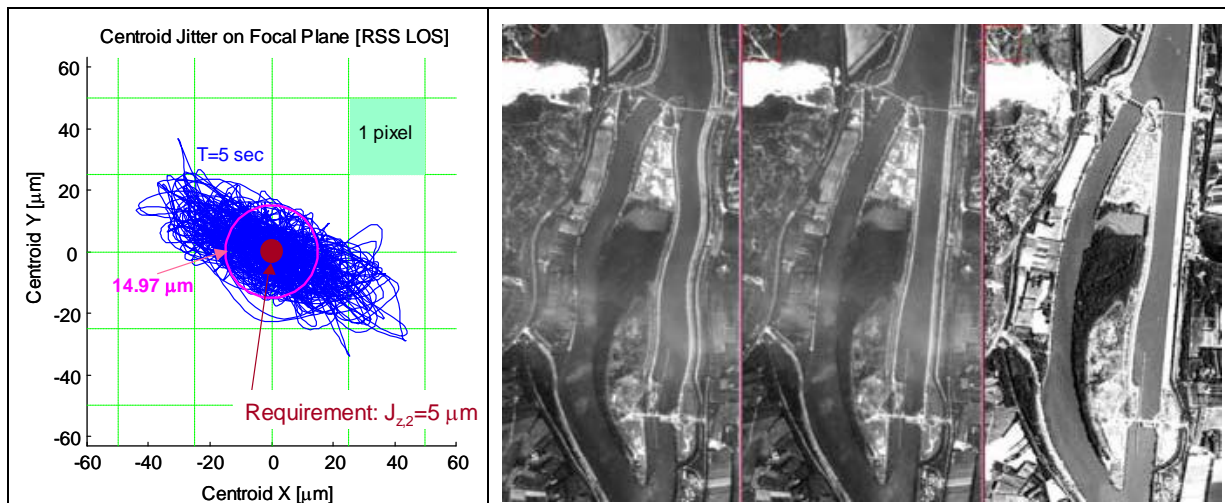


**Figure 13-16: LoS pointing as a function of time (left) and resulting effects on image quality (right)**

**Table 13-1: Typical short, medium & long term pointing stability requirements [7]**

	Time	Unit	Requirements		note
Solar Optical Telescope (SOT)	10 s	arcsec $3\sigma$	0.09*	-	Integration of images
	1hr	arcsec 0-p	2*	200	FOV (10'')/5, slit scanning
	Mission period		20	-	FOV (164'')/8
X-Ray Telescope (XRT)	1 s	arcsec $3\sigma$	0.7	-	Standard exposure
	1 min		1.7	-	Longest exposure
	1 hr	arcsec 0-p	16	400	FOV(256'')/16
	Mission period		32	-	FOV(256'')/8
EUV Imaging Spectrometer (EIS)	2 s	arcsec $3\sigma$	0.6	-	Exp. for active regions
	20 s		1.1	-	Exp. for quiet regions
	1min		1.7	-	Exp. for coronal holes
	10 min	arcsec 0-p	2.0	-	Slit scanning
	1 hr		5.0	800	FOV (256'')/50
	Mission period		50	-	FOV(512'')/10

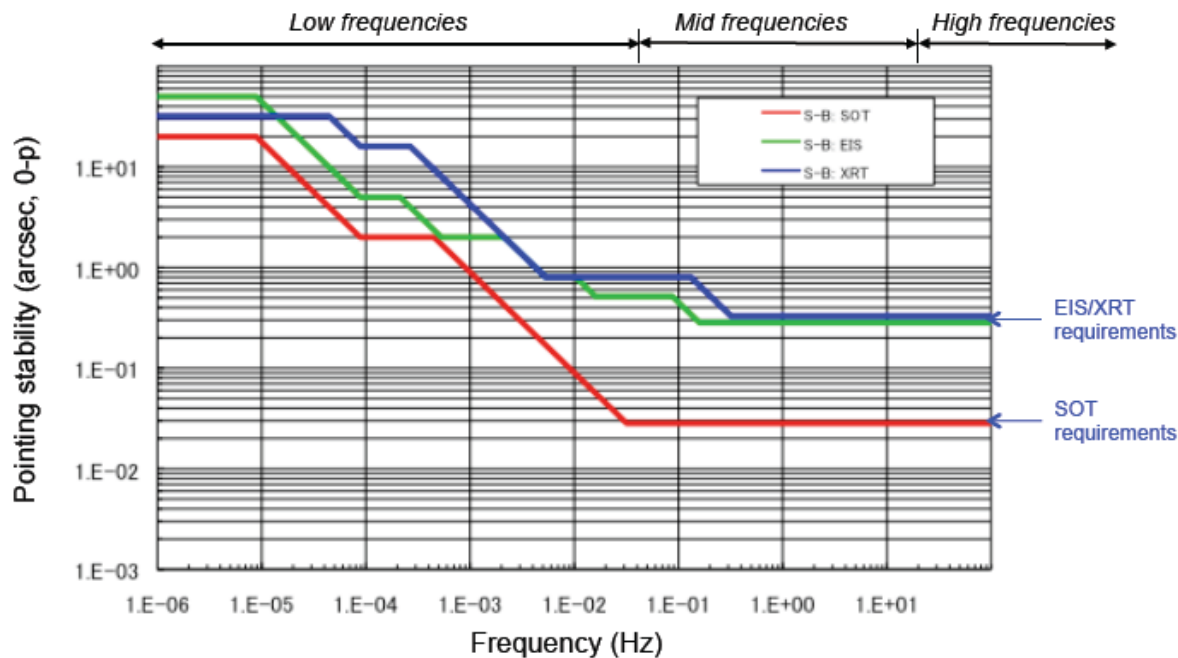


**Figure 13-17: Frequency dependent pointing stability requirements [7]**

Accuracy requirements of pointing and scanning mechanisms are typically ranging from small fractions of a degree (for high gain antennas), down to micro-radians for inter-satellite optical links, and even nano-radians for instrument optical delay lines applications. As an example the short, medium and long term as well as frequency dependent pointing stability requirements for JAXA's HINODE/SOLAR-B mission are given in Table 13-1 and Figure 13-17, respectively.

In general even relatively small oscillatory forces emitted to the spacecraft platform may generate micro-vibrations when on-board moving devices are being operated. The most important aspect to be considered in the assessment of micro-vibration environments and its severity is the transmission of the relevant spacecraft internal disturbances to the sensitive receiver locations, i.e. how the disturbances are propagating through the structure, Figure 13-18.

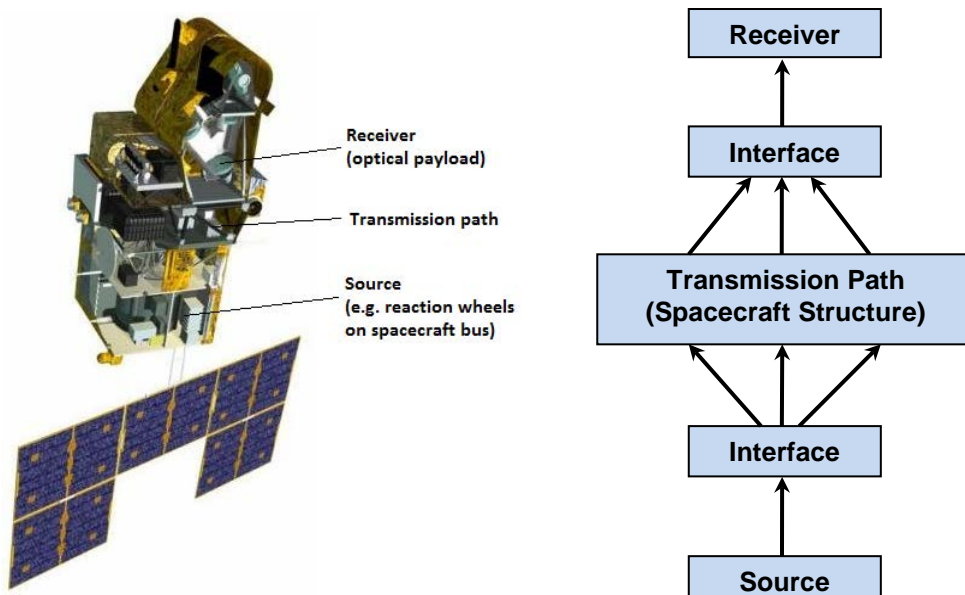


**Figure 13-18: Micro-vibration transmission through spacecraft structure**

Based on this knowledge relevant measures could be then identified to reduce the micro-vibration problem, e.g. by isolating the disturbers from the spacecraft platform in the relevant frequency range of the dynamic excitations or by vibration attenuation along the transmission path (due to improved structural damping).

The verification of the micro-vibration performances is usually based on a combination of analytical predictions and hardware tests, [8]. Such approach is necessary since the micro-vibration tests suffer from the fact that

- the performances cannot be validated on ground in a representative on-orbit environment (e.g. zero gravity, in-vacuum, perfectly unconstrained “free-free” condition), or
- end-to-end tests could not be performed due to the complexity of the test setup or since hardware needed for the test is not yet available, in particular the disturbance source and/or the micro-vibration sensitive instrument.

### 13.3.2 Micro-vibration analysis

#### 13.3.2.1 Introduction

Micro-vibration analyses are performed with the objective to predict and assess the mission critical satellite performances under the influence of micro-vibration disturbance sources. The most common approach applied in practice is based on using finite element models for predicting the spacecraft structure transfer functions and therefore the transmission of the disturbances from their source location to the receiver location. Other methods are the power approach and the energy approach based on an extension of the statistical energy analysis (SEA) as used for vibro-acoustic response predictions.

The validity of the FEM method is however usually limited to low and mid frequency ranges depending on the grade of the refinement of the model (mesh density). The energy approach is rather applicable to the higher frequency range where the modal density is sufficient to justify the use of SEA methods.

#### 13.3.2.2 Finite element model approach

##### 13.3.2.2.1 Introduction

The accuracy of the micro-vibration performance predictions depend strongly on the complexity of the spacecraft structure model, i.e. in particular concerning potential model uncertainties along the expected transmission path for the disturbances, and the frequency range where the FEM can be considered representative. In order to determine the robustness of the prediction model the sensitivities to relevant structural parameters could be assessed.

##### 13.3.2.2.2 Finite element model configuration

The FEM to be used for the micro-vibration analysis should be representative for the on-orbit configuration. The on-orbit configuration is usually significantly different from the launch configuration due to the following:

- All flexible appendages should be deployed and put in the right flight position. This concerns in particular the solar arrays and antenna booms.
- Where applicable, the launch locks and any other clamping mechanisms should be released.

Note: This could result to singularities in the stiffness matrix and particular attention should be given to properly deal with these numerical issues.

- The filling of the propellant tanks should be taken into account, in particular if the filling ratio of the tanks changes significantly for the mission phases to be considered for the micro-vibration analyses. The spacecraft modal basis might be significantly influenced, too.
- Last but not least, the analysis should be performed in a free-free configuration, i.e. 6 rigid body modes should be taken into account.

For example Figure 13-19 shows the Nexus spacecraft in its launch and on-orbit configuration.

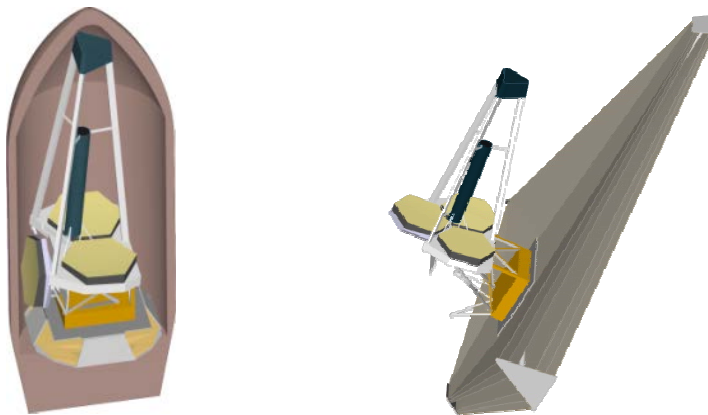


**Figure 13-19: Nexus spacecraft concept in stowed (left) and on-orbit deployed configuration (right)**

Ideally the rigid body modes should be predicted at a frequency of 0 Hz. However, due to numerical inaccuracies the rigid body modes are calculated at frequencies slightly above zero Hz for most finite element models. This should be taken into account concerning the transfer functions to be used for the assessment of the impact of the disturbance sources on the sensitive payload. They should cover only the frequency range above the rigid body mode frequencies.

Figure 13-20 provides an example of a satellite transfer function where rigid body modes are calculated for frequencies between 0.001 and 0.01 Hz. At very low frequencies the acceleration response is expected to be a constant acceleration: the excitation force divided by the satellite mass. However, this is only the case for the frequencies above 0.01 Hz until the characteristics of the transfer function are significantly changed by the appearance of elastic modes of the satellite structure.

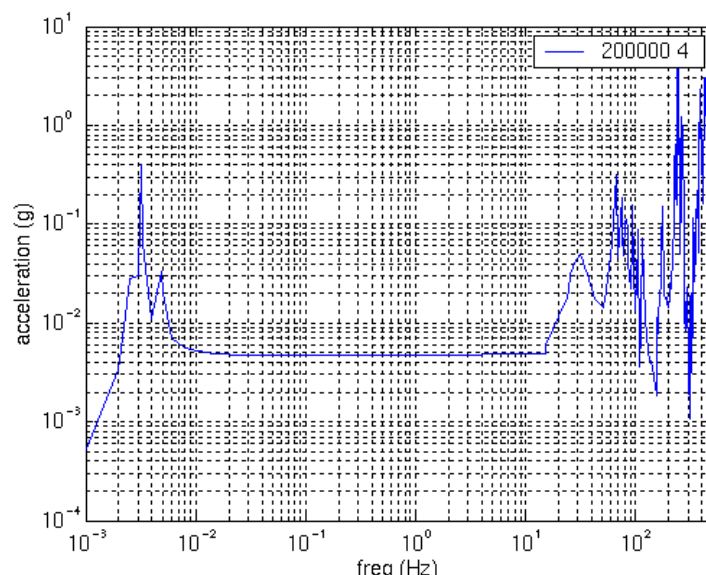


**Figure 13-20: Satellite transfer function with rigid body modes present at low frequencies [9]**

### 13.3.2.2.3 Line-of-sight definition

The most sensitive information expected from the micro-vibration analysis is the distortion of the line-of-sight (LoS) of optical instruments. Therefore the instrument LoS should be represented in the analysis model as accurate as possible to properly estimate the effect of the disturbance sources on the instrument performances. In general a detailed model of the instrument is required in order to take into account potential modal couplings between instrument and spacecraft. A simplified model representation might be sufficient if the expected instrument modal behaviour is higher than the frequency range of interest.

Furthermore the analysis output (instrument distortions) should be located as close as possible to the instrument imager location in order to significantly improve the accuracy of the micro-vibration assessment. It is recommended to define the LoS representation in the analysis model in close collaboration with the instrument development team in order to determine the relation between critical optical subsystem representations (e.g. mirror, lens, focal plane) and the overall instrument performance.

### 13.3.2.2.4 Damping

Assuming a representative damping value is of major importance for the validity of the micro-vibration performance predictions. For the on-orbit configuration usually very low damping values should be used, typically a viscous (modal) damping of  $\xi \leq 0.5\%$  (percentage of critical damping) is applied for conventional satellite structures. Since

$$Q = \frac{1}{2\xi} \quad [13-33]$$

this relates to a dynamic amplification factor of  $Q=100$  at the resonance frequency.

Other damping representations could be used as e.g. structural damping where the damping is strongly dependent on material characteristics or Rayleigh damping for transient analyses. The decision to select a specific damping assumption amongst the others or to apply a combination of different types of damping might be driven by the following:

- the type of the structure to be studied,
- the type of analysis to be performed, and
- the type of excitation to be applied.

Most often, commonly used assumptions are coming from experience acquired during past programs and accurate prediction of the damping ratio is hardly achieved throughout the whole frequency band of interest.

Two methods are usually applied to estimate the damping factor  $Q$  from test results, Figure 13-21:

1. Using the dynamic amplification factor at the resonance frequency  $f_n$ :

$$A = \left| \frac{X(f_n)}{X_{stat}} \right| \approx Q_n \quad [13-34]$$

2. Using the frequency bandwidth  $\Delta f$  at the half-power points defined by  $P_1$  and  $P_2$ :

$$Q_n = \frac{f_n}{\Delta f} = \frac{f_n}{f_{P_2} - f_{P_1}} \quad [13-35]$$

The modal damping factor  $\xi$  is then estimated according to Eq. [13-33]. Note that this method should be used only for peaks being well isolated.

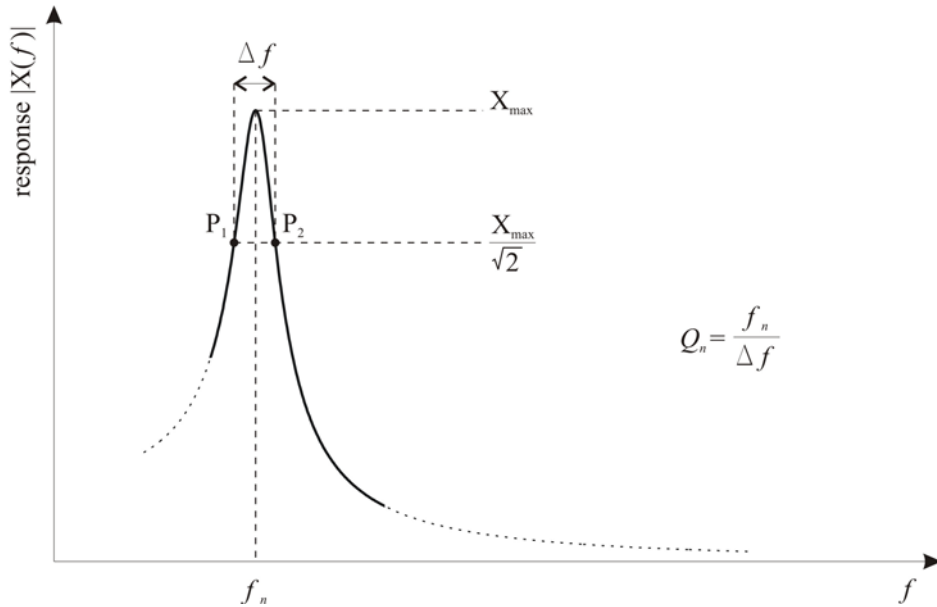


**Figure 13-21: Estimation of modal damping from response plot**

To get a proper estimation of the test damping factor the analysis results should be satisfactorily correlated with the test ones and the modal basis identified from the test should be closely matching the one obtained from the prediction model, i.e.

$$\xi_{test} = \xi_{FEM} \frac{Q_{test}}{Q_{FEM}} \quad [13-36]$$

The estimation of the damping characteristics for the on-orbit configuration from ground tests suffers from the fact that several air damping mechanisms exists on ground that would be absent for the on-orbit situation:

- damping by sound radiation into the air,
- damping by the reactive sound field around the structure,
- viscous damping due to the air trapped between components.

In some cases the damping distribution across the structure might be significantly non-homogeneous, e.g. an elastomer damper might be present in the structure for vibration isolation purposes. Then a frequency-dependent equivalent modal damping might be derived from a mixing rule. This rule requires for each mode the evaluation of the percentage of strain energy in each sub-system of the FEM, [10].

An example for the application of the mixing rule is given in Eq. [13-37] where significantly larger damping is present in the modules A and B as compared to the remaining structure:

$$\xi_{equiv} = \varepsilon_A * \xi_A + \varepsilon_B * \xi_B + (1 - \varepsilon_A - \varepsilon_B) * \xi_{structure} \quad [13-37]$$

where  $\varepsilon_k = \frac{\text{strain energy in module } k}{\text{total strain energy}}$  gives the ratio of the strain energy in module  $k$  to the total strain energy in the structure.

The application of the mixing rule should provide representative response levels associated to the modes involving the modules with large damping. Nevertheless care should be taken to not impose unrealistic damping values for modes involving modes of the usually lower damped satellite structure.

### 13.3.2.2.5 Disturbance source modelling

The disturbance source forcing functions could be defined by analytical formulation or numerical analysis or could be taken from relevant disturbance characterisation tests in the case the aforementioned approaches are not sufficiently accurate. More details are provided in Section 13.4.3 and e.g. in [11].

### 13.3.2.3 Model requirements

The finite element model used for the calculation of the transfer functions between the disturbance and the receiver locations, respectively, should be compliant with the following:

- Sufficient mesh refinement to be able to adequately predict the normal modes in the excitation frequency range.
- Sufficient detail of the disturber models to apply the input loads (excitation forces) at the correct locations considering the disturber internal transfer characteristics (from the load application point to the disturber interface with its mounting structure).
- Sufficient detail of the receiver models to properly recover the induced deformations.

Additional specific modifications of the analysis model might be required at those locations where the disturbance loads should be introduced into the structure model. In the case of a rotating mechanism these inputs are relative torque inputs meaning that opposite and equal torques are applied at the two sides of the mechanism, e.g. the reaction wheel and its housing. A reaction wheel can be modelled by adding a new node collocated with the existing and structurally attached node representing the location of the reaction wheel on the spacecraft structure. The degrees of freedom of this additional node are then constrained to follow the attached node except for the rotational degree of freedom that serves as the mechanism. The corresponding rotational inertia values are then added to the new grid point. The inertia values can be calculated from the reaction wheel masses and the estimated mass distribution.

### 13.3.2.4 General micro-vibration analysis flow

In general the micro-vibration analyses are performed in three steps:

1. Determination of the transfer function characteristics between the disturbance and the receiver location, respectively. This information is usually derived from a finite element model assembly of the satellite platform, the disturbance sources (as far as necessary) and the payloads (as far as necessary), all in the on-orbit configuration.
2. Application of the disturbance source forcing functions (either in time or frequency domain).
3. Evaluation of the responses at the receiver locations based on the relevant transfer function characteristics.

The final result, the deviation of the instrument line-of-sight from the nominal position, is then determined as the linear combination of all disturbances acting simultaneously. The analysis is usually performed in the frequency domain.

For the analysis step 1 usually a Nastran modal analysis is performed followed by a transfer to the dedicated post-processing software of the eigenfrequencies in the frequency range of interest and the associated mode shapes (mass-normalized).

The post-processing of the Nastran data, analysis steps 2 and 3, is frequently done with MATLAB where the disturbance source forcing functions are taken as inputs and the disturbances at the receiver locations are calculated by relevant matrix operations.

### 13.3.2.5 Power approach

The power approach allows estimating - without any precise knowledge of the spacecraft model - the order of magnitude of the impact of micro-vibration disturbance sources on the sensitive instruments. The main assumption of this "macroscopic" approach concerns the integral transmission of the power of the disturbance source to the instrument interface.

At mid frequencies the power injected tends to be independent from the whole structure and the behaviour is strongly linked to the local impedance at the disturbance location. In case no information on the spacecraft structure is available then the power injected to the instrument is taken equal to the power injected by the source. It is calculated thanks to displacements and forces predicted (or measured) at the perturbation interface: an accurate model of the disturbance source support is then needed. The maximum power is determined for each harmonic frequency and may be imposed to the local modes of the payload.

As an example of the power approach the application to the Envisat/GOMOS spectrometer is briefly outlined hereafter in Figure 13-22. The system coupled analysis results have been used for the GOMOS analysis with the instrument clamped at its interface.

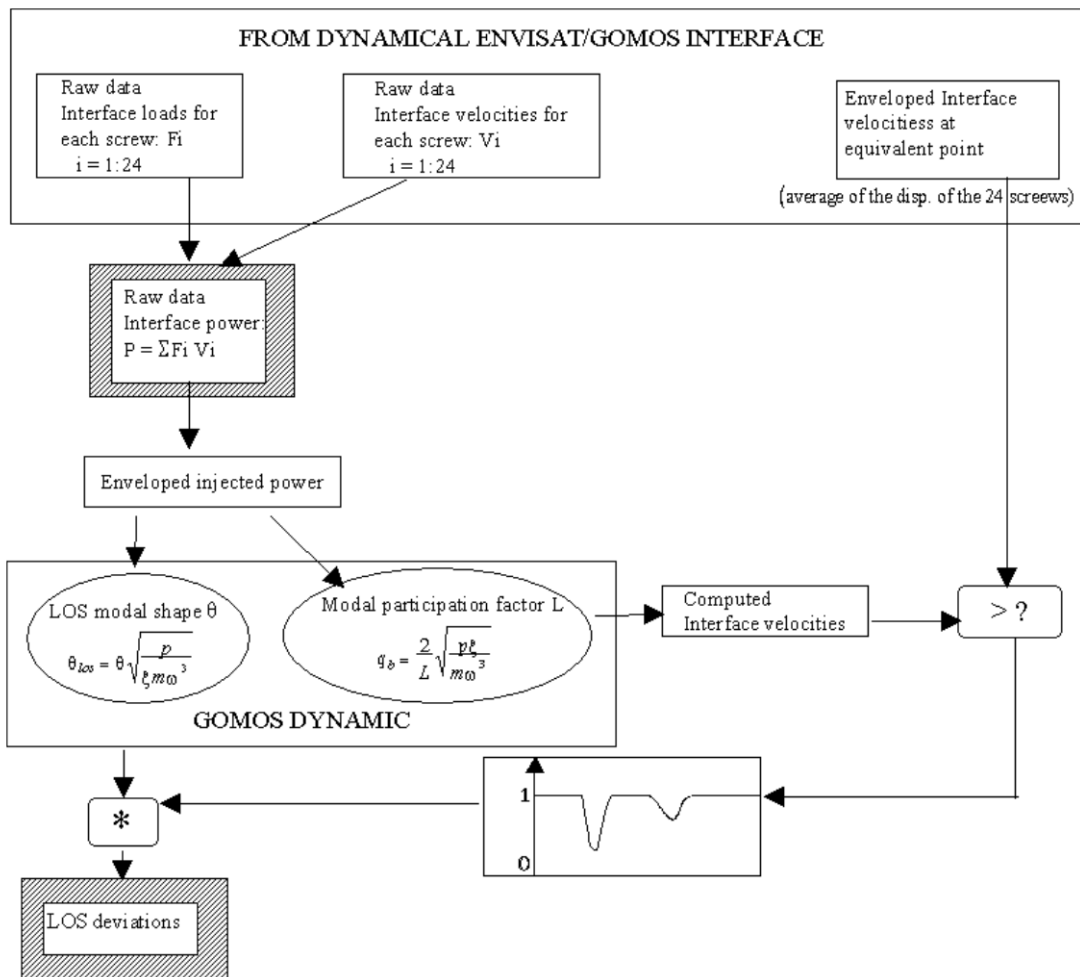


Figure 13-22: Power approach applied to Envisat/GOMOS instrument [9]

The power injected to GOMOS has been computed from the loads and velocities for all interface screws. The line-of-sight (LoS) deviation is depending on the injected power  $p$ , the LoS mode shape  $\theta$ , the damping factor  $\xi$  but not on the modal participation factor  $L$  of the mode (or effective masses).

This corresponds to the case where all power can be injected into GOMOS independently of the velocity available at the interface to generate this power. Therefore it is necessary to assess this velocity (or displacement  $q_b$ ) in order to verify that it is consistent with the interface velocity found in the satellite system coupled analysis. If this is not the case then a notching of the power for the modes with low excitabilities needs to be applied.

This is considered a quite conservative approach. In order to obtain more accurate predictions the evaluation of the power dissipation throughout the whole spacecraft structure should be improved.

### 13.3.2.6 Energy approach

#### 13.3.2.6.1 Introduction

In order to better control the on-orbit micro-vibration environment it is necessary to extend the frequency range of interest to high frequencies, e.g. up to about 4000 Hz for observation satellites. In this frequency range the finite element models have generally only a limited validity and their usage should be avoided. The Statistical Energy Analysis (SEA) method recommended for use in micro-vibration analyses for performance predictions in the mid to high frequency bands is an extension of the classical SEA which was originally developed for the vibro-acoustic analysis of complex structural and fluid systems based on the energy interaction between plate and cavity, see also Section 9.6.3.

The SEA approach has been demonstrated already in several space programs to be a useful tool for micro-vibration analyses in the high frequency range. The extended SEA furnishes the analysis of couplings between any sub-domains of a linear dynamical system in order to provide relevant information for the micro-vibration analyses.

#### 13.3.2.6.2 SEA model definition

The SEA theory is based on a fundamental simple model consisting of two linear, weakly coupled oscillators exchanging energy when excited by uncorrelated random forces. Here weak coupling means that the uncoupled eigenfrequencies of both oscillators are only slightly perturbed by the coupling condition. The relevant analysis variables are the total energy stored in the local modes of the respective sub-domains.

When introducing the vibrational energy  $E$  as the sum of potential and kinetic frequency-band-integrated energies and the power  $P$  as the mean rate of change of energy in the time domain the two oscillators exchange, under steady-state conditions, a power proportional to their energy difference:

$$\frac{P_{12}}{\omega} = B(\omega_1, \omega_2) [E_1 - E_2] \quad [13-38]$$

The coefficient  $B$  depends on specific system parameters as e.g. the coupling stiffness and/or mass, the damping loss factor and the uncoupled eigenfrequencies by  $\omega_1$  and  $\omega_2$  of both oscillators. The power exchange  $P_{12}$  is reaching a maximum value when both eigenfrequencies are the same and is rapidly decaying when  $\omega_1$  and  $\omega_2$  are much different.

Considering an analysis frequency band of width  $\Delta\omega$  and centre frequency  $\omega_c$  Eq. [13-38] has been extended to the coupling of continuous subsystems assuming that their band-integrated energy is proportional to their local modal density  $n$ , expressed in mode/Hz, or their mode number  $N$  where  $N$  is defined as follows:

$$N = n \frac{\Delta\omega}{2\pi} \omega \quad [13-39]$$

A continuous subsystem is then seen as a distribution of discrete local modal oscillators per band.

Statistics may be then applied on the modal set instead of trying to identify precisely each modal parameter. In SEA theory it is assumed that the modes are uniformly distributed over  $\Delta\omega$  reducing their description to a mode count  $N$ , the number of modes resonating in the frequency band  $\Delta\omega$ . Individual modal amplitudes are assumed uniform in a frequency band which may be considered as a maximum entropy hypothesis.

For continuous subsystems, Eq. [13-38] may be then rewritten as:

$$\frac{P_{12}}{\omega} = N_1 N_2 \langle B \rangle_{\Delta\omega} [\varepsilon_1 - \varepsilon_2] \quad [13-40]$$

The modal data set is restricted to the local modes of subsystems 1 and 2 resonating in the same analysis frequency band in which pairs of modes  $N_1 N_2$  exchange energies through a mean modal B coefficient following the relationship (1), each mode (or oscillator) carrying a mean modal energy  $\varepsilon$ .

A power balance for each subsystem can then be established which relates the power injected from applied loads, the internally dissipated power and the exchanged power:

$$\begin{Bmatrix} P_1 \\ P_2 \end{Bmatrix} = \begin{Bmatrix} \eta_1 \omega N_1 \varepsilon_1 + N_1 N_2 \omega \langle B \rangle [\varepsilon_1 - \varepsilon_2] \\ N_1 N_2 \omega \langle B \rangle [\varepsilon_2 - \varepsilon_1] + \eta_2 \omega N_2 \varepsilon_2 \end{Bmatrix} = \omega \begin{bmatrix} \eta_1 N_1 + N_1 N_2 \langle B \rangle & -N_1 N_2 \langle B \rangle \\ -N_1 N_2 \langle B \rangle & \eta_2 N_2 + N_1 N_2 \langle B \rangle \end{bmatrix} \begin{Bmatrix} \varepsilon_1 \\ \varepsilon_2 \end{Bmatrix} \quad [13-41]$$

or, in short, with [L] being the loss matrix:

$$\begin{Bmatrix} P_1 \\ P_2 \end{Bmatrix} = \omega [L] \{ \varepsilon \} \quad [13-42]$$

When a-priori portioning into weakly coupled subsystems is possible, then  $N_1$  and  $N_2$  may be estimated from the uncoupled-subsystem-wave-equation eigenvalue problem.  $\eta_1$  and  $\eta_2$  are the hysteretic mean modal damping loss factors which can be measured and given as spectral data.

On the other hand, B cannot be obtained from the coupled equation of motion since the exact coupling conditions are unknown due to the "weak coupling" assumption. In practice, B is derived from wave theory assuming all local modes can be decomposed into plane waves, reducing the problem of computing B to a well-posed problem of wave transmission through a junction under a given incidence. Due to the large number of interacting modes (in the high frequency domain), the incidence is assumed to be random and B is obtained as proportional to the diffuse field wave transmission coefficient.

The modal energies  $\varepsilon$  may then be simply calculated by inverting the loss matrix [L]. The coupling coefficient is generally defined in terms of the coupling loss factor  $\eta_{12}$ , i.e. the amount of total energy lost by a subsystem in the coupling:

$$\eta_{12} = N_2 \langle B \rangle \quad [13-43]$$

resulting to

$$\frac{P_{12}}{\omega} = N_1 \eta_{12} \varepsilon_1 - N_2 \eta_{11} \varepsilon_2 = \eta_{12} E_1 - \eta_{11} E_2 \quad [13-44]$$

where  $E = m \langle v^2 \rangle$  is the total energy stored in local modes by subsystems with total mass m and mean spaced-frequency averaged velocity  $\langle v^2 \rangle$ . A SEA model is then set up from interacting weakly-coupled subsystems which exchange power in proportion to the difference of their mean modal energy.

Despite its restrictive assumptions the SEA method has been proven to give a correct description of high frequency interactions. Regarding the frequency domain where the SEA models are valid it can be noticed that they act as quasi high-pass filters. Below a certain cut-off frequency the SEA is no longer representative of the system dynamics and this frequency is related to the size of the subsystems that determine locations in the frequency plane of the lowest local resonances.

Some limitations arise from both SEA modelling practice and theory:

- In a subsystem, the probability of the energy distribution of individual modal oscillators is generally unknown which leads to only mean value prediction.
- Wave theory used to compute Coupling Loss Factors (CLF) limits their prediction to subsystems directly connected on a common boundary.
- Link to global modes is lost due to the a-priori weak coupling assumption.
- Local modal eigenfrequencies are restricted to resonant modes (the eigenfrequency of which is included in  $\Delta\omega$ ).
- There are no well-defined rules for the division into sub-domains. This is left to the expertise of the user who may encounter some trouble when modelling complex non-homogeneous systems.

In Figure 13-23 a SEA model used for OLYMPUS micro-vibration predictions is shown.

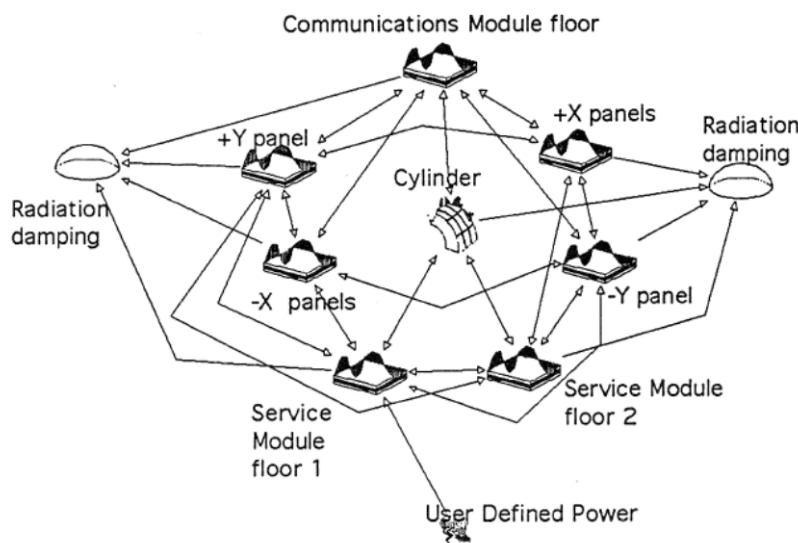


Figure 13-23: SEA model of OLYMPUS satellite with radiation damping [9]

### 13.3.3 Micro-vibration budget assessment

#### 13.3.3.1 Introduction

Usually there are several micro-vibration disturbance sources on a satellite platform. All their contributions to the line of sight distortion of a sensitive instrument (the receiver) should be taken into account to obtain the final pointing budget that describes the performance of this specific instrument under the influence of the expected satellite micro-vibration environment. The same procedure should be applied then for each micro-vibration sensitive instrument on the satellite in order to complete the overall assessment of the impact of the micro-vibration environment on the satellite performance.

The overall satellite pointing error synthesis is established by taking into account the micro-vibration perturbations and the effects of other perturbations of the instrument line of sight, e.g. resulting from thermo-elastic distortions of the satellite structure. Such synthesis is briefly addressed in Section 13.3.4.

In order to obtain the final pointing budget resulting from the satellite micro-vibration disturbances the following steps can be applied:

- Computation of all transfer functions required to describe the transmission of the perturbations from their respective input locations to the receiver location;
- Evaluation of the impact of each elementary perturbation source of each disturbance source, e.g. the impact of a single harmonic along a single excitation degree of freedom;
- Summation on the excitation degrees of freedom;
- Summation on the elementary components of the perturbation (e.g. harmonics) for each disturbance source;
- Summation on the disturbance sources.

The following complimentary approaches for the budget calculation are available:

1. Statistical approach based on pointing performance analyses where multiple simulations in the time domain are carried out taking into account dispersions of relevant parameters influencing the pointing performance;
2. Envelope approach based on the computation of the pointing performance using disturbance amplitudes and transfer functions in the frequency domain.

The goal is to more accurately assess the effects deal of coincidences of frequencies of the perturbation harmonics and the resonant modes of the satellite structure. To create a worst case pointing budget these coincidences could be enforced by assuming that each harmonic might vary within a certain frequency interval, to be defined as function of the uncertainties around the nominal frequency.

### 13.3.3.2 Summation rules

The following summation rules are frequently applied in practice, [9]:

- Summation on the excitation / response degrees of freedom:  
Practically, most micro-vibration disturbers generate the perturbation forces and moments simultaneously along several degrees of freedom, e.g. for a reaction wheel radial rotating forces, axial forces and tilting rotating torques are simultaneously acting at the interface with the satellite platform. Proper accumulation of all contributions of the different excitation degrees of freedom should be done to adequately assess the impact of the perturbations.

The following options are possible:

- Direct linear summation: realistic summation taking into account the phases between the different degrees of freedom when they are available;
- Amplitude summation: “worst case” summation to be used as a tool to maximize the effects when no information on the phases is available;
- Quadratic summation: approach corresponding to a “mean statistical case” also used when the phases are not available or not well known.

Other methods could also be applied. However, the choice depends upon the kind of disturbance and the type of result expected (realistic or worst case).

- Summation on the harmonics (in the case of a disturbing source for which the spectral content is composed of several harmonics):
  - Amplitude summation: worst case summation since the accumulation of peak response values is not frequency consistent, i.e. peak values at different frequencies are added up;
  - Quadratic summation: approach leading to the total energy of the response;
  - Maximum harmonic response: no summation is performed, instead the harmonic giving the maximum peak response is retained.

Because of the great number of harmonics often present a linear summation would be too pessimistic; on the other hand, a quadratic summation might be too optimistic.

- Summation on the disturbance sources:

In the case where several disturbance sources are operated simultaneously, similar rules of summation as for the summation on excitation degrees of freedom may be proposed: either a quadratic sum or a linear sum depending on the perturbation profile knowledge, on the number of sources and on the phase of the project.

### 13.3.3.3 Statistical approach

The so-called statistical analysis, implemented e.g. into the  $\mu$ VISION micro-vibration effect analysis software [12] [13], uses dispersions on relevant parameters at satellite level and at mission level in order to compute image quality performances at typically 99.7% of all dispersed satellites and 90% of the images. Usually the number of simulations performed is in the order of  $10^4$  to  $10^5$  and each simulation is computing the performances over fixed image durations.

In the case of the  $\mu$ VISION software only small parameter variations can be taken into account (linearity hypothesis) and therefore the impact of large mechanical uncertainties involving non-linear effects cannot be assessed.

The simulation consists of injecting dynamic perturbations (e.g. harmonics force levels for a reaction wheel) into the satellite structural mathematical model which includes the disturbance source, the platform and the sensitive instrument. The induced instrument line-of-sight angular rotations are computed and, based on the availability of instrument and detector models in on-orbit configuration, these rotations are then converted into relevant image quality criteria.

The dispersed parameters are typically:

- at satellite level:
  - the amplitude and phase of the perturbation (harmonics), ideally based on values measured on the flight hardware;
  - the structural damping (usually between 0.5% and 1%);
  - the structural parameters (if possible);
- at mission level:
  - the pointing bias;
  - the guidance parameters.

The dispersions of the structural parameters (typically thickness, Young's modulus, etc.) have a direct impact on the structural mode frequencies and consequently the transfer functions. Considering that there are usually significant difficulties to properly define representative dispersions for the satellite structural parameters this is further increasing the accuracy of the assessment since usually it is already difficult to have a representative satellite finite element model for the complete frequency

range of interest (thus having significant impact, too, on the structure modal characteristics and the transfer functions), hence it is more difficult.

A potential solution to this problem might be to increase the dispersion at disturbance source level (e.g. wheel speed) with a non-dispersed structure to have coincidences between the harmonics frequencies and the “nominal” structural modes.

#### **13.3.3.4 Envelope approach**

The order of magnitude of the satellite pointing errors and the detailed micro-vibration budgets can be assessed by multiplying the disturbances by the satellite mechanical transfer function and further post-process the results as necessary to get the relevant line-of-sight distortions.

The main objective of this verification is first to confirm the statistical budget, secondly to potentially predict effects at frequencies not represented in the analytical transfer function. For example, there was the case that transfer functions were measured in a frequency range significantly exceeding the applicable frequency limit for the validity of the satellite FEM. Furthermore significant transfer function peaks have been identified as well at frequencies above the FEM limit. With a simple direct method the order of magnitude of these peaks on the instrument pointing performance could be predicted which was not possible by the statistical approach based on FEM due to its limited validity at those frequencies. However, in order to have sufficient confidence in this simple method approach the satellite dynamic behaviour at those frequencies needs to be well understood.

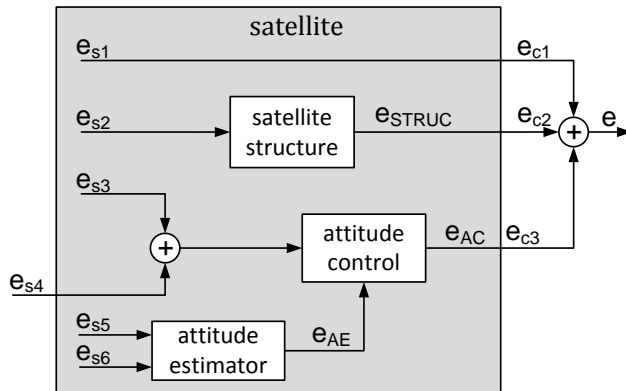
The envelope approach is also of particular interest to isolate the main contributors to the performance errors, e.g. disturbance source input degrees of freedom, harmonics number and main structural modes. It allows identifying whether the structural transfer function is driven by first or higher order modes and which structure and equipment are involved in the line-of-sight deviation. Furthermore uncertainties could be derived to support the understanding of the micro-vibration phenomena.

#### **13.3.4 Pointing error synthesis**

The pointing errors of e.g. scientific or Earth observation satellite instruments are not only influenced by the micro-vibration environment but there are also other relevant sources which might cause non-acceptable line-of-sight disturbances, e.g.:

- thermo-elastic distortions causing payload-star tracker misalignments,
- general Attitude & Orbit Control Subsystem (AOCS) errors including deviations from nominal performance for e.g. reaction wheels, star trackers and gyros,

The assessment of the contributions of all error sources and their statistical handling is described in detail in the ESA Pointing Error Engineering Handbook, [14]. In Figure 13-24 an example for a typical satellite pointing error synthesis is shown with several error sources  $e_{s1}$  to  $e_{s6}$ . The total pointing error  $e$  to be taken into account for the final pointing performance assessment is then resulting from the accumulation of all the contributors  $e_{c1}$  to  $e_{c6}$ .



PES	Type
e <sub>s1</sub>	Payload-star tracker misalignments
e <sub>s2</sub>	$\mu$ Vibrations (outside of control bandwidth)
e <sub>s3</sub>	Reaction wheel errors
e <sub>s4</sub>	External disturbances
e <sub>s5</sub>	Star tracker errors
e <sub>s6</sub>	Gyro errors

Figure 13-24: Satellite pointing example [14]

### 13.3.5 Micro-vibration verification test

Satellite micro-vibration tests are usually performed with the following main objectives:

- The verification of the satellite performances under the micro-vibration environment by employing a representative satellite configuration, applying relevant disturbance loads and measuring the responses at the sensitive receiver locations (“end-to-end” testing);
- The acquisition of relevant data to validate the micro-vibration analysis methodology and the results obtained. This concerns in particular the verification of the correctness of critical analysis parameters as e.g. the damping assumptions for the most important spacecraft modes driving the global system performances;
- Where necessary, the acquisition of relevant data to allow updating the mathematical model to perform the final micro-vibration environment predictions based on a test-validated model.

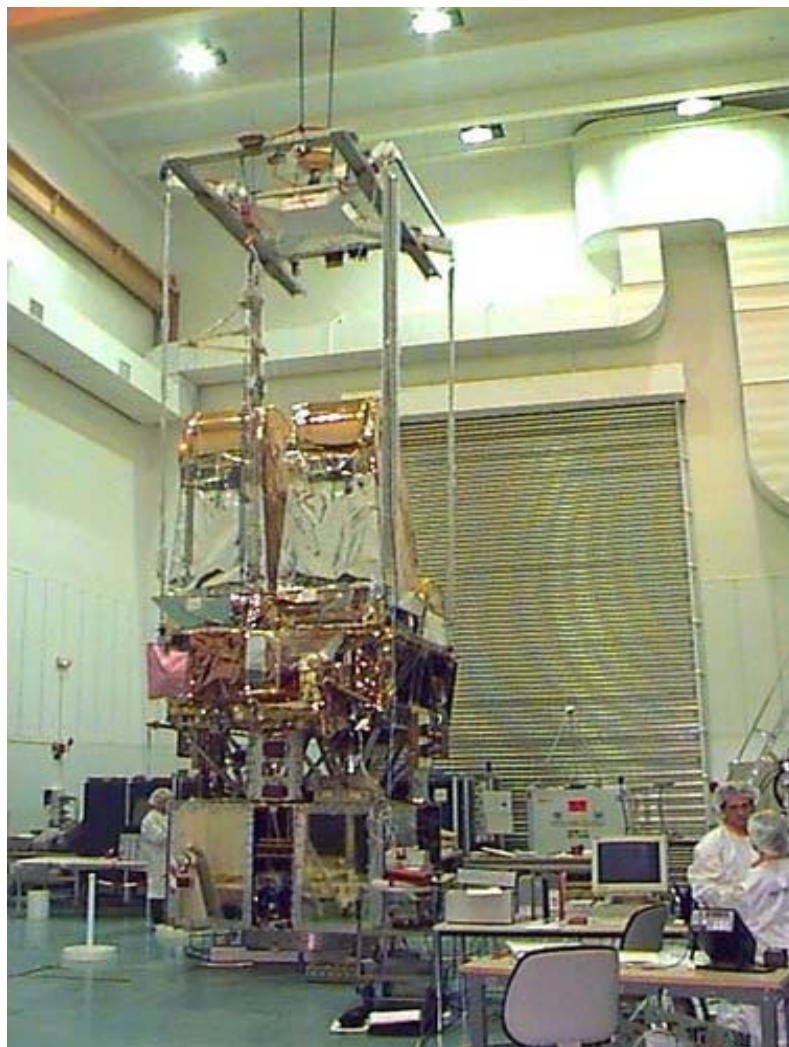


Figure 13-25: SPOT4 satellite micro-vibration test [16]

### 13.3.5.1 Test setup

The satellite micro-vibration test requires a complex setup due to the requirement that the on-orbit conditions should be simulated as close as possible in order to get reliable estimates for the expected on-orbit performances. In particular the satellite should be in a quasi “free-free” configuration and the gravity forces acting on the structure and surrounding air effects should be minimized. Consequently, much effort should be spent to define and implement the satellite.

As a general rule, the satellite should be supported in such a way that the highest natural frequency of the suspension is less than 25% of the first structural mode.

The suspension and potential gravity compensation devices could also allow isolating the test specimen from external disturbances impacting the test performance, see the section below regarding the rejection of noise sources. A typical satellite system micro-vibration test setup is shown in Figure 13-25 for the SPOT4 satellite.

An alternative test setup where the free-free boundary conditions were approximated by putting the satellite on air-cushions is described in [15]. The main purpose of this test was however to get an estimate of the applicable on-orbit structural damping rather than performing the “end-to-end” testing as mentioned above.

### 13.3.5.2 Background noise

The level of accelerations or displacements that should be measured during micro-vibration tests is usually very low. These measurements can be significantly influenced by background noise caused by exterior disturbing sources, e.g. road traffic, air-conditioning noise etc. A classification of relevant noise sources together with the affected frequency range and potential countermeasures is provided in Table 13-2, [17].

Prior to starting the test activities the background noise level should be identified by measuring – with the test unit being inactive – the parasitic acceleration levels on the test support structures and the test article itself. An example for the quantification of background noise as acceleration PSD is shown in Figure 13-26 where the magenta spectrum indicates the response of the supporting structure whereas the other (lower) spectra are for the accelerometers attached to the test article. The efficiency of the test article suspension system is clearly demonstrated. However, the graph shows also clearly the presence of electrical noise and other high frequency disturbances.

The measured background noise should be compared with the acceptable disturbance level requirement in order to assess whether the test setup has the capability to provide the expected information regarding the micro-vibration environment.

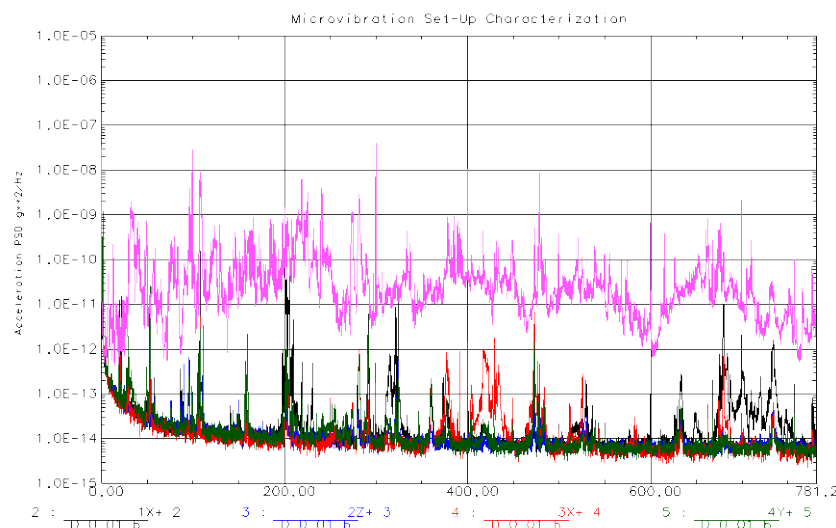


Figure 13-26: Typical background noise acceleration PSD [18]

**Table 13-2: Classification of noise sources affecting micro-vibration tests [17]**

Noise source	Frequency band	Countermeasures
<b>• Electromagnetic noise:</b>		
electrical noise from main supply (50 Hz and harmonics)	narrow band noise appearing on spectra lines	proper grounding of equipment - remove light sources - appropriate shielding
tonal noise induced by rotating machinery and illumination systems		
internal amplifiers and acquisition system noise	in general 1/f broadband noise, characteristic of equipment	selection of high quality, low noise electronics
instrumentation noise (piezo-electric accelerometers, force cells)		use of high sensitivity sensors, with reduced amplifier volt level
signal conditioning, amplification and acquisition		use of very low noise electronics
<b>• Acoustic noise:</b>		
coupling of test article with surrounding air	broadband noise with relevant frequency components in the band of interest for the test	- test at night without air-conditioning, laminar flux off and reduced human activity close to the test room, - potential encapsulation of complete test set-up in a for better isolation (while maintaining clean air conditions), - potential use of acoustic enclosure; better however to use vacuum chamber
acoustic perturbations reaching the satellite structure		
<b>• Ground-borne noise (ground vibration input):</b>	low to mid-frequency (250 – 300 Hz) range for transportation noise (e.g. truck or train)	special seismic isolation devices for noise filtering, use of proper suspension devices for test article
<b>• Signal processing noise:</b>	broadband noise	adequate signal processing to improve signal-to noise ratio

### 13.3.5.3 Test execution

Micro-vibration tests are usually performed as “end-to-end” tests where the disturbances are applied at their root source locations and the resulting effects, the distortions of the line of sight of the sensitive instruments, are measured. Although the real disturbances (e.g. resulting from reaction wheel unbalances) might be simulated by artificial excitations, e.g. applying harmonic forces over relevant frequency bands by electro-dynamic shakers, the sensitive instruments should be present on the test configuration in order to be able to adequately determine the distortions at the imager

location. This applies in particular also to the situation where instrument modes are significantly impacting on the amplification of the disturbances.

Two basic excitation types could be used for generating the input forces:

1. Sinusoidal excitation:

Stepped sine testing is useful for examining local details around specific modes of vibrations.

2. Random noise excitation:

Random vibration input should be used if a wide frequency band needs to be excited simultaneously. The required mean square value should be equivalent to the power injected at each frequency in the sine test.

#### **13.3.5.4 Test data acquisition and evaluation**

In order to ensure high data quality for further post-processing the following important aspects should be considered for micro-vibration test measurements:

- The low levels of both excitation and response require careful monitoring to avoid errors in the measured data caused by problems of limited capture time, limited time resolution and limited amplitude resolution even if the measurement system would have worked faultless.
- The measured data are containing wanted and unwanted signals (noise) that should be separated. This is particularly important in micro-vibrations testing where the measured signals are at the lower limit of the measurement capabilities of the sensors and the difference between signal and noise is rather small.
- The coherence function can provide relevant information about the noise level in the output signal. However, it does not indicate the origin of the noise. In order to guarantee data quality, the signal-to-noise ratio of all input and output channels should be acquired.
- Emphasis should be put on assessing the responses of more sensitive receivers rather than lower noise amplifications: preference should be given to measuring strong signals rather than to be able to amplify weak ones where the risks of noise contamination is becoming even larger.
- The test data should be compliant with general test data quality requirements and verify the integrity of the test performed (in particular concerning linearity, reciprocity and repeatability of the data).

## 13.4 Micro-gravity and micro-vibration disturbance sources

### 13.4.1 Scope

This section is intended to provide the information needed to identify the potential micro-gravity and micro-vibration disturbance sources, their disturbance mechanisms and their signal types. First the relevant disturbance sources are presented and discussed; then principles for the characterisation of the disturbance source forcing functions are introduced.

### 13.4.2 Review of potential disturbance sources

Potential micro-gravity and micro-vibration disturbance sources of satellites and pressurized modules can be identified by relevant reviews of the spacecraft configuration. These reviews are in general performed e.g. in early system design phases in the frame of assessments concerning the compliance with the respective performance requirements.

In the following sections an attempt is made to classify the disturbance sources followed by a presentation of general aspects of attenuating or reducing the effects of dynamic disturbances.

#### 13.4.2.1 Disturbance source classification

The characteristics of the potential disturbance sources can be defined in either the time or frequency domain or also in a combination of both. They can be subdivided into **external** (or **natural**) and **internal** disturbers.

**External** (or **natural**) **events** have a major importance only as potential micro-gravity environment disturbances. They are resulting from:

- Micro-meteoroids and debris impacts
- Atmospheric drag
- Earth gravity field gradient
- Earth magnetic field
- Solar flux & Earth albedo
- Eclipse entry & exit

**Internal events** might create relevant disturbances for both the micro-gravity and the micro-vibration environment. They are resulting from:

- Propulsion subsystem,
- Avionics subsystem,
- Electrical power subsystem (EPS),
- Radio frequency (RFS) / telemetry & telecommand subsystem,
- Thermal control subsystem (TCS),
- Structure subsystem.

Both external and internal events can be further classified taking into account the source item, the kind of physical event, the disturber physics, and the signal type.

Typical examples of micro-gravity and micro-vibration disturbance sources, categorized according to the above mentioned classification criteria, are summarized in Table 13-3 considering external (or natural) disturbance sources for a generic satellite, in Table 13-4 considering internal disturbance sources for a generic satellite, and in Table 13-5 considering the most important disturbance sources for an ISS Manned Module.

It should be noted that the signal types, as given in Table 13-3, Table 13-4 and Table 13-5, have been described in accordance with applicable NASA ISS terminology:

- “intermittent”: excitation signal (harmonic or random) that is present for less than 8 hours,
- “continuous”: excitation signal (harmonic or random) that is present for more than 8 hours.

However, the disturbance excitations might be also classified with respect to whether they are constant frequency periodic (harmonic) or transient in nature, Table 10-1. The disturbances generated by harmonic sources are usually occurring for long-time durations. The load spectrum, e.g. for reaction wheels, control momentum gyros or cryogenic coolers, is a discrete spectrum characterised by several sinusoidal signals  $H_i$  (harmonics) the frequencies of which are multiples of the fundamental harmonic  $H_1$ . However, it should be noted that the higher frequency harmonics are not always integer multiples of the fundamental one.

**Table 13-3: Potential external (or natural) micro-gravity disturbance sources for generic satellite (applicable to spacecraft system)**

Source item	Physical event	Disturber physics	Signal type
Micro-Meteoroid Impact	Particles collision to Spacecraft	Transient Structural Vibration	Intermittent
Debris Impact	Particles collision to Spacecraft	Transient Structural Vibration	Intermittent
Atmosphere Drag	Aerodynamic drag	Quasi-steady fluctuating pressure	Continuous
Earth Gravity Field Gradient	Spacecraft mass accelerations (linear and rotational)	Quasi-steady fluctuating acceleration	Continuous
Earth Magnetic Field	Spacecraft magneto-moment interaction (rotational)	Quasi-steady fluctuating acceleration	Continuous
Sun Flux & Earth Albedo	Spacecraft orbit fluctuations (linear)	Quasi-steady fluctuating acceleration	Continuous
Eclipse entry & exit	Spacecraft orbit fluctuations (linear)	Quasi-steady fluctuating acceleration	Continuous

**Table 13-4: Potential internal micro-gravity and micro-vibration disturbance sources for generic satellite**

SUB-SYSTEM	SOURCE ITEM	ACR.	PHYSICAL EVENT	DISTURBER PHYSICS	SIGNAL TYPE
Propulsion	Ion thruster	ITA	Applied thrust	Periodic Vibration	Continuous
			Thermal clanks due to the variation in the power dissipation	Sudden Stress Release	Intermittent
			Inductive Electro-Magnetic Force due to currents in wires	Inductive Electro Magnetic Force	Continuous
	Ion Propulsion Control Unit	IPCU	Thermal clanks due to the variation in the power dissipation	Sudden Stress Release	Intermittent
			Inductive Electro-Magnetic Force due to currents in wires	Inductive Electro Magnetic Force	Continuous
	Xenon Storage Tank (bearings)	XST	Internal pressure variations & Thermal heating cycles	Sudden Stress Release	Continuous
	Prop. Xe feed Assy (with: Filter, Piping, Restrictor, Pressure Regulator, Flow Controller)	PXFA	Thermal clanks due to the variation in the power dissipation	Sudden Stress Release	Intermittent
			Internal Flow (10 Restrictor)	Flow Induced Vibration	Continuous
			Switch Mechanism (PT only)	Transient Structural Vibration	Intermittent
			Inductive Electro-Magnetic Force due to currents in wires	Inductive Electro Magnetic Force	Continuous
	Neutralizer	NTR	Thermal clanks due to the variation in the power dissipation	Sudden Stress Release	Intermittent
			Inductive Electro-Magnetic Force due to currents in wires	Inductive Electro Magnetic Force	Continuous
Avionics	Ion Thruster Alignment Mechanism	ITAM	Disturbance forces and moments due to by mechanical movement	Mechanical Vibration	Continuous
	Electronic Press. Regulator Mechanism	EPRM	Disturbance forces and moments due to by mechanical movement	Mechanical Vibration	Continuous
	Central Data Manag. Unit	CDMU	Thermal clanks due to the variation in the power dissipation	Sudden Stress Release	Intermittent
			Inductive Electro-Magnetic Force due to currents in wires	Inductive Electro Magnetic Force	Continuous
	Star Tracker Sensor Electronics	STRE	Thermal clanks due to the variation in the power dissipation	Sudden Stress Release	Intermittent
			Inductive Electro-Magnetic Force due to currents in wires	Inductive Electro Magnetic Force	Continuous
	Star Tracker Sensors	STRH	Thermal clanks due to the variation in the power dissipation	Sudden Stress Release	Intermittent
			Inductive Electro-Magnetic Force due to currents in wires	Inductive Electro Magnetic Force	Continuous
	Magnetic Torquer	MT	Thermal clanks due to the variation in the power dissipation	Sudden Stress Release	Intermittent
			Inductive Electro-Magnetic Force due to currents in wires	Inductive Electro Magnetic Force	Continuous
	Earth Sensors	CESS	Thermal clanks due to the variation in the power dissipation	Sudden Stress Release	Intermittent
			Inductive Electro-Magnetic Force due to currents in wires	Inductive Electro Magnetic Force	Continuous
	Magnetometer Electronic	MGME	Thermal clanks due to the variation in the power dissipation	Sudden Stress Release	Intermittent
			Inductive Electro-Magnetic Force due to currents in wires	Inductive Electro Magnetic Force	Continuous
	Reaction Wheel	RW	Disturbance forces and moments due to mechanical movement	Mechanical Vibration	Continuous
	Momentum Wheel	MW	Disturbance forces and moments due to mechanical movement	Mechanical Vibration	Continuous

**Table 13-4: Potential internal micro-gravity and micro-vibration disturbance sources for generic satellite (cont.)**

SUB-SYSTEM	SOURCE ITEM	ACR.	PHYSICAL EVENT	DISTURBER PHYSICS	SIGNAL TYPE
EPS	Power Control Distribution Unit	PCDU	Thermal clanks due to the variation in the power dissipation	Sudden Stress Release	Intermittent
			Inductive Electro-Magnetic Force due to currents in wires	Inductive Electro Magnetic Force	Continuous
	Li-ion Battery	Battery	Thermal clanks due to the variation in the power dissipation	Sudden Stress Release	Intermittent
			Inductive Electro-Magnetic Force due to currents in wires	Inductive Electro Magnetic Force	Continuous
	Solar Array	SA	Thermal heating cycles	Sudden Stress Release	Intermittent
			Inductive Electro-Magnetic Force due to currents in wires	Inductive Electro Magnetic Force	Continuous
	Harness	-	Inductive Electro-Magnetic Force due to currents in wires	Inductive Electro Magnetic Force	Continuous
RFS	Solar Array Drvr Mechanism	SADM	Disturbance forces and moments due to by mechanical movement	Mechanical Vibration	Continuous
	Transponder	TRSP	Thermal clanks due to the variation in the power dissipation	Sudden Stress Release	Intermittent
			Inductive Electro-Magnetic Force due to currents in wires	Inductive Electro Magnetic Force	Continuous
	RF Transfer Switch	RF Switch	Thermal clanks due to the variation in the power dissipation	Sudden Stress Release	Intermittent
			Inductive Electro-Magnetic Force due to currents in wires	Inductive Electro Magnetic Force	Continuous
	S-Band Antenna	S-BAND	Thermal clanks due to the variation in the power dissipation	Sudden Stress Release	Intermittent
			Inductive Electro-Magnetic Force due to currents in wires	Inductive Electro Magnetic Force	Continuous
TCS	Antenna Pointing Mechanism	APM	Disturbance forces and moments due to by mechanical movement	Mechanical Vibration	Continuous
	Wave Guide Switch	Switch	Disturbance forces and moments due to by mechanical movement	Mechanical Vibration	Intermittent
	MLI – Under SA	MLI	Thermal heating cycles in the eclipse entry & exit	Crackling / Buckling	Intermittent
	MLI – External	MLI	Thermal heating cycles in the eclipse entry & exit	Crackling / Buckling	Intermittent
STRUCTURE	Thermistors	-	Inductive Electro-Magnetic Force due to currents in wires	Inductive Electro Magnetic Force	Continuous
	Heaters	-	Inductive Electro-Magnetic Force due to currents in wires	Inductive Electro Magnetic Force	Continuous
STRUCTURE	Structural joints	-	Thermal heating cycles	Sudden Stress Release	Intermittent
OTHER EQUIPMENT	Std Radiation Environ. Monitor	SREM	Thermal clanks due to the variation in the power dissipation	Sudden Stress Release	Intermittent
			Inductive Electro-Magnetic Force due to currents in wires	Inductive Electro Magnetic Force	Continuous
	Laser Retro Reflector	LRR	Thermal clanks due to the variation in the power dissipation	Sudden Stress Release	Intermittent
	SSTI Electronics	SSTIE	Thermal clanks due to the variation in the power dissipation	Sudden Stress Release	Intermittent
			Inductive Electro-Magnetic Force due to currents in wires	Inductive Electro Magnetic Force	Continuous
	GPS Antenna	SSTA	Thermal clanks due to the variation in the power dissipation	Sudden Stress Release	Intermittent
			Inductive Electro-Magnetic Force due to currents in wires	Inductive Electro Magnetic Force	Continuous

**Table 13-5: Potential micro-gravity disturbance sources for ISS manned module**

SUB-SYSTEM	SOURCE ITEM	ACR.	PHYSICAL EVENT	DISTURBER PHYSICS	SIGNAL TYPE
ECLSS	Cabin Fan Assembly	CFA, IMV-S, IMV-R	Disturbance forces and moments due to by mechanical movement	Mechanical Vibration	Continuous
			Airborne disturbance loads due to acoustic noise emitted by the source	Acoustic Radiation	Continuous
			Airborne disturbance loads due to air flow noise emitted by the source	Aerodynamic Noise	Continuous
	Cabin Heat Exchanger Assy	CHXF A	Disturbance forces and moments due to by mechanical movement	Mechanical Vibration	Continuous
			Airborne disturbance loads due to acoustic noise emitted by the source	Acoustic Radiation	Continuous
			Airborne disturbance loads due to air flow noise emitted by the source	Aerodynamic Noise	Continuous
			Airborne disturbance loads due to fluid flow noise emitted by the source	Fluid Dynamic Noise	Continuous
	Condensate Water Separator Assy	CWSA	Disturbance forces and moments due to by mechanical movement	Mechanical Vibration	Continuous
			Airborne disturbance loads due to acoustic noise emitted by the source	Acoustic Radiation	Continuous
			Airborne disturbance loads due to air flow noise emitted by the source	Aerodynamic Noise	Continuous
			Airborne disturbance loads due to fluid flow noise emitted by the source	Fluid Dynamic Noise	Continuous
	IMV Shut Off Valve	ISOV	Disturbance forces and moments due to by mechanical movement	Mechanical Vibration	Intermittent
			Airborne disturbance loads due to acoustic noise emitted by the source	Acoustic Radiation	Intermittent
			Airborne disturbance loads due to air flow noise emitted by the source	Aerodynamic Noise	Intermittent
	Cabin Air Diffuser	CAD	Disturbance forces and moments due to by mechanical movement	Mechanical Vibration	Continuous
			Airborne disturbance loads due to air flow noise emitted by the source	Aerodynamic Noise	Continuous
	Return Grid Muffler	RGM	Disturbance forces and moments due to by mechanical movement	Mechanical Vibration	Continuous
			Airborne disturbance loads due to acoustic noise emitted by the source	Acoustic Radiation	Continuous
	Waste Gas Line Shut Off Valve	WGLS OV	Disturbance forces and moments due to by mechanical movement	Mechanical Vibration	Intermittent
			Airborne disturbance loads due to acoustic noise emitted by the source	Acoustic Radiation	Intermittent
	N2 Line Shut Off Valve	N2LSO V	Disturbance forces and moments due to by mechanical movement	Mechanical Vibration	Intermittent
			Airborne disturbance loads due to acoustic noise emitted by the source	Acoustic Radiation	Intermittent
	Air Ducting	-	Airborne disturbance loads due to acoustic noise emitted by the source	Acoustic Radiation	Continuous

**Table 13-5: Potential micro-gravity disturbance sources for ISS manned module  
(cont.)**

SUB-SYSTEM	SOURCE ITEM	ACR.	PHYSICAL EVENT	DISTURBER PHYSICS	SIGNAL TYPE
TCS	Water Pump Assy	WPA	Disturbance forces and moments due to by mechanical movement	Mechanical Vibration	Continuous
			Airborne disturbance loads due to acoustic noise emitted by the source	Acoustic Radiation	Continuous
			Airborne disturbance loads due to fluid flow noise emitted by the source	Fluid Dynamic Noise	Continuous
	3-Way Modulating Valve	WMV	Disturbance forces and moments due to by mechanical movement	Mechanical Vibration	Intermittent
			Airborne disturbance loads due to acoustic noise emitted by the source	Acoustic Radiation	Intermittent
			Airborne disturbance loads due to fluid flow noise emitted by the source	Fluid Dynamic Noise	Intermittent
	2-Way On-Off Valve	WOO	Disturbance forces and moments due to by mechanical movement	Mechanical Vibration	Intermittent
			Airborne disturbance loads due to acoustic noise emitted by the source	Acoustic Radiation	Intermittent
			Airborne disturbance loads due to fluid flow noise emitted by the source	Fluid Dynamic Noise	Intermittent
	Standard Cold Plate	-	Disturbance forces and moments due to by mechanical movement	Mechanical Vibration	Continuous
			Airborne disturbance loads due to acoustic noise emitted by the source	Acoustic Radiation	Continuous
			Airborne disturbance loads due to fluid flow noise emitted by the source	Fluid Dynamic Noise	Continuous
	Cold Plate ATR	-	Disturbance forces and moments due to by mechanical movement	Mechanical Vibration	Continuous
			Airborne disturbance loads due to acoustic noise emitted by the source	Acoustic Radiation	Continuous
			Airborne disturbance loads due to fluid flow noise emitted by the source	Fluid Dynamic Noise	Continuous
	Duct Network	-	Disturbance forces and moments due to by mechanical movement	Mechanical Vibration	Continuous
			Airborne disturbance loads due to acoustic noise emitted by the source	Acoustic Radiation	Continuous
			Airborne disturbance loads due to fluid flow noise emitted by the source	Fluid Dynamic Noise	Continuous
	H2O Connectors	-	Disturbance forces and moments due to by mechanical movement	Mechanical Vibration	Continuous
			Airborne disturbance loads due to acoustic noise emitted by the source	Acoustic Radiation	Continuous
			Airborne disturbance loads due to fluid flow noise emitted by the source	Fluid Dynamic Noise	Continuous

**Table 13-5: Potential micro-gravity disturbance sources for ISS manned module  
(cont.)**

SUB-SYSTEM	SOURCE ITEM	ACR.	PHYSICAL EVENT	DISTURBER PHYSICS	SIGNAL TYPE
DMS	P/L Control Unit	PLCU	Disturbance forces and moments due to by mechanical movement	Mechanical Vibration	Continuous
			Airborne disturbance loads due to acoustic noise emitted by the source	Acoustic Radiation	Continuous
	Mass Memory Unit	MMU	Disturbance forces and moments due to by mechanical movement	Mechanical Vibration	Continuous
	Vital Telecom. Computer	VTC	Disturbance forces and moments due to by mechanical movement	Mechanical Vibration	Continuous
			Airborne disturbance loads due to acoustic noise emitted by the source	Acoustic Radiation	Continuous
	Laptop	LPT	Disturbance forces and moments due to by mechanical movement	Mechanical Vibration	Continuous
			Airborne disturbance loads due to acoustic noise emitted by the source	Acoustic Radiation	Continuous
EPS	Module Lighting Unit	MLU	Airborne disturbance loads due to acoustic noise emitted by the source	Acoustic Radiation	Continuous
VIDEO	Video Cassette Recorder	VRC	Disturbance forces and moments due to by mechanical movement	Mechanical Vibration	Continuous
			Airborne disturbance loads due to acoustic noise emitted by the source	Acoustic Radiation	Continuous
	Audio Terminal Unit	ATU	Airborne disturbance loads due to acoustic noise emitted by the source	Acoustic Radiation	Continuous
SSF	-	DDCU	Disturbance forces and moments due to mechanical movement	Mechanical Vibration	Continuous
	Cold Plate	-	Disturbance forces and moments due to mechanical movement	Mechanical Vibration	Continuous
			Airborne disturbance loads due to fluid flow noise emitted by the source	Fluid Dynamic Noise	Continuous
	Ammonia Cooling Lines	-	Disturbance forces and moments due to by mechanical movement	Mechanical Vibration	Continuous
			Airborne disturbance loads due to fluid flow noise emitted by the source	Fluid Dynamic Noise	Continuous
STRUCTURE	Structural joints	-	Thermal heating cycles	Sudden Stress Release	Intermittent

**Table 13-6: Potential classification of micro-vibration disturbance sources**

Source	Harmonic	Transient
Reaction wheels	X	
Control Momentum Gyros	X	
Gyroscopes	X	
Solar array drive mechanisms	(X)	X
Antenna pointing mechanisms		X
Mirror scan mechanisms		X
Cryogenic coolers	X	
Micro-thrusters, gas flow regulators		X
Latch valve		X
Heat pipe	X	
Relay, RF switch		X
Sudden stress release		X
Clank phenomena (e.g. electromagnetic force effects, MLI foil buckling)		X

### 13.4.2.2 General aspects of disturbance attenuation and reduction

#### 13.4.2.2.1 Introduction

Flexible spacecraft structures (the overall system low frequency modes and the local higher frequency vibration modes) can become significantly excited by even very small dynamic forcing functions induced by the disturbance sources. Although in most cases the disturbances are mechanically transmitted to the sensitive payload the potential acoustic excitations and their respective sources should be taken into account in pressurized compartments.

The most efficient and most preferable way to control the performance degrading effects of micro-vibrations would be to incorporate reduction principles directly into the basic functional design of the disturbance source. If such design optimization of the disturbance equipment might not be sufficient then the vibration source could be isolated from the satellite platform in order to minimize the disturbances induced into the spacecraft structure.

Alternative methods to be implemented into the spacecraft design to ameliorate the situation would consist of attenuating the induced micro-vibrations along the transmission path to the sensitive receiver or to isolate the sensitive receiver from the satellite platform at its mounting location.

The characteristics of these vibration attenuation and isolation methods are schematically shown in Figure 13-27.

In order to provide the required low vibration or low acceleration environment for the on-orbit condition it is in general necessary to define the cut-off frequency of the isolation devices at very low frequencies. In order to survive the harsh launch environment these devices might require proper locking devices to avoid excessive dynamic amplifications due to potential coupling of the isolation system eigenfrequency with launcher induced dynamic excitations.

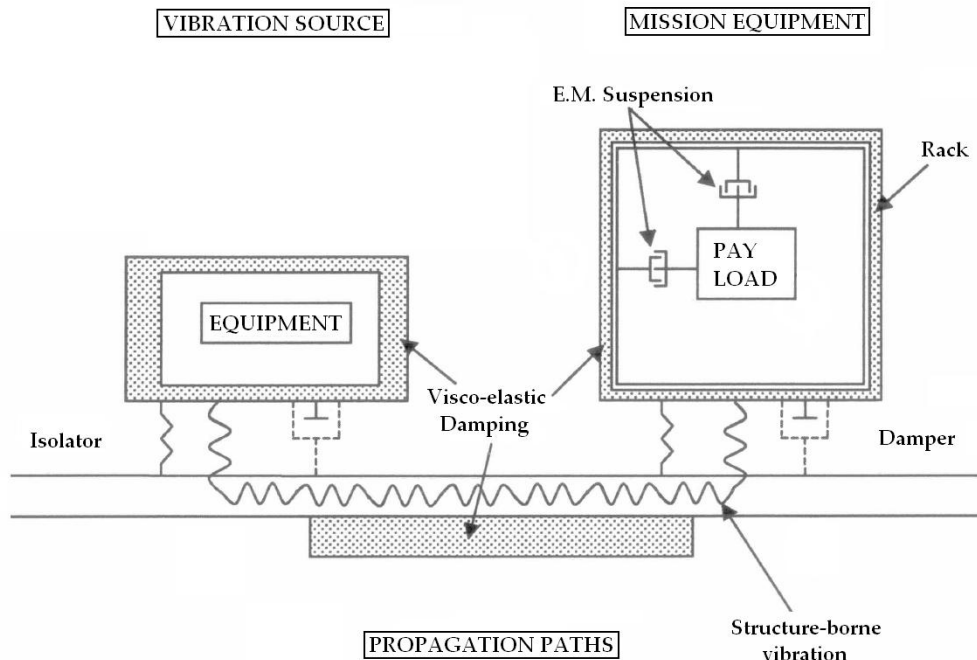


**Figure 13-27: Vibration attenuation, isolation and damping criteria**

#### 13.4.2.2.2 Vibration reduction at the source location

Controlling the generation of dynamic disturbances at the source location can be considered the most efficient and most preferable way to minimize the performance degrading effects of micro-vibrations. Methods of controlling or reducing at the source location the dynamic disturbances are listed in Table 13-7. Several potential disturbance sources have been identified.

Relevant vibration reduction strategies might be directly incorporated into the basic functional design of the disturbance source, e.g. the back-to-back operation of cryo-cooler pistons, or adequately considered when defining the operational conditions, e.g. to prepare for quickly overrunning critical speeds of reaction or momentum wheel assemblies.

Where necessary the passive vibration isolation of disturbance sources could be replaced by more sophisticated active vibration suppression systems where actuators provide the necessary counter-phase reaction forces and moments to compensate the injected disturbances.

**Table 13-7: Dynamic disturbance control/reduction methods at source location**

<p><b>Gas or Fluid Vibrations</b></p> <ul style="list-style-type: none"> <li>• Reduce flow rate</li> <li>• Use less pressure</li> <li>• Use quieter valve</li> <li>• Modify impeller</li> <li>• Smooth pipe or duct</li> <li>• Lagging of pipe or duct</li> <li>• Use flow turning vanes at bends</li> </ul> <p><b>Gear Vibrations</b></p> <ul style="list-style-type: none"> <li>• Use proper lubrication</li> <li>• Reduce speed</li> <li>• Balance gear</li> <li>• Replace worn/damaged gears</li> <li>• Use higher quality gear</li> <li>• Use different materials gear</li> </ul> <p><b>Rotor Vibrations</b></p> <ul style="list-style-type: none"> <li>• Balance rotor/coupling</li> <li>• Modify force or speed</li> <li>• Alter rotor bearings</li> <li>• Add damping</li> <li>• Reduce mass of moving elements</li> </ul> <p><b>Bearing Vibrations</b></p> <ul style="list-style-type: none"> <li>• Lubricate properly</li> <li>• adjust bearing alignment or mounting</li> <li>• Reduce speed</li> <li>• Replace worn or damaged bearings</li> <li>• Use different bearing types</li> </ul>	<p><b>Magnetic Vibrations</b></p> <ul style="list-style-type: none"> <li>• Use quieter motor, choke or transformer</li> <li>• Isolate or enclose</li> <li>• Relocate</li> </ul> <p><b>Belt/Chain Vibrations</b></p> <ul style="list-style-type: none"> <li>• Adjust tension</li> <li>• Adjust alignment</li> <li>• Lubricate properly</li> <li>• Reduce speed</li> <li>• Change material or type</li> </ul> <p><b>Pump Noise</b></p> <ul style="list-style-type: none"> <li>• Reduce speed</li> <li>• Reduce pressure</li> <li>• Alter pressure cycle</li> <li>• Isolate</li> </ul> <p><b>Combustion Noise</b></p> <ul style="list-style-type: none"> <li>• Correctly adjust burner</li> <li>• Use lower pressure barrier</li> </ul> <p><b>Impact Vibrations</b></p> <ul style="list-style-type: none"> <li>• Avoid it</li> <li>• Cushion it</li> <li>• Apply damping</li> </ul>
--	--

#### 13.4.2.2.3 Vibration reduction along the transmission path

Space structure vibrations can be excited mechanically or by air-borne noise. Increasing the losses in the vibration transmission path is a common way to reduce vibration levels at the receiver location. For this purpose the disturbing equipment should be located as remote as possible from the sensitive payload mounting location.

In case of acoustic excitation of structures like walls, floors and ceiling the vibration reduction can be obtained by the application of acoustic absorption and damping materials.

Mechanically coupled transmission can be controlled by interrupting the transmission path to the receiver or by introducing attenuating element couplings between the source and the receiver.

Table 13-8 lists common ways to reduce the vibration transmission along the transmission path through the spacecraft structure.

**Table 13-8: Design measures to reduce vibration transmission**

<p><b>Vibrating wall, floor and frames</b></p> <ul style="list-style-type: none"> <li>• Reduce area</li> <li>• Add mass</li> <li>• Change stiffness</li> <li>• Detune resonances</li> <li>• Add damping material</li> </ul>
<p><b>Gas or fluid flow vibrations</b></p> <ul style="list-style-type: none"> <li>• Use resilient pipe/duct connectors</li> <li>• Use resilient pipe hangers and support</li> </ul>
<p><b>Equipment mount vibrations</b></p> <ul style="list-style-type: none"> <li>• Isolate sections with anti-vibration mount</li> <li>• Fasten external parts at vibration nodes</li> <li>• Detune/avoid resonant built-up</li> </ul>
<p><b>Source/receiver locations</b></p> <ul style="list-style-type: none"> <li>• Position source or receiver at mass loaded areas</li> <li>• Position source or receiver at vibration nodes</li> <li>• Change position of source or receiver or both</li> <li>• Increase distance between source and receiver</li> </ul>

#### 13.4.2.2.4 Vibration reduction at the receiver/payload location

Vibration isolation of sensitive receivers can be obtained by means of passive spring/damper devices or by means of actively controlled suspension systems.

### 13.4.3 Characterisation of the disturbance sources forcing functions

#### 13.4.3.1 General aspects

For the micro-gravity and micro-vibration environment control the equipment / experiment units should follow the design verification logic shown in Figure 13-28. The determination of the disturbance sources forcing functions at equipment level (in general the reaction forces and torques at the equipment interface with the satellite platform) forms a vital part of related approach.

These forcing functions could be gained by establishing an analytical formulation, from characterisation tests, and/or by performing numerical simulations with representative models.

The analytical formulations and experimental methods that could be used in order to determine the micro-gravity and micro-vibration disturbance forcing functions generated by relevant disturbance sources are presented in detail in the following sections.

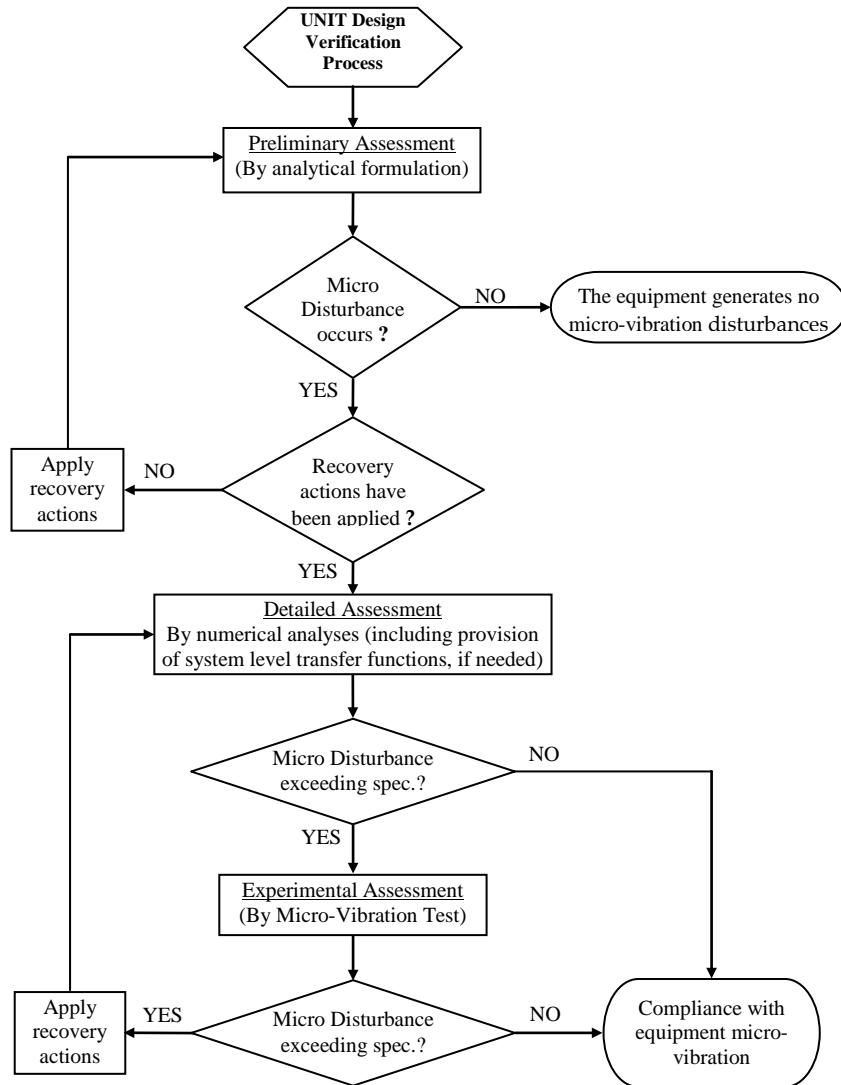


**Figure 13-28: Unit design verification approach for micro-gravity and micro-vibration environment control**

In the case of more complex equipment or assemblies where analytical formulations are not available and experimental characterisation cannot yet be performed due to non-availability of representative hardware then numerical simulations might be carried out to determine the disturbance forcing functions at the equipment or assembly interface with the satellite platform. For performing these analyses dedicated mathematical models should be used which should be able to represent, at least, the main physical characteristics of the disturbance source and to simulate the induced disturbances in the disturbance source operative conditions. The models might be based on Matlab/Simulink code for assessing e.g. electro-dynamic performances of electrical drive units and other specific software for the analysis of mechanical systems as e.g. the transmission by means of gears or clutches of the stepper motor torques to the components to be moved.

The disturbance forcing function outputs should be produced in time and/or in frequency domain whatever might be required for the further post-processing of the data generated.

However, despite best modelling efforts the uncertainties associated with these equipment and subsystem analytical models are often too large to have sufficient confidence in the validity of the analytical predictions, in particular where very stringent pointing performance requirements are applicable. Then the analysis results should be confirmed by tests as soon as representative hardware becomes available.

### **13.4.3.2 Determination of the disturbance forcing functions by analytical formulation**

#### **13.4.3.2.1 Introduction**

Design guidelines, rules and recovery actions are applicable to the disturbance sources at system, sub-system and equipment level that might impact on the specified micro-gravity and micro-vibration requirements. A comprehensive analytical assessment of their impact on the micro-gravity and micro-vibration environment should consider the computation of the relevant disturbance forcing functions, in general required to be defined at the disturber/spacecraft interface, by means of numerical simulations. The latter should be performed using dedicated mathematical models, for example based on MATLAB/Simulink code.

In order to provide relevant input needed for the assessment of the micro-gravity and micro-vibration environment the analytical formulations of the disturbance forcing functions (where applicable, together with additional data gained from experimental characterisation) are summarized hereafter for the following disturbance sources:

- high speed rotation mechanisms (reaction and momentum wheels),
- cryogenic coolers,
- electrical drive units (stepper motors),
- sudden stress release (SSR),
- clank phenomena, e.g. inductive electromagnetic forces effects resulting from equipment electrical wires and heaters, respectively, and the crackling multi-layer insulation (MLI) phenomenon.

The mathematical models should be able to represent, at least, the main physical characteristics of the disturbance source and to simulate the induced micro-gravity and micro-vibration disturbances in its operative conditions. The disturbance forcing function outputs should be produced in time and/or in frequency domain according to the envisaged further post-processing.

#### **13.4.3.2.2 High speed rotation mechanisms**

High speed continuous rotational mechanisms as reaction and momentum wheels are applied as attitude control actuators on-board 3-axes stabilized spacecraft. These mechanisms have been found in many spacecraft to be the most severe micro-vibration disturbance sources when being operated on-orbit.

The disturbances of rotating devices can be broken down into three categories:

1. rotating mass imbalances (static and dynamic imbalance),
2. ball bearing imperfections, and
3. motor imperfections.

The disturbances resulting from the reaction and momentum wheel bearings can be avoided when using actively controlled magnetic bearings instead of the conventional ball bearings. However, the drawback of using magnetic bearings is that they require a more sophisticated design and control system.

The rotating mass imbalances are considered to be the most significant source of disturbances induced from reaction wheel or momentum wheels to the spacecraft. However, the interaction of all of these speed dependent micro-vibration input sources with the structural dynamics of the rotating mechanism is usually the dominant disturbance from a typical mechanism.

The section describes first the disturbances with the necessary details, then the characteristics of the disturbances used as input to the micro-gravity and micro-vibration assessment are briefly explained.

#### Rotating mass imbalance:

The wheel static and dynamic imbalances are the result of asymmetries of the flywheel with respect to the axis of rotation. Avoiding these effects is difficult since in practice an exact balancing of a wheel, i.e. no remaining eccentricity of the rotor centre of gravity (CoG) and a perfectly axi-symmetric rotor, cannot be ensured in most cases. Even small imbalances might create significant disturbance forces and torques at high wheel speeds.

The **static imbalance**  $U_s$  is the offset of the flywheel CoG from the rotation axis, represented by a small mass  $m$  at the eccentricity  $r$  as shown in the left graph of Figure 13-29. As a result, a rotating, radial force  $F_s$  is produced which appears sinusoidal from a fixed reference, with a frequency corresponding to once per flywheel revolution, and has an amplitude proportional to the square of the wheel velocity  $\omega_w$  (assumed constant):

$$F_s = m \cdot r \cdot \omega_w^2 = U_s \cdot \omega_w^2 \quad ; \quad U_s = m \cdot r \quad [13-45]$$

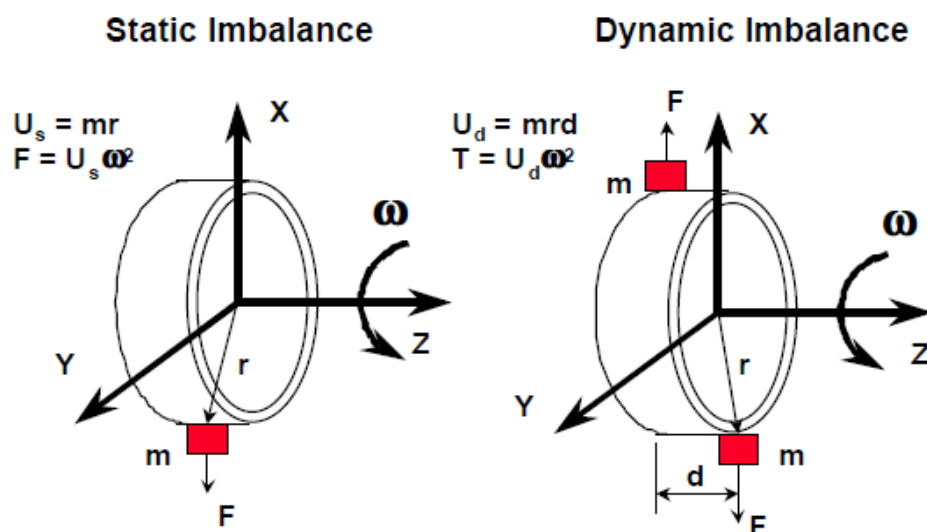


Figure 13-29: Physical models for rotating mass imbalances

The **dynamic imbalance**  $U_d$  is the cross product inertia of the flywheel, caused by angular misalignment of the principal inertia with the spin axis. This is represented by two equal masses axially spaced on the flywheel by a distance  $d$  and separated by  $180^\circ$  as shown in the right graph of Figure 13-29. The resulting disturbance torque  $T_d$  (vector perpendicular to the axis of rotation) is proportional to the wheel velocity  $\omega_w$  (assumed constant) and occurs at a frequency corresponding to once per flywheel revolution:

$$T_d = m \cdot r \cdot d \cdot \omega_w^2 = U_d \cdot \omega_w^2 \quad ; \quad U_d = m \cdot r \cdot d \quad [13-46]$$

Typical values of the static and dynamic imbalance, respectively, for reaction and momentum wheels mounted on satellites are  $U_s = 5 \text{ gcm}$  and  $U_d = 20 \text{ gcm}^2$ .

### Ball bearing imperfections

Disturbances caused by mechanical bearings (spherical or cylindrical rollers) are mainly due to imperfections of rolling elements, cage (retainer) and raceways. Disturbances due to ball-bearing imperfections can be described as a series of harmonics with frequencies which are non-integer multiples of the rotor spin speed (see the higher harmonics lines in the cascade plots shown below in Figure 13-32, Figure 13-33 and Figure 13-34, respectively). They are in fact multiples of the relative rotation rates between the moving parts of the bearing system.

Assuming an ideal motion of the ball on the raceways (no slipping), the rotation velocity  $\Omega_{c/i}$  of the balls and the cage with respect to the stator, the velocity  $\Omega_{c/o}$  of the balls and the cage with respect to the rotor, and the ball rolling velocity  $\Omega_b$  on the two raceways can be obtained as a function of the wheel spin rate  $\Omega$  as, [22]:

$$\Omega_{c/i} = \frac{r_o}{r_i + r_o} \Omega ; \quad \Omega_{c/o} = \frac{r_i}{r_i + r_o} \Omega ; \quad \Omega_b = \frac{r_i r_o}{r_b (r_i + r_o)} \Omega \quad [13-47]$$

where  $R_i$ ,  $R_o$  and  $R_b$  are the radius of inner raceway, outer raceway and rolling ball, respectively.

The ball bearing disturbance characteristics are summarized hereafter and these statements can be used to identify sub- and super-harmonics in the cascade plots according to their origin in ball bearings:

- **Disturbances due to ball irregularities:** one imperfect ball generates a disturbance at angular rate  $\Omega_b$  whereas  $N$  balls are generating a series of harmonics of  $\Omega_b$ .
- **Disturbances due to internal race irregularities:** when balls pass on flaws of the internal raceway then vibrations, depending on the angular velocity  $\Omega_{c/i}$  are generated.  $N$  balls generate a frequency  $N \times \Omega_{c/i}$ .
- **Disturbances due to external race irregularities:** when balls pass on flaws of the external raceway then vibrations, depending on the angular velocity  $\Omega_{c/o}$  are generated.  $N$  balls generate a frequency  $N \times \Omega_{c/o}$ .
- **Cage disturbances:** if the cage hits the balls then disturbances are expected at the angular rate  $\Omega_b$ . In case it hits the raceways then the pulsation depends on  $\Omega_{c/i}$  or  $\Omega_{c/o}$ .

### Motor imperfections

The motor torque characteristics, in particular the average torque and the torque stability, are the most important indicators of its overall performance. In general brushless DC motors are used to drive the flywheels of reaction and momentum wheel assemblies. Disturbances of the satellite micro-gravity and micro-vibration environment might result from torque ripple, motor cogging and motor driver anomalies. However, the latter is in general considered less significant for spacecraft micro-vibrations. An assessment of potential effects of motor driver anomalies can be found in [19].

**Torque ripple** is defined as the change in motor torque with respect to the angular position, or simply by the profile of the back-emf and the current waveform being not exactly sinusoidal. Motor ripple also manifest itself in a series of harmonics but with an amplitude proportional to the motor current. As an example Figure 13-30 shows a typical electrical cycle (0 to  $2\pi$ ) with six communication states where the torque applied by the motor can be represented as an infinite string of cosine segments. For a perfectly aligned motor with discrete commutation the torque ripple is typically about 14.3% (peak to peak) of the nominal motor torque.

Motor rippling models are usually derived by performing a Fourier Transformation (FT) on the motor torque waveform in order to determine the frequency components of the torque ripple disturbance [20].

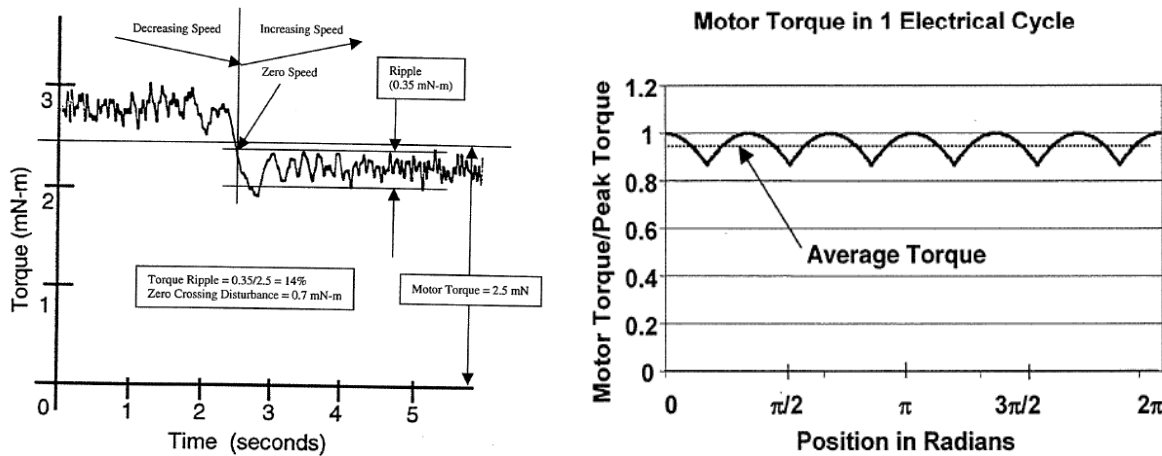


**Figure 13-30: Axial torque disturbances of reaction wheel assemblies when zero crossing and torque ripple [20]**

**Motor cogging torque** originates from the magnetic interaction between the stator slots and the rotor permanent magnets preventing the smooth rotation of the flywheel and resulting in noise. It depends only on the flywheel angular position and can be represented as a series of spatial harmonics of the motor electric step. Motor cogging disturbances can be substantially reduced e.g. by the appropriate choice of the magnet width relative to the slot pitch.

The motor cogging torque can be determined by conducting a coast down test and measuring the axial torque. For these tests it is recommended to sample the data spatially rather than at equal time intervals, [22].

#### Structural dynamics of wheel assemblies

Figure 13-31 shows a simply supported model of a rotation mechanism with a single axial degree of freedom and two degrees of freedom in the radial direction. Three fundamental resonance modes are found:

- axial translation mode,
- radial translation mode, and
- radial rocking mode.

The related frequencies are:

$$f_a = \sqrt{\frac{k_a}{m}} \quad ; \quad f_r = \sqrt{\frac{k_r}{m}} \quad ; \quad f_o = \sqrt{\frac{K_T}{I_{xx}}} \quad [13-48]$$

where  $K_T$  is the cross-axis torsional stiffness and  $I_{xx}$  is the cross-axis moment of inertia of the flywheel.

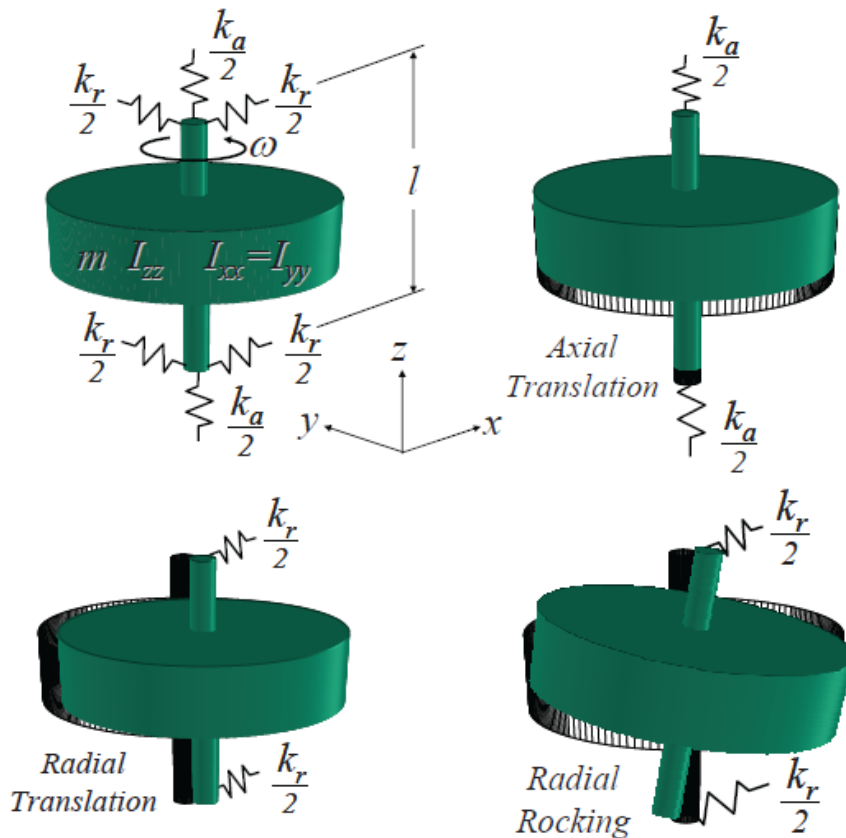


**Figure 13-31: Simply supported model of rotation mechanism and fundamental resonance modes [19]**

Due to gyroscopic precession of the rotor as the speed increases a whirl mode is created for most rotation mechanisms. Furthermore the rocking mode is split into a slow natural frequency where the whirl is opposite to the rotation and a fast one where the directions are the same. The whirl frequencies are diverging according to the following relationship:

$$f_n(\omega) = \pm \frac{I_{zz} \omega}{2I_{xx}} \pm \sqrt{\left( \frac{I_{zz} \omega}{2I_{xx}} \right)^2 + \frac{K_t}{I_{xx}}} \quad [13-49]$$

where

- $f_n(\omega)$  is the force amplitude of the fundamental at the drive frequency,
- $I_{xx}$  the polar moment of inertia of the flywheel,
- $K_t$  cross-axis torsional stiffness of the suspension, and
- $\omega$  the wheel speed.

In Figure 13-32 a modified Campbell diagram is presented where speed dependent disturbances resulting from rotating mass imbalances, bearing imperfections and the motor are superimposed with the whirl frequencies and the fundamental static resonance frequency of the wheel assembly. From this graph the “critical speeds” can be identified.

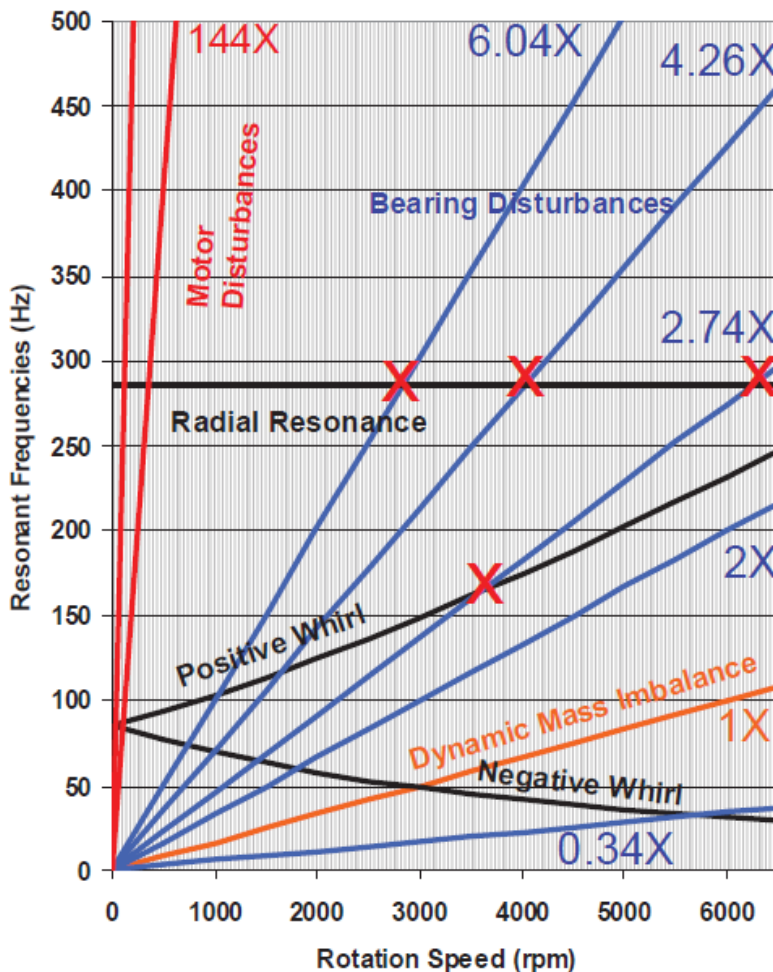


**Figure 13-32: Modified Campbell diagram showing significant coincidences of wheel assembly resonances and speed dependent disturbances (mass imbalance, bearings, motor) [19]**

#### Disturbance spectra generated by rotation mechanisms

The disturbances generated by rotation mechanisms like reaction and momentum wheels are generally sinusoidal and tonal in nature and they occur at distinct frequencies. The related disturbance spectra are typically presented as cascade or waterfall plots where a noise or vibration spectrum as a function of time or speed is shown in a 3D view. These plots are particularly useful for providing an excellent overview of the frequency content of a signal related to the incremental time or speed. Examples of such cascade or waterfall plots are shown in Figure 13-33 and Figure 13-34.

The flywheel imbalances (static and dynamic) produce steady disturbances as the wheel speed changes. The resulting force and torque are proportional to the spin speed squared and occur at a frequency equal to the flywheel spin rate. As a result, the disturbance appears as a continuously growing diagonal ridge (as the fundamental harmonic) as the wheel speed continuously increases from zero rpm, Figure 13-33.

The sub- and super-harmonics are also tonal disturbances but occur at either fractions or integer multiples of the flywheel spin rate. These disturbances have much smaller amplitudes and are often due to bearing imperfections, motor cogging, motor drive errors, bearing friction and lubricant dynamics plot, [19] [21]. Large amplifications may however occur when harmonics meet internal structural resonances of the wheel assembly as shown in Figure 13-30.

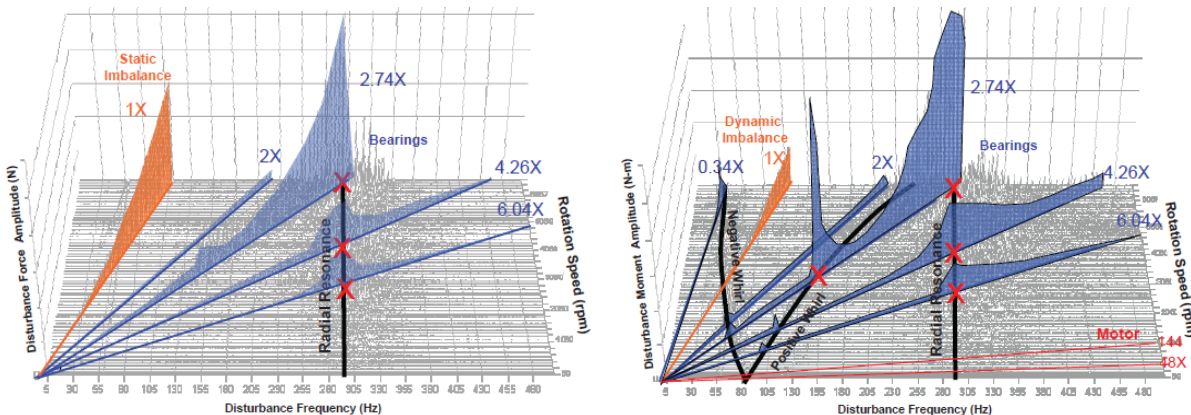


Figure 13-33: Radial force and moment disturbance waterfall plot [19]

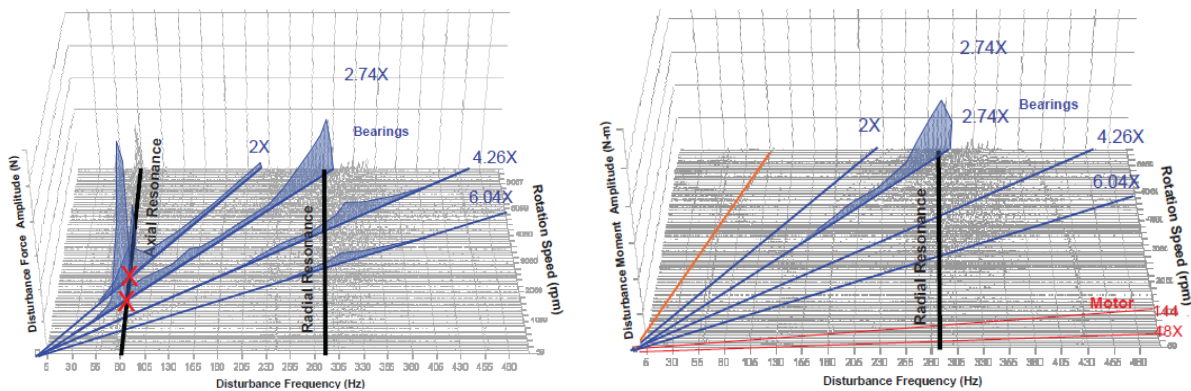


Figure 13-34: Axial force and moment disturbance waterfall plot [19]

### 13.4.3.2.3 Cryogenic coolers

Cryogenic coolers or in short cryo-coolers are often required for scientific satellite applications in order to cool down to cryogenic temperatures the focal plane detectors of their instruments. An example of a typical long-life (continuously operating) space cryo-cooler is shown in Figure 13-35.

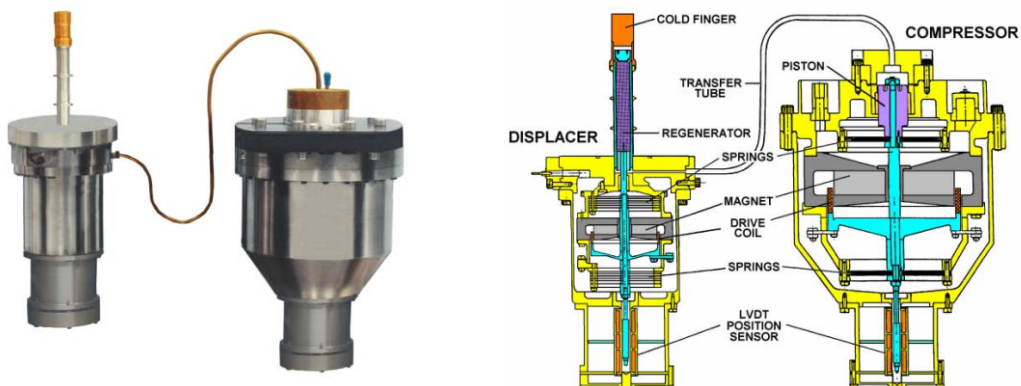


Figure 13-35: Example of long-life space cryo-cooler:  
Oxford University ISAMS 80K Stirling cooler

Cryo-coolers have been identified quite early as an important contributor to the satellite micro-vibration environment. For this reason their application for certain spacecraft missions, in particular for imaging missions with high precision pointing requirements, becomes a major design issue. The

vibrations generated by cryo-coolers are resulting from (reciprocating) movements of mechanical parts as the compressor piston and the displacer.

Most space cryo-coolers incorporate compressors operating with a fixed fundamental drive frequency in the range of 30 to 60 Hz and the vibratory forces generated are showing up at that frequency and its multiples. The resulting micro-vibrations are a combination of the harmonic signals at integer multiples of the cryo-cooler operating frequency with significant magnitude up to a higher order, i.e. the loads are at constant fundamental frequency and multiple harmonics.

Figure 13-36 depicts a typical example for the perturbation generated by a Stirling cryo-cooler. Typical vibration levels for the axial force direction of such coolers are between 0.001 N and 50 N at the fundamental drive frequency [23].

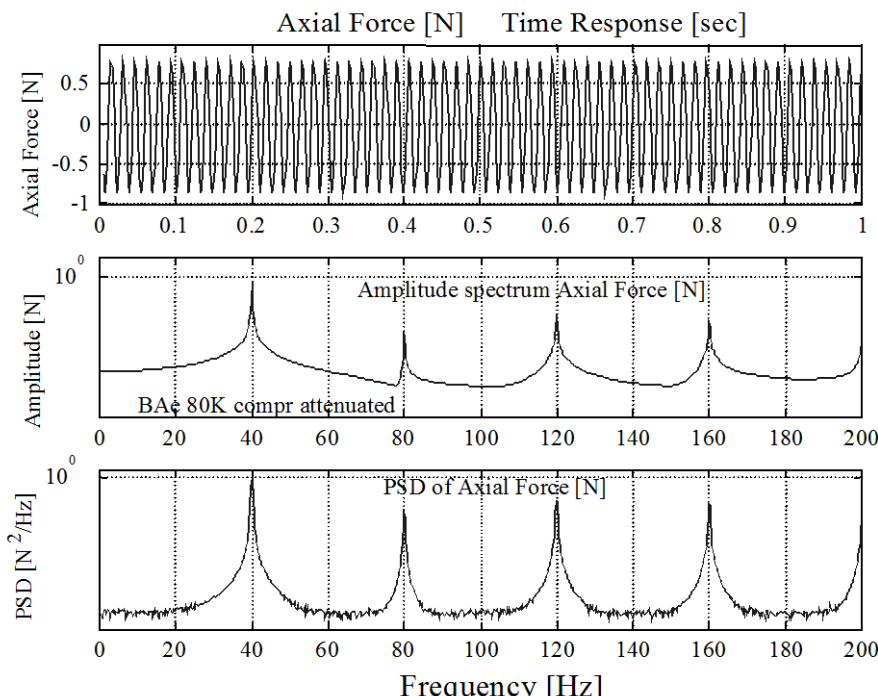


**Figure 13-36: Time domain signal, amplitude spectrum and PSD for axial force generated by BAe 80K Stirling cryo-cooler [23]**

Two basic approaches are available for the cryo-cooler disturbance model in order to assess the vibrational energy induced into the mounting structure:

1. Physical vibration modelling with assigning realistic values to the physical parameters of the model,
2. Creating an empirical model of the disturbance via the analysis of experimental test data.

Following the first approach, using a single DOF model of the expander/compressor rigidly mounted, the fundamental harmonic force  $F_t$  transmitted to the expander/compressor body and the rigid foundation can be derived:

$$F_t = x_0 m_d \omega_n^2 \sqrt{1 + \left(\frac{2\zeta\omega}{\omega_n}\right)^2} \sin(\omega t + \varphi_t) \quad [13-50]$$

where

$x_0$  is the displacer stroke,

- $m_d$  the displacer mass,  
 $\omega_n = \sqrt{\frac{k}{m_d}}$  the displacer eigenfrequency,  
 $\tan \varphi_t = \frac{2\zeta\omega}{\omega_n}$  the phase angle, and  
 $\zeta$  the percentage of critical damping assumed for the SDOF model.

A coupled dynamic model was also derived and details can be found in the literature, e.g. [23].

The empirical model relies on the extraction of harmonic frequencies and amplitudes from vibration test data. The cryo-cooler disturbance can be represented as a superposition of the fundamental frequency and higher harmonics:

$$f_k(k\Delta t) = P_0 \sin(\omega k\Delta t + \varphi) + \sum_{n=2}^N f_n \sin(n\omega k\Delta t + \varphi) \quad [13-51]$$

where

- $P_0$  is the force amplitude of the fundamental at the drive frequency,  
 $f_n$  are the coefficients of the higher harmonics,  
 $N$  is the number of samples in the time sequence, and  
 $\Delta t$  the sampling interval.

Then a Power Spectral Density (PSD) function of the disturbance can be obtained:

$$S_{PSD}(f) = \frac{2\Delta t}{N} F_k(f) F_k^*(f) \quad [13-52]$$

where

- $F_k(f)$  is the discrete Fourier transform of the sampled time signal  $f_k(k\Delta t)$ :

$$F_k(f) = \sum_{r=0}^{N-1} f_r e^{\frac{2i}{N} kr} \quad [13-53]$$

- $F_k^*(f)$  the complex conjugate of  $F_k(f)$ , and  
 $f$  the frequency in Hertz.

Experience has shown that for a Stirling cryo-cooler as shown in Figure 13-35 only the disturbance forces in the three orthogonal directions ( $x$ ,  $y$ ,  $z$ ) and the moment about the spindle axis ( $z$ ) are important. With the assumption of no coupling between each direction the Spectral Density Matrix (SDM) of the cryo-cooler mechanical disturbances can be expressed as:

$$S_{ww}^{cryo}(f) = \begin{bmatrix} S_{F_x}(f) & 0 & 0 & 0 \\ 0 & S_{F_y}(f) & 0 & 0 \\ 0 & 0 & S_{F_z}(f) & 0 \\ 0 & 0 & 0 & S_{M_z}(f) \end{bmatrix} \quad [13-54]$$

The SDM can be used for the disturbance analysis in the frequency domain. For time domain analysis the disturbance time signals can be recreated from the amplitude spectrum with arbitrary phase (uniform probability density from  $0\pi$  to  $2\pi$ ).

## 13.4.3.2.4 Gimballed Mechanisms

Gimballed mechanisms such as solar array drive mechanisms (SADM), antenna pointing mechanisms (APM), scan mechanisms, mobile mirror drives, etc. are present in some form on almost every satellite. They are all driven by electrical drive units (stepper motors) that may produce disturbances which might have significant impacts on instrument performances. However, the gears, transmitting the motor torque, and their bearings might be also significant disturbance sources. As a result, a large number harmonics across a wide frequency spectrum is produced.

Whereas the disturbance characterisation of high speed rotation mechanisms is mainly based on experimental methods the characterisation approach for gimballed mechanisms as e.g. SADM's and APM's mainly involves numerical modelling and empirical modelling based on experimental data.

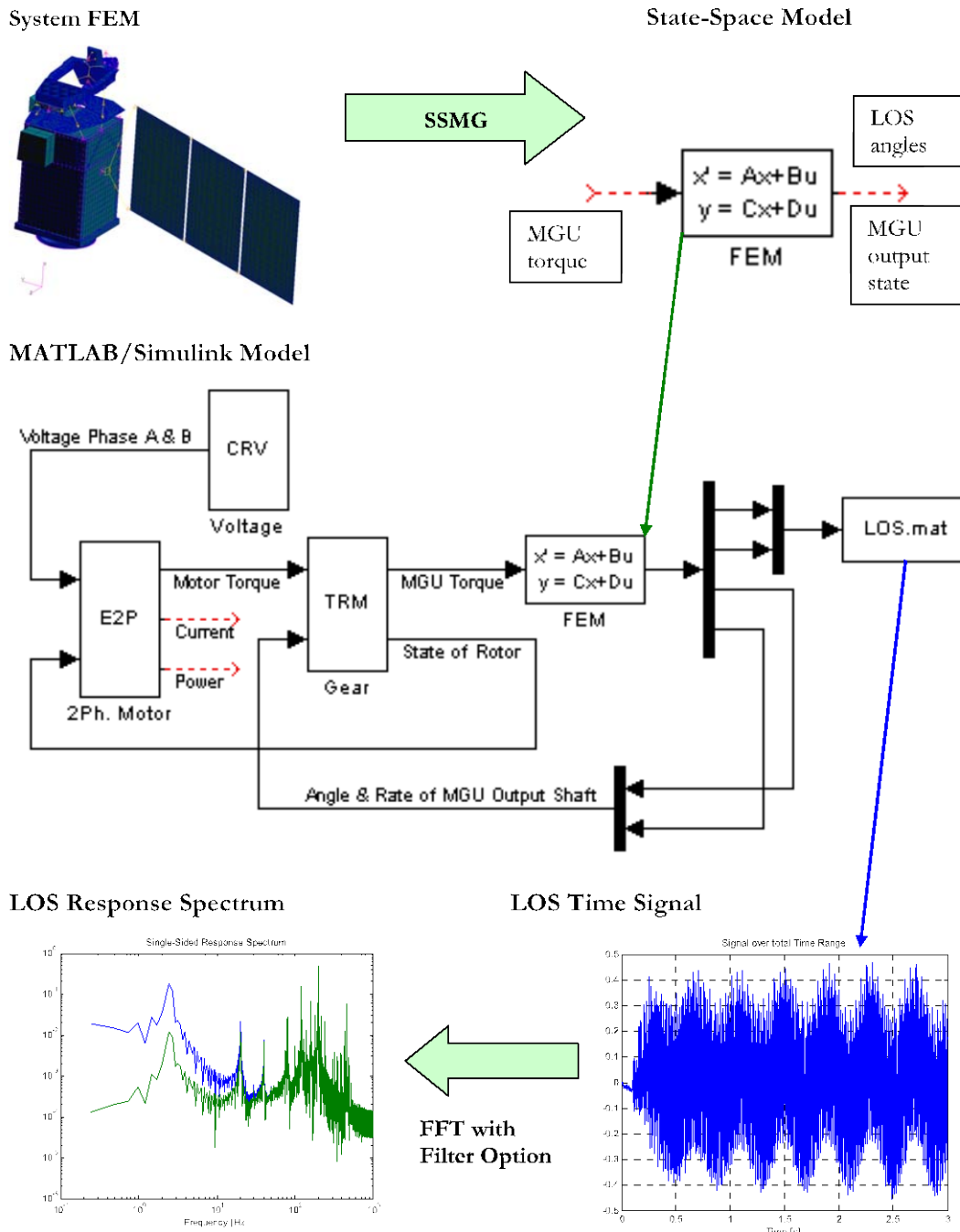


Figure 13-37: Stepper motor transient disturbance approach [9]

The analysis process frequently applied in practice is based on a combination of MATLAB/Simulink based tools for the control simulation and structural analysis tools (in general the finite element method) for the provision of relevant information to describe the dynamic characteristics of the disturbance transmission path from the source to the receiver location.

An example for such complete end-to-end analysis scheme (evaluation of disturbance transmission from source to performance critical location on receiver unit) is shown in Figure 13-37. In the first part the system FEM which includes all relevant sub-systems (mechanisms, spacecraft bus and payload structure, solar arrays in case of assessing SADM induced disturbances, other subsystems as necessary) is used to prepare a condensed modal model of the spacecraft. This model is then further processed by specific software tools (in the case shown: the Astrium in-house MATLAB-based software tool "SSMG") to generate a system state-space model which has one input channel for the Motor Gear Unit (MGU) torque and output channels for the state of the MGU output shaft and for the performance values (e.g. the line-of-sight, LoS, angles).

The state-space model is then inserted as a subsystem block into a MATLAB/Simulink model representing the mechanism drive model. The results of the time simulation performed in MATLAB/Simulink are the relevant performance values, e.g. the LoS disturbances. Finally, the time simulation results are further post-processed to evaluate the predicted performances with respect to e.g. the LoS stability requirements.

Example of coupled electro-mechanical dynamic simulation of a scan mechanism:

In Figure 13-38 the flowchart for a coupled electro-mechanical dynamic simulation of a scan mechanism for pointing a mirror to its target is provided, [24]. The key model parts and the feedback logic of such coupled simulation are shown. As for the previous example the simulation is basically performed in the MATLAB/Simulink environment, however the MECHMACS library of mechanical building blocks for MATLAB/Simulink, [25], is used for the modelling of the torque transmission effects and the structure modal properties where the latter have been derived from finite element analysis.

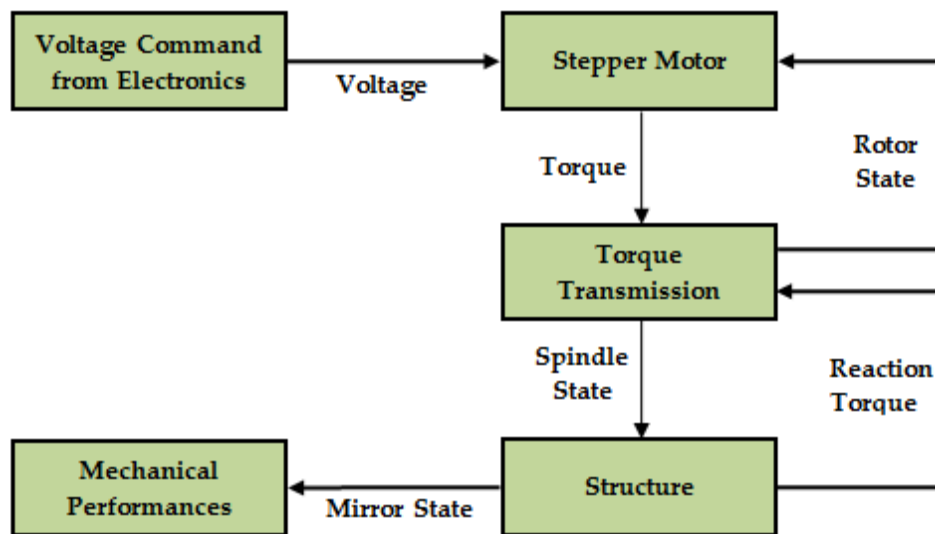


**Figure 13-38: Coupled electro-mechanical dynamic simulation [24]**

The comprehensive mathematical model of the assembly should properly cover all these influences and take into account the related interactions. In the following the relevant torque equations for the stepper motor with two electrical phases are provided.

The current  $i$  in one of the electrical phases A or B is calculated from the differential equation [13-55]:

$$L \frac{di}{dt} + R i = u_{app} - u_{emf} \quad [13-55]$$

where L is the inductance and R the resistance, respectively, of the related phases A or B winding. The current  $i$  is due to the applied voltage  $u_{app}$  and the voltage  $u_{emf}$  induced by the motion of the winding in the magnetic field (back-emf effect).  $u_{emf}$  depends on the angular position  $\alpha$  and the velocity  $\dot{\alpha}$  of the rotor according to Eq. [13-55]:

$$u_{emf} = \dot{\alpha} K_v \sin\left(\frac{\pi}{2\alpha_{step}} \alpha + \alpha_{shift}\right) \quad [13-56]$$

where  $K_v$  [V/rad] is a motor constant and  $\alpha_{step}$  [rad] the angular stepping increment of that motor, e.g. a motor with e.g. 90 pole pairs has a corresponding stepping angle  $\alpha_{step} = \frac{\pi}{180}$ .  $\alpha_{shift}$  defines the respective shift angles of the electrical phases of the stepper motor.

The torque  $T_{mot}$  generated by the actual winding is proportional to the current  $i$  and the motor torque constant  $K_T$  [Nm/A] according to Eq. [13-56]:

$$T_{mot} = i K_T \sin\left(\frac{\pi}{2\alpha_{step}} \alpha + \alpha_{shift}\right) \quad [13-57]$$

The detent torque  $T_d$  is defined according to Eq. [13-58]:

$$T_d = \sum_i K_{Di} \sin\left(\frac{2\pi}{\alpha_{deti}} \alpha\right) \quad [13-58]$$

where the harmonic amplitude values are defined by  $K_{Di}$  and the detent angles  $\alpha_{deti}$  belong to the harmonics of the detent torque characteristic. In practice the limitation to 3 detent harmonics has been shown sufficient. The superposition of the detent torque  $T_d$  with the motor torque  $T_{mot}$  contributions is giving the resulting output torque of the motor.

#### 13.4.3.2.5 Sudden Stress Release

The sudden stress release, also called thermal creak or thermal snap, is a phenomenon where thermally induced stored elastic energy is released via a slip internal to a joint or due to another nonlinear (e.g. frictional) mechanism. It might be a particular issue in deployable space structures.

A simplified (2 DOF) model for the thermal creak element is shown in Figure 13-39, [26], where inertia terms have been included in the components of the creak element. The model is able to capture the thermo-elastic response, the friction characteristics, and the dynamic response of the attached mechanical system.

In this model a pin with mass  $m_1$  is sitting on a slider with mass  $m_2$ . A mechanical system with mass M is attached to the thermal creak element via a spring (with stiffness K) and a damper (with damping coefficient C). A normal load N is applied to the pin and slider holding them together under the influence of the friction force  $F_f$  acting in the contact surface due to the applicable friction coefficient  $\mu_s$  (Coulomb friction). The pin is connected to a spring with stiffness  $k_1$ , length  $l_1$ , and coefficient of thermal expansion (CTE)  $\alpha_1$ . The slider is connected to a spring with stiffness  $k_2$ , length  $l_2$ , and CTE  $\alpha_2$ .

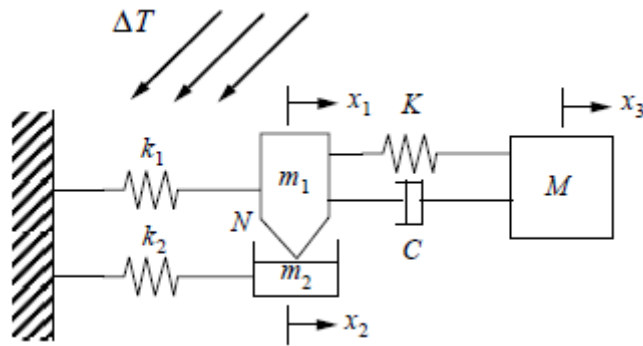


**Figure 13-39: Simplified model representation of thermal creak [26]**

The system is assumed stress free and at rest at the temperature  $T_{ref}$  but when applying a temperature increase  $\Delta T$  then the temperatures of the pin and slider are raised to  $T_1$  and  $T_2$ , respectively, and internal stresses are building up in the springs due to different stiffnesses, temperatures and CTE's. The pin and slider are moving together as long as the shear force  $F_s$  is lower than the friction force  $F_f$ , i.e.  $F_s < F_f = \mu_s N$  where  $N$  is the normal load applied to the pin and slider. However, if  $F_s$  becomes greater than  $F_f$  then the pin should slip relative to the slider.

Furthermore, the mechanical system is excited by the slip motion due to the thermal creak element acting as a disturbance source. After the stored elastic energy has been released and the pin and slider have moved to a new equilibrium state internal stresses might build up again until the next slip occurs.

The creak analysis is performed in two steps:

1. Static analysis of the thermal creak element ( $m_1$  and  $m_2$ ) assumed to be massless and without the attached mass  $M$ .
2. Assessment of the dynamic disturbances induced by the thermal creak phenomenon into the

Details of the thermal creak analysis are provided in [26], hereafter only the basics of the calculation principle and the main results obtained are presented.

#### Static thermal creak analysis:

For the static thermal creak analysis the creak element ( $m_1$  and  $m_2$ ) is considered massless. The static assumption can be considered valid for a creak element whose natural frequency is much higher than that of the attached structure, e.g. a flexible system with a stiff component. First, the response of the static thermal creak element without the attached mass  $M$  is obtained, then the dynamic response of the attached mass is calculated.

The states of pin and slider are determined based on the equilibrium condition, the constitutive relations and the compatibility relation. The creak response is the sum of a linear thermo-elastic response and a non-linear friction induced function

$$\Delta\xi = \xi_1 - \xi_2 = \frac{x_1}{x_1^*} - \frac{x_2}{x_1^*} \quad [13-59]$$

where the characteristic length  $x_1^*$  is the critical displacement at which a slip would occur under the condition that the pin has zero thermal strain ( $x_1' = 0$ ). It has been found to be dictated by the following dimensionless parameters:

- 1)  $\alpha_r = \frac{x_2}{x_1}$  thermal strain mismatch parameter being the ratio of the thermal strains of the pin and the slider, respectively,
- 2)  $f_k = \frac{F_k}{F_s}$  ratio of the kinetic and the static friction,
- 3)  $\kappa = \frac{k_2}{k_1}$  ratio of the stiffness of the springs connected to pin and slider, respectively.

The disturbance induced by the creak element to surrounding the structure is characterised by the profile, the magnitude and the frequency of  $\Delta\xi$ .  $\Delta\xi$  has a step profile at each slip point since it jumps then instantaneously to a new constant value. The magnitude  $A_c$  of these steps is found from the difference in the relative displacements just before and after the slip:

$$A_c = \left(1 + \frac{1}{\kappa}\right) (1 - f_k) \quad [13-60]$$

The creak frequency  $\omega_c$  is related to the period of the creak  $P_c$  (the time elapsed between two successive slips) and can be determined explicitly from an integral evaluating the energy storage over one period where the latter is determined by the fact that a critical thermal displacement is reached at which initial slip occurs. For a ramp thermal displacement rate  $C_t$ , the creak frequency  $\omega_c$  can be computed as follows:

$$\omega_c = 2\pi\omega C_t \left| \frac{1 - \alpha_r}{\kappa + 1} \right| \left( \frac{\kappa}{(1 - f_k)} \right) \quad [13-61]$$

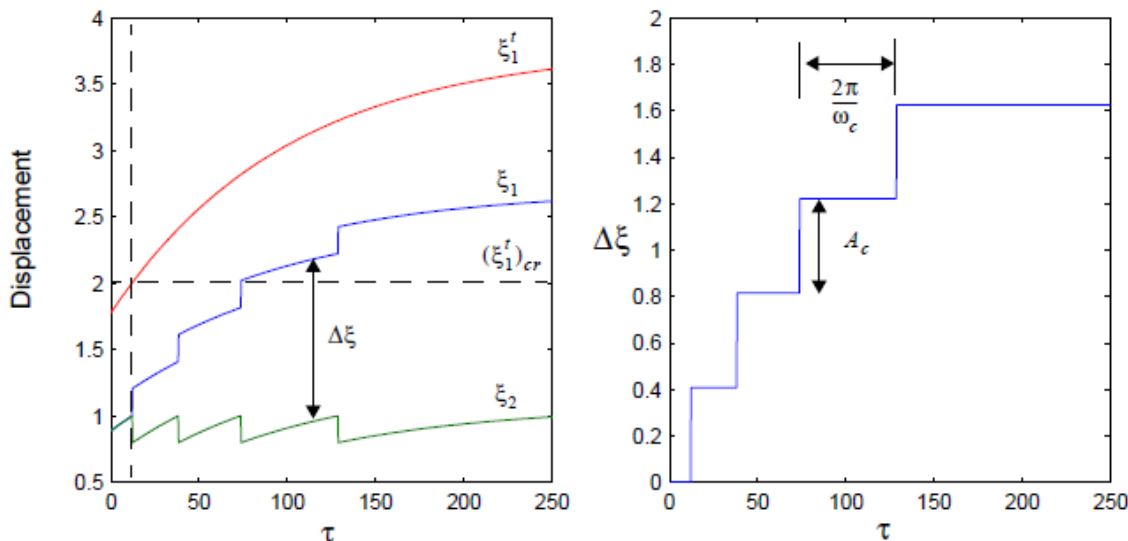


**Figure 13-40: Displacements of static creak element (left) and relative displacement in static creak element (right) [26]**

Figure 13-40 shows the displacements of static creak element and the relative displacement in this element computed for a typical exponential thermo-elastic response of the pin. Prior to attaining the critical state the pin and the slider move together, then the pin begins to follow the thermo-elastic

response in discrete steps. The initial slip occurs when the thermal displacement  $\xi'_1$  reaches the (dimensionless) critical thermal displacement  $(\xi'_1)_{cr}$ .

As expected the step size of remains constant ( $A_c = 0.4$ ). However, the creak frequency is a function of time as can be seen from the increasing time between each slip.

The periodic step displacements of the creak element are causing oscillations of the attached SDOF system (mass M, stiffness K, damping C). In case of weak coupling of the creak element and the structure ( $\kappa_0 = \frac{K}{k_1} \ll 1$ ) the creak response can be computed independent from the structural response. The SDOF system can be excited by two types of thermally induced forcing functions:

1. Significant dynamic responses are occurring if the characteristic thermal response time is of about the same or similar order of the structural characteristic response time.

Note: In most cases the dynamics induced by the thermo-elastic response can be however neglected due to the thermal response time being much greater than the structural response time.

2. The thermal creak response  $\Delta\xi$  is a series of discrete relative motion of the components in the system. The governing equation for thermal creak induced vibrations implies that this non-linear response appears as a series of step loads to the system.

The characteristics of the dynamic response are depending on the load path from the creak element to the SDOF system, given by , and the characteristics of the thermal creak response  $\Delta\xi$ .

Figure 13-41 shows the creak response  $\Delta\xi$  and the corresponding structural response  $\ddot{\xi}_3$  for an example case where the thermo-elastic response  $\xi'_1$  has been a constant ramp, the thermal response time is much greater than the structural response time, and the thermal strain mismatch parameter  $\alpha_r \geq 0$ . The SDOF system behaviour was explored by varying the ratio between the creak frequency  $\omega_c$  and the structural frequency  $\omega$  (the natural frequency of the linear system with the pin and slider sticking together).

In the first case the energy storage capacity is large and after nothing has happened for long periods a sudden large amplitude slip is occurring. The second case (more frequent) shows a lower magnitude slipping. It should be noted that the creak frequency is high enough to prevent the structural response from dying out noticeably before the next creak occurs. In the last case the creak frequency is close to the structure frequency and large motions are visible due to resonance. The plot of the forcing function shows that the creak frequency is not constant due to the coupling between the structure and the disturbance.

Figure 13-42 shows the transmissibility H for a weakly coupled system ( $\kappa_0 \ll 1$ ) and for a given set of parameters. The transmissibility H is defined as:

$$H\left(\frac{\omega_c}{\omega}\right) = \frac{\left|\ddot{\xi}_3\right|_{max}}{1-f_k} \quad [13-62]$$

where  $\left|\ddot{\xi}_3\right|_{max}$  is the performance metric for the structural response of the SDOF system.

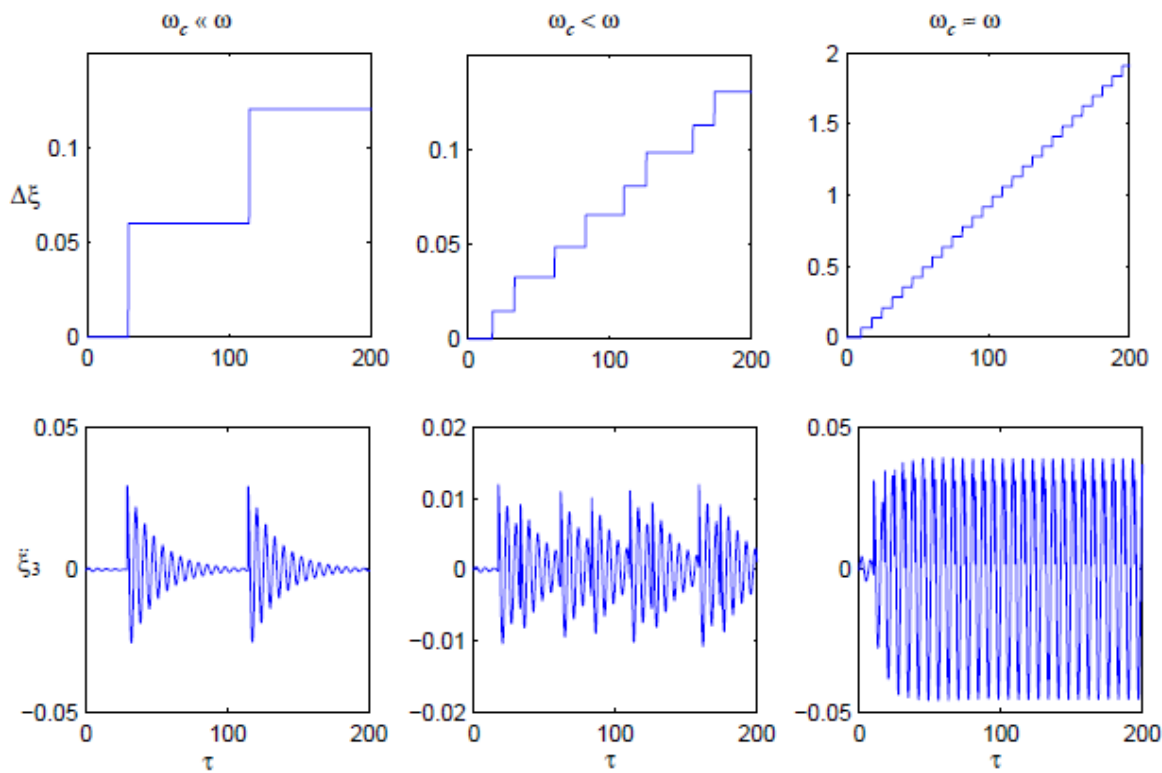


Figure 13-41: Structural response at various creak frequencies [26]

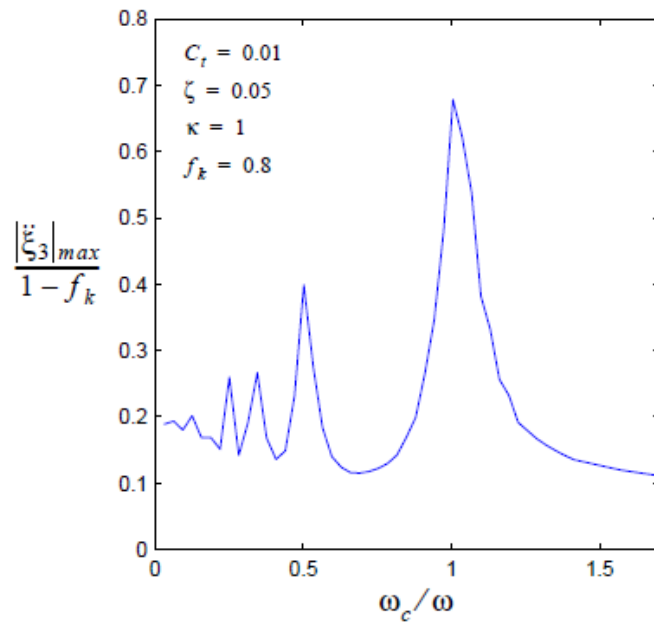


Figure 13-42: Transmissibility of static creak response to system response  
(weakly coupled system:  $\kappa_0 \ll 1$ ) [26]

Dynamic thermal creak analysis:

For the dynamic thermal creak analysis the mass of the creak elements ( $m_1$  and  $m_2$ ) is incorporated in the model. As for the static thermal creak element the response of the creak element is first obtained, then the dynamic response of the coupled two DOF system with thermal creak is calculated.

Although the equations governing the dynamic creak response are more complex than those governing the static creak response these responses are qualitatively the same. The relative motion in the system occurs as a result of the non-linear energy release via friction inducing then disturbances to the attached structure. The difference is however that the dynamic response of the creak element is resulting due to the inertia. This creak element can be therefore used to represent a structure with system level thermal creak.

The magnitude  $A_c$  of the change in  $\Delta\xi$  during the stick-slip transition is given as follows:

$$A_c = 2(1 + \frac{1}{\kappa})(1 - f_k) ; \quad \frac{\kappa}{\mu} = 1 \quad [13-63]$$

where  $\mu = \frac{\mu_2}{\mu_1}$  is the ratio of the mass of the pin and slider, respectively.

Due to the dynamic overshoot caused by the inertia the magnitude  $A_c$  is greater than that introduced by the static creak element. As shown above the magnitude  $A_c$  for the dynamic creak element is twice the one for the static creak element in the special case of  $\kappa = \mu$ . This value is an upper limit for the dynamic creak element with a given stiffness ratio  $\kappa$ .

For the same thermo-elastic response the creak frequency of a dynamic creak element has been found to be half of the creak frequency of the static creak element. This is due to the inertia causing more energy to be released per creak than the static case. The creak frequency for  $\kappa = \mu$  is a lower bound on the dynamic creak element.

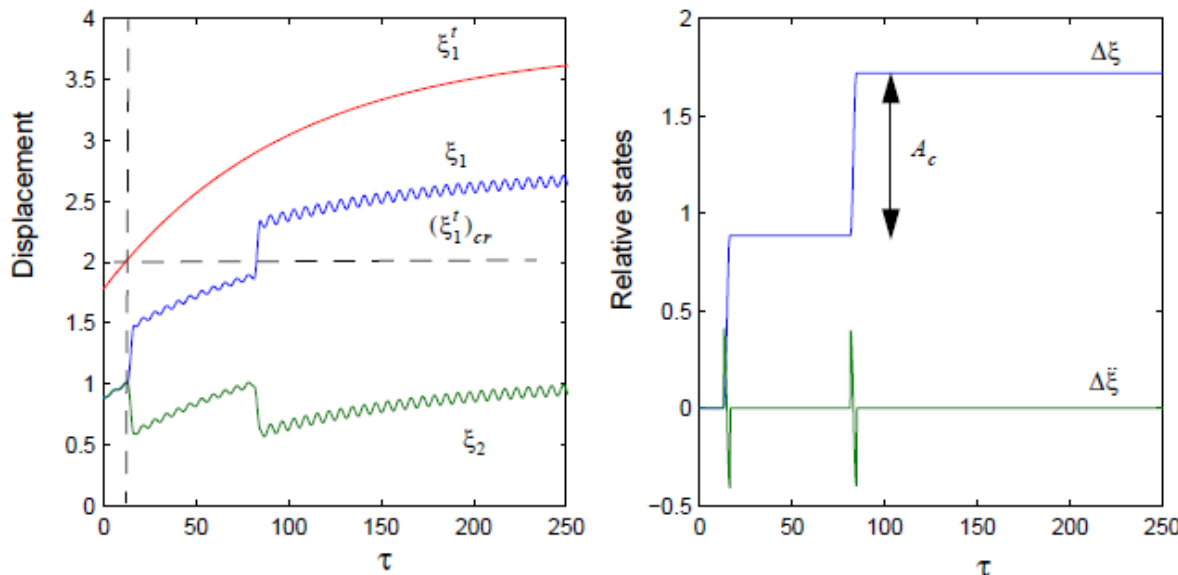


**Figure 13-43: Displacements of dynamic creak element (left) and relative acceleration in dynamic creak element (right) [26]**

Figure 13-43 shows the dynamic creak response for an exponential thermo-elastic response and for a model having the same parameters as those for the static creak example shown in Figure 13-40. The mass ratio has been set to 1.

The displacements of the creak element (pin and slider) follow the thermo-elastic response in gross slips, however not being step functions, with additional oscillatory motions. As for the static creak response the initial slip occurs when the thermal displacement  $\xi_1^t$  reaches the (dimensionless) critical thermal displacement  $(\xi_1^t)_{cr}$ .

The right graph shows the relative motions in the creak element (relative displacement  $\Delta\xi$  and relative acceleration  $\Delta\ddot{\xi}$ ). The magnitude of change of  $\Delta\xi$  is twice as large as for the static creak response. It is however almost constant at each slip.

For the purpose of calculating the dynamic response of the fully coupled system, as shown in Figure 13-39, the damping coefficients for the pin and slider ( $c_1$  and  $c_2$ , respectively) are introduced. The two DOF system for the case when pin and slider are sticking together is extended by an additional DOF for the case that the static friction is exceeded and the pin and slider are moving relative to each other. The response of the system is strongly depending on the characteristics of the forcing function  $f_{nl}$ :

$$f_{nl} = \mu \Delta\ddot{\xi} + \gamma \Delta\dot{\xi} + \kappa \Delta\xi \quad [13-64]$$

where  $\gamma = \frac{c_2}{c_1}$  is the ratio of the damping coefficients for the pin and slider, respectively, and  $\Delta\dot{\xi}$  the relative velocity of pin and slider.

The structural responses, i.e. the behaviour of the mass  $M$  as predicted by the dynamic thermal creak analysis, are shown in Figure 13-44. The creak frequency  $\omega_c$  is varied relative to the frequency of the attached system defined as  $\omega_0 = \frac{\kappa_0}{\mu_0}$  where  $\mu_0 = \frac{M}{m_1}$ .

The upper graphs show the disturbance force  $f_{nl}$  and the corresponding structural response  $\ddot{\xi}_3$  is shown in the lower graphs. Although the response contains multiple frequencies due to the introduction of the creak element dynamics the behaviour is qualitatively quite similar to the behaviour seen for the static creak element analysis. It should be also noted that the transmissibility of the thermal creak disturbance to the system performance is a strong function of the average creak frequency. This was already noticed for the static case.

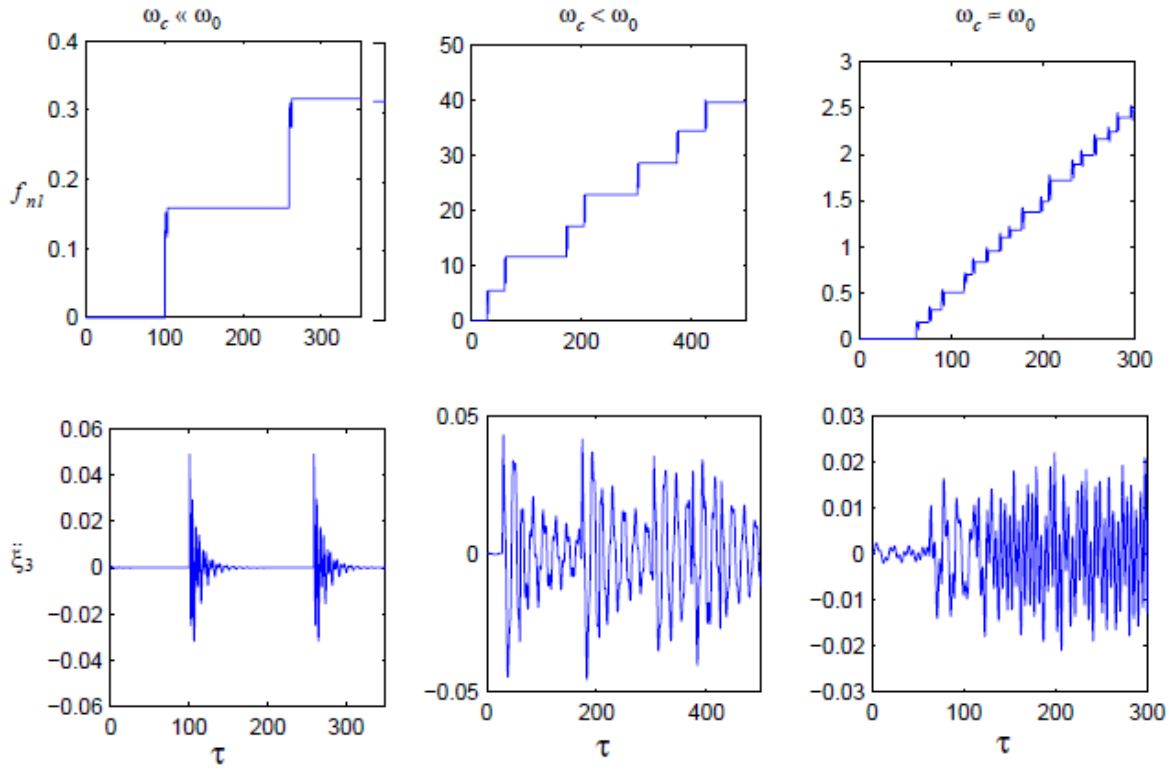


**Figure 13-44: Structural response at various creak frequencies [26]**

#### Control of sudden stress release (thermal snap) in bolted joint:

Proper design might prevent the occurrence of thermal snap effects in bolted joints. The control flow method to be followed should consist of the following steps, [4]:

1. Computation of the thermal force  $F_{TH}$  induced by the internal thermal gradient and the internal structural joint(s) thermal expansion coefficient:
  - Data are available only for one side of the unit internal junction:

$$F_{TH} = E \cdot A \cdot \alpha \cdot \Delta T \quad (\text{N}) \quad [13-65]$$

- Data are available for both sides (with subscripts 1 and 2, respectively) of the unit internal junction:

$$F_{TH} = \frac{(E_1 \cdot A_1) \cdot (E_2 \cdot A_2)}{E_1 \cdot A_1 + E_2 \cdot A_2} \cdot (\alpha_2 \cdot \Delta T_2 - \alpha_1 \cdot \Delta T_1) \quad (\text{N}) \quad [13-66]$$

where  $\Delta T$  ( $^{\circ}\text{C}$ ) is the temperature variation, and the junction material type is defined by the Young's modulus  $E$  ( $\text{N/m}^2$ ) and the linear thermal expansion coefficient  $\alpha$  ( $1/\ ^{\circ}\text{C}$ ).

The junction dimensions are given by the length  $L_0$  (m) along the expansion direction and the cross section area  $A$  ( $\text{m}^2$ ) normal to the expansion direction.

2. Computation of the maximum allowable static friction force  $F_f$  induced by the pre-load force  $F_{PLD}$  and the static friction coefficient  $\mu_s$  of the junction material:

$$F_{PLD} = \frac{T}{0.2 \cdot \phi} \quad (\text{N}) \quad ; \quad F_f = \mu_s \cdot F_{PLD} \quad (\text{N}) \quad [13-67]$$

where the pre-load of the junction is depending on the screw torque T (Nm) and the screw diameter  $\Phi$  (m).

3. Comparison of the static friction force  $F_f$  with the thermo-elastic force  $F_{TH}$  and verification whether slippage might occur at the unit/assembly moveable parts or at internal structural joints:

- $F_f > SF \cdot F_{TH}$  : *no motion should occur,*
- $F_f < SF \cdot F_{TH}$  : *the junction is expected to slip.*

#### 13.4.3.2.6 Clank Phenomena

Clank phenomena may be understood as those micro-perturbations that are caused by relatively rapid displacements of a part of a satellite, [4]. However, it should be noted that the disturbances generated are in general much smaller in amplitude compared with other sources as e.g. reaction wheels, cryo-coolers or stepper motors. Nevertheless they might be considered relevant for spacecraft without other moving parts or where very stringent micro-gravity and micro-vibration requirements are applicable.

It should be noted that the sudden stress release belongs to clank phenomena, too, but has been specifically covered in the preceding section due to its wider importance. Other relevant clank phenomena are electro-magnetic force effects resulting from equipment electrical wires and heaters, respectively, and crackling (multi-shocks) of multi-layer insulation (MLI). The procedures to derive the related disturbance functions for the assessment of their impact on the micro-gravity and micro-vibration environment are presented in this section.

By using the maximum force estimated for the different clank phenomena and assuming the spacecraft to behave as rigid body the acceleration level at the receiver location might be simply calculated as:

$$a = \frac{SF \cdot F^*}{M} \quad \text{where } M \text{ (kg) is the spacecraft mass and SF might be any applicable safety factor.}$$

The force  $F^*$  depends on the clank phenomenon being investigated, e.g.  $F^* = \Delta F$  for the inductive electromagnetic force effects resulting from equipment electrical wires,  $F^* = \max(F(t))$  for the inductive electromagnetic force effects resulting from heaters, and  $F^* = F_c$  for the crackling phenomenon (multi-layer insulation).

When employing the force spectral density  $SDF(\omega)$  as applicable disturbance function the relevant structural transfer functions should be considered for the assessment of the effects at the receiver location.

##### Inductive electromagnetic force effects resulting from equipment electrical wires:

Electrical wires inside the spacecraft and also inside the equipment may induce a micro-vibration disturbance due to the internal electrical power fluctuation that induces an attractive or repulsive electromagnetic force among parallel set of wires. Potential measures to minimize the electromagnetic force effects could include the reduction of the free-standing length (FSL, Figure 13-45) of the wires, the increase of the mechanical stiffness of the wires, the reduction of the current fluctuation, and the limitation of the current rise/fall time.

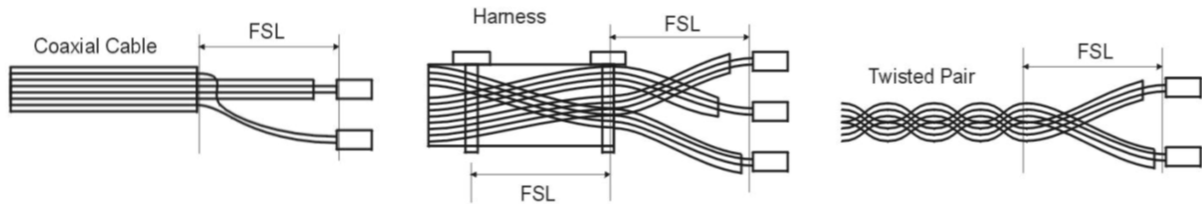


**Figure 13-45: Free-standing length (FSL) of electrical wires [4]**

The derivation of the relevant disturbance forcing function should be performed following these steps:

1. Review of the design for potential electrical wire movements due to the income and outcome wires positioning, its free-standing length and the specified/actual electric current fluctuation:
  - Identification of all “free-standing wires”, i.e. the wires that can easily displace because not benefiting from a high mechanical stiffness.
  - Computation of the maximum value L of the relevant FSL’s found for all free-standing wires:

$$L = \max(FSL_i) \quad , \quad i = 1, \dots, N_w \quad [13-68]$$

where  $N_w$  is the number of free-standing wires.

Note: Examples of FSL are illustrated in Figure 13-45.

2. a) Computation of the worst case variation  $\Delta F$  of the electromagnetic force between all possible pairs of the free-standing wires:

$$\Delta F = \mu_0 \cdot \left( \frac{\Delta I^2 + 2I_0\Delta I}{2 \cdot \pi \cdot d} \right) \cdot L \cdot \frac{1}{2} N_w (N_w - 1) \quad [13-69]$$

where

$\mu_0 = 4\pi * 10^{-7}$  is the vacuum magnetic permeability, given in  $\frac{H}{m}$  or  $\frac{N}{A^2}$ ,

$\Delta I = \max(\Delta I_i)$  the max. variation of all currents flowing in the free-standing wires

$(i = 1, \dots, N_w)$ , and

$I_0 = \text{mean}(I_i)$  the mean value of all currents flowing in the free-standing wires

$(i = 1, \dots, N_w)$ .

- b) Computation of the variation  $\Delta F_i$  ( $i = 1, \dots, N_w$ ) of the electromagnetic force between all possible pairs of the free-standing wires and subsequent derivation of the electromagnetic force variation  $\Delta F$  as the maximum of all  $\Delta F_i$ :

$$\Delta F_i = \mu_0 \cdot \left( \frac{\Delta I^2 + 2I_0\Delta I}{2 \cdot \pi \cdot d} \right) \cdot L \cdot \frac{1}{2} N_w (N_w - 1) \quad [13-70]$$

$$\Delta F = \max(\Delta F_i) \quad [13-71]$$

3. Computation of the minimum lateral oscillation pulsation of all free-standing wires:

$$\omega_{\min} = \min(\omega_i) \quad , \quad i = 1, \dots, N_w \quad [13-72]$$

where

$$\omega_i = \sqrt{\frac{k_i}{m_i}} \text{ and } k_i = \frac{48}{4} \pi E \frac{r_i^4}{FSL^3} \quad [13-73]$$

- $r_i$  the radius of the wire core,
- $E$  the wire core material,
- $m_i$  the mass of the free-standing wire.

4. Finally, the computation of the force spectral density  $FSD(\omega)$  at the disturber location:

$$FSD(\omega) = 2 \Delta F \frac{\sin(\pi\omega_{\min}\Delta t)^2}{\pi\omega_{\min}\sqrt{\Delta t}} \quad (\frac{\text{N}}{\sqrt{\text{Hz}}}) \quad [13-74]$$

$$\text{with } \Delta t = \frac{1}{\omega} = \sqrt{\frac{m}{k}} \quad [13-75]$$

#### Inductive electromagnetic force effects resulting from heaters:

Heaters mounted inside the spacecraft and also inside equipment units might create micro-vibration disturbances due to current fluctuations. The latter induce electromagnetic forces that can be attractive or repulsive among a set of wires, and between the induced currents in the metallic substrate on which the heater is mounted and the heater itself (as shown in the left graph of Figure 13-46).

These electromagnetic forces could be however minimized by increasing the structural stiffness, reducing the current fluctuation, limiting the current rise/fall time, avoiding heaters on metallic substrates, and increasing the distance between the heater and its substrate.

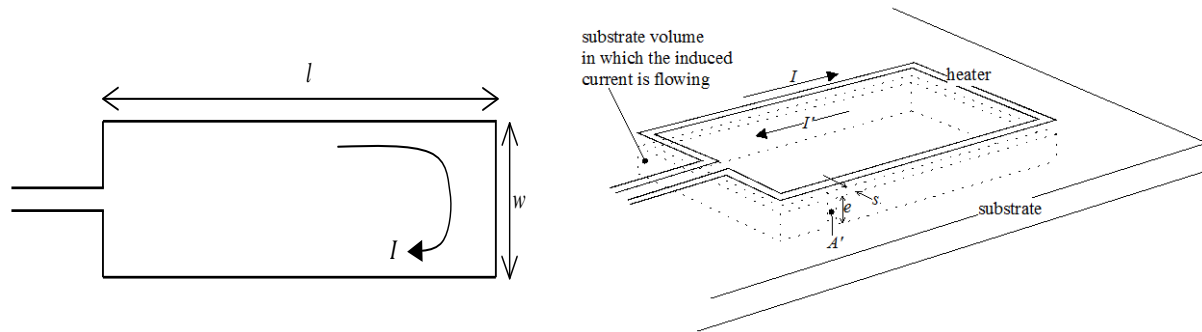


**Figure 13-46: Equivalent heater model (left) and model of the induced current path in the heater substrate (right) [4]**

In order to simplify the computation of these forces the heater is modelled as a conductive wire shaped in a rectangular path of width  $w$  and length  $l$  in which a current  $I$  is circulating, Figure 13-46.

The derivation of the relevant disturbance forcing function should be performed following these steps:

1. Computation of the modulus of the magnetic field at the centre of the rectangle circumscribed by the wire:

$$B = \frac{2\mu_0}{\pi} I \frac{\sqrt{l^2 + w^2}}{l \cdot w} = \frac{2\mu_0}{\pi} I \frac{\sqrt{l^2 + w^2}}{A} \quad [13-76]$$

where

$\mu_0 = 4\pi * 10^{-7}$  is the vacuum magnetic permeability, given in  $\frac{H}{m}$  or  $\frac{N}{A^2}$ , and

$$A = l * w \quad \text{the area of the rectangle.}$$

2. Computation of the flux  $\Phi_B$  of this magnetic field through the area A of the metallic substrate to which the heater is glued:

$$\Phi_B = B \cdot A = \frac{2\mu_0}{\pi} I \sqrt{l^2 + w^2} \quad [13-77]$$

The flux produces an which in turn induces an:

3. Computation of the electromotive force (emf)  $\varepsilon$  in the substrate caused by the time variation of the flux  $\Phi_B$ :

$$\varepsilon = -\frac{d\Phi_B}{dt} = -\frac{2\mu_0}{\pi} \sqrt{l^2 + w^2} \frac{dI}{dt} \quad [13-78]$$

4. Computation of the electric current  $I^*$  in the substrate induced by  $\varepsilon$  (assuming that the substrate is conductive):

$$I^* = \frac{\varepsilon}{R} \quad [13-79]$$

where R is the resistance of the substrate.

With  $R = \rho \frac{2(l + w)}{s \cdot e} = \rho \frac{L}{s \cdot e}$  the current  $I^*$  becomes:

$$I^* = -\frac{2\mu_0}{\pi} \sqrt{l^2 + w^2} \frac{dI}{dt} \frac{s \cdot e}{\rho \cdot L} \quad [13-80]$$

where

- L is the perimeter of the heater (length of the path in which  $I^*$  is flowing),
- s the width of the heater conductive track,
- e the thickness of the heater substrate,
- I the current circulating in the heater, and
- $\rho$  the resistivity of the substrate material, e.g.  $2.8 \cdot 10^{-8} \Omega \text{m}$  for aluminium.

5. Computation of the electromagnetic force  $F(t)$  between an equivalent heater and its conductive substrate:

$$F(t) = \left( \frac{\mu_0}{\pi} \right)^2 \sqrt{l^2 + w^2} \frac{s \cdot e}{d} \frac{I}{\rho} \frac{dI}{dt} \quad [13-81]$$

where d is the distance of the heater from its substrate.

6. Computation of the force spectral density FSD( $\omega$ ) at the disturber location:

$$FSD(\omega) = PSD[F(t)] \left( \frac{N}{\sqrt{\text{Hz}}} \right) \quad [13-82]$$

Crackling Phenomenon (on multi-layer insulation):

Multi-layer insulation (MLI) type thermal control blankets have been identified as spacecraft structural element that might deform (expansion or contraction) under temperature variations as caused by varying thermal irradiation on orbit. Sudden geometry changes, e.g. due to buckling of foils, might exert tiny forces which may cause small reactions resulting to micro-vibration disturbances.

The derivation of the relevant disturbance forcing function should be performed following these steps:

1. Computation of the MLI mass  $M_{MLI}$  subjected to crackling:

$$M_{MLI} = S_{MLI} \cdot T_{Layer} \cdot \rho \quad [13-83]$$

where

$S_{MLI}$  is the involved surface,

$T_{Layer}$  the thickness of one MLI layer, and

$\rho$  the MLI layer density.

2. Computation of the crackling force  $F_C$  generated by the MLI subjected to crackling:

$$F_C = M_{MLI} \cdot \frac{8 \cdot \Delta x}{\Delta t^2} \quad [13-84]$$

where

$\Delta x$  is the displacement, and

$\Delta t$  the total event duration.

Note: The force  $F_C$  is calculated assuming a constant acceleration and deceleration of the MLI with a time duration of  $\Delta t/2$ .

3. Computation of the force spectral density  $FSD(\omega)$  at the disturber location:

$$FSD(\omega) = 2 F_C \frac{\sin(\pi \omega \Delta t)^2}{\pi \omega \sqrt{\Delta t}} \quad (\frac{N}{\sqrt{Hz}}) \quad [13-85]$$

$$\text{with } \Delta t = \frac{1}{\omega} = \sqrt{\frac{m}{k}}$$

### 13.4.3.3 Determination of the disturbance forcing functions by test

#### 13.4.3.3.1 General aspects

Disturbance characterisation tests serve the purpose to provide relevant input for the micro-gravity and micro-vibration analyses, respectively. This is often necessary for disturbance sources (e.g. reaction wheels or various mechanisms) that have complex behaviour that cannot be properly defined e.g. by analytical functions.

In the case that recovery actions have been implemented to attenuate the impact of the disturbance sources then additional equipment characterisation tests might be necessary to measure the efficiency of the disturbance reduction.

Since the micro-gravity and micro-vibration analyses and predictions are strongly depending on data assumptions and approximations the disturbance characterisation tests provide the earliest

information about the system performance. Consequently they should be performed as early as possible in the program starting with breadboard, development and engineering units.

In most cases these tests are performed with the source clamped at its interface on a dynamometric table and interface loads are measured while operating the device. Results are either temporal or frequency response profiles depending on the typology of the perturbation.

It should be however noted that the test boundary conditions are not representative for the real interface of the equipment with the spacecraft platform and that the boundary conditions might have a large influence on the high frequency signature. Limitations might also exist with respect to those devices that cannot be operated on ground in a flight representative manner.

The full experimental characterisation of each disturbance source under flight representative conditions is not practical in many situations due to cost and schedule constraints. In this case the remaining uncertainties should be carefully assessed and covered e.g. by applying an appropriate margin policy.

The following aspects should be taken care of when performing disturbance source characterisation tests:

- The measurement device should be well isolated from the external disturbances coming from the facility. Concerning the mechanical perturbations this can be achieved by placing the test fixture on a highly damped suspension system. Frequently seismic foundations acting as mechanical low pass filter might be used to improve the isolation system.
- Gravity compensation devices may be needed to unload mechanisms from gravity forces during the on-ground tests, e.g. consisting of a set of elastomeric cables with very low natural frequency (about 1 Hz). More generally the presence of gravity may have a direct stiffening effects.

As a generic test sequence for the noise source characterisation the following steps can be performed:

- Facility characterisation, through verification of the test set-up dynamic behaviour (achieving very high frequencies for the table when loaded by the equipment);
- Background noise characterisation, by means of measurements of acceleration autospectra (equipment switched off);
- Calibration of the measurement device, through excitation of the table with a known input signal;
- Noise source characterisation tests.

Due to the complex nature of micro-vibration disturbance and vibration control, iterative steps should be planned for vibration reduction measures supported by equipment tests.

Final verification of the equipment related micro-vibration requirements in terms of

- base forcing functions/vibrations,
- effectiveness of vibration reduction, and
- radiated sound power

should be performed on flight standard qualification type equipment or Prototypical Models.

In the verification test program the testing of the equipment and structural samples should be planned depending on the severity of the micro-gravity requirements and considering the available knowledge of disturbance induced by the sources.

A plan should be established to determine which items should be gone along a verification approach by test and which can be verified by analysis. A priority could be assigned for the equipment under test in order to minimize the total amount of micro-gravity tests to be planned.

#### 13.4.3.3.2 Coupling of source and supporting structure

In practice most of the mathematical models of the sources are derived considering the source mechanism in isolation, and also the testing is generally carried out in a "blocked" condition i.e. rigidly grounding (i.e. blocking) the equipment at its mounting points.

This means that the hardware which produces the micro-vibration, e.g. a reaction wheel, or a cryo-cooler is typically tested mounted on a rigid multi-axis dynamometric platform (also known as "force table" or Kistler table, Figure 13-47) which measures the total reaction forces ( $F_x$ ,  $F_y$ ,  $F_z$ ) and moments ( $M_x$ ,  $M_y$ ,  $M_z$ ) transmitted to the ground. The accuracy of these systems is usually in the micro-Newton range, and the useful frequency range goes from about 1 to 2 Hz up to a few hundred Hz, depending on the stiffness of the particular hardware.



**Figure 13-47: Kistler table type 9253B**

However, in reality, the loads produced by the vibrating equipment (source) on its supporting structure depend on both, the dynamic characteristics of the source itself and those of the supporting structure.

For example the maximum magnitude of the force produced by the simple systems with two counter-rotating masses shown in Figure 13-48 a) and b), when the source is blocked ( $x=0$ ), is given by Eq. [13-86]:

$$F = ml\omega^2 \quad [13-86]$$

where  $\omega$  is the angular velocity (assumed constant), and the meaning of the other symbols is shown in Figure 13-48.

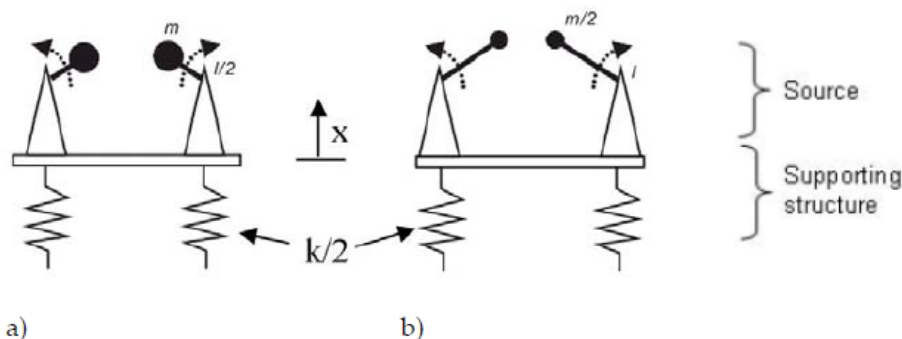


**Figure 13-48: Schematic of possible source of vibrations**

This simple formula is accurate for both systems shown in Figure 13-48 (provided the supporting structure is rigid, i.e.  $k \rightarrow \infty$ ), and measurements on a Kistler table should validate such a model; however when the equipment is actually mounted on a real, flexible structure, the system shown in Figure 13-48 b) can produce up to twice the force as that in Figure 13-48 a).

To demonstrate this, let's examine the system in Figure 13-48 a) and allow movement of the support ( $x \neq 0$ ), which in practice corresponds to the source supported by a structure with a finite stiffness equal to  $k$ . The vertical equilibrium can be expressed as:

$$2m\left(-\frac{l}{2}\omega^2 \sin(\omega t) + \ddot{x}\right) + kx = 0 \quad [13-87]$$

where  $t$  is the time (the angle  $\omega t$  is taken from the horizontal axis), and the solution of Eq. [13-87] can be written as:

$$x = \frac{ml\omega^2}{k - 2m\omega^2} \sin(\omega t) \quad \text{with} \quad \omega \neq \omega_0 = \sqrt{\frac{k}{2m}} \quad [13-88]$$

Therefore for a high rotation speed  $\omega \gg \omega_0$  the displacement  $x$  tends to become equal to  $l/2$  and consequently the force transmitted to the support is given by Eq. [13-89]:

$$F_a \Big|_{\omega \gg \omega_0} = kx = k \frac{l}{2} \quad [13-89]$$

If we now consider the system in Figure 13-48 b), the vertical equilibrium can be written as:

$$m(-l\omega^2 \sin(\omega t) + \ddot{x}) + kx = 0 \quad [13-90]$$

and its solution

$$x = \frac{ml\omega^2}{k - m\omega^2} \sin(\omega t) \quad \text{with} \quad \omega \neq \omega_0 = \sqrt{\frac{k}{m}} \quad [13-91]$$

If high angular velocity ( $\omega \gg \omega_0$ ) is considered then the displacement  $x$  tends to  $l$  and consequently the force transmitted to the support is given by Eq. [13-92]:

$$F_b \Big|_{\omega \gg \omega_0} = lk \quad [13-92]$$

which is twice the force generated by the source in Figure 13-48 a).

In fact the loads exchanged at the interface between the source and supporting structure depend on the source internal dynamics (i.e. the forces and moments in the blocked configuration, produced for example by mass unbalances, possible internal resonances of the source etc.) and the reactions due to the coupling (and consequent motion of the interface).

Intuitively, it can be said that a portion of the force that the source generated in its blocked configuration ( $\mathbf{f}_B$ ) is now used to move the source itself (as its mounting interface has acceleration  $\ddot{\mathbf{x}}_c$  different from zero). Therefore the force that the source can actually transmit to the coupled supporting structure is given by Eq. [13-93]:

$$\mathbf{f}_C = \mathbf{f}_B - \mathbf{M}_w \ddot{\mathbf{x}}_c \quad [13-93]$$

where  $\mathbf{f}_C$  is the vector of forces and moment at the interface with the supporting structure,  $\mathbf{f}_B$  is the vector of the forces and moments in the blocked configuration,  $\mathbf{M}_w$  is the dynamic mass (frequency dependent ratio between force or moment applied at the mounting of the source free-free and

accelerations at the same location) of the equipment (say a reaction wheel, hence the subscript  $w$ ) and  $\ddot{\mathbf{x}}_c$  contains the acceleration of the interface's degrees of freedom.

The forces  $\mathbf{f}_C$  obtained from Eq. [13-93] can then be multiplied by the transfer functions between input loads at the source mounting location and any relevant parameter describing the structural response of the satellite or payload. The output of these transfer functions can be for example displacements or rotations of mirrors or lenses, and these transfer functions can be obtained from the FEM of the whole satellite or experimentally (possibly simulating a free-free condition suspending the satellite with elastic cords).

It should be noted that the equilibrium expressed in Eq. [13-93] can be described using velocity and mechanical impedance rather than acceleration and dynamic mass, and also the theory described in this section can be articulated using different parameters.

The issue is to obtain the terms on the right hand side of Eq. [13-93].  $\mathbf{f}_B$  is relatively straight forward, as it is the vector containing the reactions when the source is blocked ( $\ddot{\mathbf{x}}_c = 0$ ) and can be obtained from measurements (e.g. Kistler table) or mathematical models of the source.

$\mathbf{M}_w$  is the dynamic mass of the source and for example can be obtained with the source switched off and unit loads are applied one at the time to the degrees of freedom of the source interface allowing to recover one by one the columns of the inverse of  $\mathbf{M}_w$  as shown in Eq. [13-94].

$$\begin{aligned} \mathbf{f} &= \mathbf{0} - \mathbf{M}_w \ddot{\mathbf{x}} \\ \ddot{\mathbf{x}} &= -\mathbf{M}_w^{-1} \mathbf{f} \Rightarrow \mathbf{M}_w \end{aligned} \quad [13-94]$$

Note that in practice recovering the dynamic mass experimentally can be quite challenging, and therefore this can be calculated using an accurate FEM of the source.

Finally to determine  $\ddot{\mathbf{x}}_c$  some knowledge of the supporting structure is necessary, and in particular its response at the driving point (location of the source), when loads are applied at the degrees of freedom of the interface with the source. In this circumstance, denoting with  $\mathbf{M}_{Str}$  the dynamic mass of the supporting structure (e.g. satellite) with respect to the mounting interface degrees of freedom (note that  $\mathbf{M}_{Str}$  can be obtained from the satellite FEM or experimentally), we can write

$$\mathbf{f}_C = \mathbf{M}_{Str} \ddot{\mathbf{x}}_c \quad [13-95]$$

which can be inverted to obtain the accelerations of the interface as a function of the loads applied at the interface:

$$\ddot{\mathbf{x}}_c = \mathbf{M}_{Str}^{-1} \mathbf{f}_C \quad [13-96]$$

Finally Eq. [13-96] is substituted into Eq. [13-93] to obtain:

$$\mathbf{f}_C = \mathbf{f}_B - \mathbf{M}_w \mathbf{M}_{Str}^{-1} \mathbf{f}_C \quad [13-97]$$

which can be solved for  $\mathbf{f}_C$  to yield

$$\mathbf{f}_C = (1 + \mathbf{M}_w \mathbf{M}_{Str}^{-1})^{-1} \mathbf{f}_B \quad [13-98]$$

The procedure described above represents the most general case, and allows calculating precisely the force produced by a source, including the dynamic effect produced by the interaction of sources and supporting structure. Following simpler approaches (e.g. just modelling and testing the source in a blocked condition) the coupling effects, which might be quite important, are neglected. Whether or

not the dynamics due to the coupling must be considered or can be neglected depends on the particular circumstances under consideration.

The theory above can also be implemented using typical of random vibrations parameters. The blocked force can be described by the Power Spectral Density (PSD) matrix of the reaction forces and moments  $\Phi_B$  produced by the source in its blocked configuration. The reactions produced by the flexible structure supporting the source in operation can also be expressed as a PSD matrix:

$$\Phi_C = \mathbf{M}_{\text{Str}} \ddot{\mathbf{X}}_c \mathbf{M}_{\text{Str}}^H \quad [13-99]$$

where  $\ddot{\mathbf{X}}_c$  is the PSD matrix of the accelerations input in the supporting structure, and  $\mathbf{M}_{\text{Str}}^H$  is the hermitian of the dynamic mass matrix (note that this equation is analogous to Eq. [13-94]).

Using the same method described above the PSD matrix of the coupled input force can then be written as:

$$\Phi_C = (1 + \mathbf{M}_w \mathbf{M}_{\text{Str}}^{-1})^{-1} \Phi_B (1 + \mathbf{M}_w \mathbf{M}_{\text{Str}}^{-1})^{-H} \quad [13-100]$$

which corresponds to the previously derived Eq. [13-98].

### Practical example of coupling

As mentioned before in this section, usually the structure is characterised experimentally measuring transfer functions between inputs at the source/s (using an impact hammer or mini-shaker/stinger) and output at receiver/s location (typically using high sensitivity accelerometers). When these tests are carried out, generally the real source is not available and so the test is carried out either without the source or using a representative dummy mass at the source location.

The example below shows the importance of the dynamic coupling between the source and the supporting satellite structure, and how this effect can be accounted for.

Consider a source modelled with one DOF system as shown in Figure 13-49 a) where inside the source a force of PSD equal to  $\mathbf{f}_i$  is generated. Assuming that  $\mathbf{f}_i$  is given by

$$\mathbf{f}_i = \frac{\omega}{2\pi f_i^*} \quad [13-101]$$

where  $\omega [\frac{1}{s}]$  is the frequency and  $f_i^* = 2000 [\frac{1}{Ns}]$  is assumed hereafter.

Note: This theory remains valid for other types of  $\mathbf{f}_i$ , e.g. being a constant or other function of  $\omega$ .

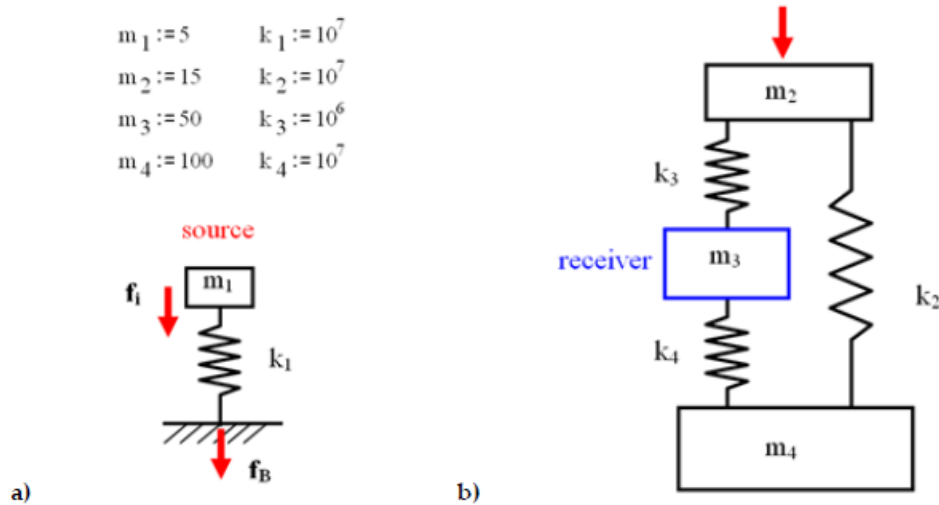


**Figure 13-49:** Model of source and supporting structure

When the source is grounded (or blocked) the PSD of the reaction force  $\mathbf{f}_B$ , generated at the support, is given by Eq. [13-102]:

$$\mathbf{f}_B(\omega) = (k_1(-m\omega^2 + k_1(1+0.02i))^{-1})^2 \mathbf{f}_i(\omega) \quad [13-102]$$

where hysterical damping with  $\eta=0.02$  has been assumed. Figure 13-50 shows both the PSD of the source internal force ( $\mathbf{f}_i$ ) and that generated at the support ( $\mathbf{f}_B$ ).

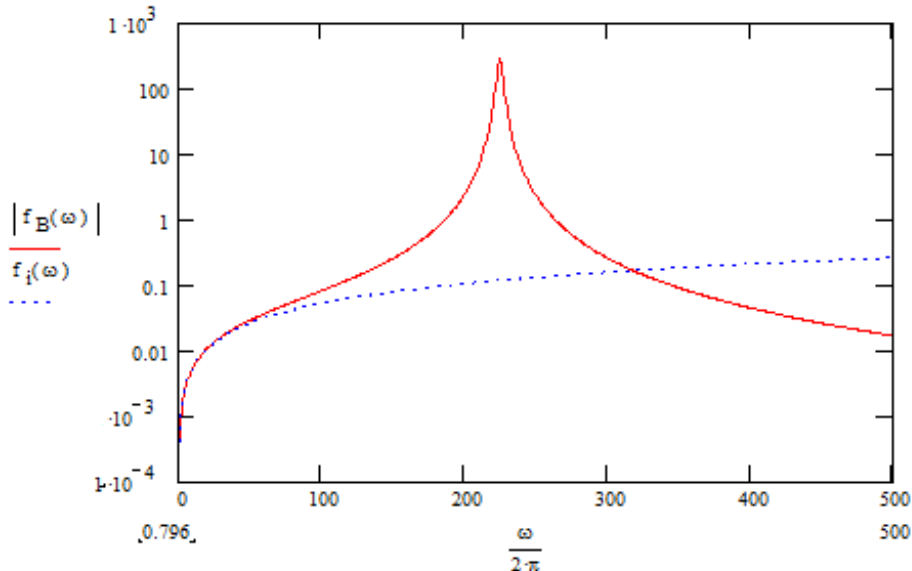


Figure 13-50: PSD of source internal force and of force at the support (blocked)

If the whole system can be assembled (as shown in Figure 13-51), then the PSD of the response at the receiver location can be calculated using the equations for the whole system (see Eqs. [13-103] to [13-106]) and applying  $\mathbf{f}_B$  at the mounting location of the source or applying  $\mathbf{f}_i$  at the source itself, respectively. The graphs in Figure 13-52 show that the response at the receiver location is exactly the same.

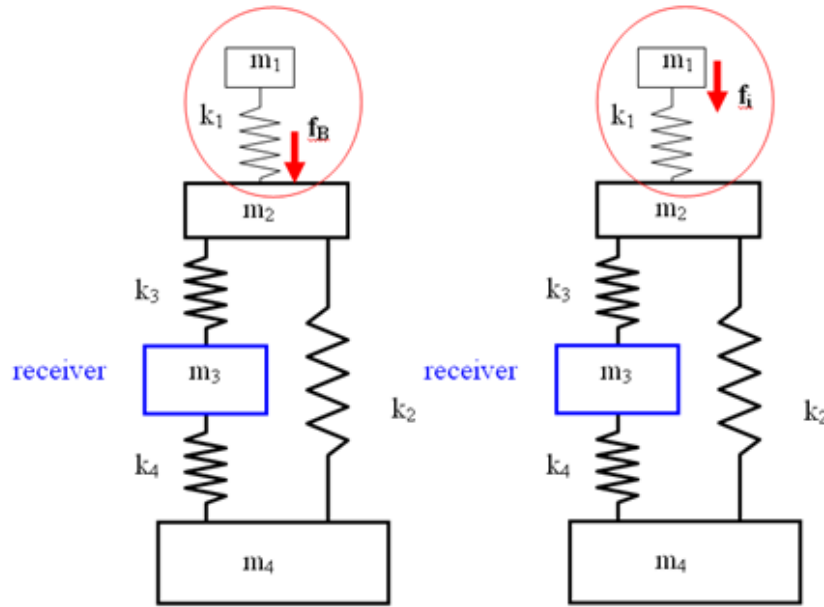


Figure 13-51: Example of application of the source loads

$$M := \begin{bmatrix} m_1 & 0 & 0 & 0 \\ 0 & m_2 & 0 & 0 \\ 0 & 0 & m_3 & 0 \\ 0 & 0 & 0 & m_4 \end{bmatrix} \quad K := \begin{bmatrix} k_1 & -k_1 & 0 & 0 \\ -k_1 & k_1 + k_2 + k_3 & -k_3 & -k_2 \\ 0 & -k_3 & k_3 + k_4 & -k_4 \\ 0 & -k_2 & -k_4 & k_4 + k_2 \end{bmatrix} \quad [13-103]$$

$$Inp_1(\omega) := \begin{bmatrix} 0 & 0 & 0 & 0 \\ 0 & f_B(\omega) & 0 & 0 \\ 0 & 0 & 0 & 0 \\ 0 & 0 & 0 & 0 \end{bmatrix} \quad Inp_0(\omega) := \begin{bmatrix} f_i(\omega) & 0 & 0 & 0 \\ 0 & 0 & 0 & 0 \\ 0 & 0 & 0 & 0 \\ 0 & 0 & 0 & 0 \end{bmatrix} \quad [13-104]$$

$$TF_{23}(\omega) = \left( \frac{-M\omega^2 + K(1+0.02i)}{\omega^2} \right)^{-1} \quad [13-105]$$

$$OUT_{B23}(\omega) = TF_{23}(\omega) Inp_1 TF_{23}(\omega)^H \quad OUT_{i23}(\omega) = TF_{23}(\omega) Inp_0 TF_{23}(\omega)^H \quad [13-106]$$

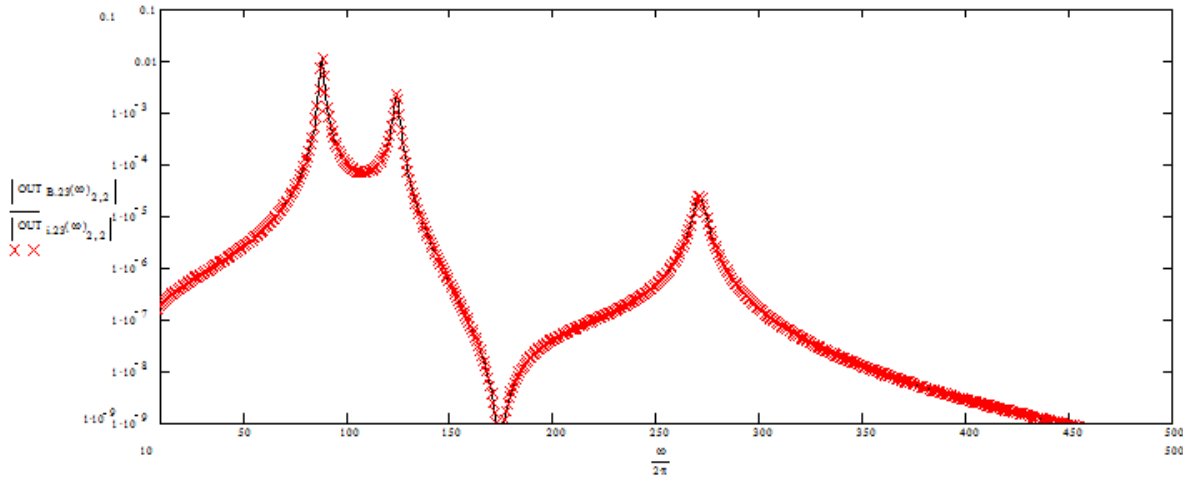


**Figure 13-52: Responses at receiver location for force input applied at the mounting location of the source or at the source itself, respectively**

However it might be not possible to have the full system assembled for example to **carry out tests and often it is necessary to treat separately the source and the satellite structure**. The uncoupled mass and stiffness matrices for the satellite structure (index nos := without the source) and the source (index SS) are:

$$M_{nos} = \begin{bmatrix} m_2 & 0 & 0 \\ 0 & m_3 & 0 \\ 0 & 0 & m_4 \end{bmatrix} \quad K_{nos} = \begin{bmatrix} k_2 + k_3 & -k_3 & -k_2 \\ -k_3 & k_3 + k_4 & -k_4 \\ -k_2 & -k_4 & k_4 + k_2 \end{bmatrix} \quad [13-107]$$

$$M_{ss} = \begin{bmatrix} m_1 & 0 \\ 0 & 0 \end{bmatrix} \quad K_{ss} = \begin{bmatrix} k_1 & -k_1 \\ -k_1 & k_1 \end{bmatrix} \quad [13-108]$$

In addition there is the complication that often the internal mechanisms that produce the loads within the source are difficult to model; so the only input available is  $\mathbf{f}_B$ .

In this case if  $\mathbf{f}_B$  is simply directly applied to the structure (without the source), or if the mass of the source is included as a lumped mass, the results are the green and red curves, respectively, shown in Figure 13-53 and none of these two curve is the exact solution.

However, if the theory of the coupling is applied as described above and the dynamic mass of the source:

$$\mathbf{M}_{\text{Source}}(\omega) = \left( (-\mathbf{M}_{ss}\omega^2 + \mathbf{K}_{ss}(1+0.02i))^{-1} \omega^2 \begin{bmatrix} 0 \\ -1 \end{bmatrix} \right)^{-1} \quad [13-109]$$

as well as that of the supporting structure, or its accelerance (being the inverse of the dynamic mass):

$$\mathbf{A}_{23nos}(\omega) = \left( (-\mathbf{M}_{nos}\omega^2 + \mathbf{K}_{nos}(1+0.02i))^{-1} \omega^2 \begin{bmatrix} -1 \\ 0 \\ 0 \end{bmatrix} \right) \quad [13-110]$$

is used in Eq. [13-100], i.e. to produce the coupled force as a function of the blocked force, then it is possible to obtain the response at the receiver location as:

$$\mathbf{OUT}_C(\omega) = \mathbf{TF}_{23nos,0,1} \overbrace{\left( 1 + \mathbf{M}_{\text{Source},1} \mathbf{A}_{23nos,0} \right)^{-1} \mathbf{f}_B \left( 1 + \mathbf{M}_{\text{Source},1} \mathbf{A}_{23nos,0} \right)^{-H}}^{\Phi_C} \mathbf{TF}_{23nos,0,1}^H \quad [13-111]$$

This is an exact solution as can be seen in Figure 13-53.

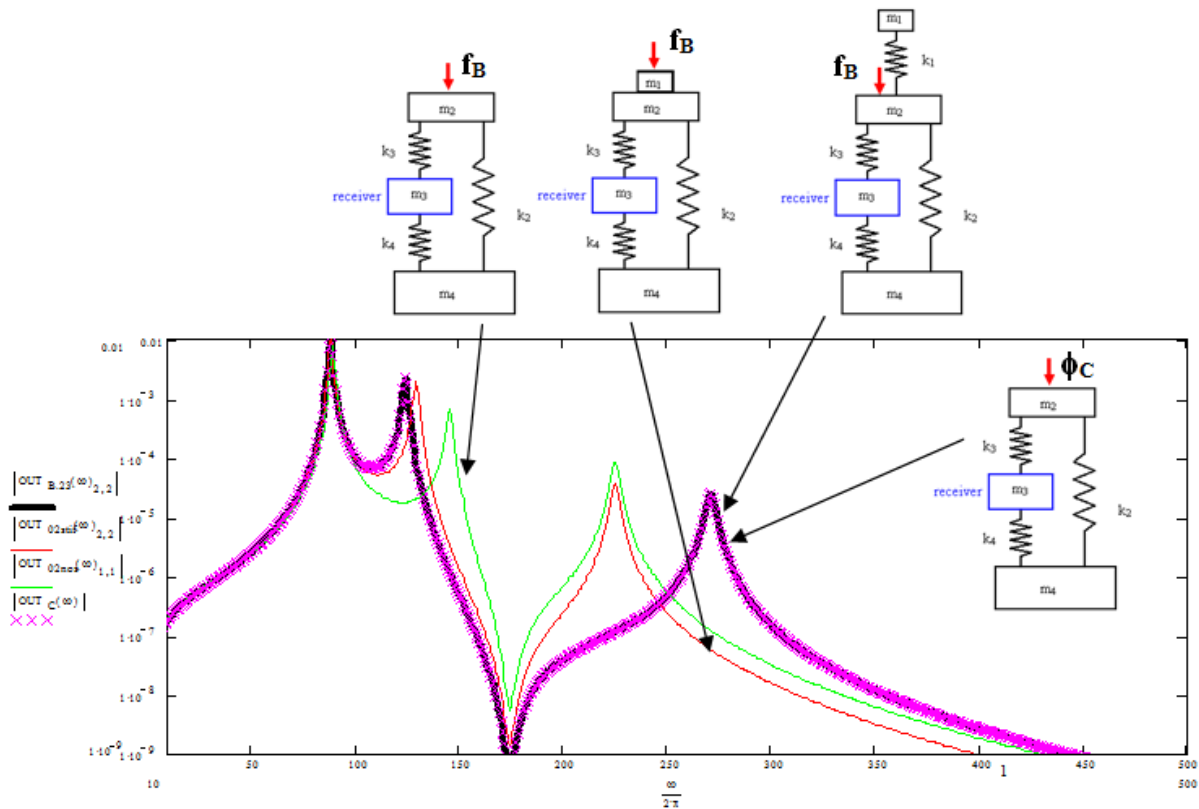


**Figure 13-53: PSD at the receiver from various implementations of the input**

Further information on a coupled disturbance analysis method including the dynamic mass matrix of each body can be found in [27].

#### 13.4.3.3.3 Test facilities for disturbance characterisation

Several micro-dynamics characterisation test facilities exist in Europe within industry and national space research institutions (e.g. CNES). The data acquired with such facilities can then be used as input to analytical models allowing more accurate investigations of the contributions of unit level operational dynamics to subsystem or system level micro-vibration performances.

As an example for such test facilities the “ESA Reaction Wheel Characterisation Facility (RCF)” located at the ESA Technology and Research Centre (ESTEC) in Noordwijk in the Netherlands is presented in more detail hereafter, [28][29]. The purpose is to introduce the general capabilities of these test facilities and the procedures to be followed for the test preparation and execution.

The setup of the RCF is shown in Figure 13-54 and the main performance characteristics in ambient conditions are given in Table 13-9.

The RCF is capable to measure the interface forces and moments (simultaneously for all 6 degrees of freedom) that are introduced by an item under test mounted onto the test table. Furthermore measurements under “low” vacuum conditions can be performed when using the vacuum bell and a dedicated pumping system.

Four tri-axial Kistler force links are located in the corners of the test table and attached to a load cell support structure that in turn rests on the marble seismic block. Furthermore the test table is equipped with 6 accelerometers to monitor the induced accelerations at low frequencies. These accelerometers

are placed at 2 diagonal corners of the test table and sense the accelerations in three degrees of freedom of the table.

The achievable measurement accuracy and resolution depends on the full-scale range to be selected and of the influence of the first eigenmode of the combined system.



**Figure 13-54: ESA Reaction Wheel Characterisation Facility; test table with standard adapter plate installed (left), RCF with vacuum bell mounted (right)**

**Table 13-9: Nominal RCF performances in ambient conditions (no vacuum bell)**

<b>Max. payload mass:</b>	20 kg (assessment needed for higher masses)
<b>Test table dimensions:</b>	320 x 320 mm <sup>2</sup>
<b>Measurement range:</b>	
lateral forces F <sub>x</sub> , F <sub>y</sub>	20 mN - 200 N
vertical forces F <sub>x</sub> , F <sub>y</sub>	40 mN - 200 N
moments M <sub>x</sub> , M <sub>y</sub>	2 mNm - 20 Nm
torques M <sub>z</sub>	6 mNm - 25 Nm
<b>Usable frequency bandwidth:</b>	2 – 1000 Hz (depending e.g. on payload mass)
<b>Measurement resolution:</b>	< 20 mN (depending on full scale range)
<b>Linearity:</b>	< 1.5%
<b>Cross-talk:</b>	< 1.6%
<b>Empty table eigenfrequencies:</b>	
lateral directions (f <sub>x</sub> , f <sub>y</sub> )	> 1200 Hz
vertical direction (f <sub>z</sub> )	> 1750 Hz
<b>Achievable vacuum level:</b>	1 mbar - 10 <sup>-1</sup> mbar
<b>Background noise level:</b>	< 5 · 10 <sup>-5</sup> N

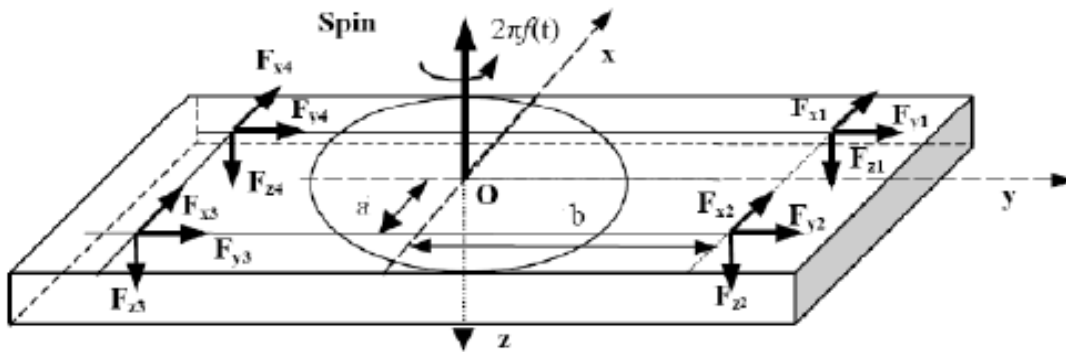


**Figure 13-55: Schematic of the RCF functional principle**

In order to derive the overall interface moments and forces the equations of static equilibrium are used. The test table is regarded to act as rigid body in the frequency range of interest and from the geometry of the test table and the instrumentation setup the following equations (applied to the measured time domain data of the individual load cells) can be derived, Figure 13-55:

$$\begin{aligned} F_x &= F_{x1} + F_{x2} + F_{x3} + F_{x4} \\ F_y &= F_{y1} + F_{y2} + F_{y3} + F_{y4} \\ F_z &= F_{z1} + F_{z2} + F_{z3} + F_{z4} \end{aligned} \quad [13-112]$$

$$\begin{aligned} M_x &= b * (F_{z1} + F_{z2} - F_{z3} - F_{z4}) \\ M_y &= a * (F_{z2} + F_{z3} - F_{z1} - F_{z4}) \\ M_z &= b * (F_{x4} + F_{x3} - F_{x2} - F_{x1}) + a * (F_{y4} + F_{y1} - F_{y2} - F_{y3}) \end{aligned} \quad [13-113]$$

Typical results obtained from further data post-processing are time histories of resulting moments and forces (filtered/unfiltered), moments and forces as function of frequency or the rotation speed of reaction wheel, and waterfall diagrams.

In order to allow assessing the time and costs impacts of performing a disturbance source characterisation test campaign it should be noted that such test campaign at the ESA Reaction Wheel Characterisation Facility might last about 8 to 10 days. The operational sequence includes the facility preparation and the test setup, the test execution, the preliminary data post-processing for the post-test review and the subsequent detailed data processing and reporting.

The particular issue of measuring micro-vibration disturbance levels at very low (cryogenic) temperatures has been dealt with in [30]. To perform the required high accuracy measurements the sensitivity fluctuations with the temperature need to be known for the high-sensitive and lightweight accelerometer to be used for the micro-vibration measurements. This calibration curve was acquired with the help of a classical, heavier accelerometer whose sensitivity at very low temperatures was known.

## 13.5 References

- [1] Eilers D., Kotzias B., Portigliotti S., "Microgravity environment dynamic disturbance study", Final Report, ESA Contract 7641/88/NL/PP, 1992
- [2] Eilers D., Kotzias B., Eckert L., Wollendorfer R., Szadeczky A., "Microgravity payload disturbance study (Volume 1)", Final Report, ESA Contract 10001/92/NL/PP, 1994
- [3] Marucchi-Chierro P. C., Ullio R., Destefanis S., Martini M., "Audible Noise and Micro-gravity Control of Pressurized Module Under On-Orbit Vibro-Acoustic Environment" European Conference on Spacecraft Structures, Materials & Mechanical Testing, Noordwijk The Netherlands, 2005
- [4] Ullio, R. "GOCE Micro-Vibration Control Plan", Thales Alenia Space Italy (TAS-I) document GO-PL-AI-0040, issue 01, 20-May-2003
- [5] Francesconi D., Marucchi-Chierro P. C., "Microgravity Control by Design: a Methodological Study of Numerical Acoustic/Structural Approaches for Manned Space Modules", 1st International Symposium Space Microdynamics and Accuracy Control, 1992
- [6] Marucchi-Chierro P. C., Ullio R., "Micro-gravity (micro-dynamic) test facility for disturbance sources characterization through indirect method technique", European Conference on Spacecraft Structures, Materials and Mechanical Testing, Noordwijk The Netherlands, 1996
- [7] Katsukawa, Y., et.al. "Pointing stability of HINODE and requirements for the next solar mission SOLAR-C", International Conference on Space Optics (ICSO), 2010
- [8] Ullio R., Marta F., "ARTEMIS micro-vibration environment prediction", European Conference on Spacecraft Structures, Materials and Mechanical Testing, Braunschweig Germany, 1998
- [9] Soula L. "Methodology for analysis of structure-borne micro-vibrations (METAMIC) – State of the art of structural micro-vibration analysis and test", Work Package Report, ESA Contract 4000101886/10/NL/RA, 2011
- [10] Soula L., Laduree G. "Modelling micro-vibrations by finite element model approach", European Conference on Spacecraft Structures, Materials & Environmental Testing, Noordwijk The Netherlands, 2012
- [11] Aglietti G. "Methodology for analysis of structure-borne micro-vibrations - Disturbance source modeling and associated experimental techniques ", Technical Note 2, ESA Contract 4000101914/10/NL/RA, 2010
- [12] Pradines A., et al. "Development of the microvibrations analysis software  $\mu$ Vision for Earth observation applications", European Conference on Spacecraft Structures, Materials and Mechanical Testing, Toulouse France, 2002
- [13] Carte G., Spalinger E., "Strategies in micro-vibrations predictions for high resolution Earth observation satellites", European Conference on Spacecraft Structures, Materials & Mechanical Testing, Toulouse France, 2009
- [14] ESSB-HB-E-003, ESA Pointing Error Engineering Handbook, Issue 1, July 19 2011
- [15] Jourdon N., Guillaud V., "Influence of microvibrations on spacecraft performances", European Conference on Spacecraft Structures, Materials and Mechanical Testing, Noordwijk The Netherlands, 1991
- [16] Privat, M. "On ground and in orbit micro-vibrations measurement comparison", 8th European Symposium on Space Mechanisms and Tribology, ESA-SP-438, 1999

- [17] Munoz Sevilla L., "Microvibration tests of the ARTEMIS structural model", European Conference on Spacecraft Structures, Materials and Mechanical Testing, Braunschweig Germany 1998
- [18] Grillenbeck A., Deutsch G., Pouilloux B. "Micro-vibration measurements on thermally loaded multi-layer insulation samples" 1st CEAS European Air and Space Conference (CEAS), Berlin Germany, 2007
- [19] Bialke B., "Microvibration disturbance fundamentals for rotating mechanisms", 34th Annual Guidance and Control Conference, American Astronautical Society, 2011
- [20] Stromswold E., Bialke B., "Behavior of reaction wheels near zero speed", 27th Annual Guidance and Control Conference, American Astronautical Society, 2004
- [21] Seiler R., Allegranza C. "Mechanism noise signatures: identification modelling", ESA SP-670, 13th European Space Mechanisms and Tribology Symposium (ESMATS), 2009
- [22] Laurens P., Decoux E. "Microdynamic behaviour of momentum and reaction wheels", Proceedings of the 2nd Space Microdynamics and Accurate Control Symposium, Toulouse France, 1997
- [23] De Weck O., Miller D. "Integrated modelling and dynamics simulation for the Next Generation Space Telescope (NGST)", MSc Thesis, Massachusetts Institute of Technology, 1999
- [24] Specht B., "Dynamic simulation of scan mechanism with electrical drive unit", European Conference on Spacecraft Structures, Materials & Mechanical Testing, Braunschweig Germany, 1998
- [25] MECHMACS - Library of mechanical building blocks for MATLAB/Simulink, BAUSCH-GALL GmbH, <http://www.bausch-gall.de>
- [26] Kim Y. A., "Thermal creak induced dynamics of space structures", PhD Thesis, Massachusetts Institute of Technology, 1999
- [27] Elias, L. M., Miller, D. W. "A coupled disturbance analysis method using dynamic mass measurement techniques", 43rd AIAA/ASME/ASCE/AHS/ASC Structures, Structural Dynamics, and Materials Conference, Denver USA, 2002
- [28] TEC-TCP/2011/59/MW, ESA Reaction Wheel Characterisation Facility Description , issue 2, November 2011
- [29] Wagner M., et al. "ESA New Reaction Wheel Characterisation Test Facility (RCF)", European Conference on Spacecraft Structures, Materials and Environmental Testing, Noordwijk The Netherlands, 2012
- [30] Clerc C., Duvermy L. "Herschel / Planck project: Microvibration measurement at low temperature", European Conference on Spacecraft Structures, Materials & Mechanical Testing, Toulouse France, 2009

# 14

## Soft stowed packaging

### 14.1 Introduction

The transport of sensitive electronic and mechanical hardware systems to the International Space Station on board the cargo carriers currently used, e.g. ATV, HTV or Progress, and the Space Shuttle used in the past has often employed “soft stowed packing” of these items. The term “soft stowed packaging” refers to conditions where the cargo items are not attached to the internal structure of the transport vehicle in a typical hard mounted configuration but wrapped in foam or bubble-wrap. They are then allocated in strapped bags or hard containers that are restrained to the vehicle internal structures (as e.g. racks or adapter plates).

A typical foam packaging of a cargo item is shown in Figure 14-1. The left picture, taken from [1], shows the pieces making up the “packed payload” which is then put into a typical Cargo Transfer Bag (CTB) for stowage inside the cargo rack.



Figure 14-1: Typical foam packaging of cargo items

Foam packing offers a soft, highly damped and distributed system of support for space flight hardware items. As a result, highly isolated/mitigated load environments are created resulting in simplified hardware certification, lower structural weight, easier physical hardware integration and de-integration, greater probability of mission success, etc. Furthermore, the exploitation of the damping effects of the available foams offers increased flexibility for the transportation of the cargo items in soft stowed conditions with several of the available carriers.

Existing requirement documents do not specifically address the verification of items packed in foam since they are usually oriented towards hardmounted verification aspects. This chapter provides some guidelines to assess the compatibility of the cargo item with the attenuated environments found for soft stowed packaging, by defining the tests which should be performed and/or the analyses to satisfy the requirements.

## 14.2 Packaging guidelines

When the general cargo item compatibility with the candidate cargo carriers has been identified (in terms of dimensions, allocation, pressurization & temperature environment, need of power, etc.) the hardware mechanical compatibility with respect to the chosen vehicle requirements can be obtained by using soft stowed packaging solutions.

An extensive test campaign, performed by Boeing in 2009 under NASA responsibility, confirmed the foam capability in significantly attenuating the applicable vibration environments: sinusoidal, random and shock. These environments are drastically reduced in the case of soft packaging conditions, in particular in the upper frequency range.

In general, the governing isolation system characteristics should:

- be relatively soft and have high damping characteristics,
- assure that the isolation material and area of contact are such that the material adequately supports the cargo item and assists in avoiding excessive shock induced motions,
- yield a low resonance frequency and a greater isolation that begins at lower frequencies, while not resulting in excessive amplifications due to potential coupling with the launch vehicle transient excitations.

Once the available cargo item integration method (either bag or container) has been identified for the selected cargo carrier it is important to choose the correct foam for a proper and efficient packaging of the hardware.

The mechanical attenuation of random, sinusoidal and shock environments due to soft-packaging is treated in Section 14.3.2.

In general, the cargo developer should

1. specify to the cargo integrator the cargo item flight packaging configuration, or
2. deliver the cargo item in its final packaging configuration.

In the first case, the cargo integrator follows the cargo developer indications. If this is not possible, the cargo integrator should propose an alternative solution with proper justification to be agreed with the cargo developer.

Guidelines for packaging of particular cargo items, in terms of "shape" or "sensible parts" are reported in Section 6 of MIL-HDBK-304C, [2].

A correct packaging should also take into account:

- the need to preserve certain areas (connectors, quick disconnectors, tubing) or protuberating parts of the hardware surface to prevent the contact with the foam during transport and launch phases,
- the need to avoid sharp edges/hard points in contact with the rest of the item (i.e. quick disconnects on lines connected to the hardware),
- the need to know whether the cargo item hardware contains batteries, liquids, brittle materials (like glass) or other objects that would result in an hazard for the launch vehicle or the crew,
- the maximum allowable foam compression in order to maintain the foam in a region of desirable and approximately constant Young's modulus (E).

Note: For this purpose it is common practise to limit the foam average compression to approximately 25% of its thickness.

It should be underlined that the vehicle *quasi-static loads* are not significantly influenced by soft stowage dampening effects. The static deflections of the foam wrapping the hardware should therefore be systematically evaluated, considering the

- quasi-static accelerations (limit load factors) experienced by the hardware,
- the contact area between the foam and the hardware, and
- the foam properties.

The foam materials commonly used for packaging are reported in Section 14.3.1.

## 14.3 Materials for packaging

### 14.3.1 Physical properties

#### 14.3.1.1 Introduction

This section summarizes the typical physical properties of the packaging materials most commonly used:

- Minicel
- Pyrell
- Zotek
- Plastazote
- Bubble Wrap

Furthermore, stress-strain diagrams obtained from static compression tests performed by NASA JSC for different thicknesses ( $\frac{1}{2}$ , 1 and 2", respectively) of Minicel, Pyrell and Zotek foam are provided, [3]. It should be noticed that the strength characteristics are slightly depending on the thickness of the foam layer being subjected to the compression forces.

The typical compression stress versus strain characteristics for low density foams used for soft stowed packaging are shown in Figure 14-2. In this diagram the following characteristic stress values and distinct regions can be identified:

1. The stress  $\sigma_A$  indicates the end of the (quasi-)linear relationship between stress and strain (segment OA) and the related strain  $\varepsilon_A$  is usually not more than about 5 - 10%. The foam modulus of elasticity (Young's modulus) is defined by the slope of OA.  
 $\sigma_A$  determines also the ultimate stress which the foam can withstand without failure of its macrostructure and which is recommended to be used for the evaluation of the compressive strength of the foam as load-carrying element.
2. The stress  $\sigma_B$  indicates the end of a flexural deformation process taking place in the cell walls and causing the walls to loose stability (buckling of cells).  $\sigma_B$  corresponds to the maximum possible compaction of damaged elements of the foam macrostructure. The related strain  $\varepsilon_B$  indicates approximately 70% compression.
3. Beyond the stress  $\sigma_B$  is there is "flattening" of the foam due to the damaged elements of the foam macrostructure (densification zone). In this region the cell walls are almost completely collapsed and the foam cell structures are interfering directly with each other.

When recording both the loading and unloading of the compression test samples the deflection curve provides valuable information regarding the energy absorption and impact cushioning characteristics of the foam material, [4]. The amount of energy absorbed by the foam material during the compression is indicated by the area between the distinct deflection curves for the loading and unloading process. This hysteretic behaviour is illustrated in the NASA JSC stress-strain diagrams where both curves are shown and the unloading deflection curve is always below the respective loading curve.

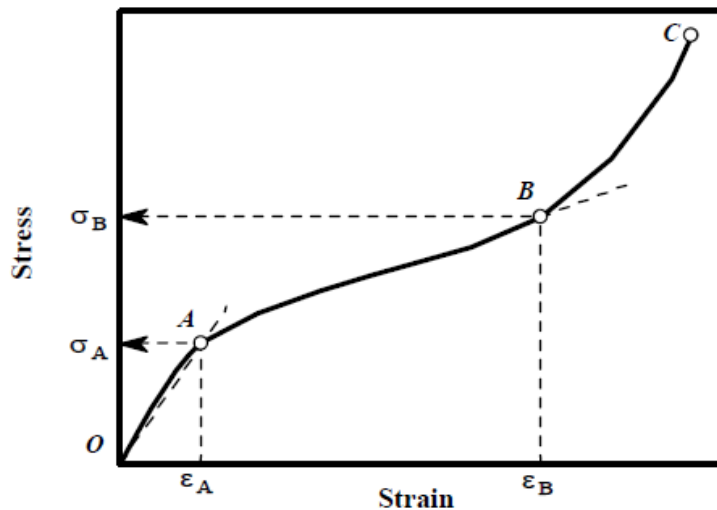


**Figure 14-2: Typical foam compression stress-strain characteristics [5]**

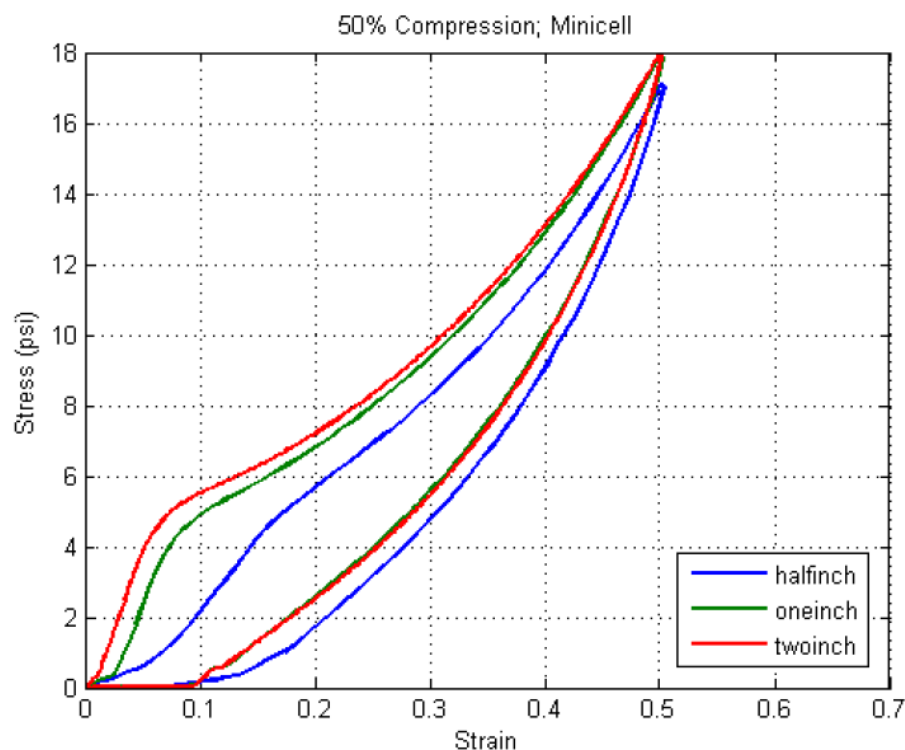
#### 14.3.1.2 Minicel

Minicel is a closed-cell cross-linked polyethylene foam resulting to a smooth surface with a very fine cell structure. There are different types of Minicel manufactured by Sekisui Voltek. The main characteristics listed in Table 14-1 are referring to Minicel L200, L300 and L380 which are especially suited for e.g. cushion packaging, [6].

Stress-strain diagrams obtained from Minicel L200 compression tests performed by NASA JSC are shown in Figure 14-3.

**Table 14-1: Minicel foam properties (for L200, L300 and L380 types), [6]**

Property	Test Method	Typical Values		
		L200	L300	L380
Density [kg/m <sup>3</sup> ]	ASTM D3575-84	32.1	48.1	60.9
Compression strength [kPa] (25% deflection)	ASTM D3575	48.3	74.5	99.3
Compression set (% of original thickness)		12.7	11.1	10.4
Tensile strength [kPa]	ASTM D3575-84	216.5	341.3	443.3
Elongation to break [%]		156	179	195
Tear strength [N/m]		981	1576	2066
Temperature range [°C]		-79 / +102		

**Figure 14-3: Minicel L200 compression tests (from NASA JSC, 1 psi = 6.895 kPa)**

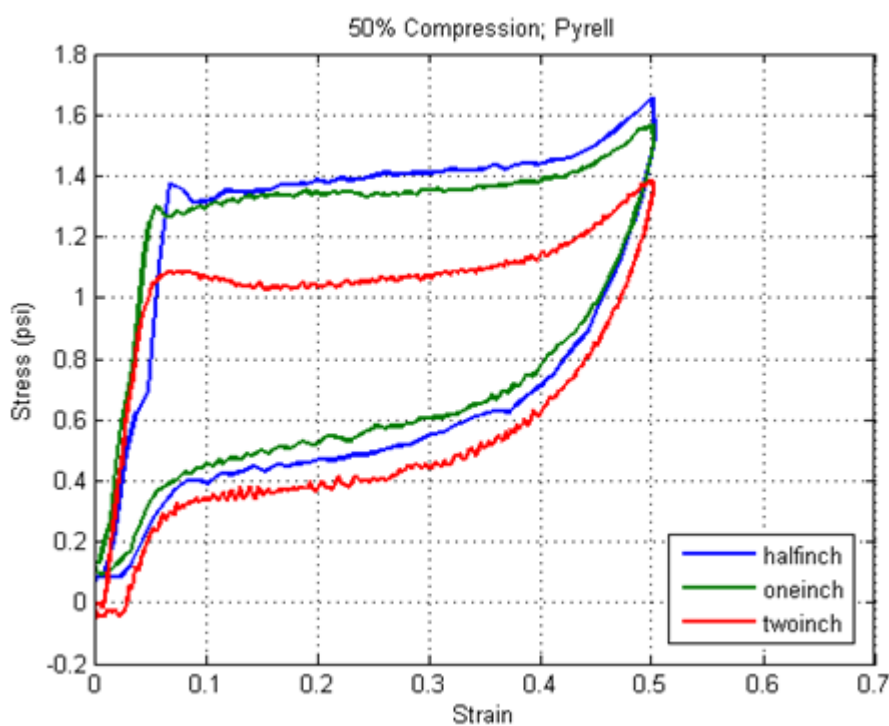
**14.3.1.3 Pyrell**

Pyrell® foam is a flexible polyester polyurethane open cell foam. The data reported in Table 14-2 are referring to the Pyrell foam manufactured by Foamex [7]. It should be noted that Pyrell is by far the “softest” foam when comparing its compression strength at 25% deflection with those of the Minicel, Zotec F30 and Plastazote LD33 foams having similar density.

Stress-strain diagrams obtained from Pyrell compression tests performed by NASA JSC are shown in Figure 14-4.

**Table 14-2: Pyrell foam properties [7]**

Property	Test Method	Typical Values	
Density [kg/m <sup>3</sup> ]	ASTM D3575-84	32.1	64.1
Compression strength [kPa] (25% deflection)	ASTM D3575	4.8	7.6
50% compression set (% of original thickness)		10	12
Tensile strength [kPa]	ASTM D3575-84	151.7	172.4
Elongation at break [%]		210	200
Tear strength [N/m]		438	525
Temperature range [°C]		-40 / +107	

**Figure 14-4: Pyrell compression test (from NASA JSC, 1 psi = 6.895 kPa)**

#### 14.3.1.4 Zotek

Zotek is a closed-cell foam. The data reported in Table 14-3 are referring to Zotek F30 [8] made from Kynar PVDF (poly vinylidene fluoride) available in sheet form.

Stress-strain diagrams obtained from Zotek F30 compression tests performed by NASA JSC are shown in Figure 14-5.

**Table 14-3: Zotek F30 foam properties [8]**

Property	Test Method	Typical Value
Density [kg/m <sup>3</sup> ]	ISO 845	30.5
Compression strength [kPa] (25% deflection)	ISO 7214 (1 <sup>st</sup> compression)	46.9
Compression set (% of original thickness)	ASTM D3575-84	12.7
Tensile strength [kPa]	ISO 1798	399.9
Elongation at rupture [%]		151.0
Tear strength [N/m]	ISO 8067	1051.0
Max. operating temperature [°C]		110

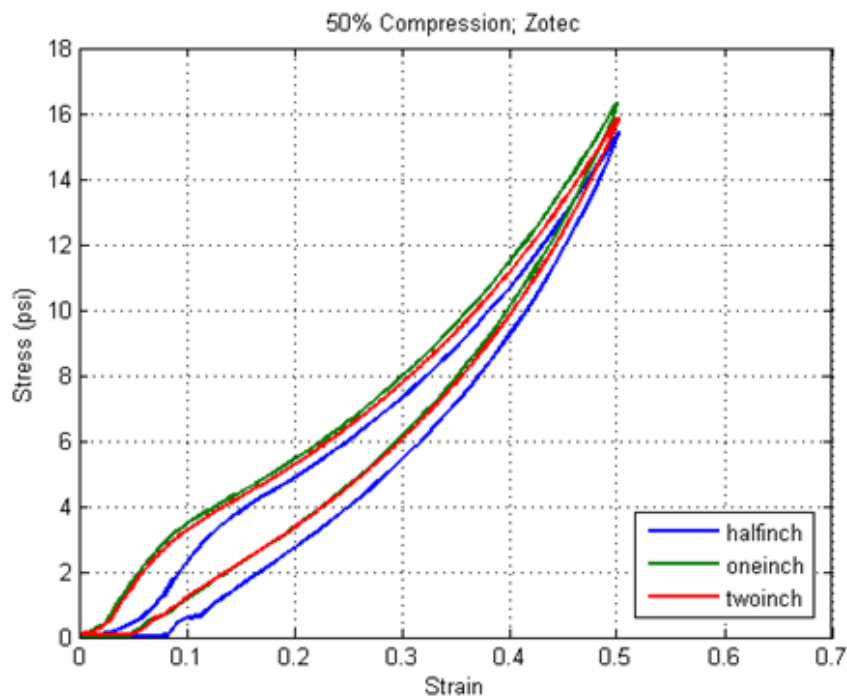


**Figure 14-5: Zotek F30 compression test (from NASA JSC, 1 psi = 6.895 kPa)**

#### 14.3.1.5 Plastazote

Plastazote is a closed cell cross-linked polyethylene foam available in sheet form [9]. Typical physical properties of the Plastazote low density foam types LD24FR, LD33 and LD45FR are listed hereafter in Table 14-4 and the respective compression strength curves are compared in Figure 14-6.

Note: At the time of writing this handbook data sheets for Plastazote foams were available from several sources showing significantly different compression strength values e.g. for LD24FR, LD33 and LD45FR. These differences are due to different test standards being applied. The supplier Zotefoams Inc. has confirmed that the data sheets available from Quality Foam Packaging Inc. are the ones that should be used.

**Table 14-4: Plastazote foam properties [9]**

Property	Test Method	Typical Values		
		LD24FR	LD33	LD45FR
Density [kg/m <sup>3</sup> ]	BS ISO 7214 1998	24	33	45
Compression strength [kPa] (25% deflection)	BS ISO 7214 1998	51	69	86
Compression set (% of original thickness), 25% compression, 22 hr, ½ hr recovery	BS ISO 7214 1998	13	10	8.5
Tensile strength [kPa]	ISO 7214 1998	240	440	435
Elongation at break [%]		115	155	180
Tear strength [N/m]	BS EN ISO 8067 1995	475	785	1200
Temperature range [°C]		-70 / +100		

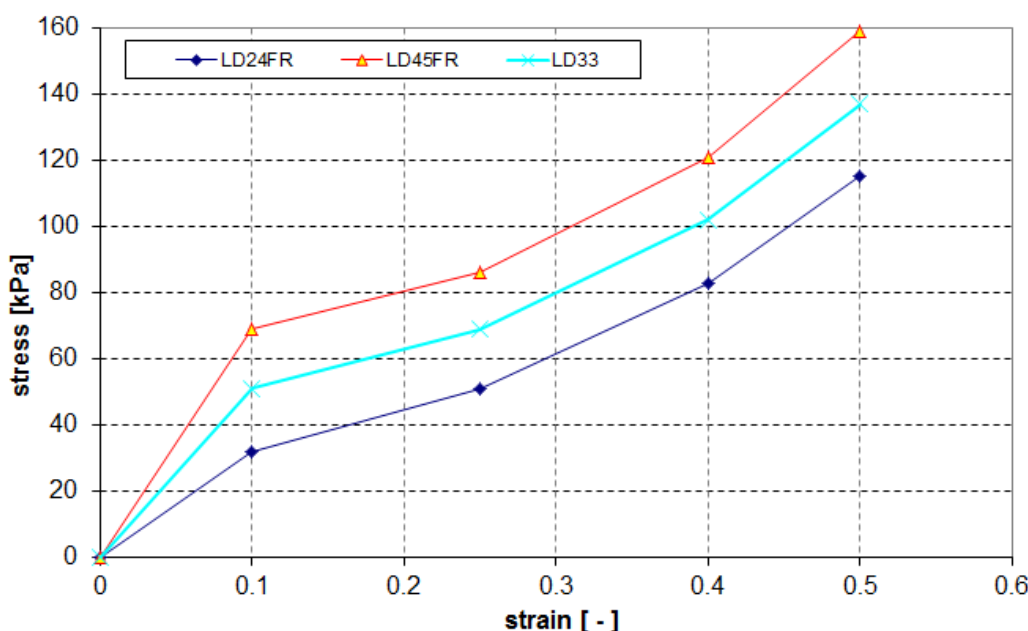


**Figure 14-6: Stress strain characteristics of Plastazote foam types**

### 14.3.1.6 Bubble Wrap

Bubble Wrap mentioned here refers to type SECO 88 manufactured by Seco Industries, 6909 East Washington Blvd, Montebello, CA 90640. However, no supplier data sheet is available.

In order to provide an indication of the Bubble Wrap mechanical characteristics the stress-strain diagrams obtained from NASA JSC compression tests for material thicknesses of  $\frac{1}{2}$ , 1" and 2", respectively, are provided in Figure 14-7.

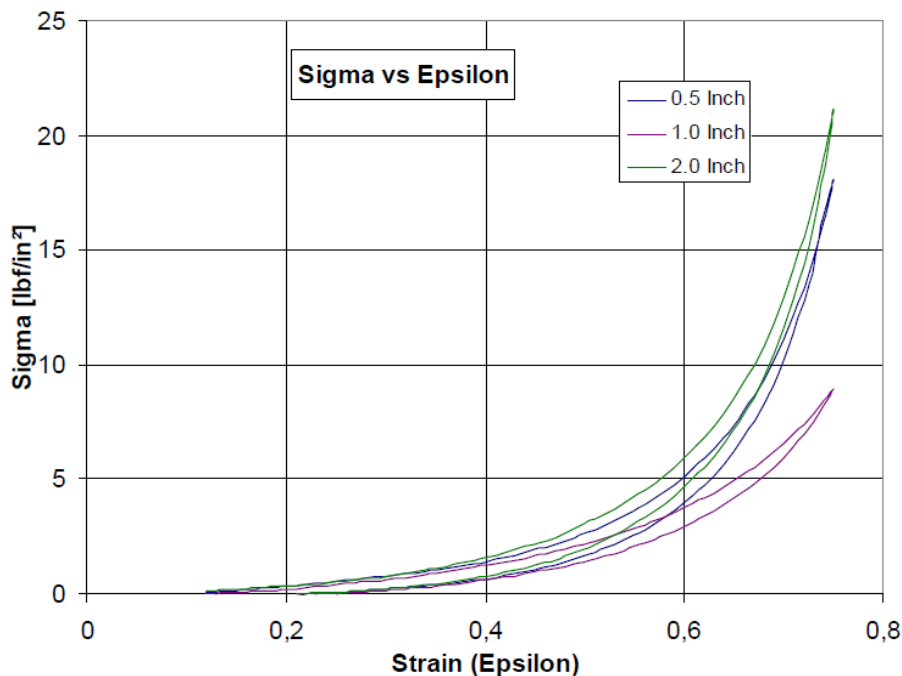


Figure 14-7: Stress strain characteristics for Bubble Wrap (1 psi = 6.895 kPa)

### 14.3.1.7 Foam safety aspects

As reported in [10] for materials that are considered unacceptable because of flammability (Pyrell, Minicel, Bubble Wrap) it should be underlined that their overwrapping in Nomex Bag negates these problems.

Whether possible concerns related to Zotek, Minicel and Pyrell electro-static discharge behaviour are valid is still under investigation by NASA. It is however common practice to enclose the hardware in a foil of LABESTAT A100 (multilayer antistatic polyethylene) prior of wrapping it into the chosen foam.

## 14.3.2 Attenuation data for foam packed items

### 14.3.2.1 Introduction

This section summarizes the vibration attenuation capabilities, related to the different foam types (Pyrell, Minicel and Zotek). The random vibration attenuation data are derived from the results of tests conducted at NASA JSC for end items packed in foam or bubble wrap inside hard containers ("component foam vibration tests") and inside soft stowed bags ("system foam vibration tests"), respectively. The first tests aimed at simulating the relevant dynamic properties and obtaining related SDOF attenuation data whereas the latter simulated the bag dynamics in order to obtain packaged attenuation data. Detailed test results are reported in Appendix I of [10] and annex A4 of [3].

For foam packed items the attenuation curves are influenced by the

- type of item accommodation (hard container or CTB),
- item weight ( $W$ ),
- foam thickness ( $t$ ),
- contact area ( $A$ ) between foam and item,
- weight per area ratio ( $W/A$ ).

The attenuation curves provide the information needed to calculate the expected flight random environments of cargo items for the respective cargo carriers (e.g. ATV or HTV) and for different packing configurations. The procedure that should be followed is presented in Section 14.4.4.2.3.

#### 14.3.2.2 Accommodation in hard containers

The test setup for the vibration tests is shown in Figure 14-8. A rigid mass of weight  $W$  is supported by a cylindrical isolation material sample of thickness  $t$ . From this test the dynamic responses of cargo items being accommodated inside hard containers with foam wrapping were determined.

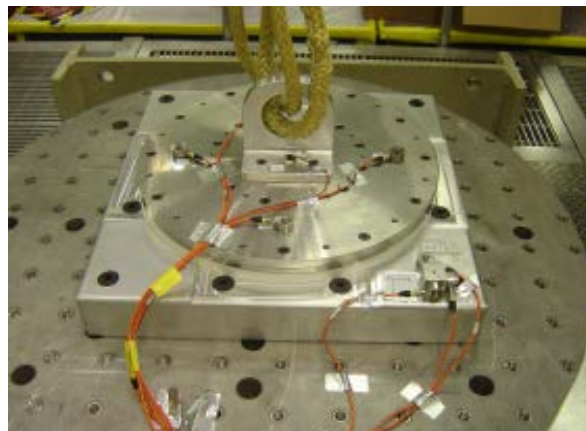


**Figure 14-8: Test set-up for assessment of cargo item dynamic responses when accommodated in a hard container**

In the following plots the random vibration attenuation capability of three different foams (Pyrell, Minicel and Zotek) is compared. A package inside a hard container with a foam thickness of  $\frac{1}{2}$  and 2 inches, respectively, and a  $W/A$  ratio of 0.2 psi is considered.

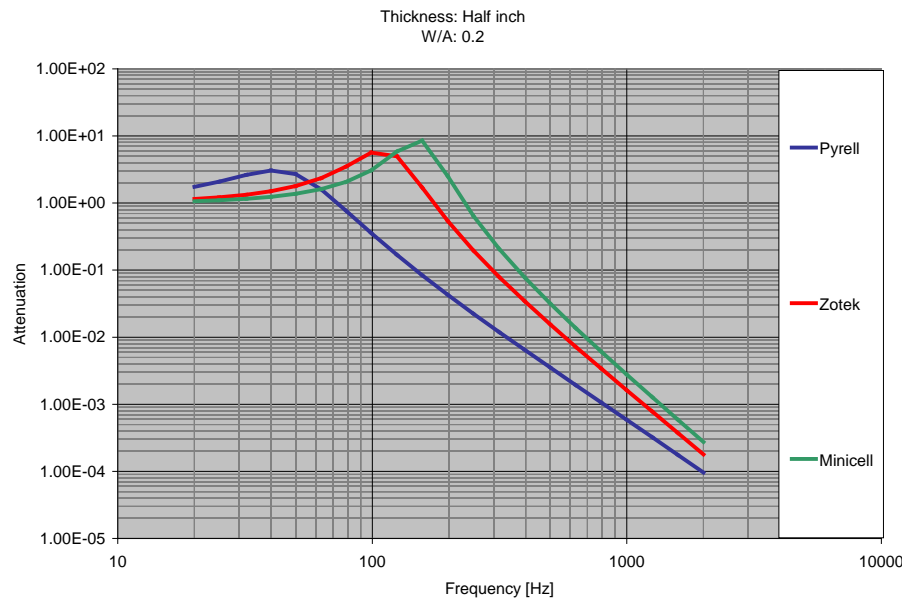


**Figure 14-9: Attenuation of  $\frac{1}{2}$  inch foam (W/A=0.2 psi)**

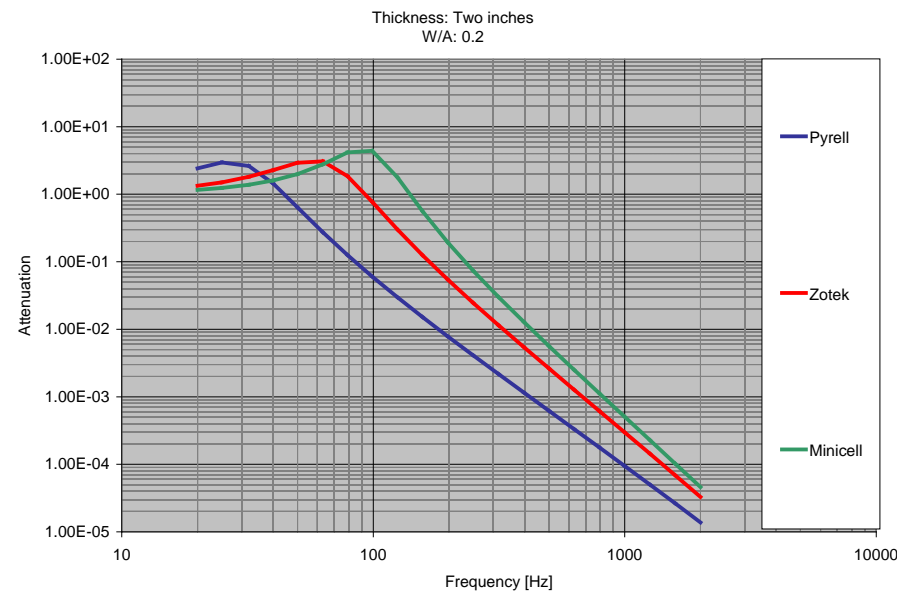


**Figure 14-10: Attenuation of 2 inch foam (W/A=0.2 psi)**

From Figure 14-9 and Figure 14-10, Pyrell appears to be the foam with the lower peak of the random attenuation factor ( $Q^2$ ) as compared to Zotek and Minicel. However, Pyrell also exhibits a significantly lower resonance frequency which is in line with the fact that its compression strength characteristics are significantly lower than those for the other foam materials as mentioned before in Section 14.3.1.3.

In Figures Figure 14-11, Figure 14-12 and Figure 14-13 the envelopes of the attenuation curves with different W/A ratios (0.2 psi to 0.7 psi) are reported for a foam thickness of  $\frac{1}{2}$ , 1 and 2 inch, respectively. The different foam response behaviours are also confirmed by the envelope plots.

In conclusion, for items packed inside hard containers it is more useful to use softer, thicker, and slightly more heavily damped materials (like Pyrell or Bubble Wrap).

In addition, for heavier end items (e.g. W/A = 0.7 psi) the resonance frequencies (and hence the attenuation curves) are shifted to the left, improving the attenuation at higher frequencies. However, care should be taken that the drop of the resonance frequency of the cargo item / foam system does not interfere with any low frequency dynamic excitations induced by the launch vehicle.

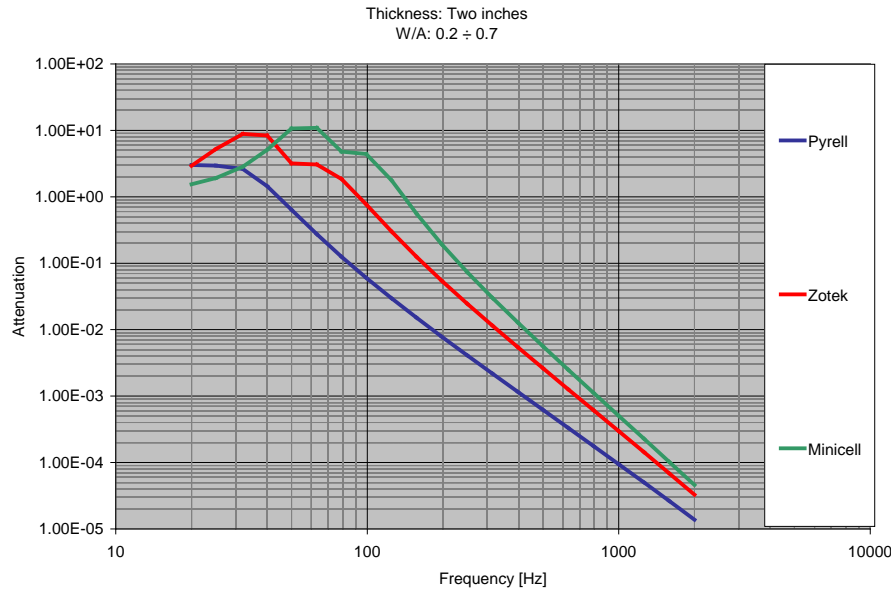


**Figure 14-11: Attenuation envelope of 2 inch foam (W/A=0.2 to 0.7 psi)**

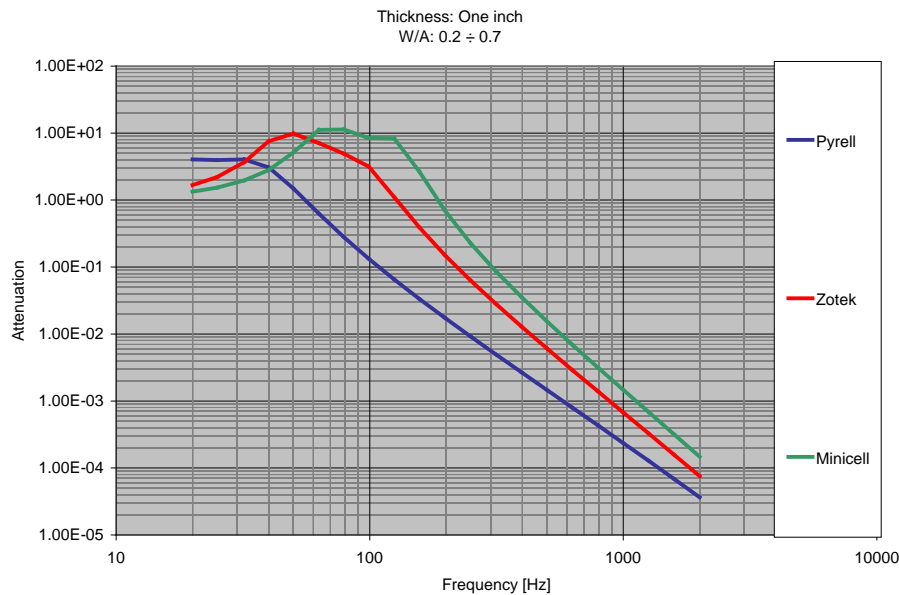


**Figure 14-12: Attenuation envelope of 1 inch foam (W/A=0.2 to 0.7 psi)**

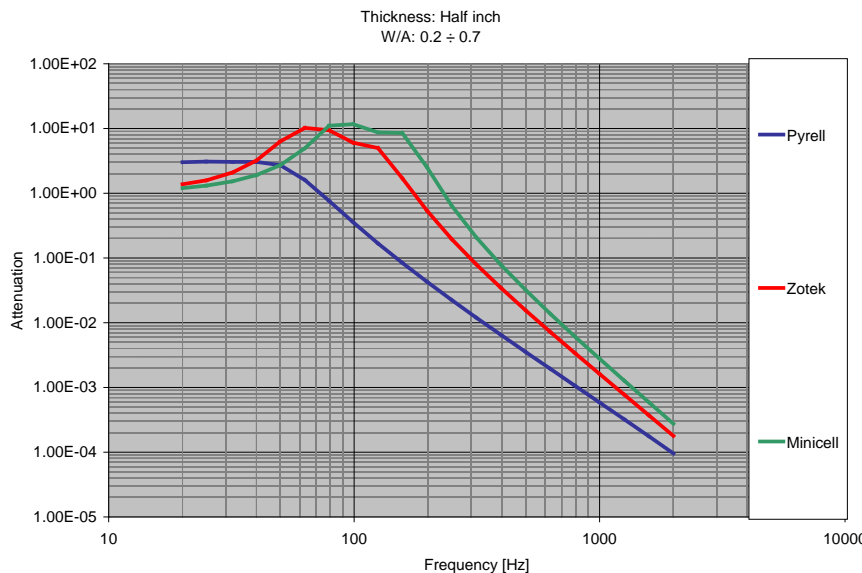


**Figure 14-13: Attenuation envelope of  $\frac{1}{2}$  inch foam ( $W/A=0.2$  to  $0.7$  psi)**

#### 14.3.2.3 Accommodation in strapped Cargo Transfer Bags (CTB)

The test setup for the vibration tests to determine the dynamic responses of cargo items when being accommodated inside soft stowed bags with foam wrapping around them is shown in Figure 14-14. In these tests mass simulators were packed in isolation materials (foam), enclosed in bags and strapped to the vibration shaker table.

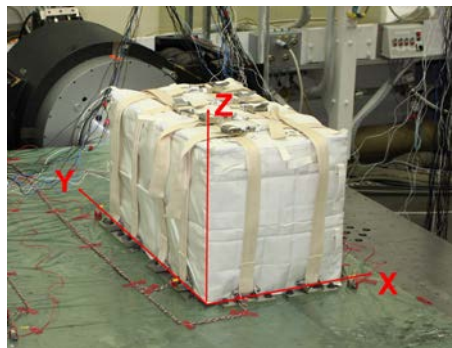


**Figure 14-14: Test set-up for assessment of cargo item dynamic responses when accommodated inside soft stowed bag**

In case the item wrapped in foam is accommodated inside a soft stowed bag (CTB) then there is an increase of the attenuation with respect to the packaging with foam alone and also with respect to the accommodation inside a hard container, as shown in Figure 14-15. Also in this case, the vibration of the heavier end item is attenuated more than that of the lighter one. It should be however noted that the constant attenuation factor of 0.001 in the high frequency range for the item inside the strapped Triple CTB is an artifact because the tabulated attenuation values used to construct this curve were set to 0.001 if being equal or less than this value. In reality the attenuation should decrease in the high frequency range with the same slope as seen e.g. between 70 and 150 Hz.

In addition the attenuation, in case of using a strapped CTB, is also a function of the excitation axis shown in Figure 14-14. For example, Figure 14-16 reports the comparison of the attenuation function in-plane and out-of-plane for an item packed in a M01 bag: for the in-plane excitation axes (X & Y

directions) the influence of the belts constraints is more evident than for the out-of-plane excitation axes (Z direction). In particular the shape of the response curve for the Z direction is very similar to those seen for the “items accommodated in hard containers”, Figure 14-9 to Figure 14-13. This becomes immediately evident when comparing the load path in the axial direction for the item inside the CTB and the test mass on top of the cylindrical isolation material, Figure 14-8, respectively. The attenuation curves for the in-plane excitation axes (X & Y) do not show the characteristic amplification at the resonance frequency. However, as experienced during similar bag testing in the frame of the ATV Enhancement activity these resonances occur at very low frequencies for even quite common cargo item masses and are therefore not seen in this figure because the low frequency range under 20 Hz has been excluded.

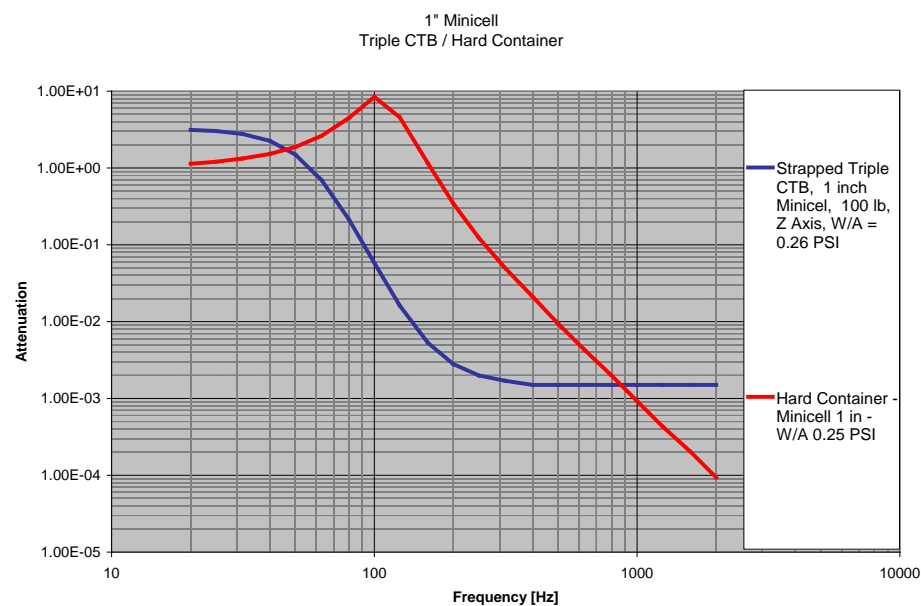


**Figure 14-15: Attenuation for items packed in Minicel inside a hard container and inside a Triple CTB**

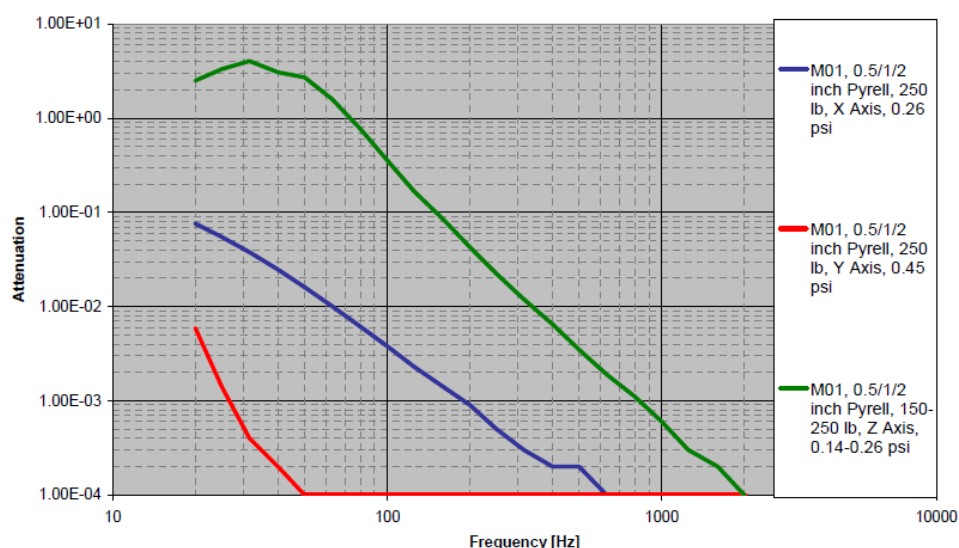


**Figure 14-16: Attenuation for items inside strapped soft bags (in-plane X & Y and out-of-plane Z attenuation)**

It should be further noted that the attenuation curves for the “items accommodated in hard containers”, Figure 14-9 to Figure 14-13, appear to be applicable, too, for cargo items soft stowed in CTB’s but where these CTB’s are then placed inside the rack compartments and safeguarded by belts. This conclusion is based on the evaluation of dummy cargo responses measured during the ATV PFM acoustic noise test where these response curves (for all directions) were found to show similar characteristics as seen in Figure 14-9 to Figure 14-13. For these particular CTB accommodation cases the rack panels surrounding the compartment might be assumed to form the “hard container”.

A full set of attenuation factors, related to items packed in different types of foam and with different foam thicknesses, inside soft bags or hard containers is provided in [10].

## 14.4 Soft stowed equipment verification flow

### 14.4.1 Hardware categories and criticality

The guidelines provided hereafter for the verification of soft stowed equipment concern two different hardware categories:

- Usage of off-the-shelf (OTS) items and already existing equipment, and
- Development of new space equipment / hardware.

The methods to achieve the structural verification of the applicable requirements are slightly different for these categories and are also depending on the definition of the cargo item criticality, i.e. whether safety critical, reliability critical or not critical. The latter categorization of the equipment to be launched in a soft stowed condition also determines the model philosophy to be applied for the requirement verification.

### 14.4.2 General verification aspects

#### 14.4.2.1 Introduction

The mechanical verification of any equipment whether an OTS item, an existing equipment or a new space hardware development comprises the following:

- Strength verification (including flight quasi-static accelerations, belt tightening loads, and loads imposed by adjacent bags),
- Verification of compatibility with the flight dynamic environments (sine, random vibration, shock).

The particular aspects of the strength verification for soft stowed equipment are outlined in detail in Section 14.4.2.2.

The verification of the compatibility with the applicable flight dynamic environments of the selected launch vehicles and cargo carriers adopts the foam attenuation factors as already reported in the previous sections for different packaging configurations. It should be however noted that the verification methodology, i.e. the model philosophy, the tests to be performed, the minimum test levels to be applied and the required workmanship verification, might differ with respect to the agency responsible for the cargo integration, the launch service provider and the authority under which responsibility the equipment is finally operated on board or as external payload to the International Space Station (ISS).

- Verification methodology for non safety critical items procured by ESA and being operated in space by ESA

For new space hardware / equipment a prototype approach is recommended based on the usage of two hardware sets: a Qualification Model (QM) for verification testing and one or more Flight Models (FM) for flight).

Preference should be given to perform the verification tests in soft mounted conditions to ensure that the test configuration and, as a result, the loading of the soft stowed equipment is as representative as possible with respect to the flight configuration. Verification tests in hard mounted conditions might be however performed if agreed by the supplier.

In general dedicated workmanship testing in hard mounted condition is not required as part of the acceptance process when relevant random vibration tests in soft mounted conditions are performed. However, such test might be still recommendable in particular for electronic and electrical equipment below 50 kg. The test input to be applied at the shaker table should be the envelope of the expected (attenuated) flight random vibration environment and the Acceptance Vibration Test (AVT) levels as given in Table 14-5. The AVT is considered the minimum test level sufficient to detect workmanship defects for some particular hardware.

If workmanship tests in hard mounted condition are part of the FM acceptance campaign then a corresponding test should be performed for the QM in order to ensure that no unexpected equipment / hardware structure integrity problem occurs when the FM is subjected to the AVT levels, in particular in those frequency ranges where the attenuation effects of the soft stowed packaging have largely reduced the input levels applied during the qualification tests in soft-mounted condition.

**Table 14-5: Acceptance Vibration Test (AVT), minimum workmanship test level [11]**

Frequency [Hz]	Level	
20	0.01	$g^2/Hz$
80-350	0.04	$g^2/Hz$
2000	0.007	$g^2/Hz$
overall	6.06	$g_{rms}$

- Verification methodology for items procured by ESA but being operated in space by other space agencies or for safety critical items

The verification procedures of the respective agencies should be followed e.g. for NASA as specified in SSP 52005, [12], and SSP 41172, [11], respectively.

In general the verification approach outlined in Section 14.4.3 for OTS items and already existing equipment and in Section 14.4.4 for new equipment / hardware follows the one recommended for items procured by ESA and being subsequently operated in space by ESA. More rigorous verification methodologies covering the variety of available cargo carriers as well as the requirements imposed by the corresponding launch authorities and other space agencies under which the equipment is operated in space are described in more detail in [3].

#### 14.4.2.2 Strength verification

##### 14.4.2.2.1 Introduction

Due to the soft stowed configuration, in addition to the flight quasi-static loads resulting to inertia loads, the cargo item is also loaded by a foam pressure. The latter can be evaluated mainly on the basis of quasi-static accelerations and belt preload (as indicated hereafter); it is therefore recommended to

identify an allowable compression pressure  $p_{all}$  for the estimation of a relevant margin of safety (MoS).

For items already qualified, this MoS value can be obtained from available documentation and performed verification campaigns but it cannot be excluded that specific additional investigations might become necessary.

As already mentioned in Section 14.2 the maximum foam compression should be limited such to maintain the foam in a region of desirable and constant Young's modulus (E). It is common practise to limit the foam average compression to approximately 25% of its thickness for that purpose.

#### 14.4.2.2.2 Flight quasi-static accelerations

If  $M$  is the mass of the cargo item, then Eq. [14-1] gives the average value of pressure  $p_1$  due to a quasi-static acceleration load  $n \cdot g$  acting along a given axis (e.g. X axis) on an effective area  $A_{eff}$  of the cargo item perpendicular to this axis:

$$p_1 = \frac{M \cdot n \cdot g}{A_{eff}} \quad [14-1]$$

Note:  $n$  represents the quasi-static acceleration, in a given direction, of the chosen cargo carrier. It is assumed that the pressure  $p_1$  is mainly due to this quasi-static acceleration load, neglecting the potential influence of other loading effects.

#### 14.4.2.2.3 Belt tightening load

The belt preload  $P$  is creating in the foam a pressure  $p_2$  which depends on the belt width  $W$  and the length  $L$  where  $L$  conforms to the bag dimension in the belt direction and on the bag belted face perpendicular to the considered pressure axis.  $p_2$  is varying inside the foam with the distance from the mentioned bag belted face, from a maximum value of  $2P/WL$  to a minimum depending on the shear-lag effect inside the foam.

If a shear-lag angle of  $45^\circ$  is assumed for the introduction of such a pressure into the foam, then a corresponding  $w_i$  can be computed for each belt. If  $k$  is the total number of parallel belts acting simultaneously on the same cargo item surface, then the corresponding pressure  $p_2$  is given by Eq. [14-2]:

$$p_2 = 2 \frac{P}{L} \sum_{i=1}^k \frac{1}{w_i} \quad [14-2]$$

Table 14-6 provides some examples of possible positions of cargo items with respect to the belts and shows how the pressure  $p_2$  can be calculated under the assumption that the belt compressed area is spread out at an angle of  $45$  degree.

#### 14.4.2.2.4 Loads due to adjacent bags

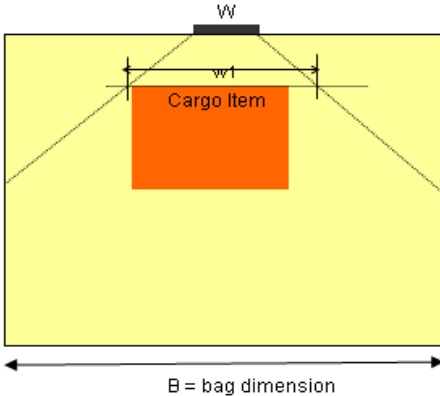
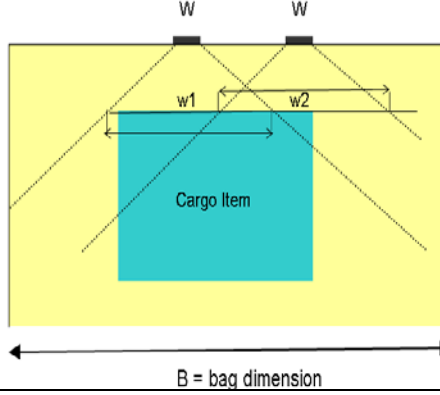
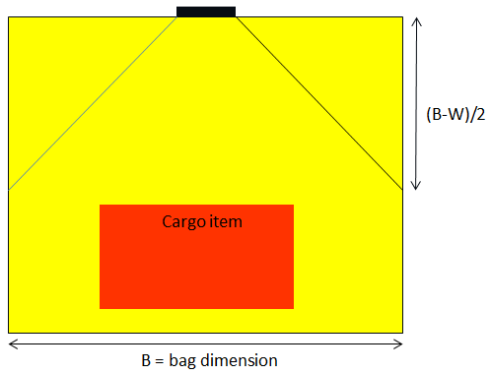
In case more bags are in contact with each other during their transportation the effects of adjacent bag inertia loads induced on the cargo item should be evaluated following the same approach.

If  $M_{bag}$  is the mass of the bag adjacent to the bag in which the cargo item is soft stowed, then Eq. [14-3] gives the average value of pressure  $p_3$  due to a quasi-static acceleration load  $n \cdot g$  along a given axis (e.g. X axis) on the contact area  $A_{bag}$  between the adjacent bags :

$$p_3 = \frac{M_{bag} \cdot n \cdot g}{A_{bag}} \quad [14-3]$$

For the quasi-static acceleration factor  $n$  the same note as mentioned above in Section 14.4.2.2.2 is applicable.

**Table 14-6: Estimation of pressure  $p_2$  depending on cargo item position with respect to belt(s)**

Example	Configuration	Pressure estimate
1 Cargo item located near to a single belt		$p_2 = \frac{2P}{L} \frac{1}{w_1}$
2 Cargo item located near to two parallel belts		$p_2 = \frac{2P}{L} \left( \frac{1}{w_1} + \frac{1}{w_2} \right)$
3 Cargo item located far away from the belt(s) and below the base of the shear cone (width $w_i$ defined then by bag dimension $B$ )		$p_2 = \frac{2P}{L} \frac{1}{B}$

The following comments can be made:

- 1) For all examples presented in the table the relevant length  $L$  is given as the bag dimension in the direction perpendicular to the cross-section shown. Then  $L$  and  $B$  would be identical to the internal width and depth of the bag.
- 2) The calculation of pressure  $p_2$  according to the formula of example 3 is applicable if the following inequality is fulfilled for the distance  $h$  of the cargo item top surface from the bag belted face:

$$h > \frac{B - W}{2} \quad [14-4]$$

#### 14.4.2.2.5 Margin of safety relevant to pressure on cargo items

The margin of safety MoS relevant to the verification of the quasi-static loads (considering all contributions) is calculated according to Eq. [14-5]:

$$\text{MoS} = \frac{P_{all}}{[\text{FoS}_1 * (p_1 + p_3) + \text{FoS}_2 * p_2]^{-1}} \quad [14-5]$$

$P_{all}$  is the allowable compression pressure of the cargo item and  $\text{FoS}_1$  and  $\text{FoS}_2$  are the applicable or recommended factors of safety.

$\text{FoS}_1$  should be applied as per Table 5.1.2-1 of [12] where 1.25 at yield and 2 at ultimate level are recommended for analysis only, and 1.4 at ultimate level for launch loads in case of verification by test.

$\text{FoS}_2$  should be the same as  $\text{FoS}_1$  if significant uncertainties are associated with the calculation of the pressure  $p_2$ , e.g. resulting from inaccurately controlled belt tightening loads or significant deviations of the actual shear load distribution in the foam from the analysis assumptions. Where these uncertainties can be demonstrated to be low then the factor of safety  $\text{FoS}_2$  might be reduced provided the agreement of the launch authority is obtained.

In case of a negative MoS the belt preload might be reduced accordingly to obtain a positive MoS. However, as for the reduction of  $\text{FoS}_2$  this requires the approval of the launch authority.

If the shape of the cargo item and the packaging design is complex and the load path cannot be simply predicted, the presented approach is not considered suitable and it should be replaced by more detailed analyses accounting for foam properties and local deformation, bag and belt modelling, stiffness of the complete system belt-bag-foam-hardware.

#### 14.4.2.2.6 Requirement applicability

The applicability of the requirements relevant to

- belts tightening ( $p_2$ )
- adjacent bag ( $p_3$ )

should be mandatory for safety critical and reliability critical cargo items, while it is only suggested for non-critical hardware .

The customer, together with the cargo integration authority, have therefore the responsibility to categorize the cargo item taking into account mainly the hardware value (e.g. a delicate and expensive experiment), its robustness and potential hazards in case of failure during transportation (pressurized equipment, hazardous materials containers, shatter-prone materials, sensitive equipment).

The categorization flow concerning the need for quasi-static load verification is shown in Figure 14-17.

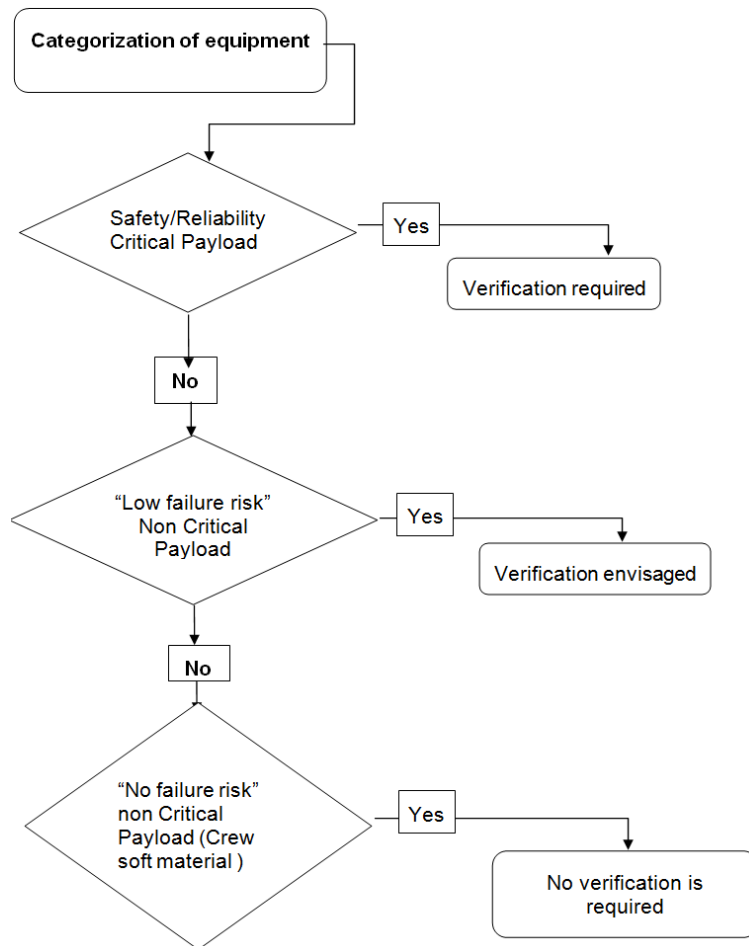


**Figure 14-17: Categorization flow concerning quasi-static load verification needs**

### 14.4.3 Off-the-shelf (OTS) items and already existing equipment

#### 14.4.3.1 Introduction

In this section the criteria are defined to assess the qualification status of cargo items to be flown in soft stowed packaging condition but previously qualified in hard mounted condition.

In this case, the assessment of the new launch levels should be requested in terms of both quasi-static loads and expected flight dynamic environment (sine, random, shock).

#### 14.4.3.2 Strength verification

The strength verification should follow the logic described in Section 14.4.2.2. The design documentation for the OTS item or existing equipment should be evaluated to determine whether the item or equipment external structure is capable to withstand the loads induced by the belt tightening.

In the absence of sufficient evidence the following options should be considered:

1. Analytical verification in order to demonstrate sufficient margins of safety with respect to the belt loads.
2. Belt load verification by test in soft stowed condition.

3. Definition of the launch position of the OTS item or equipment in a region where the loading effects of the belt loads are negligible.
4. Packaging of the soft stowed item such that the belt loads are not passing through the soft stowage materials (foam) to the stowed item, e.g. by implementing stiffening elements within the packaging to carry the belt loads.

#### 14.4.3.3 Verification of compatibility with dynamic flight environments

For OTS items and already existing equipment it may be assumed that relevant mechanical qualification test campaigns have already been performed. Careful examination and review of existing hardware verification documentation should be performed to limit any additional environmental testing to what is needed to demonstrate compliance with the new requirements.

The existing flight hardware concerned is provided as Flight Model (FM) or Protoflight Model (PFM) with corresponding qualification and acceptance heritage.

The demonstration of the cargo item ability to withstand the launch vibration environment on the selected cargo carrier concerns the following environments:

##### 1) Random vibration environment

The expected cargo item flight random vibration environment (estimated on the basis of the relevant attenuation factors reported in [10] and taking into account the applicable qualification margin) is compared to the original random vibration qualification test levels. In case of an undefined packaging configuration the envelope of all possible transmissibilities should be used.

An example for the re-definition of the flight environment due to soft stowed packaging is provided in Section 14.4.4.2.3.

If for all frequencies, the original qualification environment exceeds the expected flight environment at qualification level, then the packaged item has demonstrated its ability to withstand the launch vibration environment on the chosen cargo carrier.

Where this is not the case the design documentation should be carefully examined to identify whether sufficient margins exist to cover the deficiency. In case of insufficient margins delta testing should be performed in hard or soft mounted conditions with the respective attenuated or unattenuated cargo carrier qualification random vibration environment.

Workmanship verification is expected to have been carried out already within the original qualification and acceptance process. Renewed workmanship tests using the Acceptance Vibration Test (AVT) levels should become necessary only if design modifications have been implemented into the existing hardware.

##### 2) Sine vibration environment

If applicable, similar to the procedure for the random vibration environment, the expected (attenuated) cargo item flight sine environment is compared to the corresponding qualification sinusoidal environment.

The transmissibility of foam materials under swept sine or random vibration excitation can in fact be assumed essentially identical. As a result, the attenuated cargo item flight sine environment can be derived from the relevant unattenuated cargo carrier specification considering the square root of the attenuation factors reported in [10].

3) Shock environment

As for the random and sine vibration environments, the expected cargo item shock environment is compared to the corresponding shock qualification heritage.

In conclusion, all the data available relevant to a cargo item already qualified should concur to provide the confidence that no risk is associated with the new flight conditions excluding the need of a delta qualification test campaign.

## **14.4.4 New equipment / hardware**

In this section the criteria for the design and the qualification process relevant to the development of a new hardware are summarized.

### **14.4.4.1 Design of new equipment / hardware**

In case of a new cargo item design and in addition to the worst case flight loads depending on the cargo carrier used, the cargo developer should also consider the pressures due to the belt preloads and the adjacent cargo loads as described in Section 14.4.2.2.

The effects of these pressures should be summed up to the worst case load conditions deriving either from the quasi-static accelerations or vibration environments or from a superposition of the different contributions, consistent with the requirements reported in the applicable launcher and cargo carrier user manuals.

### **14.4.4.2 Qualification of new equipment / hardware**

#### **14.4.4.2.1 Introduction**

The qualification process should take into account the effective launch environment (attenuated by the soft stowed packaging) and the environments that should be adopted for the acceptance/qualification process of the Flight Models (FM).

As reported in the previous sections, the effective (attenuated) random vibration, sinusoidal and shock launch environments at the cargo item location can be derived from the corresponding foam and packaging attenuation data reported in [10].

The qualification tests can be performed:

- in soft mounted condition (suggested when all the data relevant to the soft stowed packaging are available and for delicate hardware that is not designed for hard-mounted tests),
- in hard mounted condition (suggested if the launch configuration is not completely defined).

Usually preference is given to performing the qualification test in soft mounted condition because the test configuration should be as close as possible to the launch configuration in order to inject into the test item in particular dynamic loads which are most representative for the in-flight conditions.

#### **14.4.4.2.2 Qualification test in soft-mounted conditions**

This section covers the qualification of new hardware to be flown in soft stowed packaging conditions, for which the qualification test is consistently performed in soft-mounted condition, too. The test environments are applied at the mounting points and surfaces of the hard container or CTB, respectively, which is accommodating the soft stowed equipment.

### 1) Random vibration environment

The random vibration qualification input for the new equipment / hardware Qualification Model (QM) test performed in soft-mounted conditions is determined by the applicable cargo carrier qualification environment (derived from the flight environment by applying relevant margins). Relevant enveloping of the candidate cargo carriers might be applied in case none has been chosen yet.

Usually, there is no QM test in hard mounted conditions when following the soft mounted verification methodology. However, if a workmanship test with applying the AVT levels is foreseen on the FM's (in particular for electronic and electrical equipment) then an additional test in hard mounted condition should be performed for the QM by applying to the shaker table the AVT levels (see Table 14-5).

The purpose of this additional test should be to verify already on the QM that there are no unexpected equipment / hardware structure integrity problem when the FM is subjected to the AVT levels, in particular in those frequency ranges where the attenuation effects of the soft stowed packaging have largely reduced the input levels applied during the qualification tests in soft-mounted condition.

### 2) Sine environment

Sine tests are required for several cargo carriers, e.g. ATV, HTV, Progress, Soyuz and Dragon. The sine test should be performed with the item in soft mounted condition (as in flight) by applying to the shaker table the applicable cargo carrier sine qualification environment (or an envelope of all candidate cargo carriers) as per hard mounted condition.

### 3) Shock environment

As for the sine environment the required qualification test levels are applied to the shaker table without considering the attenuation factors due to the soft stowed packaging.

#### 14.4.4.2.3 Qualification test in hard-mounted conditions

This section covers the qualification of new hardware to be flown in soft stowed packaging conditions for which the qualification test is however performed in hard mounted condition. Such verification approach might be particularly suitable e.g. if the packaging material and configuration is not fully defined yet. As a result, a test input being an envelope of the candidate packaging materials and configurations should be applied.

In this case of the qualification test performed in hard mounted condition the expected flight environments for the cargo item should be applied to the shaker table. These environments (random, sine, shock) are derived by applying to the environment specification of the candidate cargo carriers the attenuation factors provided in [10] and, where necessary, considering the envelope of all possible packaging configurations for the cargo item.

Furthermore, if the cargo carrier has not yet been identified, then the envelope of all the possible flight environments for the candidate cargo carriers should be considered.

### 1) Random vibration environment

The qualification random vibration input is found by enveloping two spectra:

- the cargo carrier qualification environment (taking into account the foam influence),
- the Acceptance Vibration Test (AVT) levels, see Table 14-5.

The consideration of the AVT levels should take into account whether acceptance tests in hard mounted condition are foreseen on the equipment flight models.

**Note:**

In accordance with the verification guidelines for soft stowed equipment, [3], it might be however also considered appropriate in case of a prototype approach to define the qualification random vibration input spectrum by enveloping the cargo carrier qualification environment (taking into account the foam influence) and the Qualification Acceptance Vibration Test (QAVT) levels, as given in [3] in Table 7.6-1. These more conservative qualification levels would be justified by the following:

- Maintaining a margin between the qualification test and the acceptance test should prevent possible overstressing of the flight hardware during the acceptance test,
- Having a margin between the qualification model and the flight model might be useful in case of re-testing (e.g. after a repairing activity) where it is usually required to demonstrate that sufficient useful life remains in the component for retest and subsequent service operations.

The recommended procedure to use the flight attenuation factor tables for the estimation of the applicable cargo item flight environment is described in Appendix I of [10] and briefly repeated hereafter for convenience:

For each  $F_n = 20 \text{ Hz}, 25 \text{ Hz}, \dots, 2000 \text{ Hz}$  the attenuated cargo item random vibration environment, given by the respective power spectral density values  $\text{PSD}_{n,\text{attenuated}}$ , is calculated according to Eq. [14-6]:

$$\text{PSD}_{n,\text{attenuated}} = \text{PSD}_n * \text{AF}_n \quad [14-6]$$

where:

$\text{PSD}_{n,\text{attenuated}}$  the new attenuated PSD value at frequency  $F_n$ ,

$\text{PSD}_n$  the PSD value at frequency  $F_n$  according to the cargo carrier random vibration environment specification,

$\text{AF}_n$  the applicable attenuation factor at frequency  $F_n$ , either specific to a pre-defined packaging configuration or enveloping all possible packaging configurations.

**Example:**

A cargo item with a W/A ratio of 0.20 psi, launched in a hard container and packaged with a yet undefined foam (either Pyrell, Minicel or Zotek) of 2 inch thickness is considered.

ATV has been chosen as the carrier for this cargo item.

Table 14-7 provides the attenuation factors relevant for the possible packaging solutions and their envelope considering the aforementioned candidate foams.

Table 14-8 and Figure 14-18 show the qualification random vibration environment related to hardware to be flown on ATV, with and without the foam influence. The attenuated environment is obtained by applying frequency by frequency the attenuation factors to the unattenuated environment specification.

Figure 14-19 shows the applicable qualification test profile obtained as envelope of the AVT levels and the envelope (maximum) of the attenuated cargo item flight random vibration environments taking into consideration all the candidate foams.

**Table 14-7: Foam 2 inch – W/A 0.2 Psi attenuation factors [10]**

Freq. [Hz]	Attenuation Factors W/A= 0.2 PSI			
	Pyrell 2"	Minicell 2"	Zotec 2"	Attenuation Fact. Envelope
20	2.42E+00	1.16E+00	1.33E+00	2.42E+00
25	2.95E+00	1.24E+00	1.50E+00	2.95E+00
31.5	2.63E+00	1.38E+00	1.81E+00	2.63E+00
40	1.45E+00	1.60E+00	2.28E+00	2.28E+00
50	6.39E-01	1.98E+00	2.92E+00	2.92E+00
63	2.74E-01	2.76E+00	3.07E+00	3.07E+00
80	1.25E-01	4.17E+00	1.85E+00	4.17E+00
100	6.05E-02	4.40E+00	7.70E-01	4.40E+00
125	2.96E-02	1.77E+00	2.99E-01	1.77E+00
160	1.52E-02	5.60E-01	1.25E-01	5.60E-01
200	7.83E-03	1.93E-01	5.43E-02	1.93E-01
250	4.09E-03	7.32E-02	2.45E-02	7.32E-02
315	2.17E-03	3.00E-02	1.15E-02	3.00E-02
400	1.16E-03	1.28E-02	5.44E-03	1.28E-02
500	6.19E-04	5.62E-03	2.62E-03	5.62E-03
630	3.31E-04	2.50E-03	1.27E-03	2.50E-03
800	1.77E-04	1.12E-03	6.12E-04	1.12E-03
1000	9.44E-05	5.05E-04	2.97E-04	5.05E-04
1250	5.01E-05	2.28E-04	1.43E-04	2.28E-04
1600	2.64E-05	1.02E-04	6.89E-05	1.02E-04
2000	1.38E-05	4.59E-05	3.29E-05	4.59E-05

**Table 14-8: Random vibration environments**

	ATV Env. Unattenuated [g <sup>2</sup> /Hz]	Attenuation Fact. Envelope	ATV Env. Attenuated [g <sup>2</sup> /Hz]
<b>20</b>	1.00E-02	2.42E+00	2.42E-02
<b>25</b>	1.25E-02	2.95E+00	3.69E-02
<b>31.5</b>	1.58E-02	2.63E+00	4.14E-02
<b>40</b>	2.00E-02	2.28E+00	4.55E-02
<b>50</b>	2.50E-02	2.92E+00	7.31E-02
<b>63</b>	3.15E-02	3.07E+00	9.67E-02
<b>80</b>	4.00E-02	4.17E+00	1.67E-01
<b>100</b>	5.00E-02	4.40E+00	2.20E-01
<b>125</b>	5.00E-02	1.77E+00	8.84E-02
<b>160</b>	5.00E-02	5.60E-01	2.80E-02
<b>200</b>	5.00E-02	1.93E-01	9.64E-03
<b>250</b>	5.00E-02	7.32E-02	3.66E-03
<b>315</b>	5.00E-02	3.00E-02	1.50E-03
<b>400</b>	5.00E-02	1.28E-02	6.40E-04
<b>500</b>	2.90E-02	5.62E-03	1.63E-04
<b>630</b>	1.66E-02	2.50E-03	4.15E-05
<b>800</b>	9.27E-03	1.12E-03	1.04E-05
<b>1000</b>	5.40E-03	5.05E-04	2.73E-06
<b>1250</b>	3.13E-03	2.28E-04	7.13E-07
<b>1600</b>	1.72E-03	1.02E-04	1.76E-07
<b>2000</b>	1.00E-03	4.59E-05	4.59E-08

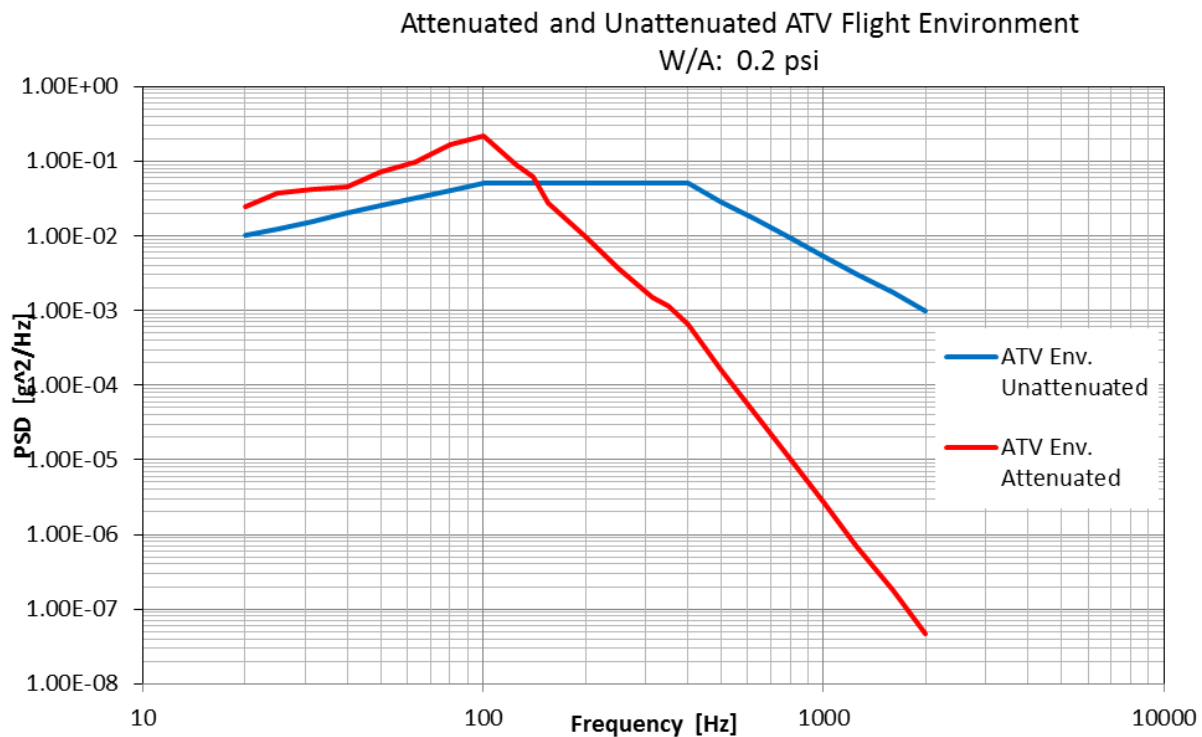


Figure 14-18: ATV attenuated and un-attenuated random vibration environment

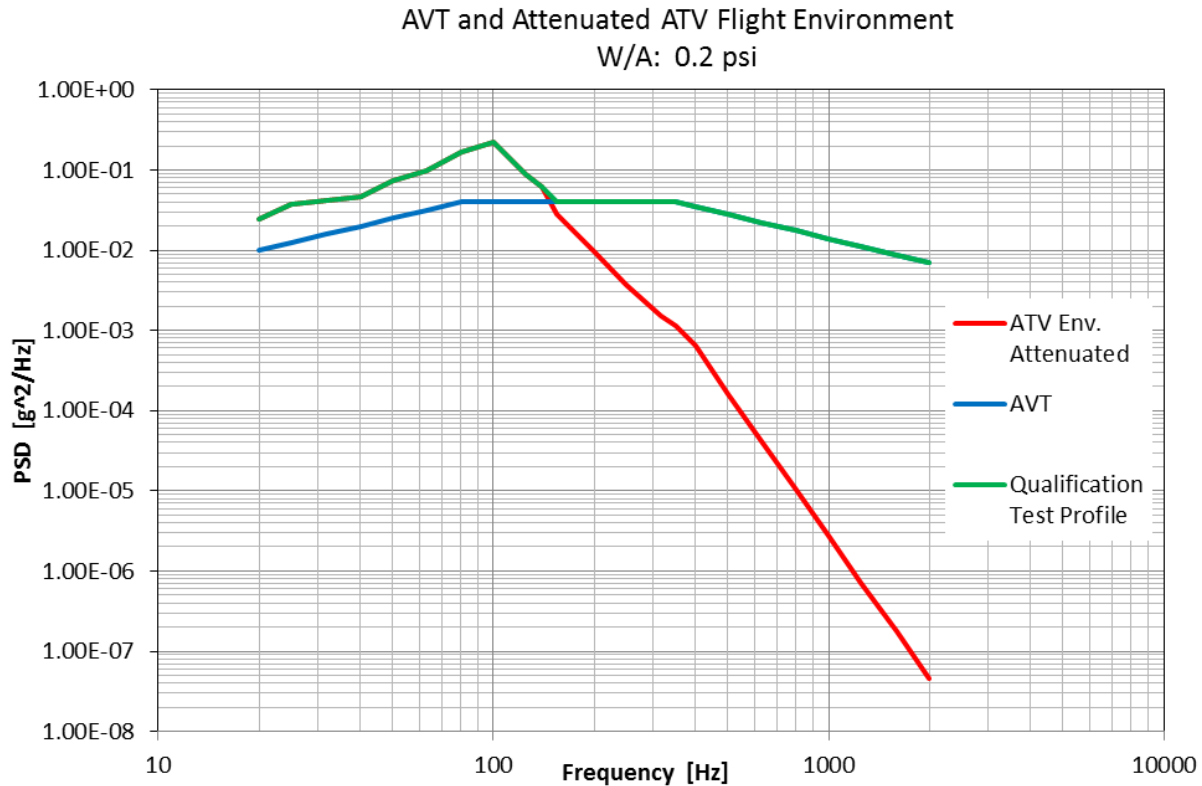


Figure 14-19: Attenuated ATV environment, AVT and qualification test profile

## 2) Sine environment

As mentioned before sine tests are required by several cargo carriers as e.g. ATV, HTV, Progress, Soyuz and Dragon. The expected cargo item flight sine environment, to be taken into account for the qualification test profile, can be derived in accordance with the procedure described for the random vibration environment, however considering the square root of the attenuation factors reported in [10].

## 3) Shock environment

Similar to the methodology applied for the verification of the sine environment in hard mounted test condition, only the expected (attenuated) cargo item flight shock environment should be taken in account for the definition of the qualification level. The attenuated shock environment is derived from the cargo carrier shock qualification test profile by considering the square root of the attenuation factors.

## 14.2 References

- [1] Cronwelge O., et al. "Vibration Attenuation Effectiveness of Foam Sandwich Enclosure", NASA TM-2011-216163, 2011
- [2] MIL-HDBK-304C, "Package Cushioning Design", 1997
- [3] ESO-IT-PR-0092, " Mechanical Environment Verification Guideline for Soft Stowed Equipment", Issue 2, March 2011
- [4] Tang H., "Portable Life Support System Packaging Phase III – Foam Protection Materials Evaluation and Selection Phase I", NASA CTSD-CX-5502, May 2008
- [5] Gnip I., et al. "Assessment of Strength under Compression of Expanded Polystyrene (EPS) Slabs", Materials Science, Vol. 10 No. 4, 2004
- [6] Minicel data sheets from [www.sekisuvoltek.com](http://www.sekisuvoltek.com) (VOLTEK – 100 Shepard Street, Lawrence, MA 01843, USA)
- [7] Pyrell data sheet from [www.qualityfoam.com](http://www.qualityfoam.com) (Foamex, 1500 E. 2<sup>nd</sup> St., Eddystone, PA 19022-1589, USA)
- [8] Zotek F30 data sheet from [www.zotefoams.com](http://www.zotefoams.com) (Zotefoams Inc., 55 Precision Drive, Walton, Kentucky, 41094, USA)
- [9] Plastazote data sheets from [www.qualityfoam.com](http://www.qualityfoam.com) (supplier: Zotefoams Inc.)
- [10] SSP 50835, "ISS Pressurized Volume Hardware Common Interface Requirements Document for International Space Station", Rev. C, November 2011
- [11] SSP 41172, " ISS Qualification & Acceptance Environmental Test Requirements", Rev. U, March 2003
- [12] SSP 52005, "Payload Flight Equipment Requirements and Guidelines for Safety-Critical Structures - International Space Station Program", Rev. D, March 2008

# 15

## Nonlinear structures

### 15.1 Introduction

Nonlinearity is a frequent occurrence in engineering structures including spacecraft structures. It can take different forms, and it is at the origin of various dynamical phenomena with no linear counterpart. These phenomena include jumps, harmonics, bifurcation and non-uniqueness of the solutions. Even when they are local, nonlinearities can affect the global dynamical behaviour of a structure and have a substantial impact on spacecraft loads.

What makes nonlinear dynamics challenging to analyse and model is the well-known result that the principle of linear superposition does not (generally) apply to nonlinear systems. Even if linearisation may suffice in some cases, the rigorous analysis of nonlinear structures requires adequate and dedicated numerical and experimental methodologies.

The main objective of this chapter is to describe how to handle nonlinearities for an accurate estimation of loads in spacecraft structures. Specifically, guidelines for both modelling and testing are provided.

### 15.2 Common spacecraft structure nonlinearities

It may be assumed that practically all spacecraft structures contain nonlinear elements. However, in most cases these structural nonlinearities are relatively weak or not substantially activated by the mechanical environment encountered during the launch phase or during ground vibration testing. As a result, the assumption of a (quasi-) linear structure is adequate for design and development purposes.

A survey of most common spacecraft structure nonlinearities encountered in past satellite programmes, in particular during sine or modal survey tests, has been performed as part of the NOLISS study [2]. Their nature can be classified in three main categories:

1. damping,
2. contact, and
3. nonlinear stiffness.

The aforementioned nonlinear phenomena are depending on the input levels. For each case a minimum input level is required to significantly activate the nonlinearity, otherwise the behaviour remains linear.

All other spacecraft structure nonlinearities have been found to be very specific and they are not expected to occur regularly on classical satellite programmes. Table 15-1 recalls the classification of all the nonlinear effects identified during the survey.

Table 15-1: Classification of nonlinear effects, [2]

non linear example	nature				effect			impact on project	global / local
	damping	gap / rattling / contact	non linear stiffness	other	freq.	levels	noise		
damping - general	x				x	x			g
gaps - general		x			x		x		l
Rattling on microsat	x					x			l
contact in hold down system		x				x	x		l
antenna Hold Down System	x		x		x	x			l
Metop solar array		x					x		l
Elastomer dampers			x		x	x	x	x	l
SASSA		x			x	x	x	x	g
Supporting blades		x			x	x			l
variable damping in dummy instrument	x							x	l/g
gyroscopic effect				gyroscopic	x				l
telecom platform with struts	x		x		x	x			g
hydrogen battery				sub harmonic	x				l
gimbal engine		x					x		l
bellows		x			x		x		l
friction damping	x		x		x	x			g
energy transfer between modes				modes coupling	x	x			g
excitation of modes with lower frequencies				modes coupling	x	x			g

## 15.2.2 Damping

Nonlinear damping is a frequently occurring effect in spacecraft structures when the input levels are increased. This nonlinear damping might originate from e.g. increased friction when a threshold value has been passed to enforce relative movement between contact surfaces which was not the case at lower levels due to the sticking friction value.

An example for nonlinear damping behaviour and its effects on the responses at the resonance frequency is given in Figure 15-1. It shows the evolution of frequency and amplification for the first lateral mode of the tested structure. The inconsistencies seen for the low level runs have been identified to result from poor frequency resolution and noisy pilot measurement used for the transfer function calculation.

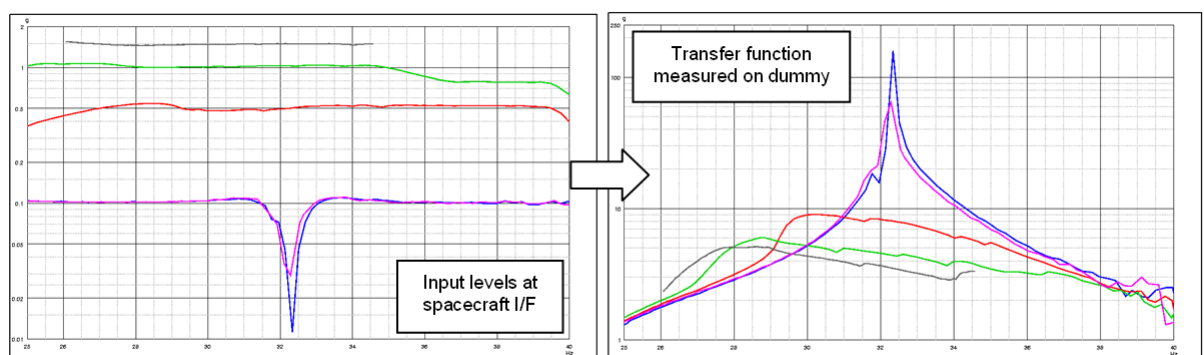
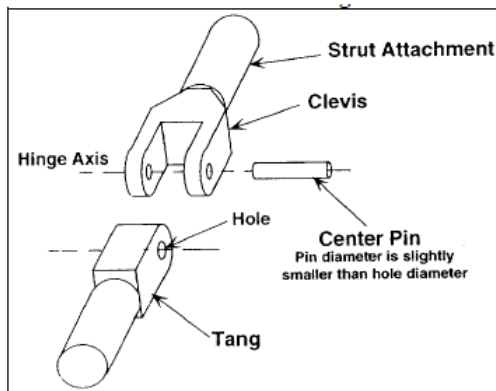


Figure 15-1: Effects of nonlinear damping seen on transfer functions for different input levels (g-levels vs. frequency), [2]

### 15.2.3 Contact

Contact nonlinearities are frequently occurring in structural joints (e.g. pinned connections) where due to manufacturing and assembly tolerances a small gap exists between the parts being connected, as shown in Figure 15-2. These effects are also frequently called play or backlash.



**Figure 15-2: Example of contact nonlinearity: joint with play due to manufacturing tolerances**

As a result of the gap, the part on which a force is acting might move first freely before getting in contact with the other part. The theoretical force / displacement relationship and therefore the consequences for the local stiffness of gaps in structural assemblies are presented in Figure 15-3.

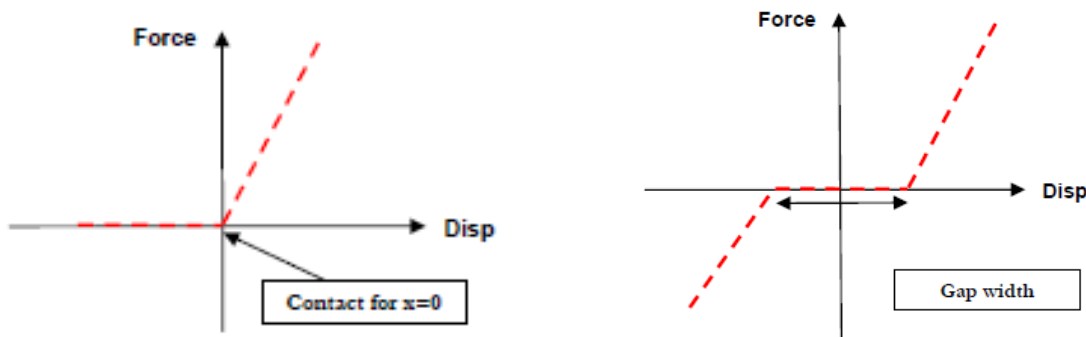


**Figure 15-3: Theoretical force/displacement relation for one-sided contact (left) and symmetric gap (right)**

Small gaps, e.g. at strut ends, may explain variable damping without visible frequency shifts. In that case the nonlinearity could be considered due to a friction effect and thus be part of the previous section related to nonlinear damping. However, when the gap is wider (although the width might be difficult to estimate) then stronger nonlinear effects may appear with modal frequency shifts and even modal shape modifications.

The effects of gap nonlinearities frequently seen during spacecraft hardware tests are shown in Figure 15-4. The time signal shows the hammering effects when repeated contacts are occurring and the nonlinear behaviour becomes visible in the response plot for a sweep-up and down, respectively, where the resonance peak occurs at a lower frequency for the sweep-down than for the sweep-up.

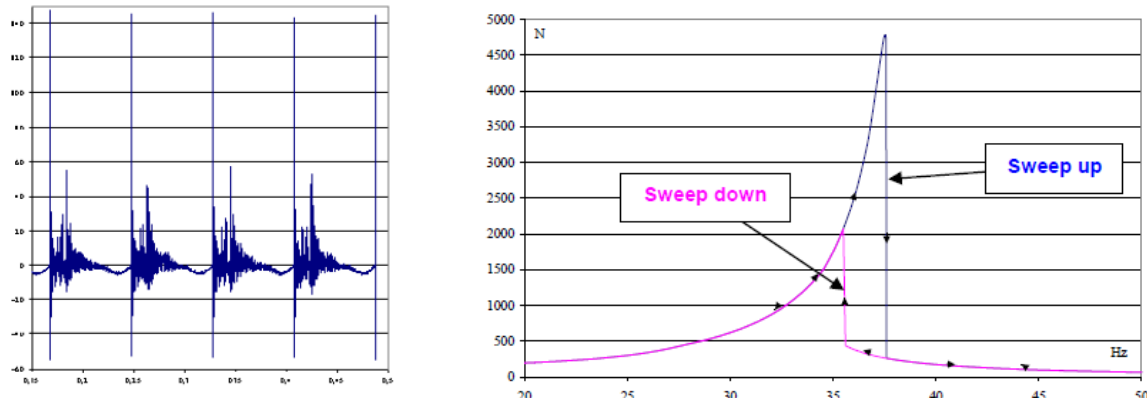


**Figure 15-4: Effects of gap nonlinearity as seen during hardware tests (left graph showing temporal signal, g vs. seconds), [2]**

### 15.2.4 Nonlinear stiffness

Nonlinear stiffness assemblies are typically introduced in spacecraft structures for specific mission objectives, e.g. by making use of stiffness variations due to the input levels to respond as needed to different mechanical environments. This is e.g. the case for elastomer dampers developed for micro-vibration attenuation needs (using the elastomer softness and associated viscous damping to filter and damp low level micro-vibrations during flight). Mechanical stops are added to the dampers in order to limit the displacements and therefore the damaging effect of large strains in the elastomers induced by high vibration levels during the launch phase.

The characteristic force / displacement curve for a typical mechanical stop is given in Figure 15-5. It shows that the initial stiffness governed by the elastomer properties is dramatically increasing when the stop is reached. In the case that the excitation levels are low the stop might not be reached and the behaviour remains in the linear domain. However, as soon as the displacement reaches the stops strong nonlinear effects show up.

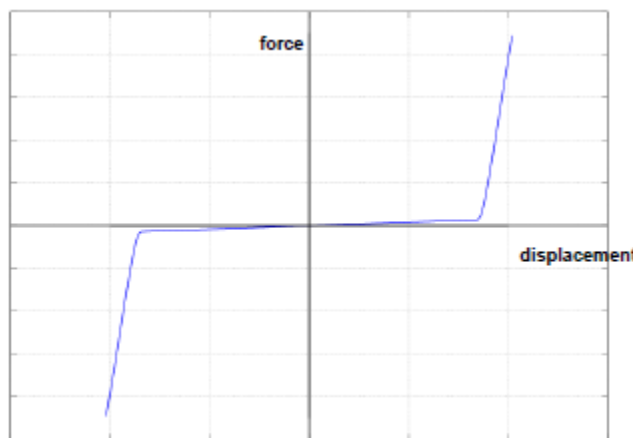


**Figure 15-5: Nonlinear stiffness due to mechanical stop**

As shown by tests the major effects of the mechanical stop nonlinearity are the modification of the shape, level and frequency of the peak of the transfer functions, Figure 15-6. The stop appears to be not reached at low level and the behaviour remains linear. For the larger acceptance level the nonlinear behaviour is clearly shown: the peak shape is non-symmetric with a sharp drop after the resonance has been passed.

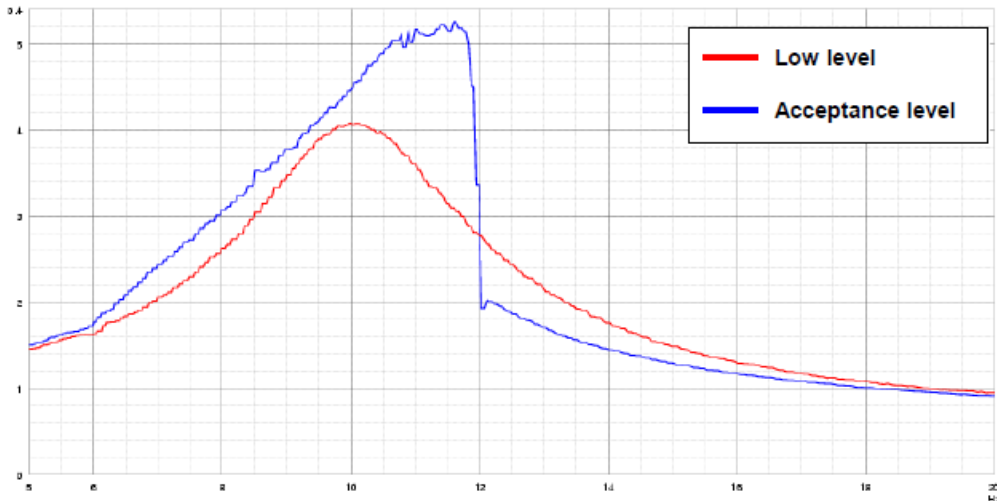


Figure 15-6: Transfer function evolution with increasing input levels in case of mechanical stop, [2]

### 15.3 Nonlinearity detection

Nonlinearity detection amounts to highlight the presence of nonlinear dynamical phenomena. As shown in the previous section, the mere inspection of the time series can sometimes be sufficient to detect nonlinearity through, e.g., the presence of signal distortions. In that regard, and, unlike random excitation, sine sweep excitation is particularly convenient.

However, more robust detection methodologies are often needed. Various concepts for the analysis of linear systems do not directly apply to nonlinear theory. The breakdown of the principle of superposition is a possible means of detecting the presence of a nonlinear effect.

Let  $y_1(t)$  and  $y_2(t)$  be the responses of a structure to the input forces  $x_1(t)$  and  $x_2(t)$ , respectively. The principle of superposition is violated if  $ay_1(t)+by_2(t)$  is not the structural response to the input  $ax_1(t)+bx_2(t)$ . However, it is of limited practical utility, and simpler procedures should be employed.

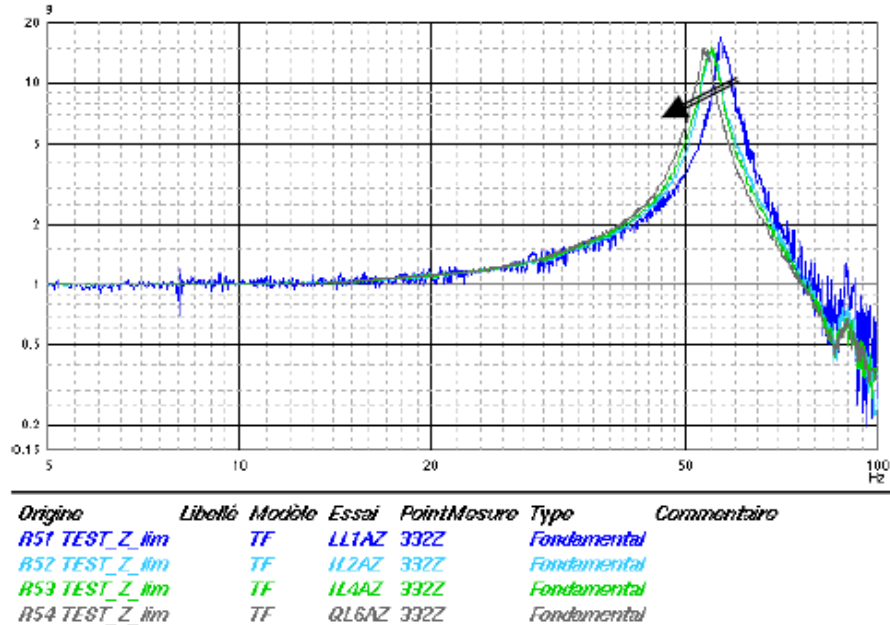


Figure 15-7: Transfer function evolution due to increasing excitation levels, [2]

The test for homogeneity, which is a restricted form of the principle of superposition ( $b$  is set to 0), is one of the most popular detection techniques. Homogeneity violation is best visualised in the frequency domain through distortions of frequency response functions (FRF). Even though sine sweep excitation is well-established for testing space structures, it is important to note that such excitation may introduce distortions in the FRFs of linear systems. It is not the ideal candidate for verifying homogeneity. For illustration, the FRFs (transfer functions) of the SmallSat spacecraft at different excitation levels are compared in Figure 15-7. The resonance peak corresponds to the first axial mode of the spacecraft. Its frequency decreases when the excitation level increases, a clear indication of nonlinear behaviour.

Due to the symmetry of the dynamic compliance matrix  $H(\omega)$ , to measure a FRF by impacting point A and measuring the response at point B is equivalent to measure a FRF by impacting point B and measuring the response at point A. The reciprocity test is not infallible either because reciprocity can hold for symmetrical nonlinear systems.

The ordinary coherence function is normally used for assessing the quality of data measured under random excitation. The coherence function is required to be unity for all accessible  $\omega$  if and only if the system is linear and noise-free. We can therefore utilise it as a detection tool for nonlinear behaviour, because it is a rapid indicator of the presence of nonlinearity in specific frequency bands or resonance regions. It is arguably the most often-used test, by virtue of the fact that almost all the commercial spectrum analysers allow its calculation; however, it does not distinguish between the cases of a nonlinear system and noisy signals.

More sophisticated diagnostic tools are provided by the Hilbert transform, time-frequency analysis (e.g., wavelet transform) and higher-order FRFs. The description of these techniques is beyond the scope of this chapter. The reader is referred to [1] [3] for further details and references about them.

Nonlinear detection is also meant to provide a quantitative assessment of the importance of nonlinear phenomena. It is therefore a very important first step: at the end of this process, the analyst should decide whether or not he decides to model the observed nonlinear behaviours.

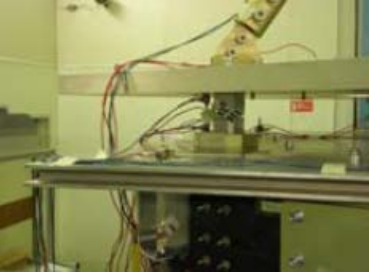
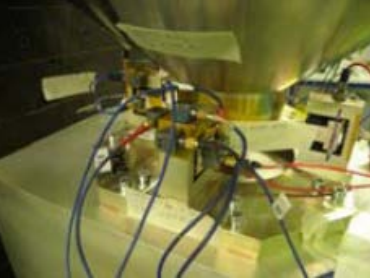
## 15.4 Handling of spacecraft structure nonlinearities

### 15.4.1 Introduction

If nonlinear effects in spacecraft structures are expected to significantly impact on the design verification process (concerning both structural analyses and subsequent hardware testing) then major efforts are frequently required to properly handle these structural nonlinearities. The latter concerns in particular the execution of adequate flight load predictions from launcher coupled loads analysis, the pre-test assessment of the shaker performance and subsequently the successful execution of the structure qualification tests.

Proper understanding of the potential effects of strong nonlinearities on the spacecraft structure performance is of outmost importance in order to reduce the risk and potential cost impacts during the spacecraft structure design and development process. Relevant guidelines to handle nonlinearities at spacecraft level have been derived in the frame of the NOLISS study, [2]. These guidelines should be currently considered being far from exhaustive but are nevertheless presented hereafter for the benefit of possibly adapting accordingly the nonlinear analyses and hardware testing.

In order to support the better understanding of the guidelines, in particular those regarding the testing aspects, the SmallSat satellite configuration employed in the experimental phase of the NOLISS study is briefly introduced in Figure 15-8. The two nonlinear components being present in the SmallSat test configuration are highlighted.

Overall SmallSat satellite configuration	Nonlinear components
 <p>The photograph shows the overall SmallSat satellite configuration. It consists of a dark, monocoque octagonal CFRP tube structure standing vertically. A white cylindrical instrument dummy base plate is attached to the bottom of the satellite. A tripod assembly is mounted on top of the satellite. Numerous red and black wires are visible, connecting the various components. The satellite is positioned within a blue triangular frame, likely a test fixture.</p>	<p><b>SASSA (Shock Attenuation System for Spacecraft and Adaptor) modules</b></p>  <p>A photograph of a SASSA module. It is a rectangular metal box with various electronic components, sensors, and wiring visible. The module is part of the shock attenuation system for the spacecraft and adaptor.</p> <p>located between SmallSat top floor and instrument dummy base plate; instrument dummy assembly supported by three SASSA modules</p>
<p>main satellite structure (monocoque octagonal CFRP tube structure; height: 1200 mm; diameter: 1000 mm) total test configuration mass: 216.9 kg of which 142 kg are contributed by the instrument dummy assembly (dummy mass + tripod + base plate)</p>	<p><b>WEMS (Wheel Elastomer Mounting System) device</b></p>  <p>A photograph of the WEMS device. It is a mechanical assembly mounted to a side panel of the SmallSat. It includes a central actuator supported by four elastomer dampers with displacement limiters (mechanical stops).</p> <p>mounted to side panel of SmallSat octagonal structure; dummy actuator (about 8 kg) supported by four elastomer dampers with displacement limiters (mechanical stops)</p>

**Figure 15-8: SmallSat satellite configuration employed in experimental phase, [2]**

## 15.4.2 Guidelines for testing

### 15.4.2.1 Suitable excitation signals

Swept sine tests are usually performed at satellite level to demonstrate that the satellite is able to sustain the mechanical launch environment, even if most flight load events are of transient nature. Most modal parameter estimation tools provide good results for swept sine excitation even if some are more adapted to other types of excitation, [2]:

- Advanced modal parameters estimation methods need a measurement of the input load to calculate FRF(s) and so are genuinely adapted to modal survey. Nevertheless they might be also applied to sine results thanks to the calculation of transmissibilities. Welch's method, traditionally used in combination with random data, provides more accurate results, however some adjustments are needed for a sine sweep application.

- If system identification techniques dedicated to nonlinear structures are employed for a proper estimation of nonlinearities, random excitation is the most versatile since it can be handled by most of the methods used for detection, characterisation or parameter estimation. In addition, force measurements are required by most nonlinear system identification methods.

### 15.4.2.2 Vibration control strategy

The vibration control strategy has shown to be a key issue when testing nonlinear spacecraft. If the spacecraft structure nonlinearities are not adequately included into the test prediction model then potential impact of the nonlinear structure behaviour on the shaker control may not be sufficiently anticipated and may threaten the integrity of the structure.

A control strategy based on “filtered” accelerations (using the harmonic estimator) ensures that the required fundamental frequency acceleration levels are obtained during the test and this was found particularly true when notching criteria are applied to control channels to protect the structure, [2]. However, such a piloting has a major disadvantage insofar as acceleration spikes due to nonlinearities (with high frequency content involved, shocks) may appear resulting to severe difficulties to estimate and limit these peaks at control level. In order to restrict these spikes, a peak or rms control strategy may be adopted; however, in this case the fundamental acceleration levels are not guaranteed and no phase information is available.

The following recommendations apply for the sine controller:

- Sweep rate:  
Lower sweep rates result to better control performance (i.e. the “measured” sine profile is closer to reference profile) and, furthermore, more frequent control updates are possible.
- Number of periods:  
Fewer periods yield slightly better control, but noisier amplitude estimates. If fewer periods are used to estimate the sine amplitudes, then more control updates are possible.
- Compression factor:  
Low compression factors give usually better control whereas higher factors yield more stable control in the sense that the spectrum becomes smoother and that less beating occurs.

### 15.4.2.3 Test instrumentation

In order to properly characterise the structural nonlinearity a dedicated test instrumentation plan is needed. Most nonlinear system identification methods require measuring the responses on either side of nonlinear components. More precisely, if a nonlinearity is located between two degrees of freedom, both degrees of freedom should be measured. Where a spacecraft component is supported by several nonlinear elements (mostly in a parallel arrangement) then each of these nonlinear elements needs to be instrumented in order to properly characterise the overall component behaviour by means of the measured test data. This requirement does not hold for nonlinear finite element model updating techniques.

There might be a need for adapted accelerometers in case repeated shocks are expected to be measured, e.g. in the case of metal / metal contact when a mechanical stop is reached. Sensors close to the nonlinearity might then measure high levels of acceleration and if these sensors are standard ones as usually used for sine tests they might not be able to sustain the high acceleration shocks (due to possibly exceeding the maximum allowable acceleration level).

#### 15.4.2.4 Data sampling and time recording

Time histories of the measured acceleration responses should be recorded during the test: this allows the use of advanced data analysis methods for the estimation of relevant dynamic parameters or to evaluate the frequency content of the responses. Because nonlinear systems excited at a specific frequency can generate harmonics, the sampling rate should be chosen as high as possible to allow proper evaluation of the response peaks in the whole frequency band of interest. However, setting the sampling rate too high drastically increases the amount of data being recorded and might be not compatible with the data acquisition system used by the test facility.

#### 15.4.3 Nonlinearity characterisation and parameter estimation

The complete nonlinear system identification process is presented in Figure 15-9. According to this scheme, the characterisation of nonlinearity is the second step of the process, after the detection step.

A nonlinear system is said to be characterised when the location, type and functional form of all the nonlinearities throughout the system are determined. It is of crucial importance to have an accurate characterisation of the nonlinear elastic and dissipative behaviour of the physical structure prior to parameter estimation. Without a precise understanding of the nonlinear mechanisms involved, the identification process is bound to failure. Characterisation is a very challenging step because nonlinearity may be caused by many different mechanisms and may result in plethora of dynamic phenomena.

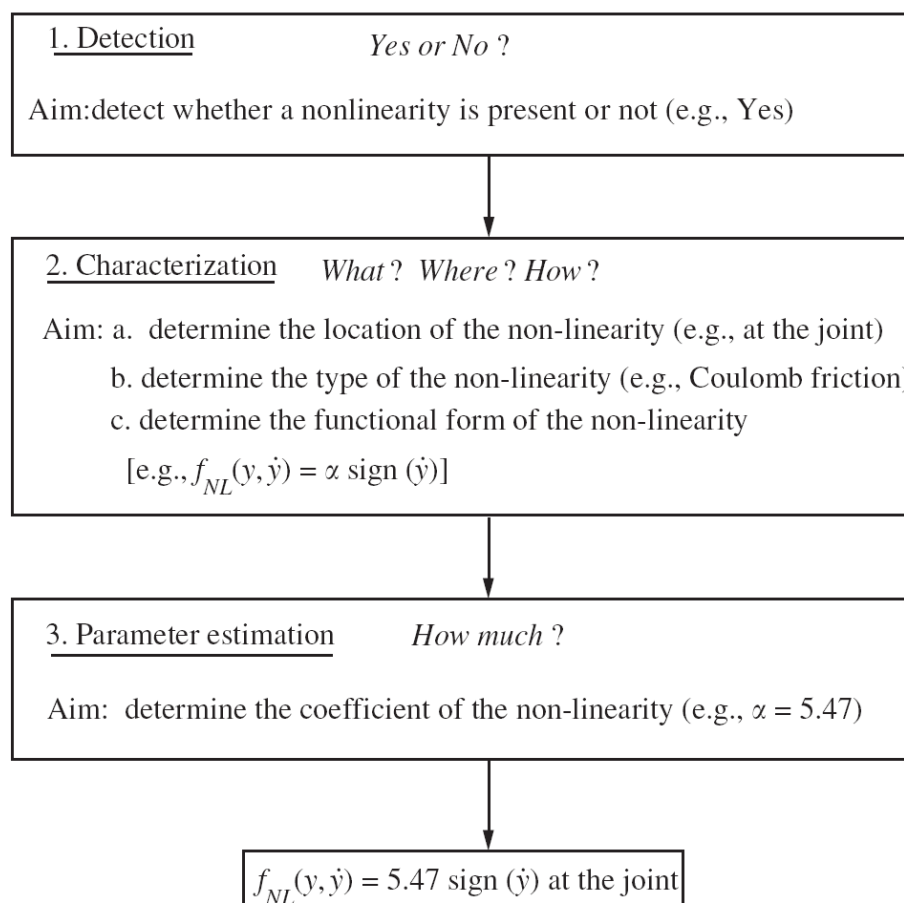


Figure 15-9: Nonlinear system identification process

Determining the location of nonlinearities is usually not difficult, because a priori knowledge is often available. If this is not the case, some information may be gleaned by studying FRFs at various excitation levels and examining the deformation shapes of the modes which are most corrupted by the nonlinear response; nonlinearities may be assumed where the relative displacements of these mode shapes are the largest.

A useful method for determining the type and functional form of the nonlinear components is the restoring force surface (RFS) method [4]. It is based on Newton's second law, which, for a single-degree-of-freedom system, is:

$$m\ddot{y}(t) + f_{nl}(y(t), \dot{y}(t)) = x(t) \quad [15-1]$$

where  $f_{nl}(y(t), \dot{y}(t))$  is the restoring force, i.e. a nonlinear function of displacement and velocity. This quantity can be computed through the measurement of the acceleration and the external force and through the knowledge of the mass coefficient:

$$f_{nl,i} = x_i - m\ddot{y}_i \quad [15-2]$$

where the subscript  $i$  refers to the  $i$ -th sampled value.

For each sampling instant, a triplet  $(y_i, \dot{y}_i, f_{nl,i})$  is found, which means that the restoring force is known for each sampled point  $(y_i, \dot{y}_i)$  in the phase plane. By representing the restoring force as a function of the displacement and velocity in a three-dimensional plot, the nonlinearity can be conveniently visualised. A characterisation of the elastic and dissipative forces can be obtained by taking a cross section of this three-dimensional plot along the axes where either the velocity or the displacement is equal to zero, respectively. The resulting plots are termed stiffness and damping curves, respectively.

The experimental stiffness curve for one of the WEMS nonlinearities is shown in Figure 15-10. The impacts with the mechanical stops, and therefore the piecewise-linear nature of the nonlinearity, are clearly visible in this plot. The experimental stiffness curve for one of the SASSA nonlinearities is shown in Figure 15-11. It highlights the softening nonlinearity of the SASSA devices.

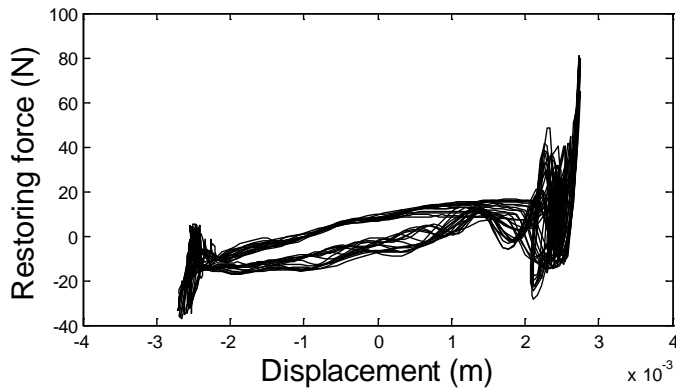


**Figure 15-10: Stiffness curve of one of the WEMS nonlinearities of the SmallSat spacecraft, [2]**

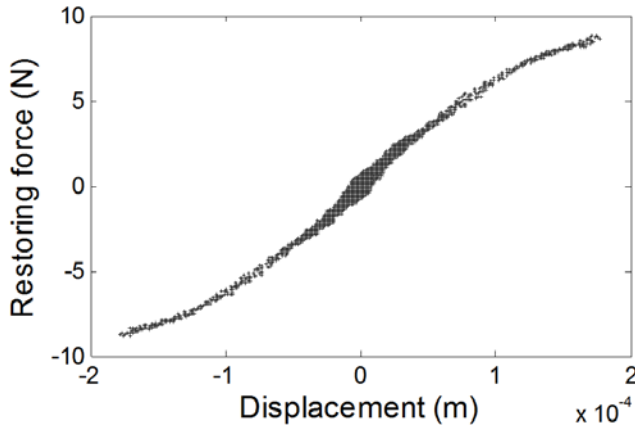


**Figure 15-11: Stiffness curve of one of the SASSA nonlinearities of the SmallSat spacecraft, [2]**

Once the nonlinear effects have been properly characterised, the last step of the identification process is parameter estimation. This step aims at determining the coefficients of the model that was chosen to represent the nonlinearities during the characterisation step. The RFS method can also be used in this context. For instance, if a polynomial model for the restoring force

$$f_{nl}(y(t), \dot{y}(t)) = \sum_{i=0}^m \sum_{j=0}^n a_{ij} y^i \dot{y}^j \quad [15-3]$$

is selected, then the coefficients  $a_{ij}$  can be determined directly by solving an overdetermined system. The method is particularly attractive for spacecraft structures, because it can be applied in the presence of sine sweep excitation.

Another interesting method is the conditioned reverse path method [6] [7]. This method computes the FRFs of the underlying linear system, which is often the nonlinear system at low excitation levels, together with the coefficients of the nonlinearity. It also generalises the concept of ordinary coherence function to nonlinear systems. The nonlinear coherence function is a very useful indicator of the accuracy of the identification process. The method is known to be more robust and accurate than the restoring force surface method, but it requires random excitation, and, hence, dedicated tests.

Nonlinear parameter estimation is difficult and demanding in terms of test instrumentation. But there has been considerable progress in this field. For instance, nonlinear generalisations of classical linear algorithms, such as the stochastic subspace identification method, have been recently proposed, which opens up new horizons for nonlinear system identification of real-life structures. A review of the literature on the subject can be found in [3].

## 15.4.4 Guidelines for structure modelling and analysis

### 15.4.4.1 Understanding the nonlinear model behaviour

Prior to using particular nonlinear features in a large, complicated finite element model the proper handling of this feature should be verified and well understood by using very simple models, e.g. consisting only of a few elements. Furthermore, preliminary insight into the nonlinear structure behaviour can be gained by performing first an analysis for a simplified model, e.g. consisting only of spring-masses systems, or a linear analysis might reveal which nonlinearities are activated first and at which load levels this can be expected to happen.

#### 15.4.4.2 Model condensation

To perform nonlinear simulations of structural behaviour under different load environments is a complicated and time-consuming task. In order to significantly reduce the computational effort for such nonlinear simulations a model simplification is usually applied to the detailed physical finite element model.

Most frequently a dynamic condensation (e.g. using the Craig-Bampton method) is performed where physical degrees of freedom (DOF) are usually maintained at the structure interfaces (or elsewhere inside the structure according to particular response restitution needs) and modal degrees of freedom are included as necessary to adequately predict the responses without being severely affected by modal truncation effects. The latter should always be carefully verified for the frequency band of interest.

In order to implement a representative and easily tuneable nonlinearity inside the spacecraft structural mathematical model the condensation should also include the physical DOF in the vicinity of the nonlinear element. In the particular case of e.g. a nonlinear stiffness the existing local stiffness between these DOF should be removed and replaced by a soft spring (typically 1 N/m) during the condensation. By doing so, the physical links between the different sub-parts of the structure are maintained and the stiffness can be easily tuned in order to perform sensitivity studies with the condensed model (e.g. by modifying the linear or nonlinear stiffness characteristics).

Numerical issues or singularities in the condensed mass and stiffness matrices were encountered during the simulations using the condensed model, [2]. These problems might be avoided by choosing physical DOF which have always associated some mass and stiffness values, even only low ones.

#### 15.4.4.3 Damping assumptions

The damping modelling for nonlinear calculations needs particular attention, in particular where the nonlinear elements are associated with large local damping effects, e.g. elastomer dampers. As a result, the damping cannot be specified as modal damping (percentage of critical damping  $\xi$ ) prohibiting also performing a modal transformation for improved computational efficiency.

Where the damping distribution across the structure is significantly non-homogeneous then a frequency-dependent damping might be derived from a mixing rule. This rule requires for each mode the evaluation of the percentage of strain energy in each sub-system of the FEM. Consequently an equivalent modal damping is calculated in order to perform the modal transformation as for equally distributed damping properties. Note that this approach is not restricted to nonlinear calculations but may be equally applied for linear calculations.

An example with large damping present in the modules A and B is given here-below:

Damping	Module A	Module B	Remaining structure
Amplification factor Q	7	10	25
Percentages of critical damping $\xi$	0.07	0.05	0.02

The equivalent modal damping is then calculated by the following mixing rule:

$$\xi_{equiv} = \varepsilon_A * 0.07 + \varepsilon_B * 0.05 + (1 - \varepsilon_A - \varepsilon_B) * 0.02 \quad [15-4]$$

where  $\varepsilon_k = \frac{\text{strain in module } k}{\text{total strain energy}}$  is the ratio of the strain energy in module  $k$  to the total strain energy in the structure.

The strain energy distribution in the example structure and the resulting modal damping due to the mixing rule is presented in Figure 15-12.

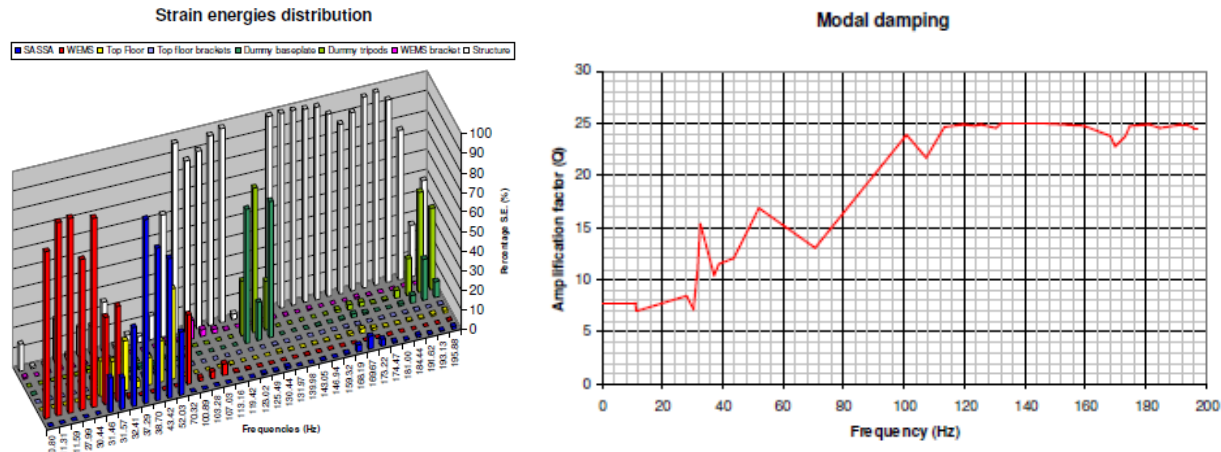


**Figure 15-12: Strain energy distribution and resulting modal damping based on mixing rule, [2]**

The concept of modal damping is no longer applicable in the case of nonlinear analyses requiring direct solution methods, e.g. for transient response analyses the calculations are made for each time step and the damping matrix needs to be evaluated for each time step, too (e.g. as stiffness matrix if nonlinear elements are present).

In NASTRAN there are two different possibilities to apply damping:

- 1) viscous damping as a characteristic of each element;
- 2) Rayleigh damping through a pair of parameters ( $\alpha_1$ ,  $\alpha_2$ ) applied on the mass and stiffness matrix, respectively.

$\alpha_1$  and  $\alpha_2$  are determined to have two values of damping  $\zeta_1$  and  $\zeta_2$  fixed at two specific frequencies  $f_1$  and  $f_2$ :

$$\begin{pmatrix} \alpha_1 \\ \alpha_2 \end{pmatrix} = \frac{2\omega_1\omega_2}{\omega_2^2 - \omega_1^2} \begin{pmatrix} \omega_2 & -\omega_1 \\ -\frac{1}{\omega_2} & \frac{1}{\omega_1} \end{pmatrix} \begin{pmatrix} \zeta_1 \\ \zeta_2 \end{pmatrix} \quad [15-5]$$

where  $\omega_1 = 2 * \pi * f_1$  and  $\omega_2 = 2 * \pi * f_2$ .

However, this definition has the major disadvantage that the damping can be precisely specified only at the frequencies from  $f_1$  and  $f_2$  but not in the whole frequency range of interest. Figure 15-13 shows that the damping deviates significantly from the specified one the more the frequency gets away from  $f_1$  and  $f_2$ .

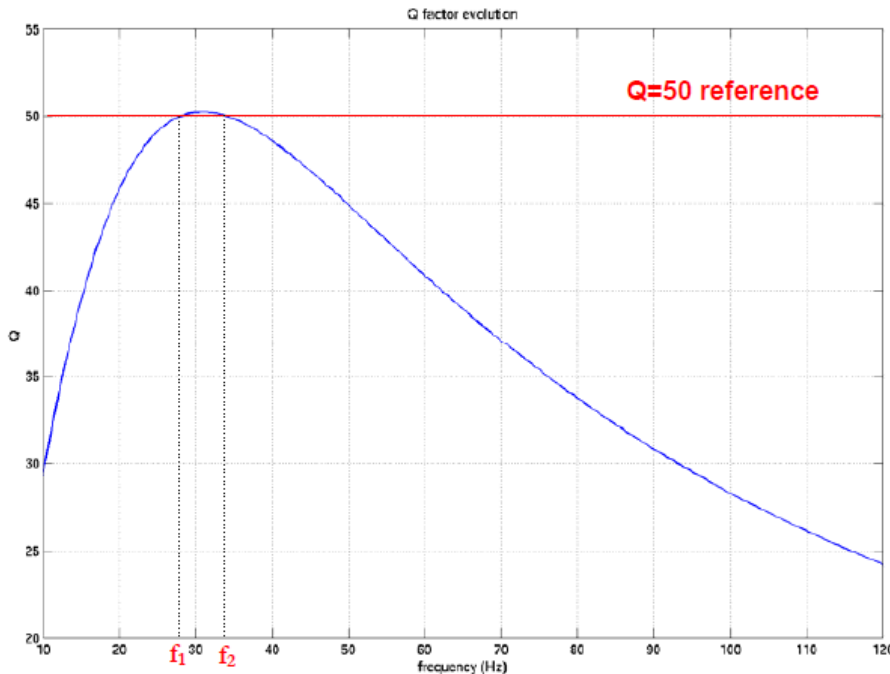


**Figure 15-13: Damping evolution versus frequency as result of chosen parameters  $(\alpha_1, \alpha_2)$**

For a better approximation of the frequency-dependent modal damping as shown in Figure 15-12 this kind of global damping may be combined with the local damping values used for those modules where quite different damping from the global one exists. This local damping may be defined in the “spring and damper” element properties (e.g. NASTRAN CBUSH1D cards) in terms of a force-velocity relationship as well as the stiffness is defined in terms of a force-displacement relationship.

The way how global and local damping is mixed for the direct transient response analysis appears different from what was used for the modal solution. However, concerning the above assumptions (damping considered at module level much greater than damping at structure level) it has been verified that the adjustment of the global damping has little impact on the main responses and that the overall damping is driven by the local damping level “c”, [2].

Monitoring a desired damping in direct transient response analyses remains difficult since the way how global and local damping is mixed is not well mastered. Some fitting is needed, keeping in mind that local damping often drives the global damping at local mode resonances.

#### 15.4.4.4 Nonlinear stiffness definition

Abrupt changes of nonlinear stiffness properties might result in significant convergence problems in numerical simulations. In order to alleviate these problems the transition phases should be smoothed, thereby in general improving the convergence behaviour.

Figure 15-14 shows an example where a 3<sup>rd</sup> order polynomial form is used to modify the transition between two different slopes of the force-displacement curve but maintaining the overall shape of the curve.

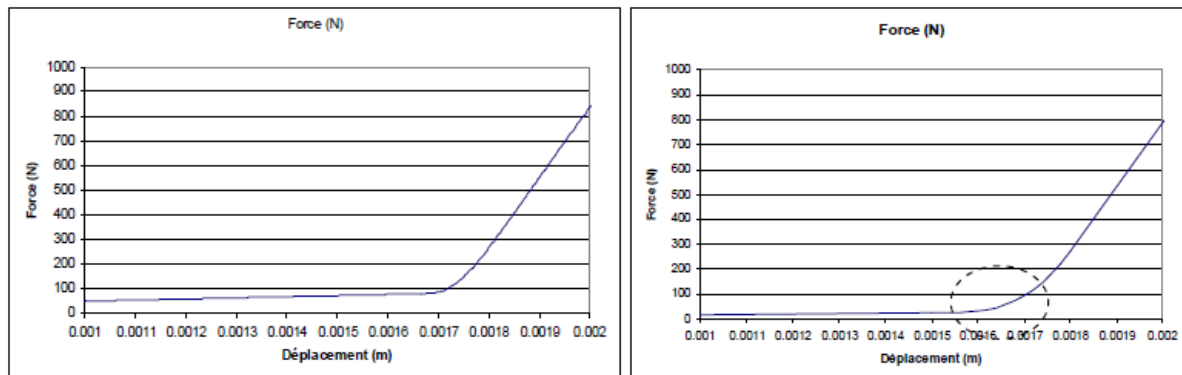


**Figure 15-14: Smooth transition in stiffness definition, [2]**

#### 15.4.4.5 Influence of gravity effects

For certain configurations the effect of gravity should not be neglected. As a result, the nonlinear stiffness definition becomes non-symmetrical. Relevant experience has been gained during hardware testing of the NOLISS study, [2].

#### 15.4.4.6 Nonlinear stiffness parameters

Nonlinear simulations, and in particular their convergence behaviour can be significantly influenced by inappropriate parameter settings:

- Number of time steps per period:

When Newmark's algorithm is used for time integration, the periodicity error for the average acceleration algorithm in the linear case is equal to  $\omega^2 h^2 / 12$  where  $\omega$  and  $h$  are the pulsation of interest and the time step, respectively. For instance, this formula shows that choosing 20 time steps per period leads to an error of 0.8%. In the nonlinear case, significantly smaller time steps may be necessary, in particular when higher harmonics of the excitation frequency are considered.

- Convergence parameters:

Convergence parameters based on displacement and energy were found to give better results than those based on loading but may require more iterations per time step.

- Smoothening of transition phases:

As for the nonlinear stiffness definition sharp transitions in the excitation signal or load application should be avoided. This should make the calculations more stable e.g. because the derivative functions are continuous in that case. Experience has shown that interpolation with a 3<sup>rd</sup> order polynomial might be appropriate.

#### 15.4.4.7 Control simulation

Proper set-up of the control parameters such as sweep rate or compression factor is crucial for a smooth performance of vibration tests of nonlinear structures. Figure 15-15 shows a comparison of control harmonic spectra calculated for both appropriate and inappropriate controller parameters. In the left graph the case is shown where the controller is tuned in such a way to perform smoothly during the sweep. From the zoom it is evident that the beating phenomenon after the first resonance is perfectly simulated and in full agreement with the test.

However, it is also important to correctly predict control instabilities in case the controller parameters are not appropriate for the test at hand. The right graph of Figure 15-15 shows that in such case the

control quality in both the test and simulation is evenly poor. The dramatic impact the control parameters have on such a vibration test is evident as well as how the availability of more sophisticated controller model could help the test engineers to set up proper test conditions, thereby speeding also up the test productivity.

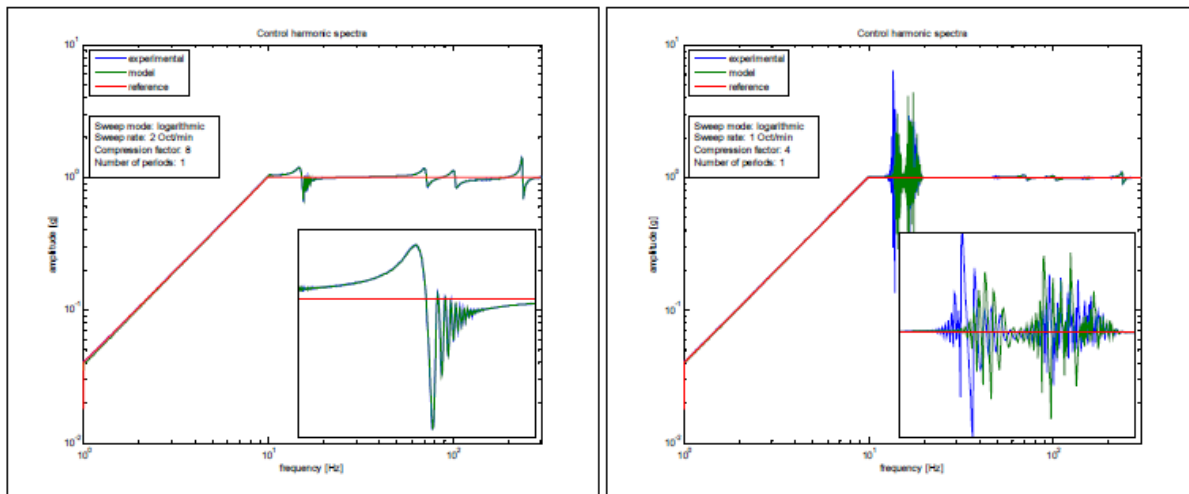


**Figure 15-15: Control harmonic spectra (response zoomed around 1<sup>st</sup> resonance), [2]**

### 15.4.5 Impact of nonlinearities on CLA flight load predictions

Launcher/spacecraft coupled loads analyses (CLA) performed by the launcher authority are usually carried out as linear analyses. In [2] it is shown that this approach was adequate for spacecraft structures for which the structural nonlinearity is relatively weak or not significantly activated by the launcher induced load environment, e.g. the displacements predicted at the location of a mechanical stop are not large enough to reach the stop. Under such assumptions, the inaccuracies imposed by the linearised CLA can be considered negligible and the results should stay within reasonable margins with respect to performing fully nonlinear CLA calculations.

The decision whether a nonlinearity should be considered weak or strong can be made e.g. on the basis of evaluating the effects on a shock response spectrum as shown in Figure 15-16.

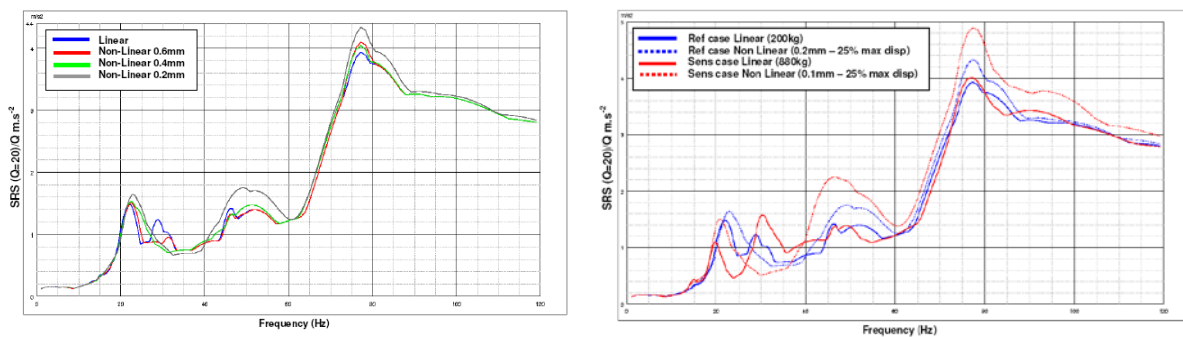


**Figure 15-16: Effects of weak (left) and significant (right) structural nonlinearity on shock response spectrum, [2]**

If the nonlinearity strongly affects the structure performances and involves large masses (e.g. greater than 10% of the total spacecraft mass) then a linearised CLA is no longer representative to adequately perform flight load predictions. However, as shown in [2], nonlinearity could be handled at spacecraft level through an uncoupled analysis approach by applying to the nonlinear spacecraft model the acceleration output from a linearised CLA. For the latter the linearisation of the structural nonlinearity inside the spacecraft was specifically adapted in order to fit the expected excitation range (nonlinearity functioning points).

In the case the expected excitation range and therefore the nonlinearity functioning points, where the linearisation needs to be performed, cannot be adequately determined prior to performing the linearised CLA then, as far as necessary, a few number of linearised spacecraft models might be delivered to the launcher authority. This allows performing multiple flight load predictions using the different linearised spacecraft models and subsequently the results obtained with the most appropriate one might be used to perform the necessary post-CLA analyses at spacecraft level with the nonlinear model.

The linearisation principle and the uncoupled CLA approach are shown in Figure 15-17 and Figure 15-18, respectively.

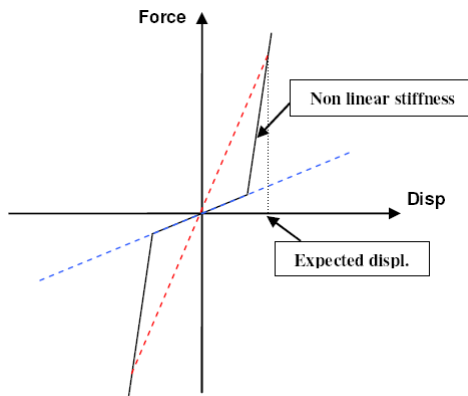


**Figure 15-17: Linearisation principle, [2]**

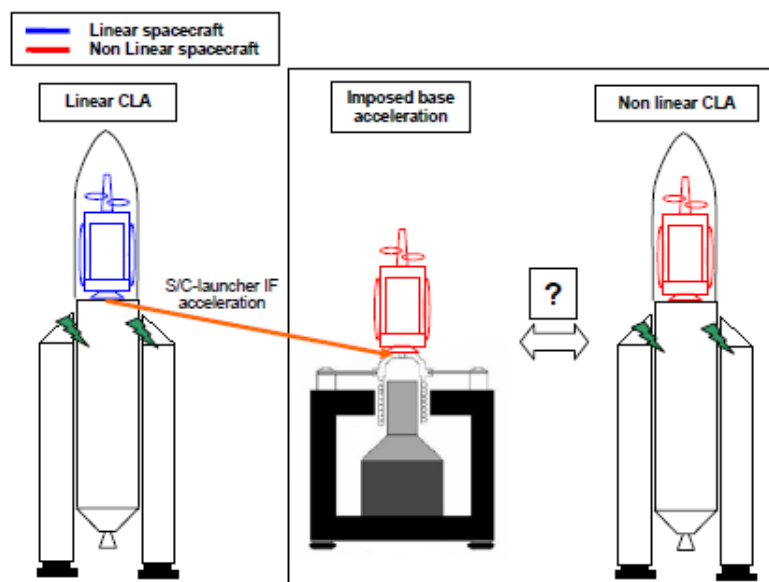


**Figure 15-18: Uncoupled CLA approach for nonlinear spacecraft structure, [2]**

## 15.5 References

- [1] Worden, K., Tomlinson, G.R. "Nonlinearity in Structural Dynamics: Detection, Identification and Modelling", Taylor & Francis (UK), 2001
- [2] "Advancement of Mechanical Verification Methods for Non-linear Spacecraft Structures (NOLISS)", Final Report, ESA Contract 21359/08/NL/SFe, 2011
- [3] Kerschen, G., Worden, K., Vakakis, A.F., Golinval, J.C. "Past, Present and Future of Nonlinear System Identification in Structural Dynamics", Mechanical Systems and Signal Processing 20, p. 505-592, 2006
- [4] Masri, S.F., Caughey, T.K. "A Nonparametric Identification Technique for Nonlinear Dynamic Problems", Journal of Applied Mechanics 46, p. 433-447, 1979
- [5] Roughen, K., Huang, J., Hammerand, D., Stuewe, D., Hertz, S. "Efficient Simulation of Structural Dynamic Systems with Discrete Nonlinearities", 52<sup>nd</sup> AIAA/ASME/ASCE/AHS/ASC Structures, Structural Dynamics and Materials Conference, 2011
- [6] Richards, C., Singh, R. "Identification of multi-degree-of-freedom non-linear systems under random excitations by the reverse-path spectral method", Journal of Sound and Vibration 213, p. 673-708, 1998
- [7] Kerschen, G., Lenaerts, V., Golinval, J.C. "Identification of a continuous structure with a geometrical non-linearity, part I: conditioned reverse path method", Journal of Sound and Vibration 262, p. 889-906, 2003
- [8] "Non-linear Dynamic Analyses (DYNOLI)", Astrium-F reports for CNRS R&D activity R-S06/TG-0002-011, March 2008

# 16

## Finite element models

### 16.1 Introduction

The concept of model is of primary importance in all the fields of the science. In engineering disciplines - and specifically in structure mechanics - a model is a representation able to describe and predict the behaviour of a system in terms of quantifiable variables. A first step to build a model is to choose the variables which are relevant to the studied phenomenon (e.g. displacements, stress, or frequencies) and the types of relationships among them (e.g. the theories provided by elasticity, plasticity, stability, statics, or dynamics): this representation is called the conceptual model (note: sometimes it is also called the “physical model”, however this term is potentially misleading since it is used with a different meaning within the present chapter). The second step is to build a mathematical representation (e.g. using differential equations, integral equations, or probability methods): this representation is called the mathematical model. A third step is to build a numerical (or computational) model, which is a formulation of the mathematical model by means of numerical algorithms, based on several approaches (e.g. the finite element method, the boundary element method, or the finite difference method). A finite element model of a structure is such a type of numerical model of structure behaviours.

For example the structural response of the spacecraft to low frequency mechanical environment of the launch and ascent phase is simulated by spacecraft-launcher coupled dynamic loads analysis which is based on the finite element method and modal synthesis techniques. The loads of the spacecraft derived from the analysis are taken as a basis to verify the dimensioning of the spacecraft. The quality of the recovered structural response on the spacecraft depends on the quality of the mathematical models and loads used for such simulations. Therefore it is crucial that the mathematical models and external loads acting on the launcher are adequately representative of the actual hardware and load condition. For the mathematical models this is done by a correlation and update process, where test results are compared to predicted results and the mathematical model updated till representativity is judged satisfactory within a certain tolerance. When the distance between the model and the experimental results is sufficiently “close”, the model is said to be “valid” or “test-verified”.

This chapter addresses the mathematical models of space structures with a special emphasis on the finite element models used for loads analysis. In particular it provides some guidelines for ensuring FE analysis quality, i.e. the correct use of this specific technology – the finite element method - and the acceptance of the results.

This handbook promotes the verification and validation (V&V) guidance proposed in the ASME Guide for V&V [1]. Some definitions are here recalled:

**model:** the conceptual, mathematical, and numerical representations of the physical phenomena needed to represent specific real-world conditions and scenarios. Thus, the model includes the geometrical representation, governing equations, boundary and initial conditions, loadings, constitutive models and related material parameters, spatial and temporal approximations, and numerical solution algorithms.

**conceptual model:** the collection of assumptions and descriptions of physical processes representing the solid mechanics behaviour of the reality of interest from which the mathematical model and validation experiments can be constructed.

**mathematical model:** the mathematical equations, boundary values, initial conditions, and modelling data needed to describe the conceptual model

**computational model:** the numerical implementation of the mathematical model, usually in the form of numerical discretization, solution algorithm, and convergence criteria.

## 16.2 Requirements for structure mathematical models

The ECSS requirements related to or relevant for structure mathematical models are reported in the following documents:

- ECSS-E-ST-32 Structural general requirements [2] (e.g. requirements for verification by analysis, data exchange for structural mathematical models, DRDs for mathematical model description and delivery)
- ECSS-E-ST-32-03 Structural finite element models [3] (e.g. general requirements, reduced mathematical models, model checks and test-analysis correlation)
- ECSS-E-ST-32-10 Structural factors of safety for spaceflight hardware [4] (e.g. requirements for model factor  $K_M$ )
- ECSS-E-ST-32-11 Modal survey assessment [5] (e.g. requirements for mathematical model validation, test-analysis correlation, mathematical models supporting modal survey tests, reduced mathematical models)

## 16.3 Introduction to V&V in computational mechanics

The following sections provide general guidance for implementing verification and validation of computational models for spacecraft and payloads. The guidance is based on [1].

The primary objective of V&V is to build confidence in the predictive capability of computational models. Specifically:

- a. Verification assesses the numerical accuracy of a computational model, irrespective of the physics being modelled.

The following definition can be established:

**Verification (of computational solid mechanics model):** the process of determining that a computational model accurately represents the underlying mathematical model and its solution.

A working definition of verification could be “solving the equations right”. This is a mathematics issue.

- b. Validation assesses the degree to which the computational model is an accurate representation of the physics being modelled. It is based on comparisons between numerical simulations and relevant experimental data. Validation assesses the predictive capability of the model in the physical realm of interest, and it addresses uncertainties that arise from both experimental and computational procedures.

The following definition can be established:

**Validation (of computational solid mechanics model):** the process of determining the degree to which a model is an accurate representation of the real world from the perspective of the intended uses of the model.

A working definition of validation could be “solving the right equations”. This is a physics issue.

The manner in which the mathematics and physics interact in the V&V process is illustrated in the flow chart in Figure 16-1. After the selection of the conceptual model, the V&V process has two branches: the left branch contains the modelling elements and the right branch the physical testing (experimental) elements.

Figure 16-1 also illustrates the paramount importance of physical testing in the V&V process, as ultimately, it is only through physical observations (experimentation) that assessments about the adequacy of the selected conceptual and mathematical models for representing the reality of interest can be made. Close cooperation among modellers and experimentalist is required during all stages of the V&V process, until the experimental outcomes are obtained.

The guidance provided by [1] is based on the following key principles:

- a. Verification (addressing programming errors and estimating numerical errors) precedes validation (assessing a model's predictive capability by comparing calculations with experiments).
- b. The need for validation experiments and the associated accuracy requirements for computational model predictions are based on the intended use of the model and should be established as part of V&V activities.
- c. Validation of a complex system should be pursued in a hierarchical fashion from the component level to the system level.
- d. Validation is specific to a particular computational model for a particular intended use.
- e. Simulation results and experimental data providing a meaningful assessment of uncertainty.

The “adequacy” of the computational model is strictly related to the successful completion of the V&V processes of the model. In principle the V&V processes begin with a statement of the intended use of the model so that the relevant physics are included in both the model and the experiments performed to validate the model. Modelling activities and experimental activities are guided by the response features of interest and the accuracy requirements for the intended use.

Ideally the V&V processes end with acceptable agreement between model predictions and experimental outcomes after accounting for uncertainties in both, allowing application of the model for the intended use. In principle if the agreement between model and experiment is not acceptable, the processes of V&V are repeated by updating the model and performing additional experiments.

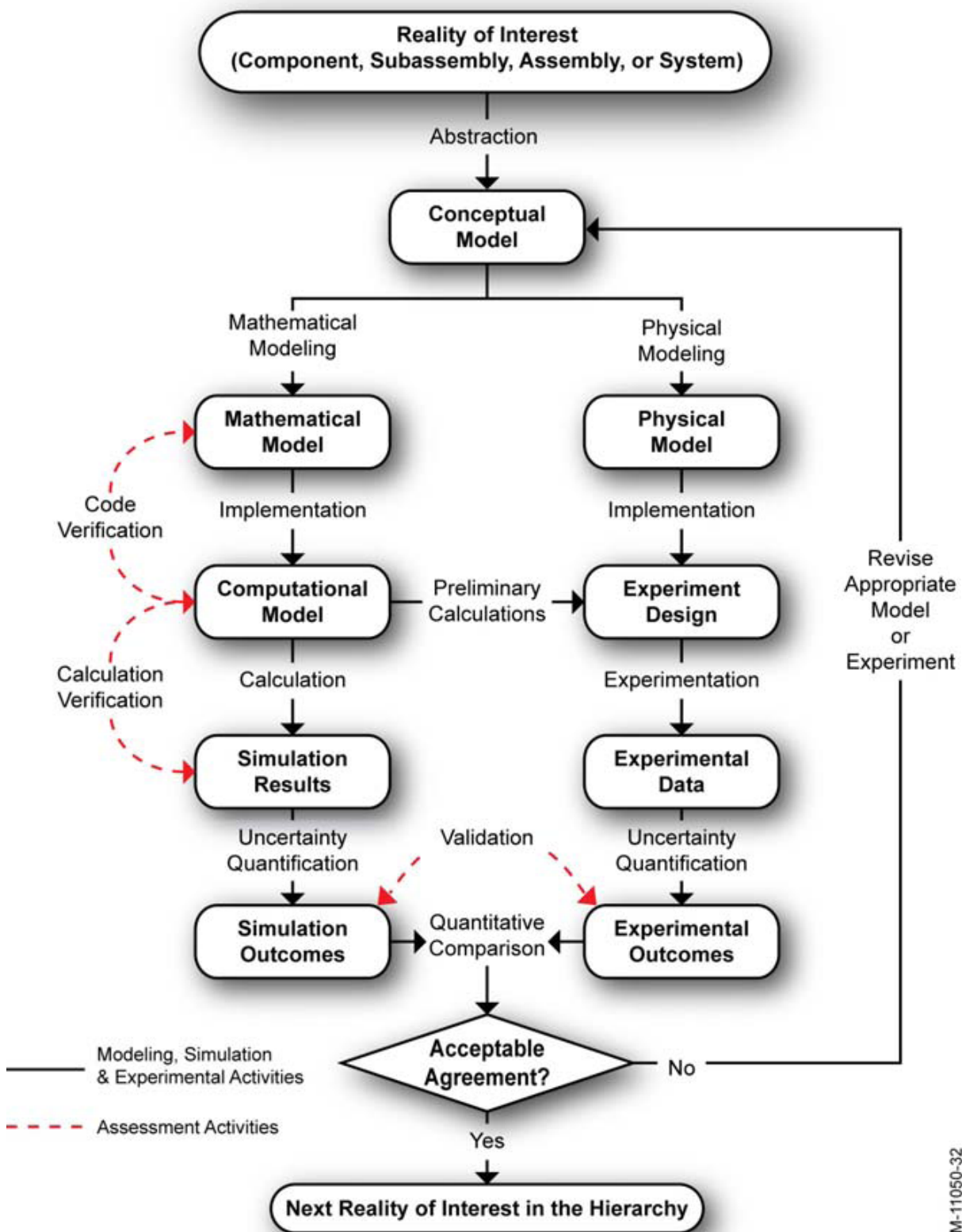


Figure 16-1: V&amp;V Activities and products [1]

## 16.4 Spacecraft finite element model complexity and validation test

Mathematical models of spacecraft and payloads have a “natural evolution” from simple to detailed models in line with the progress of the project. In any case the primary goal is to include the relevant physics in the model. Guidelines on how to develop an adequate mathematical model, specifically a FE model of a generic spacecraft, are beyond the scope of this handbook. However the following key aspects are pointed out:

- a. The dynamic models should be able to represent the major modal characteristics of the spacecraft. The model includes the elastic representations of all the items (e.g. appendages, science instruments) which have fixed base frequencies less than a defined frequency cut-off, consistently with the relevant physics (e.g. taking into account the frequency content of the forcing functions). Components with fixed base frequencies greater than the frequency cut-off are usually represented as lumped masses in the spacecraft model.
- b. The dynamic models include load transformation matrices (LTMs) for recovering items used in structural assessments. These loads recovery items consist of, for example, forces at all primary interfaces, member loads, stresses or stress indicators, CoG net accelerations, and section net loads in critical primary structural elements.
- c. The dynamic loads for final verification are developed from a dynamic model that reflects the use of experimental values of dynamic characteristics as obtained from appropriate tests and modal surveys.

Concerning the validation test (i.e. the experiment that is designed and performed to generate data for the purpose of model validation) this is usually a modal survey or a vibration test. The following key aspects are mentioned:

- a. The spacecraft validation test provides data to verify significant mode shapes and frequencies of the spacecraft dynamic mathematical model up to the relevant frequency cut-off when constrained at the launcher attach point interfaces. The significant mode shapes and frequencies are those which are primary contributors to launcher/spacecraft interface loads and internal loads.
- b. The validation test provides data to verify the dynamic characteristics of the spacecraft/launcher interface. A test configuration which imposes flight-like constraints (fixed-base) at the spacecraft/launcher interfaces is normally preferred for meeting this scope.
- c. Appropriate techniques are employed to evaluate nonlinearities in the flight hardware. Two examples are measuring test article response with respect to varying input force levels and checking for the input/output relationship, i.e. reciprocity. Nonlinearities should be evaluated as to their significance in the loads analysis. In the presence of significant nonlinearities consideration are given to measuring the affected modes and frequencies under increased load levels.
- d. Proper techniques are also used to accurately measure modal damping for all modes.

## 16.5 Uncertainty quantification during load cycles

### 16.5.1 Overview

According to [1] the uncertainty quantification is the process of characterizing all uncertainties in the model (or experiment) and of quantifying their effect on the simulation (or experimental) outcomes.

The uncertainty quantification is a complex issue and methods can be found in literature on the topic (e.g. based on Monte Carlo simulations and sensitivity analyses). However for the purpose of this handbook the practical approach by means of “factors” is presented.

This approach is based on the following assumptions:

- that recognized methodologies are used for the determination of the limit loads, including their scatter, that are applied to the hardware and for the stress analyses;
- that the structural and mechanical system design is amenable to engineering analyses by current state-of-the-art methods and is conforming to standard aerospace industry practices.

The factors are selected to cover chosen load level probability, assumed uncertainty in mechanical properties and manufacturing but not a lack of engineering effort.

In practice the following factors are used:

- The dynamic variability or uncertainty factor  $K_V$ . It is applied to the elastic portion (or to the “dynamic” portion) of the response calculated in the launcher-spacecraft CLA for calculating the Limit Loads (LL). Typically this factor is used for Space Shuttle missions.
- The model factor  $K_M$ . It is applied for calculating the Design Limit Loads (DLL) from the LL, [4].

It should be noted that in some cases applying both factors could be over-conservative at spacecraft system level, since the factors  $K_V$  and  $K_M$  partially cover the same uncertainty. On the other hand some launcher authorities can require the application of the  $K_V$  factor to the total response calculated in the launcher-spacecraft CLA.

### 16.5.2 Dynamic variability or uncertainty factor $K_V$

#### 16.5.2.1 Introduction

The dynamic variability or uncertainty factor  $K_V$  is applied to the elastic portion (or to the “dynamic” portion) of the response calculated in the launcher-spacecraft CLA for calculating the LL. It provides a margin for load increases due to variability and uncertainty in definition of the CLA dynamic models and forcing functions and, for Space Shuttle missions, location in the Orbiter cargo bay [6].

Coupled loads analyses are typically performed at each major step in the design process. For example: PDR, CDR, Preliminary Verification Load Cycle, and Final Verification Load Cycle. This is the case addressed in the next sections, basically reflecting the approach applied for the Space Shuttle payloads. Additional load cycle analyses may be required during the design process to evaluate the effects of changes in either spacecraft design or launcher criteria. The flow describing a typical coupled (cargo element/Space Shuttle) loads cycle is provided in Figure 16-2 [6].

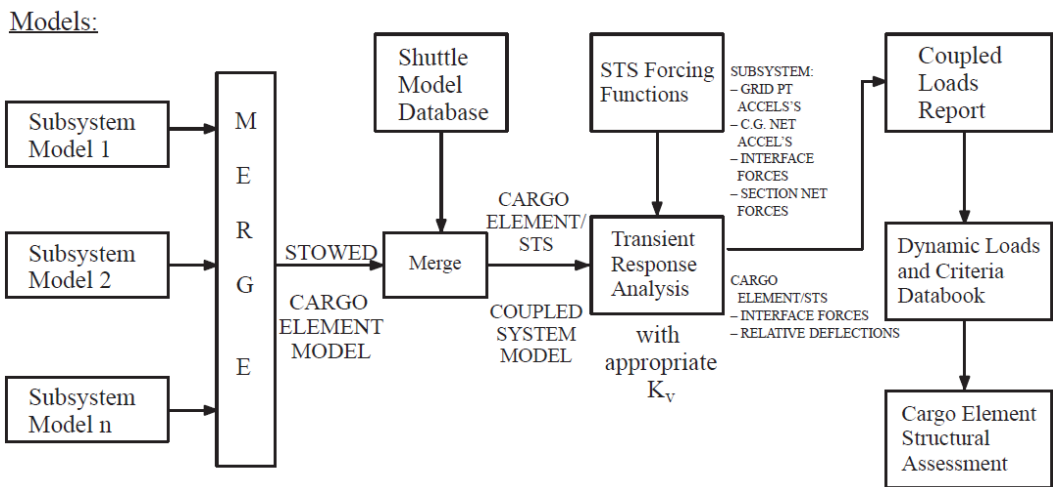


**Figure 16-2: Flowchart of a typical load cycle for Shuttle-Payload lift-off and landing conditions [6]**

### 16.5.2.2 Phase B load criteria development and PDR load cycle

Generic load criteria or loads data from detail analysis of previously analysed, similar spacecraft and payloads may be used to establish the initial design loads. These design loads are used for PDR member sizing and margins assessment. A coupled dynamic loads analysis is normally accomplished for the PDR design configuration. The PDR loads cycle uses, for example, a dynamic uncertainty/variability factor  $K_v = 1.5$  applied to the dynamic response. The loads from the dynamic analysis are compared with the initial design loads. The initial design loads are adjusted based on the results of the PDR coupled loads analysis especially when the loads predicted by the PDR dynamic analysis are greater or when significant cost and weight savings can be realized by using the lower PDR dynamic loads. These adjusted design loads criteria are used to perform detail stress and safe-life assessment for hardware drawing release.

### 16.5.2.3 CDR load cycle

A coupled dynamic loads analysis is accomplished for the CDR design configuration. The CDR load cycle is based on finite element models developed using, wherever possible, the detailed hardware drawings. The coupled dynamic loads analysis uses, for example,  $K_v = 1.25$  applied to the dynamic response. The loads from the CDR coupled dynamic loads analysis are compared to the design loads used for the release of the manufacturing drawings. The design loads are superseded with the results of dynamic loads analysis where the CDR analytical loads are higher; or, with approval from the Prime Contractor, when significant cost and weight savings can be realized by using CDR loads that are lower than current design loads. Released drawings are reassessed for higher CDR loads as required. Design loads are used to qualify hardware during the static loads test.

### 16.5.2.4 Preliminary verification load cycle

This load cycle is the spacecraft verification load cycle using models updated with CDR released drawings and some test verification. The dynamic loads analysis uses, for example,  $K_v = 1.1$  when test verified models are available and  $K_v = 1.25$  when test verification has not been completed. The results of this analysis are compared with design loads and qualification test loads to ensure that the loads are enveloped by both the design loads used in structural integrity assessment and by the qualification test loads.

### 16.5.2.5 Final verification load cycle

The final verification loads analysis cycle is performed prior to each flight. This analysis develops the predictions of flight loads and deflections which are used for the structural integrity verification of the spacecraft. In general, this analysis uses  $K_V = 1.0$  but it may be higher depending on the model correlation test results. The dynamic mathematical models used in the spacecraft preliminary verification load cycle are updated based upon the results of the structural assessment and/or additional tests. A margin of safety assessment using the results from this analysis is accomplished.

### 16.5.3 Model factor $K_M$

The model factor ( $K_M$ ) is defined as the factor which takes into account the representativity of mathematical models [4]. It is applied to account for uncertainties in mathematical models when predicting dynamic response, loads and evaluating load paths.

The model factor is part of the Design Factor (DF) which allows calculating the Design Limit Loads from the Limit Loads (DLL = LLxDF; [4]). It is applied at every level of the analysis tree system where predictive models are used. It encompasses the lack of confidence in the information provided by the model, e.g. hyperstaticity (uncertainty in the load path because of inaccuracy of the mathematical model), junction stiffness uncertainty, non-correlated dynamic behaviour. While going through the design refinement loops,  $K_M$  can be progressively reduced to 1.0 after demonstration of satisfactory correlation between mathematical models and test measurements.

The value for the model factor is based on relevant historical practice, analytical or experimental means. Typical values of  $K_M = 1.2$  are used for satellites at the beginning of new developments and  $K_M = 1.0$  for internal pressure loads for pressurized hardware.

## 16.6 Verification and quality assurance for spacecraft finite element analysis

It is possible to distinguish between code verification, addressing errors in the software, and calculation verification, estimating numerical errors due to under-resolved discrete representations of the mathematical model [1] (see Figure 16-1).

*Code verification* is the process of determining that the numerical algorithms are correctly implemented in the computer code and of identifying errors in the software. Code verification is the domain of software developers who hopefully use modern Software Quality Assurance techniques along with testing of each released version of the software. Users of software also share in the responsibility for code verification, even though they typically do not have access to the software source.

*Calculation verification* is the process of determining the solution accuracy of a particular calculation. It basically means estimating the errors in the numerical solution due to discretization. Any comparison of the numerical and analytical results contains some error, as the discrete solution, by definition, is only an approximation of the analytical solution. So the goal of calculation verification is to estimate the amount of error in the comparison that can be attributed to the discretization. Discretization error is most often estimated by comparing numerical solutions at two more discretizations (meshes) with increasing mesh resolution, i.e. decreasing element size. The objective of these mesh-to-mesh comparisons is to determine the rate of convergence of the solution. The main responsibility for calculation verification rests with the analyst, or user of the software. The lack of mesh-refinement studies in solid mechanics is often the largest omission in the verification process. This is particularly distressing, since it is relatively easy to remedy using available adaptive meshing techniques.

In practice the verification process for spacecraft FE analysis typically entails *checks of the model* and *analysis methods*. The model checks that are relevant for the verification process are reported in [3] and are here listed:

- a. Model geometry checks for unreduced models.
- b. Elements topology checks for unreduced models.
- c. Rigid body motion checks for reduced and unreduced models.
- d. Static analysis checks for reduced and unreduced models
- e. Stress free thermo-elastic deformation check for unreduced models.
- f. Modal analysis checks for reduced and unreduced models.
- g. Reduced model versus non reduced model consistency checks.

When a system level model is developed by coupling (merging) several substructure models, such as for launch loads analysis, the above-mentioned checks should be performed for each substructure model and then again for the system model.

An effective way to check the *analysis method* is to perform a second analysis using a different method or mathematical model and see if similar results are obtained. For complex analyses, such as the CLA to predict launch loads, specific checks are performed (e.g. on condensed mass and stiffness matrices and LTM generation, see Section 6.2.5).

To ensure quality, it is also crucial to document the finite element analyses which have been performed and control the electronic files [7]. It should be noted that verification of requirements depends heavily on finite element models. Even in a structural test to verify strength, the load cases or environments used in the test are based on analyses and are nearly always traceable to one or more FE models.

Some of the most important things to document for FEA are:

- a. Objectives
- b. Assumptions
- c. Reference to a drawing number for the structure being modelled
- d. Model configuration, including geometry, element properties, interface nodes, and boundary conditions
- e. Description of how key areas such as joints are modelled
- f. Derivation of loading conditions and references for traceability
- g. Input files that document submitted loading conditions and analyses
- h. Model checks
- i. Analysis results and conclusions, including any sensitivity studies done

The ECSS standard regarding structural general requirements, [2], includes the relevant Document Requirement Definitions (DRD) for structural analysis and mathematical models. In particular:

- a. Design loads (DL) - DRD
- b. Mathematical model description and delivery (MMDD) – DRD
- c. Modal and dynamic response analysis (MDRA) – DRD
- d. Test-analysis correlation (TAC) - DRD

## 16.7 Mathematical model validation

### 16.7.1 General concepts and terminology

The concepts of test-analysis correlation, error localization, model updating and validation are strongly related. This section reviews some general concepts and the terminology.

*Correlation* is the process of quantifying the degree of similarity and dissimilarity between two models [8]. Different indices can be involved to provide the most useful measures of correlation for the intended uses of the model. Correlation implies the choice of the *correlation metrics*.

*Error localisation* is the process of determining which areas of the model need to be modified. This is a pre-requisite before updating can take place. The aim of error localization is to give a hint where to search for an error, i.e. to identify locations likely to contain errors.

For *model update or updating*, two definitions from the literature are here reported:

*Model update* is the process of changing the basic assumptions, structure, parameter estimates, boundary conditions, or initial conditions of a model to improve model accuracy [1].

*Model updating* is the process of correcting the numerical values of individual parameters in a mathematical model using data obtained from an associated experimental model such that the updated model better describes the dynamic properties of the subject structure [8].

The first definition is probably more general and more relevant for what concerns the spacecraft mathematical model validation. In fact in real life cases model updating is not only parameter identification and model calibration but also consists of partial re-modelling as for example remeshing, change of element type and modification of boundary conditions.

The aim of the *model updating* in structural dynamics is to generate improved numerical models (i.e. "valid models") which may be applied in order to obtain predictions for alternative loading arrangements and modified structural configurations. For spacecraft structures normally the primary goal of the updating process is to find a mathematical model able to reproduce the test data used for updating. This goal is considered necessary but not sufficient. In fact reproducing test data does not guarantee predictability away from the region in the design space that relates to the test data. In order to make the updated model applicable to an environment which deviates from the test environment (e.g. following a modal survey test, the model is used for launcher-spacecraft coupled analysis) it should be necessary to identify the real sources and locations of the "error". This can be a difficult task.

The scenario is even more complicated by the fact that, within a deterministic approach which uses a single-test single-analysis correlation metrics, which is often the case in the space business, where is no guaranty that a "better test-analysis correlation" provides a "better model" [9]. In this context it is useful to introduce the concepts of consistent updating and inconsistent updating. If the error assumptions in the updating process are the same as the true erroneous areas in the model, this is called *consistent updating*. Vice versa if the error assumptions are not the same as the true erroneous areas, this is called *inconsistent updating*. This could bring to a "false validation".

In principle only in cases where all the erroneous parameters (or model areas) have been located and included in the updating process, a "fully consistent" updating can be performed. That is an ideal case. In practice in most of real life cases the solution, i.e. the "updated model" (or "improved model" also improperly called "correlated model") is a compromise which is often of rather unknown quality.

Finally, it should be noted that the model updating is a process fraught with numerical difficulties. These arise from inaccuracy in the finite element model and imprecision and incompleteness in the measurements [10].

It has been already reported that *validation* is “the process of determining the degree to which a model is an accurate representation of the real world from the perspective of the intended uses of the model” [1]. In the context of structural dynamics and loads analysis a valid model is a model which predicts the required dynamic behaviour of the subject structure with an acceptable degree of accuracy, or “correctness” [8].

Unfortunately there are no well-established and generally accepted criteria to judge the soundness or accuracy of the model. As mentioned, a numerical simulation is not necessarily validated after the output has been compared to test data and the model has been updated. Of course the purpose of a model (that is, what the model needs to predict) is of paramount importance because it dictates the features and metrics on which the validation should focus. Often, in practical cases, the mathematical model is declared to be “valid” on the base of the “correlation criteria”, “engineering judgement” and agreement of all parties involved. In some cases “extra factors” (e.g.  $K_V$  and  $K_M$ ) are used for output recovery to take into account test-analysis mismatches and uncertainties.

In conclusion the scenario is very complex. In practice the acceptance of a spacecraft computational model for loads analysis is usually and mainly based on the evaluation of predicted and measured modal properties such as natural frequencies, mode shapes and effective masses [5] [6], which are important characteristics that affect the structure response to applied forces. In fact natural frequencies affect response amplitude, mode shapes affect how loads distribute in the structure and modal effective masses seen from the launcher interface directly relates to the forces across the spacecraft-launcher interface. The acceptance of the model is then based on some “*correlation criteria*” or “*goals*”. They can be defined as the degree of similarity or dissimilarity establishing that the correlation between measured and predicted values is acceptable. The European Cooperation for Space Standardization (ECSS) [5] and the American space agency NASA [6] have established criteria mainly based on natural frequency deviations, modal assurance criterion (MAC), cross-orthogonality checks and effective modal mass values. It should be noted that this approach slightly mixes up the notion of “*validation*” with the one of “*certification*”. In practice, for model correlation, the criteria are somewhat arbitrarily selected, so violating them merely means that an expansion of sensitivities studies to broader tolerances is necessary.

## 16.7.2 Why a mathematical model validation process

The reasons for validating a spacecraft mathematical model can be categorized as follows:

- Need to validate “critical analysis” results (e.g. launcher-spacecraft CLA results)
- Need to verify the structural design and complement test measurements (e.g. “real time validation” [11] during sine qualification test for notching reassessment)
- Need (or opportunity) to substantiate/improve the analysis to reduce programmatic risks (e.g. validation of an instrument FE model vs. base-drive random test in order to use the FE model for satellite system vibro-acoustic predictions)

Depending on the reasons for validating and on the criticality of the analysis, different correlation criteria can be established. In this context and for the purpose of establishing adequate correlation criteria, the following aspects should be taken into account:

- The loads analysis is probably the most important single step in the design of space structures: it is the basis for static design (quasi-static loads) and test loads as well as the basis for identifying the target responses and “notching criteria” in sine tests.
- Non-representative loads analysis would result to structure design and test verification on the basis of wrong loads.
- It is important to be very confident in loads analysis, which means checking the sensitivity of our assumptions and validating the loads analysis that is the basis of strength analysis and static testing.

### 16.7.3 Categorization of the uncertainty and sources of disagreement between simulation and experimental outcomes

It has been mentioned that the aim of validation for computational mechanics models is to take into account the uncertainties associated with both simulation results and experimental data. It is useful to categorize uncertainties as being either irreducible or reducible [1].

*Irreducible uncertainty* (also called "*aleatory uncertainty*") refers to inherent variations in the physical system being modelled. This type of uncertainty always exists and is an intrinsic property of the system. Examples of irreducible uncertainty are variations in geometry, material properties, loading environment, and assembly procedures.

*Reducible uncertainty* (also called "*epistemic uncertainty*") refers to deficiencies that result from a lack of complete information or knowledge. Two important sources of reducible uncertainty are statistical uncertainty and model form uncertainty. *Statistical uncertainty* arises from the use of limited samples. *Model form uncertainty* refers to the uncertainty associated with modelling assumptions.

The main sources for the disagreement between analytical predictions and test results can be also categorized. For example:

- Modelling uncertainties and errors. The model is not completely physically representative due to missing physics (uncertainties in the stiffness of bolted or bonded joints, lack of damping representation, nonlinearities etc.) and mistakes (input errors, oversights, etc.). This is mainly a reducible uncertainty, especially a model form uncertainty.
- Scatter in manufacturing. For example the uncertainty in manufacturing tolerances (material and physical properties, etc.). This is mainly an irreducible uncertainty but can include some statistical uncertainty.
- Error and uncertainties in testing. For example the test related scatter (uncertainties in the test set-up and input loads, measurement errors, boundary conditions, etc.). This includes reducible and irreducible uncertainties.

In real life cases, the above mentioned uncertainties are normally used to justify poor or bad correlation and mathematical model modifications, following a model updating process.

### 16.7.4 Specific aspects of the validation of spacecraft FEM for coupled loads analysis

#### 16.7.4.1 Introductory aspects

The following sections provide an example on how the concepts and terminology which have been presented are applicable to the specific issue of the FEM validation for LV/SC coupled loads analysis.

The following short "dictionary" makes explicit reference to the ASME Guide for V&V [1] and shows how the terminology which has been presented is used with respect to the validation of spacecraft FEM for coupled loads analysis:

- Reality of interest: spacecraft low frequency transient environment
- Intended use of the model: launcher-spacecraft CLA (to predict system behaviour for cases that are not tested)
- Response features of interest: "CLA loads", i.e. forces, accelerations, etc.
- Validation testing: modal survey test or base-drive sine test
- Experimental data: e.g. accelerations, forces (time histories, transfer functions etc.)

- Experimental features of interest: natural frequencies, mode shapes etc.
- Metrics: relative errors (e.g. natural frequency deviations), MAC, etc.
- Accuracy requirements: e.g. see [5] (mainly in terms of correlation criteria)
- Computational model: NASTRAN F.E. model (eigenmodes analysis)
- Validation documentation: e.g. test-analysis correlation DRD in [2]

### **16.7.4.2 Phases of the validation process**

In the following the major phases of the validation process are shortly depicted.

#### **16.7.4.2.1 Modal survey (or vibration test) pre-test analysis**

A pre-test analysis prior to the modal survey is normally performed. The main purpose of this analysis is to identify all target mode shapes and frequencies for the modal survey test and to identify any coupling between the test fixture and the test article. The pre-test model is analysed in the modal survey test configuration using the same boundary conditions.

The pre-test analysis generally addresses the following objectives and activities:

- To identify all target modes
- To identify any coupling between test fixture and test article
- To confirm the adequacy of the test configuration
- To provide an appropriate instrumentation layout (e.g. for exciters and accelerometers)
- To provide a condensed mass matrix to perform, for example, the orthogonality checks
- To draw a test article simplified geometry (also called wireframe or silhouette) to visualize test (and analysis) mode shapes

#### **16.7.4.2.2 Acquisition of modal data (by test & FE analysis)**

There are basically two categories of vibration tests for the acquisition of the structure modal data:

- Modal survey tests, which are dedicated tests to provide data for dynamic mathematical model validation. A modal survey requires more effort, both in financial and time terms, however it provides results of higher quality, especially when phase resonance techniques are used.
- Base drive vibration tests, usually a sine test. This has the advantage to be performed within the structure qualification or flight acceptance test campaigns of the spacecraft. However a base drive vibration test normally provides modal data of lesser quality.

NOTE 1 Modal survey tests are often performed on structural models (SM or STM) in flight representative configuration.

NOTE 2 Modal parameters (natural frequencies, mode shapes, damping, effective masses, etc.) can be determined in two ways:

- by a method with appropriation of modes, sometimes called phase resonance, which consists of successively isolating each mode by an appropriate excitation and measuring its parameters directly;
- by a method without appropriation of modes, sometimes called phase separation, which consists of exciting a group of modes whose parameters are then determined by processing the measurements.

#### 16.7.4.2.3 Test-Analysis Correlation

This phase includes:

1. The selection of the features of interest for quantitative comparison
2. The choice of the correlation metrics

For quantitative comparisons, the characteristics that most affect the structure response to applied forces are considered. These are:

- Natural frequencies
- Mode shapes
- Modal effective masses
- Modal damping
- Total mass and, mass distribution
- Centre of Gravity and inertia properties
- Static stiffness
- Interface forces

The correlation of the reported characteristics is in most cases performed by calculating the test-analysis deviations (e.g. in percentage). The modal damping is only available by processing the measured data. The correlation of mode shapes is addressed in next section.

#### 16.7.4.2.4 Error Localization

This is normally an iterative process which can include:

- Analyst's knowledge of uncertain modelled regions
- Sensitivity analysis & selection of "updating parameters" (i.e. design variables of the optimization process, such as stiffness parameters modelling joints etc.)
- "A posteriori" evaluation of preliminary optimization processes
- Other specific error localization techniques

Error localization and model updating by sensitivity and optimization is addressed in Section 16.7.5.

#### 16.7.4.2.5 Model Updating

Conceptually the model updating phase follows the error localization phase. Often, in real cases, the two phases cannot be easily distinguished since the same methods, procedures and software are used to both localize the model errors and improve the model behaviour with respect to the experimental results. In principle, within a sensitivity and optimization approach (Section 16.7.5) it is possible to "identify" the model updating phase as the "final" optimization process which minimizes the correlation metrics. The computational model produced by the updating process is called "updated model" or "improved model" (sometimes improperly called "correlated model").

#### 16.7.4.2.6 Validation assessment

Validation assessment consists on a critical evaluation of the simulation and experimental outcomes. In particular, for example for the "updated model", it means answering the following questions:

- Are the test/analysis discrepancies acceptable?
- Are the modifications applied to the model realistic and justifiable?

- Does the model need further revision? (such as re-modelling, debugging, etc.)

A mathematical model should be considered valid only if the test-analysis discrepancies are acceptable. This is usually considered a necessary condition but not sufficient. Moreover, in order to limit the chances that an inconsistent updating has been performed, it is important that the FEM modifications be realistic and justifiable.

In this context it should be noted that the “valid” (also called “test-verified”) mathematical model is normally used to predict the structural response to different load conditions and in different spacecraft configurations (e.g. spacecraft test configuration could be rather different from the launch configuration). If the FEM parameters are “incorrect” the recovered structural response can be “incorrect” as well. This is the major reason to avoid an inconsistent updating or false validation, where the correlation could be even good, however the parameters modelling the structure are “incorrect”. In conclusion, for a valid model, it is crucial to identify and correct the true locations of error.

#### 16.7.4.3 Mode shape correlation

Generally, the analysis and test mode shapes cross-orthogonality and MAC terms, along with the natural frequency deviations, are used as the main criteria for judging the degree of correlation.

The cross-orthogonality check provides a way of checking the correlation between the analytical model mode shapes  $\Phi_a$  and the measured mode shapes  $\Phi_m$ , thereby identifying the analysis mode shape that matches with the measured mode shape. Given a measured mode shape matrix  $\Phi_m$  of size  $(n, N_m)$ , a symmetric positive definite matrix  $\mathbf{M}$  of size  $(n, n)$  corresponding to the analytical model mass matrix, and the analytical model mode shape matrix  $\Phi_a$  of size  $(n, N_a)$ , the cross-orthogonality between the analysis and test mode shapes with respect to the mass matrix is given by

$$\mathbf{C} = \Phi_m^T \mathbf{M} \Phi_a \quad [16-1]$$

Therefore the generic term of  $\mathbf{C}$ , related to the  $r$ -th measured mode shape  $\phi_{mr}$ , where  $r = 1, 2, \dots, N_m$ , and the  $s$ -th analytical mode shape  $\phi_{as}$ , where  $s = 1, 2, \dots, N_a$ , is:

$$C_{rs} = \phi_{mr}^T \mathbf{M} \phi_{as} \quad [16-2]$$

Both measured and analytical mode shapes can be normalised using the mass matrix  $\mathbf{M}$  in the following way:

$$\phi_{mr}^T \mathbf{M} \phi_{mr} = 1 \quad r = 1, 2, \dots, N_m \quad [16-3]$$

$$\phi_{as}^T \mathbf{M} \phi_{as} = 1 \quad s = 1, 2, \dots, N_a \quad [16-4]$$

A unity matrix for  $\mathbf{C}$  would mean a precise correlation between the analytical and measured mode shapes. That is an ideal case. In real cases  $\mathbf{C}$  is an unsymmetric full matrix, and the  $r$ -th measured mode is correlated to the  $s$ -th analytical mode as much as  $C_{rs}$  is closer to the unity and the other elements of the  $r$ -th row of  $\mathbf{C}$ , i.e. the coupling terms, are closer to zero. There are two major difficulties that restrict the use of orthogonality checks, namely the measurement of complex modes and the incompleteness of the measured data. The incompleteness is due to the limited number of measurement locations, which means that the mass matrix must be reduced or the mode shapes must be expanded.

The MAC between a measured mode  $\phi_{mr}$  and an analytical mode  $\phi_{as}$  is defined as:

$$MAC_{rs} = \frac{(\phi_{mr}^T \phi_{as})^2}{\phi_{mr}^T \phi_{mr} \phi_{as}^T \phi_{as}} \quad [16-5]$$

Eq. [16-5] determines the correlation between two modes for all the measurement locations. The value of the MAC is between 0 and 1. A value of 1 means that one mode shape vector is a multiple of the other. The experimental and analytical mode shapes must contain the same number of elements, although their scaling is not necessarily the same. Further discussions involving the MAC including its use in the case of complex modes can be found in [12] and [13].

#### 16.7.4.4 Correlation criteria

The test-analysis correlation criteria proposed by [5] are reported in Table 16-1:

**Table 16-1: Test-analysis correlation criteria**

Item	Quality criterion <sup>a</sup>	
Fundamental bending modes of a spacecraft	MAC: Eigenfrequency deviation:	> 0,9 < 3 %
Modes with effective masses > 10 % of the total mass	MAC: Eigenfrequency deviation:	> 0,85 < 5 %
For other modes in the relevant frequency range <sup>b</sup>	MAC: Eigenfrequency deviation:	> 0,8 < 10 %
Cross-orthogonality check	Diagonal terms: Off-diagonal terms:	> 0,90 < 0,10
Damping	To take measured values as input for the response analysis. To use realistic test inputs for this purpose.	
Interface force and moment measurements	For modes with effective masses > 10 %: deviations of interface forces and moments < 10 %.	

a The quality criteria given are not normative and are given as examples for achieving a satisfactory test-analysis correlation.

b The relevant frequency range is, in general, determined by the launcher excitation spectrum up to 100 Hz. This frequency range can, however, be extended due to, for example, high frequency launcher dynamic excitations or specific requirements for AOCS control purposes.

It should be noted that the characteristics considered for the quantitative comparison, including cross-orthogonality check and MAC, provide a quantitative measure of the test-analysis correlation, however they do not give a "useful" measure of the error. In other words there is no established procedure which directly links the prediction (e.g. accuracy) of the loads acting on the spacecraft (which for example are calculated via CLA), to the "validity" (e.g. correlation data) of the structural mathematical model.

## 16.7.5 Error localization and model updating by sensitivity and optimization

### 16.7.5.1 Parameter estimation

The problem of error localisation and model updating has been attacked by a number of researchers who have employed variety of approaches. The introduction of robust optimisation codes has led to the use of a concept which attempts to directly minimise an objective function which estimates the differences between measured and computed results. A series of papers have been published which use frequency matching as an objective function in order to bring computed and measured results into line, e.g. [14] and [15]. In this context the terminology used for design optimisation is normally used in model updating technology, e.g. the design variables of the structural optimisation scheme are the updating parameters of the model updating procedure, similarly the “optimum design” is the “optimum test-analysis correlation”.

For example, the minimisation of the differences between test-analysis natural frequencies, using structural sizing parameters as design variables, could be cast in the following form. Find the set of design variables  $\mathbf{X}$  that minimise:

$$E(\mathbf{X}) = w_g \sum_{j=1}^P w_j \left( \frac{\lambda_{aj} - \lambda_{mj}}{\lambda_{mj}} \right)^2 \quad [16-6]$$

$$\text{Subject to: } x_i^l \leq x_i \leq x_i^u$$

where  $E(\mathbf{X})$  is the objective or error function to be minimised,  $\lambda_m$  and  $\lambda_a(\mathbf{X})$  are the test and analysis eigenvalues,  $P$  is the number of paired modes,  $x^l$  and  $x^u$  are the bounds on the design variables and,  $w_j$  and  $w_g$  are weighting factors.

It was soon recognised that frequency matching alone is very often not sufficient to assure both complete correlation and really improved numerical models. In consequence other matching objectives have been employed, as reported, for example, in [16] and [17].

It should be noted that the approach normally assumes that the test results accurately depict the true behaviour of the structure being analysed; an assumption which may not be correct but the validity of test data is normally not addressed in the mentioned approach.

To assess and quantify the uncertainties in sine vibration test data has been one of the objectives of the study [18].

Finally it should be noted that the exploitation of static load test data, especially within procedures based on sensitivity and optimization is usually rather limited. This is probably due to a number of reasons. For example the correlation and validation criteria are not completely mature or agreed. Furthermore the static test is typically performed in a different test configuration (e.g. primary structure only) with respect to dynamic test and in a different phase of the project. This can bring to practical difficulties or inconsistencies. However it is recommended that the static test data be exploited in a preliminary model validation process, e.g. based on optimization procedures similar to the one indicated by Eq. [16-6]. For example, computed and measured displacements, forces and strains could be used. This should lead to more effective error localization and improved models.

### 16.7.5.2 Modelling errors and selection of the updating parameters

The issue of the location of modelling errors is strictly related to the criteria for the selection of the design variables to be used in the updating procedure. In fact it is essential that regions of the analytical model containing errors be identified and model parameters affecting these regions tailored to achieve the desired correlation. Therefore, in general, the updating parameters should be chosen with the aim of correcting recognised “weaknesses” in the model and the data should be sensitive to them. For example the design variables should be selected for those elements or element groups which have an influence on the natural frequencies and mode shapes which are targeted during the correlation-updating process, in addition to analyst's knowledge of uncertain modelled regions of the structure.

In short the underlying criterion to design variable selection and error localisation consists on determining how effective certain physical property changes might be in reducing the difference between measured and calculated data. However that the data (model output) are sensitive to a candidate parameter is not generally a sufficient reason for its selection.

In practice two basic strategies are possible for the selection of the design variables. The first consists on performing sensitivity analyses by using the initial mathematical model; the latter consists on “*a posteriori*” approach, i.e. the most effective design variables are selected at the end of a number of preliminary design optimisation processes which make use of a preliminary set of design variables.

### 16.7.5.3 Limitations of the “sensitivity and optimisation” approach

The “sensitivity and optimisation” approach to error localization and model updating has a number of limitations:

- Largest changes can be in the most sensitive parameters rather than those in error. This can be a serious inconvenient since it produces misleading “error localization” and “inconsistent updating”.
- Errors of insensitive regions cannot be detected. Generally this is not a crucial issue.
- The success of the updating procedure can strongly depend on the selection of the design parameters to be updated. It means that it could be necessary to consider several sets of design parameters to detect erroneous regions of the model.
- The approach could be “short-sighted” due to possible convergence to local minima. This issue can be strongly mitigated by means of global sensitivity strategies, for example by using Monte Carlo simulations.

### 16.7.6 Specific aspects concerning base-drive sine vibration testing and “real-time” model validation

The main objective of spacecraft base-drive sine vibration tests, (e.g. a qualification test) is to show that the spacecraft structure and units are able to withstand (with a certain margin) the launch loads. Unfortunately direct verification is quite difficult since the dynamic launch loads can be simulated only approximately by shaker motions. Furthermore it has been already mentioned that the structural response of the spacecraft to low frequency mechanical environment is simulated by spacecraft-launcher coupled dynamic analysis. The spacecraft loads derived from the analysis (e.g. interface loads and internal forces or accelerations), are taken as a basis to verify the dimensioning of the spacecraft. The objective of the vibration test is then to apply such loads. Such an approach requires that the finite element model be “valid enough” since the spacecraft interface and internal loads are dependent upon the satellite dynamic characteristics. Some kind of spacecraft modal identification is then necessary

- to verify that the discrepancies with the mathematical model are acceptable and
- to assess the actual loads on the satellite.

When the FE analysis results do not correlate well with test data the model is updated in order to determine more accurate sets of loads. The “*real-time*” model correlation-validation, i.e. the process to assess the adequacy of the FE model during the test, brings also further benefit. It validates the indirect determination of internal loads which cannot be easily measured. Load monitoring can then be achieved through accelerometer measurements after test-analysis good correlation has been demonstrated. Needless to say, when or if such a validation can be performed in real time, input spectrum notching in correspondence of appendage modes, which are often critical, can be determined more quickly and much more safely. Specimen modal characterisation and FE model updating should therefore be performed prior to running high level tests.

Generally rather crude modal identification is performed during base-drive vibration tests, basically restricted to the main spacecraft modes. Other modes, especially solar array or antenna reflector appendage modes are at best coarsely characterised. One of the major objectives of the study [11] has been to get accurate modal information in real time just after having performed the reference low level sine test.

The development of procedures and tools to extract quickly and accurately the modal characteristics from the transfer functions has been the core of the work. Of course quick access to the FEA results is necessary to perform fast correlation between test and analysis output. The study has also shown that “quasi real-time” model update is both feasible and helpful, although it is clear that only limited model modification can be performed during a real test sequence.

### **16.7.7 Stochastic approaches for model validation**

Since experiments produce noisy and fuzzy data due to numerous sources of scatter and uncertainty that are inherently present in all physical systems, and similarly in their numerical simulation models, the problem of correlating numerical and experimental data is in principle best approached on statistical grounds and the concept of model validation should be strongly coupled to uncertainty quantification. In addition, using a deterministic approach, there is usually no assessment on the robustness of the correlation. The question which is raised is really the sensitivity of the model to the known (or assumed) uncertainties. Satisfactory test-analysis correlation does not guarantee that in later events, such as the launch where environment conditions are different, the spacecraft behaves as predicted. For example it should be noted that the configuration of the tested specimen may be rather different from the flight configuration. Within the above scenario, the mathematical model validation process should be robust enough to provide “correct” extrapolations. In short, the success of any model validation depends on the ability to quantify uncertainty and it should be assessed on the basis of an acceptable stochastic distance, which implies the selection of an adequate stochastic metrics between the numerical and experimental models.

One of the major objectives of the EDIS (Enhancement of Dynamic Identification for Spacecraft) study was to develop and implement stochastic techniques for the validation of spacecraft structural dynamic models. An additional challenge came from the need to maintain compatibility with certain deterministic notions such as the MAC and mode pairing in order to provide a transitional and comparative link with current practice. A number of papers (e.g. [19] [20]) have been published which present the objectives, the logic and results of the EDIS study.

The EDIS study has shown that the stochastic approach is more complex and much more computationally expensive than the deterministic approach and the characterisation of structural uncertainties necessary to implement the approach can be difficult and time-consuming. Moreover the stochastic validation logic is not straightforward and rather complex. Finally the definition of the “acceptable correlation criteria” remained a partially open point. All the above reasons currently prevent the use of a complete stochastic approach within the industrial environment.

On the other hand the stochastic model validation approach developed within the EDIS study provides a larger and important amount of additional information on the correlation and updating processes and allows assessing the robustness of the correlation. In fact the approach can take into account the uncertainties associated with the input variables of the finite element model as well as the scatter in test data, if available.

An important final remark concerns the use of Monte Carlo simulation (MCS) techniques, which can also be used within a “determinist logic”, for example to minimize a “deterministic distance” between the numerical and experimental models. In this case, by MCS, input/output relationships may be examined over the entire design space instead of being limited to a localized gradient, therefore the updating process is, potentially, much more powerful in terms of correlation and error localization performances [21]. In particular it should be noted that specific post-processing techniques are available which visualize the results of the global sensitivity analysis performed by MCS, allowing to know, for example, which inputs or combination of inputs are responsible for changing an output quantity.

## 16.8 References

- [1] Guide for Verification and Validation in Computational Solid Mechanics, ASME V&V 10-2006, New York, NY, USA, 2006
- [2] Space engineering, Structural general requirements, ECSS-E-ST-32C Rev. 1, Noordwijk, The Netherlands, November 2008
- [3] Space engineering, Structural finite element models, ECSS-E-ST-32-03C, Noordwijk, The Netherlands, July 2008
- [4] Space engineering , Structural factors of safety for spaceflight hardware, ECSS-E-ST-32-10C Rev. 1, Noordwijk, The Netherlands, March 2009
- [5] Space engineering, Modal survey assessment, ECSS-E-ST-32-11C, Noordwijk, The Netherlands, July 2008
- [6] Guidelines for loads analyses and dynamic model verification of Shuttle cargo elements, MSFC-HDBK-1974, NASA October 1991
- [7] Sarafin T.P. (editor), Spacecraft structures and mechanisms-from concept to launch, Kluwer Academic Publishers, Dordrecht, The Netherlands, 1995
- [8] Ewins D. J. – Modal Testing: Theory, Practice and Applications – Research Studies Press LTD, Baldock, England, Second Edition, 2000
- [9] Calvi A. - Uncertainty-based loads analysis for spacecraft: Finite element model validation and dynamic responses – International Journal on Computers & Structures, 83 (2005) 1103-1112
- [10] Friswell M.I., Mottershead J.E. - Finite element model updating in structural dynamics - Kluwer Academic Publishers, Dordrecht, The Netherlands, 1995
- [11] Lefevre Y.M., Bonetti J.C., Girard A., Roy N., Calvi A., Real-Time Modal Identification Techniques for Improved Satellite Vibration Testing – Proc. European Conference on Spacecraft Structures, Materials and Mechanical Testing, Toulouse, France, December 11-13, 2002
- [12] Vacher P., Jacquier B., Bucharles A., Extensions of the MAC criterion to complex modes, Proceedings of ISMA International Conference on Noise and Vibration Engineering, Leuven, Belgium, 2010

- [13] Allemand R.J., The Modal Assurance Criterion - Twenty Years of Use and Abuse, *Sound and Vibration*, 37(8):14-21, August 2003
- [14] Blakely K., Bush R. - Using MSC/NASTRAN to Match Dynamic Test Data. Proceedings of the International Conference on Structural Dynamics Modelling, Milton Keynes, UK, pp. 411-420, July 1993
- [15] Brooker S. M., Morris A. J. - Correlation of Helicopter Test and Finite Element Analysis via Structural Optimisation. Proceedings of the International Conference on Structural Dynamics Modelling, Milton Keynes, UK, pp. 159-169, July 1993
- [16] Blelloch, P. A. - Direct Correlation of Test-Analysis Cross-Orthogonality. *Modal Analysis: the International Journal of Analytical and Experimental Modal Analysis*, v. 8, n. 3, July 1993, pp. 247-255
- [17] Calvi A., Morris A.J. - Updating of large-scale structural dynamic models by a semi-automatic two-level optimisation procedure – Proc. of the European Conference on Spacecraft Structures, Materials and Mechanical Testing, Noordwijk, The Netherlands, December 2000
- [18] Assessment and improvement of dynamic test data (DYNAMITED) – EADS Astrium Final Report MTF.AIDT.TN.2168 – ESA Contract 20307/06/NL/IA, September 2010
- [19] Calvi A., Canay M.A., Pavón M.T. – Validation of Spacecraft Structural Dynamic Models based on a Stochastic Methodology - Proc. of the 7th International Conference on Computational Structures Technology, Lisbon, Portugal, 7-9 September 2004
- [20] Roy N., Garcia De Paredes S. - A Stochastic Approach to the Validation of Spacecraft Structural Dynamic Models - Proc. of the European Conference on Spacecraft Structures, Materials and Mechanical Testing, Noordwijk, The Netherlands, May 2005
- [21] Calvi A., Petitti I.A. – Application of a Stochastic Approach for the Validation of Spacecraft Structural Dynamic Models - Proc. of the Sixth European Conference on Structural Dynamics - Paris, France, September 4-7, 2005